frontiers | Research Topics

Network mining and propagation dynamics analysis

Edited by
Xuzhen Zhu, Wei Wang, Shirui Pan and Fei Xiong

Published in
Frontiers in Physics

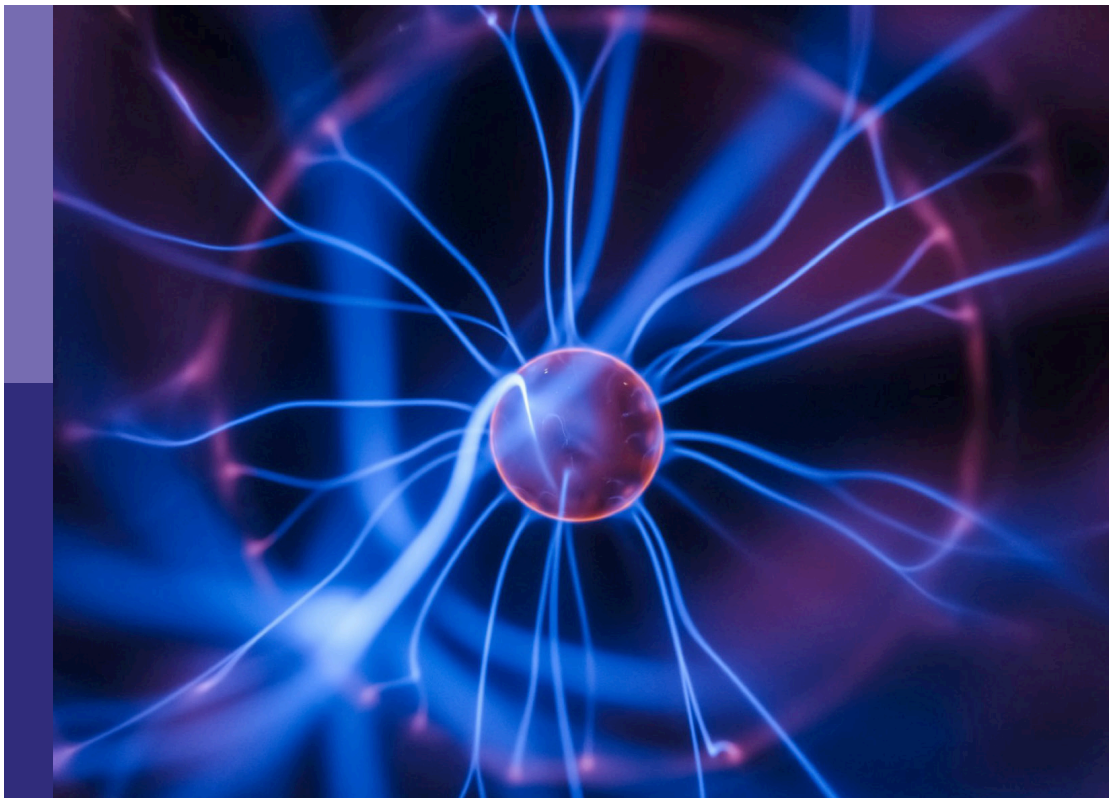

ISSN 1664-8714
ISBN 978-2-83251-614-0
DOI 10.3389/978-2-83251-614-0

About Frontiers

Frontiers is more than just an open access publisher of scholarly articles: it is a pioneering approach to the world of academia, radically improving the way scholarly research is managed. The grand vision of Frontiers is a world where all people have an equal opportunity to seek, share and generate knowledge. Frontiers provides immediate and permanent online open access to all its publications, but this alone is not enough to realize our grand goals.

Frontiers journal series

The Frontiers journal series is a multi-tier and interdisciplinary set of open-access, online journals, promising a paradigm shift from the current review, selection and dissemination processes in academic publishing. All Frontiers journals are driven by researchers for researchers; therefore, they constitute a service to the scholarly community. At the same time, the *Frontiers journal series* operates on a revolutionary invention, the tiered publishing system, initially addressing specific communities of scholars, and gradually climbing up to broader public understanding, thus serving the interests of the lay society, too.

Dedication to quality

Each Frontiers article is a landmark of the highest quality, thanks to genuinely collaborative interactions between authors and review editors, who include some of the world's best academicians. Research must be certified by peers before entering a stream of knowledge that may eventually reach the public - and shape society; therefore, Frontiers only applies the most rigorous and unbiased reviews. Frontiers revolutionizes research publishing by freely delivering the most outstanding research, evaluated with no bias from both the academic and social point of view. By applying the most advanced information technologies, Frontiers is catapulting scholarly publishing into a new generation.

What are Frontiers Research Topics?

Frontiers Research Topics are very popular trademarks of the *Frontiers journals series*: they are collections of at least ten articles, all centered on a particular subject. With their unique mix of varied contributions from Original Research to Review Articles, Frontiers Research Topics unify the most influential researchers, the latest key findings and historical advances in a hot research area.

Find out more on how to host your own Frontiers Research Topic or contribute to one as an author by contacting the Frontiers editorial office: frontiersin.org/about/contact

Network mining and propagation dynamics analysis

Topic editors

Xuzhen Zhu — Beijing University of Posts and Telecommunications (BUPT), China
Wei Wang — Chongqing Medical University, China
Shirui Pan — Monash University, Australia
Fei Xiong — Beijing Jiaotong University, China

Citation

Zhu, X., Wang, W., Pan, S., Xiong, F., eds. (2023). *Network mining and propagation dynamics analysis*. Lausanne: Frontiers Media SA. doi: 10.3389/978-2-83251-614-0

Table of contents

05 Editorial: Network mining and propagation dynamics analysis
Xinyi Wang, Yuexia Zhang, Xuzhen Zhu, Fei Xiong, Wei Wang and Shirui Pan

09 Cascade Prediction With Self-Exciting Point Process and Local User Influence Measurement
Yingsi Zhao and Chu Zhong

20 Ambient Air Pollution and Hospitalization for Acute Myocardial Infarction in Chongqing, China: A Time-Stratified Case Crossover Analysis
Mingming Zhao, Xing Liu, Ming Yuan, Ying Yang, Hao Chen, Mengmeng Li, Pan Luo, Yong Duan, Jie Fan, Leqi Liu and Li Zhou

28 Analysis of information propagation and control of a layered SITR model in complex networks
Dawei Pan and Yuexia Zhang

42 Effect of social media rumors on stock market volatility: A case of data mining in China
Hua Zhang, Yuanzhu Chen, Wei Rong, Jun Wang and Jinghua Tan

59 The study of new energy vehicle choice in China from the perspective of complex neural network
Hui Liu and Lei Feng

77 Asymmetric evolutionary game analysis of emergency cooperative social networks for magnitude emergencies: Evidence from the Beijing-Tianjin-Hebei region in China
Rui Nan and Jingjie Wang

95 City network mining in china's yangtze river economic belt based on "two-way time distance" modified gravity model and social network analysis
Duo Chai, Jiaze Du, Zongqi Yu and Dong Zhang

117 Modeling hierarchical attention interaction between contexts and triple-channel encoding networks for document-grounded dialog generation
Yuanyuan Cai, Min Zuo and Haitao Xiong

129 Social contagion influenced by active-passive psychology of college students
Jianmeng Ye and Yi Chen

138 A spatial network analysis of vegetable prices based on a partial granger causality approach
Chen Shen, Liang Chi, Ximeng Wang, Shuqing Han, Jing Zhang and Mengshuai Zhu

146 MPDNet: A Transformer-based real-time passenger detection network in metro stations
Jun Yang, Mengjie Gong, Xueru Dong, Jiahua Liang and Yan Wang

156 MERP: Motifs enhanced network embedding based on edge reweighting preprocessing
Shaoqing Lv, Ju Xiang, Yiyang Li, Xincheng Ren and Guangyue Lu

167 Role of degree and weighted coreness based on endpoints in link prediction
Jiaqi Hao, Zheng Li, Zhanhe Wu and Jinming Ma

176 Hawkes processes for understanding heterogeneity in information propagation on Twitter
Liwen Wang and Lin Zhang

188 An opinion dynamics model based on affinity and social noise
Jusheng Liu, Jianjia He, Zhiping Qiu and Shengxue He

199 Combining NSP and NER for public opinion event extraction model
Qingchuan Zhang, Siwei Wei, Zihan Li and Wenjing Yan

frontiers | Frontiers in Physics

TYPE Editorial
PUBLISHED 24 January 2023
DOI 10.3389/fphy.2022.1130473

OPEN ACCESS

EDITED AND REVIEWED BY
Matjaž Perc,
University of Maribor, Slovenia

*CORRESPONDENCE
Xuzhen Zhu,
zhuxuzhen@bupt.edu.cn

SPECIALTY SECTION
This article was submitted to Social Physics, a section of the journal Frontiers in Physics

RECEIVED 23 December 2022
ACCEPTED 29 December 2022
PUBLISHED 24 January 2023

CITATION
Wang X, Zhang Y, Zhu X, Xiong F, Wang W and Pan S (2023), Editorial: Network mining and propagation dynamics analysis. *Front. Phys.* 10:1130473. doi: 10.3389/fphy.2022.1130473

Editorial: Network mining and propagation dynamics analysis

Xinyi Wang[1], Yuexia Zhang[2], Xuzhen Zhu[3]*, Fei Xiong[4], Wei Wang[5] and Shirui Pan[6]

[1]Key Laboratory of Information and Communication Systems, Ministry of Information Industry, Beijing Information Science and Technology University, Beijing, China, [2]Key Laboratory of Modern Measurement and Control Technology, Ministry of Education Beijing Information Science and Technology University, Beijing, China, [3]State Key Laboratory of Networking and Switching Technology, Beijing University of Posts and Telecommunications, Beijing, China, [4]School of Electronic and Information Engineering, Beijing Jiaotong University, Beijing, China, [5]School of Public Health, Chongqing Medical University, Chongqing, China, [6]School of Information and Communication Technology, Griffith University, Nathan, QLD, Australia

KEYWORDS

complex network, propagation dynamics, link prediction, recommendation, network mining

Editorial on the Research Topic
Network mining and propagation dynamics analysis

1 Introduction

Many phenomena in the fields of computer science, biology, sociology, and economics can be described as transmission dynamics on complex networks. Propagation dynamics on complex networks can be used to describe many propagation phenomena in the real world [1, 2]. The modeling of communication dynamics based on complex networks and its intervention research are of great practical significance. For example, they can provide decision-making bases for the prevention and control of diseases, rumor control, and product marketing. In many real-life propagation phenomena, we often wonder about the mechanisms and laws of their propagation on complex networks and their predictive methods and means of control. We can have a clear and comprehensive understanding of the evolution mechanism, propagation process, and steady state of real phenomena by clarifying the above questions. Furthermore, it also provides some necessary theoretical support for predicting and controlling real systems.

The study of link prediction mainly uses the known information of various network structures to compute the similarity between the nodes in a network without a connection and to obtain the possibility of the lost connection in a network or the connection that will be generated in the future. With the rapid development of network science, the study of link prediction is closely related to the structure and evolution of networks. At the same time, these studies can also help us to theoretically understand the evolution mechanism of complex networks, thus better deriving the propagation dynamics of complex networks.

For this purpose, this Research Topic in Frontiers in Physics intends to clarify the contribution of the rapidly developing research field of complex networks. We encourage articles that use multidisciplinary methods for complex network data mining, such as machine learning, information theory, applied mathematics, and computational statistical physics. We also invite researchers to write original research articles. Potential topics include but are not limited to the following.

- Trend analysis of social network information dissemination
- Analysis of the spread trend of infectious diseases
- Analysis of the computer virus transmission process
- Link prediction on social networks
- Behavior analysis on social networks
- Network state prediction
- Behavior pattern recognition
- Personalized recommendation systems

2 Presentation of the papers

The first paper, titled "*Ambient Air Pollution and Hospitalization for Acute Myocardial Infarction in Chongqing, China: A Time-Stratified Case Crossover Analysis*" [3](Zhao et al.), focuses on short-term exposure to ambient air pollution on acute myocardial infarction (AMI) with limited and inconsistent evidence; investigates the relationship between air pollution and acute myocardial infarction hospitalization in Chongqing, China; and further studies and determines, from the epidemiological and physiological perspective, the causal relationship between air pollution, meteorological factors, and acute myocardial infarction. The experimental results suggest that short-term exposure to PM2.5, PM10, SO2, NO2, and CO helps to increase AMI admissions, which have public health implications for primary prevention and emergency health services. This paper provides clear evidence that AMI hospitalization can be increased by ambient air pollution in Chongqing, China.

The second paper, titled"*Cascade Prediction with Self-Exciting Point Process and Local User Influence Measurement*" [4] (Zhao et al.), proposes a prediction model of information cascades in social networks based on the Hawkes process, which considers post influence, user influence, and user response time to describe the occurrence probability of forwarding events. The authors present a new method of calculating user influence, combined with semi-local centrality and local clustering coefficients. A regression tree algorithm is used to determine time correction coefficients to reveal dynamic post influence, and the popularity prediction of posts on social networks is realized. Comparison experiments of different models are carried out on real-world datasets and the results show that our method outperforms other counterparts.

The third paper, titled "*Analysis of information propagation and control of a layered SITR model in complex networks*" [5] (Pan et al.), proposes a novel L-SITR model that stratifies information propagators based on nodal influences and improves the traditional SIRS model by adding rational propagators. Through the study of the theoretical analysis of dynamics equations, the authors determine the spread of the L-SITR model threshold and, combined with numerical simulation, prove the stability of the equilibrium point. To suppress the large-scale spread of online public opinion information, optimal control is applied to the L-SITR model. The results show that the proposed L-SITR model has higher accuracy than the traditional SIRS model and is more suitable for information propagation prediction in the presence of rational communicators. The optimal control method proposed in this paper can effectively reduce the influence of public opinion propagation.

The fourth paper, titled "Asymmetric evolutionary game analysis of emergency cooperative social networks for magnitude emergencies: Evidence from the Beijing-Tianjin-Hebei region in China" [6] (Nan et al.), uses social network analysis (SNA) and an asymmetric evolutionary game model based on the data set of the cooperative fight against COVID-19 of the Beijing-Tianjin-Hebei region in China. The authors found that the asymmetry between regions is comprehensively determined by resource endowment, administrative level, geographical distance, regional vulnerability, political pressure, and other factors; vertical control is still the main operating mechanism of ECSNs. Network derivation is caused by the superposition of multiple factors, and obstacles may arise from which political factors are very important and asymmetry.

The fifth paper, titled "*Effect of social media rumors on stock market volatility: A case of data mining in China*" [7] (Zhang et al.), identifies patterns from social media rumors from financial forums using machine learning, quantifying social media rumors based on statistics and analyzing the mechanism of propagation and influence of social media rumors on stock market volatility using econometric models. The results show that rumors have an important information transmission effect on stock market volatility and the constructed Internet Financial Forum Rumor Index is helpful in understanding the potential impact of rumors. These research results are of guiding significance for optimizing the information environment and are conducive to promoting the healthy and stable development of the securities market.

The sixth paper, titled "*The study of new energy vehicle choice in China from the perspective of a complex neural network*" [8] (Liu et al.), uses the Bert-wwm-ext model structure, data mining, and deep learning to study the new energy vehicle selection and also analyzes the positioning of domestic and foreign new energy vehicle brands and their brand development from the perspective of complex networks. The results show that: 1) Consumers are paying increasing attention to the quality of new energy vehicles; 2) Consumer satisfaction with the endurance of pure electric vehicles and plug-in hybrid electric vehicles varies significantly; 3) Consumer evaluation is positively correlated with car prices; and 4) The head effect of Chinese brands is significant, and foreign brands have formed strong brands with high brand premium.

The seventh paper, titled "*Role of degree and weighted coreness based on endpoints in link prediction*" [9] (Hao et al.), proposes a weighted hybrid influence model based on the degree and coreness (WDCHI) and compares the prediction results of the WDCHI with those of CN, AA, RA, LP, SRW, CSRW, HSRW, and SHI. The results show that WDCHI exhibits the same computational complexity and performs better than other models on the metric AUC. Moreover, this finding can be used to improve social networks, computer networks, communication networks, and other types of networks.

The eighth paper, titled "*MPDNet: A Transformer-based real-time passenger detection network in metro stations*" [10] (Yang et al.), suggests a subway passenger detection network based on the transformer model (MPDNet), which can detect dense passenger flow in the installation angle of the subway video surveillance system. Moreover, the authors propose a MetroStation dataset based on subway surveillance video to better evaluate the performance of the model in the metro. This dataset reflects multiple scenarios in subway stations compared to other pedestrian detection datasets. The experiments on the MetroStation dataset show that the MPDNet performed better.

The ninth paper, entitled "*City network mining in China's Yangtze river economic belt based on "two-way time distance"modified gravity model and social network analysis*" [11] (Chai et al.), studies the inter-urban connectivity strength, structure, density, and distribution

pattern of urban networks along the Yangtze River Economic Belt in China using the SNA method, "Dual-direction time distance" modified gravity model, and ArcGIS geographic visualization method. The results show that the modified gravitational model can better reveal the interaction differences between cities and reflect the current and potential economic, population, and resource relations between cities, and this finding has a high application value for the mining of regional urban network structures.

The 10th paper, titled "*Social contagion influenced by active-passive psychology of college students*" [12] (Ye et al.), explores the effects of behavioral psychology on social transmission on campus and establishes a threshold model of active and passive student behavior in weighted networks to conceptually study the effects of psychological heterogeneity. The theoretical study and simulation results show that active students encourage the acceptance of new behaviors and the dissemination of information. However, as the proportion of active students declines, the growth pattern shifts to a discontinuous phase transition.

The 11th paper, titled "*Hawkes processes for understanding heterogeneity in information propagation on Twitter*" [13] (Wang et al.), discusses the heterogeneity of study users during information dissemination and, finally, proposes an improved Hawkes model. The theoretical study and simulation results show that the improved Hawkes model has higher prediction accuracy for wave peaks during propagation and is more accurate in the prediction of peak occurrence. The improved Hawkes model is an effective communication model for detecting and quantifying the super-spreaders in the transmission process, which has a certain guiding significance in the control and prediction of information transmission in social media.

The 12th paper, titled "*A spatial network analysis of vegetable prices based on a partial granger causality approach*" [14] (Shen et al.), takes garlic as an example and presents a vector autoregression model, analyzing relations of the price transmission between producing and selling cities. The authors use the partial Granger causality test to determine the direction and path of price transmission between the main producing areas and the main consuming areas. The theoretical study and simulation results reveal the features of agricultural product price transmission in China and provide reasons and evidence for market regulation.

The 13th paper, titled "*Modeling hierarchical attention interaction between contexts and triple-channel encoding networks for document-grounded dialog Generation*" [15] (Cai et al.), proposes a neural network generative model with attention mechanisms for document-based, multi-session conversations. The model encodes the discourse context containing a given document, dialog history, and last speech as a distributed representation through three channels. The authors introduce hierarchical attention interactions between conversation context and previously generated utterances to generate appropriate responses. Comparing the model with the various baselines on the dataset, CMU_DoG shows that the proposed model performs better than the other related models.

The 14th paper, titled "*An opinion dynamics model based on affinity and social noise*" [16] (Liu et al.), introduces affinity and social noise in the Hegselmann–Krause model of opinion dynamics and proposes an affinity and social noise Hegselmann–Krause model (ASNHK) based on the social influence theory and the Hegselmann–Krause model of opinion dynamics. The model incorporates affinity and noise into the HK model and studies the influence of affinity, the affinity threshold, social noise, and human heterogeneity on the evolution of opinions. The results show that, first of all, affinity between people can improve their opinions toward forming a consensus positively, but the affinity threshold has a negative role. The authors state that this study introduces affinity and social noise in the Hegselmann–Krause model of opinion dynamics, provides a new perspective on the social influence theory, and enriches the application of this theory in opinion dynamics.

The 15th paper, entitled "*Combining NSP and NER for public opinion event extraction mode*" [17] (Zhang et al.), proposes an opinion event extraction model combining NSP and NER (NN-EE) to alleviate the deficiency of the combined event parameter extraction performance by introducing NER technology. At the same time, the authors incorporate the event-triggered features into the NSP mechanism of the pre-trained language model, BERT, prompting the model to learn the deep semantic interaction between event-triggered and the original text. Experimental results show that the model achieves the optimal performance on the authors' self-constructed food opinion report dataset FD-OR, which verifies the effectiveness of the model.

The last paper published in this Research Topic, entitled"*MERP: Motif-enhanced network embedding based on edge reweighting preprocessing*" [18] (Lv et al.), proposes a motif-enhancement framework for network embedding based on edge reweighting. Through edge reweighting, the weight of redundant noise edges between motifs is decreased. The authors apply edge reweighting as a preprocessing phase in network embedding and construct the motif-enhanced network by incorporating enhanced motif structures with the original network, allowing the embedding of vectors from the enhanced network for better performance in downstream network analysis tasks. The results show that this framework performs better than state-of-the-art network embedding methods.

We thank all the authors for their contributions and hope that this Research Topic will encourage more scientists to deepen their research on the development of complex network mining and the analysis of propagation dynamics.

Author contributions

XZ, XW, and YZ organized the idea. XZ, XW, and YZ wrote the paper. FX, WW, and SP reviewed the paper and made revisions.

Funding

The work was supported in part by the Sub Project of the National Key Research and Development plan in 2020 No. 2020YFC1511704, Beijing Information Science and Technology University Nos 2020KYNH212, 2021CGZH302. Beijing Science and Technology Project (Grant No. Z211100004421009), and in part by the National Natural Science Foundation of China (Grant No. 61971048).

Acknowledgments

We are grateful for the contributions to this Research Topic made by Frontiers editorial staff members. We also thank the reviewers who provided valuable input for each manuscript.

Conflict of interest

The authors declare that the research was conducted in the absence of any commercial or financial relationships that could be construed as a potential conflict of interest.

Publisher's note

References

1. Zhong C, Xiong F, Pan S, Wang L, Xiong X. Hierarchical attention neural network for information cascade prediction. *Inf Sci* (2023) 622:1109–27. doi:10.1016/j.ins.2022.11.163

2. Li Z, Xiong F, Wang X, Chen H, Xiong X. Topological influence-aware recommendation on social networks. *Complexity* (2019) 2019:1–12. doi:10.1155/2019/6325654

frontiers | Frontiers in Physics

ORIGINAL RESEARCH
published: 08 July 2022
doi: 10.3389/fphy.2022.951729

Cascade Prediction With Self-Exciting Point Process and Local User Influence Measurement

Yingsi Zhao[1]* *and Chu Zhong*[2]

[1]School of Economics and Management, Beijing Jiaotong University, Beijing, China, [2]School of Electronics and Information Engineering, Beijing Jiaotong University, Beijing, China

With the rise and large-scale applications of social networking service, the prediction of information cascades has attracted extensive attention of researchers. User influence is an important factor affecting the dissemination of posts in online social networks. However, current studies usually take the number of users' neighbors as their influence, and do not accurately describe the role of participating users in information dissemination. In this paper, a prediction model of information cascades in social networks is established based on the Hawkes process, and the model considers three factors, i.e., post influence, user influence and users' response time, to describe the occurrence probability of forwarding events. In order to utilize abundant information of local network topology, we present a new method of calculating user influence, combining with semi-local centrality and local clustering coefficients. Then, a regression tree algorithm is used to determine time correction coefficients to reveal dynamic post influence, and the popularity prediction of posts in social networks is realized. Comparison experiments of different models are carried out on real-world datasets to evaluate the effectiveness and prediction performance of the proposed model, and results show that our method outperforms other counterparts.

Keywords: cascade prediction, self-exciting point process, user influence, dynamic post correction, social network

OPEN ACCESS

Edited by:
Xuzhen Zhu,
Beijing University of Posts and Telecommunications (BUPT), China

Reviewed by:
Junyu Xuan,
University of Technology Sydney, Australia
Lin Hui,
Tamkang University, Taiwan
Zhangbing Zhou,
China University of Geosciences, China

***Correspondence:**
Yingsi Zhao
yszhao@bjtu.edu.cn

Specialty section:
This article was submitted to Social Physics, a section of the journal Frontiers in Physics

Received: *24 May 2022*
Accepted: *17 June 2022*
Published: *08 July 2022*

Citation:
Zhao Y and Zhong C (2022) Cascade Prediction With Self-Exciting Point Process and Local User Influence Measurement. Front. Phys. 10:951729. doi: 10.3389/fphy.2022.951729

1 INTRODUCTION

With massive user-generated contents and closely intertwined user relationship networks, the phenomena of information cascades become more and more common [1–3], and the work of information cascade prediction has also received notable attention of researchers [4–6]. The cascade prediction focuses on the cascade of social networks, which aims to estimate the future information diffusion ways. The final size of an information cascade directly indicates the popularity and influence depth of the information, and it is the reflection of information importance. That is, the larger the final scale of an information cascade, the higher its popularity and the wider the influence. Taking Twitter as an example, users can express their views and opinions on this platform. When a user posts a tweet, some users who follow it may retweet the tweet because they like it or approve of it, and then, the users who follow those retweeters have an opportunity to see the tweet [7–9]. After the tweet is received, it may also be forwarded, and the retweeting process is repeated continuously, forming a cascade of information in the network.

Existing work on information cascade prediction can be generally divided into two aspects: prediction methods based on feature learning and those based on model generation. The basic idea of feature learning is to use related algorithms of machine learning to formalize information cascade

prediction as a classification or regression problem, and to extract relevant features of user-generated contents and initial cascade process, such as information disseminator [10, 11], information contents [12–14], and network structure [15–17], etc. Then, this kind of methods use different algorithms to mine the extracted features, so as to establish a mapping relationship between correlated characteristics and the future size of an information cascade. Wang et al. [18] proposed a combined social media popularity prediction framework based on multimodal feature extraction, implemented feature generalization and temporal modeling, and adopted a sliding window average to model short-term dependency of each user among visual and textual features. Kong et al. [19] focused on predicting multiple stages of popularity such as outbreak, plateau, rise, and fall. They adopted a pattern matching method to predict the future popularity stage by extracting multiple dynamic factors such as the number of retweets, the number of users, and network structure features at the micro level, and extracting the overall evolution pattern of the popularity stage at the macro level. Zhang et al. [20] extracted the time, structure and content features from the diffusion process of embedded web pages in WeChat moments and predicted the growth of content popularity. The results showed that the popularity scale was strongly correlated with the initial network structure of the cascade. Due to the diversity of features in the process of information cascades, it is very difficult to extract the optimal feature set. How to minimize the calculation and optimize the dynamic feature extraction process is an urgent problem to be solved.

On the other side, the methods with model generation directly simulate the process of information diffusion in a network, and formalize the cascade process into a parameterized model by analyzing the factors that affect the diffusion. After the diffusion model is established, various parameters of the model are estimated according to the cascade data observed in the initial stage, so as to predict the future cascade [21–27]. Zhao et al. [28] used the time-varying tweet influence to measure the forwarding rate, and identified whether a cascade is in the supercritical state or in the subcritical state. Chen et al. [29] proposed a marked self-exciting point process model to capture the retweeting dynamics and predict the tweet popularity. They selected the specific parameter form of the function in the model by comparing the goodness of fit of retweet cascades in the training data set. Palmowski et al. [30] described moments method of estimation of the parameters of Hawkes point process by using the generator theory to analyze and model the cascade effect of forwarding in social networks. Srivathsan et al. [31] presented a detailed Bayesian model of the information by incorporating prior knowledge of unobserved user information, which removed the high influence of the first observed user behavior. The results show that users make weighted choices between adoption and rejection, but do not always choose the most likely option, and adding prior user information will delay the cascade effect. Due to various assumptions on many factors affecting propagation process in the modeling, compared with prediction methods based on feature learning, model generation methods do not have the learning process of cascading features, so their prediction performance may be limited to a certain extent. Therefore, model generation methods should be incorporated with feature learning to improve the expressions of propagation details.

Existing models of cascade prediction only consider the number of followers for each forwarding user, that is, the in-degree of a node, when modeling the arrival intensity of forwarding events. The number of user's followers can indeed represent the influence of a user to a certain extent, but this measurement also has certain shortcomings. Users with more followers do not necessarily have higher activity. Higher activity of a user in social networks means that the user may frequently post or repost a message, contributing to the growth of the forwarding cascade. In addition, fake online users are often used to construct fake popularity of influencers. If a user has a large number of fake fans, its influence will be overestimated when only measured by the number of fans.

We mainly focus on the problem of information cascades formed by the diffusion of posts (tweets on Twitter) after the posts are published in social networks, and investigate the prediction method based on model generation. We analyze the factors which affect the spreading of posts, and take the final number of reposts to measure the size of a cascade. Then, we construct the cascade prediction model based on the Hawkes process (also known as a self-exciting point process) to explore the final scale and influence range of an information cascade. In addition, we integrate the model with feature learning by introducing a cascading parameter to reflect the timeliness of posts. The main work of this paper is as follows:

1) We model the forwarding times of posts as a counting process, and characterize the arrival intensity of forwarding events by three factors, i.e., the influence of posts themselves, the influence of forwarding users, and the response time of users. Finally, the prediction model of the final forwarding number is obtained by integrating the theory of a branching process.
2) We propose a method of calculating the influence of forwarding users and predict the influence of posts. Then, we use a regression tree algorithm to train the cascading parameter, and a prediction algorithm is realized to obtain the final forwarding numbers of posts.
3) We conduct performance evaluation and comparative analysis of the cascade prediction model on two datasets from real social networks, and confirm the effectiveness of our model.

The rest of the paper is structured as follows. Our cascade prediction method is presented in **Section 2**. **Section 3** provides experiments and empirical results of the model. Our conclusions are presented in **Section 4**.

2 METHODS

In this section, firstly, we describe the specific problem discussed in this paper, and introduce the goal of information cascade prediction. Then, in terms of the theory of a counting process, we

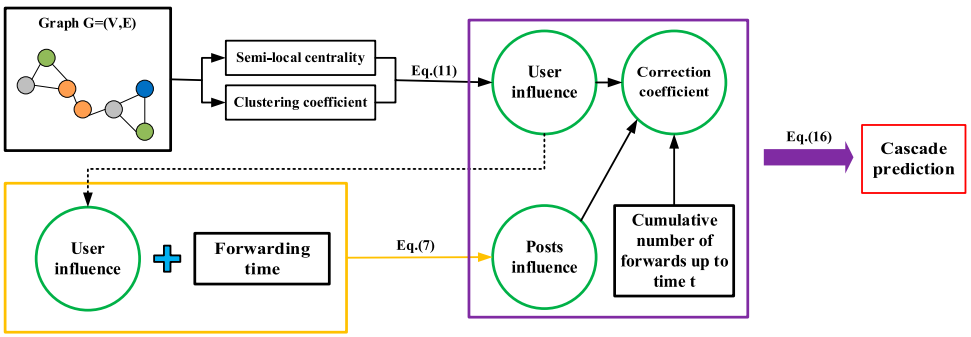

FIGURE 1 | Overview of the proposed framework.

TABLE 1 | Notations.

Symbol	Description
i	the ith forward, $i = 0$ indicating the original post
t	the time to make a prediction
t_i	the time of ith forwarding event
u_i	the influence of ith forwarding user
$\|N(i)\|$	number of nearest neighbor nodes of user i
$\|\Gamma(i)\|$	sum of the numbers of nearest neighbor and next nearest neighbor nodes of user i
c_i	local clustering coefficient of user i
β	the parameter to balance user influence
$R(t)$	cumulative number of forwards up to time t
$\hat{R}(\infty)$	the predicted value of the final number of forwards
$R(\infty)$	the real final number of post forwards
U_t	sum of influence of forwarding users up to time t
U_t^e	sum of effective values of forwarding user influence up to time t
$\lambda(t)$	arrival intensity of forwarding events for $R(t)$
$p(t)$	influence of the post at time t
$\Phi(t)$	memory kernel function
μ_t	correction coefficient of predicted results

model the arrival intensity of post forwarding events based on the Hawkes process. Finally, we combine our generative model with intergenerational characteristics of a branching process, and obtain the predicted value of the final forwarding number. **Figure 1** illustrates the overview of our proposed model.

2.1 Problem Definition

We assume that the publishing time for a post is t_0. According to forwarding events of the post in the time period $[t_0, t]$ which include forwarding time and relevant information of forwarding users, we arrange these forwarding events in the order of forwarding time. The occurrence time of the i-th forwarding event is defined as t_i, and u_i is used to represent the corresponding forwarding user. Then, the relevant information chain $\{(t_1, u_1), (t_2, u_2), \ldots, (t_i, u_i), \ldots\}$ at the initial stage of the post forwarding cascade is obtained as known information. It is worth noting here that the relevant information of forwarding users is reflected by the user relationship network, and it is mainly used to extract the influence of users in the network. The influence determines the size of the user group that may take further forwarding behaviors. The counting process $R(t)$ as a representative of point process is used to describe the cumulative number of forwards obtained by the post in the time period $[t_0, t]$. Then, the task of information cascade prediction is to predict the final number of forwards $\hat{R}(\infty)$ obtained by the post at the time t according to the information chain $\{(t_1, u_1), (t_2, u_2), \ldots, (t_i, u_i), \ldots\}$. **Table 1** shows the notations involved in this paper.

2.2 Forwarding Probability Modeling

Apparently, in the study of a counting process, how to characterize event arrival intensities in the process is a key problem. According to the features and growth mechanism of a forwarding cascade, each time a post is forwarded by a user, it may gain the attention of more users. Therefore, the number of potential users that may take forwarding behaviors increases due to forwarding events, and then more subsequent forwards are stimulated.

We characterize the probability of post forwarding events based on the intensity function of the Hawkes process. The intensity function of an event arrival in the classical Hawkes process is expressed as follows [32]:

TABLE 2 | Statistics of datasets.

Dataset	Description	Detailed Information
Dataset 1	Twitter without relationship information between users	The dataset contains information of each post includes its ID, publishing time, the ID and number of fans of the publisher, a series of forwarding time and the forwarding users
Dataset 2	Twitter with relationship information between users	The dataset contains related forwarding information of 3,553 posts, and 1,731,658 relationships between 71,367 users

$$\boldsymbol{\lambda}(\boldsymbol{t}, \mathrm{H}_t) = \boldsymbol{\nu} + \int_{-\infty}^{t} \boldsymbol{\gamma}(\boldsymbol{t} - \boldsymbol{u}) \boldsymbol{dR}(\boldsymbol{t}) \tag{1}$$

where H_t represents the historical data in the counting process $R(t)$ up to time t. ν indicates the external incentive intensity, which describes the impact of the post background on subsequent forwarding cascade. For instance, in the process of information dissemination, some emergencies in real world affect information cascades in the social network, and the influence belongs to external factors other than forwarding events themselves. $\gamma(t)$ is a self-excited kernel function, which characterizes the self-excited effect of historical forwarding events on the current event, i.e., the self-excited effect of the current event on subsequent forwarding cascade. In order to quantify the growth mechanism of an information cascade, the original Hawkes process is simplified to exclude the influence of external incentive factors, and the function of event arrival intensity in the cascade process is expressed as the linear sum of self-excited kernel functions over time. The intensity function is given as follows:

$$\boldsymbol{\lambda}(\boldsymbol{t}) = \sum_{t_i \le t} \boldsymbol{\gamma}(\boldsymbol{t} - \boldsymbol{t_i}) \tag{2}$$

We refine the self-excited effect and decompose the self-excited kernel function in the intensity function $\lambda(t)$. Then, we obtain

$$\boldsymbol{\lambda}(\boldsymbol{t}) = \boldsymbol{p}(\boldsymbol{t}) \sum_{t_i \le t} \boldsymbol{u_i} * \boldsymbol{\Phi}(\boldsymbol{t} - \boldsymbol{t_i}), \boldsymbol{t} \ge \boldsymbol{t_0} \tag{3}$$

where $p(t)$ represents the influence of the post itself, which quantifies the possibility of being forwarded for the post when it is observed by users at time t. $p(t)$ is time-dependent. For example, a post always gets more attention when it is just released. With the time elapsed, the attraction of the post decreases, and it will be crowded out by a large number of newly released information on the platform. In addition to the factor of timeliness, the influence of the post is also related to its content, release time and geographical location of the author. We synthesize all the relevant influencing factors of a post by $p(t)$. u_i is the influence of forwarding user i, which quantifies the probability that the post will be forwarded when it is seen by users at time t from the perspective of network topology. In another word, u_i represents the set of users that may take forwarding behaviors in the future, and therefore, we should give more weights to nodes with greater influence. $\Phi(t)$ is a memory kernel which indicates users' reaction time. After a post is published, it will appear in the information flow of continuous post generation. After users see the post, they may wait for a certain time to decide whether to forward it. Therefore, $\Phi(t)$ is just the function of quantifying the probability density distribution obeyed by this time interval.

Eq. 3 is the expression of the arrival intensity of post forwarding events in the information cascade, and $\lambda(t)$ describes the rate at which the post is forwarded. We have the following additional explanations of $\lambda(t)$. After the post is forwarded for the i time, users are affected by the influence of antecedent spreaders to consider participating in the diffusion. These users see the post in turn and decide whether to take forwarding behaviors according to $\Phi(t)$ which characterizes a certain response time. Therefore, $\sum_{t_i \le t} u_i * \Phi(t - t_i)$ refers to the arrival intensity of the users who see the post in the subsequent user groups and may take forwarding behaviors when influenced by the cascade events until time t, and then, we can multiply the intensity of users by $p(t)$ to obtain the arrival intensity of forwarding events at time t. The arrival intensity means the probability of a forwarding event occurring in an infinitesimal time interval.

The arrival intensity of forwarded events $\lambda(t)$ includes three factors: the influence of the post itself, the influence of forwarding users and the response time of forwarding. The quantification and parameter estimation of these three factors will be introduced in detail below.

2.3 Tweet Attraction

The influence $p(t)$ of a post comprehensively involves many factors affecting the forwarding related to the post itself, but the forms of parameters in $p(t)$ are not determined in the modeling. Instead, we model the influence $p(t)$ in a nonparametric form, and then, and estimate the value of $p(t)$ according to the observed information chain at the initial stage of the forwarding cascade.

Firstly, we consider the case that $p(t)$ does not change with time, that is, $p(t) = p$ is a constant. The sample density of forwarding cascade process based on the intensity function $\lambda(t)$ is

$$\boldsymbol{P}\{\boldsymbol{R}(\boldsymbol{t}) = \boldsymbol{r}; \boldsymbol{t}_1, \ldots, \boldsymbol{t}_r\} = \Pi_{i=1}^{R(t)} \boldsymbol{\lambda}(\boldsymbol{t}_i) \, \boldsymbol{exp}\left(- \int_{\boldsymbol{t_0}}^{\boldsymbol{t}} \boldsymbol{\lambda}(\boldsymbol{\tau}) \boldsymbol{d\tau} \right) \tag{4}$$

In order to explain the process more clearly and concisely, the graphical expression of the model for the arrival process is shown in **Figure 2**. To simplify the representation of $\boldsymbol{P}\{\boldsymbol{R}(\boldsymbol{t}) = \boldsymbol{r}; \boldsymbol{t}_1, \ldots, \boldsymbol{t}_r\}$, we roughly use variable $\boldsymbol{P}$ with subscripts to denote the sample density at different times during the forwarding cascade process. The yellow area shows the initial cascading information chain, where the sample density at each moment is marked by $\boldsymbol{P}$. $\boldsymbol{P}_1$ indicates the density at the

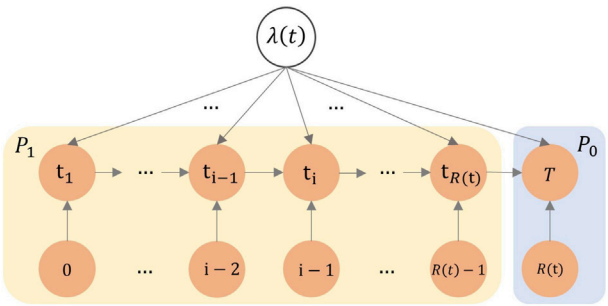

FIGURE 2 | Graphical representation of the model for the arrival process.

initial moment. The blue area indicates the sample density $\boldsymbol{P_T}$ to be calculated of the current time T with known historical information.

Eq. 4 also represents the likelihood function of $p(t)$ when the initial cascading information chain is given. Taking the derivative of the logarithmic function for **Eq. 4** and combining with **Eq. 2**, the maximum likelihood estimation of $p(t)$ is

$$U_t^e = \sum_{i=0}^{R(t)} u_i \int_{t_i}^{t} \Phi(\tau - t_i) d\tau \tag{5}$$

$$\hat{p}(t) = \frac{R(t)}{U_t^e} \tag{6}$$

Here, U_t^e can be understood as the sum of effective values for the influence of forwarding users until time t. It represents the users who have seen the post up to time t among the users who are influenced and may take forwarding behaviors. Then, the estimated value of the influence of the post itself $\hat{p}(t)$ can be explained as the proportion of the cumulative forwarding number of the post until time t in the users who have seen the post.

In order to consider the time-varying characteristic of $p(t)$, the unilateral kernel function $K_t(s), s > 0$ is introduced here to smooth $p(t)$ and weight different forwarding cascades. The weighted estimation value of $p(t)$ is obtained by using the observation information chain closer to time t [28]:

$$\hat{p}(t) = \frac{\int_{t_0}^{t} K_t(t-s) dR(s)}{\int_{t_0}^{t} K_t(t-s) dU_s^e} = \frac{\sum_{i=0}^{R(t)} K_t(t-t_i)}{\sum_{i=0}^{R(t)} u_i \int_{t_i}^{t} K_t(t-s)\Phi(s-t_i) ds} \tag{7}$$

where the unilateral kernel function $K_t(s)$ is defined as $K_t(s) = max\{1 - s/L, 0\}, s > 0$. L is the interval between the observation point and the prediction time, that is, the size of the observation cascade window. The data in the window is used for the prediction of the final cascade size. Here, we heuristically set L to 0.5, and the latter half of the information chain in the initial stage of the forwarding cascade is used as the observation interval. In this way, the forwards earlier than $t/2$ will be ignored by the kernel function. The function gives more weights to the events closer to the prediction time t in the window, and gradually reduces the weights of old forwarding events, so as to make the estimated value $\hat{p}(t)$ closer to the real dynamic post influence.

In social networks, users' forwarding behaviors have a certain delay time. After a post is published, users need a period of response time to notice the post and decide whether to forward it. The probability density distribution of response time is determined by the memory kernel function $\Phi(t)$ in the Hawkes model, which characterizes the relaxation response of the system. In social networks, the probability density distribution of users' response time obeys the heavy-tailed distribution [28], and therefore, the power-law memory kernel function is used here, as shown below:

$$\boldsymbol{\Phi(t)} = \begin{cases} \boldsymbol{c}, & \boldsymbol{0 < t \le t_0} \\ \boldsymbol{c(t/t_0)^{-(1+\theta)}}, & \boldsymbol{t \ge t_0} \end{cases} \tag{8}$$

where $t_0 = 300s$, because it is observed that the memory kernel function remains unchanged for the first 5 min, and then it shows the characteristic of power-law attenuation. The deceleration rate is obtained as $\theta = 0.242$ by fitting, which is obtained by experimentally fitting the distribution of the user's forwarding time in the training set. In addition, we notice the truth that the probability density function is integrated as one on the whole integration interval $[0, +\infty)$, and then, we obtain the parameter $c = 6.27 \times 10^{-4}$.

2.4 User Influence Modeling

We measure the influence of the ith forwarding user u_i from the perspective of network topology. **Figure 3** shows a simple network with 23 nodes and 37 edges. Obviously, node 1 has the largest number of nearest neighbors, but the posts published by node one do not necessarily generate a faster and wider cascade, because the degrees of its neighbor nodes are very small. In contrast, although node 23 does not have more nearest neighbors, the statuses of its neighbors may make it have more influence.

Combined with two indicators of node influence, i.e., semi-local centrality [33] and local clustering coefficients, we expand the measurement of forwarding user influence by using more information of local network topology. The calculation method of semi-local centrality is as follows:

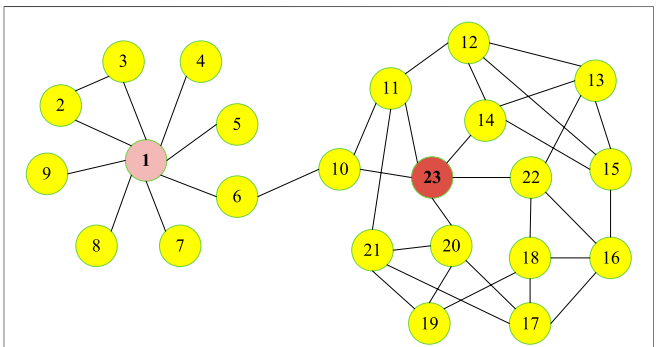

FIGURE 3 | Illustration of user influence analysis.

$$\begin{aligned}\mathbf{Q}(\mathbf{w}) &= \sum_{\mathbf{u}\in\mathbf{N}(\mathbf{w})} |\boldsymbol{\Gamma}(\mathbf{u})|,\\ \mathbf{LC}(\mathbf{i}) &= \sum_{\mathbf{w}\in\mathbf{N}(\mathbf{i})} \mathbf{Q}(\mathbf{w})\end{aligned} \tag{9}$$

Where $N(w)$ represents the set of nearest neighbor nodes (including in-degree and out-degree of node w), $\Gamma(u)$ represents the set of nearest neighbor and next nearest neighbor nodes of node u (i.e., the adjacent nodes of the nearest neighbor nodes), and $LC(i)$ is the semi-local centrality size of node i. This measurement method expands the range of involved neighbor nodes to within the fourth order neighbors, which is a trade-off between low correlation centrality measure and high time-consuming global measure. Therefore, it can not only improve the calculation accuracy, but also ensures low time complexity. However, this method ignores the influence of the connectivity between nodes in the local topology which reflects the clustering degree of nodes in the network. Therefore, considering the connectivity between neighbor nodes of a node can improve the measurement accuracy of node influence. The closer the relationships between the neighbors of a node are, the higher the degree of mutual influence will be, and the greater the influence of the node will be. The clustering coefficient is an indicator which measures the degree of connectivity between nodes. The local clustering coefficient reflects the degree of interactions between neighbor nodes of the current node. The formula is as follows:

$$\boldsymbol{c_i} = \frac{\sum_j \boldsymbol{e_{ij}} \sum_{k,k\neq j} \boldsymbol{e_{ik}} \boldsymbol{e_{jk}}}{|\boldsymbol{N}(\boldsymbol{i})|\,(|\boldsymbol{N}(\boldsymbol{i})|-\mathbf{1})/\mathbf{2}} \tag{10}$$

Where e_{ij} indicates whether nodes j and k are connected, and $|N(i)|$ is the number of nearest neighbor nodes. Considering the two indicators of semi-local centrality and local clustering coefficients, the influence of user i is quantified as

$$\begin{aligned}\boldsymbol{u_i} &= \sum_{\boldsymbol{w}\in\boldsymbol{N}(\boldsymbol{i})} \left(\boldsymbol{\beta} * |\boldsymbol{\Gamma}(\boldsymbol{w})| + (\mathbf{1}-\boldsymbol{\beta}) * \sum_{\boldsymbol{u}\in\boldsymbol{\Gamma}(\boldsymbol{w})} \boldsymbol{c_u} \right)\\ &= \boldsymbol{\beta} * \sum_{\boldsymbol{w}\in\boldsymbol{N}(\boldsymbol{i})} |\boldsymbol{\Gamma}(\boldsymbol{w})| + (\mathbf{1}-\boldsymbol{\beta}) * \sum_{\boldsymbol{w}\in\boldsymbol{N}(\boldsymbol{i})} \sum_{\boldsymbol{u}\in\boldsymbol{\Gamma}(\boldsymbol{w})} \boldsymbol{c_u}\end{aligned} \tag{11}$$

Where $\beta\,(0\le\beta\le1)$ is the balance parameter for user influence. For each nearest neighbor node w of node i, $|\Gamma(w)|$ is the sum of the number of w's nearest neighbor and next nearest neighbor nodes. For each node $u\in\Gamma(w)$, c_u is the local clustering coefficient of node u. The first part of **Eq. 11** considers the number of nodes whose distances from the nearest neighbor node w of node i are within two steps, and the second part considers the connectivity between neighbor nodes of node u in $\Gamma(w)$. In other words, user influence represented by **Eq. 11** considers not only the local influence of the nearest neighbor nodes, but also the degree of interactions between nodes in the local network. In addition, we consider both in-degrees and out-degrees of the nearest neighbor nodes, and this measurement makes up for the deficiency of considering only node in-degrees in a sparse directed network.

2.5 Predicting an Information Cascade

After the modeling and parameter estimation of the arrival intensity for post's forwarding events, this section will discuss how to predict the final number of forwards, that is, the final size of an information cascade. We define G_k as the total number of forwards formed by the descendants of the k-generation forwarding users, i.e., the users who may take forwarding behaviors driven by the influence of the k-generation forwarding users. If the cumulative forwarding users until time t are treated as the first generation with the count $R(t)$, then G_1 represents the total number of forwards in the next generation affected by $R(t)$ users. Based on this scenario, the information cascade chain after time t is obtained as $\{G_1, G_2, \ldots G_k\}$.

The final scale of the information cascade to be predicted is expressed as

$$\hat{\boldsymbol{R}}(\infty) = \boldsymbol{R}(\boldsymbol{t}) + \sum_{\boldsymbol{k}=\mathbf{1}}^{\infty} \boldsymbol{G_k} \tag{12}$$

We assume that the own influence of the post remains unchanged after the prediction time t is $p(t)$, and the number of users that may take forwarding behaviors caused by user influence is expected to be u_*. Therefore, u_* indicates the expected value of the forwarding user influence, which can be obtained from the dataset. Then, the branching factor of the cascade process is defined as $\rho = pu_*$. The branching factor represents the expected value of descendants' forwarding events, so we have $G_k = \rho G_{k-1}$. When $\rho<1$, i.e., $p<1/u_*$, the final scale of the information cascade is always bounded, and the social system enters a subcritical state. The forwarding process will gradually slow down and finally stop, and the final forwarding number can be predicted. However, when $\rho>1$, the final scale of the information cascade is unbounded, and the system state is called a supercritical state. The forwarding process never stops, and the final forwarding number cannot be predicted. Obviously, this outcome is usually not in line with the actual situation. Therefore, when $\rho<1$, $\sum_{k=1}^{\infty} G_k$ can be regarded as the summation of geometric series, that is

$$\sum_{\boldsymbol{k}=\mathbf{1}}^{\infty} \boldsymbol{G_k} = \frac{\boldsymbol{G_1}}{\mathbf{1}-\boldsymbol{\rho}} \tag{13}$$

Where G_1 represents the users who have seen the post and may forward it after time t. If U_t represents the sum of the influence of forwarding users up to time t, we obtain

$$\boldsymbol{G_1} = \boldsymbol{p}\left(\boldsymbol{U_t} - \boldsymbol{U_t^e}\right) \tag{14}$$

Based on **Eq. 14**, the predicted final scale of the information cascade can be obtained, [28] that is, the final forwarding number is

$$\hat{\boldsymbol{R}}_{\infty}(\boldsymbol{t}) = \boldsymbol{R}(\boldsymbol{t}) + \sum_{\boldsymbol{k}=\mathbf{1}}^{\infty} \boldsymbol{G_k} = \boldsymbol{R}(\boldsymbol{t}) + \frac{\boldsymbol{p}\left(\boldsymbol{U_t} - \boldsymbol{U_t^e}\right)}{\mathbf{1}-\boldsymbol{pu_*}} \tag{15}$$

In order to eliminate the inaccurate assumption that $p(t)$ remains unchanged after time t, a distinct correction coefficient $\mu_t\,(0<\mu_t<1)$ is introduced for each post to adjust the predicted value of the final forwarding number. μ_t reflects the reduced influence of a post due to obsolescence, and we use a machine

learning method to obtain dynamic μ_t. The predicted value of the final forwarding cascade size is

$$\hat{\boldsymbol{R}}_{\infty}(\boldsymbol{t}) = \boldsymbol{R}(\boldsymbol{t}) + \boldsymbol{\mu_t}\frac{\hat{\boldsymbol{p}}(\boldsymbol{t}) * (\boldsymbol{U_t} - \boldsymbol{U_t^e})}{\boldsymbol{1} - \hat{\boldsymbol{p}}(\boldsymbol{t}) * \boldsymbol{u_*}} \tag{16}$$

Eq. 16 is the final prediction model of an information cascade. We use the regression algorithm of a decision tree to solve and quantify μ_t. The selection process of the feature set is as follows:

$$\begin{aligned} \boldsymbol{f_1} &= \boldsymbol{R}(\boldsymbol{t}), \\ \boldsymbol{f_2} &= \hat{\boldsymbol{p}}(\boldsymbol{t}), \\ \boldsymbol{f_3} &= \boldsymbol{U_t}, \\ \boldsymbol{f_4} &= \boldsymbol{U_t^e}. \end{aligned} \tag{17}$$

After selecting the feature set, we use the data in the training set to train the regression tree. In the test set, we input the feature set $\{f_1, f_2, f_3, f_4\}$ into the trained regression tree model so as to obtain the corresponding correction coefficient μ_t. The whole algorithm of information cascade prediction is shown in

Algorithm 1. Final scale prediction of an information cascade

Input: All forwarding time up to time t, ID of each forwarding user, the follower relationship e_{ij} of a forwarding user
Output: Predicted value of the final cumulative number of forwards for the current post
1: $U_t = 0, U_t^e = 0$
2: Calculate the influence of the forwarding user u_i according to Eq. (11)
3: Calculate the current self-influence $\hat{p}(t)$ of the post at time t according to Eq. (7)
4: for $i = 0,1, \ldots, R(t)$ do
$U_t \leftarrow U_t + u_i$
$U_t^e \leftarrow U_t^e + u_i * \int_{t_i}^{t} \Phi(s - t_i) ds$
5: #Extract the feature set
$f_1 = R(t)$
$f_2 = \hat{p}(t)$
$f_3 = U_t$
$f_4 = U_t^e$
6: Input the feature set in the trained regression tree f_1, f_2, f_3, f_4, output the correction coefficient μ_t
7: $\hat{R}_{\infty}(t) = R(t) + \mu_t\,(\hat{p}(t) * (U_t - U_t^e))/(1 - \hat{p}(t) * u_*)$
8: Return $\hat{R}_{\infty}(t)$

3 EXPERIMENT RESULTS

We use two real-world datasets in the experiments. The first dataset was collected from the Twitter platform and disclosed by Zhao et al. [28] in their research on the prediction of tweet forwarding. This dataset contains all the posts published on Twitter and their forwarding information within 1 month from 7 October 2011. The information of each post includes its ID, publishing time, the ID and number of fans of the publisher, as well as a series of forwarding time and the forwarding users. However, this dataset does not contain the structure information of the forwarding network, that is, there is no relationship information between users. Therefore, we introduce only the correction coefficient μ_t on dataset one to advance the prediction model. In order to improve the efficiency, we select the posts with the forwarding numbers greater than 500 in the dataset for cascade prediction. We split the posts published in the first 8 days as the training set, and the test set contains the posts published in the next 7 days. The forwarding number formed in the remaining days is regarded as the final size of an information cascade. The second dataset was collected from Twitter available on the website[1], which not only contains related forwarding information of 3,553 posts, but also includes 1,731,658 relationships between 71,367 users. The purpose of introducing this dataset is to expand the measurement method of user influence in the original Hawkes process from the perspective of network topology. The descriptions of the datasets are shown in **Table 2**. In the experiments, we randomly select 1,000 posts as the research subset in which forwarding cascades of 723 posts are used as the training set.

We use the absolute percentage error (APE) and Kendall rank correlation coefficient as the evaluation metrics of prediction performance. APE is calculated as follows:

$$\boldsymbol{APE} = \frac{\left|\hat{\boldsymbol{R}}_{\infty}(\boldsymbol{t}) - \boldsymbol{R}(\infty)\right|}{\boldsymbol{R}(\infty)} \tag{18}$$

Where $\hat{R}_{\infty}(t)$ is the predicted value of the cascade size, and $R(\infty)$ is the real value. Obviously, smaller values of APE indicate higher prediction accuracy. The Kendall rank correlation is usually used to count the correlation of two attributes for n objects, which is defined as follows

$$\boldsymbol{k} = (\boldsymbol{4P/n} * (\boldsymbol{n} - \boldsymbol{1})) - \boldsymbol{1}, \quad -\boldsymbol{1} < \boldsymbol{k} < \boldsymbol{1} \tag{19}$$

Where P represents the number of concordant pairs of objects between the predicted values and real values. In other words, we suppose that there are n objects, each of which has two attributes, corresponding to the predicted value and the real value, respectively. Then, we sort the n objects according to the predicted values and real values, respectively. If both the ranks of $\hat{R}_{\infty}(t)$ and $R(\infty)$ for object i are larger than those for object j, the pair of i and j are called a concordant pair. Then, P counts the number of concordant pairs of objects [34]. Obviously, the larger the value of k, the higher the matching degree between the predicted values and real values, so that the better prediction performance is achieved.

Here, we use the Hawkes model proposed by Zhao et al. [28] as the benchmark for experimental evaluation. The original Hawkes model uses the same correction coefficient for all posts, and the measurement of user influence only considers the number of users' fans, so we address the role of our method of calculating user influence for the prediction performance. Note that the two datasets do not play the same role. We distinguish between two datasets to evaluate the impact of different modules on prediction performance. Dataset one does not have user relationships, so we validate on this dataset the effect on prediction performance of having different correction factors for different posts that we learned through machine learning without calculating user influence. Dataset 2 has user relationships, so influence can be calculated. We mainly extend the user influence on dataset two and verify the impact of this module on the prediction performance. For each post, 300s, 600s, 900s, 1,200s and 1,800s are selected as the prediction time to obtain the final sizes of forwarding cascades.

[1]https://github.com/ShinyZC/dataset.

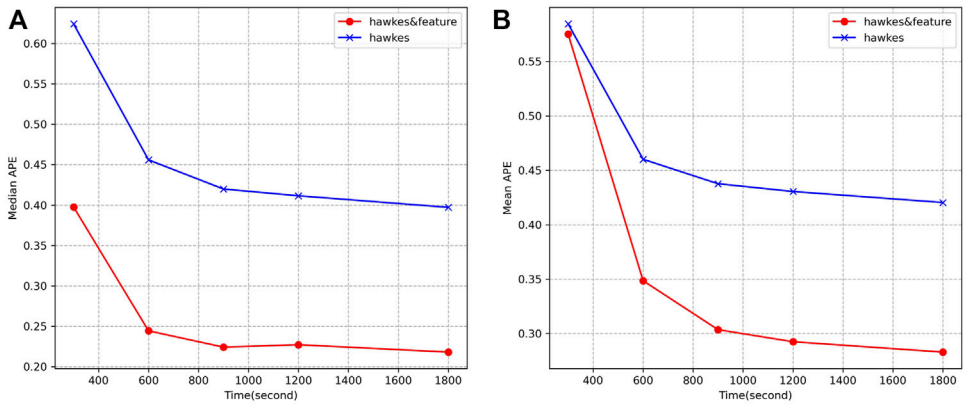

FIGURE 4 | Comparison of APE of two models on dataset 1. **(A)** Evolutionary trend of the median APE with prediction time t, **(B)** Evolutionary trend of mean APE with prediction time t.

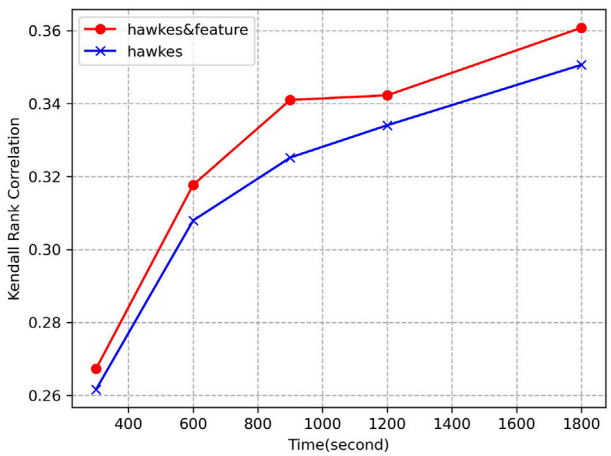

FIGURE 5 | Comparison of Kendall rank correlation for two models on dataset 1.

The comparison results on dataset one are shown in **Figure 4** and **Figure 5**. In both figures, the curve 'Hawkes' represents the original Hawkes model, and the curve 'Hawkesandfeature' represents the model by introducing the idea of feature learning and using the regression tree algorithm to improve only correction coefficients. **Figure 4A** shows the evolutionary trend of the median of APE as a function of the prediction time t, and **Figure 4B** shows the evolutionary trend of the mean of APE with the prediction time t. As can be seen from **Figure 4**, different correction coefficients μ_t varying with time are generated for each post through the feature set of the initial cascade process, and the performance of Hawkesandfeature is improved both for the median or mean value of APE compared with the original model. Specifically, at time 300s, 600s, 900s, 1,200s and 1,800s, the improvement in median APE compared to the Hawkes process is 36.28%, 46.38%, 46.58%, 44.77% and 45.07%, respectively in **Figure 4A**. For the mean APE, the best improved performance reaches 36.70% in time 1800s compared to the Hawkes process **Figure 4B**. The value of APE decreases with the increase of prediction time t, indicating that when more historical cascade information is used, the performance of the prediction method will be improved.

Figure 5 shows the evolutionary trend of Kendall rank correlation for the above two models with prediction time t. It can be seen that the model Hawkesandfeature also performs better than the original process model in the correlation between the predicted values and real values, and the value of Kendall rank correlation also increases with time, indicating that the correlation between the predicted values and real values is also improved due to the use of more historical cascade information.

In the experiments on dataset 2, the measurement of user influence is expanded and the influence balance factor is set at $\beta = 0.7$. The improved correction coefficients are also included. The relevant experimental results are shown in **Figure 6**. The curve 'Hawkesandinfluence' represents the model only expanding user influence measurement on the basis of the original process model, and the curve 'Hawkesandfeature&influence' represents our cascade prediction model which comprehensively improves the correction coefficients and expands user influence measurement. **Figure 6A** shows the evolutionary trend of the median of APE with the prediction time t, and **Figure 6B** shows that of the mean of APE. It can be seen that although the model Hawkes and influence which only expands user influence measurement has a certain performance improvement over the original process model, it is not as effective as the model Hawkesandfeature which only improves the correction coefficients. Therefore, the prediction method based on feature learning has more advantages in prediction accuracy than the method based on a generative model. Combining the improvement of correction coefficients and user influence, the final model Hawkesandfeature&influence has the smallest APE value, and its prediction performance is the best. For the median APE, the performance of final model improves 71.60% than Hawkes at time 300s in **Figure 6A**. For the mean APE, the performance improves 78.46% at time 300s in **Figure 6B**. With

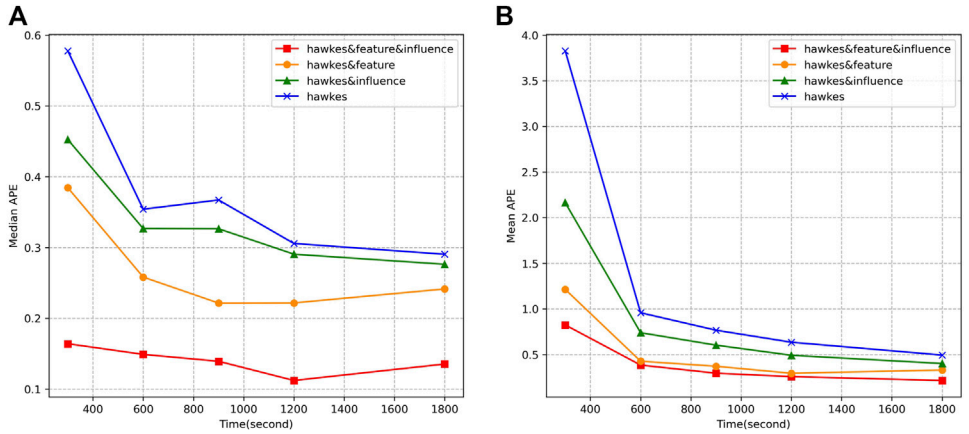

FIGURE 6 | Comparison of APE of different models on dataset 2. **(A)** Evolutionary trend of the median APE with prediction time *t*, **(B)** Evolutionary trend of mean APE with prediction time *t*.

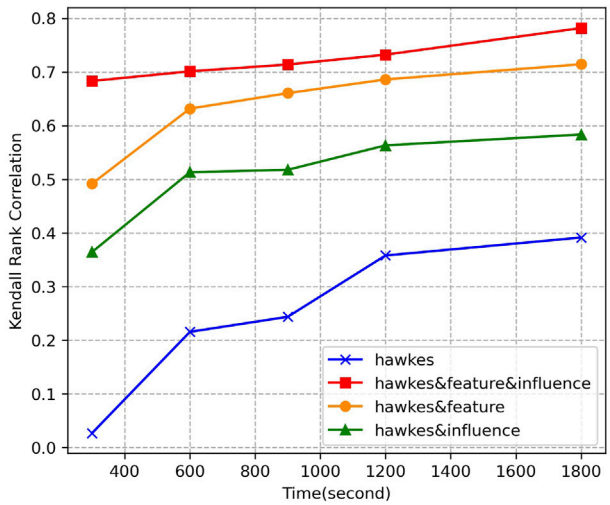

FIGURE 7 | Comparison of Kendall rank correlation for different models on dataset 2.

the increase of the prediction time, the median and mean of APE show an overall downward trend, which once again reveals the fact that using more historical cascade information can improve the prediction accuracy. Meanwhile, from **Figure 4** and **Figure 6**, the decline rate of APE gradually slows down with the passage of the prediction time, indicating that the amount of historical information available at the initial stage of the forwarding cascade increases rapidly, and then the growth rate of cascade information slows down. This phenomenon to some extent shows the rapid dissemination in social networks and the timeliness of posts, that is, posts are easier to obtain more forwards not long after publication, and with the time elapsed, the propagation of the posts eventually becomes stable.

Figure 7 shows the evolution trend of Kendall rank correlation of the above four models with prediction time *t*. It can be seen from the figure that our model represented by Hawkesandfeature&influence has larger Kendall rank correlation, indicating that the correlation between predicted values and real values is the highest, and the prediction performance of the model is the best. The value of Kendall rank correlation increases with the passage of prediction time, and also reflect the fact that the prediction accuracy is improved with the increase of historical cascade information.

We also notice that the performance of the models on the two datasets is slightly different. For instance, the mean APE of hawkesandfeature and Kendall rank correlation in dataset two are higher than it in dataset 1, which could be caused by the differences of the two networks. Dataset one contains a longer timeline of users' actions, which leads to the better results.

Above all, through the experiments on real-world datasets, it can be concluded that our proposed method can effectively predict the final size of an information cascade, and has obvious performance improvement compared with the current process model.

4 CONCLUSION

Information cascades reflect a kind of user clustering behaviors, and the prediction of them has important theoretical significance and practical applications. In this paper, the prediction method based on model generation was proposed to solve the problem of cascade prediction. By analyzing the factors affecting information diffusion, we studied the growth mechanism of information cascades. On the basis of the Hawkes process, we modeled the arrival intensity of post forwarding process in combination with post attraction, forwarding user influence and users' response time. We combined semi-local centrality with local clustering coefficients to measure the influence of forwarding users, and used the regression tree algorithm to improve the correction coefficients. Finally, the prediction model of the final number of

forwards was obtained. The performance evaluation of the proposed method was carried out on real-world datasets, and results demonstrated that our method improves the prediction accuracy compared with representative models, indicating our method effectively realizes the prediction of information cascades.

In future, we will use deep learning methods to exploit forwarding paths and extract more latent features of information cascades, and incorporate deep learning with model generation methods. In addition, we will study the effective calculation methods of user influence in the propagation process, and investigate their roles in popularity prediction.

DATA AVAILABILITY STATEMENT

The original contributions presented in the study are included in the article/Supplementary Material, further inquiries can be directed to the corresponding author.

AUTHOR CONTRIBUTIONS

YZ designed the research and wrote the paper, CZ performed the experiments, and YZ conducted the validation and analyzed the results.

REFERENCES

1. Davis JT, Perra N, Zhang Q, Moreno Y, Vespignani A. Phase Transitions in Information Spreading on Structured Populations. *Nat Phys* (2020) 16: 590–596. doi:10.1038/s41567-020-0810-3
2. Chen X, Wang R, Tang M, Cai S, Stanley HE, Braunstein LA. Suppressing Epidemic Spreading in Multiplex Networks with Social-Support. *New J Phys* (2018) 20:013007. doi:10.1088/1367-2630/aa9cda
3. Velásquez-Rojas F, Ventura PC, Connaughton C, Moreno Y, Rodrigues FA, Vazquez F. Disease and Information Spreading at Different Speeds in Multiplex Networks. *Phys Rev E* (2020) 102:022312. doi:10.1103/PhysRevE.102.022312
4. Bao Q, Cheung WK, Zhang Y, Liu J. A Component-Based Diffusion Model with Structural Diversity for Social Networks. *IEEE Trans Cybern* (2017) 47(4): 1078–1089. doi:10.1109/tcyb.2016.2537366
5. Li D, Zhang S, Sun X, Zhou H, Li S, Li X. Modeling Information Diffusion over Social Networks for Temporal Dynamic Prediction. *IEEE Trans Knowl Data Eng* (2017) 29(9):1985–97. doi:10.1109/tkde.2017.2702162
6. Cui P, Jin S, Yu L, Wang F, Zhu W, Yang S. Cascading Outbreak Prediction in Networks: a Data-Driven Approach. In: Proceedings of the 19th ACM SIGKDD international conference on Knowledge discovery and data mining; 2013 Aug 11-14; New York, USA. Association for Computing Machinery (2013). p. 901–909.
7. Zhao J, Wu J, Xu K. Weak Ties: Subtle Role of Information Diffusion in Online Social Networks. *Phys Rev E Stat Nonlin Soft Matter Phys* (2010) 82:016105. doi:10.1103/PhysRevE.82.016105
8. Ma Z, Sun A, Cong G. On Predicting the Popularity of Newly Emerging Hashtags in Twitter. *J Am Soc Inf Sci Tec* (2013) 64:1399–1410. doi:10.1002/asi.22844
9. Xiong F, Liu Y, Zhang Z, Zhu J, Zhang Y. An Information Diffusion Model Based on Retweeting Mechanism for Online Social media. *Phys Lett A* (2012) 376(30-31):2103–2108. doi:10.1016/j.physleta.2012.05.021
10. Bakshy E, Hofman J, Mason W, Watts D. Everyone's an Influencer: Quantifying Influence on Twitter. In: Proceedings of the Fourth ACM International Conference on Web Search and Data Mining; 2011 Feb 9-12; Hong Kong, China. ACM Press (2011). p. 65–74.
11. Flamino J, Szymanski B. A Reaction-Based Approach to Information cascade Analysis. In: 28th International Conference on Computer Communication and Networks; 2019 Jul 29-Aug 1; Valencia, Spain. IEEE (2019). p. 1–9. doi:10.1109/icccn.2019.8847096
12. Tsur O, Rappoport A. What's in a Hashtag? : Content Based Prediction of the Spread of Ideas in Microblogging Communities. In: Proceedings of the Fifth ACM International Conference on Web Search and Data Mining; 2012 Feb 8-12; Seattle, Washington, USA. ACM Press (2012). p. 643–652.
13. Bakshy E, Hofman JM, Mason WA, Watts DJ, Watts D. Everyone's an Influencer: Quantifying Influence on Twitter. In: Proceedings of the 4th ACM International Conference on Web Search & Web Data Mining; 2011 Feb 9-12; Hong Kong, China. ACM Press (2011). p. 65–74.
14. Wang J, Li W, Weili W. Predicting Information Popularity Degree in Microblogging Diffusion Networks. *Int J Multimedia Ubiquitous Eng* (2014) 9(2):21–30. doi:10.14257/ijmue.2014.9.2.30
15. Weng L, Menczer F, Ahn Y-Y. Virality Prediction and Community Structure in Social Networks. *Sci Rep* (2013) 3:2522. doi:10.1038/srep02522
16. Tsugawa S. Empirical Analysis of the Relation between Community Structure and Cascading Retweet Diffusion. In: Proceedings of the Thirteenth International AAAI Conference on Web and Social Media; 2019 Jun 11-14; Münich, Germany. AAAI Press (2019). p. 493–504.
17. Hong L, Dan O, Davison BD. Predicting Popular Messages in Twitter. In: Proceedings of the 20th International Conference Companion on World Wide Web; 2011 Mar 28-Apr 1; Hyderabad, India. ACM (2011). p. 57–58. doi:10.1145/1963192.1963222
18. Wang K, Wang PH, Chen X, Huang Q, Mao Z, Zhang Y. A Feature Generalization Framework for Social Media Popularity Prediction. In: Proceedings of the 28th ACM International Conference on Multimedia (MM '20); Seattle, WA; October 12–16, 2020. Association for Computing Machinery (2020). p. 4570–4574. doi:10.1145/3394171.3416294
19. Kong Q, Mao W, Chen G, Zeng D. Exploring Trends and Patterns of Popularity Stage Evolution in Social Media. *IEEE Trans Syst Man Cybern, Syst* (2020) 50(10):3817–3827. doi:10.1109/tsmc.2018.2855806
20. Zhang B, Wu Q, Chen X, Chen L. Information Cascades over Diffusion-Restricted Social Network: A Data-Driven Analysis. In: IEEE INFOCOM 2019 - IEEE Conference on Computer Communications Workshops (INFOCOM WKSHPS) (2019). 29 April 2019 - 02 May 2019, Paris, France, p. 151–156. doi:10.1109/infcomw.2019.8845264
21. Crane R, Sornette D. Robust Dynamic Classes Revealed by Measuring the Response Function of a Social System. *Proc Natl Acad Sci U.S.A* (2008) 105(41):15649–15653. doi:10.1073/pnas.0803685105
22. Li Q, Wu Z, Yi L, N K, N. H, Ma X. WeSeer: Visual Analysis for Better Information cascade Prediction of WeChat Articles. *IEEE Trans Vis Comput. Graphics* (2020) 26:1399–1412. doi:10.1109/tvcg.2018.2867776
23. Szabo G, Huberman BA. Predicting the Popularity of Online Content. *Commun ACM* (2010) 53:80–88. doi:10.1145/1787234.1787254
24. Yu L, Cui P, Wang F, Song C, Yang S. From Micro to Macro: Uncovering and Predicting Information Cascading Process with Behavioral Dynamics. In: 2015 IEEE International Conference on Data Mining; 2015 Nov 14-17; Atlantic City, USA. IEEE (2015). p. 559–568. doi:10.1109/icdm.2015.79
25. Zaman T, Fox EB, Bradlow ET. A Bayesian Approach for Predicting the Popularity of Tweets. *Ann Appl Stat* (2014) 8(3):1583–1611. doi:10.1214/14-aoas741
26. Shen H, Wang D, Song C, Barabási AL. Modeling and Predicting Popularity Dynamics via Reinforced Poisson Processes. In: Proceedings of the 28th AAAI Conference on Artificial Intelligence; 2014 Jul 27-31; Québec, Canada. AAAI Press (2014). p. 291–297.
27. Kobayashi R, Lambiotte R. TiDeH: Time-dependent Hawkes Process for Predicting Retweet Dynamics. In: the 10th International AAAI Conference on Web and Social Media; 2016 May 17-20; Cologne, Germany. AAAI Press (2016). p. 191–200.
28. Zhao Q, Erdogdu MA, He HY, Rajaraman A, Leskovec J. SEISMIC: A Self-Exciting point Process Model for Predicting Tweet Popularity. In: Proceedings of the 21th International Conference on Knowledge Discovery and Data Mining; 2015 Aug 10-13; Sydney, Australia. ACM (2015). p. 1513–1522.

29. Chen F, Tan WH. Marked Self-Exciting Point Process Modelling of Information Diffusion on Twitter. *Ann Appl Stat* (2018) 12(4):2175–2196. doi:10.1214/18-aoas1148
30. Palmowski Z, Puchalska D. *Modeling Social media Contagion Using Hawkes Processes*. New York, NY: Cornell University (2020). ArXiv, abs/2010.14623.
31. Srivathsan S, Cranefield S, Pitt J. *A Bayesian Model of Information Cascades*. New York, NY: Cornell University (2021). p. 03166. ArXiv, abs/2105.
32. Hawkes AG, Oakes D. A Cluster Process Representation of a Self-Exciting Process. *J Appl Probab* (1974) 11(3):493–503. doi:10.2307/3212693
33. Chen D, Lü L, Shang M-S, Zhang Y-C, Zhou T. Identifying Influential Nodes in Complex Networks. *Physica A: Stat Mech its Appl* (2012) 391(4):1777–1787. doi:10.1016/j.physa.2011.09.017
34. van Doorn J, Ly A, Marsman M, Wagenmakers E-J. Bayesian Inference for Kendall's Rank Correlation Coefficient. *The Am Statistician* (2018) 72(4): 303–308. doi:10.1080/00031305.2016.1264998

Conflict of Interest: The authors declare that the research was conducted in the absence of any commercial or financial relationships that could be construed as a potential conflict of interest.

frontiers | Frontiers in Physics

ORIGINAL RESEARCH
published: 22 July 2022
doi: 10.3389/fphy.2022.941181

Ambient Air Pollution and Hospitalization for Acute Myocardial Infarction in Chongqing, China: A Time-Stratified Case Crossover Analysis

*Mingming Zhao[1†], Xing Liu[1†], Ming Yuan[2], Ying Yang[3], Hao Chen[1], Mengmeng Li[1], Pan Luo[1], Yong Duan[1], Jie Fan[1,4], Leqi Liu[5] and Li Zhou[1]**

[1]Department of Epidemiology, School of Public Health and Management, Chongqing Medical University, Chongqing, China, [2]Chongqing Medical and Pharmaceutical College, Chongqing, China, [3]Bureau of Ecology and Environment of Jiulongpo District, Chongqing, China, [4]Nanan District Center for Disease Control and Prevention, Chongqing, China, [5]Jiangjin District Center for Disease Control and Prevention, Chongqing, China

OPEN ACCESS

Edited by:
Xuzhen Zhu,
Beijing University of Posts and Telecommunications (BUPT), China

Reviewed by:
Yuewei Liu,
Sun Yat-sen University, China
Suzana M. Blesic,
University of Belgrade, Serbia

***Correspondence:**
Li Zhou
zhouli@cqmu.edu.cn

[†]These authors have contributed equally to this work and share first authorship

Specialty section:
This article was submitted to Social Physics, a section of the journal Frontiers in Physics

Received: 11 May 2022
Accepted: 22 June 2022
Published: 22 July 2022

Citation:
Zhao M, Liu X, Yuan M, Yang Y, Chen H, Li M, Luo P, Duan Y, Fan J, Liu L and Zhou L (2022) Ambient Air Pollution and Hospitalization for Acute Myocardial Infarction in Chongqing, China: A Time-Stratified Case Crossover Analysis. Front. Phys. 10:941181. doi: 10.3389/fphy.2022.941181

Previous studies have demonstrated that short-term exposure to ambient air pollution was associated with hospital admissions for cardiovascular diseases, but the evidence of its effects on acute myocardial infarction (AMI) in East Asian countries is limited and inconsistent. We aimed to investigate the association between air pollution and AMI hospitalizations in Chongqing, China. This time-stratified case-crossover study included 872 patients with AMI from three hospitals in Chongqing from January 2015 to December 2016. Exposures were compared between days with AMI (case days) and days without AMI (control days). Spearman's correlation coefficient was applied to explore the correlation between air pollutants and meteorological conditions. Conditional logistic regression was used to assess the associations between air pollution exposure with different lag periods and AMI hospitalizations. Stratification analysis was further implemented by sex, age, and season. Hospitalizations for AMI were significantly associated with air pollution. All analyzed air pollutants showed lag-specific at lag 0 day and lag 01 day, whereas a 10 μg/m^3 increase of average concentrations in $PM_{2.5}$, PM_{10}, SO_2, NO_2, and CO was associated with 1.034% (95% CI: 1.003–1.067%), 1.035% (95% CI:1.015–1.056%), 1.231% (95% CI: 1.053–1.438%), 1.062% (95% CI: 1.018–1.107%), and 1.406% (95% CI: 1.059–1.866%) increase in hospitalizations for AMI, respectively. No effect modifications were detected for sex, age, and season. Our findings suggest that short-term exposure to $PM_{2.5}$, PM_{10}, SO_2, NO_2, and CO contributes to increase AMI hospitalizations, which have public health implications for primary prevention and emergency health services.

Keywords: acute myocardial infarction, air pollution, environment, hospitalization, risk factor

INTRODUCTION

Acute myocardial infarction (AMI) is a specific manifestation of coronary artery disease which has the characteristics of arrhythmias, heart failure, and angina pectoris with typical distribution [1]. As with the common heart attack event, the global fatality rate of AMI is estimated at more than 2.4 million deaths in the United States, more than four million fatalities in Europe and northern Asia, and is higher in most industrialized countries and low-income countries [2]. In China, AMI has a significant fatality rate and a large economic burden, where it is responsible for over 0.6 million deaths annually [3].

It was previously reported that the underlying influencing factors of AMI may involve genetic background, emotional state, and socioeconomic status, which have been found to be significantly and positively associated with the incidence and pathogenic condition [4], wherea, recent epidemiological studies have reported an association between ambient air pollution and AMI. In Europe, a comprehensive meta-analysis that included 17 time-series studies and 17 case-crossover studies suggested that all the main air pollutants (with the exception of ozone) were significantly associated with an increase in AMI risk [5]. In addition, a time-stratified case-crossover research conducted in England showed significant correlations [6]. It has been shown that ambient air pollution has been connected to deleterious effects on cardiovascular mortality. Furthermore, ambient air pollution has been linked to elevated risks of AMI, including worsening pre-existing symptoms and exacerbating the development of atopic diseases [7–10]. Environmental variables are also thought to be responsible for 24% of global morbidity and 23% of mortality, according to the World Health Organization. Given the ongoing interaction between human beings and the environment, variables such as air pollutants may be potential predictors of cardiovascular diseases [11, 12].

Over the past few decades, the evidence linking air pollution to cardiovascular disease has grown substantially. A time-series study that covered 16 administrative districts of Beijing found an ambient particulate matter of diameter ≤10 μm (PM_{10}), and nitrogen dioxide (NO_2) had a significant influence on deaths from cardiovascular diseases [13]. Another cross-sectional study in Shanghai suggested that the particulate matter of diameter ≤2.5 μm ($PM_{2.5}$) was significantly associated with increased AMI risk on a concurrent day [14]. Meanwhile, Yu's research about significant adverse effects focused on the city of Guangzhou, which is the central city of South China, and this study found that increased daily levels of $PM_{2.5}$ increase the daily morbidity of myocardial infarction [15].

All the aforementioned studies indicated that exposure to air pollutants may trigger AMI symptoms or development; however, most of these studies were conducted in the coastal region, and there are currently no studies on heavy industry cities such as Chongqing in inland China. Chongqing is different from the countries or regions mentioned earlier, which are mainly related to the light industry and tertiary industry. The secondary sector in Chongqing accounts for 40% of the total, according to the 2021 Economic Development report, and its value-added has climbed by 4.9 percent. Furthermore, the medical care visits for AMI are clinically meaningful and need to be evaluated for potentially differentiated effects of air pollution in southwest China.

Therefore, this study has selected a major heavy industry city in China as the research site. We conducted a case-crossover analysis to evaluate the associations between short-term exposure to major air pollutants and daily hospital admissions for AMI in Chongqing, a non-coastal region in southwest China.

MATERIALS AND METHODS

Study Population

Data on daily hospitalizations for AMI from 1 January 2015 to 31 December 2016 were extracted from three top-level and general hospitals (the Second Affiliated Hospital of Chongqing Medical University, the University-Town Hospital of Chongqing Medical University, and the Southeast Hospital) with approximately 3,500, 1,500, and 1,200 inpatient beds, respectively. The AMI (the International Classification of Diseases-10 codes: I21) hospitalization was defined as our study outcome. For each AMI death case, we retrieved information on age at hospital admission, sex, diagnosis, dates of admission, and admitted hospital. All the medical information was recorded on the Platform of Medical Data Science Academy of Chongqing Medical University.

Study Design

We used a time-stratified case-crossover design, which has been widely applied to investigate the acute effects of air pollution on various health outcomes, to examine the relationship between short-term exposure to air pollution and AMI hospitalizations [16, 17]. To control the potential confounding effects of day of the week, long-term trend, and seasonality, the ambient air exposure on the case day (admission day) was matched with the exposure on a series of reference days within the same month on the same day of the week for each AMI case [18].

Exposure Assessment

We obtained daily mean concentrations of $PM_{2.5}$, PM <10 μm in aerodynamic diameter (PM_{10}), sulfur dioxide (SO_2), nitrogen dioxide (NO_2), and carbon monoxide (CO) between 1 January 2015 and 31 December 2016 from the National Urban Air Quality Real-Time Publishing Platform in China. In Chongqing, there were 17 air pollution monitoring stations. Due to the high number of missing data at some monitoring stations, 14 monitoring sites were finally retained. To assess air pollutant exposures, we used the inverse distance weighting (IDW) method. Specifically, the Baidu Maps API (http://lbsyun.baidu.com/) was used to geocode the locations of all monitoring and hospital addresses. To analyze the IDW method's performance in the exposure assessment, we used a 10-fold cross-validation procedure and estimated the coefficient of determination (R^2) and root mean square error based on the observed and projected concentrations across the research period. For each AMI case, we calculated the predicted concentration of his/her inpatient hospital as an inverse distance weighted average

TABLE 1 | Distribution of daily AMI admissions and meteorological factors in Chongqing, China (January 2015–December 2016).

Baseline characteristics	Hospital A	Hospital B	Hospital C	Value
AMI, *n*	22	781	69	872
Case days, *n*	22	781	69	872
Control days, *n*	72	2,526	232	2,960
Sex, *n* (%)				
M	17 (77.3)	520 (66.6)	45 (65.2)	582 (66.7)
F	5 (22.7)	261 (33.4)	24 (34.8)	290 (33.3)
Age				
Mean (SD), yr	77.27 (15.01)	74.93 (12.11)	76.22 (10.26)	75.38 (12.27)
Median (IQR), yr	78 (22)	76 (17)	79 (14)	77 (18)
n (%)				
<75	9 (40.9)	350 (44.8)	25 (36.2)	384 (44.0)
≥75	13 (59.1)	431 (55.2)	44 (63.8)	488 (56.0)
Season, *n* (%)				
Cold	11 (50.0)	356 (45.6)	40 (58.0)	409 (46.9)
Warm	11 (50.0)	425 (54.4)	29 (42.0)	463 (53.1)

of concentrations (1/d2) at all monitoring stations on each of the case and control days. In the present study, we estimated single-day lag exposures (lag 1 day to lag 5 days) and moving average day exposures (lag 01 day to lag 05 days).

Covariates

Weather conditions including daily mean temperature and mean relative humidity were sourced from the National Meteorological Information Centre of China and weather conditions were included in all models to account for their potential confounding effects. We did not take into account the other individual-level covariates, including sex, age, and marital status, because they were held constant in comparing case days to the corresponding control days.

Statistical Analysis

Spearman's correlation coefficient was applied to investigate the correlation between air pollutants and meteorological conditions. Conditional logistic regression was used to assess the associations between air pollution exposure with different lag periods and AMI hospitalizations. Daily average temperature and relative humidity were included as natural cubic spline functions (with a df of 6 and 3, respectively) in all models to account for potential confounding by meteorologic conditions. The risk estimates were expressed in terms of the odds ratio in AMI hospitalizations per 10 μg/m^3 increment of air pollutants (except that CO was per 1 mg/m^3) and their respective 95% confidence intervals (CIs). Stratified and sensitivity analyses were performed on the basis of reaching the maximum effect of $PM_{2.5}$, PM_{10}, SO_2, NO_2, and CO in the moving average lag structure.

We explored the potential effect modification of AMI risk by age (≥75 years and <75 years), gender, and season (warm season as 1 April to 30 September and cold season as 1 October to 31 March). The statistical significance of subgroup differences was assessed as $(\hat{Q}1 - \hat{Q}2)/\sqrt{S\hat{E}1^2 + S\hat{E}2^2}$, such that the $\hat{Q}1$ and $\hat{Q}2$ represent the estimates for the two subgroups and SE1 and SE2 represent their respective standard errors.

The robustness of our results was evaluated by several sensitivity analyses. First, we fitted a two-pollutant model to exclude the confounding effects of other pollutants. However, correlation coefficients >0.5 were not included to avoid collinearity. Second, the degrees of freedom for temperature and humidity are selected as 4–6 and 7–9, respectively. All analyses were performed using R version 3.6.3. P-value less than 0.05 was considered statistically significant.

RESULT

There were 872 cases of AMI between 1 January 2015 and 31 December 2016 from the Platform of Medical Data Science Academy of Chongqing Medical University. **Table 1** summarized the statistics on AMI patients during the study period. Of the 872 AMI patients, 582 (66.7%) were male and 409 (46.9%) were female, hospitalized in the cold season. The mean age at hospital admission was 75.38 years, and 56.0% of the cases were ≥75 years old.

Table 2 shows the distributions of air pollutants and meteorological conditions. The mean exposures to $PM_{2.5}$, PM_{10}, SO_2, NO_2, and CO were 58.170 μg/m^3, 94.046 μg/m^3, 113.631 μg/m^3, 61.410 μg/m^3, and 0.998 mg/m^3, respectively. The annual average temperature and relative humidity were 20°C and 75%, respectively, reflecting the typical subtropical climate of Chongqing.

Spearman's correlation coefficients between air pollutants and meteorological factors are listed in **Table 3**. $PM_{2.5}$, PM_{10}, and CO were positively and moderately correlated, while SO_2 and NO_2 displayed a weak correlation with other air pollutants. Temperature was negatively associated with PM_{10}. Relative humidity was negatively associated with NO_2 but not statistically associated with other air pollutants.

Figure 1 (risk of AMI cases for each pollutant at various lags) lists ORs in daily admissions for AMI associated with 10 μg/m^3 increase in air pollutant concentrations for different lag structures. All analyzed air pollutants showed consistent significant associations at lag 0 day and lag 01 day. The ORs of $PM_{2.5}$, PM_{10}, SO_2, NO_2, and CO peaked at the lag 02 days, lag 0 day, lag 02 days, lag 0 day, lag 01 day, and the corresponding

TABLE 2 | Summary statistics of air pollutant concentrations and meteorological factors.

Variable	Mean	SD	Min	P25	Median	P75	Max
Air pollutant							
$PM_{2.5}$	58.17	32.06	7.13	35.89	51.03	71.70	223.08
PM_{10}	94.06	46.46	10.15	60.30	85.69	115.16	329.80
SO_2	13.63	6.97	2.28	8.76	12.65	17.13	49.56
NO_2	61.41	19.44	7.66	47.99	59.65	72.82	152.90
CO	1.00	0.36	0.30	0.78	0.99	1.18	12.26
Meteorologic condition							
Temperature	20.05	7.36	1.20	13.70	21.03	25.70	36.20
Relative humidity, %	75.36	11.10	43.00	67.50	76.00	84.30	96.25

$PM_{2.5}$, particles with aerodynamic diameter <2.5 μm; PM_{10}, particles with aerodynamic diameter <10 μm; SO_2, sulfur dioxide; NO_2, nitrogen dioxide; CO, carbon monoxide.

TABLE 3 | Spearman's correlation coefficients between air pollutants and meteorological factors.

Variables	CO	$PM_{2.5}$	PM10	SO_2	NO_2	Temperature	Relative humidity
CO	1.000						
$PM_{2.5}$	0.581	1.000					
PM_{10}	0.519	0.858	1.000				
SO_2	0.178	0.158	0.135	1.000			
NO_2	0.081	0.169	0.214	0.385	1.000		
Temperature	−0.334	−0.128	−0.009**	−0.309	0.081	1.000	
Relative humidity	0.124	−0.085	−0.283	0.078	−0.007**	−0.410	1.000

$PM_{2.5}$, particles with aerodynamic diameter <2.5 μm; PM_{10}, particles with aerodynamic diameter <10 μm; SO_2, sulfur dioxide; NO_2, nitrogen dioxide; CO, carbon monoxide.

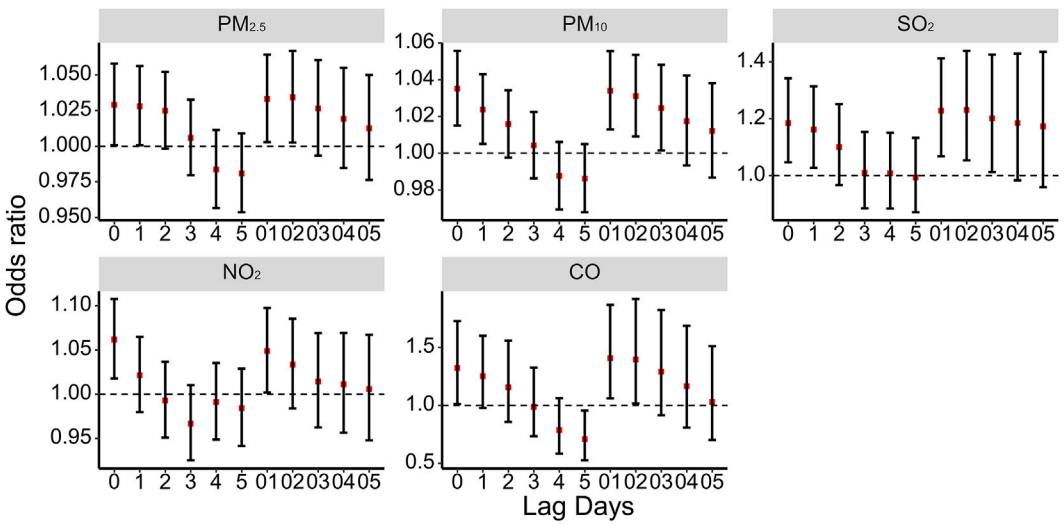

FIGURE 1 | Risk of AMI cases for each pollutant at various lags.

values were 1.034 (95% CI: 1.003–1.067), 1.035 (95% CI: 1.015–1.056), 1.231 (95% CI: 1.053–1.438), 1.062 (95% CI: 1.018–1.107), and 1.406 (95% CI: 1.059–1.866), respectively. The estimated effects in 10 μg/m^3 increments are presented in **Supplementary Table S1**.

The associations between air pollutant exposures and the hospitalizations for AMI were evaluated in the subgroups based on sex, age, and season (**Table 4**). Although the ORs for $PM_{2.5}$, PM_{10}, NO_2, SO_2, and CO varied to some extent, no significant effect modification by sex, age, or season was observed (all p for effect modification >0.05).

Table 5 provides the results of the two-pollutant model. When adjusting for co-pollutants, the effect estimates for PM_{10}, NO_2, SO_2, and CO were slightly reduced but remained statistically significant, and further adjustment for other pollutant exposures did not materially change the associations between $PM_{2.5}$

TABLE 4 | Risks for AMI hospitalizations with per 10 μg/m^3 increase of exposure to $PM_{2.5}$, PM_{10}, SO_2, NO_2, and except that CO was per 1 mg/m^3 stratified by age, sex, and season.

Variable	$PM_{2.5}$	*p* value	PM_{10}	*p* value	SO_2	*p* value	NO_2	*p* value	CO	*p* value
	OR (95%CI)		OR (95%CI)		OR (95%CI)		OR (95%CI)		OR (95%CI)	
Male	1.034 (0.995–1.075)		1.033 (1.008–1.059)		1.283 (1.062–1.55)		1.06 (1.006–1.117)		1.66 (1.097–2.513)	
Female	1.037 (0.984–1.093)	0.924	1.041 (1.007–1.077	0.706	1.113 (0.842–1.47)	0.407	1.063 (0.989–1.142)	0.960	1.243 (0.844–1.828	0.316
<75	1.003 (0.955–1.053)		1.032 (1.001–1.064)		1.348 (1.065–1.707)		1.077 (1.012–1.147)		1.816 (1.075–3.067)	
≥75	1.057 (1.015–1.101)	0.109	1.038 (1.012–1.066)	0.761	1.156 (0.938–1.424)	0.339	1.047 (0.989–1.109)	0.515	1.263 (0.904–1.764)	0.252
Warm	1.024 (0.957–1.095)		1.023 (0.984–1.065)		1.305 (1.016–1.676)		1.081 (1.017–1.149)		1.151 (0.625–2.119)	
Cold	1.024 (0.985–1.064)	0.998	1.033 (1.007–1.058)	0.712	1.175 (0.941–1.467)	0.540	1.034 (0.973–1.099)	0.315	1.38 (0.973–1.956)	0.613

$PM_{2.5}$, particles with aerodynamic diameter <2.5 μm; PM_{10}, particles with aerodynamic diameter <10 μm; SO_2, sulfur dioxide; NO_2, nitrogen dioxide; CO, carbon monoxide; CI, confidence interval.

TABLE 5 | Risks of AMI for each pollutant in the two-pollutant model.

Air pollution	Variable	OR (95%CI)
$PM_{2.5}$	NULL	1.034 (1.003–1.067)
	SO_2	1.028 (0.997–1.061)
	NO_2	1.031 (0.999–1.065)
PM_{10}	NULL	1.035 (1.015–1.056)
	SO_2	1.032 (1.011–1.052)
	NO_2	1.031 (1.011–1.052)
SO_2	NULL	1.231 (1.053–1.438)
	$PM_{2.5}$	1.205 (1.029–1.411)
	PM_{10}	1.188 (1.014–1.393)
	NO_2	1.238 (1.029–1.489)
	CO	1.210 (1.034–1.416)
NO_2	NULL	1.062 (1.018–1.107)
	$PM_{2.5}$	1.057 (1.013–1.103)
	PM_{10}	1.050 (1.006–1.096)
	SO_2	1.043 (0.994–1.094)
	CO	1.058 (1.014–1.104)
CO	NULL	1.406 (1.059–1.866)
	SO_2	1.349 (1.016–1.789)
	NO_2	1.367 (1.029–1.815)

$PM_{2.5}$, particles with aerodynamic diameter <2.5 μm; PM_{10}, particles with aerodynamic diameter <10 μm; SO_2, sulfur dioxide; NO_2, nitrogen dioxide; CO, carbon monoxide; CI, confidence intervals.

exposures and AMI. Sensitivity analysis is presented in **Supplementary Table S2**. The use of an alternative df value for temperature (4–6) and relative humidity (7–9) had no significant effect on the effect estimates of the associations between air pollution and daily hospital admissions for AMI.

DISCUSSION

Over the past few decades, a growing body of epidemiological and clinical evidence has raised concerns about the influence of air pollution on cardiovascular health in the context of global environmental change, but the data in developing countries are still limited, especially in East Asia. Chongqing is a major heavy industry city with a population of more than 8.6 million in southwest China, and its basin structure has a great impact on ambient air pollution. Therefore, we conducted this time-stratified case-crossover study to evaluate the short-term effects of ambient air pollutants on hospitalizations for AMI in Chongqing.

In the present study, we identified that ambient air pollutants were associated with hospitalizations for AMI. The data indicated that short-term exposure to $PM_{2.5}$, PM_{10}, SO_2, NO_2, and CO was significantly associated with increased clinical visits for AMI. In the single-pollutant models, we found that each 10 μg/m^3 increase in $PM_{2.5}$, PM_{10}, SO_2, NO_2, and CO was associated with a 1.03, 1.03, 1.23, 1.06, and 1.41% increase in AMI hospitalizations, respectively. In the two-pollutant models, the estimated effects of PM_{10}, SO_2, and NO_2 were all statistically significant when adjusting for co-pollutants. Also all the air pollutants and meteorological factors showed lag effects in the present study. Despite the relatively small effect sizes of unit changes in exposure variables, our results still have considerable public health implications due to ubiquitous exposure. Our results contribute to the limited scientific evidence that ambient air pollution and meteorological factors may influence the incidence of AMI.

It was indicated that air pollutants were positively associated with AMI incidence in previous similar studies [19–21]. For example, a study conducted in Brisbane city has shown that AMI hospitalizations increased by 12.34% (95% CI: 1.44–24.42%) per 10 μg/m^3 increase in $PM_{2.5}$ [19]. Another case-crossover research on fine particulate air pollution and AMI hospitalization rate in 26 Chinese cities also indicated that short-term elevations in $PM_{2.5}$ concentration may increase the risk of STEMI [20]. Meanwhile, a European multicenter cohort study reported that cardiac readmissions increased by 1.014% (95% CI: 1.001–1.026%) per 200 microg/m^3 increase in CO and increased by 1.032% (95% CI: 1.013–1.051) for per 8 microg/m^3 NO2 [21].

In China, the evidence of the effects of air pollutant exposure on AMI risk is still controversial in the previous studies. A research study in Hubei province was also a retrospective study with a similar theme but with different observational outcomes [17]. They discovered that short-term elevations of PM and NO_2 can increase AMI mortality, and the difference in dependence time lags may be related to different observational outcomes or variation in $PM_{2.5}$ constituents across. Meanwhile, a study conducted in Hongkong found that PM_{10} and NO_2 were significantly and positively associated with AMI hospitalizations

both in the single-pollutant model and multipollutant model [22]. Another research study conducted in Shanghai indicated that PM_{10}, SO_2, and NO_2 were related to visit for AMI [23], which was consistent with our results. However, a research study from Changzhou observed a negative association between ambient NO_2 concentrations and AMI hospitalizations [15]. In addition, several other studies in China found no association between CO, SO_2, and AMI risk [24–26].

The reason why the change of air quality index concentration in this study affects the change in AMI hospitalization rate can be explained from both medical and environmental aspects. On the one hand, according to the recent mechanistic studies in cells and animal models, the positive association between air pollution and AMI was biologically plausible [27–29]. In addition to inflammatory effects [30], ambient air pollutants have been linked to arterial vasoconstriction and decreased heart rate variability [31]. Air pollutants could aggravate the cardiopulmonary symptoms of AMI or weaken the protection of the respiratory system. Among these hypotheses is the possibility that particles could directly induce the production of reactive oxygen species, resulting in oxidative stress, damage, and inflammation reactions in the immune system [32, 33]. On the other hand, a series of environmental studies have proven that atmospheric aerosol is a composite of various inorganic and organic components, and its physical and chemical properties under the fluctuating environmental conditions determine its impact on air quality and human health [34–37]. Aerosol particles such as $PM_{2.5}$ and their precursors can have a significant impact on air quality, the ozone layer, and climate on scales ranging from regional to global as anthropogenic activities increase. In terms of $PM_{2.5}$ particle composition, the creation of $PM_{2.5}$ particles from atmospheric pollutants (NO_x, SO_2, etc.) heterogeneously interacted with and condensed on the surfaces of other aerosols in the atmosphere is a process that accelerates toxic gas deposition [38]. Under high relative humidity circumstances, H_2O is both a major component of $PM_{2.5}$ and speeds up the transformation and deposition of accumulated hazardous gases. In this study, we verified the correlation between relative humidity and air pollutants, and the relationships also are rationally followed through other studies [39]. Apart from water-soluble ions, $PM_{2.5}$ mainly contains sulfate–nitrate–ammonium (SNA) ions, and the sulfate and nitrate are formed by their precursors SO_2 and NO_x, respectively [40]. High levels of reactive oxygen species (ROS) can be generated from environmentally persistent-free radicals (EPFRs) in $PM_{2.5}$, and atmospheric pollutants can boost the radical production and EPFR degradation rates through photochemical processes. The capacity of ambient PM to generate ROS can be a reliable predictor of particle-induced unfavorable health effects [41]. It has been shown above that SNA and organic matter can promote the formation of haze and are the main chemical components in the pollution events. That is to say, it proves the relationship between CO, NO_2, or SO_2 studied in this article, and the relationship between toxic gases accelerates their transformation and deposition. When its emissions increase, it promotes the generation of aerosols and changes the physical and chemical properties of atmospheric aerosols, accelerates the deposition of $PM_{2.5}$ in the lungs, and then affects the incidence of AMI through pathological reactions [42–44].

The acute influences of air pollutants and climate factors on AMI hospital visits were investigated based on a large database in Chongqing, China. Chongqing's high air pollution levels and distinct seasons provided ample opportunities to investigate the effects of environmental risk factors on AMI conditions. Nevertheless, our study has some potential limitations. First, this is the disadvantage of this research that we do not have, according to the residential address, to perform air pollution exposure assessment, and the exposure misclassification results in an underestimation of the sensitivity of air pollution, which might lead to lower statistical power. Second, this time-stratified study is inherently an ecological analysis, which may limit the ability to adjust for the individual confounders and might understate the effects of air pollution. Last, the data were only collected in Chongqing with a subtropical humid climate, and therefore the results of this study can only be generalized to cities with the same environmental and socioeconomical characteristics.

CONCLUSION

In summary, this study provided clear evidence that ambient air pollution could increase the hospitalization of AMI in Chongqing, China. Further studies from both an epidemiological and a physiological perspective are needed to establish the causal relationship between air pollution, meteorological factors, and AMI.

DATA AVAILABILITY STATEMENT

The raw data supporting the conclusion of this article will be made available by the authors, without undue reservation.

AUTHOR CONTRIBUTIONS

MMZ wrote the manuscript and analyzed the data. XL collected and inputted the data. MY, YY, HC, MML, PL, YD, JF, LQL, and LZ reviewed the results and provided guidelines for presentation and interpretation.

ACKNOWLEDGMENTS

We thank the Medical Data Science Academy of Chongqing Medical University for providing the population health data.

SUPPLEMENTARY MATERIAL

The Supplementary Material for this article can be found online at: https://www.frontiersin.org/articles/10.3389/fphy.2022.941181/full#supplementary-material

REFERENCES

1. Anderson JL, Morrow DA. Acute Myocardial Infarction. *N Engl J Med* (2017) 376(21):2053–64. doi:10.1056/nejmra1606915
2. Reed GW, Rossi JE, Cannon CP. Acute Myocardial Infarction. *The Lancet* (2017) 389(10065):197–210. doi:10.1016/s0140-6736(16)30677-8
3. Xu A, Mu Z, Jiang B, Wang W, Yu H, Zhang L, et al. Acute Effects of Particulate Air Pollution on Ischemic Heart Disease Hospitalizations in Shanghai, China. *Int J Environ Res Public Health* (2017) 14(2):168. doi:10.3390/ijerph14020168
4. Santurtún A, Sanchez-Lorenzo A, Villar A, Riancho JA, Zarrabeitia MT. The Influence of Nitrogen Dioxide on Arrhythmias in Spain and its Relationship with Atmospheric Circulation. *Cardiovasc Toxicol* (2017) 17(1):88–96. doi:10.1007/s12012-016-9359-x
5. Mustafic H, Jabre P, Caussin C, Murad MH, Escolano S, Tafflet M, et al. Main Air Pollutants and Myocardial Infarction: a Systematic Review and Meta-Analysis. *JAMA* (2012) 307(7):713–21. doi:10.1001/jama.2012.126
6. Butland BK, Atkinson RW, Crichton S, Barratt B, Beevers S, Spiridou A, et al. Air Pollution and the Incidence of Ischaemic and Haemorrhagic Stroke in the South London Stroke Register: a Case-Cross-Over Analysis. *J Epidemiol Community Health* (2017) 71(7):707–12. doi:10.1136/jech-2016-208025
7. Brunekreef B, Beelen R, Hoek G, Schouten L, Bausch-Goldbohm S, Fischer P, et al. Effects of Long-Term Exposure to Traffic-Related Air Pollution on Respiratory and Cardiovascular Mortality in the Netherlands: the NLCS-AIR Study. *Res Rep Health Effects Inst* (2009) 139(139):5–71. https://pubmed.ncbi.nlm.nih.gov/19554969/.
8. Kriit HK, Anderson EM, Carlsen HK, Anderson N, Ljungman PLS, Pershagen G, et al. Using Distributed Lag Non-linear Models to Estimate Exposure Lag-Response Associations between Long-Term Air Pollution Exposure and Incidence of Cardiovascular Disease. *Int J Environ Res Public Health* (2022) 19(5). doi:10.3390/ijerph19052630
9. Stockfelt L, Andersson EM, Molnár P, Gidhagen L, Segersson D, Rosengren A, et al. Long-term Effects of Total and Source-specific Particulate Air Pollution on Incident Cardiovascular Disease in Gothenburg, Sweden. *Environ Res* (2017) 158:61–71. doi:10.1016/j.envres.2017.05.036
10. Stockfelt L, Andersson EM, Molnár P, Rosengren A, Wilhelmsen L, Sallsten G, et al. Long Term Effects of Residential NOx Exposure on Total and Cause-specific Mortality and Incidence of Myocardial Infarction in a Swedish Cohort. *Environ Res* (2015) 142:197–206. doi:10.1016/j.envres.2015.06.045
11. Li Q, Yang Y, Chen R, Kan H, Song W, Tan J, et al. Ambient Air Pollution, Meteorological Factors and Outpatient Visits for Eczema in Shanghai, China: A Time-Series Analysis. *Int J Environ Res Public Health* (2016) 13(11). doi:10.3390/ijerph13111106
12. Royé D, Zarrabeitia MT, Fdez-Arroyabe P, Álvarez Gutiérrez A, Santurtún A. Role of Apparent Temperature and Air Pollutants in Hospital Admissions for Acute Myocardial Infarction in the North of Spain. *Revista Española de Cardiología (English Edition)* (2019) 72(8):634–40. doi:10.1016/j.rec.2018.07.009
13. Li W, Cao Y, Li R, Ma X, Chen J, Wu Z, et al. The Spatial Variation in the Effects of Air Pollution on Cardiovascular Mortality in Beijing, China. *J Expo Sci Environ Epidemiol* (2018) 28(3):297–304. doi:10.1038/jes.2016.21
14. Hu J, Tang M, Zhang X, Ma Y, Li Y, Chen R, et al. Size-fractionated Particulate Air Pollution and Myocardial Infarction Emergency Hospitalization in Shanghai, China. *Sci Total Environ* (2020) 737:140100. doi:10.1016/j.scitotenv.2020.140100
15. Yu Y, Yao S, Dong H, Ji M, Chen Z, Li G, et al. Short-term Effects of Ambient Air Pollutants and Myocardial Infarction in Changzhou, China. *Environ Sci Pollut Res* (2018) 25(22):22285–93. doi:10.1007/s11356-018-2250-5
16. Carracedo-Martínez E, Taracido M, Tobias A, Saez M, Figueiras A. Case-crossover Analysis of Air Pollution Health Effects: a Systematic Review of Methodology and Application. *Environ Health Perspect* (2010) 118(8):1173–82. doi:10.1289/ehp.0901485
17. Liu Y, Pan J, Fan C, Xu R, Wang Y, Xu C, et al. Short-Term Exposure to Ambient Air Pollution and Mortality from Myocardial Infarction. *J Am Coll Cardiol* (2021) 77(3):271–81. doi:10.1016/j.jacc.2020.11.033
18. Bateson TF, Schwartz J. Control for Seasonal Variation and Time Trend in Case-Crossover Studies of Acute Effects of Environmental Exposures. *Epidemiology* (1999) 10(5):539–44. doi:10.1097/00001648-199909000-00013
19. Cheng J, Tong S, Su H, Xu Z. Hourly Air Pollution Exposure and Emergency Department Visit for Acute Myocardial Infarction: Vulnerable Populations and Susceptible Time Window. *Environ Pollut Barking, Essex* (1987) 288:2021117806.
20. Liu H, Tian Y, Cao Y, Song J, Huang C, Xiang X, et al. Fine Particulate Air Pollution and Hospital Admissions and Readmissions for Acute Myocardial Infarction in 26 Chinese Cities. *Chemosphere* (2018) 192:282–8. doi:10.1016/j.chemosphere.2017.10.123
21. von Klot S, Peters A, Aalto P, Bellander T, Berglind N, D'Ippoliti D, et al. Ambient Air Pollution Is Associated with Increased Risk of Hospital Cardiac Readmissions of Myocardial Infarction Survivors in Five European Cities. *Circulation* (2005) 112(20):3073–9. doi:10.1161/circulationaha.105.548743
22. Yu IT-s., Qiu H, Wang X, Tian L, Tse LA. Synergy between Particles and Nitrogen Dioxide on Emergency Hospital Admissions for Cardiac Diseases in Hong Kong. *Int J Cardiol* (2013) 168(3):2831–6. doi:10.1016/j.ijcard.2013.03.082
23. Xie J, He M, Zhu W. Acute Effects of Outdoor Air Pollution on Emergency Department Visits Due to Five Clinical Subtypes of Coronary Heart Diseases in Shanghai, china. *J Epidemiol* (2014) 24(6):452–9. doi:10.2188/jea.je20140044
24. Chen C, Wang X, Lv C, Li W, Ma D, Zhang Q, et al. The Effect of Air Pollution on Hospitalization of Individuals with Respiratory and Cardiovascular Diseases in Jinan, China. *Medicine* (2019) 98(22):e15634. doi:10.1097/md.0000000000015634
25. Goggins WB, Chan EYY, Yang C-Y. Weather, Pollution, and Acute Myocardial Infarction in Hong Kong and Taiwan. *Int J Cardiol* (2013) 168(1):243–9. doi:10.1016/j.ijcard.2012.09.087
26. Li J, Liu C, Cheng Y, Guo S, Sun Q, Kan L, et al. Association between Ambient Particulate Matter Air Pollution and ST-Elevation Myocardial Infarction: A Case-Crossover Study in a Chinese City. *Chemosphere* (2019) 219:724–9. doi:10.1016/j.chemosphere.2018.12.094
27. Nemmar A, Hoylaerts MF, Hoet PH, Dinsdale D, Smith T, Xu H, et al. Ultrafine Particles Affect Experimental Thrombosis in an *In Vivo* Hamster Model. *Am J Respir Crit Care Med* (2002) 166(7):998–1004. doi:10.1164/rccm.200110-026OC
28. Nemmar A, Nemery B, Hoet PHM, Van Rooijen N, Hoylaerts MF. Silica Particles Enhance Peripheral Thrombosis. *Am J Respir Crit Care Med* (2005) 171(8):872–9. doi:10.1164/rccm.200409-1202oc
29. Peters A, Dockery DW, Muller JE, Mittleman MA. Increased Particulate Air Pollution and the Triggering of Myocardial Infarction. *Circulation* (2001) 103(23):2810–5. doi:10.1161/01.cir.103.23.2810
30. Ghio AJ, Kim C, Devlin RB. Concentrated Ambient Air Particles Induce Mild Pulmonary Inflammation in Healthy Human Volunteers. *Am J Respir Crit Care Med* (2000) 162(3 Pt 1):981–8. doi:10.1164/ajrccm.162.3.9911115
31. Brook RD, Brook JR, Urch B, Vincent R, Rajagopalan S, Silverman F. Inhalation of fine Particulate Air Pollution and Ozone Causes Acute Arterial Vasoconstriction in Healthy Adults. *Circulation* (2002) 105(13):1534–6. doi:10.1161/01.cir.0000013838.94747.64
32. Boovarahan SR, Kurian GA. Mitochondrial Dysfunction: a Key Player in the Pathogenesis of Cardiovascular Diseases Linked to Air Pollution. *Rev Environ Health* (2018) 33(2):111–22. doi:10.1515/reveh-2017-0025
33. Huang SK, Zhang Q, Qiu Z, Chung KF. Mechanistic Impact of Outdoor Air Pollution on Asthma and Allergic Diseases. *J Thorac Dis* (2015) 7(1):23–33. doi:10.3978/j.issn.2072-1439.2014.12.13
34. Farmer DK, Cappa CD, Kreidenweis SM. Atmospheric Processes and Their Controlling Influence on Cloud Condensation Nuclei Activity. *Chem Rev* (2015) 115(10):4199–217. doi:10.1021/cr5006292
35. Shiraiwa M, Li Y, Tsimpidi AP, Karydis VA, Berkemeier T, Pandis SN, et al. Global Distribution of Particle Phase State in Atmospheric Secondary Organic Aerosols. *Nat Commun* (2017) 8:15002. doi:10.1038/ncomms15002
36. Kuwata M, Martin ST. Phase of Atmospheric Secondary Organic Material Affects its Reactivity. *Proc Natl Acad Sci U.S.A* (2012) 109(43):17354–9. doi:10.1073/pnas.1209071109
37. Brunekreef B, Holgate ST. Air Pollution and Health. *The Lancet* (2002) 360(9341):1233–42. doi:10.1016/s0140-6736(02)11274-8
38. Liang C-S, Duan F-K, He K-B, Ma Y-L. Review on Recent Progress in Observations, Source Identifications and Countermeasures of PM2.5. *Environ Int* (2016) 86:150–70. doi:10.1016/j.envint.2015.10.016

39. Martin ST. Phase Transitions of Aqueous Atmospheric Particles. *Chem Rev* (2000) 100(9):3403–54. doi:10.1021/cr990034t
40. Velali E, Papachristou E, Pantazaki A, Choli-Papadopoulou T, Planou S, Kouras A, et al. Redox Activity and *In Vitro* Bioactivity of the Water-Soluble Fraction of Urban Particulate Matter in Relation to Particle Size and Chemical Composition. *Environ Pollut* (2016) 208(Pt B):774–86. doi:10.1016/j.envpol.2015.10.058
41. Gehling W, Khachatryan L, Dellinger B. Hydroxyl Radical Generation from Environmentally Persistent Free Radicals (EPFRs) in PM2.5. *Environ Sci Technol* (2014) 48(8):4266–72. doi:10.1021/es401770y
42. Kampa M, Castanas E. Human Health Effects of Air Pollution. *Environ Pollut* (2008) 151(2):362–7. doi:10.1016/j.envpol.2007.06.012
43. Franchini M, Mannucci PM. Particulate Air Pollution and Cardiovascular Risk: Short-Term and Long-Term Effects. *Semin Thromb Hemost* (2009) 35(7): 665–70. doi:10.1055/s-0029-1242720
44. Maitre A, Bonneterre V, Huillard L, Sabatier P, de Gaudemaris R. Impact of Urban Atmospheric Pollution on Coronary Disease. *Eur Heart J* (2006) 27(19): 2275–84. doi:10.1093/eurheartj/ehl162

Conflict of Interest: The authors declare that the research was conducted in the absence of any commercial or financial relationships that could be construed as a potential conflict of interest.

frontiers | Frontiers in Physics

TYPE Original Research
PUBLISHED 23 August 2022
DOI 10.3389/fphy.2022.985517

OPEN ACCESS

EDITED BY
Xuzhen Zhu,
Beijing University of Posts and Telecommunications (BUPT), China

REVIEWED BY
Guanghui Song,
Xidian University, China
Yilun Shang,
Northumbria University, United Kingdom
Qisheng Zhang,
China University of Geosciences, China
Wang Fengli,
Institute of Computing Technology (CAS), China

*CORRESPONDENCE
Yuexia Zhang,
zhangyuexia@bistu.edu.cn

SPECIALTY SECTION
This article was submitted to Social Physics, a section of the journal Frontiers in Physics

RECEIVED 04 July 2022
ACCEPTED 22 July 2022
PUBLISHED 23 August 2022

CITATION
Pan D and Zhang Y (2022), Analysis of information propagation and control of a layered SITR model in complex networks.
Front. Phys. 10:985517.
doi: 10.3389/fphy.2022.985517

Analysis of information propagation and control of a layered SITR model in complex networks

Dawei Pan[1] and Yuexia Zhang[2,3,4]*

[1]School of Information and Communication Engineering, Beijing Information Science & Technology University, Beijing, China, [2]Key Laboratory of Modern Measurement & Control Technology, Ministry of Education, Beijing Information Science & Technology University, Beijing, China, [3]State Key Laboratory of Networking and Switching Technology (Beijing University of Posts and Telecommunications), Beijing, China, [4]Key Laboratory of Information and Communication Systems, Ministry of Information Industry, Beijing Information Science and Technology University, Beijing, China

In the field of complex network research, complex network information transmission models based on infectious disease models are often used to study the mechanism of information transmission. This is helpful for the prediction of information transmission trends and the formulation of control strategies. However, the classification of node types in traditional information transmission models is too simple and cannot reflect the characteristics of each node. To solve the above problems, this study proposes a layered SITR complex network information transmission model. The model is layered according to the influence of nodes, and rational propagator nodes are added to optimize it. The propagation threshold of the model is deduced theoretically and the stability of the model is proved. To reduce the dissemination scale of the network's public opinion information, an optimal control strategy is proposed based on the Pontryagin maximum principle to optimize the information dissemination process. Finally, combined with real events from social network platform, the simulation results show that the layered SITR model can describe the process of network information dissemination more accurately, and the optimal control strategy can effectively reduce the dissemination scale of the network's public opinion information.

KEYWORDS

complex networks, infectious disease model, propagation dynamics, stability analysis, optimal control

1 Introduction

With the development and progress of Internet technology, a variety of online social platforms has enriched the ways people use to exchange information, but they have also accelerated the spread of online rumors. When false and malicious information spreads on a large scale, it triggers heated discussions among netizens, thus resulting in many online public opinions, which will have a negative impact on social stability and economic development. Because of the high similarity between network information and virus transmissions,

researchers have begun to combine the structural characteristics of information networks to apply complex networks and infectious disease models to the field of information transmission and simulate the process of information transmission in social networks based on mathematical models [1]. Therefore, it is of great practical significance to establish an information transmission model for realistic scenarios based on infectious disease models and complex networks, analyze and study the mechanism of information transmission, and formulate specific prevention and control strategies.

At present, numerous achievements have been accomplished in the research of infectious disease models in the field of information transmission. Among them, Kermack and McKendrick proposed the most classic infectious disease model in 1927, that is, the susceptible-infected-recovered (SIR) model [2]. Subsequently, scholars proposed various optimized models of infectious diseases on this basis and studied the mechanism of information transmission [3–6]. Based on a simple susceptible-infected-susceptible (SIS) model, Wang et al. innovatively established an ESIS information transmission model based on emotion weighting, which weighted different links according to user emotions, effectively improving the accuracy of the model [7]. Based on the traditional SIRS model, Wang et al. proposed the SPIRS model with potential propagation nodes and applied it to different real networks, thus indicating that the number of potential nodes can predict the peak of information propagation [8]. After the introduction of the time-varying rate of immune loss in the SIRS model, Shaji et al. proposed a new SIRS model and conducted simulation verification on an artificial network [9]. Zhao et al. proposed the SIHR social network information transmission model and added hibernation nodes to the model to study the mechanism of forgetting and memory associated with the process of information transmission. The results showed that nodes with a hibernation state can reduce the overall impact of rumors [10].

Owing to the continuous progress of communication technology, the abilities associated with the reception and spreading of information are not identical and the individual network user nodes are influenced by many factors that lead to a complicated propagation behavior mechanism. Thus, single information propagation models cannot accurately describe the information in the network transmission process. Accordingly, scholars have established a complex network of multilayer information dissemination model to solve these problems effectively. These efforts have rendered the multilayer information transmission model the hot spot of current research. In a multilingual environment, Li et al. stratified the infectious disease model based on whether people transmitted information through their first or second languages, improved the information exchange mechanism between layers, and established a stratified ISR model [11]. Yagan et al. improved the information transmission mechanism based on the characteristics of the SIR virus transmission model and established a social–physical, two-layer network information diffusion model to explore the occurrence of the seepage effect in multilayer networks [12]. Scholars divide the model into consciousness layer and propagation layer and study the influence of consciousness on propagation dynamics. Wang et al. stratified the transmission channels of viruses in the network into consciousness and viral transmission layers, so as to establish the hierarchical transmission model of virus and information, and studied the impact of information on viral transmission [13]. Wu et al. proposed an aware-susceptible-infected model (ASI) to explore the effect of awareness on the spreading process in multiplex networks. Experiment found that epidemic information can help to suppress the epidemic diffusion only when individuals' abilities of transforming awareness into actual protective behaviors attain a threshold [14]. Li et al. built a dynamic model to describe the transmission of two competing complex information, in which individuals in the network can only accept one of the two messages. The results show that the heterogeneity of the distribution of multiple network degrees has no qualitative influence on the results [15]. Although scholars have conducted in-depth studies on the multilayer information transmission model in recent years, the node types are very limited and cannot accurately describe the influence of various nodes in the network on information transmission.

To make the model reflect the process of information transmission more accurately, scholars have enriched the nodal types in the network according to the characteristics of information transmission. Jiang et al. added the truth disseminator node in the model, established a two-stage SPNR rumor propagation model, and studied the influence of official information on online rumor propagation [16]. Wang et al. established the 2SI2R model by considering the simultaneous spread of two types of rumors in the population [17]. Sang et al. proposed a SFTRD information transmission model based on heterogeneous network, added controlled nodes into the model, and studied the information transmission process combined with optimal control theory [18]. Zhu considered the influence of the user's psychological state on information dissemination when facing major public opinions, classified nodes according to different attitudes associated with believing and resisting public opinions, and established the SBD (Susceptible–Believed–Denied) public opinion dissemination model [19]. Li et al. proposed a UAU-SIS information transmission model and conducted simulations in a network composed of a static information transmission network and temporal physical network to study the influence of spatiotemporal characteristics on information transmission [20]. Zhao et al. improved the SEIV information transmission model by introducing vigilance nodes to improve the SEIR model and solved the information transmission control problem by using a group-based stochastic optimization strategy, effectively improving the accuracy of the model [21].

The traditional model has two major limitations: The division of the SIRS model of node state is relatively simple, all the nodes in the model have the same properties, part of the connection among

the nodes are ignored, and the network users in the situation differ markedly with reality. Especially in the process of public opinion communication, different communicators have different groups of people in contact, and the influence of communicator groups is also different. Therefore, the model needs to be considered stratified according to node influence. In addition, in the traditional SIRS model, only communicators can influence susceptible people. However, in practice, communicators have different attitudes toward public opinion events. Thus, they also influence each other. Therefore, we propose the layered SITR (L-SITR) model to solve the above problems.

This paper discusses the emergency in the Sina Weibo information dissemination process and proposes the L-SITR model. According to the different number of neighbors of nodes, information propagators are divided into influential propagator node and normal propagator node, and the rational propagator node is added to represent the information dissemination of rational thinking to spread the correct information of nodes. The mechanism of influential propagators and rational guidance are established to make the model more appropriate to the actual situation. Through the dynamic analysis of the L-SITR model, the propagation threshold of the model is theoretically solved, and the stability of the equilibrium point is proved [22–25], and the optimal control problem of information propagation is solved using Pontryagin's maximum principle. Our main contributions of this work can be listed as follows:

(1) Considering the differences between nodes in the network, the complexity of node behaviors and the different attitudes of communicators toward public opinion information, rational propagator nodes were added to the study and a new L-SITR information dissemination model was proposed in accordance with optimization of the traditional SIRS model.
(2) The propagation threshold of the L-SITR model was calculated using the reproduction matrix method, and the stability of the model was proved according to the Routh–Hurwitz criterion and Lyapunov methods.
(3) The traditional SIRS and proposed L-SITR models were simulated using the data obtained from Sina Weibo and the performances of the different models were compared and evaluated using the least-squares criterion.
(4) The information transmission process of the L-SITR model was optimized and an optimal control strategy was proposed for the information transmission process according to the maximum principle of Pontryagin.

The organization of this paper is as follows. Section 2 is the L-SITR model formulation and preliminaries. In Section 3, the information propagation threshold of L-SITR model was determined by dynamic analysis, and the stability of equilibrium point was proved. In Section 4, the optimal control strategy for network information is introduced and analyzed theoretically. In Section 5, the simulation results are given and discussed. Finally, conclusions are presented in Section 6.

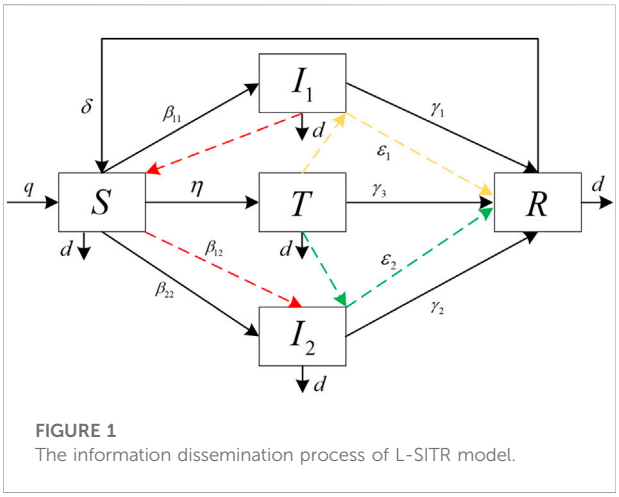

FIGURE 1
The information dissemination process of L-SITR model.

2 L-SITR information propagation model

We proposed the L-SITR model to study the dissemination process of emergency information on the network platform under the scenario of government intervention. The L-SITR model is shown in Figure 1. This model divides network nodes in five categories: uninformed persons S, influential propagators I_1, normal propagators I_2, rational propagators T, and immune R. After the occurrence of public opinion events, the uninformed person is exposed to public opinion information and becomes a propagator. Some will quickly spread all information they receive about events, while others will spread official information. According to their attitude, propagators are divided in two categories: public opinion propagators I and rational propagators T. Rational propagators T disseminate correct information in the process of information transmission and convince public opinion propagators to think rationally by contacting them so as to become restorers with a certain probability and reduce the influence of public opinion. In such emergencies with government intervention, the media will report the event and ordinary netizens will also participate in the discussion, but different groups have different influences, therefore public opinion propagators are divided in influential propagators (I_1) and normal propagators (I_2) according to their influences. Influential public opinion propagators will have a higher public opinion propagation power and uninformed persons will have a higher probability of becoming public opinion propagators after they are contacted. The L-SITR model parameters shown in Figure 1 are listed in Table 1.

On the basis of the original transmission mechanism of traditional SIRS model, this paper adds the transmission mechanism of influential propagators and rational guidance

TABLE 1 Parameters defining the L-SITR model.

Parameter	Description
β_{11}	Uninformed persons S may receive information from influential propagators I_1 and becomes I_1 with probability β_{11}
β_{22}	Uninformed persons S may receive information from normal propagators I_2 and becomes I_2 with probability β_{22}
β_{12}	Uninformed persons S may receive information from influential propagators I_1 and becomes I_2 with probability β_{12}
γ_1	The transmission probability of influential propagators I_1 turning into immune R
γ_2	The transmission probability of normal propagators I_2 turning into immune R
γ_3	The transmission probability of rational propagators T turning into immune R
ε_1	Influential propagators I_1 may receive correct information from rational propagators T and becomes immune R with probability ε_1
ε_2	Normal propagators I_2 may receive correct information from rational propagators T and becomes immune R with probability ε_2
η	The transmission probability of uninformed persons S turning into rational propagators T
δ	The transmission probability of immune R turning into uninformed persons S
q	The coming rate of uninformed persons S
d	The leaving rate of the different compartment

mechanism. The mechanism of influential propagators refers to that the uninformed person S will receive the information spread by the influential propagators I_1 and become the normal propagators I_2. This process is shown in the red dotted line in Figure 1. The rational influence mechanism means that influential propagators I_1 and normal propagators I_2 will receive the information spread by rational propagators T, and thus become immune R with a higher probability, as shown in the yellow dotted line and green dotted line in Figure 1.

L-SITR model can be expressed by the following dynamic equation,

$$\begin{aligned}
\frac{dS(t)}{dt} &= q - \frac{(\beta_{11}+\beta_{12})\bar{k}_1 S(t)I_1(t)}{N(t)} - \frac{\beta_{22}\bar{k}_2 S(t)I_2(t)}{N(t)} \\
&\quad + \delta R(t) - \eta S(t) - dS(t) \\
\frac{dI_1(t)}{dt} &= \frac{\beta_{11}\bar{k}_1 S(t)I_1(t)}{N(t)} - \frac{\varepsilon_1\bar{k}_3 I_1(t)T(t)}{N(t)} - \gamma_1 I_1(t) - dI_1(t) \\
\frac{dI_2(t)}{dt} &= \frac{\beta_{12}\bar{k}_1 S(t)I_1(t)}{N(t)} + \frac{\beta_{22}\bar{k}_2 S(t)I_2(t)}{N(t)} - \frac{\varepsilon_2\bar{k}_3 I_2(t)T(t)}{N(t)} \\
&\quad - \gamma_2 I_2(t) - dI_2(t) \\
\frac{dT(t)}{dt} &= \eta S(t) - \gamma_3 T(t) - dT(t) \\
\frac{dR(t)}{dt} &= \frac{\varepsilon_1\bar{k}_3 I_1(t)T(t)}{N(t)} + \frac{\varepsilon_2\bar{k}_3 I_2(t)T(t)}{N(t)} \\
&\quad + \gamma_1 I_1(t) + \gamma_2 I_2(t) + \gamma_3 T(t) - \delta R(t) - dR(t).
\end{aligned} \tag{1}$$

where N is the total number of nodes, $\bar{k}_1$, $\bar{k}_2$, $\bar{k}_3$ represent the average degree of nodes in states I_1, I_2, T. Therefore, we have [26] that

$$\frac{dN(t)}{dt} = q - dN(t). \tag{2}$$

To simplify the analysis process, this study assumes that the total population remains constant, that is, $q = dN(t)$ and N are constant. The normalization of N can be obtained as follows,

$$S(t) + I_1(t) + I_2(t) + T(t) + R(t) = 1. \tag{3}$$

3 The basic reproduction number and stability analysis

In this section, the next generation matrix method was used to calculate the basic reproduction number of the L-SITR model, namely the propagation threshold and to prove the global stability of the no information equilibrium and information equilibrium of the model, respectively.

The basic reproduction number refers to the expected number of secondary infections caused by an infected in an environment full of susceptible people during the disease cycle. For information propagation model, the basic regeneration number is the threshold of information propagation. Firstly, we study the basic reproduction number of model 1) through the next generation matrix method.

Because the actual number of nodes in the information transmission model cannot be negative, so the number of nodes in the model presented in this study is as follows,

$$S(t) > 0, I_1(t) \geq 0, I_2(t) \geq 0, T(t) \geq 0, R(t) \geq 0. \tag{4}$$

Let $I_1 = I_2 = 0$ and $\frac{dS}{dt} = 0$ in Eq. 1. Combined with Eq. 2, we can obtain the no information equilibrium point $E_0(S^0, I_1^0, I_2^0, T^0, R^0) = (\frac{q}{(\eta+d)}, 0, 0, 0, 0)$ of the L-SITR model. We set $\chi = (S^0, I_1^0, I_2^0, T^0, R^0)$. Eq. 5 can then be expressed as,

$$\frac{d\chi}{dt} = \mathcal{F} - \mathrm{V}, \tag{5}$$

Where $\mathcal{F}$ and V are both 5×1 matrix as follow:

$$\mathcal{F} = \begin{pmatrix} \frac{\beta_{11}\bar{k}_1 S(t)I_1(t)}{N(t)} \\ \frac{\beta_{12}\bar{k}_1 S(t)I_1(t)}{N(t)} + \frac{\beta_{22}\bar{k}_2 S(t)I_2(t)}{N(t)} \\ 0 \\ 0 \\ 0 \end{pmatrix}, \tag{6}$$

$$\mathcal{F} = \begin{pmatrix} \frac{\varepsilon_1 \bar{k}_3 I_1(t) T(t)}{N(t)} + \gamma_1 I_1(t) + dI_1(t) \\ \frac{\varepsilon_2 \bar{k}_3 I_2(t) T(t)}{N(t)} + \gamma_2 I_2(t) + dI_2(t) \\ -\eta S(t) + \gamma_3 T(t) + dT(t) \\ -q + \frac{(\beta_{11}+\beta_{12})\bar{k}_1 S(t) I_1(t)}{N(t)} + \frac{(\beta_{22}+\beta_{21})\bar{k}_2 S(t) I_2(t)}{N(t)} + \eta S(t) + dS(t) \\ -\frac{\varepsilon_1 \bar{k}_3 I_1(t) T(t)}{N(t)} - \frac{\varepsilon_2 \bar{k}_3 I_2(t) T(t)}{N(t)} - \gamma_1 I_1(t) - \gamma_2 I_2(t) - \gamma_3 T(t) \end{pmatrix}. \tag{7}$$

At the no information equilibrium point E_0, the simplified transmission matrix F and immune matrix V of 3×3 are shown in Eqs 8, 9, respectively.

$$F = \begin{pmatrix} \frac{\beta_{11}\bar{k}_1 S(t)}{N(t)} & 0 & 0 \\ \frac{\beta_{12}\bar{k}_1 S(t)}{N(t)} & \frac{\beta_{22}\bar{k}_2 S(t)}{N(t)} & 0 \\ 0 & 0 & 0 \end{pmatrix}, \tag{8}$$

$$V = \begin{pmatrix} \gamma_1 + d & 0 & 0 \\ 0 & \gamma_2 + d & 0 \\ 0 & 0 & \gamma_3 + d \end{pmatrix}. \tag{9}$$

Thus, we can calculate the basic regeneration number of the regeneration matrix FV^{-1}, that is, the propagation threshold of the L-SITR model is the spectral radius of the regeneration matrix, as shown below:

$$R_0 = \rho\left(FV^{-1}\right) = \max\left\{\frac{q\beta_{11}\bar{k}_1}{(\eta+d)(\gamma_1+d)}, \frac{q\beta_{22}\bar{k}_2}{(\eta+d)(\gamma_2+d)}\right\}. \tag{10}$$

The stability of the no information equilibrium point is detailed in Theorem 2. According to the expression of the propagation threshold R_0 and the results in the literature [27, 28], the values of $\varepsilon_1, \varepsilon_2, \delta$ do not change the propagation threshold R_0. Therefore, to simplify the calculation, $\varepsilon_1 = \varepsilon_2 = \delta = 0$ we set in the following analysis.

Theorem 1

The no information equilibrium E_0 of the L-SITR model is locally asymptotically stable if $R_0 < 1$ and unstable if $R_0 > 1$. The Jacobian matrix of the L-SITR model is given by,

$$J = \begin{bmatrix} -(\beta_{11}+\beta_{12})\bar{k}_1 I_1(t) - \beta_{22}\bar{k}_2 I_2(t) - \eta - d & -(\beta_{11}+\beta_{12})\bar{k}_1 S(t) & -\beta_{22}\bar{k}_2 S(t) & 0 \\ \beta_{11}\bar{k}_1 I_1(t) & \beta_{11}\bar{k}_1 S(t) - \gamma_1 - d & 0 & 0 \\ \beta_{12}\bar{k}_1 I_1(t) + \beta_{22}\bar{k}_2 I_2(t) & \beta_{12}\bar{k}_1 S(t) & \beta_{22}\bar{k}_2 S(t) - \gamma_2 - d & 0 \\ \eta & 0 & 0 & -\gamma_3 - d \end{bmatrix}. \tag{11}$$

By substituting $E_0(S^0, I_1^0, I_2^0, T^0, R^0) = (\frac{q}{(\eta+d)}, 0, 0, 0, 0)$ in Eq. 11, the Jacobian matrix at the no information equilibrium point can be obtained as

$$J_0 = \begin{bmatrix} -\eta - d & -(\beta_{11}+\beta_{12})\bar{k}_1 S(t) & -\beta_{22}\bar{k}_2 S(t) & 0 \\ 0 & \beta_{11}\bar{k}_1 S(t) - \gamma_1 - d & 0 & 0 \\ 0 & \beta_{12}\bar{k}_1 S(t) & \beta_{22}\bar{k}_2 S(t) - \gamma_2 - d & 0 \\ \eta & 0 & 0 & -\gamma_3 - d \end{bmatrix}, \tag{12}$$

In order to simplify the calculation process, we set:

$$\begin{cases} A = \eta + d \\ B = -\beta_{11}\bar{k}_1 S(t) + \gamma_1 + d \\ C = -\beta_{22}\bar{k}_2 S(t) + \gamma_2 + d \\ D = \gamma_3 + d \end{cases}. \tag{13}$$

As $R_0 < 1$, we can obtain $A > 0, B \geq 0, C \geq 0, D > 0$. The characteristic polynomial of matrix 12) is,

$$|\lambda E - J_0| = m_0\lambda^4 + m_1\lambda^3 + m_2\lambda^2 + m_3\lambda + m_4, \tag{14}$$

where

$$\begin{cases} m_0 = 1 \\ m_1 = A + B + C + D \\ m_2 = AB + AC + AD + BC + BD + CD, \\ m_3 = ABC + ABD + ACD + BCD \\ m_4 = ABCD \end{cases} \tag{15}$$

Because

$$\begin{aligned} m_0 > 0 m_3 m_2 - m_4 m_1 = {} & A^2B^2C + A^2BC^2 + AB^2C^2 + A^2B^2D \\ & + AB^2D^2 + A^2C^2D + A^2CD^2 + A^2BD^2 \\ & + B^2C^2D + B^2CD^2 + BC^2D^2 + 2A^2BCD \\ & + 2AB^2CD + 2ABC^2D \\ & + 2ABCD^2 > 0 m_3 m_2 m_1 - m_4 m_1^2 \\ & - m_3^2 m_0 > 0. \end{aligned} \tag{16}$$

According to the Routh–Hurwitz stability criterion [29], when $R_0 < 1$, the disease-free equilibrium point is locally asymptotically stable.

Theorem 2

If $R_0 < 1$, then the no information equilibrium point E_0 is globally asymptotically stable. In this case, we build the following Lyapunov function,

$$V(t) = I_1, \tag{17}$$

The full differential equation of V with respect to t is,

$$\frac{dV}{dt} = \frac{dI_1(t)}{dt} = \beta_{11}\bar{k}_1 S(t) I_1(t) - \gamma_1 I_1(t) - dI_1(t). \tag{18}$$

When $R_0 < 1$, we obtain $\beta_{11}\bar{k}_1 S^0 \leq \gamma_1 + d$ and $\frac{dV}{dt} \leq 0$. $\frac{dV}{dt} = 0$ if and only if the system is at an no information equilibrium point $E_0(S^0, I_1^0, I_2^0, T^0, R^0)$. Combined with the local asymptotic stability of no information equilibrium point, according to the LaSalle's invariance principle [30] indicates that the no information equilibrium point E_0 is globally asymptotically stable.

In the next theorem, we will prove the stability of the information equilibrium point.

Theorem 3

If $R_0 > 1$, then the information equilibrium point E_1 is locally asymptotically stable. By eliminating I_1 and I_2 in Eq. 1 and solving them, the endemic equilibrium point $E_1(S^*, I_1^*, I_2^*, T^*, R^*)$ of the L-SITR model can be obtained, where

$$\begin{aligned}
S^* &= \frac{\gamma_1 + d}{\beta_{11}\bar{k}_1} \\
I_1^* &= \frac{\left[(\gamma_1 + d)\beta_{22}\bar{k}_2 - (\gamma_2 + d)\beta_{11}\bar{k}_1\right]\left[q\bar{k}_1 - (\eta + d)(\gamma_1 + d)\right]}{(\gamma_1 + d)^2\beta_{22}\beta_{11}\bar{k}_1\bar{k}_2 + (\gamma_1 + d)(\gamma_2 + d)(\beta_{12} - \beta_{11})\beta_{11}\bar{k}_1^2} \\
I_2^* &= \frac{q\beta_{12}\bar{k}_1 - (\eta + d)(\gamma_1 + d)\frac{\beta_{12}}{\beta_{11}}}{(\gamma_1 + d)\beta_{22}\bar{k}_2 + (\gamma_2 + d)(\beta_{12} - \beta_{11})\bar{k}_1} \\
T^* &= \frac{(\gamma_1 + d)\eta}{(\gamma_3 + d)\beta_{11}\bar{k}_1} \\
R^* &= -(I_1^* + I_2^*) + \frac{q}{d} - \frac{(\eta + d)(\gamma_1 + d)}{d\beta_{11}\bar{k}_1} + \frac{\gamma_3(\gamma_1 + d)\eta}{d(\gamma_3 + d)\beta_{11}\bar{k}_1}
\end{aligned} \quad . \tag{19}$$

Substituting Eq. 19 into Eq. 11, we obtain,

$$\begin{aligned}
&m_0 > 0 \\
&m_3 m_2 - m_4 m_1 > 0 \\
&m_3 m_2 m_1 - m_4 m_1^2 - m_3^2 m_0 > 0
\end{aligned} \quad . \tag{20}$$

According to the Routh–Hurwitz stability criterion, when $R_0 > 1$, the information equilibrium point is locally asymptotically stable.

Theorem 4

If $R_0 > 1$, then the information equilibrium point E_1 is globally asymptotically stable. In this case, we build the following Lyapunov function,

$$V(t) = \left[(S - S^*) + (I_1 - I_1^*) + (I - I_2^*) + (T - T^*) + (R - R^*)\right]^2. \tag{21}$$

Because we assumes that the total population remains constant, that is, $q = dN(t)$ and N are constant. So we can obtain $q - dS^* - dI_1^* - dI_2^* - dT^* - dR^* = 0$, and set $Q = (S - S^*) + (I_1 - I_1^*) + (I_2 - I_2^*) + (T - T^*) + (R - R^*)$.

The derivative of $V(t)$ (see Eq. 21) is given as follow. Where, we first substitute Eq. 1 into $\frac{dV}{dt}$, and then add $q - dS^* - dI_1^* - dI_2^* - dT^* - dR^* = 0$ to the equation to get the final result.

$$\begin{aligned}
\frac{dV}{dt} &= 2Q\left(\frac{dS(t)}{dt} + \frac{dI_1(t)}{dt} + \frac{dI_2(t)}{dt} + \frac{dT(t)}{dt} + \frac{dR(t)}{dt}\right) \\
&= 2Q\left(q - d(S(t) + I_1(t) + I_2(t) + T(t) + R(t))\right) \\
&= 2Q\left[d(S - S^*) + d(I_1 - I_1^*) + d(I_2 - I_2^*) + d(T - T^*) + d(R - R^*)\right] \\
&= -2dQ^2
\end{aligned} \quad . \tag{22}$$

When $R_0 > 1$, we can obtain $\frac{dV}{dt} \leq 0$. $\frac{dV}{dt} = 0$ if and only if the system is at the information equilibrium point $E_1(S^*, I_1^*, I_2^*, T^*, R^*)$. Combined with the local asymptotic stability of information equilibrium point, according to the LaSalle's invariance principle indicates that when $R_0 > 1$, the information equilibrium point E_1 is globally asymptotically stable.

4 Optimal control strategy

This section discusses the influence of optimal control on the L-SITR model with control measures, as shown in Eq. 23. As the government continues to report the truth, it will effectively increase the probability of the uninformed becoming the recovered person, assuming that the probability of the uninformed becoming the recovered person increases by $u_0(t)$. At the same time, the report also increased the probability of the communicator who becomes the restorer by assuming that the probability of the communicator becoming the restorer from the influential propagator increased to $u_1(t)$. The probability of switching from a normal propagator to a restorer increased to $u_2(t)$.

$$\begin{aligned}
\frac{dS(t)}{dt} &= q - \frac{(\beta_{11} + \beta_{12})\bar{k}_1 S(t)I_1(t)}{N(t)} - \frac{\beta_{22}\bar{k}_2 S(t)I_2(t)}{N(t)} + \delta R(t) \\
&\quad - \eta S(t) - dS(t) - u_0(t)S(t) \\
\frac{dI_1(t)}{dt} &= \frac{\beta_{11}\bar{k}_1 S(t)I_1(t)}{N(t)} - \frac{\varepsilon_1\bar{k}_3 I_1(t)T(t)}{N(t)} - u_1(t)I_1(t) \\
&\quad - \gamma_1 I_1(t) - dI_1(t) \\
\frac{dI_2(t)}{dt} &= \frac{\beta_{12}\bar{k}_1 S(t)I_1(t)}{N(t)} + \frac{\beta_{22}\bar{k}_2 S(t)I_2(t)}{N(t)} - \frac{\varepsilon_2\bar{k}_3 I_2(t)T(t)}{N(t)} \\
&\quad - u_2(t)I_2(t) - \gamma_2 I_2(t) - dI_2(t) \\
\frac{dT(t)}{dt} &= \eta S(t) - \gamma_3 T(t) - dT(t) \\
\frac{dR(t)}{dt} &= \frac{\varepsilon_1\bar{k}_3 I_1(t)T(t)}{N(t)} + \frac{\varepsilon_2\bar{k}_3 I_2(t)T(t)}{N(t)} + (\gamma_1 + u_1(t))I_1(t) \\
&\quad + (\gamma_2 + u_2(t))I_2(t) + \gamma_3 T(t) + u_0(t)S(t) - \delta R(t) - dR(t)
\end{aligned} \tag{23}$$

The purpose of public opinion control is to reduce the number of propagators and the cost of public opinion management as much as possible during public opinion propagation. Let the cost of public resource consumption caused by the propagator be proportional to the number of propagators with the proportional coefficients being equal to ζ_1 and ζ_2. The cost generated by the control measures is proportional to the square of the control intensity with the proportional coefficients being equal to $\zeta_0, \zeta_3, \zeta_4$ respectively, and the total cost generated by the public opinion propagation period $[0, t_f]$ is defined as the objective function.

The objective function is set as [31]:

$$J(u_0,u_1,u_2)=\int_0^T[\zeta_0u_0^2(t)+\zeta_1I_1(t)+\zeta_2I_2(t)+\zeta_3u_1^2(t)+\zeta_4u_2^2(t)] \tag{24}$$

Using Pontryagin's maximum principle, we attempted to find the optimal control for u_0^*,u_1^*,u_2^* so that the objective function can be minimized. The control was defined as $\varphi=\{(u_0,u_1,u_2)|u_i\in[0,u_{i\max}],i=0,1,2\}$.

The Hamiltonian function for the control problem can be described as,

$$\begin{aligned}H&=\zeta_0u_0^2(t)+\zeta_1I_1(t)+\zeta_2I_2(t)+\zeta_3u_1^2(t)+\zeta_4u_2^2(t)\\&+\lambda_1\frac{dS(t)}{dt}+\lambda_2\frac{dI_1(t)}{dt}+\lambda_3\frac{dI_2(t)}{dt}+\lambda_4\frac{dT(t)}{dt}+\lambda_5\frac{dR(t)}{dt},\end{aligned} \tag{25}$$

where $\lambda_1,\lambda_2,\lambda_3,\lambda_4,\lambda_5$ are the covariant variables that satisfy the transversal condition, $\lambda_i(t_f)=0,i=1,2,\cdots,5$, and the following differential equation,

$$\begin{aligned}\dot{\lambda_1}&=(\lambda_1-\lambda_2)\frac{\beta_{11}\bar{k_1}I_1(t)}{N(t)}\\&+(\lambda_1-\lambda_3)\left[\frac{\beta_{12}\bar{k_1}I_1(t)}{N(t)}+\frac{\beta_{22}\bar{k_2}I_2(t)}{N(t)}\right]+(\lambda_1-\lambda_4)\eta\\&+(\lambda_1-\lambda_5)u_0(t)+\lambda_1d\\\dot{\lambda_2}&=-\zeta_1+(\lambda_1-\lambda_2)\frac{\beta_{11}\bar{k_1}S(t)}{N(t)}+(\lambda_1-\lambda_3)\frac{\beta_{12}\bar{k_1}S(t)}{N(t)}\\&+(\lambda_2-\lambda_5)\left(\frac{\varepsilon_1\bar{k_3}T(t)}{N(t)}+u_1(t)+\gamma_1\right)+\lambda_2d\\\dot{\lambda_3}&=-\zeta_2+(\lambda_1-\lambda_3)\frac{\beta_{22}\bar{k_2}S(t)}{N(t)}\\&+(\lambda_3-\lambda_5)\left(\frac{\varepsilon_2\bar{k_3}T(t)}{N(t)}+u_2(t)+\gamma_2\right)+\lambda_3d\\\dot{\lambda_4}&=(\lambda_2-\lambda_5)\frac{\varepsilon_1\bar{k_3}I_1(t)}{N(t)}+(\lambda_3-\lambda_5)\frac{\varepsilon_2\bar{k_3}I_2(t)}{N(t)}+(\lambda_4-\lambda_5)\gamma_3\\&+\lambda_4d\\\dot{\lambda_5}&=(\lambda_5-\lambda_1)\delta+\lambda_5d\end{aligned} \tag{26}$$

According to the results obtained by Panja [32] and the Pontryagin's maximum principle, the following theorem applies.

Theorem 5

There is an optimal control strategy $u^*=(u_0^*,u_1^*,u_2^*)$ used to make $J(u_0^*,u_1^*,u_2^*)=\min_{(u_0,u_1,u_2)\in\varphi}J(u_0,u_1,u_2)$ valid, and the optimal control variable is as follows,

$$\begin{cases}u_0^*(t)=\min\left\{u_{0\max},\max\left\{0,\dfrac{(\lambda_1-\lambda_5)S^*(t)}{2\zeta_0}\right\}\right\}\\u_1^*(t)=\min\left\{u_{1\max},\max\left\{0,\dfrac{(\lambda_2-\lambda_5)I_1^*(t)}{2\zeta_3}\right\}\right\}\\u_2^*(t)=\min\left\{u_{2\max},\max\left\{0,\dfrac{(\lambda_3-\lambda_5)I_2^*(t)}{2\zeta_4}\right\}\right\}\end{cases} \tag{27}$$

$$\begin{cases}\dfrac{\partial H}{\partial u_0}=2\zeta_0u_0-(\lambda_1-\lambda_5)S(t)=0\\\dfrac{\partial H}{\partial u_1}=2\zeta_3u_1-(\lambda_2-\lambda_5)I_1(t)=0\\\dfrac{\partial H}{\partial u_2}=2\zeta_4u_2-(\lambda_3-\lambda_5)I_2(t)=0\end{cases} \tag{28}$$

.It can be obtained with calculations that

$$\begin{cases}u_0=\dfrac{(\lambda_1-\lambda_5)S(t)}{2\zeta_0}\\u_1=\dfrac{(\lambda_2-\lambda_5)I_1(t)}{2\zeta_3}\\u_2=\dfrac{(\lambda_3-\lambda_5)I_2(t)}{2\zeta_4}\end{cases} \tag{29}$$

From the characteristics of the control variable that $u_i\in[0,u_{i\max}]$, we can obtain:

$$u_0=\begin{cases}0,\dfrac{(\lambda_1-\lambda_5)S(t)}{2\zeta_0}<0\\\dfrac{(\lambda_1-\lambda_5)S(t)}{2\zeta_0},0<\dfrac{(\lambda_1-\lambda_5)S(t)}{2\zeta_0}<u_{0\max}\\u_{0\max},\dfrac{(\lambda_1-\lambda_5)S(t)}{2\zeta_0}>u_{0\max}\end{cases} \tag{30}$$

$$u_1=\begin{cases}0,\dfrac{(\lambda_2-\lambda_5)I_1(t)}{2\zeta_3}<0\\\dfrac{(\lambda_2-\lambda_5)I_1(t)}{2\zeta_3},0<\dfrac{(\lambda_2-\lambda_5)I_1(t)}{2\zeta_3}<u_{1\max}\\u_{1\max},\dfrac{(\lambda_2-\lambda_5)I_1(t)}{2\zeta_3}>u_{1\max}\end{cases} \tag{31}$$

$$u_2=\begin{cases}0,\dfrac{(\lambda_3-\lambda_5)I_2(t)}{2\zeta_4}<0\\\dfrac{(\lambda_3-\lambda_5)I_2(t)}{2\zeta_4},0<\dfrac{(\lambda_3-\lambda_5)I_2(t)}{2\zeta_4}<u_{2\max}\\u_{2\max},\dfrac{(\lambda_3-\lambda_5)I_2(t)}{2\zeta_4}>u_{2\max}\end{cases} \tag{32}$$

We can obtain optimal control variable $u_0^*(t)=\min\{u_{0\max},\max\{0,\frac{(\lambda_1-\lambda_5)S^*(t)}{2\zeta_0}\}\}$. Similarly, the specific expressions for other two optimal control variables $u_1^*(t)$ and $u_2^*(t)$ can be obtained in the same way. Hence, Theorem 5 was proved.

5 Numerical example

MATLAB was used to conduct the simulations. In this section, the accuracy of the L-SITR model is verified by an example simulation and the influence of the interference strategy on each node in the model was studied. The "backward–forward sweep method" was used to solve the optimal control problem, and the fourth-order Runge-Kutta method was used to calculate the numerical solution of

L-SITR [33–35]. In this method, the equation of state of the model was solved forward in time, the equation was solved backward in time, the value of the control variable was constantly updated, and the process was repeated until convergence.

5.2 Propagation threshold and stability verification

5.2.1 Stability of no information equilibrium ($R_0 < 1$)

We set the parameters of the L-SITR model as $q = 0.01$, $d = 0.01, k_1 = 40, k_2 = 5, k_3 = 20, \gamma_1 = 0.05, \gamma_2 = 0.03, \gamma_3 = 0.06$, $\delta = 0.01, \varepsilon_1 = 0.03, \varepsilon_2 = 0.08, \eta = 0.03$. To ensure the propagation threshold $R_0 < 1$, the stability of the model at $R_0 < 1$ was verified by changing the propagation rate and initial number of nodes. At this time, the information eventually disappeared after diffusion and propagation. The simulation results in these conditions are shown in Figures 2-4. Figure 2 and Figure 3, respectively describe the influences of different propagation rates β_{11} and β_{22} on the number of nodes in the network when $R_0 < 1$, and Figure 4 describes the influence of different initial node numbers on the final equilibrium point of the model when $R_0 < 1$.

In Figure 2 and Figure 3 the horizontal and vertical coordinates represent the time step and the quantity of nodes, respectively. From Figure 2 we observe that when $R_0 < 1$, the numbers of influential propagator and normal propagator will increase rapidly in the initial stage of information transmission, but will gradually decrease over time and eventually disappear.

From Figure 3 we observe that when $R_0 < 1$, the number of uninformed persons decreases rapidly, the number of rational propagators increases slowly, and the number of immune persons increases rapidly at the beginning of information dissemination. When the information dissemination reaches the peak, the decrease rate of uninformed persons and the increase rate of restorers decrease slowly, and the number tends to be stable after a period of time. Figure 2 and Figure 3 show that when $R_0 < 1$, regardless of how the propagation rate changes, the nodes of uninformed person, rational propagator, and immune will eventually tend to be in dynamic equilibrium, which is consistent with the theoretical results and verifies the stability of the model.

In Figure 4, the x-axis represents the proportion of normal propagator nodes (%), the y-axis represents the proportion of influential propagator nodes (%), and the z-axis represents the proportion of immune nodes (%). We randomly generated ten groups of different initial node proportions and conducted ten simulations respectively. Curves of different colors in the figure represent the changes in the number of nodes of the normal propagator, influential propagator, and temporal variation of immunity at different initial proportions of different types of nodes. Irrespective of how different the initial proportions of nodes of different types are in the case in which $R_0 < 1$, the model eventually converges to no information equilibrium point, which is consistent with the results of theoretical deduction. The stability of the no information equilibrium point of the L-SITR model was verified.

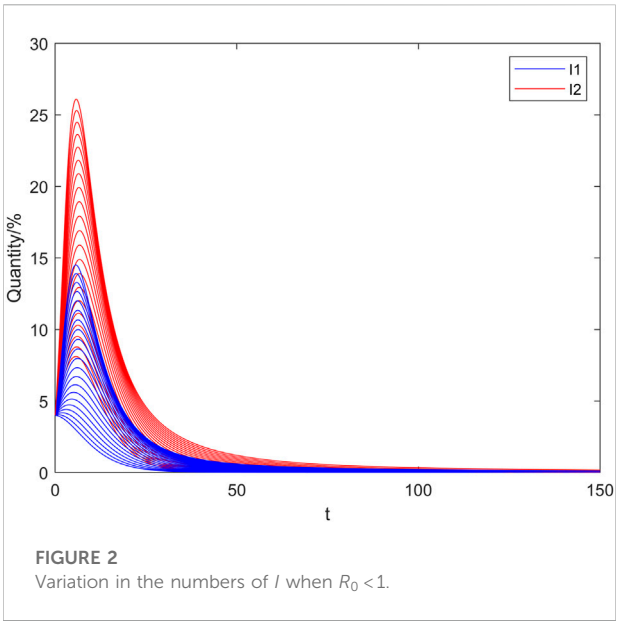

FIGURE 2
Variation in the numbers of I when $R_0 < 1$.

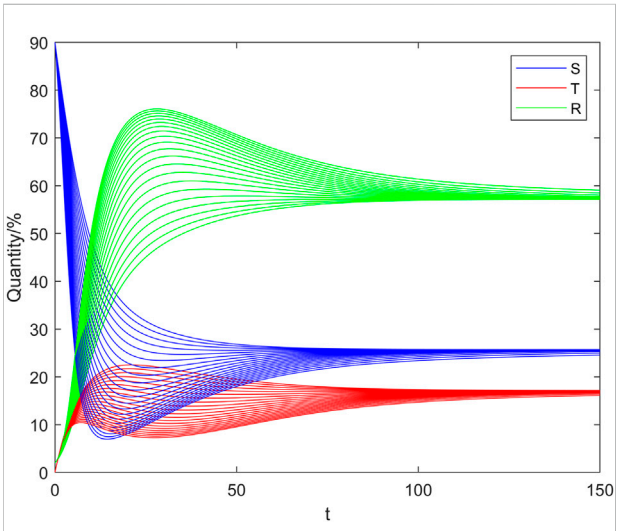

FIGURE 3
Variations in the numbers of S, T, R when $R_0 < 1$.

5.2.2 Stability of information equilibrium ($R_0 > 1$)

We set the parameters of the L-SITR model as $q = 0.01$, $d = 0.01, k_1 = 60, k_2 = 5, k_3 = 20, \gamma_1 = 0.04, \gamma_2 = 0.03, \gamma_3 = 0.06$, $\delta = 0.01, \varepsilon_1 = 0.03, \varepsilon_2 = 0.08, \eta = 0.03$, the initial proportion of

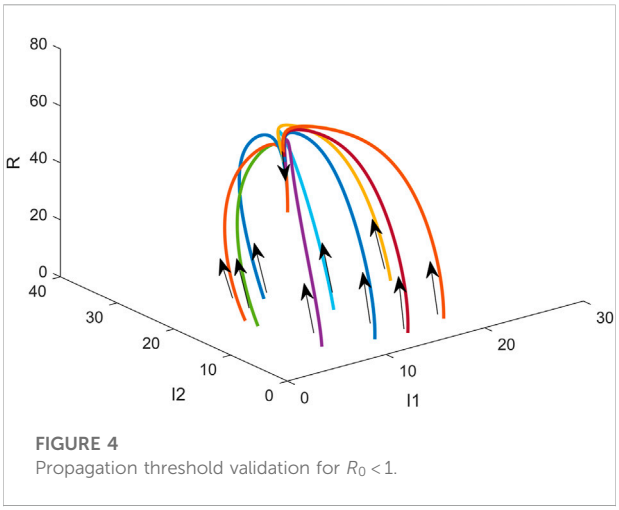

FIGURE 4
Propagation threshold validation for $R_0 < 1$.

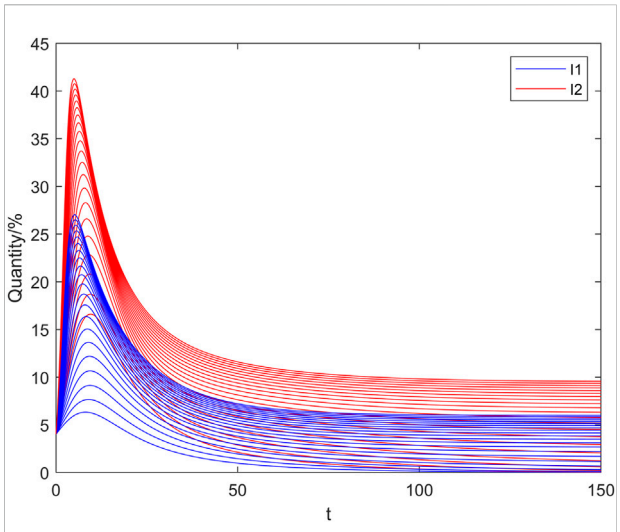

FIGURE 5
Variations in the numbers of I when $R_0 > 1$.

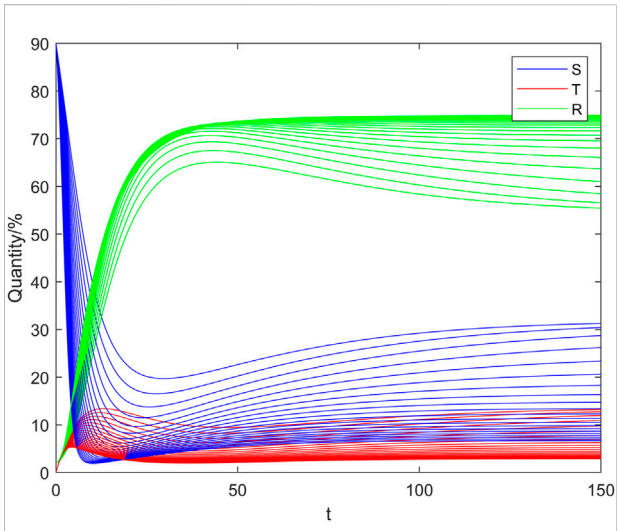

FIGURE 6
Variations in the numbers of S, T, R when $R_0 > 1$.

uninformed persons was 0.9, the initial proportion of propagator was 0.04, and the initial proportion of immune was 0.06. To ensure the propagation threshold $R_0 > 1$, the stability of the model at $R_0 > 1$ was verified by changing the propagation rate and the initial number of nodes. At this time, the information will propagate. The simulation results in these conditions are shown in Figures 5-7. Figure 5, and Figure 6 respectively, describe the influences of different propagation rates β_{11} and β_{22} on the number of nodes in the network when $R_0 > 1$, and Figure 7 describes the influence of different initial node numbers on the final equilibrium point of the model when $R_0 > 1$.

In Figure 5 and Figure 6 the horizontal and vertical coordinates represent the time step and the quantity of nodes, respectively. Figure 5 shows that when $R_0 > 1$, the number of influential propagator and normal propagator nodes increases rapidly in the early stage of information transmission, and gradually decreases after its peak, and then tends to a dynamic balance, and the number of dynamic equilibrium points is affected by the propagation rate.

From Figure 6 we observe that when $R_0 > 1$, at the beginning of information dissemination, the number of uninformed persons decreases rapidly, the number of rational propagators increases slowly, and the number of restorers increases rapidly. When the information dissemination reaches the peak, the decrease rate of uninformed persons and the increase rate of restorers decrease slowly, and the number tends to be stable after a period of time. Figure 5 and Figure 6 show that when $R_0 > 1$, regardless of how the propagation rate changes, each node eventually tends to be in dynamic equilibrium, which is consistent with the result of the theoretical derivation and verifies the stability of the model.

In Figure 7, the x-axis represents the proportion of normal propagator nodes (%), the y-axis represents the proportion of influential propagator nodes (%), and the z-axis represents the proportion of immune nodes (%). We randomly generated ten groups of different initial node proportions and conducted ten simulations respectively. Curves of different colors in the figure represent the changes in the number of nodes of the normal propagators, influential propagators and temporal variation of immunity at different initial proportions of different types of nodes. In the case in which $R_0 > 1$, irrespective of the initial proportion of nodes of different types, the model eventually converges to information equilibrium point, which is consistent with the result of the theoretical derivation and verifies the stability of the information equilibrium point of the L-SITR model.

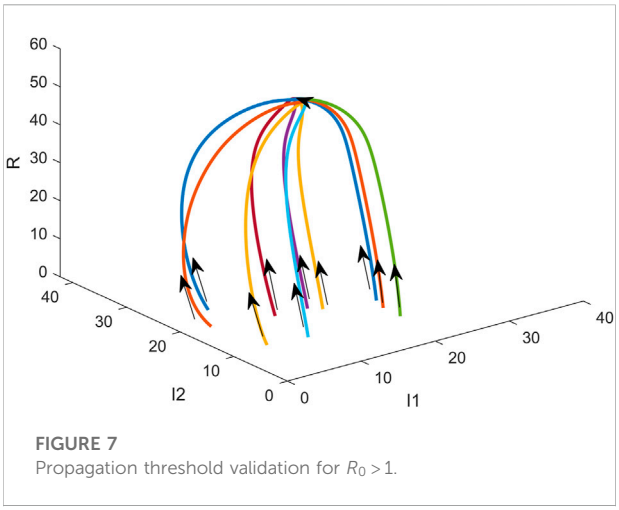

FIGURE 7
Propagation threshold validation for $R_0 > 1$.

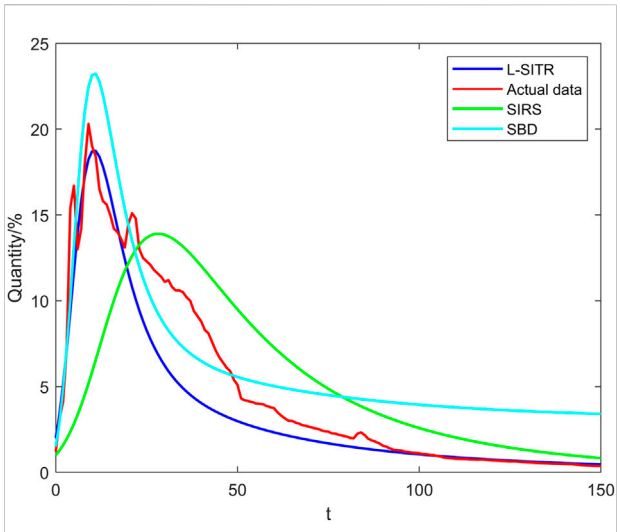

FIGURE 8
Simulation of an actual case.

5.3 Real case verification

We mainly selected some real data of "old man died by falling over a dog leash" on the official platform of Sina Weibo for the experiment. The earliest information about the incident began to spread on the Internet platform at 9:00 on 18 August 2020, which aroused wide attention and a large number of comments and forwarding on the topic of dog management and the safety of the elderly. The number of forwarding reached the peak at 22:00 in the evening, and then the number of comments and forwarding gradually decreased. The discussion on the event ended at 8:00 on August 24. It is worth noting that in this event, some articles published by official media discussed the legal issues behind the accident, guided netizens to think rationally, provided ideas for improving relevant laws and regulations, promoted the rapid end of public opinion caused by the emergency, and reduced the negative impact caused by public opinion. According to the real data of "Jiang Yi Yan" event, we have established a network with 72,000 nodes, among which the nodes are users who pay attention to that event. The average degree of the nodes in the network is about 24.76. MATLAB was used in the cases of the L-SITR simulation model, SBD model [18] and the traditional SIRS model, and outcomes were compared with real data, as shown in Figure 8. The proportions of uninformed persons, influential propagator and normal propagators, rational propagator, and immunity were set to 0.95, 0.01, 0.03, 0, and 0.01. Table 2 lists the parameters used in the experiments.

In Figure 8, the horizontal and vertical coordinates represent the time step in hours and the quantity of nodes, respectively. Curves in different colors represent the prediction results of the event by different models. Among them, blue, green and cyan are the prediction results of L-SIRS model, traditional SIRS model and SBD model respectively. The red curve is fitted with the real data obtained from Sina Weibo.

TABLE 2 Initial parameter setting.

Parameter	Value
β_{11}	0.0171
β_{22}	0.0188
β_{12}	0.0496
γ_1	0.075
γ_2	0.046
γ_3	0.053
ε_1	0.037
ε_2	0.072
η	0.051
δ	0.01
q	0.01
d	0.01

In the initial stage of information transmission, the uninformed nodes S of both L-SITR model, traditional SIRS model and SBD model quickly acquire information and become propagators. However, due to the consideration of high-influence propagators, L-SITR model showed a faster transformation rate of uninformed than traditional SIRS model, and reached the transmission peak 12.4 h later, with the number of peak propagators being 17.71%. However, the traditional SIRS model takes 31.7 h to reach the transmission peak, and the transmission range is also smaller than L-SITR model, with only 14.47% of the peak propagators. The analysis shows that the L-SITR model is more accurate compared with the traditional SIRS model in predicting the arrival time of peak

information transmission, the number of peak propagator nodes, and the end time of information transmission. This is because the traditional SIRS model ignores the difference in the influence of different nodes, thus resulting in a low-node degree average and slow information transmission rate in the network. Although the SBD model takes into account users' different attitudes towards public opinion information, it does not take into account the influence of government intervention on information transmission, resulting in the predicted value of the number of peak transmission nodes being much higher than the actual value. When the transmission peak is reached, the descending trend of the transmission node is also slower than that of L-SITR model, and the information is spread in the network for a long time, with a large deviation from the actual value. In addition, the root-mean-square error (RMSE) of each model was calculated, and yielded an RMSE value of 4.69 for the L-SITR model, while that of the traditional SIRS model was 15.38 and SBD model was 9.19. This shows that L-SITR model can more accurately describe the information propagation process of the event.

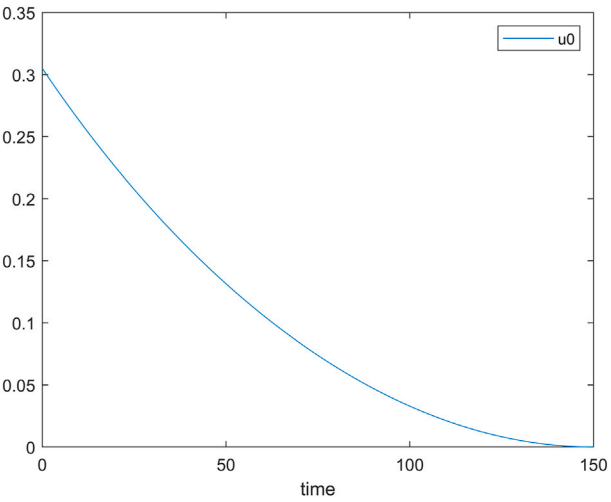

FIGURE 9
Variation in u_0 subject to the control of an uninformed person.

5.4 Information propagation subject to optimal control

The information transmission process subject to optimal control was simulated by using the real data of the event "An old man fell over the dog's leash and died," the weighting coefficients were set according to $\zeta_0 = 0.2$, $\zeta_1 = 0.3, \zeta_2 = 0.25, \zeta_3 = 0.4, \zeta_5 = 0.15$, and the maximum control intensity was set as $u_{0\max} = 0.8, u_{1\max} = 1, u_{2\max} = 1$.

5.4.1 Optimal control of uninformed person

Figure 9 shows the change in u_0 under control of an uninformed person. The horizontal and vertical coordinates represent the time step and the control strength, respectively. The control u_0 reached the highest intensity in the early stage, gradually decreased as a function of the information transmission time, and approached zero at the end of information transmission. This indicates that the government needs to report the truth with high intensity in the early stage and turn as many uninformed persons to immune persons, so as to reduce the impact of adverse events.

Figure 10 shows the changes in the number of nodes of an uninformed person S, information propagator $I(I = I_1 + I_2)$, and immune persons R subject to the control of the uninformed and without control. The control of the uninformed person can effectively reduce the information transmission time, propagator node number, and can make more people immune. The number of propagators decreased by 4.64% at the peak of information transmission, and at the end of the dissemination of information, the number of immune persons increased by 9.29%, making more people no longer pay attention to the message. But can also generate more insider access cases to the public opinion events, and can't reduce the impact of information dissemination.

5.4.2 Optimal control of propagator

Figure 11 shows the variations of u_1 and u_2 subject to the control of the propagator. The horizontal and vertical coordinates represent the time step and the control strength, respectively. The control u_1 reaches the highest intensity at an early stage, gradually decreases as a function of the increase in information transmission time, and approaches zero at the end of information transmission. The intensity of control u_2 increases gradually as a function of the increase in information transmission time, decreases gradually after reaching the peak value, and approaches zero at the end of information transmission. This shows that because of the small number of influential propagators and slower growth rate, in the early days of control, good effects can be achieved. So Thus, the government needs to reported in the early days of the truth of this class of people and controls. Additionally, the normal propagators are fewer, but the growth rate is higher. Thus, the government does not need to control the high strength at an early stage. However, with the dissemination of information, it is still necessary to gradually strengthen the reporting and control of the truth of the incident.

Figure 12 shows the changes in the number of nodes of the uninformed person S, information propagator I $(I = I_1 + I_2)$, and immune persons R, subject to the control of the propagator and without control. The control of the propagator can effectively reduce the number of information propagator

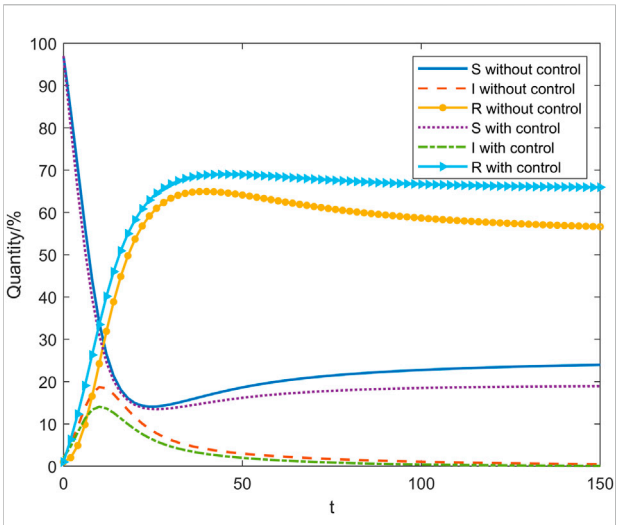

FIGURE 10
Comparison of the changes in the number of nodes without control and subject to the control of an uninformed person.

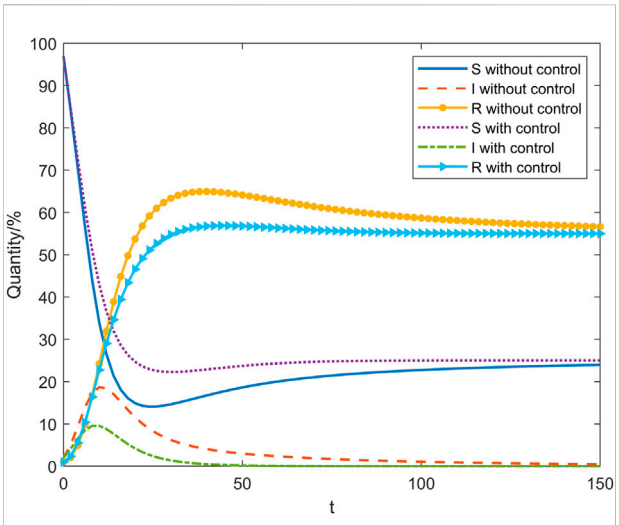

FIGURE 12
Comparison of the changes in the number of nodes without and with control of the propagator.

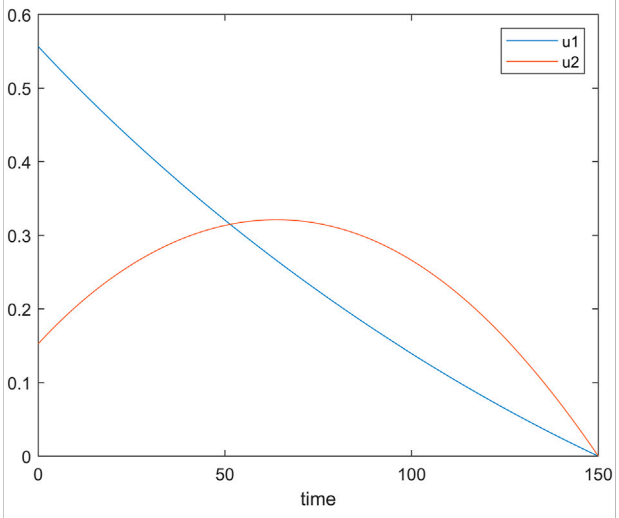

FIGURE 11
u_1 and u_2 subject to propagator control.

nodes at the peak of information dissemination so that the latter can be completed as soon as possible, the number of propagators decreased by 9.16% at the peak of information transmission. In addition, in the process of information transmission, the number of uninformed nodes is effectively reduced. At most, the number of uninformed nodes is 8.2% more than that without control, avoiding more nodes to participate in information transmission and reducing the scope of information transmission.

6 Conclusion

This study proposed a novel L-SITR model that stratified information propagators based on nodal influences and improved the traditional SIRS model by adding rational propagators. Through the study of the theory analysis of dynamics equations, we determine the spread of L-SITR model threshold, and combined with numerical simulation proved that the stability of the equilibrium point. To suppress the large-scale spread of online public opinion information, optimal control was applied to the L-SITR model and the real data obtained from Sina Weibo were used to conduct simulation experiments. Simulation results show that the proposed L-SITR model has higher accuracy than the traditional SIRS model, and is more suitable for information propagation prediction in the presence of rational communicators. Moreover, the optimal control method proposed in this paper can effectively reduce the influence of public opinion propagation.

Because of the complexity of the network information dissemination, our work is not perfect; it also needs to work in the future through the use of more accurate data collection, analysis, and information dissemination mechanism between the nodes to develop a more complete information propagation model. Among them, exploring the information transmission mechanism in line with the real scene is the basis for establishing the propagator model, and the conscious and social attributes of nodes should be taken into account in future work. Additionally, many more methods are needed to simulate and analyze the methods of the intervention process, further improving the accuracy of the models and practicality.

Data availability statement

The original contributions presented in the study are included in the article/supplementary material, further inquiries can be directed to the corresponding author.

Author contributions

All authors participated in the design of the models, methodology, and experiments, and assessment of their relevance. DP and YZ contributed the computer coding and testing. All authors participated in the writing of the article.

Funding

The work was supported in part by Sub Project of National Key Research and Development plan in 2020. (NO. 2020YFC1511704). Beijing Information Science & Technology University (NO.2020KYNH212 and NO. 2021CGZH302). Beijing Science and Technology Project (Grant No. Z211100004421009), and in part by the National Natural Science Foundation of China (Grant No. 61971048). Open Foundation of State key Laboratory of Networking and Switching Technology (Beijing University of Posts and Telecommunications) (SKLNST-2022-1-16).

Conflict of interest

The handling editor declared a past co-authorship with one of the authors YZ.

The remaining author declares that the research was conducted in the absence of any commercial or financial relationships that could be construed as a potential conflict of interest.

Publisher's note

References

1. Wang W, Liu Q, Liang J, Hu Y, Zhou T. Coevolution spreading in complex networks. *Phys Rep* (2019) 820:1–51. doi:10.1016/j.physrep.2019.07.001

2. Mckendrick W. Contributions to the mathematical theory of epidemics. III. Further studies of the problem of endemicity. *Proc R Soc Lond* (1933) 141:94–122.

3. Wang Y. The spreading of information in online social networks through cellular automata. *Complexity* (2018) 2018. doi:10.1155/2018/1890643

4. Kabir KMA, Tanimoto J. Analysis of epidemic outbreaks in two-layer networks with different structures for information spreading and disease diffusion. *Commun Nonlinear Sci Numer Simul* (2019) 72:565–74. doi:10.1016/j.cnsns.2019.01.020

5. Lu Y, Liu J. The impact of information dissemination strategies to epidemic spreading on complex networks. *Physica A: Stat Mech its Appl* (2019) 536:120920. doi:10.1016/j.physa.2019.04.156

6. Huang H, Chen Y, Ma Y. Modeling the competitive diffusions of rumor and knowledge and the impacts on epidemic spreading. *Appl Math Comput* (2021) 388: 125536. doi:10.1016/j.amc.2020.125536

7. Wang Q, Lin Z, Jin Y, Cheng S, Yang T. Esis : Emotion-based spreader – ignorant – stifler model for information diffusion. *Knowl Based Syst* (2015) 81:46–55. doi:10.1016/j.knosys.2015.02.006

8. Wang Z, Rui X, Yuan G, Cui J, Hadzibeganovic T. Endemic information-contagion outbreaks in complex networks with potential spreaders based recurrent-state transmission dynamics. *Physica A: Stat Mech its Appl* (2021) 573:125907. doi:10.1016/j.physa.2021.125907

9. Shaji A, V Belfin R, Kanaga EGM. An innovated SIRS model for information spreading. *Int Conf Bigdata Cloud Comput* (2017) 2017:1–8.

10. Zhao L, Wang J, Chen Y, Wang Q, Cheng J, Cui H. SIHR rumor spreading model in social networks. *Physica A: Stat Mech its Appl* (2012) 391:2444–53. doi:10.1016/j.physa.2011.12.008

11. Li J, Jiang H, Mei X, Hu C, Zhang G. Dynamical analysis of rumor spreading model in multi-lingual environment and heterogeneous complex networks. *Inf Sci (N Y)* (2020) 536:391–408. doi:10.1016/j.ins.2020.05.037

12. Yagan O, Qian D, Zhang J, Cochran D. Conjoining speeds up information diffusion in overlaying social-physical networks. *IEEE J Sel Areas Commun* (2013) 31:1038–48. doi:10.1109/JSAC.2013.130606

13. Wang Z, Guo Q, Sun S, Xia C. The impact of awareness diffusion on SIR-like epidemics in multiplex networks. *Appl Math Comput* (2019) 349:134–47. doi:10.1016/j.amc.2018.12.045

14. Wu J, Zuo R, He C, Xiong H, Zhao K, Hu Z. The effect of information literacy heterogeneity on epidemic spreading in information and epidemic coupled multiplex networks. *Physica A: Stat Mech its Appl* (2022) 596:127119. doi:10.1016/j.physa.2022.127119

15. Li X, Hou B. Competing complex information spreading in multiplex. *Complexity* (2021) 2021. doi:10.1155/2021/9923837

16. Jiang G, Li S, Li M. Dynamic rumor spreading of public opinion reversal on Weibo based on a two-stage SPNR model. *Physica A: Stat Mech its Appl* (2020) 558: 125005. doi:10.1016/j.physa.2020.125005

17. Wang Z, Liang J, Nie H, Zhao H. A 3SI3R model for the propagation of two rumors with mutual promotion. *Adv Differ Equ* (2020) 109. doi:10.1186/s13662-020-02552-w

18. Sang C, Li T, Tian S, Xiao Y, Xu G. Sftrd: A novel information propagation model in heterogeneous networks: Modeling and restraining strategy. *Physica A: Stat Mech its Appl* (2019) 524:475–90. doi:10.1016/j.physa.2019.04.213

19. Zhu L, Guan G. Dynamical analysis of a rumor spreading model with self-discrimination and time delay in complex networks. *Physica A: Stat Mech its Appl* (2019) 533:121953. doi:10.1016/j.physa.2019.121953

20. Wang Y, Yuan G, Fan C, Hu Y, Yang Y. Disease spreading model considering the activity of individuals on complex networks. *Physica A: Stat Mech its Appl* (2019) 530:121393. doi:10.1016/j.physa.2019.121393

21. Zhao T, Member S, Chen W, Member S, Liew AW, Member S, et al. A binary particle swarm optimizer with priority planning and hierarchical learning for networked epidemic control. *IEEE Trans Syst Man, Cybern Syst* (2019) 2019:1–15.

22. Huo HF, Yang P, Xiang H. Dynamics for an SIRS epidemic model with infection age and relapse on a scale-free network. *J Franklin Inst* (2019) 356: 7411–43. doi:10.1016/j.jfranklin.2019.03.034

23. Liu L, Wei X, Zhang N. Global stability of a network-based SIRS epidemic model with nonmonotone incidence rate. *Physica A: Stat Mech its Appl* (2019) 515: 587–99. doi:10.1016/j.physa.2018.09.152

24. Yuan X, Wang F, Xue Y, Liu M. Global stability of an SIR model with differential infectivity on complex networks. *Physica A: Stat Mech its Appl* (2018) 499:443–56. doi:10.1016/j.physa.2018.02.065

25. Huo J, Zhao H. Dynamical analysis of a fractional SIR model with birth and death on heterogeneous complex networks. *Physica A: Stat Mech its Appl* (2016) 448:41–56. doi:10.1016/j.physa.2015.12.078

26. Van Den Driessche P, Watmough J. Reproduction numbers and sub-threshold endemic equilibria for compartmental models of disease transmission. *Math Biosci* (2002) 180:29–48. doi:10.1016/s0025-5564(02)00108-6

27. Huo L, Cheng Y, Liu C, Ding F. Dynamic analysis of rumor spreading model for considering active network nodes and nonlinear spreading rate. *Physica A: Stat Mech its Appl* (2018) 506:24–35. doi:10.1016/j.physa.2018.03.063

28. Nekovee M, Moreno Y, Bianconi G, Marsili M. Theory of rumour spreading in complex social networks. *Physica A* (2008) 2008:1–23.

29. Li J, Jiang H, Yu Z, Hu C. Dynamical analysis of rumor spreading model in homogeneous complex networks. *Appl Math Comput* (2019) 359:374–85. doi:10.1016/j.amc.2019.04.076

30. O'Regan SM, Kelly TC, Korobeinikov A, O'Callaghan MJA, Pokrovskii AV. Lyapunov functions for SIR and SIRS epidemic models. *Appl Math Lett* (2010) 23:446–8. doi:10.1016/j.aml.2009.11.014

31. Wang X, Peng H, Shi B, Jiang D, Zhang S, Chen B. Optimal vaccination strategy of a constrained time-varying SEIR epidemic model. *Commun Nonlinear Sci Numer Simul* (2019) 67:37–48. doi:10.1016/j.cnsns.2018.07.003

32. Reviews B, Panja P. Optimal control analysis of a cholera epidemic model. *Biophys Rev Lett* (2019) 14:27–48. doi:10.1142/S1793048019500024

33. Bakare EA, Nwagwo A, Danso-Addo E. Optimal control analysis of an SIR epidemic model with constant recruitment. *Int J Appl Math Res* (2014) 3:273–85. doi:10.14419/ijamr.v3i3.2872

34. Li K, Zhu G, Ma Z, Chen L. Dynamic stability of an SIQS epidemic network and its optimal control. *Commun Nonlinear Sci Numer Simul* (2019) 66:84–95. doi:10.1016/j.cnsns.2018.06.020

35. Yu T, Cao D, Liu S. Epidemic model with group mixing: Stability and optimal control based on limited vaccination resources. *Commun Nonlinear Sci Numer Simul* (2018) 61:54–70. doi:10.1016/j.cnsns.2018.01.011

frontiers | Frontiers in Physics

TYPE Original Research
PUBLISHED 30 August 2022
DOI 10.3389/fphy.2022.987799

OPEN ACCESS

EDITED BY
Wei Wang,
Chongqing Medical University, China

REVIEWED BY
Genhua Hu,
Anhui University of Technology, China
Mingjie Wang,
University of Guelph, Canada

*CORRESPONDENCE
Jinghua Tan,
jinghuatan.swufe@gmail.com

SPECIALTY SECTION
This article was submitted to Social Physics,
a section of the journal
Frontiers in Physics

RECEIVED 06 July 2022
ACCEPTED 28 July 2022
PUBLISHED 30 August 2022

CITATION
Zhang H, Chen Y, Rong W, Wang J and Tan J (2022), Effect of social media rumors on stock market volatility: A case of data mining in China.
Front. Phys. 10:987799.
doi: 10.3389/fphy.2022.987799

Effect of social media rumors on stock market volatility: A case of data mining in China

Hua Zhang[1], Yuanzhu Chen[2], Wei Rong[3], Jun Wang[4] and Jinghua Tan[4]*

[1]School of Economics and Management, Sichuan Normal University, Chengdu, China, [2]School of Computing, Queen's University, Kingston, ON, Canada, [3]School of Management Science and Engineering, Southwestern University of Finance and Economics, Chengdu, China, [4]School of Computing and Artificial Intelligence, Southwestern University of Finance and Economics, Chengdu, China

The Stock Market is a typical complex network composed of investors, stocks, and market information. The abnormal fluctuation of the Stock Market has a strong effect on the economy of a country and even that of the world. Fueled by the herd effect of the increasingly abundant social media, Internet rumors, as an important source of market information and an exogenous financial risk, can lead to the collapse of investor confidence and the further propagation of financial risks, which can damage the financial system and even lead to social unrest. With additional availability of computing techniques, we attempt to uncover the media information effects in the stock market and seek to provide researchers with 1) a theoretical reference for a comprehensive understanding of such a complex network, 2) accurate prediction of future data, and 3) design of efficient and reliable risk intervention models. Based on the data of China's Stock Market, this study uses machine learning to investigate social media rumors to reveal the interplay of social media rumors and stock market volatility. In this work, we find patterns from social media rumors from financial forums using machine learning, quantify social media rumors based on statistics, and analyze the mechanism of propagation and influence of social media rumors on stock market volatility using econometric models. The empirical results show that rumors play an important information transmission effect on stock market volatility and the constructed Internet Financial Forum Rumor Index is helpful to sense the potential impact of rumors, i.e., a significant lagged negative effect. These findings are of guidance for the optimization of the information environment, and can serve to promote the healthy and stable development of the stock market.

KEYWORDS

complex network, machine learning, stock market, social media rumors, information dissemination

1 Introduction

The impact of Internet social media on the stock market is a double-edged sword. On the one hand, its ability to disseminate information widely and freely is conducive to reducing information asymmetry among market participants, improving the effectiveness of the stock market, and maintaining the stability of the financial market. On the other hand, the circulation of irregular, one-sided or unconfirmed information tends to impact stock prices, mislead investors, and can seriously affect the confidence of market participants in the transparency and truthfulness of market information, resulting in a decrease in the financing capacity of the stock market and a misallocation of social resources. For instance, the circuit breaker mechanism[1] in China's stock market has been triggered by reports on "devaluation of RMB exchange rate", "imminent release of many restricted sales", "geopolitical instability", "overseas transfer of domestic capital", and "the unstable situation". These rumors spread rapidly through the Internet social media, leading to weakened investor confidence and collective position reduction, financial risks, and even social unrest. Therefore, in the era of big data, it has become an important and urgent challenge in today's world to study the mechanism of the inherent influence of rumors on stock market volatility, capitalizing on the massive information on the Internet to ensure the sound operation of financial systems [1–3].

At present, there are two deficiencies in the research on the impact of rumors on the stock market [4–11]. First, we are yet to find any establishment of a single scalar value to quantify not only the degree of rumors in online social networks but also the general performance of the stock market. Second, although econometric regression models have been widely used to study the influence of rumors on stock market, such studies only focus on the one-way effect without considering how the stock market performance may feedback to online social networks. In view of the first deficiency, the Internet Financial Forum Rumor Index (IFFRI) is constructed based on the relative number of Eastmoney[2] forum rumors in time variation and spatial comparison according to the generalized attribute of statistical index. IFFRI is used to indicate the relative number of changes in social media rumors. It expresses the comprehensiveness and variation of rumors. Aiming at the second deficiency, IFFRI is added into the GARCH model to solve the problem of single investor sentiment variable in existing studies. When IFFRI is added, the intermediate variable reflects both rumor characteristics and stock market characteristics. This makes this paper better analyze the fluctuation law of social media rumors' influence on the stock market. Specifically, the contribution of this study is twofold. At the data level, we have collected and identified 430,424 rumors in China's Stock Market, which are of great value for further exploration of related issues supported by these sufficient data. At the rumor research level, this study provides a new perspective and opportunity to improve the effectiveness of stock market information disclosure, and plays a positive role in promoting the healthy and stable development of the capital market.

In this paper, we first review relevant research literature. Then, we present a social media rumors detection method, IFFRI generation principle, and empirical research model of rumor's impact on stock market volatility. Last, we design experiments to examine their effects and analyze ramifications from these experimental results to reveal the interaction between the informational and financial spaces.

2 Related work

2.1 Specialized social media on financial markets

Rose was the first researcher who proposed the impact of rumors on the stock market. By analyzing samples collected by hand over 2 years, he found that rumors can have a short-term impact on stock prices, leading investors to buy and sell [12]. Later on, similar studies have been increasingly conducted to explore the effects of social media on the stock market. In particular, Diefenback manually searched for each unsubstantiated rumor that appeared in the Wall Street Journal's market Rumors section [13]. Davies and Canes analyze the "Market Rumors" section of the Wall Street Journal and find that positive rumors have a positive impact on stock prices, while negative rumors have a negative impact. Pound et al. found through newspapers and magazines that rumors of corporate mergers and acquisitions had little impact on market fluctuations, and there was arbitrage behavior before rumors were announced [14]. Huth et al. found through media news that rumors have more impact on large-scale enterprises [15]. Barber et al. filter rumors by manually reading the "rumors" section of Business Week [16]. Kiymaz et al. detect rumors by analyzing stock market rumors in the Turkish media one by one, and found that rumors in the categories of "earnings" and "foreign takeover" had a more significant impact on stock market

1 The circuit breaker mechanism is a mechanism that sets a melting price for a contract before it reaches a stop, so that contract buying and selling quotes can only be traded within this price range for a period of time.

2 Eastmoney is one of the most visited and influential financial and securities portals in China, and has always been in a leading position among financial and economic websites in China.

volatility by collating media information [17]. Clarkson et al. investigated the relationship between rumor and abnormal returns by manually selecting rumor posts as rumor events [18]. Spiegel et al. manually selected the rumors on Israeli Internet forums and found that the rumors confirmed the significant abnormal returns in the stock market in the first 5 days [19]. Zhao et al. used false or misleading information publicly published in official media and clarified by listed companies as the study sample [5]. However, most studies mainly relied on manual identification of rumors, which is time consuming and with human bias. Some researchers have taken a further step by utilizing machine learning algorithms to identify rumors. For example, Li carried out research on network rumor recognition based on Naive Bayes classification [20]. Liu researched the detection technology of microblog rumors of unexpected events based on machine learning [21].

This paper uses machine learning method to realize the detection of social media rumors in stock market. Based on the results, we analyze the performance characteristics of social media rumors in Chinese stock market, such as sentiment polarity, time, sector and inter-industry and so on.

2.2 Sentiment polarity classification

In the study of sentiment classification in financial media, Das et al. mine investor sentiment from stock message boards and compare the efficiency of different classifiers. Their research method has a significant effect on noise removal, and they try to apply their method to different language fields [22]. Zhu used naive Bayes classification algorithm to classify six million posts into "positive", "neutral" and "negative" categories by emotion and constructed a sentiment index and opinion dispersion index [23]. Chen et al. used the evaluation theory to classify the emotional words and behavioral words in the stock market and obtained the emotional polarity of stock news by using the statistics of financial lexicon [24]. Xu et al. used support vector machine (SVM), Bayes classifier and Rough Set Theory to predict industry and individual stock news respectively and introduced a theory of sentiment classification evaluation [25]. Meng et al. obtained a keyword lexicon of investor sentiment in China [26]. Yin et al. constructed the emotional characteristics of users and microblogs by conducting emotional analysis on the rumor texts of detection microblogs and users' historical microblogs [27]. These methods provide a promising solution for sentiment classification.

In fact, research on emotional classification based on financial media has been paid more and more attention. Nowadays, network forum becomes an important form of social media, and the influence of its information dissemination has undergone great changes from breadth to depth. Most of its manifestations are semi-structured or unstructured text, such as stock forum. When studying forum information, accurate sentiment classification is the basis of quantitative impact analysis of stock market. Based on the Chinese Financial sentiment Lexicography [67] and machine learning, we will classify the rumors in the forum of Eastmoney. We use supervised learning to extract emotion information and use evaluation indexes of Chinese emotion analysis technology to evaluate the performance of emotion classification. This paper obtains more accurate emotional polarity, which provides an important basis for capturing the relationship between rumor and stock market volatility.

2.3 Quantification of social media texts

We believe that the quantification of media information is essentially the quantification of investor sentiment based on rumors. The measurement of investor sentiment is the basic work of studying the influence of media on stock market. After obtaining the rumor text and its emotional polarity, it is necessary to conduct data standardization processing first, quantify investor sentiment, and make data preparation for studying the impact of rumor on the stock market. However, because investors are affected by subjective factors such as physiology and psychology, as well as objective factors such as social environment and macroeconomy, the quantification of investor sentiment has always been a difficult problem in academia. So far there has not been a completely ideal unified measurement method.

The index of investor sentiment can be divided into market level and company level [28]. At the market level, researchers use investor sentiment factors through investor survey, closed-end fund discount, IPO offering and first-day return, market trading volume, principal component analysis, least square, HAR-RV GAS and other sentiment measurement methods [29–40]. At the firm level, researchers measure investor sentiment by discretionary accruals, decomposed Tobin, Momentum Index, market-to-book ratios, and deviation of analyst earnings forecasts [41–49].

At present, investor sentiment has not been studied by combining market and company. The main reason is the large difference of individual investors [50]. Individual investors have a greater degree of irrationality than institutional investors [51]. The biggest characteristic of China's stock market is the majority of individual investors. With the rapid development of social media in China, investors participate in discussions and express their opinions through forums, which has become a "window" for Chinese shareholders to express their emotions. At this time, rumors gather in the forum, and through investors' reading and reprinting, the

influence of rumors is expanded, and investors' emotions and behaviors are triggered. This study will use forum information to quantify investors' subjective judgment on the market and companies, discover investor sentiment hidden in rumors, and provide a new method for extracting and measuring investor sentiment.

2.4 Effect of rumors on stock market volatility

Shiller and Le Roy were among the first to discover the "volatility puzzle" of stock returns [52, 53]. Later, more and more researchers observed the influence of investor sentiment on stock market volatility. For example, Browna et al. find that investor sentiment is positively correlated with stock market returns at weekly frequencies and vice versa at monthly frequencies [54]. Wang et al. find that changes in investor sentiment have a significant impact on Shanghai and Shenzhen stock markets returns and have an inverse correction effect on the volatility of the two markets [55]. Arindam study finds that stock returns are determined by trader sentiment on the day and investor sentiment can explain stock market return volatility [56]. Clarkson et al. found that rumors react quickly to the stock market after 10 min of appearing in online forums, realizing as abnormal returns and volume [57]. Verma finds that both individual and institutional investors' sentiments have a negative impact on stock market volatility [58]. Tetlock empirically demonstrates that pessimistic media coverage predicts downward pressure on stock market prices [59]. Kaniel et al. argue that investor sentiment has an inverse relationship with short-term stock returns [60]. Patrick argues that investor sentiment changes investors' risk aversion and has a seasonal impact on the stock market [61]. Sabherwald et al. state that online forum investor sentiment has a negative impact on next-day stock returns and volatility [62]. Antonios et al. found that investor sentiment is idiosyncratic and positively associated with abnormal returns on tender announcements during corporate takeovers, a result that goes beyond previous scholarly research on the relationship between investor sentiment and the stock market [63]. Chi et al. studied the relationship between investor sentiment and ACSI information mispricing based on CAPM, Fama-French three-factor model, and Carhart four-factor model, and found that negative investor sentiment causes asset prices to deviate from value, confirming that customer satisfaction is a valuable intangible asset in capital markets [64]. Demetrios et al. studied the impact of investor sentiment in the Greek stock market, and mid-sized stocks were most significantly affected by investor sentiment [65]. Woan-lih incorporates investor sentiment factors into the Carhart four-factor model. He found that companies that were sensitive to investor sentiment earned more outlier returns in stock repurchase. At the same time, information asymmetry will exacerbate investor sentiment and lead to a greater degree of asset mispricing [66]. These studies unveil that investor sentiment has a significant impact on stock market fluctuations, but there are few researches based on social media, especially on spreading rumors.

This paper studies the influence of rumors on stock market volatility through investor sentiment reflected in social media rumors, which is of great practical significance. In particular, we explore such rumor influence according to the different stages of rumor spreading, including generation, evaluation, and dissemination.

3 Methods

In this section, we first crawl forum data (Section 3.1) and use machine learning to detect rumors (Section 3.2). Next in Section 3.3, we define a scalar value for all rumors of each day to quantify their collective significance and positivity. Such an index is used to construct the trend evolution over time. Last, in Section 3.4, we use the GARCH model to quantitatively analyze the transmission mechanism of rumors on stock market volatility.

3.1 Data acquisition

In recent years, China's stock market experienced a major stock market crash caused by information asymmetry in 2016. Within the first four trading days of that year, the Chinese stock market triggered the circuit breaker mechanism twice and closed early, setting a precedent for the world stock market. This event is providing important data for our study, and We try to discover the mechanism of propagation dynamics of social media rumors on the stock market. Therefore, this paper focuses the sample data on the Chinese stock market from 2015 to 2016. The stock data used in this paper are obtained from the China RESSET[3] database, specifically using individual stock opening price, closing price, high price, low price, turnover rate, volatility, number of shares traded, amount traded, basic information of individual stocks, the Shanghai Composite Index (SSE) and Shenzhen Component Index (SZI).

3 RESSET (Beijing Juyuan RuiSi Data Technology Co., Ltd): The company's main business is to provide financial data services, which is one of the important databases of interest to financial practitioners, researchers and investors in China.

This paper uses the text of Eastmoney stock bar as the base data. The Eastmoney stork bar is one of the most important stock forums in China: 1) According to ALEXA[4], Eastmoney ranks among the top ten Chinese websites in the world and the first financial website in China, with a daily average page view of over 100 million, which is far ahead of domestic financial websites; 2) According i-research[5], the average monthly coverage of user visits of Eastmoney reaches 63.57 million people, occupying half of the industry, and has developed into one of the most successful Internet platforms and financial data platforms in China. It providing researchers with a massive data base; 3) Eastmoney stock bar provides an interactive exchange platform for investors, and is one of the largest financial interactive platforms in China in terms of user volume. According to the data from Ariadne, Stock Bar ranks first in China in terms of user visits and user stickiness. It posting time is accurate and high, with "seconds" as the timing unit, more accurate, and the forum data is more complete. Therefore, this paper of Chinese stock market forum rumors through the Eastmoney stock bar has considerable representativeness and reference value.

We start from the URL of Eastmoney, get the initial list of pages, and keep crawling new URLs from the current page until the URL is empty or meets the crawl termination condition. We used a train crawler (an open-source web crawler) with fast crawling speed and high accuracy for adaptive modulation to meet the crawling requirements. We collected stock posts in stock bar from 2015 to 2016, totaling about 37.8 million, with a quantity of 10 GB and a data accuracy of seconds, and the content of the crawl included: stock code, posting IP address, posting title, post content, crawl URL, reading volume, following volume, and posting time.

We pre-process the data as follows. Step 1: We write the collected data into the MYSQL database, and then export the text in the database according to the information in each piece of data and export the data of the same stock into a CSV file, so as to realize the classification by stock code. Step 2: We use the program to eliminate "distorted information, mis recorded and inappropriate samples" in the database, such as very small (less than 4 kb) or very large (more than 100 kb) text, zero reading volume, long-term suspension stocks, etc. Through the pre-processing of the crawl information, 200,000 noisy posts were eliminated, and 37.6 million stock posts were made.

3.2 Rumor detection

After obtaining the forum text, we follow the route of "text representation - feature generation - feature extraction - text classification" to distinguish "rumor" and "non-rumor".

(1) Text representation. In this paper, let the information of the share Eastmoney stock bar be D and the weight of the feature term be W_k, that is, if there is a feature term $T_i$in a forum information D_i, the vector of feature terms of $T_i$is expressed as 1, otherwise it is 0. The size of the correlation between the content of two documents is measured by the distance between the vector document vectors, which is generally calculated using the inner product or the cosine of the angle, the smaller the angle the higher the similarity (Eq. 1).

$$Sim(D1, D2) = \cos\theta = \frac{\sum_{k=1}^{n} w_{1k} \times w_{2k}}{\sqrt{\left(\sum_{k=1}^{n} {w_{1k}}^{2}\right) \times \left(\sum_{k=1}^{n} {w_{2k}}^{2}\right)}} \quad (1)$$

(2) Feature Extraction. Based on the characteristics of rumor in stock market, five feature sets are used in this paper. F_a: post content features (word frequency features, word nature features, sentiment word features, etc.); F_b: followers features (number of followers, word frequency features, word nature features, sentiment word features, etc.); F_c: publisher behavior features (number of posters' posts, number of their followers, etc.); F_d: information credibility features (website credibility, posting time period, original post or repost, authority of posters, etc.); F_e: stock market features (stock index change rate, price change of corresponding stocks, volume change and turnover rate in the time period before and after posting, etc.).

(3) Feature weight calculation. Based on the *TF-IDF* model, we added a lexical weight determination method and calculated the text feature weights based on the set of stock bar information features [67]. We form a comprehensive weight for each word item of each document in the rumor sample, from which we judge that if a word item appears in a rumor sample with high frequency and the number of texts containing it in the whole rumor sample set is small, then it has a high *TF-IDF* (Eq. 2).

4 Alexa ranking refers to the world ranking of websites, mainly divided into comprehensive ranking and classification ranking, Alexa provides a number of evaluation index information including comprehensive ranking, arrival ranking, page visit ranking, etc. Most people take it as the current more authoritative evaluation index of website visits.

5 i-research is the leading brand in China's new economy and industry digital insight research and consulting services, providing professional industry analysis, data insight, market research, strategic consulting and digital solutions to help clients improve their cognitive level, profitability and overall competitiveness.

$$TF\text{-}IDF_{i,j} = tf_{i,j} \times idf_i \quad (2)$$

The weight of lexical item i in the rumor sample $j$is noted as $tf_{i,j} = \frac{n_{i,j}}{\sum_k n_{k,j}}$, If the fewer documents containing lexical item i in the rumor sample, it means that lexical item i has good category differentiation ability, which will be noted as $IDF_{i,j}$, and the larger its idf will be, noted as $idf_i = log\frac{N}{df_i}$. To deal with the situation when word$i$ does not exist in the set of rumor sample and the denominator df_iin the formula is 0, the above formula is modified as follows $idf_i = log\frac{N}{df_i+1}$.

(4) Text Classification. In this paper, we use Support Vector Machine (SVM) as a classifier for rumor recognition of stock bar text messages. This paper directly uses the most representative *LIBSVM package*[6], *LIBSVM-2.88 JAVA* program to build the SVM classifier.

To check the accuracy of SVM classifier in classifying rumors on the Internet, after the SVM finished the sample test, this paper used "*Precision (P) + Recall (R) + F-measure (F)*" to ensure the accuracy of classification of all samples. $P = \frac{a}{a+b}$, $R = \frac{a}{a+c}$ (a is the number of rumors correctly classified as "rumor", b is the number of "non-rumor" incorrectly classified as rumors, c is the number of rumors incorrectly classified as "non-rumor"), $F = \frac{2 \times P \times R}{P+R}$.

(5) Emotional polarity judgment. Due to the lack of a Chinese financial sentiment lexicon, most researchers in the face of the Chinese stock market have had to use manual reading discrimination methods in order to improve the accuracy of sentiment analysis, which greatly limits the sample size and increases the subjective variability of judgment results.

We design an unsupervised sentiment analysis algorithm for a large number of documents based on the Chinese Financial Sentiment Thesaurus (CFST) [67]. Step 1, the sentiment tendency of rumor is determined using CFST and combined with syntactic analysis, and the sentences with the determined tendency are used as the training set to train a sentiment determination model for rumor sentences using SVM. Step 2, the sentences in the quasi-training utterances that are larger than a certain threshold are proposed by the SVM to determine the positive and negative polarity, and are used as new training utterances to improve the SVM. Step 3, for a new rumor, the trained SVM is used to determine the positive and negative sentiment polarity of the statements in the text, and the sentiment polarity of the whole rumor message is determined based on the sentiment polarity of the sentences in the document and the importance of the position of the sentences in the text. The advantage of this method is that it uses machine learning algorithms to overcome the low recall rate of sentiment determination based on sentiment dictionaries alone. At the same time, it avoids the time-consuming of constructing training samples manually on a large scale and is suitable for mass text processing.

(6) Validation. In this paper, the experiment is evaluated using 10-fold cross-validation.

Step 1: Find any 10,000 rumor samples (A), and then find any 10,000 non-rumor samples (B), totaling 20,000 forum text messages, as the experimental data samples. Step 2: Build the training set. From the sample data, 90% rumor samples (C) and 90% non-rumor samples (D) are randomly selected as the training set and divided into 10 copies equally as the training set. Step 3: Construct the test set. The remaining 10% of rumor samples ($E = A - C$) and 10% of non-rumor samples ($F = B - D$) are used as the test set and divided into 10 copies on average as the test set.

Finally, we obtained the performance evaluation metrics of SVM classifier: *Precision = 76.82%, Recall = 72.32%, F-measure = 74.50%*. Therefore, we consider that: 1) the classifier has good performance in classifying rumors, and can detect rumor in stock bar forums crawled by the crawler; 2) the average accuracy of the SVM classifier in classifying the emotional polarity of rumors reaches *71.5%*, which can be considered as good performance in classifying emotional polarity. The trained SVM classifier can be used to discriminate the emotion of rumors.

3.3 Rumor quantification

Based on the social media rumors data obtained in Section 3.2, this paper further constructs the Internet Financial Forum Rumor Index (IFFRI) to comprehensively measure the degree and direction of social media rumors changes, which provides the prerequisites for analyzing the mechanism of social media rumors' impact on stock market volatility in Section 4 of this paper. IFFRI is the relative number of rumors in terms of time variation and spatial comparison, which conforms to the generalized attributes of statistical indexes.

3.3.1 IFFRI

To consider the comprehensiveness and variation of rumors, IFFRI is constructed according to the different stages of rumor spreading. In fact, the characteristics of social media rumors are

6 LIBSVM package: The strong principle, high efficiency, and easy operation SVM identification and regression package developed and designed by Professor Chih-Jen Lin of National Taiwan University. The package provides open-source code, which has been compiled to be executable in WINDOWS system environment. It provides tested default parameters, and the applicant has less parameter adjustment for SVM algorithm design, and provides common kernel functions such as linear and polynomial for selection, which can easily solve specific problems in SVM algorithm.

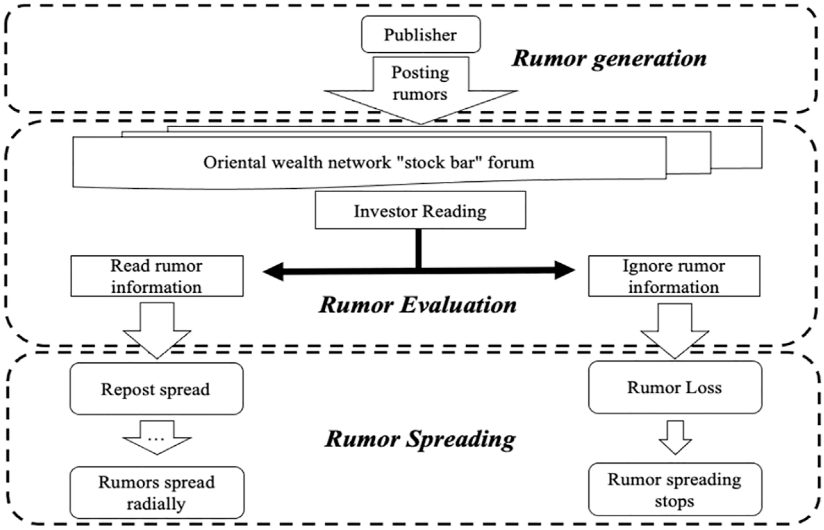

FIGURE 1
Rumor spreading behavior diagram.

essentially the same as those of traditional rumors, and their spread goes through three stages: generation, evaluation, and dissemination [68]. Rumor spreading behavior of stock forum readers is shown below (Figure 1).

1) **Rumor generation.** As the publisher's subjective evaluation and independent judgment of a listed company, rumor reflects investors' uncertainty and anxiety, which are the basis for the breeding of rumors. The publisher spontaneously generates and disseminates the information through forums, and audience receives it independently, which is typical of spontaneity and originality. The rumor at this time is "original", without interference from outside, and most truly reflects the psychological and emotional characteristics of investors. Therefore, Rumor in a forum can reflect publishers' views about companies and extract the emotional polarity of investors.

2) **Rumor Evaluation.** When investors receive rumors, they determine whether to believe them based on their own judgment. When considering other people's judgment, investors often engage in herding behavior, which is irrational, although reasonable, and is brought about by the "information cascade theory" [69]. As the survey of CNNIC (China Internet Network Information Center) shows, Chinese netizens still lack the awareness of questioning the authenticity of online news, and direct forwarding of unverified news is common. The data show that 60.3% of Internet users do not verify the authenticity of information before forwarding it directly, which plays a role in promoting the spread of false news information. Therefore, the amount of reading and commenting on rumor in a forum can reflect the extent to which investors are affected by rumor, and the emotional polarity characteristics of publishers are retained and continued.

3) **Rumor Spreading.** First, in terms of forum rumor spread, when an investor reads a rumor and believes it to be a rumor, investor quickly and actively spreads it to close friends. Rumors are passed on by people who are known and trusted (also known as "opinion leaders"), whose opinions and views are highly persuasive and are spread to increase its credibility. At the same time, rumors can flow between different social groups, with the communicator maintaining horizontal relations with other members of the group and reaching different groups through other "opinion leaders". In this way, rumor flows smoothly among multiple groups [70]. After the rumor is spread, it retains the meaning and emotional polarity of the poster, and the number of forum readings is an important indicator of the breadth of its spread. Secondly, the depth of the spread of rumors from the forum. Since there are scale differences among stocks and different sizes of impact and influence on the stock market, from a statistical perspective, the factor of market value weighting of stocks of the companies involved in rumors should also be considered. Therefore, from the comprehensive consideration of the breadth and depth of

forum rumor spread, the composition of rumor indicators should include the reading volume indicator and the market value indicator of the company involved in the rumor.

Therefore, the content and reading volume (including comment volume) of rumor in online forums imply the whole process of a rumor from generation to investors' evaluation and then dissemination, reflecting the breadth and depth of rumor dissemination, that is, the extent to which rumor "infects" the audience through "radial dissemination". We propose Attention Rate (*AR*) and Market Capitalization (*MC*); at the same time, forum rumors also contain the emotional polarity of investors' judgment on information of listed companies, that is, the emotional tendency of investment decision psychology for listed companies, and we propose Sentimental Polarities (*SP*).

$IFFRI_t$ denotes the index of financial forum rumors on day t; $AR_{i,t}$ denotes the attention index of social media rumors on day t; $MC_{i,t}$ denotes the market capitalization index of companies involved in social media rumors on day t; $SP_{i,t}$ denotes the sentiment polarity index of social media rumors on day t (Eq. 3).

$$IFFRI_t = \sum_{i=1}^{n} AR_{i,t} \times MC_{i,t} \times SP_{i,t} \tag{3}$$

In this paper, the IFFRI values of each social media rumors were calculated separately for each day in the sample period, and then summed by day to obtain the daily *IFFRI* values in the sample period. *IFFRI* provides important explanatory variables for the analysis of "social media rumors and the underlying mechanism of stock market volatility" in Section 4.

3.3.2 IFFRI factors

1) **Attention Rate (*AR*).** At day t, there are n pieces of rumor. It is necessary to weigh the importance of each piece of rumor in the attention index. The reading weight of each piece of rumor is given as follows. $AR_{i,t}$ denotes the attention index of the i^{th} rumor; $ar_{i,t}$ denotes the number of readers of the i^{th} rumor on day t; $\sum_{i=1}^{n} ar_{i,t}$ denotes the total number of rumors read at day t (Eq. 4).

$$AR_{i,t} = \frac{ar_{i,t}}{\sum_{i=1}^{n} ar_{i,t}} \tag{4}$$

2) **Market Capitalization (*MC*).** This paper matches daily market capitalization data with the market capitalization of companies involved in social media rumors on day *t*. In order to weigh the severity of the impact of the rumor on the stock market for the companies involved in the rumor, the proportion of the company involved in the market value of all listed companies (set as *J*) on t day is taken as the weight coefficient. $MC_{i,t}$ denotes the market capitalization indicator of the company involved in the i^{th} rumor; $mc_{i,t}$ denotes the market value of the company involved in rumor i at day t; $\sum_{i=1}^{j} mc_{i,t}$ denotes the total market capitalization of all listed companies in the stock market (j) at day t (Eq. 5).

$$MC_{i,t} = \frac{mc_{i,t}}{\sum_{i=1}^{j} \mathrm{mc}_{i,t}} \tag{5}$$

3) **Sentimental Polarities (*SP*).** This study divides the emotional polarity of rumor into "positive rumor" and "negative rumor". When quantifying emotional polarity indicators, *1*represents "positive rumor" and*−1* represents "negative rumor" (Eq. 6).

$$SP_{i,t} = \begin{cases} 1, if = positive\,rumor \\ -1, if = negative\,rumor \end{cases} \tag{6}$$

3.4 GARCH modeling

This study investigates the degree and direction of the effect of rumors on the volatility of the stock market. If the daily return on stocks unexpectedly rises or falls, investors will increase their expectations of variance in the next period. In this regard, a GARCH model can be used to analyze fluctuations in the effect of rumors on the stock market based on the IFFRI index and daily stock return data.

The GARCH model is the most classical model proposed by Tim Bollerslev in 1986 for describing volatility [71]. The basic principle is that the residuals reflect the magnitude of the deviation of the dependent variable from the fitted value of the mean equation, and the variance of period t can be predicted by the weighted average of the constant variance (k), the predicted value of the variance of the previous q periods (h_{t-i}) and the new information of the previous period (ε_{t-i}^2), which is particularly suitable for analysis of stock market volatility. The general GARCH model can be expressed as follows:$r_t$is the daily stock return at day t (Eq. 7), ε_t is the random error term (Eq. 8), and$h_t$is the conditional variance (Eq. 9).

$$r_t = c_1 + \sum_{i=1}^{R} \varnothing_i r_{t-i} + \sum_{j=1}^{M} B_j \varepsilon_{t-j} + \varepsilon_t \tag{7}$$

$$\varepsilon_t = u_t \sqrt{h_t} \tag{8}$$

$$h_t = k + \sum_{i=1}^{q} G_i h_{t-i} + \sum_{i=1}^{p} A_i \varepsilon_{t-i}^2 \ldots\ldots \tag{9}$$

This paper investigates the extent and direction of the impact of social media rumors on the volatility of the stock market. If the daily stock returns unexpectedly rise or fall, investors will increase their expectations of the variance of

TABLE 1 ADF test result.

Variables	T	*p*	ADF result
R_t	−16.41570	0.0000	Stable
IFFRI	−5.720275	0.0000	Stable

the next day, when a GARCH model can be used. Based on the IFFRI index and daily stock return data, we analyze the volatility pattern of the impact of social media rumors on the stock market. The process for the GARCH model is described below (Eq. 10), *m*takes the value of five in this paper[7], $IFFRI_i$ is the rumor index at day *i*. The rest of the variables are consistent with the GARCH model.

$$h_t = \mathrm{k} + \sum_{i=1}^{q} G_i h_{t-i} + \sum_{i=1}^{p} A_i \varepsilon_{t-i}^2 + \sum_{i=-m}^{m} \beta_i IFFRI_i \tag{10}$$

3.4.1 Data validation

1) **Stability test (CHANGE to enumeration).** The GARCH model requires that each variable must be a smooth time series, i.e., with a stable trend, volatility, and cross-sectional linkage, in order to prevent pseudo-regressions. Therefore, before formally model for regression analysis, ADF unit root tests are required for daily return Rt and IFFRI values. After the ADF test, there is no unit root for both daily return Rt and IFFRI values (Table 1). It can be seen that both time series of daily return Rt and IFFRI values are smooth and can be subjected to time series model.
2) **Yield autocorrelation test**. Since the premise of the ARMA model is that the dependence between variables is manifested in the continuity of the original data in time, that is, the existence of autocorrelation of daily returns is required. Therefore, an autocorrelation test is required here for the daily return data. The test results show that there is autocorrelation in daily returns, indicating that the ARMA model can be used for model.
3) **ARMA order fixing**. From the above results, it is shown that the ARMA model can be used for model analysis, and the orders of autoregression and moving average need to be further determined. Since the order of the time series should not be too high, a total of 15 models were tried with order 3 as the maximum order, and AIC, SC, and sum of residual squares were used as judgment criteria to select the optimal model. From the fixed-order results, it can be seen that the ARMA (3, 2) model corresponds to the smallest AIC and SC, so it is determined that the ARMA (3, 2) model is used for model and analysis.
4) **Residual test.** If the residual series after ARMA model is white noise[8] series, it indicates that the ARMA model is good, and if there is heteroskedasticity in the residuals, further model of the residual series by GARCH model should be considered.

Step 1: **Residual squared autocorrelation test.** After the residual squared autocorrelation test, the autocorrelation (AC) and partial autocorrelation (PAC) coefficients show that the residuals are autocorrelated.

Step 2: **Residual variance test (ARCH-LM test).** The residual difference variance test with lags of 5 and 10 order shows that there is heteroskedasticity in the residual series by the F-value, TR value, and the corresponding *p*-value.

From the above autocorrelation test and heteroskedasticity test, it is shown that there is autocorrelation in the residual squared series and heteroskedasticity in the residual series, so further GARCH model is performed on the residual series.

3.4.2 Application of GARCH

GARCH model first requires determining the lag order of ARCH and GARCH terms. In this paper, we try to use four models GARCH (1, 1), GARCH (1, 2), GARCH (2, 1) GARCH (2, 2) and use AIC, SC as model selection criteria. From the AIC and SC values of the four models, it can be seen that GARCH (2,1) has the smallest AIC and SC values and significant regression coefficients, indicating that the model works best, indicating that the GARCH model is not autocorrelated. In summary, an ARMA (3,2)-GARCH (2,1) model is used to study the effect of rumors on stock market volatility.

4 Experiments

4.1 Descriptive statistics of detected rumors

A total of more than 400,000 social media rumors were detected according to machine learning methods (Table 2), and their descriptive statistics and feature analysis are as follows.

7 Based on the existence of short-term effects of social media rumors on the Stock Market, this paper intends to investigate whether social media rumors have an effect on Stock Market returns in the range of $[t-5, t+5]$. For the purpose of the study, this paper advances the IFFRI by five periods, thus determining $m = 5$.

8 White noise: a purely random process with expectation of 0 and a constant variance.

TABLE 2 Stock Bar volume.

Year	Information (item)	Rumors (item)	Rumor ratio (%)
2015	15,640,623	195,271	1.25
2016	22,054,662	235,153	1.07
Total	37,695,285	430,424	1.14

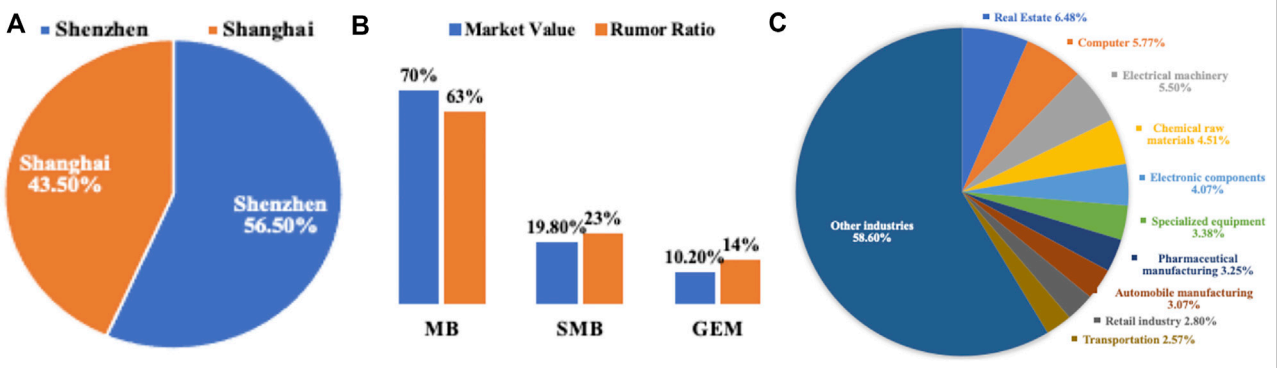

FIGURE 2
Distribution of trading venues, sectors and industry.

4.1.1 Breakdown by Trading Venues, Sectors and Industry

The stock exchange markets in China that are dominated by individual investors are Shenzhen and Shanghai. From Figure 2A, it can be seen that the Shenzhen market is significantly more than the Shanghai market. It indicates that social media rumors makers pay more attention to the Shenzhen market, which may have some relationship with the structure of China's Stock Market. Small and medium-sized stocks and GEM[9] stocks are concentrated in the Shenzhen market, and compared to the Shanghai market, there are more small and medium-sized companies and private enterprises, which are more vulnerable to the impact of social media rumors, and therefore rumor-mongers are more enthusiastic about the Shenzhen market.

When compared with the market capitalization ratio of sectors, the proportion of social media rumors involving SMB[10] and GEM is higher than that of the Main Board of Shanghai and Shenzhen (MB) (Figure 2B), indicating a higher relative concentration of SMB social media rumors in the Chinese stock market.

In terms of the distribution of social media rumors by industry, according to the 143 subcategories divided into industries by the CSRC[11], the top 10 industries in terms of social media rumors are all closely related to people's lives (Figure 2C). Among them, the three major industries, namely real estate development and operation, computer application services, and electrical machinery and equipment manufacturing, all had more than 20,000 social media rumors during the sample period, and the combined number of social media rumors for the three industries accounted for 42.9% of the top 10 social media rumors industries. Such a concentrated distribution of social media rumors reflects the high attention of media and capital to the real estate market, the use of Internet plus and intelligent manufacturing representing Industry 4.0, which is synchronized and consistent with social hot issues.

4.1.2 Temporal patterns

In terms of 1 day distribution (Figure 3A), there are two distinct peaks in social media rumors during the day: 10:00–12:00 and 14:00–15:00. It can be seen that the release of social media rumors basically coincides with the trading hours of the Chinese stock market, indicating to a certain extent that investors are

9 GEM: Growth Enterprise Market

10 SMB: Small and medium-sized board

11 CSRC: China Securities Regulatory Commission

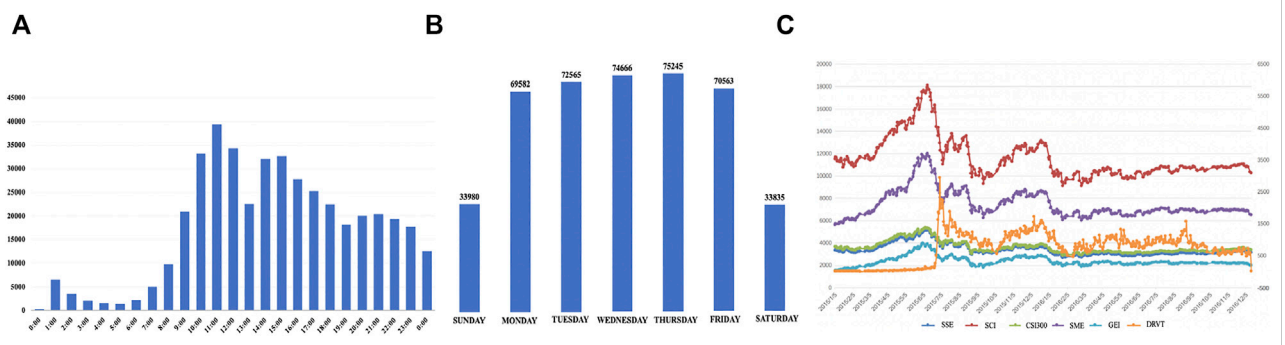

FIGURE 3
Distribution of Time. The vertical coordinate is the number of rumors, and the horizontal coordinate is the different time distribution **(A)**: 1 day; **(B)** 1 week; **(C)** observation period).

TABLE 3 AR descriptive statistics.

Statistic	Maximum	Minimum	Mean	Median	Standard deviation
AR	1	0	0.179293	0.162946	0.132082

easily influenced by the information in stock bar forums during stock trading. This is basically consistent with the Internet Report of CNNIC, which shows that "social apps have a small peak at 22:00", indicating that Chinese investors are already relying on mobile devices to a large extent. To a large extent, Chinese investors have relied on mobile devices, and it has become a habit to participate in stock market discussions through mobile APPs. From the graph, it can be seen that in addition to the two period of 10:00–12:00 and 14:00–15:00 during the day, there is also a small peak of posting at 20:00–23:00 in the evening.

According to CNNIC the Latest Internet report, "Chinese Internet users spend 28.5 h online per capita", and on which day of the week are social media rumors the most frequent? In terms of 1 week distribution (Figure 3B), we can see that the number of social media rumors gradually rises on Monday and reaches a peak on Thursday, and then drops to a slightly lower level on Friday and a trough on Saturday and Sunday. This coincides with the "Friday effect"[12] in the stock market, where rumor mongers start "warming up" on Thursday to "prepare" for trading under the "Friday effect". Public opinion preparation. Statistics show that the volume of social media rumors on national holidays (including weekends) is lower than the weekly average, indicating that Chinese investors pay the least attention to stock bar forums during holidays.

During the whole observation period (Figure 3C), the "Daily Rumor Volume Trend (DRVT)" of social media rumors basically coincides with the trend of the five stock indices: SSE, SCI, CSI300, SME and GEI[13].

4.2 Descriptive statistics of quantified rumors

4.2.1 AR

According to the AR calculation formula 1, the AR value of each social media rumors per day during the observation period was obtained as a statistical value (Table 3).

From Table 8, it can be seen that the attention level is generally small and concentrated between 0.1 and 0.2, indicating that the proportion of each social media rumors message in the total attention level of the day is between 10 and 20%. Social media rumors attention is more concentrated to reflect the extremely easy automatic alliance of online individuals with shared interests, similar interests and the same stance, driven by various factors such as information screening and filtering and the spiral of silence. As social media rumors spread interactively,

12 Friday effect: Friday usually predicts what changes in policy will occur over the weekend for 2 days and makes a move to buy or sell stocks.

13 SSE: Shanghai Composite Index; SCI: Shenzhen Component Index; CSI300: Shanghai and Shenzhen 300 Stocks index; SME: SSE SME composite; GEI: Growth Enterprise Index.

TABLE 4 MC descriptive statistics.

Statistic	Maximum	Minimum	Mean	Median	Standard deviation
MC	0.043765	0.0000088	0.0008388	0.00024916	0.002512995

TABLE 5 IFFRI descriptive statistics.

Statistic	Maximum	Minimum	Mean	Median	Standard deviation
IFFRI	0.005886	0.00001729	0.00076	0.000472	0.000781

TABLE 6 ARMA-GARCH model result (IFFRI factor is not added).

Variable	Coefficient	Std. Error	z-Statistic	Prob.
AR (1)	-0.498364***	0.035401	-14.07764	0.0000
AR (2)	-0.521428***	0.031818	-16.38769	0.0000
AR (3)	0.401244***	0.035882	11.18244	0.0000
MA (1)	0.954137***	0.006331	150.7024	0.0000
MA (2)	0.980187***	0.006682	146.6990	0.0000
Variance Equation				
C	5.31E-07**	3.66E-07	2.452029	0.0465
RESID (-1)2	0.244192***	0.058644	4.164008	0.0000
RESID (-2)2	-0.200193***	0.059398	-3.370357	0.0008
GARCH(-1)	0.953329***	0.006911	137.9479	0.0000

Note: ***0.01level significant, **0.05 level significant, *0.1level significant.

TABLE 7 ARMA-GARCH model result (IFFRI factor is added).

Variable	Coefficient	Std. Error	z-Statistic	Prob.
AR (1)	0.176209***	0.410661	11.429086	0.0000
AR (2)	0.440349***	0.301024	3.209737	0.0035
AR (3)	0.044834***	0.033055	3.077273	0.0050
MA (1)	-0.157808**	0.403087	-2.503621	0.0254
MA (2)	-0.425043**	0.290870	-2.170462	0.0439
Variance Equation				
C	-2.15E-06	6.39E-07	-3.367238	0.0008
RESID (-1)2	0.289353	0.082471	3.508521	0.0005
RESID (-2)2	-0.264836	0.081637	-3.244084	0.0012
GARCH(-1)	0.966563	0.006404	150.9424	0.0000
IFFRI (5)	0.031634	0.026267	1.204323	0.2285
IFFRI (4)	-0.046835	0.027929	-1.676922	0.0936
IFFRI (3)	0.021234	0.024839	0.854846	0.3926
IFFRI (2)	0.011335	0.030260	0.374589	0.7080
IFFRI (1)	-0.043466**	0.019225	-2.506311	0.0243
IFFRI	0.082588**	0.042403	2.488217	0.0317
IFFRI (-1)	0.141135***	0.040618	3.474665	0.0005
IFFRI (-2)	0.157343	0.032807	0.792202	0.4221
IFFRI (-3)	-0.012868	0.019596	-0.656691	0.5114
IFFRI (-4)	-0.017211	0.020295	-0.848050	0.3964
IFFRI (-5)	0.048120	0.017079	0.817472	0.4048

Note: ***0.01 level significant, **0.05 level significant, *0.1 level significant.

investors with similar attitudes, positions and judgments begin to gradually differentiate and reorganize to form cohesive subgroups. The AR value can be used to determine the concentration trend and dispersion of attention over a period of time.

4.2.2 MC

According to the MC calculation formula 2, the MC value of each social media rumors per day during the observation period was obtained as a statistical value (Table 4).

The maximum MC value is 0.043765, and the listed company involved is "PetroChina", while the minimum MC value is 0.0000088, and the listed company involved is "Xintai Electronics". The median value is 0.00024916 and the standard deviation is 0.002512, which indicates a large degree of dispersion. MC values are distributed as follows, and it can be seen that the companies involved in rumors are most concentrated in small and medium-sized companies with MC values less than 0.008, and there is relatively little rumor about large and very large-sized listed companies, which is basically consistent with the analysis results of 4.3.2.

4.2.3 SP

From the perspective of rumor sentiment polarity, positive rumors for 82%, while negative rumors for only 18%. The overall characteristics of rumor polarity are unevenly distributed, indicating that positive rumors predominate among stock rumors in China. The biggest reason is related to the lack of a shorting mechanism in the Chinese stock market, as rumor-mongers cannot make profits by suppressing the stock market through negative rumors, while it is easier to make profits by creating and spreading positive rumors in an attempt to raise stock prices.

TABLE 8 Robustness test result (IFFRI factor not added).

Variable	Coefficient	Std. Error	z-Statistic	Prob.
AR (1)	0.829516***	0.136773	6.064913	0.0000
MA (1)	-0.388203***	0.139910	-2.774652	0.0055
MA (2)	-0.100298**	0.080923	-2.528561	0.0152
MA (3)	-0.164216***	0.056503	-2.906347	0.0037
Variance Equation				
C	2.26E-06***	5.15E-07	4.382215	0.0000
RESID (-1)2	0.282862***	0.060494	4.675847	0.0000
RESID (-2)2	-0.239141***	0.059202	-4.039440	0.0001
GARCH(-1)	0.952541***	0.007985	119.2930	0.0000

Note: ***0.01 level significant, **0.05 level significant, *0.1 level significant.

TABLE 9 Robustness test result (IFFRI factor is added).

Variable	Coefficient	Std. Error	z-Statistic	Prob.
AR (1)	0.256550***	0.667377	7.984415	0.0000
MA (1)	0.186862**	0.669367	2.321136	0.0301
MA (2)	0.096648**	0.309043	2.373544	0.0253
MA (3)	-0.005294**	0.149115	-2.522035	0.0117
Variance Equation				
C	0.000306***	4.96E-05	6.171424	0.0000
RESID (-1)2	0.292074***	0.067003	4.359094	0.0000
RESID (-2)2	0.214970**	0.084681	2.538586	0.0111
GARCH(-1)	-0.056850*	0.146570	-1.687869	0.0881
IFFRI (5)	0.009562	0.027771	0.344313	0.7306
IFFRI (4)	-0.040098	0.024450	-1.640017	0.1010
IFFRI (3)	0.010373	0.027976	0.370774	0.7108
IFFRI (2)	-0.016124	0.033186	-0.485871	0.6271
IFFRI (1)	-0.053343***	0.007190	-7.419483	0.0000
IFFRI	0.032761	0.024523	1.335959	0.1816
IFFRI (-1)	0.045723**	0.030420	2.400840	0.0228
IFFRI (-2)	0.013860**	0.025613	2.195575	0.0416
IFFRI (-3)	-0.030547	0.018712	-1.632492	0.1026
IFFRI (-4)	0.012949	0.018256	0.709281	0.4782
IFFRI (-5)	-0.024424	0.024564	-0.994283	0.3201

Note: ***0.01 level significant, **0.05 level significant, *0.1 level significant.

4.2.4 IFFRI

The "Internet Financial Forum Rumor Index" (IFFRI) constructed in this paper consists of Attention Rate (AR), Market Capitalization (MC), and Sentimental Polarities (SP). According to the IFFRI definition (Eq. 4), the IFFRI values were calculated for each day of the sample period (Table 5).

4.3 Impact of social media rumors on stock market volatility

4.3.1 Empirical results

Step1: **Without IFFRI factor.** ARMA (3,2)-GARCH (2,1) is used for model without the IFFRI value regression results. The coefficient of variance equation variable is significant (at the 1% level) (Table 6), indicating that there is no sequence autocorrelation in the model.

Step2: **ARCH-LM test.** To test whether the ARMA (3,2)-GARCH (2,1) model eliminates the ARCH effect of the residual error sequences, ARCH-LM tests of 5 and 10 orders of lag are carried out for residual error sequences. The results show that the corresponding p values of F and the TR^2 values of 5 and 10 orders of lag are all greater than 0.1. We thus accept the null hypothesis of "the ARCH effect does not exist in residual errors"; that is, residual errors no longer have an ARCH effect, and residual information is extracted cleanly. This shows that the variance equation estimation is correct, and the model has strong explanatory power.

Step3: **Incorporation of IFFRI.** To study the influence of rumors on Stock Market volatility, the IFFRI value is added to the variance equation. The regression results show (Table 7) that rumors have a significant effect on stock volatility in $t-1$, t, $t+1$. In the $t-1$ *and* t, rumors have a positive response to stock market volatility while in $t+1$, there is a negative response. This indicates that rumors affect stock volatility in the current and next period, and both have positive response. However, as rumors may spread in advance and be fed back into stock volatility, rumors appear relatively backward, showing negative responses.

4.3.2 Robustness test

To test the robustness of the ARMA-GARCH model, we use the CSI 300 instead of the SSE Composite Index to conduct ARMA-GARCH model for all samples during the observation period. The specific processes for data preparation and model construction are similar to those mentioned above and are not repeated here. The regression results are described below.

Step 1: **IFFRI factor not added.** ARMA (1,3)-GARCH (2,1) is used for model, and the regression results for values without IFFRI are obtained (Table 8). The coefficient of variance equation variable is significant (at the 1% level), indicating that there is no sequence autocorrelation in the model.

Step 2: **ARCH-LM test is performed.** To test whether the ARMA (1,1)-GARCH (1,1) model eliminates the ARCH effect of the residual error sequence, the ARCH-LM test of the residual error sequence lagged by 5 and 10 orders is carried out. The results show that the corresponding P values of F and the TR^2 values of lag orders of 5 and 10 are all greater than 0.1. The null hypothesis of "the ARCH effect does not exist in residual error" is accepted; that is, the residual error no longer has an ARCH effect, and the residual error information is extracted cleanly. This shows that

the variance equation estimation is correct, and the model has strong explanatory power.

Step 3: **Add the IFFRI factor.** To study the influence of rumors on stock volatility based on the CSI 300 Index, the IFFRI value is added to the variance equation. The regression results show (Table 9) that rumors have a significant effect on the volatility of stocks in $t-2, t-1$, *and* $t+1$. The coefficient signs and significance of $t-1$ *and* $t+1$ remain unchanged. This is consistent with the regression results obtained based on the Shanghai Composite Index, indicating the robustness of the ARMA-GARCH model. Although $t-2$coefficient changes from insignificant to significant, the time span is close and small. Thus, we can conclude that it does not affect the empirical results of the ARMA-GARCH model.

4.3.3 Experiment summary

The ARMA-GARCH model and the variance equation regression results indicate that rumors affect stock market volatility. Specifically.

(1) The empirical results corroborate the behavioral finance perspective. In the stock investment process, a person as a system, when acquiring external information, encodes and evaluates it to form a unique investor sentiment and then makes behavioral decisions [72]. Since the information may not be complete or accurate feedback of truth, it can lead to a large amount of judgment bias in the cognitive process of investors [73]. Coupled with the fact that investors have limited cognitive resources and do not follow Bayes' law completely, they may take uncertain information as true and accurate information as long as the probability of its occurrence is higher [74]. As a result, people psychologically feel anxious when presented with unknown information and try to reduce this anxiety, leading to a level of irrationality in investor cognition that is exacerbated by the fact that people do not readily change their previously made, although suboptimal, decisions. Under the effect of investor sentiments, investors exhibit limited rationality, such as herd behavior, under- or over-reaction, and other behavioral characteristics, which in turn affect stock market volatility. The empirical results confirm that social media rumors trigger changes in investor sentiments, and that investors' behavioral decisions deviate from the optimum. Thus, rumors play an important information transmission effect on stock market volatility through investor sentiments.

(2) Consider the stock volatility at time t, and quantification of rumors *a priori*. Rumors at time $t-1$and t have a positive response to stock market volatility at t. That is, empirical results show that there is a positive effect on the stock market volatility at time t of rumors at $t-1$ and t. The greater the IFFRI at $t-1$ and t, the greater its effect on the stock market volatility at t. It owns the attitude of "rather believe it" overconfidence which coincidently matches that of House Money Effect. At the same time, we can find that if there is a positive response of rumors to stock market volatility at $t-1$, it supports the explanation that rumors have some advance effect on stock market volatility; that is, even though rumors have been spread on the Internet, investors show moderate caution about rumors and do not make decisions easily, driving investment decisions and triggering stock market volatility only on the day following the receipt of rumors, t.

(3) On the other hand, interestingly at $t+1$, rumors have a negative response to stock market volatility; i.e., have a significant lagged negative effect. In other words, the higher the stock market volatility at t, the weaker the rumor at $t+1$. It is probable that the network spammers who generated significant rumors at $t-1$ have achieved driving the market volatility at t, and then become less motivated to continue at $t+1$.

These findings suggest that social media rumor has a short-term effect on stock market volatility, which consolidates the previous studies that digital information, including news, social media, rumors, etc., has quick effects on stock market after it is released [4, 67]. In addition, the IFFRI is able to sense the potential impact of rumors on stock market movements, thus helping market regulators make more timely risk warnings and interventions to serve the promotion of healthy and stable stock market development.

5 Concluding remarks

This paper identifies a large number of stock forum rumors through machine learning methods and constructs a framework around IFFRI to quantify stock market investor sentiment. The empirical results show that the constructed IFFRI has a good ability to explain the influence trend of the Chinese stock market, and it is a comprehensive and timely index that accurately reveals the linkage of social media rumors on the stock market. This indicates that IFFRI is a suitable index for measuring investors' sentiment in the stock market. In particular, this study uses machine learning to find patterns from social media rumors and quantifies rumors based on statistical data, which sheds light on the application of large-scale market data in stock market volatility tracking, especially with the explosive growth of online data. On the application side, this study uses an econometric model to analyze the impact of rumors on the volatility of China's stock market and has a preliminary understanding of the interplay between the two, which provides a new perspective and concrete practice for the research on the transmission mechanism of social media information in the stock market.

This paper is based on a study of the Chinese stock market, and hence has two limitations. First, there is no short selling mechanism in the Chinese stock market, and profits can only be

made when stocks rise. For the same reason, as long as the house controls the majority of shares outstanding, the price is likely to move up and down in accordance with the house's will. Therefore, in China's stock rumors, rumor spammers cannot reap profits by suppressing the stock market through negative rumors; instead, they can only rely on positive rumors. Second, China's stock market implements the inter-day trading patterns, where traders cannot sell stocks purchase on the same day regardless of the degree of fluctuation in the rest of the day. In contrast, stock markets in many major economies does not have the inter-day trading patterns, which allows investors to immediately act on novel information about the stock market. This constitutes a substantial difference in the impact of rumors on stock market volatility.

This work can be extended in a few interesting ways as future research. 1) We intend to study the linkage and compound effect of rumors on the stock market. The current research mainly focuses on the direct impact of online rumors on listed companies or the impact of the entire stock market, and does not involve the more general one-to-many, many-to-one, many-to-many, or even secondary impacts of online rumors on listed companies. Therefore, we will try to use the results from the area of complex networks to study the behavior characteristics of listed companies in Internet media. By building an enterprise media relation network and analyzing the topological features of the network, we will study the overlapping effects of multiple social media rumors on the intersection companies. 2) We will conduct research on the impact of social network spammers to unveil the mechanism of rumors' influence on the stock market. At present, the research of rumors is mainly focus on general rumors identified from forum, and few involve the rumors generated by network spammers. Through the comprehensive and intelligent application to identify various rumors, we will fathom the extent of different rumors and analyze their impact on the stock market.

Through this research, we found that social media information including rumors has become an important part of external information in the stock market and even the entire financial market. How to establish a prevention mechanism with effective participation and joint supervision of all parties in the market is our next research goal. We also look forward to similar research in this vein, so as to facilitate benign interactions between financial markets and their external information environments.

Data availability statement

The raw data supporting the conclusions of this article will be made available by the authors, without undue reservation.

Author contributions

HZ, YC, RW, WR and JT designed the research, performed the research, analyzed the empirical data and wrote the paper.

Funding

This work was partially supported by The Ministry of Education of Humanities and Social Science Project of China (No.19YJA630110).

Conflict of interest

The authors declare that the research was conducted in the absence of any commercial or financial relationships that could be construed as a potential conflict of interest.

Publisher's note

All claims expressed in this article are solely those of the authors and do not necessarily represent those of their affiliated organizations, or those of the publisher, the editors and the reviewers. Any product that may be evaluated in this article, or claim that may be made by its manufacturer, is not guaranteed or endorsed by the publisher.

References

1. Jin BW, Zhang Q. Stock market reactions to adverse ESG disclosure via media channels. *Br Account Rev* (2022) 54(1):101045. doi:10.1016/j.bar.2021.101045)

2. Wu B, Wang S, Zeng C. Forecasting the U.S. Oil markets based on social media information during the COVID-19 pandemic. *Energy* (2021) 226:120403. doi:10.1016/j.energy.2021.120403

3. Yeşiltaş S, Şen A, Arslan B, Altuğ S. A twitter-based economic policy uncertainty index: Expert opinion and financial market dynamics in an emerging market economy. *Front Phys* (2022) 10:864207. doi:10.3389/fphy.2022.864207

4. Tetlock PC. Does public financial news resolve asymmetric information? *SSRN J* (2010) 23(9):3520–57. doi:10.2139/ssrn.1303612

5. Zhao J, He X, Wu F. Research on rumors in Chinese stock market: Spreading, refuting and impact on stock price. *Manag World* (2010) 11:38–51. doi:10.19744/j.cnki.11-1235/f.2010.11.005

6. Jiang CQ, Liang K, Chen H, Ding Y. Analyzing market performance via social media: A case study of a banking industry crisis. *Sci China Inf Sci* (2014) 57(5):1–18. doi:10.1007/s11432-013-4860-3

7. Yang SY, Yin S, Mo K, Liu A. Twitter financial community sentiment and its predictive relationship to stock market movement. *Quantitative Finance* (2015) 15(10):1637–56. doi:10.1080/14697688.2015.1071078

8. Luss R, D'Aspremont A. Predicting abnormal returns from news using text classification. *Quantitative Finance* (2015) 15(6):999–1012. doi:10.1080/14697688.2012.672762

9. Dimpfl T, Stephan J. Can Internet search queries help to predict stock market volatility? *Eur Financial Manag* (2016) 22(2):171–92. doi:10.1111/eufm.12058

10. Kumar A, Raj Sangwan S. Rumor detection using machine learning techniques on social media. *Int Conf Innovative Comput Commun* (2018) 2: 213–21. doi:10.1007/978-981-13-2354-6_23

11. Pathak AR, Mahajan A, Singh K, Patil A, Nair A. Analysis of techniques for rumor detection in social media. *Proced Comp Sci* (2020) 167:2286–96. doi:10.1016/j.procs.2020.03.281

12. Rose AM. Rumor in the stock market. *Public Opin Q* (1951) 15(3):461–86. doi:10.1086/266330

13. Diefenbach RE. How good is institutional brokerage research? *Financial Analyst J* (1972) 28(1):54+56–60.

14. Davies PL, Canes M. Stock prices and the publication of second-hand information. *J Business* (1978) 51(1):43–56. doi:10.1086/295983

15. Huth WL, Maris BA. Large and small firm stock price response to "heard on the Street" recommendations. *J Account Auditing Finance* (1992) 7(1):27–44. doi:10.1177/0148558x9200700103

16. Barber BM, Douglas L. The "dartboard" column: Second- hand information and price pressure. *J Financial Quantitative Anal* (1993) 28(2):273–84. doi:10.2307/2331290

17. Kiymaz H. The stock market rumours and stock prices: A test of price pressure and size effect in an emerging market. *Appl Financial Econ* (2002) 12(7):469–74. doi:10.1080/09603100010005852

18. Peter M, Joyce D, Tutticci I. Market reaction to takeover rumour in Internet discussion sites. *Account Finance* (2006) 46(1):31–52. doi:10.1111/j.1467-629X.2006.00160.x

19. Spiegel U, Tavor T, Joseph T. The effects of rumours on financial market efficiency. *Appl Econ Lett* (2010) 17(15):1461–4. doi:10.1080/13504850903035873

20. Li. W. Research on Internet rumor identification based on plain bayesian classification. *Comp Eng Sci* (2022) 44(03):495–501. doi:10.3969/j.issn.1007-130X.2022.03.015

21. Liu X, Chen L. Research progress of rumor identification technology for breaking news microblogs based on machine learning. *Netw Security Tech Appl* (2022) 5:54–6. doi:10.3969/j.issn.1009-6833.2022.05.031

22. Das SR, Chen MY. Yahoo! For amazon: Sentiment extraction from small talk on the web. *Manag Sci* (2007) 53(9):1375–88. doi:10.1287/mnsc.1070.0704

23. Zhu Y. The influence of network information on stock market. [PhD thesis]. Zhejiang, China: Zhejiang university (2013).

24. Chen Q, Lian W. Sentiment classification of Internet stock news based on text mining technology. *China Market* (2015) 24:234–5. doi:10.13939/j.cnki.zgsc.2015.24.234

25. Xu W, Li Y. Quantitative analysis of the impact of industry and individual stock news on stock price. *Money China* (2015) 20:31–2. doi:10.16266/j.cnki.cn11-4098/f.2015.13.025

26. Meng X, Meng X, Hu Y. Research on investor sentiment index based on text mining and baidu index. *Macroeconomics* (2016) 1:144–53. doi:10.16304/j.cnki.11-3952/f.2016.01.014

27. Yin P, Cheng P, Pan W. Early detection of microblog rumors based on integrated learning. *Microelectronics Comp* (2021) 38(01):83–8. doi:10.19304/j.cnki.issn1000-7180.2021.01.015

28. Huang H. *Investor sentiment, credit financing and corporate investment*. Beijing, China: Economic Science Press (2015).

29. Brown GW, Cliff MT. Investor sentiment and the near-term stock market. *J Empirical Finance* (2004) 11(1):1–27. doi:10.1016/j.jempfin.2002.12.001

30. Lee CMC, Shleifer A, Thaler RH. Investor sentiment and the closed-end fund puzzle. *J Finance* (1991) 46(1):75–109. doi:10.1111/j.1540-6261.1991.tb03746.x

31. Pang B, Lee L, Vaithyanathan S. Thumbs up? Sentiment classification using machine learning techniques. *Proc EMNLP* (2002) 79–86. doi:10.48550/arXiv.cs/0205070

32. Pontiff J. Closed-end fund premia and returns implications for financial market equilibrium. *J Financial Econ* (1995) 37(3):341–70. doi:10.1016/0304-405X.(94)00800-G

33. Loughran T, Ritter JR, Rydqvist K. Initial public offerings: International insights. *Pacific-Basin Finance J* (1994) 2:165–99. doi:10.1016/0927-538x(94)90016-7

34. Alexander L, Nanda V, Singh R. Hot markets, investor sentiment, and IPO pricing. *The J Business* (2006) 79(4):1667–702. doi:10.1086/503644

35. José A. Scheinkman and wei xiong. Overconfidence and speculative bubbles. *J Polit Economy* (2003) 111(6):1183–219. doi:10.1086/378531

36. Cheng X, Lu J. Research on validity of investor sentiment index based on technical analysis index. *J Manag Sci* (2018) 31(01):129–48. doi:10.3969/j.issn.1672-0334.2018.01.01

37. Baker M, Stein JC. Market liquidity as A sentiment indicator. *J Financial Markets* (2004) 7(3):271–99. doi:10.1016/j.finmar.2003.11.005

38. Huang G-B, Zhou H, Ding X, Zhang R. Extreme learning machine for regression and multiclass classification. *IEEE Trans Syst Man Cybern B* (2012) 42(2):513–29. doi:10.1109/TSMCB.2011.2168604

39. Wang Z, Hao G. Managing hypercholesterolemia and preventing cardiovascular events in elderly and younger Chinese adults: Focus on rosuvastatin. *Clin Interv Aging* (2014) 7:1–8. doi:10.2147/CIA.S41356

40. Shen Y, Yan X. Volatility and VAR prediction of CSI 300 index: Har-rv GAS model based on investor sentiment. *J Zhejiang Univ (Science Edition)* (2022) 49(1): 66–75.

41. Polk C, Paola S.The real effect of investor sentiment. Working Paper. National Bureau of Economic Research (2004). p. 105. 63. doi:10.3386/w10563

42. Goyal VK, Yamada T. Asset price shocks, financial constraints, and investment: Evidence from Japan. *J Business* (2004) 77(1):175–99. doi:10.1086/379866

43. Gao Y, Yang X, Wei X, He Y. Investor sentiment and real business performance. *Mod Business* (2022) 5:83–6. doi:10.14097/j.cnki.5392/2022.05.036

44. Zhang G, Wang M. Investor sentiment and actual investment of Chinese listed companies. *South China J Econ* (2007) 3:3–14. doi:10.3969/j.issn.1000-6249.2007.03.001

45. Jegadeesh N, Titman S. Returns to buying winners and selling losers: Implications for stock market efficiency. *J Finance* (1993) 48(1):65–91. doi:10.1111/j.1540-6261.1993.tb04702.x

46. Hua G, Zhou S, Liu Z, Jin G. Industrial policies, investor sentiment and enterprise resource allocation efficiency. *J Finance Econ* (2021) 47(01):77–93. doi:10.16538/j.cnki.jfe.20200917.303

47. Ma Y, Yang W, Jiang Y. How does investor sentiment affect a company's share price? *Finance Forum* (2020) 25(05):57–67. doi:10.16529/j.cnki.11-4613/f.2020.05.007

48. Baker M. Capital market driven corporate finance. *Annu Rev Financ Econ* (2009) 1:181–205. doi:10.1146/annurev.financial.050808.114245

49. Gilchrist S, Himmelberg CP. Gur huberman. Do stock price bubbles influence corporate investment. *J Monetary Econ* (2005) 52(4):805–27. doi:10.1016/j.jmoneco.2005.03.003

50. Huang S, wang Z. An analysis of the impact of investor sentiment on asset price: An empirical study based on Chinese stock market. *Price: Theor Pract* (2015) 11:109–11. doi:10.19851/j.cnki.cn11-1010/f.2015.11.038

51. Li G, Tang G, Liu L. Irrational linkage between stock name and stock price -- A study on China's A-share market. *J Manag World* (2011) 01:40–188. doi:10.19744/j.cnki.11-1235/f.2011.01.007

52. Shiller RJ. Do stock prices move too much to Be justified by subsequent changes in dividends? *Am Econ Rev* (1981) 71:421–36.

53. LeRoy SF, Porter RD. The present-value relation: Tests based on implied variance bounds. *Econometrica* (1981) 49(3):555–74. doi:10.2307/1911512

54. Browna GW, Cliff MT. Investor sentiment and the near-term stock market. *J Empirical Finance* (2004) 11(1):1–27. doi:10.1016/j.jempfin.2002.12.001

55. Wang M, Sun J. Chinese stock market returns, earnings volatility and investor sentiment. *Econ Res J* (2004) 10:75–83.

56. Bandopadhyaya A, Jones AL. Measuring investor sentiment in equity markets. *J Asset Manag* (2005) 7(3):208–15. doi:10.1057/palgrave.jam.2240214

57. Clarkson PM, Joyce D, Irene T. Market reaction to takeover rumour in Internet discussion sites. *Account Finance* (2006) 46(1):31–52. doi:10.1111/j.1467-629x.2006.00160.x

58. Verma R, Verma P. Noise trading and stock market volatility. *J Multinational Financial Manag* (2007) 17(3):231–43. doi:10.1016/j.mulfin.2006.10.003

59. Paul C. Tetlock. Giving content to investor sentiment: The role of media in the stock market. *J Finance* (2007) 62(3):1139–68. doi:10.1111/j.1540-6261.2007.01232.x

60. Kaniel R, Saar G, Titman S. Individual investor trading and stock returns. *J Finance* (2008) 63(1):273–310. doi:10.1111/j.1540-6261.2008.01316.x

61. Kelly PJ, Meschke F. Sentiment and stock returns: The SAD anomaly revisited. *J Banking Finance* (2010) 34(6):1308–26. doi:10.1016/j.jbankfin.2009.11.027

62. Sabherwal S, Sarkar SK, Zhang Y. Do Internet stock message boards influence trading? Evidence from heavily discussed stocks with No fundamental news. *J Bus Finance Account* (2011) 38(9-10):1209–37. doi:10.1111/j.1468-5957.2011.02258.x

63. Danbolt J, Siganos A, Vagenas-Nanos E. Investor sentiment and bidder announcement abnormal returns. *J Corporate Finance* (2015) 33(3):164–79. doi:10.1016/j.jcorpfin.2015.06.003

64. Peng C-L, Lai K-L, Chen M-L, Wei AP. Investor sentiment, customer satisfaction and stock returns. *Eur J Marketing* (2015) 5(6):827–50. doi:10.1108/ejm-01-2014-0026

65. Demetrios G, Shah C. *Investor sentiment and stock returns: Evidence from the athens stock exchange*. Munich Personal RePEc Archive (2016). Online at: https://mpra.ub.uni-muenchen.de/71243/ (Accessed August 11, 2020).

66. Woan-lih L. Sensitivity to investor sentiment and stock performance of open market share repurchases. *J Banking Finance* (2016) 71:75–94. doi:10.1016/j.jbankfin.2016.06.003

67. Qing L, Wang T, Gong Q, Chen Y, Lin Z, Sa-kwang S, et al. Media-aware quantitative trading based on public web information. *Decis Support Syst* (2014) 61:93–105. doi:10.1016/j.dss.2014.01.013

68. DiFonzo N, Bordia P, Ralph L. Reining in rumors. *Organ Dyn* (1994) 23(1):47–62. doi:10.1016/0090-2616(94)90087-6

69. Bikhchandani S, Hirshleifer D, Welch I. A theory of fads, fashion, custom, and cultural change as informational cascades. *J Polit Economy* (1992) 100(5):992–1026. doi:10.1086/261849

70. Cai Y. *Research on rumor propagation of emergent group events in digital new media environment*. Jiangxi, China: Jiangxi People's Publishing House (2014).

71. Bollerslev T. Generalized autoregressive conditional heteroskedasticity. *J Econom* (1986) 31(3):307–27. doi:10.1016/0304-4076(86)90063-1

72. Tversky A, Kahneman D. Availability: A heuristic for judging frequency and probability. *Cogn Psychol* (1973) 5(2):207–32. doi:10.1016/0010-0285(73)90033-9

73. Akerlof GA, Yellen JL. A near-rational model of the business cycle,with wage and price inertia. *Q J Econ* (1985) 100:823–38. doi:10.2307/1882925

74. Tversky A, Kahneman D. Judgment under uncertainty: Heuristics and biases. *Science* (1974) 185:1124–31. doi:10.1126/science.185.4157.1124

frontiers | Frontiers in Physics

TYPE Original Research
PUBLISHED 23 September 2022
DOI 10.3389/fphy.2022.1015103

OPEN ACCESS

EDITED BY
Fei Xiong,
Beijing Jiaotong University, China

REVIEWED BY
Zhuyin Sui,
Yantai University, China
Junfeng Xiang,
Northwestern Polytechnical University, China
Zheng Liu,
Tianjin University, China
Junsong Fu,
Beijing University of Posts and Telecommunications (BUPT), China

*CORRESPONDENCE
Lei Feng,
522131568@qq.com
Hui Liu,
305145855@qq.com

SPECIALTY SECTION
This article was submitted to Social Physics, a section of the journal Frontiers in Physics

RECEIVED 09 August 2022
ACCEPTED 09 September 2022
PUBLISHED 23 September 2022

CITATION
Liu H and Feng L (2022), The study of new energy vehicle choice in China from the perspective of complex neural network.
Front. Phys. 10:1015103.
doi: 10.3389/fphy.2022.1015103

The study of new energy vehicle choice in China from the perspective of complex neural network

Hui Liu[1,2]* and Lei Feng[2,3]*

[1]Faculty of Applied Economics, University of Chinese Academy of Social Sciences, Beijing, China, [2]Center for Brand Leadership, University of Chinese Academy of Social Sciences, Beijing, China, [3]Faculty of Economics, University of Chinese Academy of Social Sciences, Beijing, China

China has become the world's largest market for the production and sales of new energy vehicles. In the Internet era, online review data is becoming more and more important, and it is a great challenge for new energy vehicle manufacturers and consumers to quickly obtain and find out the effective information in the review data. In view of the above understanding, this study uses the Bert-wwm-ext model structure, data mining, and deep learning to study the new energy vehicle selection, and also analyzes the positioning of domestic and foreign new energy vehicle brands and their brand development from the perspective of complex networks. The research results found that: 1) Consumers pay more and more attention to the quality of new energy vehicles. 2) The comparative analysis of BEV and PHEV reveals that consumers' evaluation of both types of vehicles is roughly comparable, but the difference in satisfaction with the endurance of both types of vehicles is very obvious. 3) Most of the brands of new energy vehicles are concentrated in the price range of RMB80,000 to RMB350,000, and within this range, consumers' evaluation is positively correlated with the price of the vehicle. Among the new energy vehicle brands over RMB350,000, consumer evaluation does not rise with the price of the vehicle. 4) The head effect of Chinese brands is significant, Foreign brands have formed strong brands with high brand premiums.

KEYWORDS

complex networks, new energy vehicles, data mining, deep learning, natural language processing

1 Introduction

With the deepening of the global energy crisis, the depletion of oil resources and the aggravation of air pollution, urban smog, and rising global temperatures, governments around the world are planning to adopt new energy vehicles to establish new transportation systems and provide corresponding support policies [1], in a way to combat global warming and achieve carbon neutrality [2].

The attention of scholars all over the world on the research topic of electric vehicles continues to increase. The research on the choice of new energy vehicles mainly includes:

financial subsidies, tax relief, free parking and priority driving and other new energy vehicle incentive policies on the choice of new energy vehicles [3–6], the influence of technical factors such as cruising range, charging equipment, top speed, acceleration performance, and quietness on the selection of new energy vehicles [7–10], the influence of economic factors such as car purchase cost and electricity price on the choice of new energy vehicles [11–13], the influence of consumer personal characteristics such as gender, age, education level, income and occupation on the choice of new energy vehicles [14–15].

The new energy vehicle industry is characterized by a complex network [16]. Most of the previous studies were conducted through questionnaires [17, 18]. The small sample method of the questionnaire survey cannot better reflect the public and generality; in addition, in the process of filling out the questionnaire, some questions may not express real feelings, and cannot better reflect the objectivity and accuracy of the data; Finally, in the Internet age, consumers' consumption habits and behaviors have changed, and the method of questionnaires cannot reflect the attitudes of consumers at that time.

Cars are relatively high-value products, and consumers generally tend to spend longer and search for more information to make multiple comparisons before making a final purchase decision [19]. In the Internet era, consumers are more and more inclined to obtain information on products or services through online reviews, and information search before purchasing is considered an inevitable event for consumers' purchasing behavior [20]. Information about a product or brand increases product awareness and convinces people to try these things [21]. Research shows that nearly 50% of consumers spend more than 10 h searching for information when choosing a car that matches their needs [22]. Word of mouth can improve brand perception, promote the diffusion of new products, and increase sales, thereby increasing corporate profits and market competitiveness [23]. With the development of the Internet, word-of-mouth has evolved towards online word-of-mouth to a large extent.

China has become the world's largest new energy vehicle production and sales market. Self-owned brands are rising rapidly, and the number of new energy vehicle companies is growing. In the Internet era, the channels for consumers to obtain information are more and more diversified, and the information they obtain is relatively more and more abundant. Consumers' attitudes or word of mouth are becoming more and more important to manufacturers. Facing the diversified and personalized needs of consumers, how can China's new energy vehicles win in the fiercely competitive industry? How can the production of new energy vehicle companies better match the needs of consumers? From the perspective of demand, it is of great theoretical and practical significance to study the choice of new energy vehicles.

In summary, based on the complex neural network, this paper conducts data mining and deep learning on the 77,000 word-of-mouth texts of Autohome, the largest professional automobile communication platform in China, and studies the development of new energy vehicles in China from the demand side. The main contributions of the research are: establishing a consumer new energy vehicle choice model, and applying the BERT model to the research on new energy vehicles for the first time, analyzing the changes in consumers' choice of new energy vehicles from the perspective of time series; secondly, by analyzing the initial data Conduct training to study the impact of new energy vehicle brand influence on the choice of new energy vehicles and analyze the differences in the development of Chinese and foreign new energy vehicle brands through consumers' purchasing decisions, so as to provide opportunities for new energy vehicle brands to break through and the development direction of the new energy vehicle industry. The path of reference.

2 Data and methodology

2.1 Data

In terms of the development trend of new energy vehicles, China's new energy vehicle market has entered a rapid development phase since 2014, with intense competition among enterprises and the concentration of the industry beginning to increase. In 2014, China launched a total of 16 new energy vehicle policies, including exemption from purchase tax, clarifying the proportion of new energy vehicles in new public vehicles, and breaking local protectionism. These policies have promoted the development of the new energy vehicle industry.

From the supply side, during the year, new car makers such as LeTV, NIO and Xiaopeng started to enter the market, making China's new energy vehicle market show explosive growth. From the demand side, the national sales of new energy vehicles exceeded 70,000 units in 2014, more than three times the previous year. From the perspective of data availability, the rapid growth in the number of consumers purchasing new energy vehicles will lead to a rapid growth in the number of consumer reviews of new energy vehicles, which provides the data basis for big data analysis of consumer reviews.

Overall, 2014 was the first year of commercialization of new energy vehicles in China. Therefore, it is reasonable to conduct word cloud analysis of new energy vehicle data after 2014, which can see the changing trend of consumers' reasons for purchasing new energy vehicles.

The data in this article comes from the word-of-mouth reviews of Autohome, which were obtained through web crawler. Autohome is the largest auto website in China and one of the earliest established auto websites. The data of consumer reviews in the website are the most abundant among all auto websites and also span the longest period of

time. Therefore, Autohome's data has the most research value. The word-of-mouth data of Autohome is standardized. The website will provide 11 fields for consumers to make an overall evaluation of the car: most satisfied, least satisfied, space, power, control, endurance, comfort, exterior, interior, cost performance, and reasons for choosing this car. In addition, there are also indicators such as review time, the number of views per review, and the price of the car, which are standardized data for easy analysis and research.

The data crawled is all the new energy vehicle word-of-mouth data in Autohome before 12 June 2022, with 77,712 data initially collected.

After getting the raw data, we need to pre-process the data. In the raw data, there are two kinds of problems: one problem is that there are duplicates in the data, and a de-duplication operation should be performed on this part of the data; the other problem is that there are vacant fields in the data, which is not conducive to subsequent analysis, and this part of the data needs to be deleted. After these two steps, 73,322 data remain.

After removing some bad quality data, some fields in the data still need to be processed.

Since the year needs to be used for subsequent time series analysis, the year of the review needs to be extracted from the review time as a new field.

In addition, the price of the car also needs to be further processed. In the new energy car data, the data of price has three forms. The first one is that there is only a single price for that type of car. For example, the price of Tesla Model 3 is RMB279,900; the second is the price of the range. For example, the price of BYD Qin is in the price range of RMB129,900 to RMB174,800; the third type is no offer, this part of the data has no price information. This type of data is relatively small, with only 1,137 data belonging to this type. In order to facilitate the analysis of car prices, it is necessary to standardize the prices. For the first type of data, keep its original price; for the second type of data, take the average of the interval price as the price of the car; for the third type of data, leave it for now. In the price analysis, just remove this part of the data. After the above processing, we get the new field "Average Price".

2.2 Research methodology and model construction

2.2.1 Word cloud analysis

The word cloud can display the keywords in the text in a visual form. Through the word cloud analysis, it is possible to visualize the indicators that consumers are concerned about in new energy vehicles. The most important step in creating a word cloud is word separation. Only after the text has been split into words can the word frequency be counted. Jieba is a third-party library for python, which is often used for splitting words. The process of using jieba library to split words is as follows:

1) Load the default statistical dictionary

A statistical dictionary file "dict.txt" is available in the jieba library. In this dictionary file, each line contains a word and shows the frequency and lexical nature of the word.

2) Building a prefix dictionary

The prefix dictionary extracts every prefix of every word that appears in the statistical dictionary and counts the word frequency. If a prefix word does not appear in the statistical dictionary, the word frequency is counted as zero.

3) Generate directed acyclic graphs

The input text is scanned based on the prefix dictionary to generate a directed acyclic graph. For example, if the sentence "张三的新能源汽车" is entered, the directed acyclic graph is:

$$\{0:\ [0], 1:\ [1], 2:\ [2], 3:\ [3, 5], 4:\ [4, 5], 5:\ [5], 6:\ [6, 7], 7:\ [7]\}$$

This is a directed acyclic graph represented in dictionary format. Each word in the input sentence is represented by a value in its corresponding position, forming the "key" of the dictionary. The "value" corresponding to each "key" is the position of the last word that can be formed into a word. For example, 0: [0] means "张" can only be combined into "张", 3 [3, 5]: means "新" can be combined into "新" or "新能源". Therefore, the directed acyclic graph obtained from the sentence "张三的新能源汽车" has six paths.

4) Find the maximum probability path

Since there are multiple paths, it is necessary to find an optimal path from them. The jieba library uses a dynamic programming approach to find the maximum probability path on the directed acyclic graph to be the final path. By predicting the probability of each candidate path, the path with the highest probability is selected as the final path. The specific formula is as follows.

$$best_{path} = argmax_i \prod_j p\left(w_{i,j}\right) = argmax_i \prod_j \frac{Freq\left(w_{i,j}\right)}{\sum_k Freq\left(w_k\right)} \tag{1}$$

Where "i" represents the different paths, "j" is the word splitting scheme for path "i", and the probability "p" for each word is the word frequency divided by the total word frequency in the statistical dictionary.

Taking "新能源" and "新/能源" as examples, we need to compare the probabilities of p(新能源) and p(新)*p(能源), which are calculated as follows.

$$p(\text{新能源}) = 4.991517166151983e-08$$

$$p(\text{新})*p(\text{能源}) = 3.869648276424812e-08$$

The value of p(新能源) is greater than the value of p(新)*p(能源). Therefore, when splitting the word, "新能源" will become one word instead of splitting into "新" and "能源". According to this calculation, the sentence "张三的新能源汽车" would be split according to "张/三/的/新能源/汽车".

5) Handling Out-of-vocabulary

Out-of-vocabulary is the words that do not appear in the dictionary but should be split out. Although the statistical dictionary of jieba library contains hundreds of thousands of words, there are still many words that are not included in it, especially some names of people and places. If the word splitting is based on the dictionary only, many words will be missed. For example, in the sentence "张三的新能源汽车", "张三" as a person's name should be split into one word, but since the word "张三" is not in the dictionary, so "张三" is split into two words.

For such Out-of-vocabulary, the jieba library provides the option to use a Hidden Markov Model for prediction and the Viterbi algorithm to solve it [24].

The Hidden Markov Model predicts not the entire sentence at the beginning of the input, but a string of consecutive individual word parts that are reassembled after the end of the previous word splitting step. For example, the sentence "张三的新能源汽车" has been split into "张/三/的/新能源/汽车" in the previous step. Then, the successive parts of "张/三/的" that have been split into single words are put together and fed into the Hidden Markov Model for prediction.

A hidden Markov model is a probabilistic model of a time series that describes the process of generating a random sequence of unobservable states from a hidden Markov chain, and then generating an observation from each state to produce a random sequence of observations. The sequence of states randomly generated by the hidden Markov chain is called a sequence of states; each state generates an observation, and the resulting random sequence of observations is called a sequence of observations, and each position of the sequence can be regarded as a moment.

The Hidden Markov Model is determined by the initial probability distribution, the state transfer probability distribution and the observation probability distribution. It contains the following five elements.

1. The set of state values $Q = \{q_1, q_2, \ldots, q_N\}$, where N is the number of possible states.
2. The set of observations $V = \{v_1, v_2, \ldots, v_M\}$, where M is the number of possible observations.
3. Transfer probability matrix $A = [a_{ij}]_{N\times N}$, where a_{ij} denotes the probability of transfer from state i to state j.
4. Observation probability matrix $B = [b_j(k)]$, where $b_j(k)$ denotes the probability of generating observation v_k conditional on state j.
5. The initial state probability vector $\pi = (\pi_i)$.

Usually, the Hidden Markov Model can be expressed as $\lambda = (A, B, \pi)$ with a sequence of states "I" and a corresponding sequence of observations "O". The Hidden Markov model has three basic problems:

1. Probability calculation problem.

Given a model λ and an observation sequence O, calculate the probability P(O|λ) of the occurrence of the observation sequence O.

2. Learning problem.

Knowing the observation sequence O, estimate the parameters of the model λ such that the probability of the observation sequence P(O|λ) is maximized.

3. The prediction problem.

Knowing the model λ and the observation sequence O, find the state sequence I that maximizes the conditional probability P(I|O) for the given observation sequence. i.e., given the observation sequence, find the most probable corresponding state sequence.

Among them, word splitting is mainly concerned with the prediction problem.

In the jieba library, the transfer probability matrix A, the observation probability matrix B and the initial state probability vector π of the Hidden Markov Model are parameters that have been trained and can be used directly. The set of state values Q is set to {B, E, M, S}, i.e., it contains four states, which denote the beginning, end, middle and independent characters of the word, respectively. The observation sequence is a Chinese sentence. For example, the sentence "张三的新能源汽车" is the observation sequence, and the state sequence predicted by Hidden Markov Model is "BESBMEBE", then the result of word separation is "张三/的/新能源/汽车".

In fact, the prediction problem can be expressed as follows: for the string $O = \{o_1, \ldots, o_n\}$, solve for the maximum conditional probability $maxP(i_1, \ldots, i_n|o_1, \ldots, o_n)$. where i_j denotes the state corresponding to o_j. The specific solution process is computed using the Viterbi algorithm, which is actually a dynamic programming algorithm used to solve the prediction problem of Hidden Markov Model, i.e., solving the probability maximum path. Define the probability maximum among all individual paths with state i at moment t as:

$$\delta_t(i) = \max_{i_1, i_2, \cdots, i_{t-1}} P(i_t = i, i_{t-1}, \cdots, i_1, o_t, \cdots, o_1|\lambda), i = 1, 2, \cdots N \quad (2)$$

By definition, the recurrence formula can be written as:

$$\delta_{t+1}(i) = \max_{1 \le j \le N} \left[\delta_t(j) a_{ji}\right] b_i(o_{t+1}), i = 1, 2, \cdots N; t = 1, 2, \cdots, T-1 \tag{3}$$

Define the "t-1"th node of the path with the highest probability among all individual paths with state "I" at moment t as:

$$\psi_t(i) = arg \max_{1 \le j \le N} \left[\delta_{t-1}(j) a_{ji}\right], i = 1, 2, \cdots N \tag{4}$$

By initializing $\delta_1(i) = \pi_i b_i(o_1)$ and $\psi_1(i) = 0$, we can recursively obtain $\delta_t(i)$ and $\psi_t(i)$, and find the maximum probability P^* and the end point i_T^* of the optimal path, then we can gradually find the nodes $i_{T-1}^*, \cdots, i_1^*$ from backward to forward, and finally obtain the optimal path $I^* = (i_1^*, i_2^*, \cdots, i_T^*)$.

By the above five steps, the original text can be split into words. However, splitting into words in this way also creates problems. New energy vehicles have their own dictionary of nouns, and some of them will be separated if they are split according to the common word splitting logic. For example, the word "充电桩" will be split into "充电" and "桩". To solve this problem, it is necessary to create a dictionary of new energy vehicle terminology. This will ensure that the term is not be split.

In addition, there are some words that are not needed for the word cloud generation, such as tone words. These words can be filtered out by setting them as stop words. By this setting, we can get a more suitable word cloud.

2.2.2 Deep learning of complex neural networks

There are three main methods that can be used for text sentiment analysis. Sentiment analysis based on sentiment dictionary, sentiment analysis based on machine learning and sentiment analysis based on deep learning. From the current development, among these three methods, the deep learning-based sentiment analysis method works best and has the highest accuracy rate.

Deep learning for sentiment analysis is now a state-of-the-art approach. Deep learning is actually a subset of machine learning, which is an application of multilayer neural networks. The basic structure of a neural network is an input layer, a hidden layer, and an output layer. Each neuron in the input layer can be used as a feature of an object, the hidden layer can have one or more layers, which transforms the input into something that can be used in the output layer, and the output layer transforms the result of the hidden layer into the desired result.

Among the deep learning methods, there are also many models that can be chosen, such as TextCNN, LSTM, BiGRU, etc. However, after the emergence of pre-trained language models, their effect of sentiment analysis is significantly better, so they become the most cutting-edge methods in the field of sentiment classification now. The latest pre-trained models include ELMo, Bert, XL-NET, ALBERT, etc.

In 2019, HIT and IFLYTEK jointly released the Chinese Bert-wwm-ext pre-training model. This model is based on an improvement of Bert. The Bert-wwm-ext pre-trained language model is able to leverage the language prior knowledge learned during unsupervised pre-training and transfer it to downstream natural language processing tasks during fine-tuning. This model was chosen since it is one of the most effective models nowadays.

1) Bert-wwm-ext model structure

The Bert-wwm pre-trained language model consists of an Embedding layer and a Transformer layer, as shown in Figure 1.

The beginning of each sentence is [CLS], and [SEP] is the segmentation mark, which is placed at the end of each paragraph. The input sentence of the model is defined as $e = (e_1, e_2, \ldots, e_n)$,

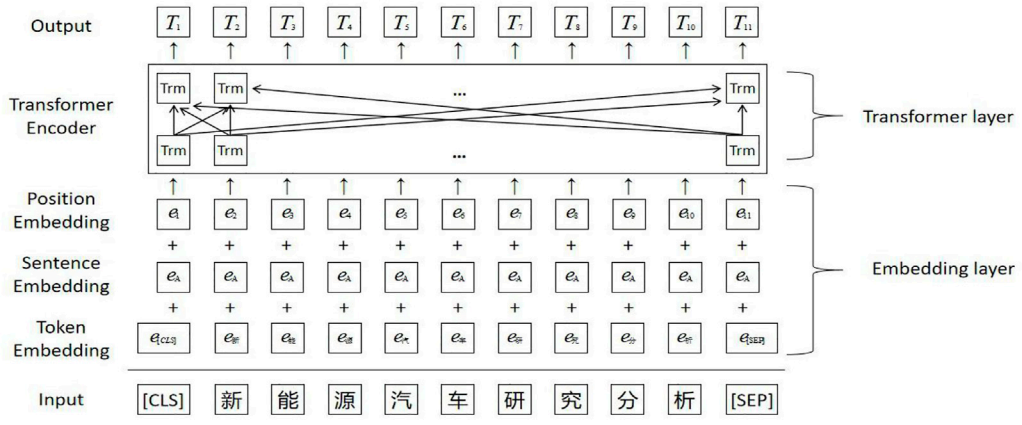

FIGURE 1
Bert-wwm-ext model.

where e_i denotes the ith character of the input sentence and n denotes the sentence length.

In the Embedding layer, the input vector "e" is obtained by summing the Token Embedding vector, the Sentence Embedding vector and the Position Embedding vector. The Token embedding vector is a static encoding of the word, and the Sentence Embedding vector represents the sentence to which the word belongs. The Position Embedding vector represents the location information of the word [25].

In this model, the Transformer layer is its main framework, which consists of multiple Transformer Encoders [26]. Among them, the structure of a single encoder is shown in Figure 2.

The structure of the Transformer Encoder has four layers: the first layer is a multi-head self-attention mechanism, the second and fourth layers are residual connection and normalization, and the third layer is a position-wise fully connected feed-forward network.

1. Multi-Head Attention layer

The main idea of multi-head attention is to adjust the weight of a word by calculating the association between words, reflecting the interrelationship between the word and all words in this sentence and the importance of each word. After the input sequence X enters the first layer, three matrices Q, K, V will be obtained by linear transformation, which is calculated as:

$$Q = X*W_Q \tag{5}$$

$$K = X*W_K \tag{6}$$

$$V = X*W_V \tag{7}$$

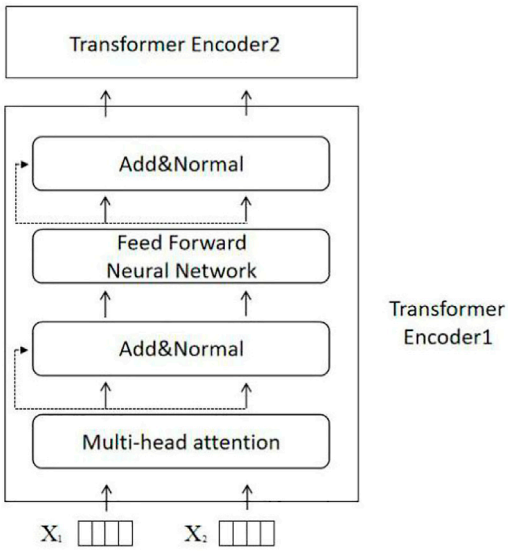

FIGURE 2
Transformer encoder.

W_Q, W_K, W_V are the weight matrices. Using the three vector matrices Q, K, and V, the output of the self-attentive mechanism can be calculated as follows.

$$Attention(Q,K,V) = Softmax\left(\frac{QK^T}{\sqrt{d_K}}\right)V \tag{8}$$

Where $Q \in R^{n\times d_K}$, $K \in R^{n\times d_K}$, $V \in R^{n\times d_V}$, $\sqrt{d_K}$ is the scaling factor. The Softmax function is to normalize each row vector after the $\frac{QK^T}{\sqrt{d_K}}$ operation so that the sum of each row vector is 1. The purpose is to calculate the weight coefficient of a word. After obtaining the output of self-attention, the output of multi-head attention can be calculated with the formula:

$$MultiHead(Q,K,V) = concat\left(Attention_1, \ldots Attention_i, \ldots, Attention_g\right)\cdot W^O \tag{9}$$

$$\text{where } Attention_i = Attention\left(QW_i^Q, KW_i^K, VW_i^V\right) \tag{10}$$

Where W^O denotes the parameter matrix, W_i^Q, W_i^K, W_i^V denote the weight matrix of the ith head attention mechanism, respectively.

2. Residual connection and normalization layer

There are two main operations done in this layer. The first operation is the residual connection, which adds up the input X of the previous layer and the output $SubLayer(X)$ of the previous layer to get:

$$X + MultiHead(Q,K,V) \tag{11}$$

The second operation is Layer Normalization, which normalizes the hidden layers in the neural network to a standard normal distribution. The formula is:

$$LayerNorm(x) = \frac{\left(x_{ij} - \mu_j\right)^2}{\sqrt{\sigma_j^2 + \epsilon}} \tag{12}$$

Where $\mu_j = \frac{1}{m}\sum_{i=1}^{m} x_{ij}, \sigma_j^2 = \frac{1}{m}\sum_{i=1}^{m}(x_{ij} - \mu_j)^2$.

3. Position-wise fully connected feed-forward network layer

At this layer, two linear transformations are done to the matrix and then activated with the activation function. Usually, the activation function uses the ReLU function.

$$X = ReLU(X*W_1*W_2) \tag{13}$$

where the ReLU function is given by

$$f(x) = \max(0,x) \tag{14}$$

2) Bert-wwm-ext pre-trained model task

The Bert-wwm-ext pre-training process consists of two unsupervised tasks: the masked language model (MLM) task and the next sentence prediction (NSP) task.

The masked language model can improve the generalization ability of the model to sentences and feature representation ability. In the original Bert model, the masked language model randomly masks 15% of the words in the input sequence, and the masked words have an 80% probability of being replaced with the symbol [MASK], a 10% probability of being replaced with any other word, and a 10% probability of remaining the original word. This allows the model to guess what the masked word is from the context, thus capturing the deeper meaning of the text. The details are shown in Figure 3.

In the Bert-wwm-ext model, this approach is improved. If a partial subword of a complete word is masked, other parts of the same word are also masked [27]. as shown in Figure 4.

The next sentence prediction task is to predict whether a sentence is the next sentence of another sentence. The next sentence prediction task allows the model to capture the relationship between sentences and sentences. Specifically, the model will randomly select sentence A from the corpus, then obtain its next sentence B, and then replace sentence B with sentence C in the corpus that is unrelated to A with 50% probability. During training, the final input corresponding to the special token [CLS] will be used as a representation of the two sentences to determine whether the two sentences are related. The details are shown in the following Figure 5.

3). Bert-wwm-ext model for classification task training

The pre-trained model can be used in downstream natural language processing tasks. By fine-tuning the Bert-wwm-ext model, it can be made applicable to a variety of different natural language processing tasks.

In this paper, the model is updated with relevant parameters by retraining on a specific word-of-mouth review dataset, which allows the model to obtain better text classification results. Compared with the traditional method, the application of fine-tuning can reduce the hardware cost and time cost to a great extent because the pre-training does not have to be turned on again.

a. Data cleaning and labeling

In the word-of-mouth reviews crawled in this paper, there are 11 fields of consumer evaluations. Among them, the “most satisfied point” and “least satisfied point” fields can be interpreted as labeled data. The “most satisfied point” indicates a positive emotional tendency and is represented by “1”, with a total of 73,322 data. The “least satisfied point” indicates the negative affective tendency and is represented by “0”, with 73,322 data. Thus, a total of 146,644 data were obtained to fine-tune the model.

b. Standardization of sentence length

Due to the different lengths of the word-of-mouth review texts, the sentence lengths were standardized to make all reviews of the same length before inputting them into the model. The average length of the “most satisfied point” and “least satisfied point” comments is 108 and the maximum length is 2,677. Because of the computation time and computer performance, the text fields cannot be unified into 2,677 length units. After experiments, the final choice is to unify the text length to 256 words. This field length covers 93% of the text data. If

FIGURE 3
Masked language model of Bert.

FIGURE 4
Masked language model of BERT-wmm-ext.

FIGURE 5
Next sentence prediction task.

the text comment exceeds 256 words, the subsequent text is truncated; if the text comment is less than 256 words, the length is made up to 256.

c. Dividing the training set and test set

The ratio of training set and test set belongs to one of the hyperparameters of the model, and the division ratio chosen in this paper is 8:2, with 80% of the data as the training set of the model and 20% of the data as the test set of the model. This is a commonly used partition ratio in deep learning.

d. Optimizer settings

The goal of deep learning is to fit the output by continuously changing the network parameters so that the parameters can perform various nonlinear transformations on the input data, which is essentially a process of finding the optimal solution to a function. One of the algorithms for updating the parameters is called an optimizer, which can be trained to optimize the parameters to minimize the loss function. The loss function is a function used to calculate the degree of deviation between the true and predicted values in the test set. The smaller the loss function is, the better the model effect is.

The optimizer chosen for this model is Adam. The Adam algorithm is one of the most popular optimizers in the field of deep learning at present. Its mathematical formula is as follows.

$$m_t = \beta_1 m_{t-1} + (1-\beta_1) g_t \tag{15}$$

$$v_t = \beta_2 v_{t-1} + (1-\beta_2) g_t^2 \tag{16}$$

$$\widehat{m_t} = \frac{m_t}{1-\beta_1^t} \tag{17}$$

$$\widehat{v_t} = \frac{v_t}{1-\beta_2^t} \tag{18}$$

$$\theta_{t+1} = \theta_t - \frac{\eta}{\sqrt{\widehat{v_t}+\varepsilon}} \widehat{m_t} \tag{19}$$

Initially, m_0、v_0 and t are set to 0. Among them, the first two formulas are sliding averages of the gradient and the square of the gradient, respectively, making each update related to the historical values. Equations three and four are bias corrections, which can correct for the larger sliding average bias in the initial period. The fifth formula is an update formula for the parameters. The initial parameters are set $\beta_1 = 0.9$、$\beta_2 = 0.999$、η = 2e-5 and ε =1e-8.

e. Classification training using [CLS]

Due to the existence of attention mechanism, the information of each token is gathered into [CLS] when the model operates, so the role of [CLS] in the Bert-wwm-ext model is not only to mark the beginning of a sentence, but also to store the basic information of a sequence. Therefore, after doing linear transform and softmax transform on the output vector of the last layer of [CLS], it can be compared with the labels of text data for classification training.

f. Model Evaluation

The commonly used evaluation metrics in classification tasks are: accuracy, precision, recall, F1-Measure, etc. The accuracy metric is chosen for this evaluation. The accuracy is the most intuitive evaluation metric, which is evaluated by the ratio of correctly classified data to the total data volume. The calculation method is:

$$Acc = \frac{TP + TN}{TP + FN + FP + TN} \tag{20}$$

Among them, TP denotes the number of samples that are actually positive and predicted to be positive; TN denotes the number of samples that are actually negative and predicted to be negative; FN denotes the number of samples that are actually positive and predicted to be negative; and FP denotes the number of samples that are actually negative and predicted to be positive.

By verifying the model effect on the test set, the final text classification accuracy obtained in this paper is 98.93%. Compared with traditional machine learning algorithms and deep learning algorithms such as LSTM, the effect of Bert-wwm-ext model is undoubtedly much better.

g. Sentiment classification for other fields

The trained model can predict the sentiment of eight dimensions of word-of-mouth reviews: space, power, control,

endurance, comfort, exterior, interior, and cost performance. The text labels with positive sentiment are saved as 1 and those with negative sentiment are saved as 0. The final text data with sentiment labels can be obtained for subsequent data analysis.

3 Analysis of the evolution of new energy vehicle options

3.1 Word cloud evolution analysis

In this paper, we plot the word cloud of the "Reasons for choosing this car" field by year to show the factors that consumers value in purchasing new energy vehicles. Since the word cloud for each year contains the word "new energy" and is the largest word in the word cloud, the word "new energy" is placed in the stop words table to highlight other information. In addition, since brand analysis is not done here, the brands of cars are also filtered out. For example, brands such as "BYD", "NIO" and "Tesla" were put into the stop words table. Based on the collected data, a word cloud was drawn for the 9 years from 2014 to 2022. The words in the word cloud are translated into English to obtain Figure 6.

The sales of new energy vehicles in China have been in an upward phase. In 2017 and before, the sales of new energy vehicles in China were within 1 million units, and from 2018 onwards, the sales of new energy vehicles in China exceeded 1 million volumes. If we divide by sales volume, 2017 and the years before it can be called the early years of new energy vehicle development. And starting from 2018, new energy vehicles are gradually accepted by the majority of consumers and become one of the main options for purchasing cars. So, we can use 2017 and 2018 as the dividing point to see the changes that have occurred in the word cloud.

According to what the word cloud shows, there is a big difference between the concerns of early consumers and those of recent years for new energy vehicles.

FIGURE 6
" Reasons for choosing this car" Word Cloud.

In the early years, consumers were more concerned about "power", "cost performance", "saving money" and "subsidies".

"Power" is the biggest difference between new energy vehicles and fuel cars. Compared with traditional fuel cars, new energy vehicles have a faster start and better power. Early consumers can easily feel this difference in driving. However, with the gradual popularity of new energy vehicles, consumers' concern for power has significantly decreased. In the 9 years from 2014 to 2022, the frequency of the word "power" was ranked first, third, fourth, fifth, fourth, sixth, eighth, eighth and eighth. This indicates that consumers have gradually become accustomed to the power of new energy vehicles.

The three indicators of "cost performance", "saving money" and "subsidies" can be viewed together. In the 9 years from 2014 to 2022, the ranking of cost performance in the word frequency is third, second, sixth, first, fifth, seventh, seventh, fifth, and sixth. The ranking of saving money in the word frequency is 23rd, 13th, third, 18th, 15th, 18th, 27th, 36th and 38th. Although there are some fluctuations, it can be seen that the importance of these two fields has been decreasing over time. For subsidies, the frequency ranking in the 5 years from 2014 to 2018 is seventh, 12th, second, 31st, and 44th in order. After 2019, the word subsidies no longer enter the top 50 words in terms of frequency. These three indicators show that early new energy vehicles are greatly influenced by policies, and consumers are more likely to be influenced by policies and choose new energy vehicles with strong subsidies.

In addition to these indicators, early consumers were more concerned about the indicator of "environmental friendly". In the 7 years from 2014 to 2020, the frequency of environmental friendly was ranked ninth, fifth, eighth, eighth, 16th, 21st, and 39th in order. In 2021 and 2022, the word does not enter the top 50 words in terms of frequency. This shows that early consumers of new energy vehicles pay more attention to green consumption, and the concept of environmental protection is one of the reasons for them to buy new energy vehicles. In recent years, consumers' concern for environmental protection has begun to decline, which indicates that the quality of new energy vehicles has improved, making those consumers who are not concerned about environmental protection willing to choose new energy vehicles for quality reasons.

In the period from 2018 to 2022, the indicators that consumers are most concerned about new energy vehicles are "exterior", "space", "endurance", "price" and "brand".

In the 4 years from 2014 to 2017, exterior ranked second, 19th, fifth, and third in word frequency. After 2018, the word exterior ranked first in word frequency for all of them. In the 9 years from 2014 to 2022, space ranked 16th, 25th, seventh, fourth, third, second, third, second, second, and second in word frequency. This means that for "exterior" and "space", consumers were also more concerned about these two indicators in the early stage. But in recent years, the concern has increased significantly, which shows that consumers have paid more attention to the quality of new energy vehicles in recent years.

In 2014, endurance was not in the top 50 in word frequency, and from 2018 to 2022, endurance ranked 10th, 20th, 10th, seventh, third, fourth, fourth, and fourth in word frequency. "Endurance" is the core indicator of new energy vehicles, and the word cloud shows that consumers hardly choose new energy vehicles because of "endurance" in the early years, but now "endurance" is one of the reasons consumers choose new energy vehicles. This shows that the endurance of new energy vehicles was poor in the early days, but now the endurance of new energy vehicles is gradually recognized by consumers.

"Price" is an important reason for consumers to purchase goods. In fact, both before 2017 and after 2018, consumers were concerned about price. However, consumers have become significantly more concerned about price in recent years. From 2018 to 2022, price ranked 10th, fourth, 27th, second, second, fourth, second, third and third in word frequency. As a comparison, earlier consumers were more concerned about the indicators associated with car subsidies rather than the price of the car itself. This change indicates that as the amount of subsidies has declined in recent years, consumers have become more concerned about price itself.

"Brand" is one of the most important reasons for consumers to choose new energy vehicles in recent years. In 2014, brand was not in the top 50 in word frequency, and from 2015 to 2022, brand ranked 26th,31st, 13th, 11th, eighth, sixth,sixth, and fifth in word frequency. It takes time for brands to form. At the early stage of the development of new energy vehicles, strong brands have not yet been formed, and it is difficult for consumers to choose a suitable new energy vehicle by brand. Therefore, the frequency of consumers mentioning brands in their comments on why they choose new energy vehicles in the early stage is very low. After several years of development, some famous brands have gradually appeared in the new energy vehicle market, and consumers are paying more and more attention to the brands. In recent years, the frequency of brand has been in the top ten of the reasons why consumers choose new energy vehicles, and the trend has been increasing. This shows that consumers are now more willing to choose new energy vehicles by the merits of the brand than before.

3.2 Emotional evolution analysis

3.2.1 Eight dimensions of emotional evolution

Using the text data with labels obtained from the model, the sentiment tendency can be calculated for the eight dimensions of word-of-mouth reviews by year. For each dimension, the ratio of its positive sentiment review volume to the total review volume for each year is calculated to obtain the overall sentiment evaluation score of the consumer for that dimension for that year, which is between 0 and 1. The results of the calculation are presented in Table 1.

Based on the results obtained from the calculations, it is possible to map the evolution of emotions in eight dimensions.

As can be seen in Figure 7, most of the indicators have a large variation until 2017; after 2017, the trend of the curve is flatter. This

TABLE 1 Emotional scores in eight dimensions.

Year	Endurance	Space	Power	Control	Comfort	Exterior	Interior	Cost performance
2014	0.73196	0.57732	0.86598	0.54639	0.55670	0.79381	0.38144	0.61856
2015	0.67347	0.58776	0.82857	0.58776	0.53061	0.66122	0.45306	0.61224
2016	0.81481	0.66204	0.89815	0.77778	0.76389	0.83796	0.65278	0.84722
2017	0.67289	0.70904	0.84458	0.65964	0.54759	0.73976	0.55241	0.74639
2018	0.64301	0.72321	0.87272	0.73693	0.56991	0.86823	0.57559	0.85427
2019	0.62542	0.74865	0.90069	0.78535	0.67489	0.89205	0.59411	0.88729
2020	0.61745	0.78852	0.88838	0.80205	0.67690	0.90814	0.63694	0.89818
2021	0.64732	0.78842	0.90438	0.81226	0.69562	0.92102	0.66639	0.90235
2022	0.64970	0.78823	0.89789	0.81316	0.68272	0.91592	0.65834	0.88225

reason is mainly due to the size of the data volume. The data volumes for the 9 years from 2014 to 2022 are 97, 245, 216, 1,660, 4,227, 7,985, 11,235, 27,640, and 20,017, respectively. The small data volumes for the earlier years result in indicators that are more susceptible to individual consumer influence. To better observe the trend, the data from 2014 to 2017 can be combined. As shown in Figure 8.

As can be seen, after combining the data from 2014 to 2017, the curve is smoother than before. From the graph, for the five indicators of power, exterior, cost performance, control and space, the overall evaluation of consumers shows an upward trend, and from 2019 onward, consumers' emotional scores for these five indicators are basically above 0.75. Among them, the exterior, power and cost performance are about 0.9.

For the two indicators of comfort and interior, consumers' sentiment scores also show an upward trend. However, until 2022, the scores of these two indicators are still low, not reaching 0.7. This indicates that in the future, these two dimensions have more room for improvement.

For the score of the indicator of endurance, it is in a decreasing trend until 2020, and in 2021 and 2022, although there is a slight increase, the overall trend is still decreasing. Moreover, this indicator is the lowest rated among all indicators.

However, according to what the word cloud shows, the endurance of new energy vehicles has been gradually recognized by consumers in recent years. This contradiction indicates that the endurance indicator is highly polarized in consumers' evaluation. Some consumers believe that the endurance of new energy vehicles has met their needs, while others believe that the endurance of new energy vehicles still needs to be improved.

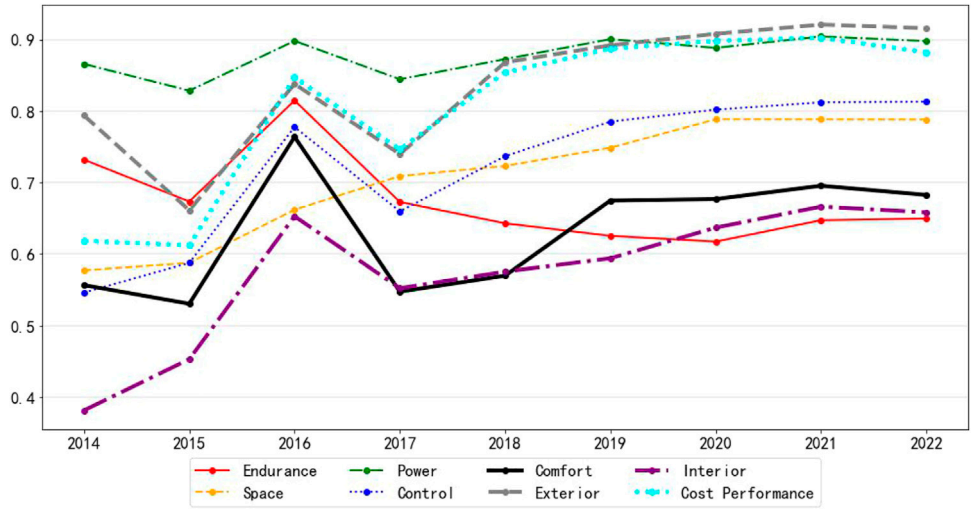

FIGURE 7
2014–2022 emotional trend chart.

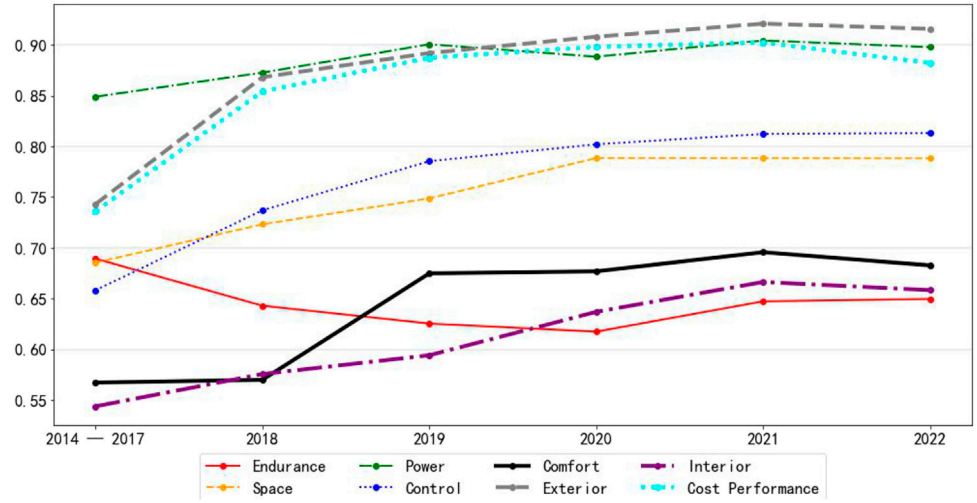

FIGURE 8
2014–2022 emotional trend chart 2

3.2.2 Comparison analysis of BEV and PHEV

For new energy vehicles, the current mainstream models are divided into three types: Battery Electric Vehicle (BEV), Plug-in Hybrid Electric Vehicle (PHEV), and Range Extended Electric Vehicle (REEV). The development of BEV can effectively relieve the pressure of energy and environment. The development of PHEV and REEV is an important path for the transition from traditional fuel vehicles to BEV. At present, PHEV and REEV are in a booming stage of development in China, and PHEV and REEV have various advantages such as high energy-saving potential, moderate cost, high market acceptance, and environmental friendliness. Therefore, for a period of time, both PHEV and REEV will continue to play an irreplaceable and important role in the transition to vehicle electrification. By clustering the data, we obtained 39,395 items of BEV, 8,447 items of PHEV, 24,829 items of BEV/PHEV, 485 for REEV and 163 for others. Among them, BEV/PHEV means that there are both BEV and PHEV of this type of vehicle. Since the amount of data for REEV is too small, we do not analyze them. The main analysis is on BEV and PHEV. Figure 9 and Figure 10 show the sentiment of BEV and PHEV, respectively.

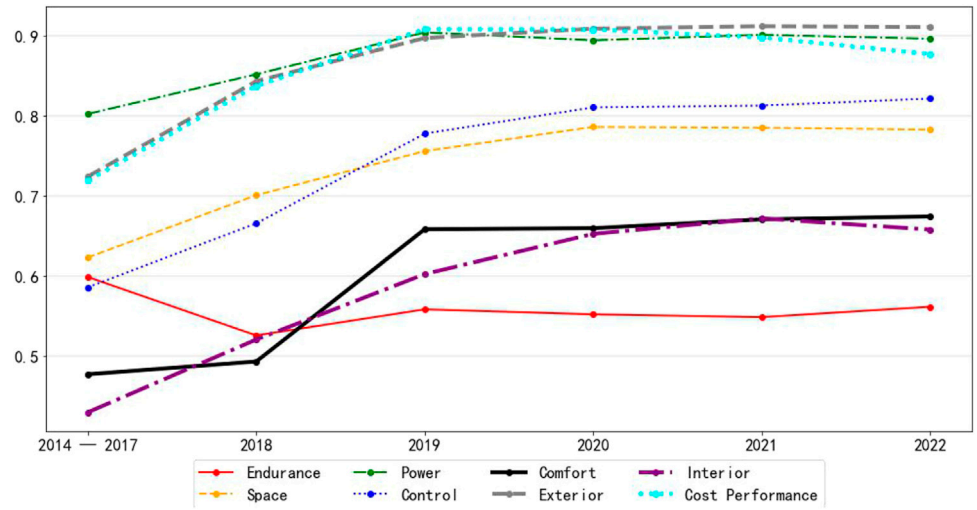

FIGURE 9
2014–2022 emotional trend of BEV

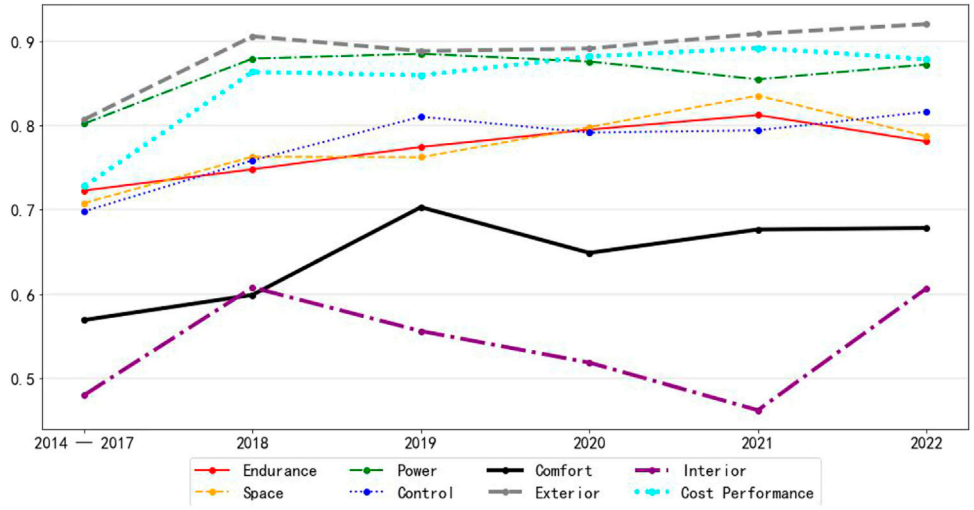

FIGURE 10
2014–2022 emotional trend of PHEVs.

As you can see from the graph, most of the indicators of the two charts have basically the same emotional trend. Only the two indicators of interior and endurance have a big difference.

For the indicator of interior, the sentiment score of BEV shows a gradual upward trend, while PHEV has a significant downward trend from 2018 onward, and only turns upward in 2022. However, from an overall perspective, both BEV and PHEV do not have high scores for this indicator of interior. It shows that the interior is the overall problem of new energy vehicles.

For the indicator of endurance, the sentiment score for BEV basically stays the same after slipping from near 0.6 in the early years to around 0.55. Moreover, from 2019 onward, this indicator has the lowest score of all indicators. As a comparison, the endurance score for PHEV has a gradual upward trend, reaching near 0.8 in recent years. From here, we can see that PHEV do not actually have an endurance problem. Endurance is only an issue for BEV.

To see the difference more clearly, the scores of the eight indicators for BEV and PHEV can be drawn in a radar chart. As you can see in Figure 11, endurance is the biggest difference between BEV and PHEV. Consumers still have greater dissatisfaction with the endurance of BEV.

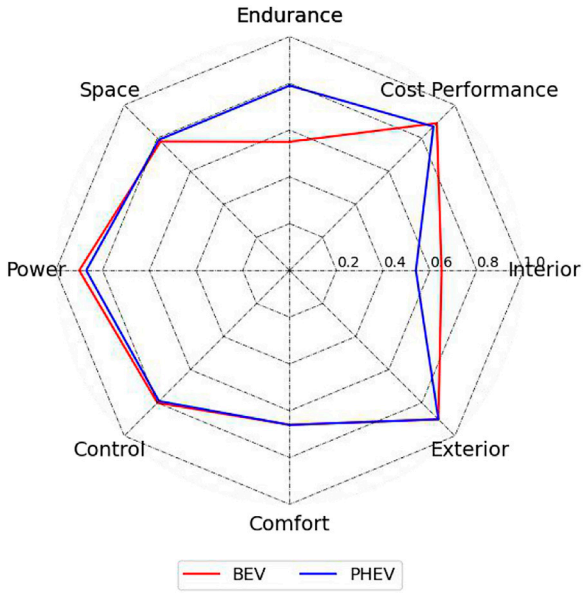

FIGURE 11
A comparative radar chart of BEV and PHEV

With the development of the new energy vehicle industry in recent years and the advancement of battery technology and infrastructure such as charging piles, new energy vehicles have seen a major improvement in both battery range and ease of charging. In the data obtained in this paper, the battery range field of the model is included. In this field, 1.6% of the data take the value of null, and 98.4% of the data can be extracted to the battery range of the car. Extracting the data of BEV whose battery range is not null and clustering them by year to find the average, we can obtain Table 2.

From Table 2, we can see that the average battery range of BEV is increasing from 2014 to 2022, and the range in 2022 is already 3.3 times higher than that in 2014. However, consumers' battery range ratings for pure electric vehicles have not risen, but have declined

TABLE 2 The battery range of BEV in 2014–2022.

Year	2014	2015	2016	2017	2018	2019	2020	2021	2022
Battery Range (km)	159	235	262	297	356	443	486	514	528

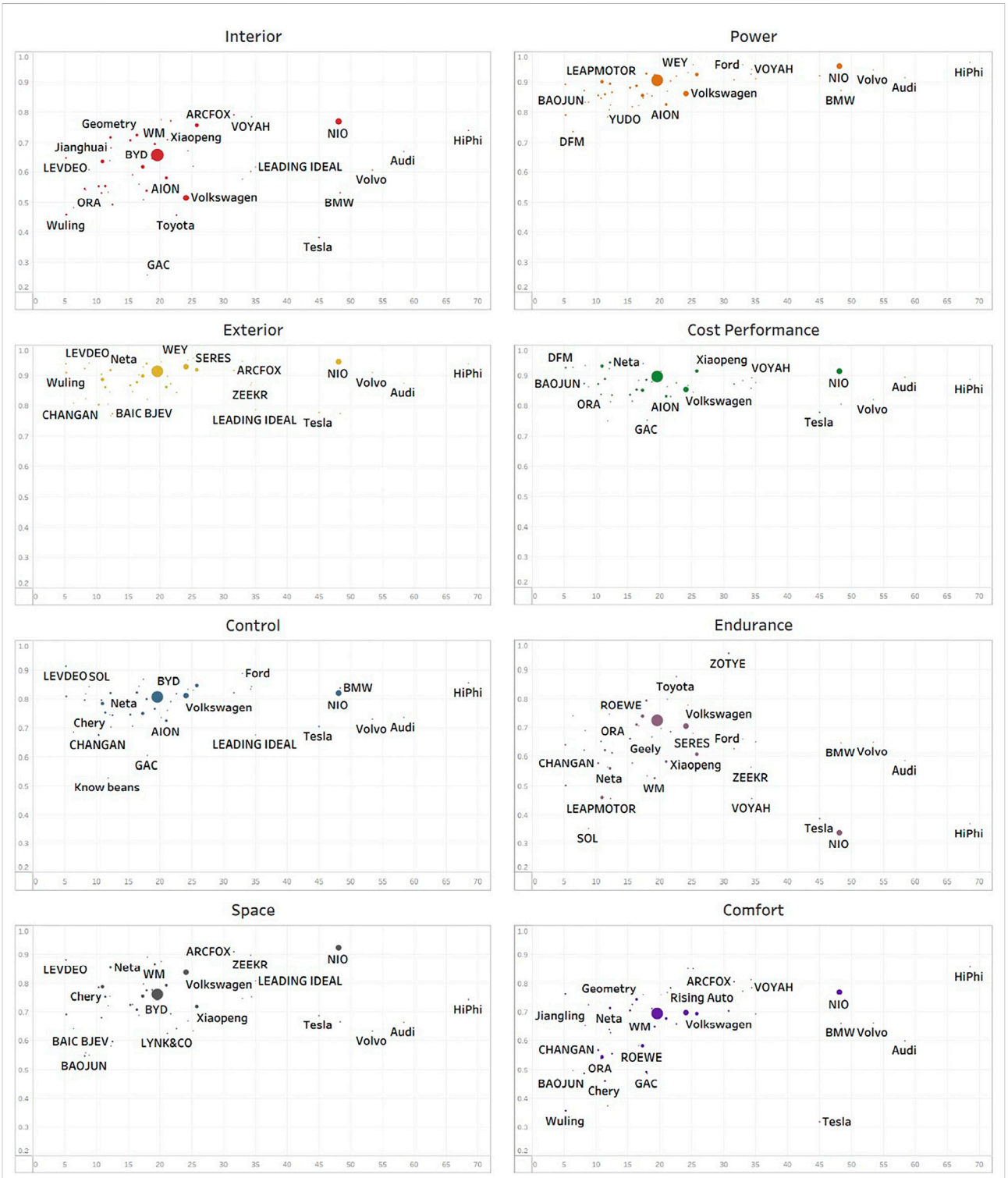

FIGURE 12
The eight-dimensional emotional distribution map of different brands of cars.

compared to earlier ratings, indicating that consumers' requirements for battery range are also rising.

According to China's subsidy policy and the development trend of new energy vehicles, BEV is the main development direction of new energy vehicles in the future. Therefore, improving the range of BEV is the most important aspect of developing new energy vehicles.

3.2.3 Price and brand analysis

In order to study the consumer evaluation of different brands of new energy vehicles, the data needs to be further processed.

In the raw data, the price of the car in each data was obtained by data pre-processing. Since the prices of different brands of new energy vehicles vary greatly, the price corresponding to a certain brand of car needs to be obtained in some way. The approach taken in this paper is to average the prices of all cars of a brand appearing in the data, and the value obtained represents the price corresponding to that car brand. In addition, the sentiment scores of the eight dimensions of each brand of car are obtained by averaging all the data of the brand. Finally, the average sentiment score of consumers for each brand of new energy vehicles is obtained by averaging the scores of the brands on the eight dimensions.

New energy vehicle brands with an evaluation volume of more than 100 can be selected, and eight scatter plots are drawn with the average price of the brand as the horizontal coordinate, the sentiment scores of the eight dimensions as the vertical coordinate, and the data volume of each brand as the sample point size.

As seen in Figure 12, for the four indicators of power, exterior, cost performance and control, there is no significant difference between brands at different prices. For the two indicators of endurance and comfort, the increase in price did not bring an increase in consumer evaluation, but rather a decline. For the two indicators of interior and comfort, they can be divided into two parts with a price of 400,000. Each of these two parts has an emotional rating that rises as the price rises. However, there is no gap between the ratings of these two parts. These indicate that consumers who buy premium new energy vehicles are more critical of the cars' evaluations.

In order to further understand consumers' comprehensive evaluation of different new energy vehicle brands, we can take the car brands with more than 100 word-of-mouth reviews, take the average price of the brand as the horizontal coordinate, the average of consumers' eight emotional scores of each brand as the vertical coordinate, and the data volume of each brand as the sample point size to draw a scatter plot.

According to what is shown in Figure 13, it can be found that most of the new energy vehicle brands are located in the price range of RMB80,000 to RMB350,000. In this range, as

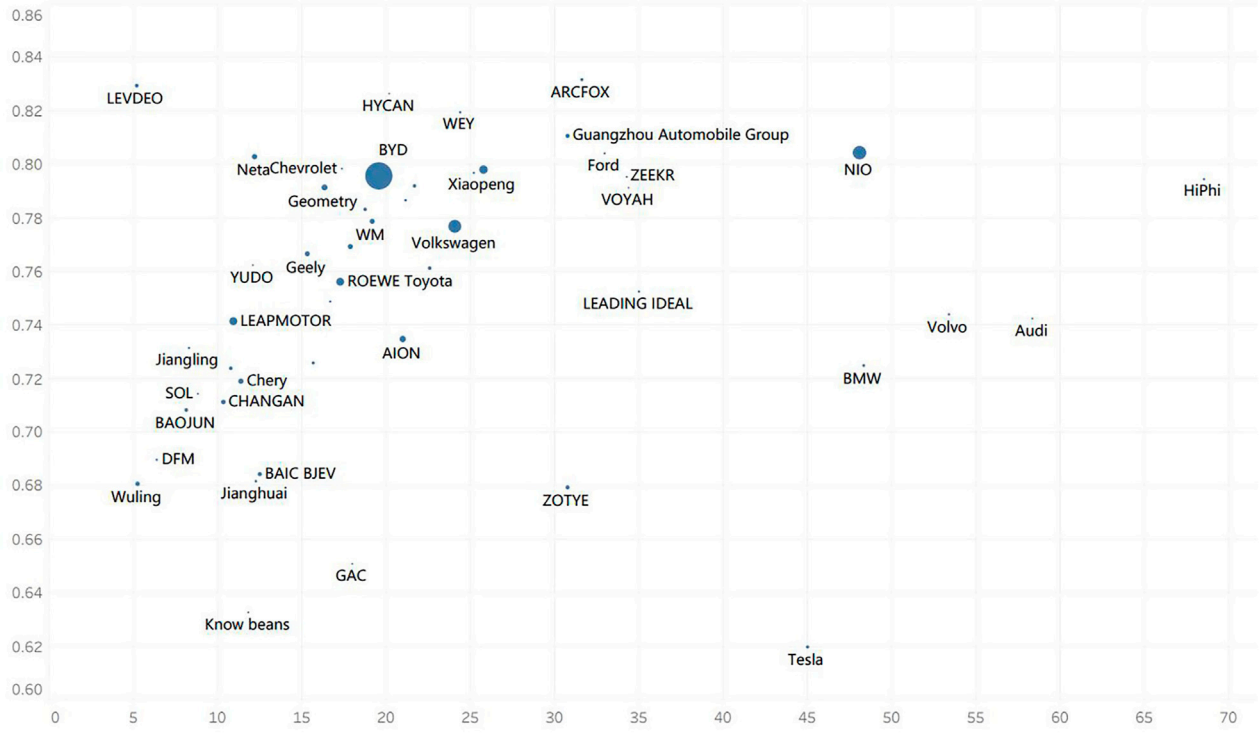

FIGURE 13
Distribution map of the average sentiment score of different brands of cars.

the price rises, the average sentiment score of consumers shows a more obvious upward trend. This indicates that as the price rises, the quality of new energy vehicles also rises and is more likely to be recognized by consumers.

However, among new energy vehicle brands with prices over RMB350,000, they do not show the same trend. This shows that compared to ordinary new energy cars, there is no significant rise in quality for high-priced new energy cars.

BYD is the mainstream brand in the new energy vehicle market. Other new energy vehicle brands have a precipitous gap in the amount of word-of-mouth review data compared to BYD. BYD is in the mainstream price range of new energy vehicles and has a relatively high overall rating, making it the most recognized brand in the market. NIO is the premium brand of new energy vehicles in China and has the highest consumer rating score among all new energy vehicle brands priced over RMB350,000, which shows that our premium new energy vehicle brand has been recognized by consumers. Chinese brands BYD and NIO already have the characteristics of strong brands in the new energy vehicle market, but the head effect of Chinese brands is significant.

In terms of brand, Tesla, the world's most well-known brand of new energy vehicles, has the lowest sentiment score. This indicates that Tesla has formed a strong brand with a high brand premium. In addition, compared to Chinese brands, foreign brands, such as Tesla, BMW, and Audi, they already have a very high reputation and reputation, and they have strong brand premium capabilities.

4 Conclusion

This study investigates new energy vehicle selection through complex neural network models, data mining, and deep learning, and also analyzes the positioning of domestic and foreign new energy vehicle brands and their brand development from the perspective of complex networks. Through theoretical analysis and empirical research, this paper obtains the following main conclusions.

1) Through word cloud analysis, we can find that the reasons why consumers choose to buy new energy vehicles are gradually changing. Consumers in the early stage are more willing to choose new energy vehicles because of the advantages of cost performance and subsidy benefits; Consumers in the later stage pay more attention to the exterior, space and other indicators of new energy vehicles. This shows that consumers are paying more and more attention to the quality of new energy vehicles.
2) From the analysis of emotional evolution, it is found that consumers' evaluation of the power of new energy vehicles has always been high, which is determined by the characteristics of new energy vehicles. Consumers' evaluation of the six indicators of exterior, space, control, cost performance, comfort and interior of new energy vehicles is increasing, which indicates that the quality of new energy vehicles is gradually recognized by consumers. Among these indicators, the overall evaluation of comfort and interior is relatively low, which indicates that there is still much room for improvement in these two indicators.
3) Through word cloud analysis, it is found that consumers are more willing to choose new energy vehicles in recent years due to their endurance. However, the sentiment evolution analysis reveals that consumers' evaluation of the endurance of new energy vehicles is on a downward trend, and the evaluation is low. This phenomenon shows that consumers' evaluation of the endurance of new energy vehicles is polarized. A part of consumers gradually recognizes the endurance of new energy vehicles, while another part of consumers is not satisfied with the endurance of new energy vehicles.
4) The comparative analysis of BEV and PHEV reveals that consumers' ratings of both types of vehicles are roughly comparable, but the gap in satisfaction with the endurance of both types of vehicles is pronounced. Consumers rated the range of PHEV higher, and rated the range of BEV very low.
5) The word cloud analysis shows that consumers are more concerned about the brand of new energy vehicles in recent years. The brand analysis reveals that most brands of new energy vehicles are concentrated in the price range of RMB80,000 to RMB350,000, and within this range, consumer ratings are positively correlated with the price of the car. In the brands of new energy vehicles over RMB350,000, consumer ratings do not increase with the price of the vehicle.
6) The brand analysis reveals that domestic manufacturer BYD's new energy vehicles are moderately priced and have high overall consumer satisfaction, making it the most mainstream new energy vehicle brand in the market. In the field of high-end new energy vehicles over RMB350,000, the domestic manufacturer Azera has the highest rating and is the mainstream choice for consumers to buy high-end new energy vehicles. Foreign brands have formed strong brands with high brand premiums.

Compared with previous studies, this study has some innovations, such as the use of Bert-wwm-ext model structure, which is more accurate compared with traditional machine learning algorithms and deep learning algorithms such as LSTM. In addition, this paper discusses the development status of BEV and PHEV from the perspective of consumers, as well as the development status of new energy vehicle brands at home and abroad,

to provide a referable path for the development direction of new energy vehicles.

Of course, there are some shortcomings in this study, such as this study is based on the data of the largest professional automotive communication platform in China, and the data classification is according to the existing classification of the platform, so the mined data may not reflect the relevant variables comprehensively. In addition, this study focuses on the selection of new energy vehicles under complex networks, but does not compare fuel vehicles and new energy vehicles [28–30].

Data availability

The data used to support the findings of this study are available from the corresponding authors upon request.

Author contributions

All authors listed have made a substantial, direct, and intellectual contribution to the work and approved it for publication.

Acknowledgments

The authors acknowledge the financial support from the National Social Science Fund of China (no. 19BH156), and Innovation Project of The University of Chinese Academy of Social Sciences.

Conflict of interest

The authors declare that the research was conducted in the absence of any commercial or financial relationships that could be construed as a potential conflict of interest.

Publisher's note

All claims expressed in this article are solely those of the authors and do not necessarily represent those of their affiliated organizations, or those of the publisher, the editors and the reviewers. Any product that may be evaluated in this article, or claim that may be made by its manufacturer, is not guaranteed or endorsed by the publisher.

References

1. Mock P, Yang Z. Driving electrification: A global comparison of fiscal incentive policy for electric vehicles. *Exp. Physiol.* (2013) 98(98): 1244–1246. doi:10.1113/expphysiol.2012.068940

2. Hill G, Heidrich O, Creutzig F, Blythe P. The role of electric vehicles in near-term mitigation pathways and achieving the UK's carbon budget. *Appl Energ* (2019) 251:113111. doi:10.1016/j.apenergy.2019.04.107

3. Li G, Luo R, Zhang H. The impact of promotion policies on the demand for new energy vehicles: Evidence from city and model level sales data. *J Shanghai Univ Int Business Econ* (2019) 26(02):49–58+68. doi:10.16060/j.cnki.issn2095-8072.2019.02.005

4. Diamond D. The impact of government incentives for hybrid-electric vehicles: Evidence from US states. *Energy Policy* (2008) 37(3):972–83. doi:10.1016/j.enpol.2008.09.094

5. Liu Y, Kokko A. Who does what in China's new energy vehicle industry? *Energy Policy* (2013) 57:21–9. doi:10.1016/j.enpol.2012.05.046

6. Green EH, Skerlos SJ, Winebrake JJ. Increasing electric vehicle policy efficiency and effectiveness by reducing mainstream market bias. *Energy Policy* (2014) 65: 562–6. doi:10.1016/j.enpol.2013.10.024

7. Jensen AF, Cherchi E, Mabit SL. On the stability of preferences and attitudes before and after experiencing an electric vehicle. *Transportation Res D: Transport Environ* (2013) 25:24–32. doi:10.1016/j.trd.2013.07.006

8. Xu G, Xu F. Study on the factors influencing the purchase decision of new energy vehicles. *China Popul Resour Environ* (2010) 20(11):91–5. doi:10.3969/j.issn.1002-2104.2010.11.016

9. Lieven T, Mühlmeier S, Henkel S, Waller JF. Who will buy electric cars? An empirical study in Germany. *Transportation Res Part D: Transport Environ* (2011) 16(3):236–43. doi:10.1016/j.trd.2010.12.001

10. Hoen A, Koetse MJ. A choice experiment on alternative fuel vehicle preferences of private car owners in The Netherlands. *Transportation Res A: Pol Pract* (2014) 61:199–215. doi:10.1016/j.tra.2014.01.008

11. Dumortier J, Siddiki S, Carley S, Cisney J, Krause RM, Lane BW, et al. Effects of providing total cost of ownership information on consumers' intent to purchase a hybrid or plug-in electric vehicle. *Transportation Res Part A: Pol Pract* (2015) 72: 71–86. doi:10.1016/j.tra.2014.12.005

12. Sovacool BK, Abrahamse W, Zhang L, Ren J. Pleasure or profit? Surveying the purchasing intentions of potential electric vehicle adopters in China. *Transportation Res Part A: Pol Pract* (2019) 124:69–81. doi:10.1016/j.tra.2019.03.002

13. Palmer K, Tate JE, Wadud Z, Nellthorp J. Total cost of ownership and market share for hybrid and electric vehicles in the UK, US and Japan. *Appl Energ* (2018) 209:108–19. doi:10.1016/j.apenergy.2017.10.089

14. Hidrue MK, Parsons GR, Kempton W, Gardner MP. Willingness to pay for electric vehicles and their attributes. *Resource Energ Econ* (2011) 33(3):686–705. doi:10.1016/j.reseneeco.2011.02.002

15. Prakash N, Kapoor R, Kapoor A, Malik Y. Gender Preferences for alternative energy transport with focus on electric vehicle. *J Soc Sci* (2014) 10(3):114–22. doi:10.3844/jssp.2014.114.122

16. Fan R, Dong L, Guo YW, Sun J. Study on the optimal supervision strategy of government low-carbon subsidy and the corresponding efficiency and stability in the small-world network context. *J Clean Prod* (2017) 168:536–50. doi:10.1016/j.jclepro.2017.09.044

17. Liao F, Molin E, Timmermans H, van Wee B. Consumer preferences for business models in electric vehicle adoption. *Transport Policy* (2019) 73:12–24. doi:10.1016/j.tranpol.2018.10.006

18. Maheshwari P, Seth N, Gupta AK. An empirical approach to consumer buying behavior in Indian automobile sector. *Ind Commercial Train* (2016) 48(3):156–62. doi:10.1108/ict-09-2015-0061

19. Mitchell VW, Prince G. *Retailing to experienced and inexperienced consumers: A perceived risk approach*. West Yorkshire, UK: International Journal of Retail & Distribution Management (1993). doi:10.1108/09590559310042323

20. Akalamkam K, Mitra JK. Consumer pre-purchase search in online shopping: Role of offline and online information sources. *Business Perspect Res* (2018) 6(1): 42–60. doi:10.1177/2278533717730448

21. Van denBulte CVD, Wuyts S. *Leveraging customer networks in the network challenge: strategy, profit, and risk in an interlinked world*. PR Kleindorfer Y Wind, Editors. Upper Saddle River, NJ: Pearson Education (2009). p. 243–58.

22. Wachter P, Widmer T, Klein A. Predicting automotive sales using pre-purchase online search datac. Proceeding of the 2019 Federated Conference on

Computer Science and Information Systems (FedCSIS). Leipzig, Germany. Sept. 2019. IEEE (2019) 1–4. doi:10.15439/2019F239

23. Liu Y. Word of mouth for movies: Its dynamics and impact on box office revenue. *J Marketing* (2006) 70(3):74–89. doi:10.1509/jmkg.70.3.74

24. Li H. *Statistical learning methods*. Beijing: Tsinghua University Press (2019). p. 193–213.

25. Devlin J, Chang MW, Lee K, Toutanova KB. Pre-training of deep bidirectional transformers for language understanding. In: *Naacl* (2018). p. 4171–86. doi:10.48550/arXiv.1810.04805

26. Vaswani A, Shazeer N, Parmar N, Uszkoreit J, Jones L, Gomez AN, et al. Attention is all you need. In: *Advances in neural information processing systems* (2017). p. 5998–6008. doi:10.48550/arXiv.1706.03762

27. Cui Y, Che W, Liu T, Qin B, Yang Z, Wang S, Hu G. *Pre-training with whole word masking for Chinese bert* (2019). arXiv preprint. doi:10.48550/arXiv.1906.08101

28. Xiong F, Wang X, Pan S, Yang H, Wang H, Zhang C. Social recommendation with evolutionary opinion dynamics. *IEEE Trans Syst Man Cybern Syst* (2020) 50(10):1–13. doi:10.1109/TSMC.2018.2854000

29. Xiong F, Liu Y, Cheng J. Modeling and predicting opinion formation with trust propagation in online social networks. *Commun Nonlinear Sci Numer Simulation* (2017) 44:513–24. doi:10.1016/j.cnsns.2016.09.015

30. Liu H, Lu S, Wang X, Long S. The influence of individual characteristics on cultural consumption from the perspective of complex social network. *Complexity* (2021) 2021:1–14. doi:10.1155/2021/7404690

frontiers | Frontiers in Physics

TYPE Original Research
PUBLISHED 27 September 2022
DOI 10.3389/fphy.2022.986605

OPEN ACCESS

EDITED BY
Fei Xiong,
Beijing Jiaotong University, China

REVIEWED BY
Yongjiao Yang,
Chongqing University, China
Wei Zhang,
Sichuan University, China
Hongshu Chen,
Beijing Institute of Technology, China

*CORRESPONDENCE
Rui Nan,
nr19841018@163.com
Jingjie Wang,
wjj15903360066@163.com

†These authors have contributed equally to this work and share first authorship

SPECIALTY SECTION
This article was submitted to Social Physics,
a section of the journal
Frontiers in Physics

RECEIVED 05 July 2022
ACCEPTED 11 August 2022
PUBLISHED 27 September 2022

CITATION
Nan R and Wang J (2022), Asymmetric evolutionary game analysis of emergency cooperative social networks for magnitude emergencies: Evidence from the Beijing-Tianjin-Hebei region in China.
Front. Phys. 10:986605.
doi: 10.3389/fphy.2022.986605

Asymmetric evolutionary game analysis of emergency cooperative social networks for magnitude emergencies: Evidence from the Beijing-Tianjin-Hebei region in China

Rui Nan*† and Jingjie Wang*†

School of Law and Humanities, China University of Mining and Technology, Beijing, China

Emergency cooperative social networks (ECSNs) play a very important role in emergency management for magnitude emergencies in China recently. Based on the data set of cooperative fight against COVID-19 of the Beijing-Tianjin-Hebei region in China, using social network analysis (SNA) and asymmetric evolutionary game model, this study finds that the asymmetry between regions is comprehensively determined by resource endowment, administrative level, geographical distance, regional vulnerability, political pressure and other factors; vertical control is still the main operating mechanism of ECSNs; network derivation is caused by the superposition of multiple factors, of which political factors are very important, and asymmetry may become an obstacle.

KEYWORDS

emergency cooperative social networks (ECSNs), magnitude emergencies, game theory, asymmetry, social network analysis (SNA)

1 Introduction

In the post-crisis era, magnitude emergencies occur frequently, involving multiple fields and spreading to a wide range. They have a large degree of influence and have complex characteristics, such as mass occurrence, diversity, and coupling of derivative secondary events. Therefore, it requires cross-regional emergency cooperation [1–3]. With the unified goal of managing magnitude emergencies, social actors at all levels in the region reach emergency cooperation relations through joint meetings, policy releases, exercises, resource assistance, and business guidance, and form the emergency cooperative social networks (ECSNs). The ECSNs are an effective organizational form to address magnitude emergencies, and have the function of coordinating emergency response, integrating emergency resources, and improving emergency response

effectiveness. This is crucial to the improvement and guarantee of emergency management capacity of countries all around the world. In recent years, literature on the ECSNs for magnitude emergencies has emerged, focusing mainly on the causes, structure, and effects of the networks, and focusing less on the operation and formation mechanisms of the networks. Therefore, based on the detailed analysis of the ECSNs, this paper analyzes their operation and formation mechanisms. This research answers three questions: 1) What are the characteristics of the ECSNs for magnitude emergencies? 2) What is the cooperation mechanism of the ECSNs for magnitude emergencies? 3) What is the mechanism of cooperative strategy selection of each subject in the networks? Based on the above questions, this paper takes the Beijing-Tianjin-Hebei (B-T-H) region in China as a sample and analyzes the emergency cooperation practices for COVID-19 from the following aspects: 1) The construction and analysis of the ECSNs for magnitude emergencies. Crawler and Social Network Analysis are used to search a large number of samples and obtain relevant data to build the ECSNs. Through the analysis of overall network characteristics, individual node attributes, and cohesive subgroup, the subject composition, connection, and operation mode of the ECSNs are deconstructed, and the cooperation mechanism is analyzed. 2) The asymmetric evolutionary game analysis of the ECSNs for magnitude emergencies. Emergency cooperation is accompanied by game behavior, and the subject strategy choice and its rules reflect the generation mechanism of the ECSNs. Asymmetry is a universal phenomenon that exists widely among the subjects in the networks. Therefore, this paper conducts asymmetric evolutionary game analysis on the ECSNs for magnitude emergencies to explore the generation mechanism and evolutionary influencing factors of the ECSNs.

The contributions of this study are significant both in theory and practice. First of all, different from the previous researches on the network structure and function at the macro level, this study makes a detailed analysis of the ECSNs structure in specific sample areas by comprehensively using the SNA, asymmetric dynamic evolutionary game and SD simulation method. On this basis, it analyzes the influencing factors, operation mechanism and generation mechanism, further focuses on the research perspective, and enriches and expands the existing researches from the meso-level. Second, the empirical analysis of the ECSNs in the B-T-H region of China can provide the world with Chinese wisdom and experience, explore the world's emergency cooperation problems with China as the incision, and provide experience for countries to improve the ECSNs and increase the quality of emergency cooperation.

The paper is arranged as follows: The second chapter summarizes the existing researches and puts forward relevant hypotheses based on the existing literatures. The third chapter introduce methods, samples and data. The fourth chapter introduces the results of social network analysis. The fifth chapter introduces the results of asymmetric evolutionary game analysis and SD simulation. The sixth chapter provides the conclusions of the study.

2 Literature review

The ECSNs is a dynamic structure formed by formal and informal cooperation between organizations of different types and scales in the context of crisis management [4, 5] having a positive role in promoting the sharing of information, financial resources and human capital, which is conducive to the improvement of emergency management efficiency [6].

The subjects in the ECSNs gather for common goals and are mutual stakeholders, and the asymmetry among stakeholders is a common problem in cooperative networks [7]. Traditional theories suggest that asymmetries of power are not conducive to the establishment of cooperative relationships [8]. This asymmetry is manifested in resource endowment, administrative level, geographical proximity, degree of disaster impact and other aspects [9–15]. If there is a serious asymmetry between network actors, the stronger party will take the initiative, and occupy the central position of the network and control network resources, while the weaker party will find it is difficult to participate effectively, leading to a crisis of confidence or void contract [6]. Moreover, the actors in the ECSNs are interconnected, which makes them vulnerable to each other's strategic behaviors [16]. In asymmetric power relations, the stronger organization may hijack the weaker organization for its own purposes [17], so that the weaker party will lose interest in participating in cooperation. Therefore, it is assumed that inter-agent asymmetry is not conducive to the formation and close operation of ECSN.

The ECSNs contribute to information transmission because of its multi-directional network connections, and its flexible and diverse network structure promotes the improvement of emergency efficiency. First of all, vertical control is the continuation of the bureaucracy structure under the conventional situation, and this mechanism has the rationality of system logic. From the perspective of institution, as part of the national administrative organization, local governments at all levels are accountable to higher levels of government. Tasks assigned by superiors are an important part of local government responsibilities. From the perspective of intrinsic motivation, obedience to leaders helps local governments maintain an edge in peer competition. In addition, as a representative of the central authority, the participating superior governments can reduce transaction costs and cooperation risks [18]. Therefore, vertical control by higher levels of governments helps to build trust and respect among local government entities at all levels and foster cooperative networks [19]. Second, in the theoretical framework proposed by Ansell and Gash (2007) [6], they point out that when the distribution of power is asymmetric or the motivation to

participate is weak, the success of cooperative governance requires leadership control. This proposition implies that vertical control is critical to social networks. Especially in China, the involvement of national/provincial governments will lead to more authoritative agreements [20]. Therefore, vertical control is assumed to be the dominant mechanism for the ECSNs, with other forms of cooperation as auxiliary.

Many studies have explored the causes of social networks. Based on previous studies, the essence of the formation of ECSNs can be summarized as follows: multi subjects form a cooperative network by establishing cooperative relations based on common emergency objectives (insert references), the causes of the network can be decomposed into the stimulation of environmental factors and the formation of emergency cooperative relations [21]. Some scholars have pointed out that environmental factors are the initial conditions for triggering social networks, especially the emergency management scenarios that give birth to ECSNs. For example, Bryson, Crosby, and stone (2006) propose a framework for understanding cross sector collaborations [22]. Some of the initial conditions for cooperation are environmental factors, such as turbulence and complexity. Head and Alford (2013) pointed out that major emergencies go beyond administrative levels and policy areas, and are complex, fuzzy and uncertain, forcing the generation of cooperative networks to deal with emergencies [23]. At the same time, the formation of emergency cooperation is caused by many factors. Social networks promote better performance through collective action rather than through individual organizational efforts [24–27]. And the development of the Internet, World Wide Web and smart mobile devices has also provided technical support for ECSNs and promoted the development process of online networks [28]. Under the Logic of Collective Action framework, authorities choose whether to participate in different mechanisms based on transaction costs and cooperation risks [29]. These factors are often intertwined, with many working together to build partnerships. Similarly, Emerson, Nabatchi, and Balogh (2012) suggested that cooperation is unlikely to continue without a combination of at least one or more other drivers (indirect incentives, interdependence, and/or uncertainty), which implicitly pointed to the generality of network generation [30]. It is worth noting that among many factors, political factor -- institutional pressure cannot be ignored. Wen Xuemei and Suo Liming (2020) pointed out that regional emergency cooperation becomes closer under political pressure [31]. In many centralized and federal systems, the central/federal governments use institutional pressure -- accountability mechanisms to enforce the will of the higher authorities at all levels below the state [32]. In China, local governance has similarities and differences with western countries [33, 34]. Considering the particularity of emergency situation, we assume that the ECSNs are caused by many factors, among which political factors have a greater impact.

Combined with the logic of network structure response operation mechanism, this paper chooses SNA to analyze the operation mechanism of ECSNs. Referring to the Logic of Collective Action framework to explain the formation mechanism of the social networks, considering the widespread existence of asymmetry between the actors in networks, the formation mechanism of the ECSNs is analyzed by using asymmetric evolutionary game combined with SD simulation analysis.

3 Methods, simples and data

3.1 Methods

3.1.1 Social network analysis (SNA)

SNA is an important method to study the interaction between action objects and the overall network structure. It provides a feasible tool for examining the structure and operation mode of a social system by visualizing the interaction between actors in the networks and evaluating them through a series of indicators [35, 36]. This paper analyzes the ECSNs for COVID-19 in the B-T-H region from overall network structure, individual network structure, and cohesive subgroup analysis.

3.1.1.1 Overall network structure

The ECSNs structure of the overall network is analyzed by measuring the density of the overall network. Density refers to the ratio of the actual number of connections in the network to the maximum possible number of connections, thereby reflecting the density of the ECSNs, and the value is between 0 and 1. The higher the network density, the closer the connection between the subjects.

3.1.1.2 Individual network structure

The indicators of individual network structure include degree centrality, betweenness centrality, and closeness centrality [37]. The network position of each subject in the ECSNs can be explored by calculating them.

Degree centrality. Degree centrality is the sum of points connected directly to other points. The central position and cooperation enthusiasm of each region in the ECSNs can be found by degree centrality analysis. Degree centrality is divided into absolute degree centrality ($C_D(n_i)$) and relative degree centrality ($C_D^{'}(n_i)$). Absolute degree centrality refers to the number of other points directly connected with the point. Relative degree centrality is the ratio of the absolute point centrality to the maximum possible degree of a point in the graph. The calculation formulas are as follows:

$$\boldsymbol{C_D(n_i) = d(n_i) = x_{i+} = \sum_j x_{ij} = \sum_j x_{ji}} \quad (1)$$

$$C_D^{'}(n_i) = d(n_i)/g - 1 \quad (2)$$

Considering the directivity of connection, the degree of centrality can be divided into out-centrality and in-centrality. Among them, out-degree centrality is the sum of a point pointing to other points, showing the degree of a region's concern on other regions. In-degree centrality is the sum of a point pointed by other points, showing the attention of a region and measuring its prominence. Its calculation formula is as follows:

$$C_D(v_i) = \sum_{i=1, i \neq j}^{n} d_i^{in} \quad (3)$$

$$C_D(v_i) = \sum_{i=1, i \neq j}^{n} d_i^{out} \quad (4)$$

Betweenness centrality. Betweenness centrality is the number of shortest paths to a point. It represents the extent to which one actor stands between the other two actors, namely, the ability to build bridges for other actors and the degree to which each region has control over emergency resources can be determined through the betweenness centrality analysis. Betweenness centrality is divided into absolute betweenness centrality and relative betweenness centrality and calculated by the ratio of geodesics at any other two points and the number of geodesics passing through that point (geodesics indicate the shortest distance between two points). The calculation formulas are as follows:

$$C_B(n_i) = \sum_{j<k} g_{jk}(n_i)/g_{jk} \quad (5)$$

$$C_B^{'}(n_i) = C_B(n_i)/[(g-1)(g-2)/2] \quad (6)$$

where g_{jk} represents the number of the shortest path connecting two actors, and $g_{jk}(n_i)$ represents the number of the shortest path connecting actors j and k including actor i.

Closeness centrality. Closeness centrality is the average length of the shortest path of each node to other nodes, and the greater the closeness centrality's value, the more it indicates that the point is not the core point of the network. The location of each region in the ECSNs can be determined by the closeness centrality analysis. The degree of closeness centrality is divided into absolute closeness centrality $[C_C(n_i)]$ and relative closeness centrality $[C_C^{'}(n_i)]$. The calculation method is to sum the distance of geodesic between the point and all other points and then derivative. The calculation formulas are as follows:

$$C_C(n_i) = \left[\sum_{j=1}^{g} d(n_i, n_j)\right]^{-1} \quad (7)$$

$$C_C^{'}(n_i) = \frac{g-1}{\sum_{j=1}^{g} d(n_i, n_j)} = (g-1)C_C(n_i) \quad (8)$$

3.1.1.3 Cohesive subgroup

A cohesive subgroup is a subset of actors in which there are relatively strong, direct, close, or positive relationships among the actors. The cohesive subgroup analysis can explore the subgroups in the network and their closeness, and refine the understanding of the structure and operation mode of the ECSNs. In this paper, the cohesive subgroup analysis of the ECSNs is carried out using clique and image matrix analyses.

Clique. The clique is a subset of actors whose relationships within the clique are closer than those outside the cliques. Clique analysis can explore the cliques and their components in the ECSNs. The calculation needs to reduce the dimension of the data "binarization" processing, the number greater than the critical value "0" is re-coded as "1", otherwise it is "0" (calculation Eq. 9). On this basis, the clique analysis in UCINET is used for clustering.

$$x_{ij}^{'} = \begin{cases} 1 & if\ x_{ij} > 0 \\ 0 & if\ x_{ij} = 0 \end{cases} \quad (9)$$

Image matrix. Image matrix analysis is a method to describe block type from the perspective of the overall network. The intimacy between subgroups can be obtained by image matrix analysis. The method of the a-density index was used to obtain the image matrix: the intimacy between each subgroup was compared with the overall network intimacy, and the value greater than the overall network intimacy (a) was recoded as "1", and vice versa as "0" to obtain the intimacy analysis table between each group. The calculation formula is as follows:

$$b_{klr} = \begin{cases} 0 & if\ \Delta_{klr} < \alpha \\ 1 & if\ \Delta_{klr} \geq \alpha \end{cases} \quad (10)$$

3.1.2 Asymmetric evolutionary game

Game theory is a branch of modern mathematics that can be used to study security issues and interactions between decision-makers competing for limited or shared resources [38–41]. Considering the asymmetry between the subjects and the dynamics of the game process, the asymmetric dynamic evolutionary game analyzes the game strategy of the cooperative subjects. In this paper, the asymmetric dynamic evolutionary game is used to deduce the choice of cooperation strategies between the actors in the ECSNs, and then the formation mechanism is analyzed.

First, the mathematical formula of asymmetry is obtained through literature summary and formula derivation. In other words, by introducing the rising Γ distribution exponential function, the multidimensional asymmetric indices are transformed into parameters in the form of a single index (Eq. 11). Normalized the index values to obtain the comprehensive value in each region (k_i) (Eq. 12). The asymmetry between the regions can be defined as $k_i/k_j\ (i, j \in 1, 2, \ldots, n, i \neq j)$, where ω_i represents the weight value of index P_i, which can be determined according to the analytic hierarchy process, and $0 < k_1 < 1$, and $\sum_{i=1}^{n} k_i = 1$. In particular, when considering the asymmetry between regions, it is defined as $k/(1-k)$ (Eq. 13).

TABLE 1 Region and abbreviation.

Region	Abbreviations
Beijing	BJ
Tianjin	TJ
Hebei	HB
Shijiazhuang	SJZ
Qinhuangdao	QHD
Tangshan	TS
Baoding	BD
Langfang	LF
Xingtai	XT
Handan	HD
Chengde	CD
Cangzhou	CZ
Hengshui	HS
Zhanjiakou	ZJK
The State Council	The State Council
Joint Prevention and control mechanism	JPCM
National health commission	NHS
Ministry of science and technology	MOST
Ministry of science and technology	the Ministry of Finance
Political Bureau of the Central Committee of the CPC	Political Bureau of the Central Committee of the CPC

$$Pi = \begin{cases} 0 & 0 \le x_i \le \delta \\ 1 - e^{-\eta \cdot (x_i - \delta)} & x_i > \delta \end{cases} \tag{11}$$

$$k_i = \frac{\omega_i P_i}{\sum_{i=1}^{n} \omega_i P_i} \tag{12}$$

$$\mu = k/(1-k) \tag{13}$$

Second, on the premise of considering asymmetry, mathematical calculation is conducted on the causes of the strategies selection in each region through the construction and solution of the model. The optimal solution is obtained by constructing Nash equilibrium and the evolutionary phase diagram is drawn to deduce the formation mechanism of the ECSNs.

3.1.3 SD simulation

SD simulation refers to the process of simulating an evolutionary game with system dynamics. The results of the asymmetric evolutionary game can be verified through SD simulation analysis, and the effects of the various factors on the evolution of the ECSNs can be analyzed.

First, the value of other variables is kept unchanged, and by adjusting the value of the asymmetry index k_i in each region, the influence of the asymmetry index on the evolution of the ECSNs is analyzed, and the conclusion of the asymmetric evolutionary game is verified.

Second, by adjusting the additional cost indices (θ, β) of emergency cooperation, the influence of the additional cost on the evolution of the ECSNs was investigated under the two conditions of one party's negative cooperation and both parties' negative cooperation. The influence of economic factors on the evolution of the ECSNs is also explored.

The effects of punishment intensity on the evolution of the ECSNs for magnitude emergencies was explored by adjusting the additional punishment index (λ) and punishment value (F). The influence of political pressure on the ECSNs is explored.

3.2 Samples and data

3.2.1 Samples

In this paper, the B-T-H region is selected as the research sample of the ECSNs.[1] The reasons are as follows. First, as the most typical urban agglomeration in China, the GDP of the B-T-H region accounts for 44% of the national total, and is a municipality directly under the Central Government and the capital. It has crucial political and economic status. Second, regional cooperation is durable and stable. As early as 2014, the emergency offices of Beijing, Tianjin, and Hebei jointly signed the Emergency Management Cooperation Agreement of Beijing,

1 There are 11 prefecture level cities in Hebei Province, including Shijiazhuang, Tangshan, Qinhuangdao, Handan, Xingtai, Baoding, Zhangjiakou, Chengde, Cangzhou, Langfang and Hengshui.

TABLE 2 Text codes and examples related to the emergency cooperation for COVID-19 in the B-T-H region.

	time	collaborative content	subject		Scale	level
			active	passive		
1	2020.11.28-29	*Some opinions on strengthening the construction of public health emergency management system in the capital*	Beijing	Tianjin-Hebei	multilateral	province
2	2020.02.25	Video conference on joint epidemic prevention and control in Beijing-Tianjin-Hebei region	B-T-H		multilateral	province
.....	.....	.....	.....	.....	.....	.....

Tianjin, and Hebei Province and held the joint meeting, providing an institutional guarantee for future emergency cooperation. A working mechanism for the COVID-19 prevention and control was established in 2020, providing stable support for regional cooperation in emergency management. Third, the administrative level and boundary structure of this region are relatively complex, and involves not only the coordination and cooperation between inter-provincial cities but also the vertical coordination at different levels, such as municipalities directly under the Central Government, provinces, sub-provincial cities, and prefecture-level cities. Fourth, the epidemic of COVID-19 at the end of 2019 has brought a huge effect of the world's public health system. China has achieved good results in the fight against the epidemic. Among them, the B-T-H region has achieved remarkable results in emergency cooperation, providing Chinese solutions and wisdom for the world's emergency cooperation.

3.2.2 Data

The data searched in this paper were from the official websites of the Central Government, Hebei, Beijing, Tianjin, 11 prefecture-level cities in Hebei (See Table 1), and the websites of the Health Commission. The time limit was from December 2019 to December 2021.

This study uses big data techniques to crawl and download the emergency cooperation information stored on the websites of local governments and the health commission. Because it is impossible to download massive website data directly, it is realized by writing programs. *Python* is a programming language library that provides efficient data structures for simple and effective object-oriented programming. It has been widely used in Web site development, artificial intelligence, spatial statistics, and other applications. In this study, we use the *Python* software to code 28 sets of programming languages, which can be divided into two steps, keywords search and content search to crawl and store data in relevant websites in various regions. On the basis of data collection, data screening and coding are carried out. First, the collected data are cleaned, that is, the retrieval results are manually selected, and the reports that do not involve the sample urban agglomeration, are not related to the research content, and do not belong to the research time range are removed to make them meet the sample conditions. Second, the report is structured by encoding from five dimensions: time, collaboration content, collaboration subject, collaboration scale, and collaboration level. Among them, the dimension of the cooperation subject is divided into positive and negative. If there is a joint document, joint attendance of meetings, long-distance investigation, or cooperation between cities, the host of the meeting, the support party, and the observer party shall be regarded as the positive cooperation subjects, while the others shall be regarded as the negative cooperation subjects. The collaboration level includes provincial, municipal, province-municipal, and central participation (Table 2). The multi-valued directed cooperation matrix is constructed through relational assignment. That is, the relationship is assigned based on structured coding. If the two places jointly send out a document or take joint action, 1 is added to the value of the emergency cooperation between the positive party, while the negative party remains unchanged.

The crawler function of *Python* was used to identify and store the regional emergency cooperation reports within the scope of data search, supplemented by manual screening, and finally, there were 153 reports left.

4 Construction and analysis of the ECSNs

4.1 ECSNs construction

Using the sorted multi-valued directed relation matrix, Net Draw software was used to draw the ECSNs map of COVID-19 in the B-T-H region (Figure 1). Each region is represented as a point, and the connection between regions is represented as a line. The ECSNs for COVID-19 in the B-T-H region have the following characteristics.

(1) The subjects of emergency cooperation are diverse. The cooperation subjects in the ECSNs involve central,

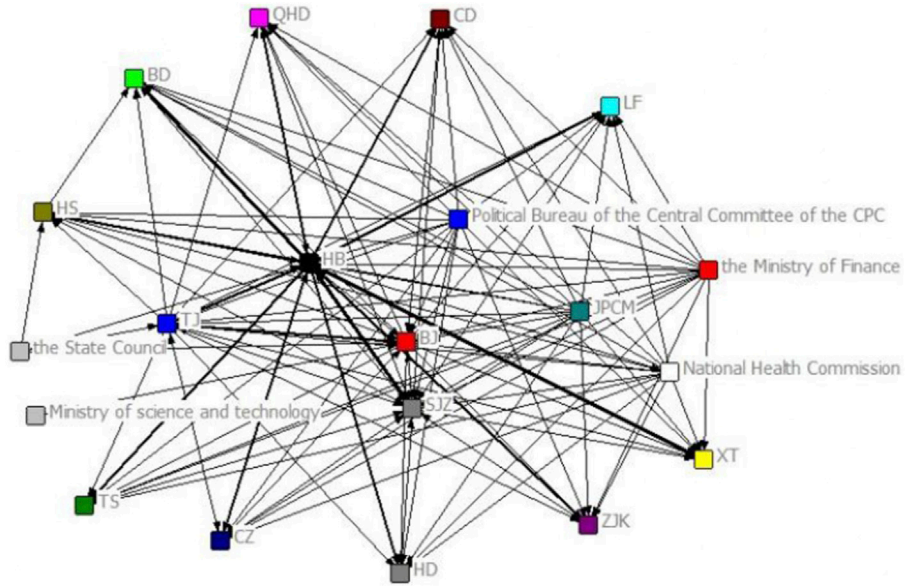

FIGURE 1
map of the ECSNs for COVID-19 in the B-T-H region.

provincial, and municipal levels. The central level includes the State Council, the Political Bureau of the Central Committee of the CPC, the National Health Commission, the Ministry of Science and Technology, the Ministry of Finance, and the State Council's Joint Prevention and Control Mechanism (JPCM) for the COVID-19. At the provincial level, it includes Beijing, Tianjin, and Hebei. The municipal level includes 11 cities in Hebei.

(2) The contacts between emergency cooperation subjects are multi-directional. The ECSNs have three types of network connections for emergency cooperation subjects: vertical, horizontal, and mixed connections. Vertical connection refers to the emergency cooperation between superior and subordinate administrative regions, including the cooperation between the central government and provinces and the cooperation between Beijing, Tianjin, Hebei, and 11 cities in Hebei. Horizontal connection refers to the emergency cooperation between regions at the same administrative level, including the cooperation at the central level, the cooperation between Beijing, Tianjin, and Hebei at the provincial level, and the cooperation between 11 cities in Hebei at the municipal level. The mixed connection refers to the connection inspired by the sudden and complex governance situation, which breaks through the restrictions of levels, regions, and departments, including the cooperation among the JPCM, provincial, and municipal regions.

(3) The structure of the ESCNs is dynamic. The network actors and their relationships in the ECSNs will change with the emergency and finally lead to the network structure with dynamic debugging. That is, the emergency has given birth to the sudden emergence of the JPCM, and resulted in temporary network connections, thereby leading to the structure of the ECSNs under the emergency, and the realization of the dynamic transformation and upgrading of the normal ECSNs.

4.2 ECSNs analysis

4.2.1 Overall network structure

The calculations of the UCINET shows that 132 connection lines can be found in the ECSNs for COVID-19 between regions in the B-T-H region (Figure 1) with an overall network density of 0.33, indicating a relatively close overall connection. At the same time, the mean value of the central potential of the overall network is 43.75, with a high-value number, indicating that a few subjects in the B-T-H region are in the center of the network, and the power of the ECSNs for magnitude emergencies is relatively concentrated. According to the map of the ECSNs, Beijing, Tianjin, and Hebei are at the center of the social network.

4.2.2 Centrality

4.2.2.1 Degree centrality

According to the degree centrality analysis, provincial (municipal) governments are at the center of the ECSNs for COVID-19 in the B-T-H region, and longitudinal coordinated leadership is its dominant mechanism. First, provincial

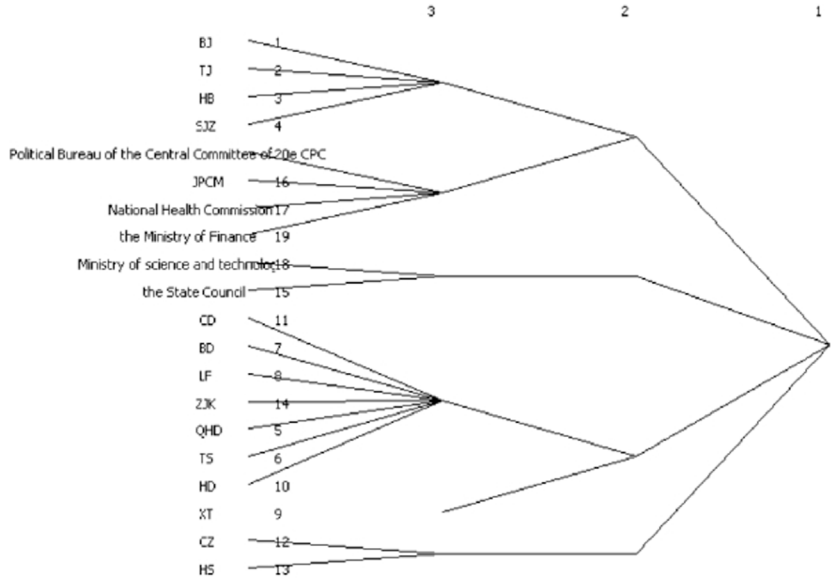

FIGURE 2
Clique analysis of the ECSNs for COVID-19 in the B-T-H region.

(municipal) governments occupy the position of cooperation center. Based on the ranking of the centrality of each subject and the thickness of the connection between subjects in Figure 1, the provincial governments, such as Beijing, Tianjin and Hebei are in the absolute network center position. It shows that the three governments have more power and resources in emergency cooperation, the highest participation and the strongest importance in the ECSNs, and a high degree of emergency cooperation with each other. Second, longitudinal coordinated leadership is its dominant mechanism of emergency management. Here is a response to hypothesis 2. It can be seen that the governance mechanism in the normal governance scenario will have spill over effects on the emergency governance scenario. This phenomenon is caused by the following reasons: 1) the rationality of the bureaucratic system. This point echoes the existing research and reaches a consensus. This system has been continued from the last century to the present, and has been recognized and used by various countries, which proves that it has the rationality of institutional logic. As a governance situation parallel with the normal governance, emergency management can also adopt this governance mechanism. 2) The ECSNs is not yet mature and complete. The situation of emergency governance is not only the same as that of normal governance, but also has higher requirements on governance efficiency and cooperation degree. The bureaucratic system represented by vertical control does not have these advantages, so it is difficult to determine that vertical control is the most suitable governance mode. But due to the present stage countries have not been able to set up flat for emergency management, the collective organization, is also not able to improve the precision of power distribution way, although the organizations established in emergency situations temporary relations of cooperation, but the norm management system still plays a leading role to its, therefore cooperation motivation and persistence are hard to guarantee, It still needs vertical control as the dominant mechanism to guarantee it. Combined with directed relationship, the out-degree centrality of Hebei province and central ministries are significantly higher than the in-degree centrality, which indicates that the Central Government and Hebei province play an important role in promoting intra-network emergency cooperation. At the central level, the National Health Commission and State Council have a high degree of centrality, indicating that the Central Government has a high degree of intervention in emergency cooperation. That is, the vertical promotion and leadership coordination of the Central Government has played a non-negligible role in the formation of the ECSNs. With the exception of Hebei province, the out-degree centrality is greater than in-degree centrality, and the in-degree centrality is greater than out-degree centrality in other cities in Hebei province, indicating that the mechanism of emergency cooperation within the province is top-down leadership and assistance (Table 3).

4.2.2.2 Betweenness centrality

Table 4 shows the betweenness centrality of Beijing, Tianjin, Hebei, and Shijiazhuang is high, accounting for 99.5% of the total. It shows that these organizations occupy the important

TABLE 3 Degree centrality analysis of the ECSNs for COVID-19 in the B-T-H region.

	OutDegree	InDegree	NrmOutDeg	NrmInDeg
BJ	88	67	4.4534	3.3907
TJ	97	50	4.9089	2.5304
HB	867	66	43.8765	3.3401
SJZ	13	143	0.6579	7.2368
QHD	3	86	0.1518	4.3522
TS	2	87	0.1012	4.4028
BD	2	101	0.1012	5.1113
LF	2	88	0.1012	4.4534
XT	5	96	0.2530	4.8583
HD	2	81	0.1012	4.0992
CD	3	84	0.1518	4.2510
CZ	8	91	0.4049	4.6053
HS	8	83	0.4049	4.2004
ZJK	2	87	0.1012	4.4028
The State Council	4	0	0.2024	0.0000
JPCM	18	0	0.9109	0.0000
NHS	58	1	2.9352	0.0506
MOST	1	0	0.0506	0.0000
the Ministry of Finance	14	0	0.7085	0.0000
Political Bureau of the Central Committee of the CPC	14	0	0.7085	0.0000

TABLE 4 Betweenness centrality analysis of the ECSNs for COVID-19 in the B-T-H region.

	Betweenness	n-Betweenness
BJ	28.4167	8.3090
TJ	5.4167	1.5838
HB	31.9167	9.3324
SJZ	94.7500	27.7047
QHD	0.0000	0.0000
TS	0.0000	0.0000
BD	0.0000	0.0000
LF	0.0000	0.0000
XT	0.0000	0.0000
HD	0.0000	0.0000
CD	0.0000	0.0000
CZ	0.0000	0.0000
HS	0.5000	0.1462
ZJK	0.0000	0.0000
The State Council	0.0000	0.0000
JPCM	0.0000	0.0000
NHS	0.0000	0.0000
MOST	0.0000	0.0000
the Ministry of Finance	0.0000	0.0000
Political Bureau of the Central Committee of the CPC	0.0000	0.0000

TABLE 5 Closeness centrality analysis of the ECSNs for COVID-19 in the B-T-H region.

	InFarness	OutFarness	InCloseness	OutCloseness
BJ	26.0000	115.0000	73.0769	16.5217
TJ	29.0000	115.0000	65.5172	16.5217
HB	27.0000	114.0000	70.3704	16.6667
SJZ	21.0000	115.0000	90.4762	16.5217
QHD	30.0000	126.0000	63.3333	15.0794
TS	30.0000	128.0000	63.3333	14.8438
BD	29.0000	128.0000	65.5172	14.8438
LF	30.0000	128.0000	63.3333	14.8438
XT	30.0000	128.0000	63.3333	14.8438
HD	30.0000	128.0000	63.3333	14.8438
CD	30.0000	127.0000	63.3333	14.9606
CZ	30.0000	124.0000	63.3333	15.3226
HS	29.0000	124.0000	65.5172	15.3226
ZJK	30.0000	128.0000	63.3333	14.8438
The State Council	380.0000	106.0000	5.0000	17.9245
JPCM	380.0000	96.0000	5.0000	19.7917
NHS	45.0000	114.0000	42.2222	16.6667
MOST	380.0000	110.0000	5.0000	17.2727
the Ministry of Finance	380.0000	96.0000	5.0000	19.7917
Political Bureau of the Central Committee of the CPC	380.0000	96.0000	5.0000	19.7917

position of bridge nodes and have strong influence and control over other cooperative entities. From the perspective of organizational structure, this may be related closely to its administrative level. The provincial government, as the administrative level between the central and local governments, and Shijiazhuang, as the capital of Hebei province, play an organizational and coordination role, and the characteristics of organizational structure affect its position in the ECSNs.

4.2.2.3 Closeness centrality

Table 5 shows that the ECSNs for COVID-19 in the B-T-H region exhibit the characteristics of close cooperation between provinces and cities with the help of the Central Government. The results of the data analysis show that at the central level, except for the Health Commission, the closeness centrality degree of other organizations is relatively small, indicating that the Health Commission is the main organization promoting emergency cooperation at the central level, and the other organizations play the role of coordination and assistance, located at the edge of the network. At the provincial level, a small gap in the value of closeness to the center can be observed, indicating that the three provinces and cities are closely linked, and the information and resources are interoperable among organizations. According to the background, there are three reasons: 1) The spillover of major public health emergencies forced neighboring regions to cooperate in emergency response. Due to its own characteristics, the COVID-19 pandemic has the characteristics of spillover, which will produce negative externalities on neighboring areas. In the face of local communities of interests, it has created the realistic need for emergency cooperation. 2) The three places have a realistic basis for emergency cooperation. As mentioned above, the three places have signed an emergency cooperation agreement, held regular cooperation meetings, and established a joint prevention and control mechanism to provide stable support for their cooperation. 3) The central government's administrative pressure boosts emergency cooperation. In accordance with the above conclusions, the vertical control mechanism is still the dominant mechanism of emergency cooperation. Therefore, the central government exerts hierarchical capabilities to promote the formation of emergency cooperation.

4.2.3 Cohesive subgroup

4.2.3.1 Clique

According to the clique analysis, provinces (municipalities) are the core component of the ECSNs for COVID-19 in the B-T-H region, and regions at the same administrative level are more likely to cooperate and form emergency cooperation. The calculation results of the clique analysis show that there are six cliques in the ECSNs (Figure 2), among which, the first clique composed of Beijing, Tianjin, Hebei, and Shijiazhuang occupies

TABLE 6 Image matrix analysis of the ECSNs for COVID-19 in the B-T-H region.

	1	2	3	4	5	6
1(BJ、TJ、HB、SJZ)	1	0	0	1	1	1
2(NHS ETC.)	1	0	0	1	1	1
3(MOST ETC.)	1	0	0	0	0	0
4(TS ETC.)	1	0	0	0	0	0
5(BD,CD)	1	0	0	0	0	0
6(CZ、HS)	1	0	0	0	0	0

the core position of the ECSNs and has the closest emergency cooperation among them. In addition, the analysis shows that national ministries, provinces, and cities are more likely to form cooperative relations with regions at the same administrative level.

4.2.3.2 Image matrix

Table 6 shows the results of the image matrix analysis.

First, close links between provinces and cities in Beijing, Tianjin, and Hebei can be observed. From Table 6, the first clique and the fourth, fifth, and sixth cliques are closely connected, indicating a strong bi-directional cooperation willingness among provinces and cities in B-T-H and a close relationship in emergency cooperation. The results show that the normal coordination mechanism in B-T-H produces positive externalities and causes them to overflow in emergencies. The geographical closeness of the three places makes them a community of interest in the face of the epidemic, generating endogenous impetus for emergency cooperation. The high position of the Central Government promotes the increase in the closeness of emergency cooperation.

Second, the emergency cooperation between the Central Government and the region of B-T-H is unilateral resource input and cooperation promotion. From Table 6, the second and third cliques unilaterally show a high degree of closeness to the first clique, which indicates that the cooperation path between the Central Government and B-T-H is top-down resource input and command coordination. Immediately after the outbreak of COVID-19, the Central Government set up the JPCM for COVID-19 and provided instructions and resources to assist the coordinated emergency response in the B-T-H region. These inputs can be categorized as political pressure and emergency assistance exerted by the Central Government on the three regions to promote their emergency cooperation.

Third, cities at prefecture-levels in Hebei do not have close cooperation between cities. Table 6 shows that the 11 cities in Hebei are scattered into three cliques. Considering that the first clique shows a high degree of closeness to the fourth, fifth, and sixth cliques, the emergency cooperation in the province is manifested mainly in the vertical cooperation between provinces and cities, while there is less horizontal cooperation between prefecture-level cities. The main reason is that although the prefecture-level cities in Hebei belong to the same administrative level, the geographical distance is different, and their economic development level differs greatly from the emergency demand. Large differences can also be found in the administrative level, economic development level, and emergency demand between Hebei and its prefecture-level cities. However, the provincial government has political responsibility for the emergency effect on prefecture-level cities because of its administrative subordination in Hebei province. Therefore, in the context of emergency response, political factors break through hierarchical constraints, affect the willingness for emergency cooperation, and political pressure is an important factor in the formation of the ECSNs in the B-T-H region. This responds to hypothesis 2

Based on the SNA analysis of the ECSNs for COVID-19 in the B-T-H region, it can be concluded that the operation mechanism of the ECSNs for magnitude emergencies is multi-directional coordination and cooperation between local governments led by vertical control, and its operation is characterized by multiple subjects, multiple connections, and dynamic structure.

5 Asymmetric evolutionary game analysis

The ECSNs are formed by the connection of various emergency subjects and their emergency cooperation relations. The combination of the different strategies among the subjects leads to different cooperative relationships and derives different ECSNs. Therefore, this paper will use an asymmetric evolutionary game to explore emergency strategy selection of each subject in the ECSNs and explore the formation mechanism of the ECSNs.

5.1 Basic assumptions

Hypothesis 1. Assume that the game subject is the central-provincial-municipal governments in the ECSNs. Local governments (provincial-municipal governments) are the leading force of emergency management, and their strategic choice based on the actual situation determines the cooperative relationship between local governments and other places. And the establishment of emergency cooperation requires at least the combination of cooperative strategies of the local governments of the two places. Therefore, based on the research

samples, this paper sets the game subject as the central-provincial-municipal governments in the ECSNs and discusses the selection process of the pair emergency cooperation strategies between them.

Hypothesis 2. Both governments adopt two strategies to participate in emergency cooperation, namely, "positive cooperation" and "negative cooperation" (including non-cooperation), namely, the strategy set is {positive, negative}, denoted as $(g1, g2)$ and $(f1, f2)$. The corresponding strategy selection probabilities are x, $1-x(0 \le x \le 1)$; $y, 1-y(0 \le y \le 1)$.

Hypothesis 3. Assume a basic income R used to represent the comprehensive income when both governments adopt positive cooperation strategies in emergency cooperation. When the government of one party is negative in emergency cooperation, the comprehensive emergency income is damaged, and the comprehensive emergency income is set as αR, $(0 \le \alpha \le 1)$. The comprehensive emergency benefit is γR when both parties adopt negative cooperative strategies.

Hypothesis 4. :Assume a basic cost C to represent the sum of costs incurred when both governments choose positive strategies. If only one party chooses the negative strategy, that is, the cooperation is not smooth, and the cooperation cost will increase because of the communication and coordination between the two parties. The following two situations may exist: 1) when only one party chooses the negative strategy, the rising cost, θC, is borne by the party that chooses the positive cooperation and meets the requirement of $0 < \theta < 1$. 2) When both parties choose the negative strategies, both parties need to pay the rising costβC, and satisfy$0 < \theta < \beta < 1$.

Hypothesis 5: In the ECSNs, the superior governments retain supervision responsibility for the actions of the subordinate governments. Therefore, if the cooperation is not smooth, the superior governments will punish the governments for the negative cooperation between the two parties. A basic punishment F is assumed to represent the punishment imposed by a superior government for unilateral negative cooperative strategies. When both governments adopt the negative cooperation strategies, the superior government adjusts the basic punishment F through coefficient λ $(\lambda \ge 1)$, which is used to punish the two governments.

5.2 Model construction

5.2.1 Regional asymmetry

In the ECSNs for COVID-19 in the B-T-H region, the administrative level, resources endowment, fragile degree, and degree of geographical approaches of each region differ, making the local governments form an asymmetric relationship between cooperation and dependence and leadership and being led in the emergency cooperation, resulting in widespread asymmetry in the emergency cooperation. This asymmetry is also reflected in the resource-advantageous parties being more likely to occupy a dominant position in emergency cooperation [9], and regional emergency cooperation becomes closer under political pressure. Regions with roughly equal administrative levels and geographically close regions are more likely to form cooperative relationships. The regions hardest hit by the crisis have a stronger willingness to cooperate and receive greater assistance [42]. Therefore, based on the model of asymmetric evolutionary game, this paper discusses the strategy selection and evolution process of local governments in emergency cooperation and attempts to deduce the formation mechanism of the ECSNs.

TABLE 7 Payment matrix of local governments in emergency cooperation.

Region B (1- k) Region A(k)	Active (y)	Passive (1-y)
Active (x)	$(R-C)/4k$	$(\alpha R-C)/4k-\theta C$
	$(R-C)/4(1-k)$	$(\alpha R-C)/4(1-k)-F$
Passive (1-x)	$(\alpha R-C)/4k-F$	$\frac{\gamma R-(1+\beta)C-\lambda F}{4k}$
	$(\alpha R-C)/4(1-k)-\theta C$	$\frac{\gamma R-(1+\beta)C-\lambda F}{4(1-k)}$

5.2.2 Construction and solution

The choice of local governments strategy includes three cases: 1) Both sides choose the positive cooperation strategy, then the local governments with power value of k can obtain the revenue $(R-C)/4k$, and the local governments with the power value of $1-k$ can obtain the revenue $(R-C)/4(1-k)$. The denominator is divided by 4 to return to the traditional equilibrium evolutionary game analysis when $k = 1/2$. 2) Both parties adopt the negative cooperation strategy, and the local governments with the strength value of k can obtain the benefits of $\frac{\gamma R-(1+\beta)C-\lambda F}{4k}$, and the game with the strength value of $1-k$ can obtain the income of $\frac{\gamma R-(1+\beta)C-\lambda F}{4(1-k)}$. 3) One party adopts a positive cooperation strategy and the other adopts a negative cooperation strategy. There are two situations. First, when region A with a power value of k chooses a positive cooperation strategy, and region B with a power value of $(1-k)$ chooses negative cooperation strategy, the two regions obtain $(\alpha R-C)/4k-\theta C$ and $(\alpha R-C)/4(1-k)-F$, respectively. Second, when region A with a power value of k chooses the strategy of negative cooperative, and region B with a power value of $(1-k)$ chooses the strategy of positive cooperative, the two regions get $(\alpha R-C)/4k-F$ and $(\alpha R-C)/4(1-k)-\theta C$, respectively. The payment matrix is shown in Table 7.

The average revenue of local government A is:

$$\begin{aligned}\overline{V}A &= xV_{A1} + (1-x)V_{A2}\\ &= xy(R-C)/4k + x(1-y)[(\alpha R - C)/4k - \theta C]\\ &\quad + (1-x)y[(\alpha R - C)/4k - F]\\ &\quad + (1-x)(1-y)\left[\frac{\gamma R - (1+\beta)C - \lambda F}{4k}\right]\\ &= \frac{x\{R[(\gamma-2\alpha)y - 2\gamma + \alpha] + y(1+4F)\} + [(\alpha-\gamma)Ry + 2\gamma R - C - 4kyF]}{4k}\end{aligned} \tag{14}$$

Therefore, the dynamic replication equation of local government A is:

$$\begin{aligned}F(x) &= \frac{dx}{dt} = x(V_{A1} - \bar{V}_A)\\ &= x(1-x)/4k\{y(R-C) + (1-y)[(\alpha R - C) - 4k\theta C]\\ &\quad + y[(\alpha R - C) - 4kF] + (1-y)[\gamma R - (1+\beta)C - \lambda F]\}\\ &= (1-x)/4k\langle y\{(1-\gamma)R - C + 4k\theta + (1+\beta)C - (4k+\lambda)F\}\\ &\quad + \{(a+\gamma)R + \beta C - 4k\theta - \lambda F\}\rangle\end{aligned} \tag{15}$$

Similarly, the replication dynamic equation of local government B can be written:

$$\begin{aligned}G(x) &= \frac{dy}{dt} = x(V_{B1} - \bar{V}_B)\\ &= \frac{y(1-y)}{4(1-k)}\{x[(1-a)R + (4-4k-\lambda)F + (1+\beta)]\\ &\quad + [(a-\gamma)R + \beta C - 4\theta(1-k) + \lambda F]\}\end{aligned} \tag{16}$$

Analysis of the above dynamic replication equation shows that the system has five equilibrium points (0,0) (0,1) (1,0) (1,1) $(\frac{(\gamma-a)R-\beta C+4\theta(1-k)-\lambda F}{(1-a)R+(4-4k-\lambda)F+(1+\beta)}, \frac{\lambda F+4k\theta-(a+\gamma)R-\beta C}{(1-\gamma)R-C+4k\theta+(1+\beta)C-(4k+\lambda)F})$.

$$\begin{aligned}\text{Set} f(y) = \langle y\{(1-\gamma)R - C + 4k\theta + (1+\beta)C - (4k+\lambda)F\}\\ + \{(a+\gamma)R + \beta C - 4k\theta - \lambda F\}\rangle\end{aligned} \tag{17}$$

$$\begin{aligned}g(x) = \{x[(1-a)R + (4-4k-\lambda)F + (1+\beta)] + [(a-\gamma)R\\ + \beta C - 4\theta(1-k) + \lambda F]\}\end{aligned} \tag{18}$$

Further analysis of the Jacobian matrix of the system can be obtained:

$$J = \begin{bmatrix} f(y)(1-2x)/4k & x(1-x)\{(1-\gamma)R - C + 4k\theta + (1+\beta)C - (4k+\lambda)F\}/4k \\ g(x)(1-2y)/4k & y(1-y)[(1-a)R + (4-4k-\lambda)F + (1+\beta)]/4k \end{bmatrix} \tag{19}$$

By calculating the value $Det(J)$and Trace $Tr(J)$ of determinant, it can be seen that (0,0) and (1,1) are not evolutionary stable points (1,0) and (0,1) are evolutionary stable points, and $(\frac{(\gamma-a)R-\beta C+4\theta(1-k)-\lambda F}{(1-a)R+(4-4k-\lambda)F+(1+\beta)}, \frac{\lambda F+4k\theta-(a+\gamma)R-\beta C}{(1-\gamma)R-C+4k\theta+(1+\beta)C-(4k+\lambda)F})$is saddle point. Therefore, the evolutionary game phase diagram of positive and negative cooperation between governments is shown in Figure 3.

It is easy to know from the above analysis $(x, y) = (\frac{(\gamma-a)R-\beta C+4\theta(1-k)-\lambda F}{(1-a)R+(4-4k-\lambda)F+(1+\beta)}, \frac{\lambda F+4k\theta-(a+\gamma)R-\beta C}{(1-\gamma)R-C+4k\theta+(1+\beta)C-(4k+\lambda)F})$is a

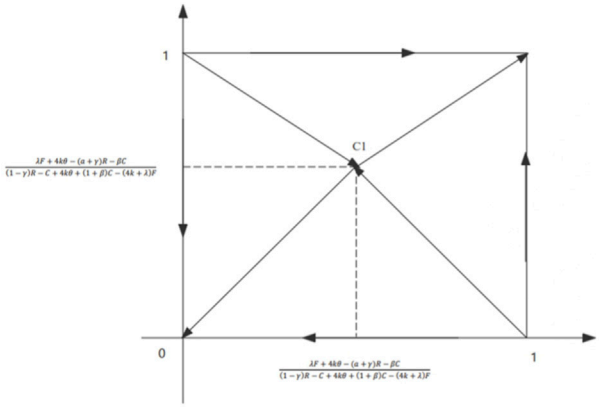

FIGURE 3
Game phase diagram.

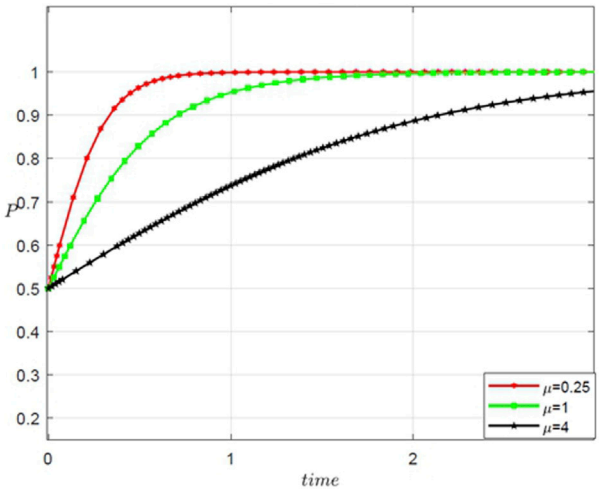

FIGURE 4
The influence of asymmetric (μ) on the evolution of ECSNs.

mixed strategy Nash equilibrium. In order to better analyze the positive cooperative intention x, Let $\mu = \frac{k}{1-k}$ denote asymmetry, then the value of x is converted to:

$$X = \frac{(\mu+1)(\gamma-a)R - (\mu+1)\beta C + 4\theta - (\mu+1)\lambda F}{(\mu+1)(1-a)R + 4F - (\mu+1)\lambda F + (1+\beta)(\mu+1)} \tag{20}$$

Derivative of $\mu$for the expression of region A's positive willingness to cooperate:

$$\begin{aligned}X'_{(\bar{\mu})} &\frac{-\lambda F^2 + [(\gamma-a)R]F + (\lambda\theta - \beta C)F - \theta(1-a) + (1+\beta)}{\{(\mu+1)(1-a)R + 4F - (\mu+1)\lambda F + (1+\beta)(\mu+1)\}^2}\\ &= \frac{F[-\lambda F + (\gamma-a)R - \beta C + \lambda\theta] - [\theta(1-a) + (1-\beta)]}{\{(\mu+1)(1-a)R + 4F - (\mu+1)\lambda F + (1+\beta)(\mu+1)\}^2}\end{aligned} \tag{21}$$

Considering that $0 < \theta, \beta, a < 1$, and $F, R, C \gg \theta, \beta, a$, since $\gamma < a$. So $|[-\lambda F + (\gamma - a)R - \beta C + \lambda\theta]| \gg |[\theta(1 - a) + (1 - \beta)]|, F[-\lambda F + (\gamma - a)R - \beta C + \lambda\theta] - [\theta(1 - a) + (1 - \beta)] < 0, X'_{(\mu)} < 0$

Therefore, the emergency cooperation willingness is inversely proportional to the asymmetric index μ, that is, the larger μ, the smaller the positive emergency cooperation willingness x between the two governments. This responds to hypothesis 1. To analyze the causes of its reality and academic theory, first of all, the different geographical location leads to the similarities and differences of regional cooperation willingness. Geographical proximity is directly proportional to the spillover effect of disasters, so the more neighboring regions have deeper interests in this scenario, the easier it is to reach emergency cooperation. Secondly, the unequal administrative level leads to the similarities and differences in the willingness of emergency cooperation among different regions. The asymmetry of administrative level contains the inequality of political status, especially under the current bureaucratic system, the emergency willingness of vulnerable regions is more easily ignored. Again, differences in cooperation needs lead to differences in emergency cooperation willingness. The need for emergency cooperation is determined by the emergency situation of different places, so the similarities and differences of emergency cooperation needs are inevitable. The greater the need for cooperation, the more likely it is to produce the collective action dilemma of "free riding", leading to the similarities and differences of emergency cooperation willingness.

5.3 SD simulation

MATLAB is used to describe the mathematical model of the ECSNs for magnitude emergencies to describe the influence of each parameter value in the ECSNs more intuitively and deduce the formation mechanism of the ECSNs based on the above asymmetric evolutionary game.

5.3.1 Influence of asymmetry on ECSNs evolution

First, the influence of asymmetry on the evolution of the ECSNs is explored. On the premise that $0 \leq \gamma < \alpha \leq 1$, $0 < \theta < \beta < 1$, $\lambda \geq 1$, $0 < k < 1$, assign values to each parameter of the system. Set the initial values as C = 14, R = 22, F = 10, α = 0.8, γ = 0.6, θ = 0.2, β = 0.3, λ = 1.2, set the initial value of x and y as 0.5, assign the value of k as 0.2, 0.5, 0.8, respectively, and the running time to [0,3], and then determine the simulation results. The result is shown in Figure 4.

The simulation results show that when μ = 0.25, the evolution of the ECSNs takes the shortest time to reach the equilibrium point, and with the increasing k value, the evolution of the ECSNs takes a longer time to reach the equilibrium, which verifies that the cooperative intention is a subtractive function of the asymmetric value μ consistent with the game conclusion.

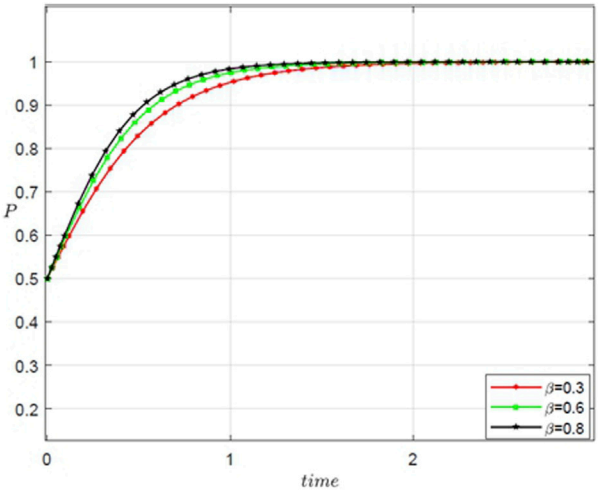

FIGURE 5
The effect of extra cost (β) on the evolution of ECSNs when both parties cooperate negatively.

5.3.2 Effect of extra cost on ECSNs evolution

Cost belongs to the category of economic factors and has always been an important factor affecting the ECSNs. The discussion of the effects of the cost on the evolutionary game is conducive to exploring the effects of the economic factors on the choice of emergency cooperation strategies. Different from traditional evolutionary games, in asymmetric evolutionary games, as long as negative cooperation exists between one party and the other, the emergency cooperation needs to pay extra costs. The simulation of the influence of extra costs on the evolutionary game can directly show the influence of economic factors on the strategy selection of emergency cooperation subjects in the ECSNs. Based on the initial value set, the asymmetry index k was assigned 0.5, When both parties cooperate negatively, the value of additional cost index β is 0.3,0.6, and 0.8; When one side cooperates negatively, the extra cost index θ was assigned 0.2,0.6, and 0.9, respectively, and the running time was [0,3], and thus, the simulation results are obtained (Figure 5,6).

The simulation results show that the extra cost index of the negative cooperation of one party and the negative cooperation of both parties have different influences on the evolution of the ECSNs, and thus, the economic factors have no significant influence on the evolution of the ECSNs for magnitude emergencies. In other words, with the increase in extra cost index θ, the time for the network to reach the evolutionary equilibrium is gradually prolonged when one party is in negative cooperation. When both parties cooperate negatively, the time for the network to reach equilibrium decreases gradually with the increase of extra cost index β.

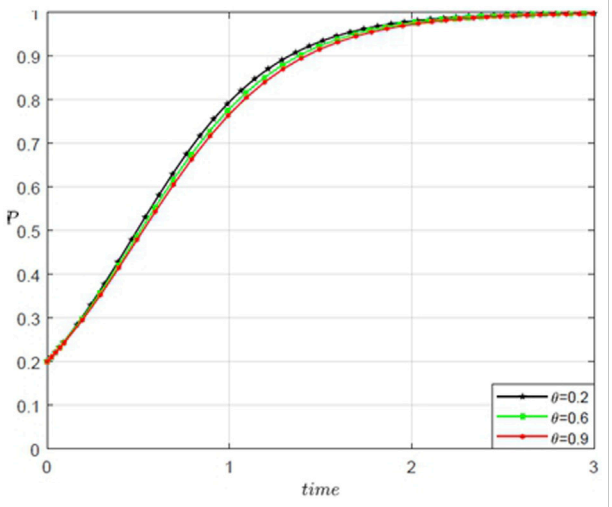

FIGURE 6
The effect of extra cost (θ) on the evolution of ECSNs when one party cooperates negatively.

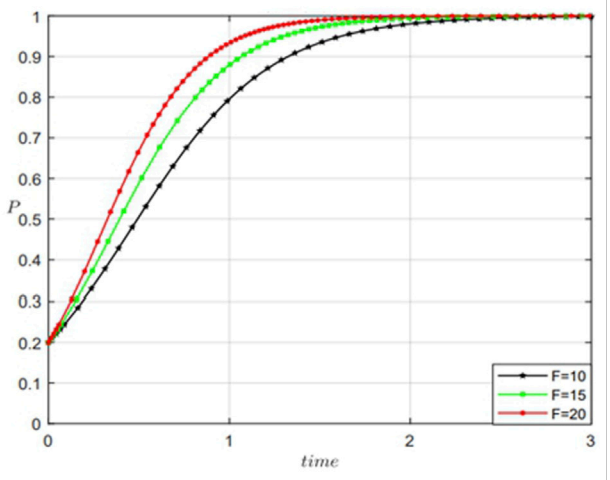

FIGURE 7
The effect of basic punishment F on the evolution of ECSNs.

5.3.3 Influence of punishment intensity on ECSNs evolution

The punishment of the superior government to the negative partner includes direct administrative punishment, unqualified political performance assessment, blocked promotion of officials, etc., which can be understood as political factors affecting the formation of the ECSNs. The simulation of the influence of punishment intensity on the evolutionary game can reveal the influence of political factors on the ECSNs for magnitude emergencies. The simulation results show that political factors affect the evolution of the ECSNs for magnitude emergencies.

First, to explore the effects of punishment intensity on the evolution of the ECSNs, the basic punishment F was assigned 10,15, and 20, respectively based on the initial value setting, and the simulation results were obtained. Second, when both parties cooperate negatively, the superior government will adjust the basic punishment through the coefficient λ. To fully explore the effect of the punishment on the evolution of the ECSNs, the influence of the punishment adjustment coefficient λ on the evolution of the ECSNs for magnitude emergencies is further simulated based on the SD simulation of the basic punishment. Based on the initial value, the penalty adjustment coefficient λ was set as 1.2, 1.6, and 2.0, respectively, and the simulation was carried out (Figure 7,8).

The simulation results show that the effects of the basic punishment intensity F and punishment adjustment coefficient λ on the evolution of the ECSNs is in the same direction, and thus, political factors will also affect the evolution of the ECSNs. This conclusion is a response to hypothesis 3. In other words, with the decrease of basic

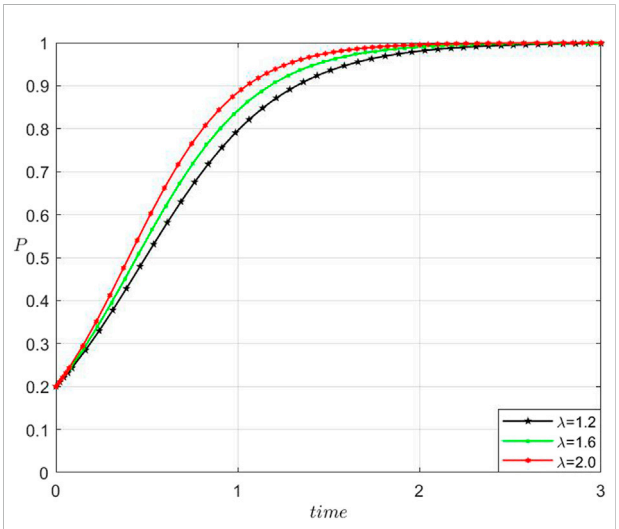

FIGURE 8
The effect of penalty adjustment (λ) on the evolution of ECSNs.

punishment intensity F and punishment adjustment coefficient λ, the time for local governments to reach the ECSN is gradually prolonged. Because the punishment of the superior to the subordinate governments can be classified under political pressure, political pressure is inversely proportional to the achievement of the ECSNs. That is, the greater the political pressure, the easier it is to form the ECSNs and the shorter the achievement time.

According to the simulation results, the asymmetry between the subjects in the ECSNs is inversely proportional to the willingness for emergency cooperation. Political factors have a considerable influence on the evolution of the ECSNs,

while economic factors have limited influence. Combined with the asymmetric evolutionary game analysis, this paper summarizes the formation mechanism of the ECSNs for magnitude emergencies as follows: the nature of the crisis contributes to the endogenous dynamics of emergency cooperation, while the influence of political factors stimulates the endogenous power to break the asymmetric restrictions and beyond the economic factors, and produces strategic and temporary ECSNs. Among them, the characteristics of magnitude emergencies lead the neighboring area to become a community of interests, generating the endogenous will of emergency cooperation.

The political factors break through hierarchical and economic constraints using coercive means and condense all parties. Thus, external coercive force pressurizes endogenous power, thereby generating the ECSNs.

6 Conclusion

This paper takes the B-T-H region in China as a sample and focuses on the emergency cooperation practice for COVID-19. First, massive search data are used to build the ESCNs for magnitude emergencies. Second, the structural characteristics and operation mechanisms of the ECSNs are analyzed using the social network analysis (SNA) method. Third, the asymmetric evolutionary game analysis is used to calculate the subject strategy selection of the ECSNs and the influence of various factors on network evolution is explored through SD simulation to explore the internal mechanism of network generation. Through the above analysis, the following conclusions are obtained:

(1) The ECSNs to meet the emergency needs of countries has been basically formed. With the acceleration of urbanization, human beings enter the risk society, the frequent outbreak of major emergencies has attracted the attention of the governments of various countries, and they have gradually realized the importance of emergency cooperation in the continuous practice of emergency management. Through a long period of continuous development and improvement, all countries have found their own mode of emergency cooperation and formed ECSNs with their own characteristics. Among them, China has formed ECSNs with Chinese characteristics through constant exploration, and played an important role in the prevention and control of the epidemic, which greatly promoted the improvement of the efficiency of emergency management in China. Taking this network as the incision can reflect the general situation of the ECSNs all over the world, and its own characteristics can provide China's experience for the world emergency cooperation. Its network has the pluralism of emergency cooperative subjects, the plurality of the connection of emergency cooperative subjects and the dynamic of the network structure.

(2) The ECSNs for magnitude emergencies have asymmetry, and the cooperative willingness among network subjects is inversely proportional to the asymmetry. First, the asymmetry of the ECSNs is the asymmetry of the subjects in the network in terms of resource endowment, administrative level, geographical distance, emergency demand, political pressure, and so on. Second, the willingness for emergency cooperation with network subjects is inversely proportional to asymmetry, that is, the greater the difference between administrative levels, the easier it is to ignore the willingness of the vulnerable areas in emergency management. The greater the gap in economic development, the more likely the asymmetric distribution of emergency cooperation resources. The greater the difference in demand, the more likely the emergency cooperation to appear as the "free rider" dilemma. Regional emergency management cooperation norms and systems should be formulated through consultation to integrate the interests of all parties in emergency management, eliminate the negative effect of the asymmetry, and promote regional emergency cooperation.

(3) The operation mechanism of the ECSNs for magnitude emergencies is multi-directional coordination and cooperation between local governments under longitudinal hierarchical control. The generation mechanism is that political factors affect the endogenous cooperation willingness, which breaks through the hierarchical and economic constraints and condenses the subject of all parties, generating the strategic and temporary ECSNs. That is, vertical level control is still the dominant mode of the ECSNs. Complex emergencies force the political pressure to break through hierarchical and economic constraints. The characteristics of magnitude emergencies catalyze the endogenous willingness of emergency cooperation in regional communities of interest. External pressure affects the endogenous willingness to produce the ECSNs for magnitude emergency that is dominated by vertical control and supplemented by horizontal coordination. Among these characteristics, political pressure is an important factor influencing the

formation and evolution of the ECSNs, while economic factors have little influence on it. This is because of the emergency management situation of a magnitude emergency on many aspects, such as economy, society, life and property security threat, is a special governance situation with political gravity. The government will take temporary tough measures to rein them in, regardless of the economic cost, resulting in a strategic and temporary form of network governance.

Data availability statement

The raw data supporting the conclusion of this article will be made available by the authors, without undue reservation.

Author contributions

RN and JW both carefully outlined the contents of the review and wrote the entire manuscript.

Funding

This study was supported by the Fundamental Research Funds for the Central Universities (Grant no.2021SKWF04), Beijing Social Science Foundation (Grant no. 20GLC044) and the National Social Science Fund of China (Grant no. 18CGL033).

Acknowledgments

Thanks to Associate Professor Lei Jiang for his help in the technique of reptiles.

Conflict of interest

The authors declare that the research was conducted in the absence of any commercial or financial relationships that could be construed as a potential conflict of interest.

Publisher's note

References

1. Kapucu N. Interagency communication networks during emergencies. *Am Rev Public Adm* (2006) 36(2):207–25. doi:10.1177/0275074005280605

2. Kapucu N, Garayev V. Designing, managing, and sustaining functionally collaborative emergency management networks. *Am Rev Public Adm* (2013) 43(3):312–30. doi:10.1177/0275074012444719

3. Kapucu N, Garayev V. Structure and network performance: Horizontal and vertical networks in emergency management. *Adm Soc* (2016) 48(8):931–61. doi:10.1177/0095399714541270

4. Snow CC, Lipnack J, Stamps J. The virtual organization: Promises and payoffs, large and small. *J Organizational Behav* (1999) 6:15. doi:10.1080/00208825.2003.11043688

5. Vangen S, Huxham C. Nurturing collaborative relations: Building trust in interorganizational collaboration. *J Appl Behav Sci* (2003) 39(1):5–31. doi:10.1177/0021886303039001001

6. Nan R, Wang J, Zhu W. Evolutionary game of social network for emergency mobilization (SNEM) of magnitude emergencies: Evidence from China. *Complexity* (2022). doi:10.1155/2022/3885934

7. Ansell C, Gash A. Collaborative governance in theory and practice. *J Public Adm Res Theor* (2007) 18(4):543–71. doi:10.1093/jopart/mum032

8. Baybeck B, Berry WD, Siegel DA. A strategic theory of policy diffusion via intergovernmental competition. *J Polit* (2011) 73(1):232–47. doi:10.1017/s0022381610000988

9. Mooney CZ. Modeling regional effects on state policy diffusion. *Polit Res Q* (2001) 54(1):103–24. doi:10.2307/449210

10. Weyland K. Theories of policy diffusion: Lessons from Latin American pension reform. *World Polit* (2005) 57(2):262–95. doi:10.1353/wp.2005.0019

11. Zakour MJ. Geographic and social distance during emergencies: A path model of interorganizational links. *Soc Work Res* (1996) 20(1):19–29. doi:10.1007/s11069-015-1925-1

12. Caruson K, MacManus SA. Disaster vulnerabilities: How strong a push toward regionalism and intergovernmental cooperation? *Am Rev Public Adm* (2008) 38(3):286–306. doi:10.1177/0275074007309152

13. Mu R, de Jong M, Koppenjan J. Assessing and explaining interagency collaboration performance: A comparative case study of local governments in China. *Public Management Rev* (2019) 21(4):581–605. doi:10.1080/14719037.2018.1508607

14. Xiong F, Wang X, Pan S, Yang H, Wang H, Zhang C. Social recommendation with evolutionary opinion dynamics. *IEEE Trans Syst Man Cybern Syst* (2020) 50(10):1–13. doi:10.1109/TSMC.2018.2854000

15. Li Z, Xiong F, Wang X, Guan Z, Chen H. Mining heterogeneous influence and indirect trust for recommendation. *IEEE Access* (2020) 8:21282–90. doi:10.1109/ACCESS.2020.2968102

16. Sedgwick D. Managing collaborative paradox: Examining collaboration between head start and the Virginia preschool initiative. *Adm Soc* (2016) 48(2):190–215. doi:10.1177/0095399714532269

17. Kwon SW, Feiock RC, Bae J. The roles of regional organizations for interlocal resource exchange: Complement or substitute? *Am Rev Public Adm* (2014) 44(3):339–57. doi:10.1177/0275074012465488

18. Yi H, Suo L, Shen R, Zhang J, Ramaswami A, Feiock RC. Regional governance and institutional collective action for environmental sustainability. *Public Adm Rev* (2018) 78(4):556–66. doi:10.1111/puar.12799

19. Xiong F, Liu Y, Cheng J. Modeling and predicting opinion formation with trust propagation in online social networks. *Commun Nonlinear Sci Numer Simulation* (2017) 44:513–24. doi:10.1016/j.cnsns.2016.09.015

20. Bryson JM, Crosby B, Stone M. The design and implementation of cross-sector collaborations: Propositions from the literature. *Public Adm Rev* (2006) 66:44–55. doi:10.1111/j.1540-6210.2006.00665.x

21. Kapucu N, Garayev V. Collaborative decision-making in emergency and disaster management. *Int J Public Adm* (2011) 34(6):366–75. doi:10.1080/01900692.2011.561477

22. Head BW, Alford J. Wicked problems: Implications for public policy and management. *Adm Soc* (2013) 47(6):711–39. doi:10.1177/0095399713481601

23. Provan KG, Kenis P. Modes of network governance: Structure, management, and effectiveness. *J Public Adm Res Theor* (2008) 18(2):229–52. doi:10.1093/jopart/mum015

24. Klijn E-H, Steijn B, Edelenbos J. The impact of network management on outcomes in governance networks. *Public Adm* (2010) 88(4):1063–82. doi:10.1111/j.1467-9299.2010.01826.x

25. Turrini A, Cristofoli D, Frosini F, Nasi G. Networking literature about determinants of network effectiveness. *Public Adm* (2010) 88(2):528–50. doi:10.1111/j.1467-9299.2009.01791.x

26. Klijn E-H, Ysa T, Sierra V, Berman E, Edelenbos J, Chen DY. The influence of network management and complexity on network performance in taiwan, Spain and The Netherlands. *Public Management Rev* (2015) 17(5):736–64. doi:10.1080/14719037.2014.957340

27. Feiock RC. The institutional collective action framework. *Policy Stud J* (2013) 41(3):397–425. doi:10.1111/psj.12023

28. Zhu X, Tian H, Cai S. Personalized recommendation with corrected similarity. *J Stat Mech* (2014) 7:P07004. doi:10.1088/1742-5468/2014/07/P07004

29. Emerson K, Nabatchi T, Balogh S. An integrative framework for collaborative governance. *J Public Adm Res Theor* (2012) 22(1):1–29. doi:10.1093/jopart/mur011

30. Wen XM, Suo LM. A study on the intergovernmental network structure of public health governance in urban agglomerations: Data from the beijing-tianjin-hebei region and the yangtze river delta (in Chinese). *Jinan J (Philosophy Soc Sciences)* (2020) 42(11):100–15.

31. Nicholson-Crotty S. Goal conflict and fund diversion in federal grants to the states. *Am J Pol Sci* (2004) 48(1):110–22. doi:10.1111/j.0092-5853.2004.00059.x

32. Ye L. Regional government and governance in China and the United States. *Public Adm Rev* (2009) 69(S1):S116–21. doi:10.1111/j.1540-6210.2009.02098.x

33. Jing Y, Savas ES. Managing collaborative service delivery: Comparing China and the United States. *Public Adm Rev* (2009) 69:S101–7. doi:10.1111/j.1540-6210.2009.02096.x

34. Ernoul L, Wardell-Johnson A. Governance in integrated coastal zone management: A social networks analysis of cross-scale collaboration. *Environ Conserv* (2013) 40(3):231–40. doi:10.1017/s0376892913000106

35. Guo X, Kapucu N. Examining collaborative disaster response in China: Network perspectives. *Nat Hazards (Dordr)* (2015) 79(3):1773–89. doi:10.1007/s11069-015-1925-1

36. Freeman L. *The development of social network analysis: A study in the sociology of science*. Vancouver: Empirical Press (2004).

37. Cheng Y, Zheng X. Emergence of cooperation during an emergency evacuation. *Appl Mathematics Comput* (2018) 320:485–94. doi:10.1016/j.amc.2017.10.011

38. Diehlmann F, Lüttenberg M, Verdonck L, Wiens M, Zienau A, Schultmann F. Public-private collaborations in emergency logistics: A framework based on logistical and game-theoretical concepts. *Saf Sci* (2021) 141(2021):105301–16. doi:10.1016/j.ssci.2021.105301

39. Zheng X, Cheng Y. Modeling cooperative and competitive behaviors in emergency evacuation: A game-theoretical approach. *Comput Mathematics Appl* (2011) 62(12):4627–34. doi:10.1016/j.camwa.2011.10.048

40. Iqbal A, Gunn LJ, Guo M, Ali Babar M, Abbott D. Game theoretical modelling of network/cybersecurity. *IEEE Access* (2019) 7:154167–79. doi:10.1109/access.2019.2948356

41. Liu F, Fu LP, Xu KB. Structure and effect measurement of inter-government and inter-city cooperation network of medical and health services: Taking jingjinji metropolitan region as an example (in Chinese). *J Northeast Univ (Social Science)* (2021) 23(04):59–66+75. doi:10.15936/j.cnki.1008-3758.2021.04.008

42. Johnson BJ, Goerdel HT, Lovrich NP, Pierce JC. Social capital and emergency management planning. *Am Rev Public Adm* (2013) 45(4):476–93. doi:10.1177/0275074013504127

frontiers | Frontiers in Physics

TYPE Original Research
PUBLISHED 30 September 2022
DOI 10.3389/fphy.2022.1018993

OPEN ACCESS

EDITED BY
Fei Xiong,
Beijing Jiaotong University, China

REVIEWED BY
Jinzhong Guo,
Xinjiang University of Finance and Economics, China
Yingjie Zhang,
Beijing Forestry University, China
Hongping Lian,
Beijing Normal University, China

*CORRESPONDENCE
Duo Chai,
chaiduobnu@126.com

SPECIALTY SECTION
This article was submitted to Social Physics,
a section of the journal
Frontiers in Physics

RECEIVED 14 August 2022
ACCEPTED 12 September 2022
PUBLISHED 30 September 2022

CITATION
Chai D, Du J, Yu Z and Zhang D (2022), City network mining in china's yangtze river economic belt based on "two-way time distance" modified gravity model and social network analysis.
Front. Phys. 10:1018993.
doi: 10.3389/fphy.2022.1018993

City network mining in china's yangtze river economic belt based on "two-way time distance" modified gravity model and social network analysis

Duo Chai[1]*, Jiaze Du[1], Zongqi Yu[1] and Dong Zhang[2]

[1]School of Government, Central University of Finance and Economics, Beijing, China, [2]School of Public Administration and Policy, Renmin University of China, Beijing, China

In order to improve the city network mining method, the inter-cities' connection strength, structure and density, and distribution patterns of city network in the Yangtze River Economic Belt of China have been empirically analyzed through the combined application of SNA method, "Dual-direction time distance" modified gravity model and ArcGIS geographic visualization method. The results show that the modified gravity model can better reveal the interaction differences between cities and reflect the current and potential economic, population and resource relations among cities. The city network density of this area has positively close relationship with the regional economic development level. The average value of degree centrality in the basin is high, but the difference between cities is obvious. The "agglomeration effect" of the central cities is significant, and the urban connections have an obvious cluster structure, showing an "M" shaped spatial distribution along the Yangtze River; The inner interaction strength of city network subgroups is high, but the connection between subgroups is low. The law of "downstream > midstream > upstream" also appears on the closeness centrality and betweenness centrality. In the future, it is essential to improve the integration and multi-level connections of urban agglomeration in the river basin and form a development pattern of "downstream driving - midstream transition - upstream connection"; strengthen the functions and connections of central and subcentral cities.

KEYWORDS

city network, dual-direction time distance, gravity model, social network analysis, Yangtze river economic belt

1 Introduction

City network mining is an important interdisciplinary research field of physics, economics and geography [1, 2]. Under the joint promotion of economic globalization, regional integration, transportation technology and information technology, relying on certain geographical elements (large rivers, traffic trunk lines, and valleys along the

mountains), cities of different scales, endowments and energy levels are interconnected [3–5]. A composite transportation network of highways, railways, water transport, air transport, intercity rail transit and three-dimensional transportation within the city has been gradually formed, and a complex information system has been built [6, 7]. The efficiency of residents' commuting, material transportation and information transmission has been greatly improved, which has promoted the cross regional flow of all kinds of production factors. The interaction pattern of material, energy and wealth among cities has become more complex [6]. A functional organic city network with multi-level connection, multi-domain cooperation and multi-path arrival has been formed. The comprehensive value of city network development is an important indicator to identify national and regional development patterns [7]. The mature city network has also become the core growth pole that represents the country to participate in global competition and compete for high-end resources [8].

By 2021, China's population reached 1.413 billion. The total number of cities reached 572, the urban resident population was 914.25 million, and the urbanization rate exceeded 64.7%; the urbanization rate of eight provinces exceeded 70%, the resident population of 91 cities reached more than five million, and the resident population of 18 cities exceeded 10 million. According to the great differences in location, functional positioning and economic development level among the east, central and west of China, the population flows from the west to the east, from the inland to the coastal, from water deficient areas to water rich areas, and from small cities to large cities. The resulting consumption, investment and resource development have affected the industrial agglomeration, diffusion and structural and layout adjustment, forming the urban functional circles, which center on megalopolis, connect several large cities outward, and then expand and connect the surrounding cities and towns [9]. These city networks, which are still evolving rapidly, provide rare observation samples for the research in this field.

For a long time, scholars have conducted systematic research on the methods of city network structure mining, connection strength measurement and core node identification [2, 10], and comprehensively used the research tools of complex networks, economics, management, sociology and regional science to analysis the formation mechanism, inter connection characteristics and influence mechanism of related factors of city network [3, 4], which helps us understand the laws of population migration and industrial distribution in the process of regional integration. It also guides the construction of regional transportation network, communication facilities and the spatial layout of population, industry and ecology in the planning [11]. However, most of the existing studies focus on depicting a certain aspect of regional traffic links, population migration, industrial transfer and division of labor, economic structure complementarity and administrative jurisdiction. The research on city network structure mining that from the comprehensive viewpoint of economic, social and transportation links and takes the possible differences of two-directions link into account is almost ignored [12].

Cities in the big river basin are of a special type. On the one hand, the resource sharing and ecological connection formed by water resources connect the cities in the basin into a community of interests [13]; on the other hand, the cities in the basin have spontaneously formed economic and industrial complexes under the organization of shipping links [14–16]. China's Yangtze River is a core economic belt with rich natural resources, superior geographical conditions, dense population and industries. However, the problem of uncoordinated urban development and large economical gap between cities in this basin has not been fundamentally solved, the living standards gap of residents between cities has widened, and the destruction of the resources and environment in the basin has intensified. The root cause is the lack of overall planning for the development of the basin, coupled with the imperfect transportation and information network, resulting in the separation of urban division of labor and the contradiction of functional positioning, which leads to resource competition, excessive development and negative environmental externalities [17]. In 2016, the State Council of China approved the regional development strategy of "Yangtze River Economic Belt" (According to the development planning outline of the Yangtze River Economic Belt in 2016) [18]. The guiding ideology of river basin development changed from "development" to "protection", forming a comprehensive transportation network of "three horizontality, six verticality, three networks and multiple points" [19]. The mining of city network in the basin is helpful to guide the formulation of development policies and the implementation of tasks.

The marginal contribution includes three aspects: First, the city network mining method is improved by the combined application of gravity model modified by dual-direction arrival time, social network analysis (SNA) calculation method and ArcGIS geographic visualization method. Second, the economic and population scale (potential connection strength) and commuting connection (actual connection degree) are integrated in the measurement of city network connection. So as to comprehensively reflect the economic, social and practical connection ability between cities. Third, the city network of 11 provinces in the Yangtze River is measured, providing guidance for formulating basin development plans and policies, optimizing the industrial and population layout of the basin, and improving the construction of inter town transportation facilities.

2 Related works

Social network analysis (SNA) believes that social connections can be quantified, so as to specify on social

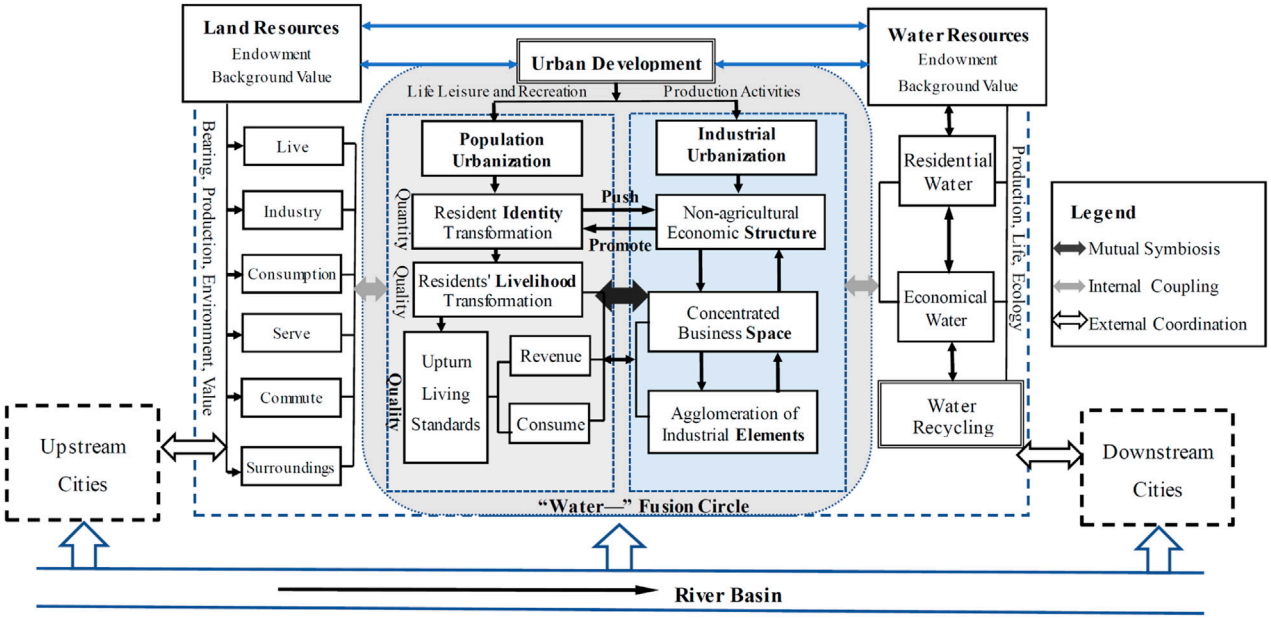

FIGURE 1
Resource and environment connection logic of basin cities.

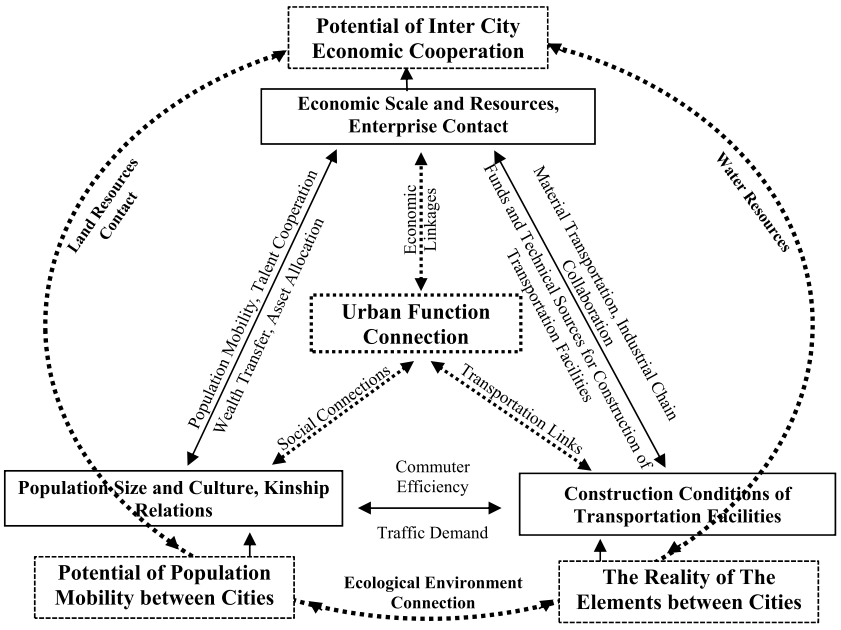

FIGURE 2
The logical relationship between economy, population, transportation and city network.

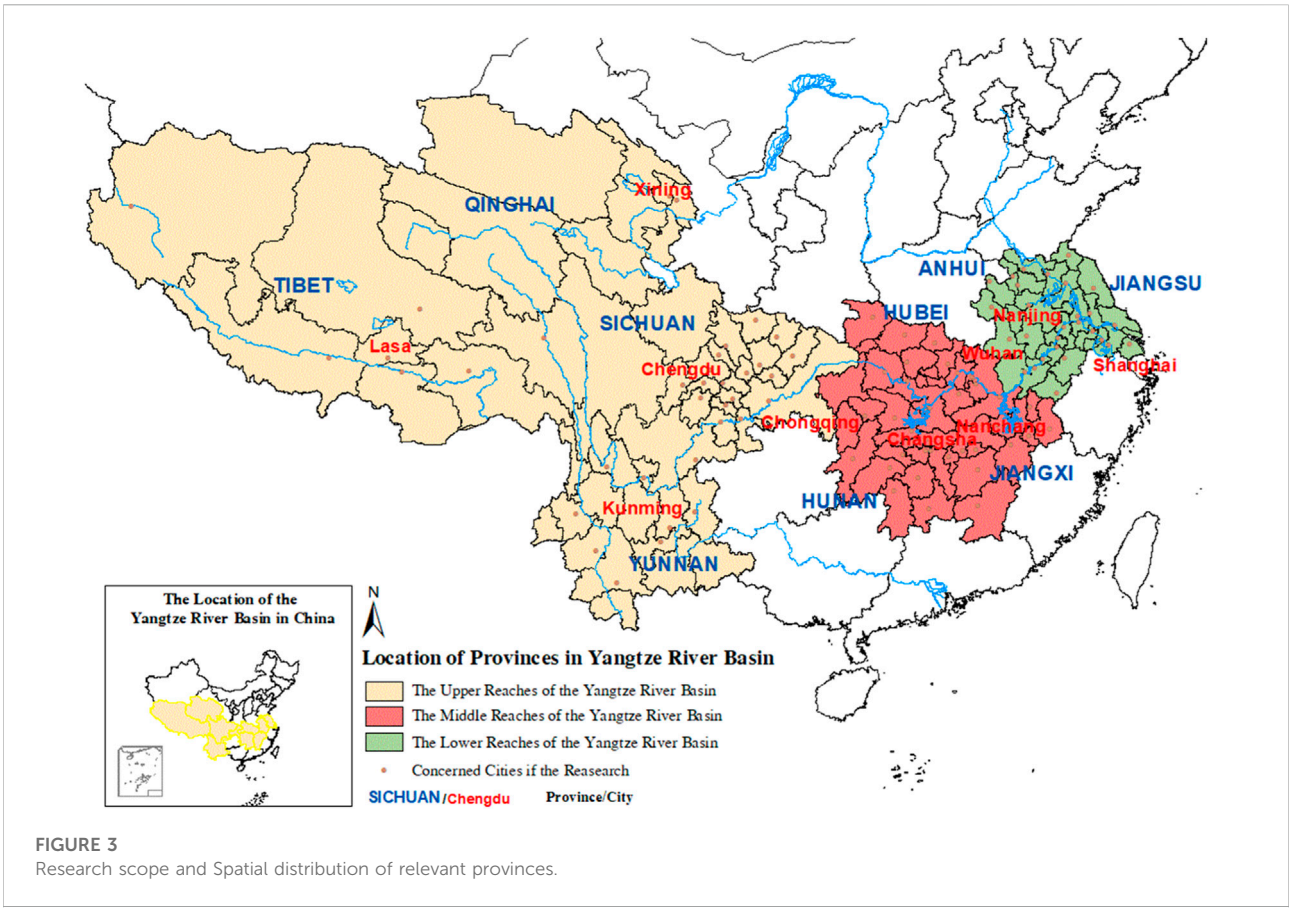

FIGURE 3
Research scope and Spatial distribution of relevant provinces.

TABLE 1 Data source of this study.

Data	Access	unit
1) Commuting time by expressway	Checking the map of Gaode, which is expressed by the point-to-point traffic time of the city government office	Minutes
2) Commuting time by railway	China 12,306 railway ticket purchasing network	Minutes
3) Commuting time by water	Checking the official website of Yangtze River Transportation	Minutes
4) Economic and social development indicators	Annual urban development statistics released by the Chinese government	RMB 100 million yuan/10 thousand people
5) Transfer experience of cities' primary officials among cities	Central and local government website and http://xinhuanet.com/	If there is transfer experience = 1; otherwise = 0

operation [20], which is widely used in sociology, psychology, geography and other fields [8, 12]. Early studies focused on explaining the principle of urban formation through social network relations and exploring the network structure and attributes within cities [21]. D. A. Smith and M. Timberlake 1995) designed the measurement technique of city network relationship such as infrastructure method and labor flow method [22]. Taylor [23] further proposed the Inter-locking Network Model and designed the measurement method of city network structure based on the data of urban business and economic relations. Taylor et al. [24] proposed the measurement methods of "absolute network relevance" and "relative network relevance". Pfliege [25] believed that the existence and development of cities depend on the internal composition network and external contact network. An et al. [26] used analytic hierarchy process, spatial visualization and SNA to analyze the spatial connection and grid pattern Urban Agglomeration based on the comprehensive traffic information flow. Zachary P. Neal [27] built the interlocking world city network model (IWCNM) and proposed the decision network

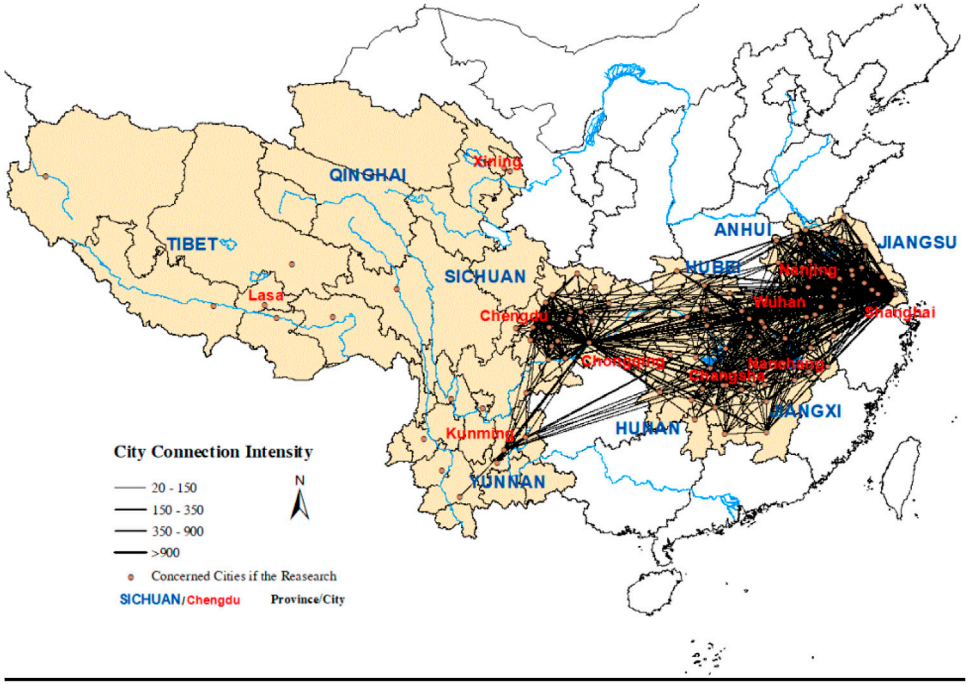

Direction of Connection	F1	F1 Ranking
Shanghai-Suzhou	2.09%	1
Chongqing-Chengdu	1.34%	2
Nanjing-Shanghai	0.99%	3
Shanghai-Wuxi	0.96%	4
Wuxi-Suzhou	0.95%	5
Shanghai-Changzhou	0.78%	6
Shanghai-Nantong	0.62%	7
Meishan-Chengdu	0.58%	8
Deyang-Chengdu	0.57%	9
Hefei-Shanghai	0.55%	10

FIGURE 4
City contact strength max-value distribution in the research area.

structure mining method and multi department network analysis method.

Because of the connection generated by natural resources and environment as well as the geographical proximity, cities in the big river basin are the hot objects of city network mining. On the basis of "flow space theory", Wang et al. [28] comprehensively applied the city flow intensity model to build an abstract city association of factor flow. Gao et al. [29] and Li et al. [14] used data envelopment analysis and gravity model to analyze the characteristics of the population and economic connection of cities in the Yangtze River basin. Wang et al. [15] used ArcGIS software spatial analysis tools to calculate the distance and mutual distance between cities and rivers as an indicator to measure the link strength between cities.

Recently, city network structure analysis using SNA has gradually increased [30–32]. Wu et al. [33] studied the economic relations and integration trend of cities. Peng et al. [34] analyzed the evolution characteristics of urban agglomeration integration. In terms of city network structure identification, Zhao et al. [35] explored the influencing factors of city network spatial structure from the perspective of multi factor flow. Wu et al. [36], based on the big data of transportation and information, analyzed the outward connection network structure and influencing factors of the urban agglomeration by SNA, SSI, modularity and other methods. Sun et al. [37] analyzed the city network structure and spatial pattern based on the high-speed railway transport data, and identified the urban agglomeration characteristics by combining the geographic network and the topological network.

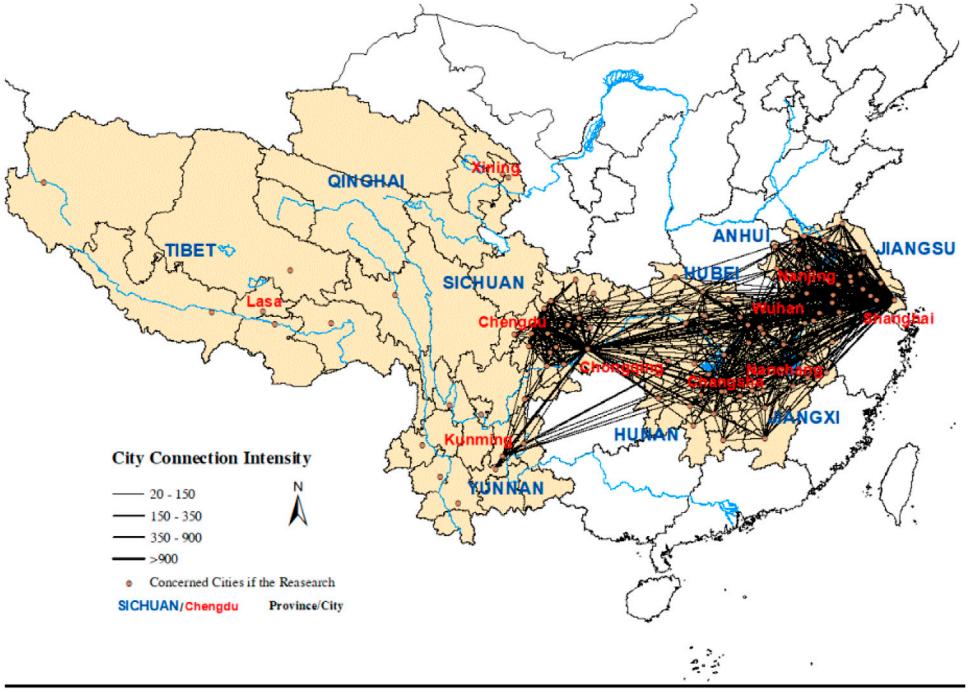

Direction of Connection	F2	F2 Ranking
Suzhou-Shanghai	1.81%	1
Chengdu-Chongqing	1.09%	2
Shanghai-Nanjing	0.89%	3
Wuxi-Shanghai	0.88%	4
Suzhou-Wuxi	0.81%	5
Changzhou-Shanghai	0.70%	6
Nantong-Shanghai	0.61%	7
Shanghai-Hefei	0.51%	8
Chengdu-Deyang	0.48%	9
Chengdu-Meishan	0.47%	10

FIGURE 5
City contact strength min-value distribution in the research area.

At present, the overall city network in the Yangtze River basin is less studied. Most studies only assess the strength of inter city Linkages Based on specific aspects such as urban transport links, population migration, industrial transfer, economic structure complementarity, and administrative and jurisdictional relations. Driven by the large-scale construction of transportation, logistics and information networks, the shortest arrival time between cities has become the best indicator to measure the strength of transportation links between cities in China, because it can reveal more realistic indicators such as economic and demographic links between cities. In addition, the exiting studies mistakenly believe that the arrival time of two directions between two cities should be the same, without distinguishing the "two-directions difference" of inter-city connections, and only one-way links are calculated. It is wise to treat all cities as the same individuals and calculate the connection strength in both directions.

3 Materials and methods

3.1 Theoretical analysis

The form of urban development is mainly manifested in the transformation of population and industry into cities [38–40]: Firstly, under the coordination of the central government, the limited land resources and various natural resources carried by

the land are distributed administratively among the cities in the basin. The scale of the bearing capacity of land space determines the potential scale of residence, industry, consumption, commuting, infrastructure and ecological environment, and then determines the subordinate relationship of the functions of the cities in the basin. Secondly, the distribution of rights to water resources in the basin, including production and domestic water and the recycling of water resources, determines the initiation, maintenance and growth of urban production and living activities. Third, the cities in the basin have a strong ecological environment relationship. Any city will have strongly external effects on the natural resources development in the basin, therefore, it is essential to coordinate and cooperate with each other. To sum up, the spatial adjacency, the distribution of land resources, the sharing of water resources and the ecological externalities jointly determine the competition and cooperation relationship between the cities in the basin (Figure 1).

Further, the links between cities are complex, and city network mining needs to find the main indicators that reflect the link strength. As shown in Figure 2, on the basis of resources and environment connection, the connection between cities in the basin is specifically manifested as measurable population flow, economic cooperation and traffic connection [40]. Therefore, theoretically, the strength of functional connections between the two cities should be determined by two aspects: first, if the economy and population scale of cities are relatively large, the potential for cooperation between them will be possibly greater [41]. The second is the transportation connection measured by commute time [42]. A developed transportation network can significantly improve the commuting efficiency between cities, thus facilitating the transformation of potential links and cooperation between cities into reality. Measuring the traffic links between cities can reflect comprehensive information: first, the flow and interaction of various resource elements between cities need the traffic network to provide media; Secondly, the construction of the transport network is also based on the past and present inter city cooperation needs. In other words, a large number of cooperation needs are the main driving force for the construction of the transport network. Third, transportation connections show the current situation and growing trend of economics, population size, and trade links among cities in the future. Fourth, traffic connections also reflect the policy intention of the state to combine cities and develop urban agglomerations.

Most of the existing studies only describe the urban connection from a certain aspect such as population migration, enterprise cooperation, administrative jurisdiction or railway, highway and transportation facilities construction, while the economic, population and traffic connections are not taken into comprehensive consideration [43]. In addition, most of the urban traffic connections are calculated by geographical spatial distance, and it is believed that the strength of inter-city connections has an inverse proportion to the geographical distance [44]. The thinking paradigm of previous research simply regards the straight distance between two points on the plane as the convenience of arrival between cities, which is divorced from reality. This analysis method does not consider the blocking effect of terrain and various geographical elements on intercity commuting, nor the impact of human factors on intercity commuting efficiency. For example, the development of high-speed railway and aviation has had a subversive impact on commuting efficiency. More importantly, previous studies have not taken into account the differences in the mutual influence between cities, especially the differences in the two-way arrival time. At present, the infrastructure construction of intercity high-speed rail transit, expressway and civil aviation in the study area is relatively complete. In view of the two-way link difference between cities ignored in previous studies, this paper constructs a matrix based on the shortest arrival time of two directions between cities, integrates indicators such as urban population and GDP, and modifies the gravitational model. The purpose of this is to comprehensively measure the existing and potential population, trade, logistics and other links between cities and the potential for cooperation. On this basis, the structure and density of city functional network and the importance of different functional nodes are measured by using various indicators of SNA.

3.2 Research object and data

China's Yangtze River, with a total length of 6,300 km, spans the three major regions of southwest, central and east China. It connects the three-river source ecological protection zone, Chengdu-Chongqing urban agglomeration, central Yunnan urban agglomeration, the middle reaches of the Yangtze River urban agglomeration and the Yangtze River Delta Urban Agglomeration. According to the Yangtze River Economic Belt regional developing plan, all 102 cities in 11 provinces are selected in this paper as research objects. The research scope is shown in Figure 3. Calculation from the data of 2021 China Statistical Yearbook, the total area accounted for 21.5% of China, the total population accounted for 43.0%, and the GDP accounted for 46.4%, while carried about 44.8% of the local fiscal revenue, 43.5% of the number of authorized patents, 45.7% of the foreign trade import and export volume, and 82.2% of foreign capital actually utilized of the whole nation, which is the most important urban cluster in China.

Table 1 shows the source of the data used in this study. It should be noted that, the shortest arrival time distance represented is mainly determined by making a comparison of various means of transportation including ships, cars, trains

10.3389/fphy.2022.1018993

TABLE 2 TOP 60 of inter-city contact strength value in the research area.

Direction	F1 (%)	Rank of F1	Direction of connection	F2 (%)	Rank of F2	F1/F2
Shanghai-Suzhou	2.09	1	Suzhou-Shanghai	1.81	1	1.15
Chongqing-Chengdu	1.34	2	Chengdu-Chongqing	1.09	2	1.24
Nanjing-Shanghai	0.99	3	Shanghai-Nanjing	0.89	3	1.11
Shanghai-Wuxi	0.96	4	Wuxi-Shanghai	0.88	4	1.09
Wuxi-Suzhou	0.95	5	Suzhou-Wuxi	0.81	5	1.16
Shanghai-Changzhou	0.78	6	Changzhou-Shanghai	0.70	6	1.11
Shanghai-Nantong	0.62	7	Nantong-Shanghai	0.61	7	1.02
Meishan-Chengdu	0.58	8	Chengdu-Meishan	0.47	10	1.24
Deyang-Chengdu	0.57	9	Chengdu-Deyang	0.48	9	1.20
Hefei-Shanghai	0.55	10	Shanghai-Hefei	0.51	8	1.08
Huanggang-Wuhan	0.47	11	Wuhan-Huanggang	0.35	13	1.34
Chengdu-Mianyang	0.39	12	Mianyang-Chengdu	0.38	11	1.02
Suzhou-Nantong	0.37	13	Nantong-Suzhou	0.36	12	1.02
Changzhou-Suzhou	0.37	14	Suzhou-Changzhou	0.33	14	1.10
Ziyang-Chengdu	0.33	15	Chengdu-Ziyang	0.27	17	1.22
Chongqing-Nanchong	0.31	16	Nanchong-Chongqing	0.26	18	1.18
Wuhan-Xiaogan	0.31	17	Xiaogan-Wuhan	0.31	15	1.00
Nanjing-Suzhou	0.30	18	Suzhou-Nanjing	0.15	50	2.03
Leshan-Chengdu	0.30	19	Chengdu-Leshan	0.24	20	1.22
Chongqing-Guangan	0.28	20	Guangan-Chongqing	0.27	16	1.02
Chongqing-Luzhou	0.27	21	Luzhou-Chongqing	0.26	19	1.06
Nanjing-Hefei	0.27	22	Hefei-Nanjing	0.18	32	1.49
Shanghai-Zhenjiang	0.26	23	Zhenjiang-Shanghai	0.22	23	1.17
Shanghai-Wuhan	0.25	24	Wuhan-Shanghai	0.24	21	1.05
Wuxi-Changzhou	0.25	25	Changzhou-Wuxi	0.22	24	1.13
Wuxi-Nantong	0.24	26	Nantong-Wuxi	0.21	25	1.11
Wuhan-Hefei	0.24	27	Hefei-Wuhan	0.22	22	1.07
Changzhou-Nanjing	0.22	28	Nanjing-Changzhou	0.20	27	1.10
Shanghai-Chuzhou	0.22	29	Chuzhou-Shanghai	0.21	26	1.04
Chengdu-Neijiang	0.21	30	Neijiang-Chengdu	0.17	37	1.22
Chongqing-Dazhou	0.21	31	Dazhou-Chongqing	0.20	29	1.08
Yuxi-Kunming	0.21	32	Kunming-Yuxi	0.20	28	1.03
Shanghai-Taizhou	0.20	33	Taizhou-Shanghai	0.16	45	1.28
Chengdu-Yibin	0.20	34	Yibin-Chengdu	0.18	33	1.09
Chongqing-Suining	0.19	35	Suining-Chongqing	0.17	38	1.13
Nanjing-Wuhu	0.19	36	Wuhu-Nanjing	0.19	31	1.02
Liuan-Hefei	0.19	37	Hefei-Liuan	0.12	55	1.56
Yancheng-Shanghai	0.19	38	Shanghai-Yancheng	0.19	30	1.00
Chongqing-Neijiang	0.19	39	Neijiang-Chongqing	0.16	40	1.15
Mianyang-Deyang	0.18	40	Deyang-Mianyang	0.15	49	1.22
Wuhu-Hefei	0.18	41	Hefei-Wuhu	0.18	34	1.04
Qujing-Kunming	0.18	42	Kunming-Qujing	0.18	35	1.02
Shanghai-Xuzhou	0.18	43	Xuzhou-Shanghai	0.16	44	1.12
Zhenjiang-Yangzhou	0.18	44	Yangzhou-Zhenjiang	0.15	48	1.16
Chengdu-Nanchong	0.17	45	Nanchong-Chengdu	0.17	36	1.00
Shanghai-Yangzhou	0.17	46	Yangzhou-Shanghai	0.17	39	1.03
Nanjing-Wuxi	0.17	47	Wuxi-Nanjing	0.15	46	1.10

(Continued on following page)

TABLE 2 (*Continued*) TOP 60 of inter-city contact strength value in the research area.

Direction	F1 (%)	Rank of F1	Direction of connection	F2 (%)	Rank of F2	F1/F2
Shanghai-Wuhu	0.16	48	Wuhu-Shanghai	0.11	57	1.56
Nanjing-Chuzhou	0.16	49	Chuzhou-Nanjing'	0.09	58	1.86
Wuhan-Huangshi	0.16	50	Huangshi-Wuhan	0.16	42	1.02
Yangzhou-Nanjing	0.16	51	Yangzhou-Nanjing	0.16	43	1.02
Ezhou-Huanggang	0.16	52	Huanggang-Ezhou	0.16	41	1.00
Suzhou-Hefei	0.16	53	Hefei-Suzhou	0.15	51	1.08
Shanghai-Bengbu	0.16	54	Bengbu-Shanghai	0.12	56	1.35
Chongqing-Yibin	0.15	55	Yibin-Chongqing	0.14	53	1.12
Hefei-Huainan	0.15	56	Huainan-Hefei	0.15	47	1.00
Chuzhou-Hefei	0.15	57	Hefei-Chuzhou	0.14	52	1.05
Nanchang-Shanghai	0.15	58	Shanghai-Nanchang	0.05	59	3.17
Wuhan-Xianning	0.15	59	Xianning-Wuhan	0.02	60	9.66
Suining-Chengdu	0.14	60	Chengdu-Suining	0.14	54	1.07

between sample cities. However, airplane is not taken into account for four reasons: ① High-speed rail and expressway in Yangtze River Economic Belt is far more developed than air transport, with high-speed trains generally easily reaching 250–350 km/h, while there is a big gap in the development level of aviation industry in the basin. ② In China, the cost of flying is much higher than that of road and rail commuting. Most Chinese residents rarely choose to travel by air. ③ According to the estimation of the urban transport data of both passengers and freight of the Ministry of Transport of China, passenger and cargo of freight traffic in the Yangtze River Economic Belt merely accounts for about 2.64% of that on expressway and railway. ④ It is known that flights are very vulnerable to delays due to weather conditions, causing much uncertainty in commute time. Thus, air transport cannot be regarded as a common mode of transportation between cities in the basin.

3.3 Dual-direction time distance modified gravity model

The gravity model originally came from classical physics, as Formula (1), the gravitational force between two objects that can be regarded as particles is equal to the gravitational constant G multiplied by the mass of two objects (M×m) and then divided by R^2, which represents the distance between two objects.

$$\boldsymbol{F} = \frac{\boldsymbol{G} \times (\boldsymbol{M} \times \boldsymbol{m})}{\boldsymbol{R}^2} \tag{1}$$

In Social Sciences, with the appropriate adjustment of definition of parameters and components, the basic form of gravity model can be transformed into a powerful model for analyzing and predicting spatial properties and interactions, which can be used in the research of spatial layout, spatial interaction (tourism, trade, population migration, *etc.*) and so on [45]. The modified gravity model is as Formula (2):

$$\boldsymbol{K_{ij}} = \frac{\sqrt{\boldsymbol{G_i P_i}}\sqrt{\boldsymbol{G_j P_j}}}{\boldsymbol{T_{ij}^2}};\ \boldsymbol{K_{ji}} = \frac{\sqrt{\boldsymbol{G_j P_j}}\sqrt{\boldsymbol{G_i P_i}}}{\boldsymbol{T_{ji}^2}} \tag{2}$$

in which K represents the contact intensity; T represents the shortest time distance; G represents the total economic output value; p represents the population size. 10,302 and 5151pairs of links between cities have been identified. Formula (3) is further defined to find out the strongest and weakest relationship and location ranking among these cities, in which, $max(R_{ij}, R_{ji})$ and $min(R_{ij}, R_{ji})$ represent the strangest and weakest contact intensity between cities; $\sum_{i,j=1}^{n=78} R_{ij}$ represents the total amount of the contact intensity. Compared with the traditional method of measuring urban links, the improved gravity model can comprehensively measure the functional links between cities and also reflect the differences between them.

$$\boldsymbol{F_1} = \boldsymbol{max}\left(\boldsymbol{R_{ij}}, \boldsymbol{R_{ji}}\right) \Big/ \sum_{\boldsymbol{i,j=1}}^{\boldsymbol{n=78}} \boldsymbol{R_{ij}};\ \boldsymbol{F_2} = \boldsymbol{min}\left(\boldsymbol{R_{ij}}, \boldsymbol{R_{ji}}\right) \Big/ \sum_{\boldsymbol{j,i=1}}^{\boldsymbol{n=78}} \boldsymbol{R_{ji}} \tag{3}$$

3.4 City network structure mining tools: SNA

The research hypothesis of SNA is that the operation of the system is determined by the nature of nodes and the network relations. By analyzing the structure, individual attributes and overall attributes of the network, the overall function of the

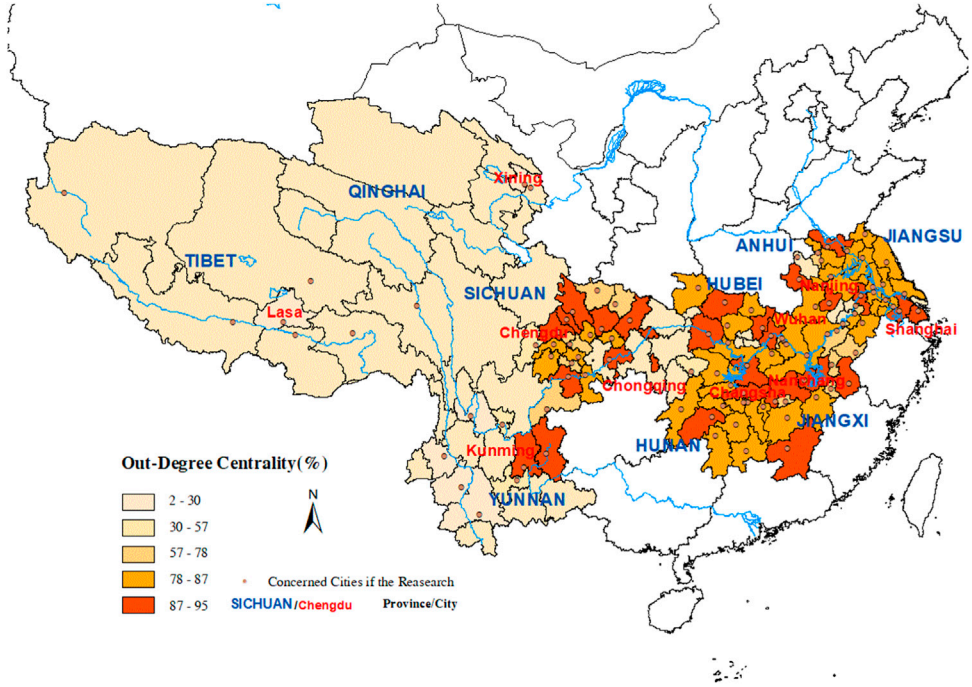

FIGURE 6
Out-degree centrality value distribution in the research area.

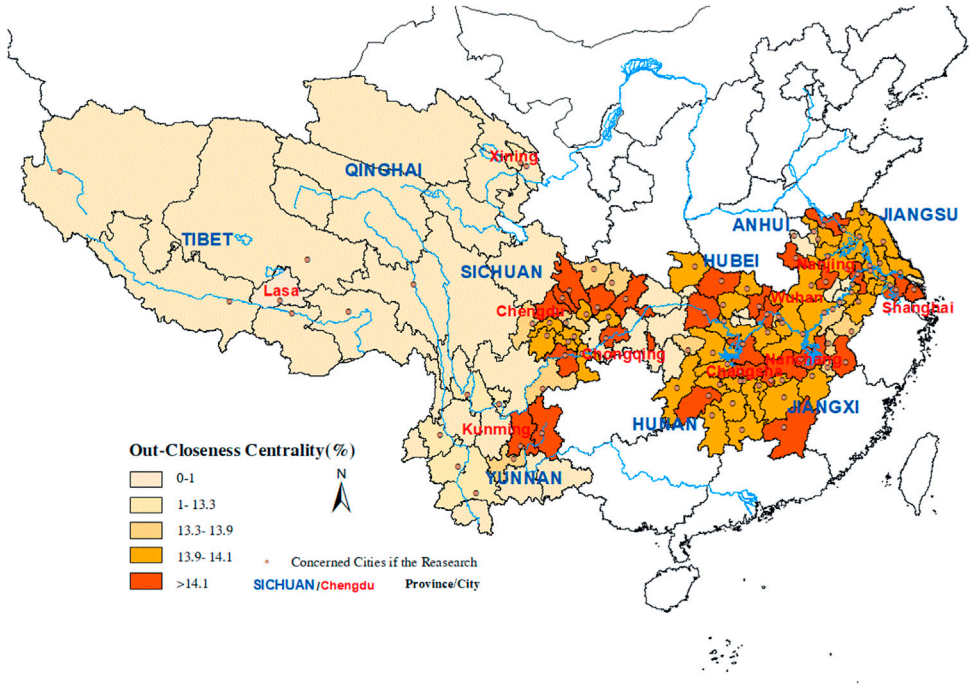

FIGURE 7
Out-closeness centrality value distribution in the research area.

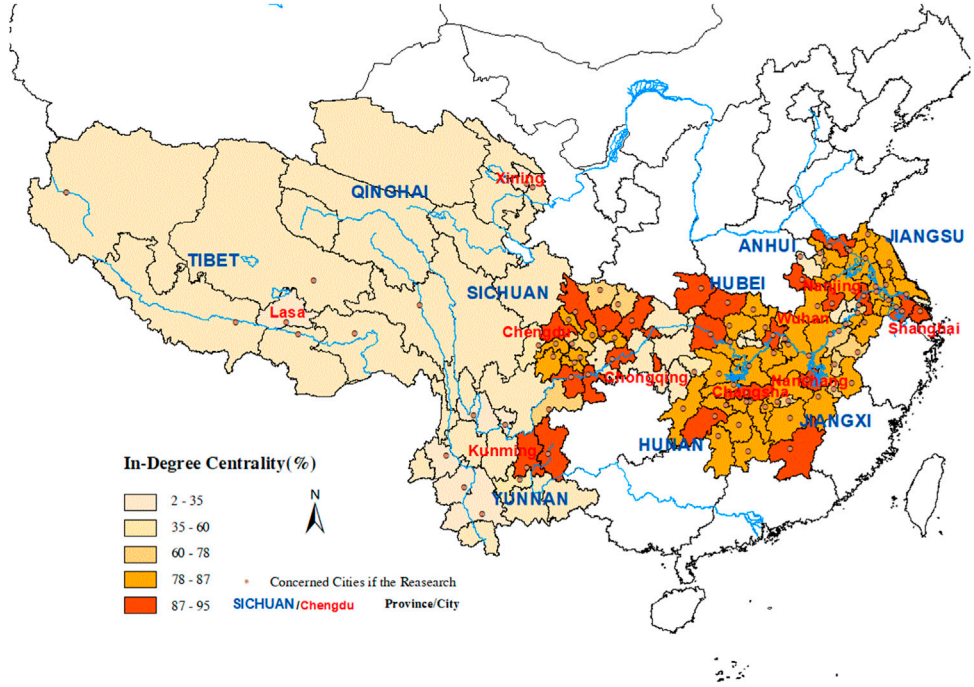

FIGURE 8
In-degree centrality value distribution in the research area.

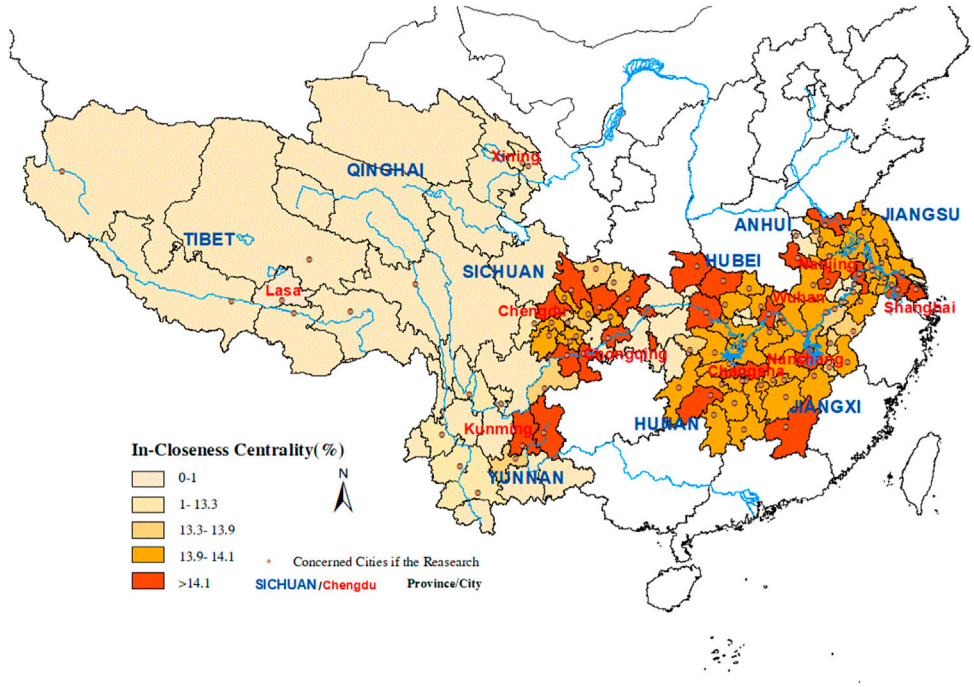

FIGURE 9
In-closeness centrality value distribution in the research area.

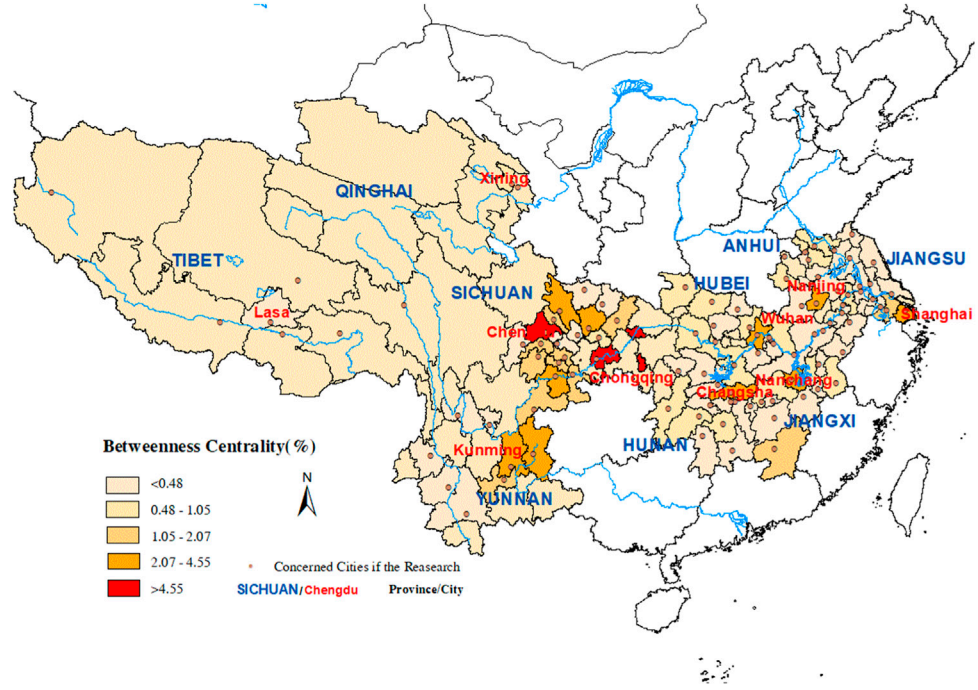

FIGURE 10
Betweenness centrality value distribution in the research area.

system can be improved from the aspects of improving the role of nodes and improving the network connection [46]. In this paper, SNA is applied to describe both the network distribution of the interconnection between cities and the importance of cities in the network. This paper will analyze from three aspects as followed.

3.4.1 Centrality

1) **Degree centrality** The more external connections a node has, the more important it is in the network composition. The degree centrality can be expressed in matrix as formula (4):

$$Cd(N_{ij}) = \sum_{i=1,i\neq j}^{n} X_{ij};\ d(N_{ji}) = \sum_{j=1,j\neq i}^{n} X_{ji} \tag{4}$$

X indicates whether there is a direct connection between node i and others. If there is a direct connection, it is one; if not, it is 0. Obviously, the larger the $Cd\ (N_{ij})$ and $Cd\ (N_{ji})$, the more important the node is in the network. When a certain weight is given to the node, a weighted undirected graph is obtained. $\sum_{i=1}^{n} W$ is the weight of the connecting edge. Then the degree centrality can be expressed as Formula (5):

$$Cd\,(N_i) = \sum_{i=1,i\neq j}^{n} W_{ij} \tag{5}$$

In this study, degree centrality is divided into "out-degree centrality" $U'_{od}(1)$ and "in-degree centrality" $U'_{id}(i)$, that are shown in Formula (6). This indicator reflects the importance of cities in the city network in terms of external and internal links.

$$U'_{od}\,(i) = \sum_{j=1}^{n} X_{ij} \Big/ (n-1);\ U'_{id}\,(i) = \sum_{i=1}^{n} X_{ji} \Big/ (n-1) \tag{6}$$

2) **Closeness centrality** is shown following in Formula (7), d is the shortest arrival time between two cities. This indicator is mainly used to measure the proximity of a city to other cities from a simple space-time distance, reflecting whether the location of the city is easy to reach in the city network, that is, whether it is easy to contact other nodes.

$$CC_i = \frac{1}{d_i};\ d_i = \sum_{j=1}^{N} d_{ij} \tag{7}$$

In this study, closeness centrality is also divided into "out-closeness centrality" C'_{oc} and "in-closeness centrality" C'_{ic}, which are shown following in Formula (8), in which, $d(i,j)$ is the shortest single-way arrival time between cities, respectively. These two indicators measure the proximity of one city to other cities (the ease of contact) and the proximity of other cities to this city (the ease of contact) in the city network.

$$C'_{oc}\,(i) = (n-1) \Big/ \sum_{j=1}^{n} d\,(i,j);\ C'_{ic}\,(i) = (n-1) \Big/ \sum_{j=1}^{n} d\,(j.i) \tag{8}$$

3) **Betweenness centrality** is shown following in Formula (9), in which, $C'_b(1)$ represents betweenness centrality. G is a value calculating the number of shortest paths for one city contacting

TABLE 3 Average city network and development level indicators values in the research area.

Urban agglomerations	Network density (%)	Outward degree Centrality (%)	Inward degree Centrality (%)	Outward closeness Centrality (%)	Inward closeness Centrality (%)	Betweenness Centrality (%)	2021 urbanization rate (%)	2021 average GDP (108 RMB)
Overall	70.67	20.8	31.3	36.7	37.6	9.78	69.78	4,459.84
Chengdu basin	75.5	90	94	14.27	14.27	168.52	72.37	6,075.33
Chongqing	74.5	95	95	14.29	14.29	262.52	73.49	6,321.62
Wuhan	75.3	93	93	14.25	14.25	53.44	71.25	6,435.59
Hefei	76.5	92	92	14.23	14.23	38.90	73.21	4,450.27
Nanjing	80.5	89	88	14.15	14.17	15.13	77.16	6,457.49
Shanghai	82.6	93	93	14.25	14.25	74.27	86.54	8,897.55
Kunming	66.6	93	93	14.25	14.25	53.43	69.29	2,832.24
Changsha	68.8	93	92	14.23	14.23	45.65	70.23	3,043.13
Nanchang	65.4	93	91	14.21	14.25	40.12	71.39	2,714.93

others. This indicator reflects the importance of a city as a "connecting transit station" to communicate with other nodes and as a functional exchange medium in the city network.

$$C'_b(i) = \frac{\sum_{j<k} g_{jk}(c_j)/g_{jk}}{(n-1)(n-2)} \quad (9)$$

3.4.2 Network density

The network density reflects the city network development level. High network density means cities in the region are closely connected, and the city network seems to be mature. Formula (10) shows the network density calculating method, in which, D is the network density; m means the exact number of connections among cities in research scope, and n means the total number of samples (cities in the research scope).

$$D = m/[n \times (n-1)] \quad (10)$$

3.4.3 Cohesive subgroups

In the study of city networks, cities usually form clusters because of their close and direct links, that is "internal cohesive subgroups." Cohesive subgroup analysis can generally deeply analyze the city networks distribution structure and classify cities with the same characteristics [43, 44]. In order to figure out the cohesive subgroups of the city network which is in the research area, a kind of network analysis software named UCINET (version6.5) has been used in this research.

3.5 Research tools for inter-city officials transfer networks

China is a unitary country, which implements the governance system of "centralized leadership by the central government—authorization to local governments to govern all regions". Through the performance evaluation, selection and promotion system, local officials are encouraged to improve work efficiency, innovate policies, compete for development resources and strengthen urban construction. Among the constituent factors of China's city network, the factor of local leadership is very special. The policies and efforts of local officials will greatly affect the local economic and social development [47]. First, since the reform and opening-up, Chinese local officials have taken the expansion of opening-up as an important means of economic development. Attracting foreign and domestic funds and expanding regional cooperation often rely on the private social relations of local officials, mainly to cooperate with their hometown or places where they have served [48]. On the other hand, China often transfers officials with excellent performance from developed cities to less developed provinces, makes more scientific development

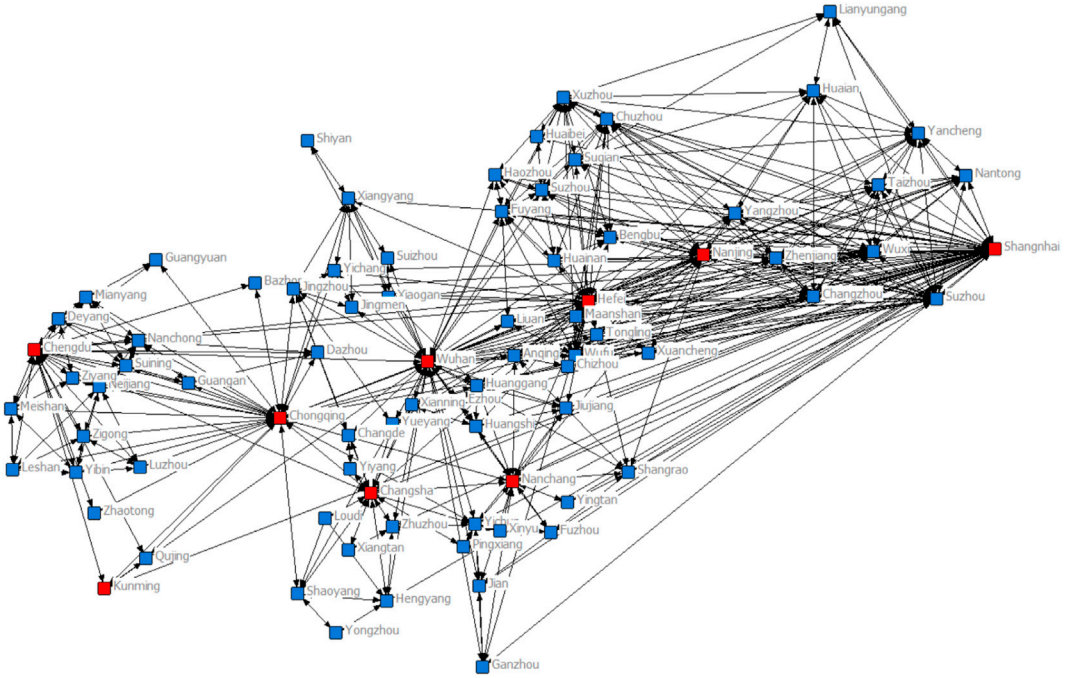

FIGURE 11
City networks structure of the Yangtze River Basin area.

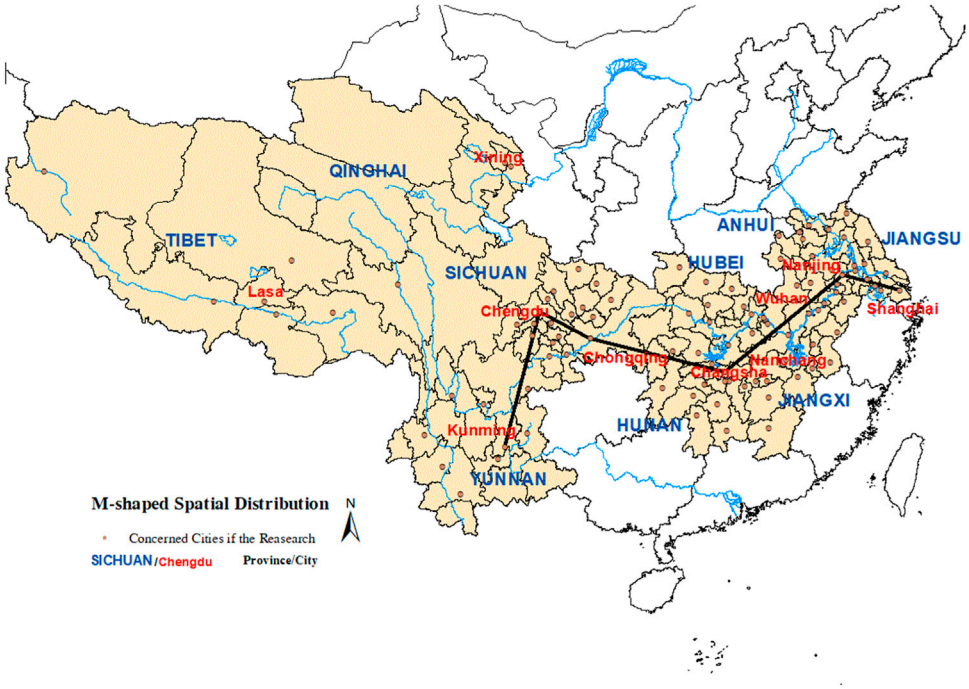

FIGURE 12
High network density value distribution shape in the Yangtze River Basin area.

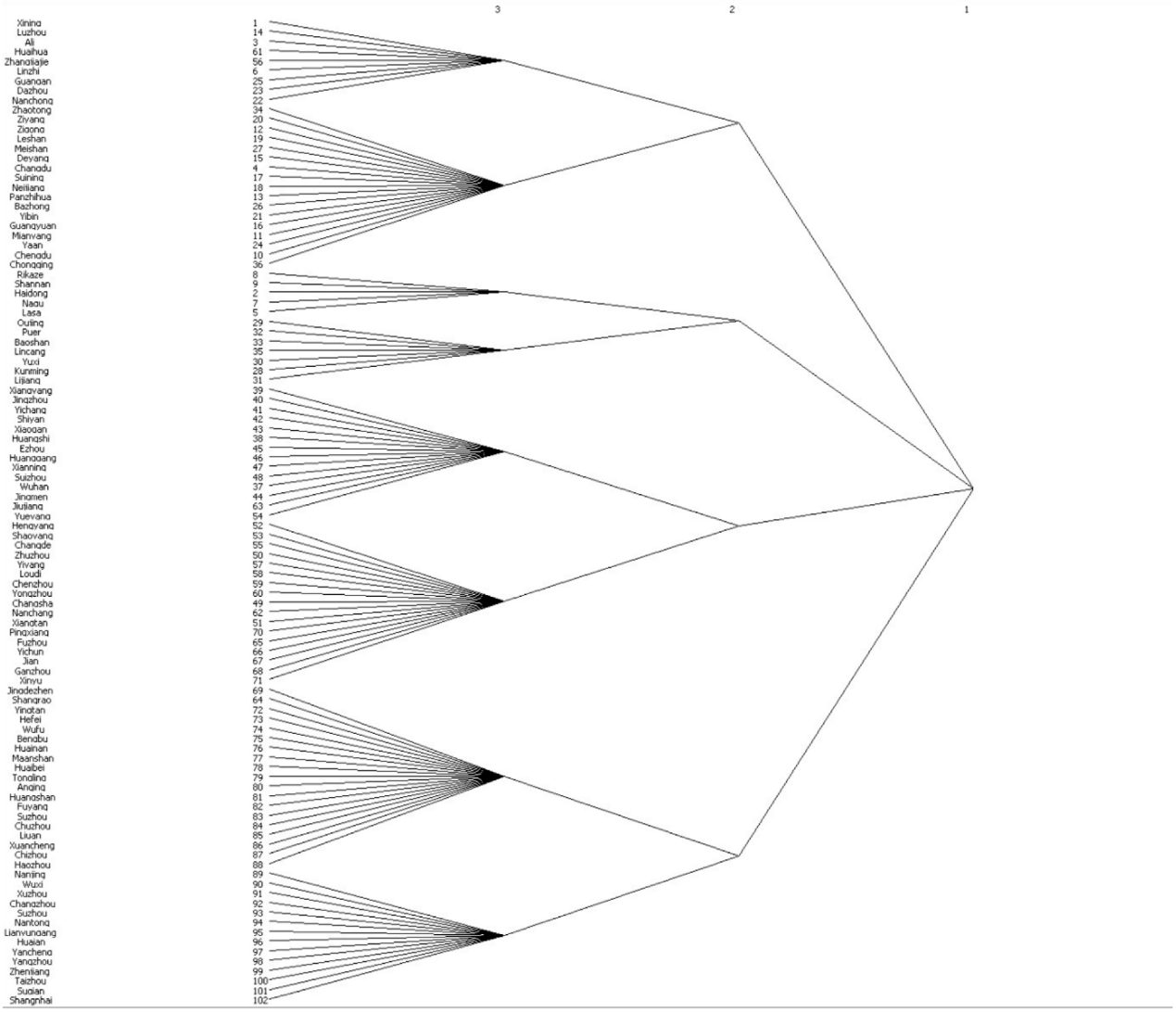

FIGURE 13
Cohesive subgroups in the research area.

plans and policies for less developed cities, and implements more efficient and powerful management behaviors. More importantly, with the help of the interpersonal relations and enterprise cooperation experience accumulated by excellent officials in developed provinces and cities, cooperation between cities and realization of the complementary resource advantages between cities can be established. Therefore, the transfer of officials between cities is also an important factor to promote the formation of city networks. Although the transfer of officials among cities in the Yangtze River Basin has not yet formed a large-scale network, which is difficult to be directly included in the gravity model and SNA, this study takes the transfer of city officials as a supplementary study to further reveal the closeness of "political cooperation" and the potential social connection potential between cities.

4 Results and discussion

4.1 Intensity analyzing of dual-direction economic connection between cities

Calculation Formulas 2 and 3 of the improved gravity model are used to calculate the Dual-direction connection strength between cities, and then the map of the Dual-direction connection strength between cities is drawn with the aid of Arc GIS10.2 software. Figure 4 shows the larger connection

TABLE 4 Cohesive subgroups of city networks in the research area.

Research area	The 2nd class subgroup		The 3rd class subgroup
	Location of region	Province list	Definition of the subgroup
The Yangtze River Basin	Northwest bank of middle reaches	Upstream Yangtze River Delta Urban Agglomerations	Sichuan, Tibet, Qinghai Adjoining District Urban Agglomeration
			Sichuan, Chongqing, and Eastern Tibet Urban Agglomeration
	Middle and upper reaches	Yunnan, Western Tibet, and part of Qinghai	Western Tibet-Qinghai Urban Agglomeration
			Yunnan Urban Agglomeration
	East bank of middle reaches	Part of Triangle of Central China	Hubei Adjoining District Urban Agglomeration
			Hunan- Southwest Jiangxi Urban Agglomeration
	Lower reaches	Part of Yangtze River Delta Urban Agglomerations	Anhui- Northeast Jiangxi Urban Agglomeration
			Jiangsu-Shanghai Urban Agglomeration

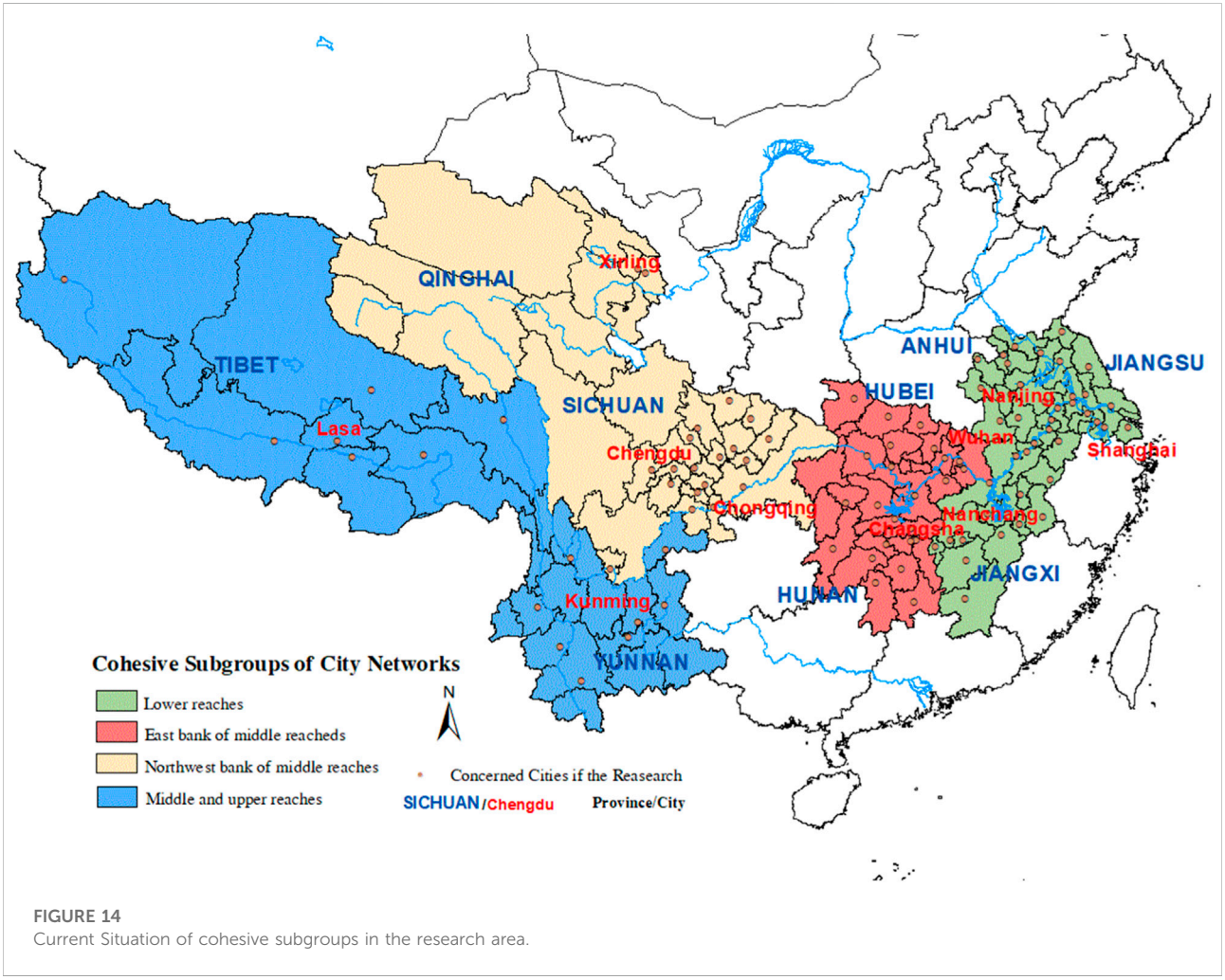

FIGURE 14
Current Situation of cohesive subgroups in the research area.

strength value F1 in each pair of urban connections, and Figure 5 shows the smaller connection strength value F2 in each pair of urban connections. In order to make the illustration clearer, Figure 4 and Figure 5 simply show the links with urban contact strength values which are larger than 2000 million × 10,000 people/minute^2.

Table 2 shows the 60 pairs of city relations with the highest connection strength and their reverse city relations among the 5,151 pairs of city links between cities:

First, the connections between the cities are mostly of little difference in strength (in both directions), indicating that most cities are of an equal relationship between each other of mutual benefit and reciprocity. Almost all of F1/F2 are close to 1, and most of them are higher than one mainly in regional central cities such as Shanghai, Chongqing, Nanjing, Wuhan, Chengdu, Suzhou, Wuxi, *etc.*, indicating that these cities have significantly stronger external connections than other cities, with distinguishing feature of central cities obviously reflected.

Second, value differentiation of contact strength within Yangtze River Economic Belt cities is more obvious. "Shanghai-Suzhou" (2.09%) shows the highest value of the contact strength between cities, which is almost twice the value between the second-placed "Chongqing-Chengdu" (1.34%). After the 10th place, the value of connection strength between cities is already less than 0.5%. The top five cities with the strongest connection with others are Shanghai, Chongqing, Suzhou, Chengdu, and Wuhan. Shigatse, Shannan, Nagqu, Nyingchi, Ali and other cities have the lowest sum of connection strength values with other cities, which is already less than one billion yuan*10,000 people/min^2. It is quite evident that the city connection has an obvious cluster structure. The urban clusters driven by the regional central cities are distributed evenly in the river basin, the "agglomeration effect" of the central cities is significant.

Third, the regional disparity in the connection strength between cities is relatively obvious, showing the law of "city connection in the lower reaches > city connection in the upper and middle regions". This is due to the fact that there are many mountains and basins in the middle and upper reaches, and topographic factors restrict the construction of economy, population interaction and transportation facilities.

4.2 City network structure analyzing

4.2.1 Centrality result

After calculating the in-degree/out-degree centrality, in-closeness/out-closeness centrality and betweenness centrality in the region according to formulas (6) 8) and (9), the following rules can be seen:

Figure 6 and Figure 7 show the current situation of the out-degree centrality and the out-closeness centrality in cities. The averages of the two are 73.4 and 13.2% respectively, with a big difference. It shows that although there seems to be not close connection to each other, the radiation and driving effect between cities is significant, which is gratifying. The out-degree centrality of Shanghai, Wuhan, Chengdu, Kunming and other cities is as high as or close to 95%, indicating that these regional central cities have strong external connection ability and high driving ability. There are many cities with strong radiative driving force being evenly distributed in the basin, which is good for the development of city network. However, the differences in the out-degree centrality between cities are also obvious. The cities in the lower reaches have the highest and more balanced out-degree centrality; and those in the middle and upper reaches of metropolitan area such as "Chengdu-Chongqing" and "Changsha-Zhuzhou-Xiangtan" also have the high out-degree centrality, but the difference is obvious. The external radiation capacity of Ya'an, Yingtan, Jingdezhen and other cities is relatively weak.

From the perspective of urban attractiveness, the average in-degree centrality and in-closeness centrality of sample cities are 73.4 and 13.2% respectively, and the difference is also obvious. It can also be seen that the attraction of cities to resources is strong with the support of factors such as transportation construction. Figure 8 and Figure 9 show that cities which are central cities located in the downstream and midstream such as Shanghai, Wuhan, and Chongqing have high in-degree centrality and in-closeness centrality. Node cities in different flow segments have good element transition and conduction effects.

The betweenness centrality of the city network in research region is 16%, but the difference is very large, and the function of the intermediary connection hub of the regional cities is obviously different. Figure 10 shows that a few cities in the midstream and upstream area can get a higher value of betweenness centrality relatively. Chongqing, Wuhan, Chengdu and Kunming have particularly prominent intermediary functions. In contrast, the intermediary functions around Wuhan, Shanghai and Suzhou are relatively scattered. It shows only a few city connection nodes exist in these areas, and the choice is not multiplied. Most surrounding cities can only rely on the central city to establish connections. The "center-edge" characteristic is obvious, and the urban agglomeration as a whole still relies heavily on a few cities as a "media" to expand the economic contact between cities. The betweenness centrality of Shannan, Nagqu, Nyingchi, Haidong and other cities in Tibet is 0, suggesting that these cities are marginal in the network.

4.2.2 City network density

As a result from formula (10), the city network density whose average value is as high as 72.67% in the research area is calculated. Regions including the "Chengdu-Chongqing" urban agglomeration and the metropolitan circles around Wuhan, Nanjing, Nanchang, Hefei, and Shanghai score much higher city network density relatively. The sum of connection

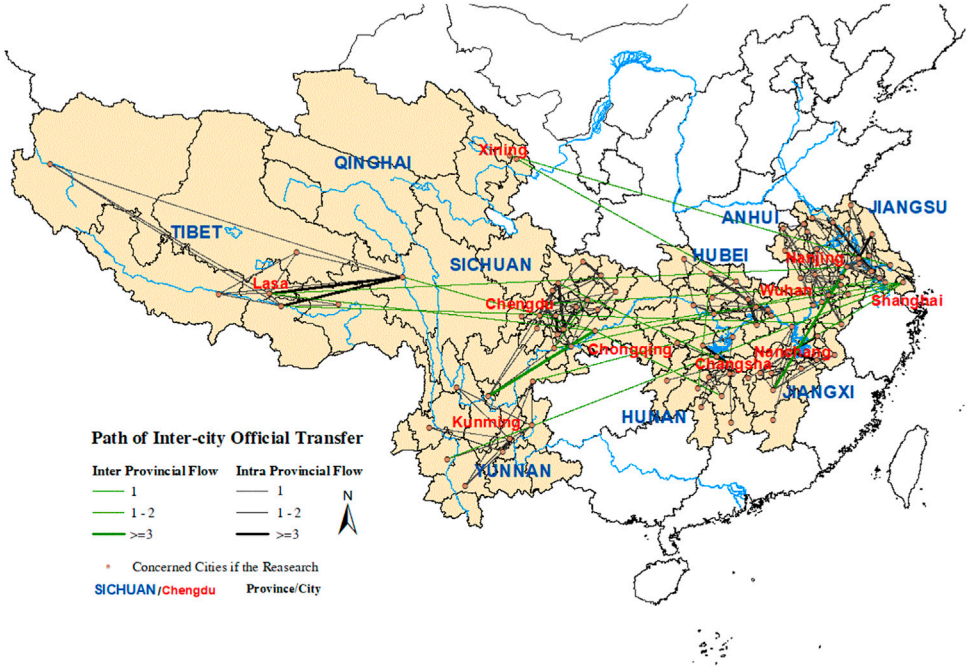

FIGURE 15
Path diagram of inter-city official transfer in the research area.

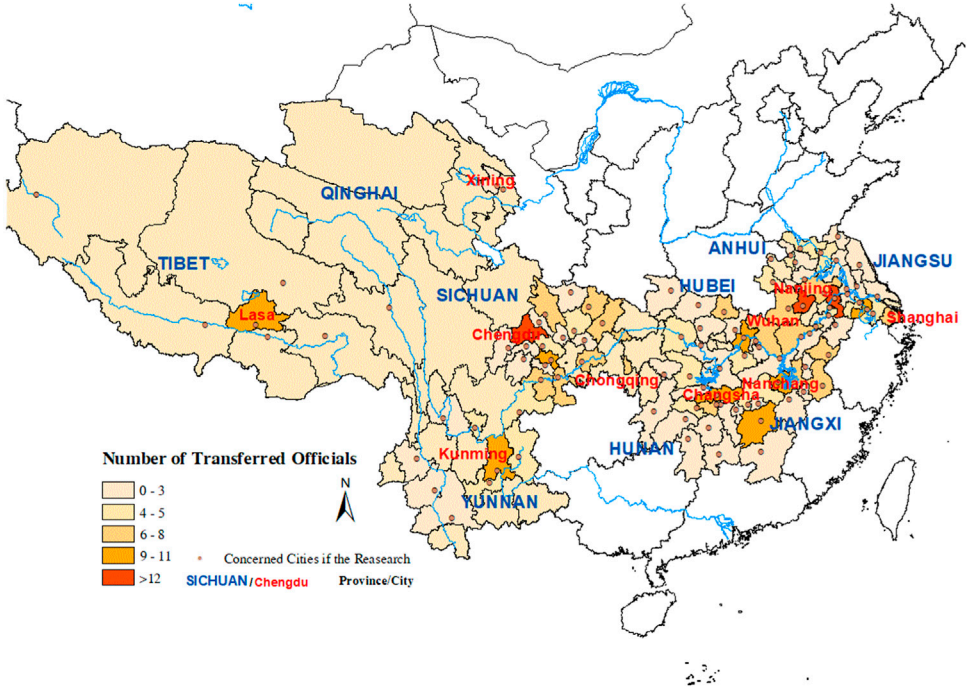

FIGURE 16
Current situation of the amount of primary city officers transferred between cities in the research area.

strength values between cities in these regions accounts for more than 90% of the sum of the 5,151 pairs of connection strength values among all cities in the research region. Table 3 shows that the betweenness centrality of each urban agglomeration in the Yangtze River Economic Belt is close to 90%, indicating relatively high level of development connection and integration. The city network density of sub-urban agglomerations is mostly higher than that of the whole region, suggesting that the internal economic and social connection is far stronger than the overall contact intensity of the basin cities, and the connection between the sub-urban agglomerations interaction needs to be strengthened.

Figure 11 shows that the overall city network density in the research area exhibits the characteristics of "balanced distribution in north and south, dense in the east and sparse in the west, high density along the river, and low density far from the riverside". The city network density in areas near the river is significantly higher, indicating that rivers play a crucial role during the formation of city networks. The network density of central cities such as Chengdu, Chongqing, Wuhan, Shanghai is significantly higher than that of other regions. The characteristics of sub-centers such as Changsha, Kunming and Nanchang are also obvious. The structure of "center-subcenter" is clear, and is evenly distributed in the river basin. The city network in the midstream region and that in its lower reaches which is also called Yangtze River Delta tends to converge.

Figure 12 shows that the city network density distribution in the study area is basically consistent with the rivers, showing the M-shaped distribution characteristic:

4.3 City cohesive subgroups result

As shown in Figure 13 and Table 4, there are of four kinds of second class subgroups and eight kinds of third class subgroups in the research scope recognized by UCINET software. The urban subgroups in the basin show a trend of cross provincial integration. The urban subgroups between Sichuan and Chongqing, Hunan and Hubei, Anhui and Jiangxi, Jiangsu and Shanghai are closely combined, and the connection intensity within different subgroups is slightly different.

Figure 14 describes the spatial distribution of current cohesive subgroups.

4.4 Transferring network result of city officers between cities

As shown in Figure 15 and Figure 16, we used ArcGIS software to draw the city level official transfer path in this area from 2015 to 2020, reflecting the potential economic cooperation and resource cooperation possibilities between cities, which are promoted by official private social relations. The results show that officials transfer between cities is mainly within provinces. It is common for officials to be transferred at the same post level between cities. Officials transferred across provinces are usually at the same level. Most of the job promotions occur when officials are transferred from non-central cities to central cities. Non-central cities also transfer officials to each other. Cities which is the five largest number of officials transferred to are Xining (16 transfers), Haidong (15 transfers), Ali (Tibet) (14 transfers), Changdu (11 transfers) and Lhasa (10 transfers), most of which are underdeveloped cities in the basin. Local officials in Chengdu, Kunming, Wuhan, Chongqing and Xining have been transferred to backward cities more frequently. It reflects that the government attach importance to the transfer of outstanding officials to help the development of backward cities.

5 Conclusion and suggestions

The "dual-direction time distance" modified gravity model can better show interaction differences between cities, and comprehensively reflect the possibility of real and potential economic cooperation, population flow and resource connection between cities. It has high application value for the mining of regional city network structure.

The city network connection strength in the area has obvious regional differentiation characteristics. The connection strength between cities in the downstream area is higher than that in the midstream and upstream area. The development level of the city network is positively correlated with the level of regional economic development. Because the level of economic development determines the level of local fiscal revenue and infrastructure construction capacity, at the same time, a larger economic scale can also generate more economic cooperation, which has a reverse role in promoting the strengthening of regional inter city ties.

The average values of "out-degree centrality" and "in-degree centrality" of the cities in the research area are high, but the difference between cities is obvious, which also shows the characteristics of "downstream area > middle and upstream area". Most dual-direction connection strength between cities is generally equal, but that of the central city to surrounding cities is dramatically higher than that of surrounding cities to their central city, indicating that the "agglomeration effect" of the central city is significant and the central status is strong. The urban connection in the basin has obvious cluster structure, and the urban agglomeration is relatively mature and closely connected. The internal connection strength of cohesive subgroups of cities is strong, while the connection strength between cohesive

subgroups of cities is relatively small. The cohesive subgroups of cities generally present an "M" shape along the river.

The results show that the construction of urban transport facilities in the river basin is generally in a satisfying condition, though the shortcomings in the middle and upper reaches still need to be made up. Chongqing, Chengdu, Kunming and other cities are very important for the interaction between cities within the region as well as in the connection between regional cities and downstream developed areas. The "center-edge" structure of urban agglomeration is more obvious.

Based on the empirical analysis, there are some practical suggestions proposed as followed:

First, the Yangtze River basin is of strong economic strength. There are many central cities with strong radiative driving power, which are evenly distributed in the river basin. Promoting the integration of urban functional groups will be a key task. In the near future, the 4 second-class subgroups of the city network may be prioritized as plans of zoning for the construction of the city network. First, strengthen the internal relations of the secondary subgroups, vigorously develop the intercity railway, promote the industrial echelon transfer and the uniform distribution of the population. On this basis, gradually strengthen the interconnection of various infrastructure between adjacent subgroups. Nanchang in Jiangxi, Kunming in Yunnan and Changsha in Hunan can be selected as key cities. Promote the further integration of several major urban agglomerations, form the urban development pattern of "downstream driving - midstream transition - upstream connection", and drive the development of cities in the upstream such as central Yunnan and the hinterland of Tibet area.

Second, further enhance the functions of central cities, expand the radiation and driving capacity, and strengthen the links between central cities. The central city plays an important role in regional economic driving, function transmission intermediary, and building a cooperation platform. The construction of central cities can refer to the current M-shaped distribution to build the core city chain in the west-east direction of "Chengdu/Chongqing - Wuhan - Hefei - Nanjing—Shanghai" connecting the upstream and downstream areas, develop the sub central city chain of "Kunming - Changsha—Nanchang", and strengthen the links between the north and south basin.

Third, give full play to China's institutional advantages can promote potential economic and resource development cooperation by strengthening the mobilization of excellent officials between developed and underdeveloped regions, so that the development achievements and resource advantages of different regions can be shared. Through the mobilization of local officials, the use of private social contacts of officials can enhance the potential complementarity between cities in the river basin into reality, enhance the cross regional transfer and cooperation of resource elements, and promote the sharing of development achievements while improving economic efficiency.

In the future, it will become a more accurate research tool to mine the city network structure by using the big data of regional population migration, economic cooperation and transportation. At the same time, the dynamic change process of city network density also deserves further study.

Data availability statement

The original contributions presented in the study are included in the article/Supplementary Material, further inquiries can be directed to the corresponding author.

Author contributions

DC, research scheme design, literature review, empirical research operation, empirical results analysis, paper organization and editing of the full paper. JD, literature review, empirical research operation, writing of a section of the paper. ZY, data collection and sorting operation. DZ, literature review, empirical research operation and GIS map making.

Funding

This study was supported by the National Natural Science Foundation of China (Grant no. 71974220).

Acknowledgments

Thank Professor Song Yan of the UNC for her enlightening suggestions on the research. At the same time, thank Li Changqing for providing English polishing and proofreading for this article.

Conflict of interest

The authors declare that the research was conducted in the absence of any commercial or financial relationships that could be construed as a potential conflict of interest.

Publisher's note

All claims expressed in this article are solely those of the authors and do not necessarily represent those of their

affiliated organizations, or those of the publisher, the editors and the reviewers. Any product that may be evaluated in this article, or claim that may be made by its manufacturer, is not guaranteed or endorsed by the publisher.

Supplementary material

The Supplementary Material for this article can be found online at: https://www.frontiersin.org/articles/10.3389/fphy.2022.1018993/full#supplementary-material

References

1. Cao X, Liang F, Chen H. Influence of different spatial forms for metropolitans on transportation network efficiency. *Scientia Geographica Sinica* (2019) 39(1): 41–51. doi:10.13249/j.cnki.sgs.2019.01.005

2. Peng F. Economic spatial connection and spatial structure of Guangdong-Hong Kong-Macao greater Bay and the surrounding area cities—an empirical analysis based on improved gravity model and social network analysis. *Econ Geogr* (2017) 37(12):57–64. doi:10.15957/j.cnki.jjdl.2017.12.008

3. Ding R, Liu M, Li D. The driving effect of Polycentric city network on coordinated regional economic development—Taking the Yangtze River economic belt as an example. *Stat Res* (2020) 37(11):93–105. doi:10.19343/j.cnki.11-1302/c.2020.11.008

4. Liu H, Shen Y, Meng D, Jin X. The city network centrality and spatial structure in the Beijing-Tianjin-Hebei metropolitan region. *Econ Geogr* (2013) 33(8):37–45. doi:10.15957/j.cnki.jjdl.2013.08.008

5. Liu K, Zhou Y, Wang S. Urban science and technology innovation efficiency and network structure characteristics:an empirical analysis based on national innovative cities. *Sci Technology Prog Policy* (2020) 37(23):36–45.

6. Taylor PJ, Derudder B. *World city network: A global urban analysis*. London: Routledge Press (2003). p. 256.

7. Castells M. *The rise of the network society*. Massachusetts: Blackwell Publishers (1996). p. 656.

8. Pan F, Cheng F, Li X. The Progress and prospect of research on Chinese city network. *Scientia Geographica Sinica* (2019) 39(7):1093–101. doi:10.13249/j.cnki.sgs.2019.07.007

9. Li D, Yi W, Wang T. Spatial and temporal evolution of urban innovation network in China. *Habitat Int* (2015) 49:484–96. doi:10.1016/J.HABITATINT.2015.05.031

10. Feng Z, Wang X, Yin J, Zhang M. An empirical study on Chinese city network pattern based on producer services. *Chin Geogr Sci* (2013) 23(3):274–85. doi:10.1007/s11769-013-0595-8

11. Zhao M, Liu X, Derudder B, Zhong Y, Shen W. Mapping producer services networks in mainland Chinese cities. *Urban Stud* (2015) 52(16):3018–34. doi:10.1177/0042098014558541

12. Wang F, Liu Y, Wang J. Transport networks, intraurban structure and system of cities:a Sino-US comparative perspective. *Prog Geogr* (2014) 33(10):1289–99.

13. Cheng Y, Zhu Y. The Tum of the world city study and Chinese world cities. *Urban Plann Forum* (2015) 5:39–44. doi:10.16361/j.upf.201505005

14. Li M, Wang C, Liu H, Wang R, Yu S. Evaluation of urban development quality and characteristics of spatial connection network in the Yellow river basin. *Econ Geogr* (2021) 41(12):84–93. doi:10.15957/j.cnki.jjdl.2021.12.009

15. Wang C, Duan Y, Zhang R. Spatial pattern evolution of cities and influencing factors in the Historical Yellow river basin. *J Nat Resour* (2021) 36(1):69–86. doi:10.31497/zrzyxb.20210105

16. Xu P, Ye Z. Review and prospect of the development of urban agglomerations in New China in the past 70 years. *Development Res* (2019) 11:18–25.

17. Lu D. The 'T'-shaped structure of land development and economic Arrangements and the Sustainable development of the Yangtze economic belt. *Macroeconomic Management* (2018) 11:43–7+55. doi:10.19709/j.cnki.11-3199/f.2018.11.008

18. Zhang G. Promote high-quality development of the comprehensive transportation system in the Yangtze economic belt. *China Transportation Rev* (2022) 44(1):1.

19. Li M, Wang L. Discussing how to extract city characteristic with the examples of ancient capital cities in the Yellow River basin. *China Ancient City* (2017) 5: 25–30.

20. Xiao H. Analysis of some Advances in Contemporary social network research. *Sociological Stud* (1999) 3:3–13.

21. Fujita M, Ogawa H. Multiple equilibria and structural transition of non-monocentric urban configurations. *Reg Sci Urban Econ* (1982) 12:161–96. doi:10.1016/0166-0462(82)90031-x

22. Smith DA, Timberlake M. Conceptualising and mapping the structure of the world System's city system. *Urban Stud* (1995) 32(2):287–302. doi:10.1080/00420989550013086

23. Taylor PJ, Catalano G, Walker DRF. Exploratory analysis of the world city network. *Urban Stud* (2002) 39(13):266–79. doi:10.1080/0042098022000027013

24. Derudder B, Taylor P. The cliquishness of world cities. *Glob Networks* (2005) 5(1):71–91. doi:10.1111/j.1471-0374.2005.00108.x

25. Pflieger G, Rozenblat C. Introduction. Urban networks and network theory: The city as the connector of multiple networks. *Urban Stud* (2010) 47(13):2723–35. doi:10.1177/0042098010377368

26. An Y, Liu J, Qiao D. Analysis of the urban spatial connection network pattern of the central Plains urban agglomeration——based on the comprehensive traffic information flow. *Scientia Geographica Sinica* (2019) 39(12):1929–37. doi:10.13249/j.cnki.sgs.2019.12.011

27. Zachary P. Fallacies in world city network measurement*. *Geogr Anal* (2021) 53(2):377–82. doi:10.1111/gean.12230

28. Wang C, Wang M. Evolution of associated network characteristics between cities in Shandong province comparing central place and flow space Theories. *Geographical Res* (2017) 36(11):2197–212.

29. Gao Z, Zhang M. Analysis of efficiency Heterogeneity and spatial effect of urban Shrinkage in the Yellow river basin. *Urban Probl* (2021) 4:4–11. doi:10.13239/j.bjsshkxy.cswt.210401

30. Zhang H, Jia S, Luo Y. Spatial network structure of tourism economic relations in the upper Reaches of the Yangtze River. *Areal Res Development* (2022) 41(2): 95–100.

31. Qiu Y, Han W, Wu J. Dynamic evolution of innovation space correlation network of urban agglomeration in the middle reaches of Yangtze River——an empirical research based on social network analysis. *J Xiangtan University(Philosophy Social Sciences)* (2021) 45(52):80–6+107. doi:10.13715/j.cnki.jxupss.2021.05.013

32. Wang S, Song Y, Wen H, Jing L. Network structure analysis of urban agglomeration in the Yangtze River economic belt under the perspective of Bidirectional economic connection:based on time distance and social network analysis method. *Econ Geogr* (2019) 39(2):73–81. doi:10.15957/j.cnki.jjdl.2019.02.009

33. Wu C, Huang X, Chen B, Li J, Xu J. Analysis of economic and spatial linkage and economic integration trend in Yangtze River economic belt from social network analysis perspective. *Econ Geogr* (2017) 37(7):71–8. doi:10.15957/j.cnki.jjdl.2017.07.010

34. Gao P, He D, Sun Z, Ning Y. Characterizing functionally integrated regions in the Central Yangtze River Megaregion from a city-network perspective. *Growth and Change* (2020) 51(3):1357–79. doi:10.1111/grow.12401

35. Zhao J, Wang C, Cao S. City network structures of the Yangtze River Basin and the Yellow River Basin based on multi-el- ement factor flows. *China Popul Resour Environ* (2021) 31(10):59–68.

36. Wu S, Zhong Y, Wu Q, Mao W. Multi-outward connection networks of urban agglomeration:an empirical study from middle reaches of Yangtze River to Yangtze River economic belt. *Resour Environ Yangtze Basin* (2021) 30(10):2360–72.

37. Sun J, Hu W, Fu Y. City network structure and spatial pattern in Yangtze River economic belt based on the analysis of HSR flow data. *Areal Res Development* (2022) 41(3):75–81.

38. Gao S, Liu J. The research of Beijing-Tianjin-Hebei urban Agglomerations'Spatial connection based on urban relation intensity and urban flow. *Areal Res Development* (2013) 32(3):57–61.

39. Lian J, Zeng G, Teng T. Research on the difference of function diffusion of the central city based on the economic connection intensity:A Case of the central city of

Hangzhou metropolitan area and its Compact cities. *Areal Res Development* (2017) 36(6):54–8.

40. Zhang H, Zhang D, He Q. Analysis of urban association intensity based on Tencent migration data and gravity model ——a Case study of urban agglomeration around Poyang lake. *Chin Overseas Architecture* (2019) 7:66–9.

41. Li E, Lu Y, Yang X, Chen Y, et al.Spatio-temporal evolution on connection strength of global city network based on passenger flight data from 2014 to 2018. *Scientia Geographica Sinica* (2020) 40(1):32–9. doi:10.13249/j.cnki.sgs.2020.01.005

42. Jun C, Zheng G, Liu Y. The spatial connection evaluation of Yangtze River Delta with the high-speed rail. *Econ Geogr* (2014) 34(8):54–60+67. doi:10.15957/j.cnki.jjdl.2014.08.037

43. Guo L, Wang R. Syudy on Accessibility and spatial connecting among the cities in Sichuan basin urban agglomeration. *Hum Geogr* (2009) 24(3):42–8.

44. Meng H, Huang X, Yang J, Lin B. Network structure and development concept in Huaihai economic zone. *Econ Geogr* (2019) 39(12):1–10. doi:10.15957/j.cnki.jjdl.2019.12.001

45. Chen L, Jin X. Measurement of spatial interaction between central towns based on the gravity model. *Scientia Geographica Sinica* (2016) 36(5):724–32. doi:10.13249/j.cnki.sgs.2016.04.005

46. Liu Y, Li G, Sun L. City network research in China:A literature review based on social network analysis. *Urban Development Stud* (2021) 28(11):16–22.

47. Wu M, Zhou L. Political Incentives and city construction: The Visibility of public Projects. *Econ Res J* (2018) 53(12):97–111.

48. Niu J, Wei X. Official mobility, Interragional connections and Interprovincial trade flows. *Finance Trade Econ* (2020) 41(6):128–43. doi:10.19795/j.cnki.cn11-1166/f.20200609.001

frontiers | Frontiers in Physics

TYPE Original Research
PUBLISHED 03 October 2022
DOI 10.3389/fphy.2022.1019969

OPEN ACCESS

EDITED BY
Fei Xiong,
Beijing Jiaotong University, China

REVIEWED BY
Qian Liu,
Nanyang Technological University, Singapore
Zhonggui Ma,
University of Science and Technology Beijing, China
Weijia You,
Beijing Forestry University, China

*CORRESPONDENCE
Haitao Xiong,
xionghaitao@btbu.edu.cn

SPECIALTY SECTION
This article was submitted to Social Physics, a section of the journal Frontiers in Physics

RECEIVED 15 August 2022
ACCEPTED 14 September 2022
PUBLISHED 03 October 2022

CITATION
Cai Y, Zuo M and Xiong H (2022), Modeling hierarchical attention interaction between contexts and triple-channel encoding networks for document-grounded dialog generation. *Front. Phys.* 10:1019969. doi: 10.3389/fphy.2022.1019969

Modeling hierarchical attention interaction between contexts and triple-channel encoding networks for document-grounded dialog generation

Yuanyuan Cai[1,2], Min Zuo[1,2] and Haitao Xiong[1,3]*

[1]National Engineering Research Centre for Agri-Product Quality Traceability, Beijing Technology and Business University, Beijing, China, [2]School of E-Business and Logistics, Beijing Technology and Business University, Beijing, China, [3]School of International Economics and Management, Beijing Technology and Business University, Beijing, China

Dialog systems have attracted attention as they are promising in many intelligent applications. Generating fluent and informative responses is of critical importance for dialog systems. Some recent studies introduce documents as extra knowledge to improve the performance of dialog generation. However, it is hard to understand the unstructured document and extract crucial information related to dialog history and current utterance. This leads to uninformative and inflexible responses in existing studies. To address this issue, we propose a generative model of a neural network with an attention mechanism for document-grounded multi-turn dialog. This model encodes the context of utterances that contains the given document, dialog history, and the last utterance into distributed representations *via* a triple-channel. Then, it introduces a hierarchical attention interaction between dialog contexts and previously generated utterances into the decoder for generating an appropriate response. We compare our model with various baselines on dataset CMU_DoG in terms of the evaluation criteria. The experimental results demonstrate the state-of-the-art performance of our model as compared to previous studies. Furthermore, the results of ablation experiments show the effectiveness of the hierarchical attention interaction and the triple channel for encoding. We also conduct human judgment to evaluate the informativeness of responses and the consistency of responses with dialog history.

KEYWORDS

document-grounded conversation generation, hierarchical attention interaction, semantic feature encoding, context-aware, transformer, encoder–decoder framework

1 Introduction

A dialog system, or conversational agent, is a computer system intended to communicate with human beings intelligently. Dialog systems have wide applications in various domains, such as open-domain chatbots and task-oriented online services [1,2]. For example, patients can quickly obtain an effective diagnosis with the assistance of the automatic medical consultation system. In terms of the way of response acquisition, traditional dialog systems are divided into retrieval-based and generative systems. The former needs to select appropriate responses from a set of candidate facts to match user requests [3], while the latter directly generates more free responses according to the questions.

In general, the task of dialog response generation (DRG) faces more challenges than answer selection, as it is difficult to generate diverse and informative responses. Thus, recent works try to introduce background knowledge such as explicit commonsense [4], keywords, or knowledge graphs [5] into dialog response generation for improving response quality [6].

Document-grounded dialog generation is a typical task in knowledge-based conversations [7]. It expects to use a great amount of relevant information learned from the given unstructured document(s) to limit the range of the output responses [8]. It commonly consists of multi-turn questions and answering, in which the history of dialog can also be used for generating responses constantly. Table 1 shows an example of multi-turn dialog in the openly available document-grounded dialog dataset CMU_DoG [9]. As shown in Table 1, document-grounded dialog generation expects smooth interlacing between multi-turn task-oriented QA (with underline) and casual chat (with underline and italics) taking a document as the background. In particular, this task requires two speakers chatting surrounding a special topic while taking many turns. The generated replies in document-grounded dialog are freer than QA, which may be a safe sentence such as "I do not know" or "I think so" for unanswerable questions, and sometimes maybe even a rhetorical question or new subject of a talk. Some studies consider that document-grounded dialog generation resembles machine reading comprehension (MRC) in the introduction of the unstructured document(s) as supplementary knowledge. However, document-grounded dialog generation comprises multi-turn conversation while the MRC involves only single-turn QA.

The impressive success of deep learning techniques in natural language processing has advanced document-grounded multi-turn dialog. In spite of the explicit knowledge resources that play an important role in generating responses, neural network models have proved effective in generative dialog systems for their strong capabilities to understand a conversation and generate fluent responses [9,10]. Neural network-based response generation does not rely on a specific answer database or template but carries out dialog generation according to the language understanding ability acquired from a large number of corpora. Most of the studies on dialog generation utilize hierarchical encoder–decoder [11,12] or Seq2Seq architecture [13] based on deep neural networks. Chen et al. proposed a dialog pre-training framework named DialogVED, which introduces continuous latent variables into the enhanced encoder–decoder framework to increase the relevance and diversity of responses [1]. These existing research works mainly use two representation methods of dialog utterances. One is treating dialog history and current dialog as an integrated sequence fed into a single encoder [7,9], while the other is recurrently encoding multi-turn utterances by hierarchical encoders, such as the RNN (recurrent neural network) and transformer [1]. Although existing works made some exploration in the conversation structure, they ignore the features of human participating in a multi-turn conversation. As shown in Table 1, a speaker may give multiple utterances

TABLE 1 Example in CMU_DoG.

Movie	**Jaws**
Document	A beach party takes place at dusk on Amity Island, where a woman named Chrissie Watkins goes skinny dipping in the ocean. She is violently pulled under. The next day, her partial remains are found on the shore. The medical examiner rules the death a shark attack which leads to Police Chief Martin Brody closing the beaches. Mayor Larry Vaughn overrules him, fearing it will ruin the town's summer economy. The coroner now concurs with the mayor's theory that Watkins was killed in a boating accident. Brody reluctantly accepts their conclusion until another fatal shark attack occurs shortly after. . .
Conversation	u1: What is it about?
	u2: I meant to say Jaws lol.
	u1: I think I have seen it at some point. Is it a scary movie?
	u2: It is a movie made in the late 70s where people are been hunted by a large shark
	u2: Well, more like action; seems people are always being attacked by the shark
	u1: I have definitely seen it. I always think about it when I am at the beach
	u2: *Really? Wow, it is kind of scary if you are in the deep*
	. . .

constantly in some scenarios. Moreover, different speakers have different backgrounds and emotional attitudes. Thus, we consider that it is unreasonable to predict the response without specifying the speaker.

The existing generative models can be divided into parallel models [14] and incremental models [15], according to the way of representing the given document and historical dialog. The incremental one preserves the temporal relationship of utterances and encodes each historical utterance in turn for response generation. Inspired by the study of incremental response generation, this work models a triple-channel encoder with self-attention networks and an incremental decoder with hierarchical attention interaction between the context of dialog for document-grounded multi-turn response generation. The proposed model uses a transformer framework [16] for the encoder and decoder, which depends entirely on an attention mechanism. The attention mechanism relates different positions of a single sequence to learn and optimize the representation of this sequence [16]. We take the given document, dialog history, and current utterance as significant context clues to create responses. Then we model the hierarchical attention interaction between contexts with self-attention under an encoder–decoder framework for document-grounded multi-turn dialog generation. The contributions of this work are as follows:

- *We propose a novel generative model within the encoder–decoder framework, which introduces a triple-channel encoder to capture global attention between documents, dialog history, and the last utterance for document-driven conversation.*
- *The triple-channel in the encoder is used to learn the distributed representation of conversational context synchronously and then integrate them with the self-attention mechanism.*
- *A hierarchical attention interaction structure is built in the decoder, which can preserve the temporal relationship and the coherence of contexts for response generation. On the basis of this structure, context knowledge is integrated within layer-wise attention to increase the relevance and diversity of next-turn responses.*

The rest of this study is organized as follows. The next section reviews related work. Our proposed model is introduced in Section 3, then the experiments and analyses are presented in Section 4, followed by the conclusion in Section 5.

2 Related work

Traditional dialog systems consist of single-turn conversations [17,18] and multi-turn conversations [12,19] according to the independence of inquiries. In multi-turn dialogs, different inquiries have certain correlations; thus, not only the current quire but also previous utterances are used as model inputs for predicting the next utterance. Wu et al. proposed a multi-hop attention with a termination mechanism in the generative neural network for multi-turn reasoning [20]. However, these previous studies only take utterances as model input regardless of the external knowledge.

In terms of the purpose of conversation, dialog systems can be also divided into task-oriented, QA, conversational recommendation, and chit-chat [21]. Task-oriented systems aim to accomplish users' goals (e.g., online shopping or restaurant reservation) through an optimal decision-making process in multi-turn dialogs. QA systems commonly retrieve useful information from background knowledge to answer single-turn user requests. Conversational recommendation systems offer a useful service or a good product without receiving explicit commands [22,23], while chit-chat systems are designed to meet the users' emotional and social needs. However, most authentic dialog scenarios consist of more than one purpose, which makes recent studies introduce external unstructured or structured knowledge [24] to generate more informative responses for various conversational purposes. Some studies [25] have proved that it is more reasonable to divide dialog systems by background knowledge to reflect the dialog tasks and datasets. Lian et al. used external knowledge to build an end-to-end neural network for single-turn dialog generation [26]. Ghazvininejad et al. extended an end-to-end neural network with real-world facts or conversation history for single-turn conversation generation [27]. Some other studies focus on multi-turn dialog with capturing useful information from the given knowledge [28].

A document-grounded dialog system is one of the representative knowledge-based systems, which uses relevant information derived from the given unstructured text to obtain (generate) responses. Generally, document-grounded dialog systems include reading comprehension in the form of QA [29] and multi-turn dialog in the form of chit-chat. Li et al. proposed a transformer-based architecture (incremental transformer) with a two-way deliberation decoder to encode utterances along with textual knowledge for multi-turn document-grounded conversations [15]. Following their works, Li et al. designed a D3G model with a doc-reader mechanism to locate the information related to the user's questions in a given document [7].

For conversational response generation, sequence-to-sequence or encoder–decoder frameworks with sequential neural networks are widely used to construct generative models for safe and ordinary responses. Qin et al. employed an RNN with memory as the decoder [30], while Shang et al. combined global and local context information in the RNN for a one-round conversation [17]. Vinyals and Quoc explored the LSTM (long short-term memory) network to produce sequential multi-turn conversations [18]. Li et al. improved the LSTM-based generator by using maximum mutual information as the

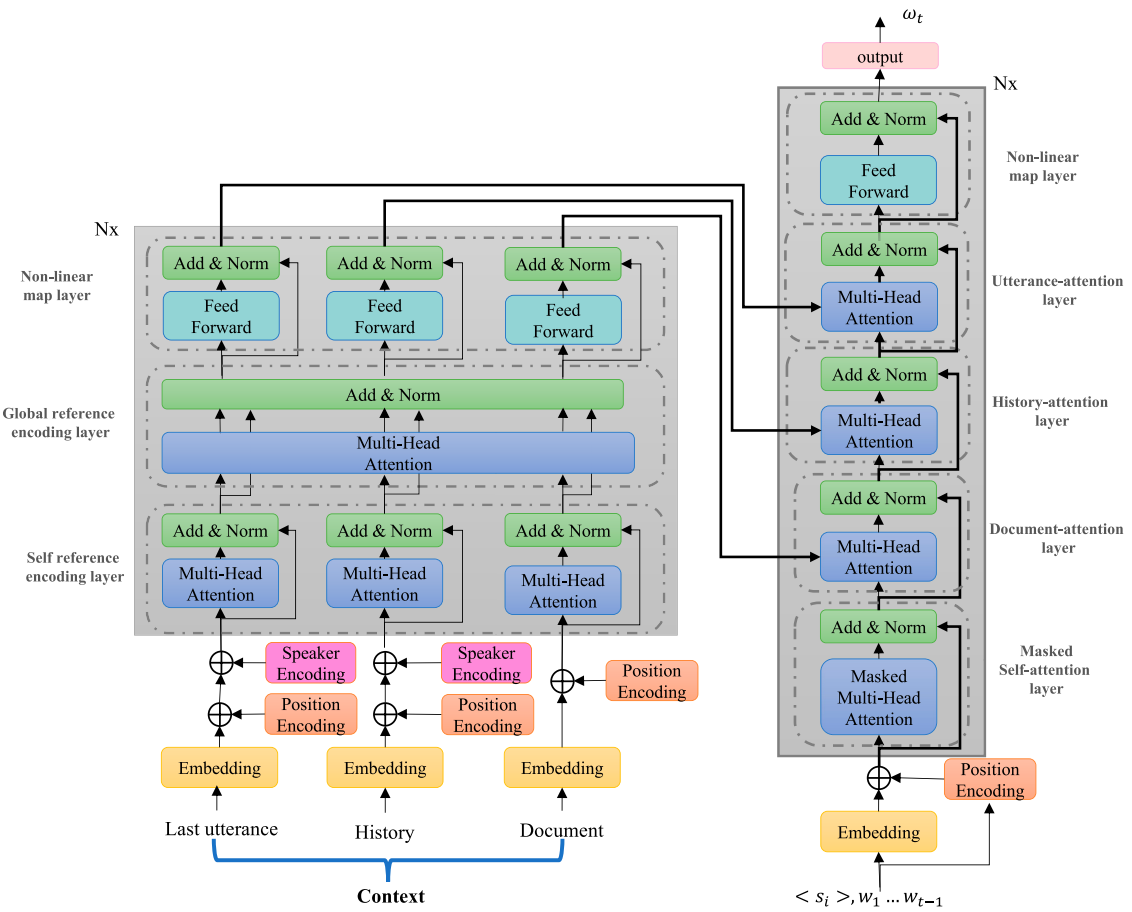

FIGURE 1
Framework of the model. The left is the context encoder with the triple channel. The right is the decoder interacted with contextual encoding for response generation.

objective function [19]. Tang et al. used a one-layer transformer as the decoder [14]. To capture the textual dependencies and key information in the sequences, attention mechanisms [16] have been used to enhance the neural networks of dialog generation and improve response quality. Andrea et al. used a multi-hop attention mechanism over memories with pointer networks to effectively incorporate external knowledge into dialog generation [31]. To emphasize the correlation between contexts, Wu et al. also proposed a multi-hop attention mechanism to learn a single-context vector by computing attention scores [20]. Xing et al. combined utterance-level attention with word-level attention in a neural network to draw the important parts for generating response [32].

3 Methodology

In this work, we propose a novel transformer-based model for document-grounded dialog, and the overall structure of the model is shown in Figure 1. It follows the encoder–decoder framework and consists of three parts: 1) a multi-view embedding module that concatenates position features, speaker features, and word-level semantic features together as input; 2) a context encoding module that learns the semantic information of the document and dialog and captures their information interaction with the triple channel; 3) a hierarchical decoding module that generates context-aware response according to the interaction with outputs of the encoder.

3.1 Problem definition

Given 1) a document D that provides the knowledge associated with the dialog, 2) the corresponding dialog history H presented as a sequence of utterances, and 3) the current (last) utterance u_{k+1}, the motivation of this work is to simulate human reading comprehension to generate a proper response utterance R and keep the conversation going.

Assume the document is a sequence of tokens with length m, which is denoted as $D = \{w_1^d, w_2^d, \ldots, w_m^d\}$. A dialog history is generally treated as a sequence of k utterances $\{u_1, u_2, \ldots, u_k\}$, and the current utterance is naturally denoted as u_{k+1}. Each utterance in the dialog $u_i = \{w_{i,1}^u, w_{i,2}^u, \ldots, w_{i,l_i}^u\}$ is a token-level sequence with length l_i. The dialog history is formalized as

$$H = \left\{w_{1,1}^u, w_{1,2}^u, \ldots, w_{1,l_1}^u, \ldots, w_{k,1}^u, w_{k,2}^u, \ldots, w_{k,l_k}^u\right\}, \quad (1)$$

where w_{k,l_k}^u denotes the kth utterance in the dialog history which has l_k tokens in total. For convenience, we further use $l = \sum_{i=1}^{k} l_i$ to denote the total length of the dialog history sequence. The generated response of our model is a sequence $R = \{w_1, w_2, \ldots, w_T\}$, where T is the length of the response sequence.

Overall, the goal of our model is to generate a reasonable reply by maximizing the conditional probability P. For all possible responses $\{R_j\}$, it can be formalized as

$$R = \arg\max_{R_j} P\left(R_j | D, H, u_{k+1}, \Theta\right), \quad (2)$$

where Θ indicates all trainable parameters in the generative model.

3.2 Multi-view embedding module

This module aims to map the symbolic representations of the given document, dialog history, and current utterance (input query) to distribution representations. In this module, each token is represented with three kinds of embedding features. As shown on the left of Figure 1, the features are listed as follows:

1) **Token embedding**: token embedding is learned to capture the lexical semantics in numerical form. According to the distributed hypothesis, the semantic dependency between words can be efficiently calculated in low-dimensional vector space, i.e., similar words have a closer distance in vector space. In our work, we use matrix $E_w \in R^{(|V|+4)\times d_e}$ to denote the word embedding of the sequence, where $|V|$ is the vocabulary size and d_e is the dimension of the embedding. The first four lines of E_w represent some special tokens: $[PAD]$ for padding the sequence to a fixed length, $[UNK]$ for representing the words out of the vocabulary, $[GO]$ is the start flag of a sequence, and $[EOS]$ is the end flag of a sequence. The rest lines in E_w are the semantic embeddings of words in the vocabulary.
2) **Position embedding**: it is obvious that the temporal information of utterance is important for semantic encoding. Existing recurrent neural networks model the temporal information with its recurrent structure. However, there is a lack of the ability to implicitly modeling the sequence information in the self-attention mechanism and feed-forward networks. Therefore, following the transformer model [16], we introduce an additional position embedding mechanism to supply the required position information for each token in the input sequence. The vector representation for each position pos is defined as

$$PE(pos, d) = \begin{cases} sin\left(pos/10000^{d/d_e}\right) & \text{if } d \text{ is even} \\ cos\left(pos/10000^{(d-1)/d_e}\right) & \text{otherwise} \end{cases}, \quad (3)$$

where d is the dth dimension of the representation.

3) **Speaker embedding**: in general, one dialog consists of multiple utterances from at least two speakers who may have different attitudes toward the same question. It is unreasonable for us to model all utterances as equals, and we consider that the same token in the historical sequence H should have different representations if derived from different speakers. Therefore, we introduce a speaker embedding for integrating the speaker feature into the token representations. In particular, we use $E_s \in R^{n\times d_e}$ to specify the speaker information, where n is the total number of speakers, and each line in E_s represents a speaker.

The synthetic embedding representations of the input sequences are obtained by the aforementioned three kinds of embedding. For historical dialog H and current utterance u_{k+1}, we sum all three kinds of embedding features mentioned previously as their representations, which are denoted as $H_0^h \in R^{l\times d_e}$ and $H_0^u \in R^{l_{k+1}\times d_e}$, respectively. For document D, we only sum the token embedding and position embedding as its representation, which is denoted using $H_0^d \in R^{m\times d_e}$.

3.3 Context encoding module

We build an encoder with a triple channel in the context encoding module of our model. The encoder synchronously learns the document, history, and current utterance and captures the interaction information between them. Previous works generally integrate the document and history information into the hidden states of the current utterance and then feed the fused representations into the decoder. In this work, we retain the representations of all inputs and implement global reference encoding on them.

The encoder is stacked by N blocks with the same structure. The inputs of the first block are the utterance embedding H_0^u, history embedding H_0^h, and document embedding H_0^d. The outputs of it are three matrices H_1^u, H_1^h, and H_1^d, which are the encoded representations of the utterance, history, and document, respectively. For the nth block ($n > 1$), the inputs of it are the outputs of the previous block, while the outputs are also three matrices H_n^u, H_n^h, and H_n^d.

As shown in the left section of Figure 1, each block of the encoder consists of three layers. The first layer is the "self-reference encoding." The second is the "global reference encoding" layer. The last one is the "non-linear map." Following the transformer, we apply an "Add & Norm" operation in each layer, and for convenience, this operation is omitted in the study.

The "self-reference encoding" layer is proposed to learn the independent representation of the utterance, history, and document. It is implemented by a multi-head attention function [16], which is defined as *MultiHead* (·, ·, ·) and the inputs of the function are the query, key, and value, respectively[1].

For *n*th block, the self-reference encoding layer is defined as

$$\begin{aligned}\bar{H}_n^u &= MultiHead\left(H_{n-1}^u, H_{n-1}^u, H_{n-1}^u\right)\\ \bar{H}_n^h &= MultiHead\left(H_{n-1}^h, H_{n-1}^h, H_{n-1}^h\right)\\ \bar{H}_n^d &= MultiHead\left(H_{n-1}^d, H_{n-1}^d, H_{n-1}^d\right)\end{aligned}. \tag{4}$$

We concatenate the outputs of the "self-reference encoding" layer,

$$H_n = \left[\bar{H}_n^u; \bar{H}_n^h; \bar{H}_n^d\right], \tag{5}$$

and then feed them into the "global reference encoding" layer.

$$\left[\tilde{H}_n^u; \tilde{H}_n^h; \tilde{H}_n^d\right] = MultiHead\left(H_n, H_n, H_n\right). \tag{6}$$

Through the aforementioned operations, the model could capture the interaction information of the utterance, history, and document.

Furthermore, we feed the outputs of the global reference encoding layer into the "non-linear map" layer to obtain the outputs of the current block. The non-linear map layer is implemented by a position-wise feed-forward network (FFN) with two layers, which is defined as

$$FFN\left(x\right) = \sigma\left(xW_1 + b_1\right)W_2 + b_2, \tag{7}$$

where σ is a ReLU function, $W_1 \in R^{d_m \times d_{in}}$, $b_1 \in R^{d_{in}}$, $W_2 \in R^{d_{in} \times d_m}$, and $b_2 \in R^{d_e}$ are trainable parameters, d_m is the hidden size of the model, and d_{in} is the inner size of the FFN. The formalization of "non-linear map" layer is, therefore, defined as

$$\begin{aligned}H_n^u &= FFN\left(\tilde{H}_n^u\right)\\ H_n^h &= FFN\left(\tilde{H}_n^h\right)\\ H_n^d &= FFN\left(\tilde{H}_n^d\right)\end{aligned}. \tag{8}$$

Finally, we define the outputs of the last block H_N^u, H_N^h, and H_N^d as the outputs of the context encoding module.

1 Since multi-head attention is a general function, we will not introduce its implementation in this study.

3.4 Hierarchical decoding module

This module is built for generating responses according to the dialog context as shown in the right section of Figure 1. We consider that people normally read through a given document and dialog history first in reading comprehension to learn and pay close attention to the required evidence, relevant to the current utterance. Thus, we designed a hierarchical information interaction structure with a multi-head attention mechanism for the conversation context and the generated replies. The three-layer structure consists of the document-attention layer, history-attention layer, and utterance-attention layer. In this module, the context representations learned from the triple-channel encoder are integrated with the previously generated responses to predict the next target reply.

As shown in Figure 1, a decoder that has N stacks and contains five layers per stack is built in this module. The response is generated token by token, that is, we first produce the first token with a start flag [*GO*], then we concatenate the start flag and the generated first token to produce the second token, and so on, until an end flag [*EOS*] is produced. At time step t, the start flag, the previous $t-1$ tokens $w_1, w_2, \ldots, w_{t-1}$, and the output of the encoder are fed into the decoder to predict the tth token in the response.

First, we convert the start flag and the generated tokens to distributed representations by the multi-view embedding module. The representation for the start flag and previous $t-1$ tokens is defined as $H_0^{r_{t-1}}$.

After that, $H_0^{r_{t-1}}$ is fed into the stacked blocks. For the nth block, we feed the inputs (embedding representations or outputs of the previous block) into the masked self-attention layer to learn the information from the generated responses. This layer is implemented by a masked multi-head attention mechanism [16], which is defined as *MaskedMultiHead* (·, ·, ·) and the inputs of it are the same as the *MultiHead* function.

$$\bar{H}_n^{r_{t-1}} = MaskedMultiHead\left(H_{n-1}^{r_{t-1}}, H_{n-1}^{r_{t-1}}, H_{n-1}^{r_{t-1}}\right). \tag{9}$$

Then, we pass the encoded responses through the document-attention layer, history-attention layer, and utterance-attention layer sequentially.

$$\begin{aligned}\tilde{H}_n^{r_{t-1}} &= MultiHead\left(\bar{H}_n^{r_{t-1}}, H_N^d, H_N^d\right)\\ \dot{H}_n^{r_{t-1}} &= MultiHead\left(\tilde{H}_n^{r_{t-1}}, H_N^h, H_N^h\right)\\ \ddot{H}_n^{r_{t-1}} &= MultiHead\left(\dot{H}_n^{r_{t-1}}, H_N^u, H_N^u\right)\end{aligned}. \tag{10}$$

Next, $\ddot{H}_n^r$ is fed into a non-linear map layer, which is the same as in the context encoding module.

$$H_n^{r_{t-1}} = FFN\left(\ddot{H}_n^{r_{t-1}}\right). \tag{11}$$

Finally, we use the outputs of the Nth block to predict the generated token at the tth time step. The generated token is selected from the pre-defined vocabulary with the highest probability, and the distributed probability is defined as

TABLE 2 Statistics of the CMU_DoG datasets.

Dataset	#Conversation	#Utterance	Average utterances per conversation	Average tokens per utterance
Train	3,373	107,792	31.96	11.03
Valid	229	7,030	30.70	12.22
Test	619	19,375	31.30	10.94
Total	4,221	134,197	31.79	11.08

$$p_t = softmax\left(H_n^{r_{t-1}}(t) \cdot E_w^T\right), \tag{12}$$

where $H_n^{r_{t-1}}(t)$ is the tth row of the output matrix $H_n^{r_{t-1}}$, indicating the output vector corresponding to the last input token, and E_w is the matrix representation of the pre-defined vocabulary.

During training, we use the negative log-likelihood of the target word as the loss at each time step, and then the final loss is defined as the summation of the losses of all time steps.

4 Experiments and result analysis

4.1 Dataset

We conduct the experiments of dialog response generation on dataset CMU_DoG which has a total of 4,221 conversations with an average of 31.79 utterances per conversation. The statistics of the dataset are shown in Table 2. This dataset presents a set of movie-themed text descriptions and their corresponding multi-turn dialogs. The extra textual descriptions contain movie names, introductions, ratings, and some other scenes. They present enough dialog-related information that may help generate context-specific and informative responses for a multi-turn conversation. The average length of the documents is approximately 200 words.

Each dialog in CMU_DoG involves two participants, and the given document is accessible to only one participant or both participants. Moreover, the dataset also provides the correspondence between each utterance and the paragraphs of the document.

4.2 Experiment settings

In our experiments, the stacks of both the encoder and decoder are set to 4. The number of attention heads is set to 8. The embedding size d_e and the hidden size d_m are set to 512, and the inner size of the FFN d_{in} is set to 2,048. We use the Adam algorithm [33] with a learning rate of 0.0001 for optimization. The batch size is set to 64, and the dropout rate is set to 0.1. In addition, we train the model for 50 epochs. To save space and training time, we take the previous three utterances as the dialog history in our experiments.

4.3 Evaluation criteria

4.3.1 Automatic evaluation

We evaluate the proposed document-driven generative model in terms of diverse metrics, including BLEU-n [34], METEOR [35], Doc_BLEU, perplexity [36], and the average length of the generated responses.

BLEU-n: it is known to correlate reasonably well with human beings on the evaluation of conversation generation. It measures n − Gram overlap between generated responses and the ground truth, which is defined as BLEU−n. We leverage multiple BLEU−n scores to evaluate the performance of generative models.

METEOR: it is also a common metric to measure the relevance between generated responses and ground truth. Compared with BLEU−n scores, METEOR pays more attention to the recall rate and applies a more generalized concept of a unigram matching method that the unigram can be matched based on their surface forms, stemmed forms, and meanings.

Doc_BLEU: we use this criterion to evaluate the relevance of generated responses with the given documents. It measures the unigram overlap between responses and documents, which is calculated by the original formula of BLEU [34] without the brevity penalty factor.

Perplexity (PPL): this indicator is used to evaluate the fluency of the response. A lower perplexity indicates the better performance of the models and higher quality of the generated sentences.

Avg_Len: generally speaking, longer sentences supply richer information. Therefore, we use the average length of generated utterances as an automatic criterion to evaluate the quality of the generated responses.

TABLE 3 BLEU–*n* scores and METEOR scores for baselines and the proposed model. The "-speaker embedding" indicates the speaker embedding is removed from the multi-view embedding module of our model.

Models	BLEU-1	BLEU-2	BLEU-3	BLEU-4	METEOR
SEQ [37]	6.12	1.52	0.59	0.30	4.18
SEQS [37]	6.57	1.65	0.67	0.35	4.30
D3G [7]	6.32	1.71	0.71	0.41	4.17
Transformer [16]	8.55	2.49	1.12	0.60	4.53
ITDD [14]	-	-	-	0.95	-
ITDD (our impl)	8.19	2.88	1.66	0.85	5.21
BCTCE [9]	9.98	3.56	2.05	1.42	5.22
Our model	**11.24**	**4.27**	2.54	1.80	5.83
-speaker embedding	10.59	3.87	**2.66**	**2.22**	**5.86**

4.3.2 Human judgment

In addition to the aforementioned quantitative evaluation, we also augment the manual evaluation in terms of fluency and coherence of dialog and the diversity of responses. These evaluation metrics are scored 0/1/2. We randomly sample multiple conversations containing 822 utterances from the test set. We ask multiple annotators to score these utterances given their previous utterances and related documents. The final score of each utterance is the average of the scores rated by three annotators.

Fluency: it is used to indicate whether the response is natural and fluent. Score 0 shows the response is not fluent and incomprehensible; 1 shows the response is partially fluent but still comprehensible; 2 shows the response is sufficiently fluent.

Coherence: it is used to evaluate whether the response is logically coherent with the dialog. Score 0 shows the response is irrelevant with previous utterances; 1 shows the response matches the topic of previous utterances; 2 shows the response is exactly coherent with previous utterances.

Diversity: it is used to reflect the lexical diversity of the response. Score 0 represents the safe response which is applicable to almost all conversations, e.g., "I agree with you;" 1 represents the response suitable to limited conversations but plain and uninformative; 2 shows the response is evidently vivid and informative.

4.4 Baselines and result discussion

We choose several studies on document-grounded conversational generation as baselines, which contain the transformer [16], ITDD [15], D3G [7], BCTCE [9], SEQ, and SEQS [37] models. The transformer, ITDD, BCTCE, and the proposed model in this work depend entirely on attention mechanisms, while others utilize sequential neural networks as encoders and decoders. The transformer takes the dialog context as a sequence of tokens and inputs it into an encoder–decoder framework without distinction. The ITDD incrementally encodes multi-turn utterances along with the knowledge in related documents and applies a two-pass decoder that focuses on context coherence and knowledge correctness to generate responses. The BCTCE proposes a binary-channel structure for context encoding. However, our proposed model in this work uses a triple-channel structure to encode the dialog contexts in parallel and employs an incremental decoder to capture the semantic dependency of contexts in a hierarchical network for response generation.

TABLE 4 Document relevance and response quality for baselines and the proposed model. The "-speaker embedding" indicates the speaker embedding is removed from the multi-view embedding module of our model.

Models	Doc_BLEU	Avg_Len	PPL
SEQ [37]	24.88	7.31	15.62
SEQS [37]	27.96	7.21	19.53
D3G [7]	26.76	6.83	18.40
Transformer [16]	27.55	7.91	13.70
ITDD [14]	-	-	15.10
ITDD (our impl)	26.96	8.52	**11.01**
BCTCE [9]	28.23	9.16	17.80
Our model	**29.10**	10.22	20.06
-speaker embedding	26.42	**11.10**	24.68

The results in Tables 3, 4 show the comparison of our model with baseline models on the dataset CMU_DoG. It can be seen that our model significantly outperforms all baselines according to the automatic evaluation criteria except PPL and achieves state-of-the-art performance. The new state-of-the-art

TABLE 5 Human evaluation of baselines and our proposed model. The "-speaker embedding" means the speaker embedding is removed from the multi-view embedding module in our model.

Models	Fluency	Dialog coherence	Diversity
SEQ [37]	1.27	0.81	0.42
SEQS [37]	1.13	0.96	0.71
D3G [7]	1.29	1.12	0.84
Transformer [16]	1.34	1.17	0.90
ITDD (our impl)	1.35	1.27	0.93
BCTCE [9]	1.34	1.29	0.95
Our model	**1.42**	**1.35**	**0.97**
-speaker embedding	1.38	1.32	0.94

performance achieved by our model indicates that the responses generated by our model correspond more with the ground truth. However, our original model gets lower scores in terms of BLEU−3, BLEU−4, and METEOR than the one without speaker embedding. In spite of its worse performance, the effectiveness of speaker information could be demonstrated by the following case study.

Moreover, we also conducted some human judgment to evaluate our model and the results are shown in Table 5. It shows that the responses generated by our model are more relevant to the context (document and dialog history) with better diversity, compared to baselines.

According to Tables 4, 5, our model has better fluency but worse PPL scores than baselines. Both PPL and fluency are used to measure whether the generated response is natural and fluent. However, PPL is hard to accurately evaluate the fluency of the response. Some research studies find that a sentence with a low PPL would not be in accord with natural language and an informative sentence usually has a higher PPL than a common sentence [38]. This fact indicates that the models with a low PPL tend to produce more generic responses. Thus, our model would generate fluent responses in spite of its higher PPL.

4.5 Ablation study

To validate the effectiveness of each layer for contextual attention interaction in the hierarchical decoder, we also conduct ablation experiments on the dataset CMU_DoG. First, we change the decoding order of the context. Some instances are explained as follows.

1) **Document=>utterance=>history:** the last utterance is exchanged with the dialog history upon our model, which means that the attention interaction between previously generated responses with it is conducted before with the dialog history.
2) **History=>document=>utterance:** we feed the embedding of the dialog history, document, and the last utterance into the decoder for the attention interaction by turn.
3) **Parallel decoder:** we replace the incremental decoder in our model with a parallel decoder. The concatenate of embedding of the dialog history, document, and the last utterance is fed into the decoder for attention interactions with previously generated responses.

The results in Tables 6, 7 show that the original model outperforms the ablation models in terms of most metrics, which indicates the decoding order used in our model is more effective. The reason is that the order is in more accordance with human custom. Human beings commonly read through the given documents to acquire background knowledge before finding out the core information of dialog by understanding historical utterances and then focus on the current utterance to give its response.

In addition, the results can also show the effectiveness of hierarchical attention interaction with a reasonable order for utterance decoding, despite of the concatenation of the context within parallel attention interaction achieving the highest BLEU−4 score.

Furthermore, we remove an attention layer from the decoder in the second ablation experiment. The results given in Tables 8, 9 also show the effectiveness of all attention interactions in the decoder. Compared to other variants, our model has better performance in terms of BLEU−*n*, METEOR, PPL, and Doc_BLEU.

4.6 Case study

To demonstrate the role of speaker embedding, we analyze two conversations in CMU_DoG shown in Table 10. In the first case, our model generates a proper response for the speaker "u2" to reply to the question from the speaker "u1," while the model without speaker embedding produces a repeated question from the speaker "u2" in the last dialog turn. In the second case, the speaker "u1" gives two continuous utterances, where the first one is a question and the second one answers the previous question from the speaker "u2." Our model generates a more proper response for the speaker "u2" to reply to the first utterance of the speaker "u1," compared to the model without speaker embedding. The case study shows that speaker embedding is an effective component for our model to identify the speaker of each utterance and improve the consistency of generated responses in a multi-turn dialog.

TABLE 6 Comparison of various decoding orders of the context on the BLEU–*n* score and METEOR. The symbol " =>" represents the decoding order from the bottom up.

Model	BLEU-1	BLEU-2	BLEU-3	BLEU-4	METEOR
Document=>history=>utterance(Ours)	**11.24**	**4.27**	**2.54**	1.80	**5.83**
Document=>utterance=>history	10.12	3.45	2.21	1.73	5.45
History=>document=>utterance	10.23	3.42	2.11	1.68	5.62
History=>utterance=>document	10.34	3.41	2.14	1.65	5.60
Utterance=>history=>document	9.96	3.40	2.16	1.72	5.44
Utterance=>document=>history	10.20	3.42	2.18	1.70	5.55
Parallel decoder	10.43	3.67	2.37	**1.91**	5.69

TABLE 7 Comparison of various decoding orders of the context on document relevance and response quality. The symbol " =>" represents the decoding order from the bottom up.

Model	Doc_BLEU	Avg_Len	PPL
Document=>history=>utterance(Ours)	**29.10**	10.22	**20.06**
Document=>utterance=>history	27.29	10.44	23.07
History=>document=>utterance	28.08	**11.41**	23.78
History=>utterance=>document	27.53	11.31	22.40
Utterance=>history=>document	26.90	10.41	22.73
Utterance=>document=>history	28.48	10.97	24.01
Parallel decoder	27.47	11.07	23.51

TABLE 8 Ablation study for the hierarchical decoding module on BLEU–*n* scores and METEOR. The symbol " =>" represents the decoding order from the bottom up.

Model	BLEU-1	BLEU-2	BLEU-3	BLEU-4	METEOR
Document=>history=>utterance(Ours)	**11.24**	**4.27**	**2.54**	**1.80**	**5.83**
Document=>history	10.35	3.43	2.11	1.60	5.63
Document=>utterance	10.20	3.34	2.04	1.58	5.47
History=>utterance	10.19	3.41	2.09	1.64	5.49
History=>document	9.71	3.29	2.07	1.62	5.49
Utterance=>history	10.41	3.53	2.23	1.77	5.61
Utterance=>document	10.06	3.39	2.09	1.62	5.22

TABLE 9 Ablation study for the hierarchical decoding module on document relevance and response quality. The symbol " =>" represents the decoding order from the bottom up.

Model	Doc_BLEU	Avg_Len	PPL
Document=>history=>utterance(Ours)	**29.10**	10.22	**20.06**
Document=>history	27.27	**11.54**	21.86
Document=>utterance	27.88	10.71	21.50
History=>utterance	27.35	10.84	22.79
History=>document	26.33	9.75	20.60
Utterance=>history	27.34	10.94	21.65
Utterance=>document	26.62	10.84	21.76

TABLE 10 Sample responses of model variants.

Document	Dialog	Responses
Home Alone is a 1990 American comedy film written and produced by John Hughes and directed by Chris Columbus. The film stars Macaulay Culkin as Kevin McCallister, a boy who is mistakenly left behind when his family flies to Paris for their Christmas vacation. Kevin initially relishes being home alone, but soon has to contend with two would-be burglars played by Joe Pesci and Daniel Stern. The film also features Catherine O'Hara and John Heard as Kevin's parents	**u1:** Hi **u2:** have you seen Home Alone? **u1:** Yes, I love that movie **u2:** [predicted response]	**ground truth:** There is a second one, isn't there? **w/ speaker:** I like the actors in it too **w/o speaker:** Have you seen it before?
La la land is a 2016 American musical romantic comedy-drama film written and directed by Damien Chazelle. It stars Ryan Gosling as a jazz pianist and Emma Stone as an aspiring actress, who meet and fall in love in Los Angeles while pursuing their dreams. The film's title refers simultaneously to music, the city of Los Angeles, and to the idiom for being out of touch with reality	**u2:** Do you like this movie? **u1:** The movie is called La La Land. Have you seen it? **u1:** Yes, I like the movie. I saw it in the theater **u2:** [predicted response]	**ground truth:** I like it. Yes, I have seen **w/ speaker:** I have not seen it yet **w/o speaker:** It is a great movie to see

5 Conclusion

In this study, we present a novel neural model for dialog response generation in document-oriented dialog systems. This model utilizes unstructured document information for response generation to exploit the knowledge hidden in the text, which will be the inevitable trend of the open domain dialog systems. To improve the quality of generated responses, we model a triple-channel encoding and a hierarchical attention interaction between dialog contexts. Comparative experiments are conducted on a public dataset CMU_DoG to evaluate the proposed model. The results show the greater performance of our model than that of several relevant models. The experiment results also confirm the effectiveness of hierarchical attention interactions between contexts with a triple channel for multi-turn dialog generation.

Data availability statement

The dataset used in our experiments is publicly available at https://github.com/festvox/datasets-CMU_DoG.

Author contributions

YC, HX, and MZ contributed to the conception and design of the study. MZ performed the statistical analysis. YC wrote the first draft of the manuscript. HX and MZ wrote sections of the manuscript. All authors agreed to be accountable for the content of the work. All authors contributed to manuscript revision and approved the submitted version.

Funding

This research was supported by the R&D Program of the Beijing Municipal Commission of Education (Grant No. KM202010011011), National Natural Science Foundation of China (Grant Nos. 72171004 and 61873027), Beijing Natural Science Foundation (Grant No. 4202014), and Humanity and Social Science Youth Foundation of the Ministry of Education of China (Grant Nos. 21YJCZH186 and 20YJCZH229).

Acknowledgments

The authors would like to thank the associate editor and the reviewers for their useful feedback that improved this study.

Conflict of interest

The authors declare that the research was conducted in the absence of any commercial or financial relationships that could be construed as a potential conflict of interest.

Publisher's note

All claims expressed in this article are solely those of the authors and do not necessarily represent those of their affiliated organizations, or those of the publisher, the editors, and the reviewers. Any product that may be evaluated in this article, or claim that may be made by its manufacturer, is not guaranteed or endorsed by the publisher.

References

1. Chen W, Gong Y, Wang S, Yao B, Qi W, Wei Z, et al. Dialogved: A pre-trained latent variable encoder-decoder model for dialog response generation. In: S Muresan, P Nakov, A Villavicencio, editors. *Proceedings of the 60th annual meeting of the association for computational linguistics (volume 1: Long papers), ACL 2022, dublin, Ireland, may 22-27, 2022*. Stroudsburg, PA: Association for Computational Linguistics (2022). p. 4852–64.

2. Adiwardana D, Luong M-T, So D R, Hall J, Fiedel N, Thoppilan R, et al. *Towards a human-like open-domain chatbot* (2020). doi:10.48550/arXiv.2001.09977

3. Park Y, Ko Y, Seo J. Bert-based response selection in dialog systems using utterance attention mechanisms. In: *Expert systems with applications* (2022).

4. Zhou H, Young T, Huang M, Zhao H, Xu J, Zhu X. Commonsense knowledge aware conversation generation with graph attention. In: *Twenty-seventh international joint conference on artificial intelligence IJCAI-18* (2018).

5. Xu J, Wang H, Niu Z, Wu H, Che W. Knowledge graph grounded goal planning for open-domain conversation generation. *Proc AAAI Conf Artif Intelligence* (2020) 34:9338–45. doi:10.1609/aaai.v34i05.6474

6. Xu Y, Ishii E, Liu Z, Winata G I, Su D, Madotto A, et al. Retrieval-free knowledge-grounded dialog response generation with adapters. In: *Proceedings of the second DialDoc workshop on document-grounded dDialog and conversational question answering*. Dublin, Ireland: Association for Computational Linguistics (2022). p. 93–107. DialDoc@ACL 2022May 26, 2022.

7. Li K, Bai Z, Wang X, Yuan C. A document driven dialog generation model. In: *Chinese computational linguistics - 18th China national conference, CCL 2019*. Kunming, China (2019). p. 508–20. October 18-20, 2019, Proceedings.

8. Gao C, Zhang W, Lam W. Unigdd: A unified generative framework for goal-oriented document-grounded dialog. In: S Muresan, P Nakov, A Villavicencio, editors. *Proceedings of the 60th annual meeting of the association for computational linguistics (volume 2: Short papers), ACL 2022, dublin, Ireland, may 22-27, 2022*. Stroudsburg, PA: Association for Computational Linguistics (2022). p. 599–605.

9. Cai Y, Zuo M, Zhang Q, Xiong H, Li K. A bi-channel transformer with context encoding for document-driven conversation generation in social media. *Complexity* (2020) 1–13. doi:10.1155/2020/3710104

10. Zhang H, Lan Y, Pang L, Guo J, Cheng X. Recosa: Detecting the relevant contexts with self-attention for multi-turn dialog generation. In: *Proceedings of the 57th annual meeting of the association for computational linguistics* (2019).

11. Zeng H, Liu J, Wang M, Wei B. A sequence to sequence model for dialog generation with gated mixture of topics. *Neurocomputing* (2021) 437:282–8. doi:10.1016/j.neucom.2021.01.014

12. Serban I V, Sordoni A, Bengio Y, Courville A, Pineau J. *Building end-to-end dialog systems using generative hierarchical neural network models* (2016). p. 3776–84.

13. Sutskever I, Vinyals O, Le Q V. Sequence to sequence learning with neural networks. In: *NIPS* (2014).

14. Tang X, Hu P. Knowledge-aware self-attention networks for document grounded dialog generation. In: *The 12th international conference on knowledge science, engineering and management* (2019).

15. Li Z, Niu C, Meng F, Feng Y, Li Q, Zhou J. Incremental transformer with deliberation decoder for document grounded conversations. In: *Proceedings of the 57th conference of the association for computational linguistics, ACL 2019*, 1. Florence, Italy (2019). p. 12–21. July 28- August 2, 2019Long Papers.

16. Vaswani A, Shazeer N, Parmar N, Uszkoreit J, Jones L, Gomez A N, et al. Attention is all you need. In: *Advances in neural information processing systems 30: Annual conference on neural information processing systems 2017*. Long Beach, CA, USA (2017). p. 5998–6008. 4-9 December 2017.

17. Shang L, Lu Z, Li H. Neural responding machine for short-text conversation. In: *Proceedings of the 53rd annual meeting of the association for computational linguistics and the 7th international joint conference on natural l anguage processing of the asian federation of natural l anguage processing*, 1. Beijing, China (2015). p. 1577–86. *ACL 2015, July 26-31, 2015*Long Papers.

18. Vinyals O, Le Q. A neural conversational model. *Comp Sci* (2015).

19. Li J, Galley M, Brockett C, Gao J, Dolan B. A diversity-promoting objective function for neural conversation models. *Comp Sci* (2015).

20. Wu X, Martinez A, Klyen M. Dialog generation using multi-turn reasoning neural networks. In: *NAACL-HLT. Association for computational linguistics* (2018). p. 2049–59.

21. Chiu S, Li M, Lin Y, Chen Y. Salesbot: Transitioning from chit-chat to task-oriented dialogs. In: S Muresan, P Nakov, A Villavicencio, editors. *Proceedings of the 60th annual meeting of the association for computational linguistics (volume 1: Long papers), ACL 2022, dublin, Ireland, may 22-27, 2022*. Stroudsburg, PA: Association for Computational Linguistics (2022). p. 6143–58.

22. Xiong F, Wang X, Pan S, Yang H, Zhang C. Social recommendation with evolutionary opinion dynamics. In: *IEEE transactions on systems, man, and cybernetics: Systems* (2018). p. 1–13.

23. Li Z, Xiong F, Wang X, Chen H, Xiong X. Topological influence-aware recommendation on social networks. *Complexity* (2019) 1–12. doi:10.1155/2019/6325654

24. WanyunXiao Y, Wang H, Song Y, won Hwang S, Wang W. Kbqa: Learning question answering over qa corpora and knowledge bases. *Proc VLDB Endowment* (2017) 10:565–76. doi:10.14778/3055540.3055549

25. Ma L, Zhang W, Li M, Liu T. *A survey of document grounded dialog systems (dgds)* (2020). doi:10.48550/arXiv.2004.13818

26. Lian R, Min X, Fan W, Peng J, Hua H. Learning to select knowledge for response generation in dialog systems. In: *Twenty-eighth international joint conference on artificial intelligence IJCAI-19* (2019).

27. Ghazvininejad M, Brockett C, Chang M, Dolan B, Gao J, Yih W, et al. A knowledge-grounded neural conversation model. In: S A McIlraith K Q Weinberger, editors. *Proceedings of the thirty-second AAAI conference on artificial intelligence, (AAAI-18), the 30th innovative applications of artificial intelligence (IAAI-18), and the 8th AAAI symposium on educational advances in artificial intelligence (EAAI-18)*. New Orleans, Louisiana, USA: AAAI Press (2018). p. 5110–7. February 2-7, 2018.

28. Xu F, Zhou S, Wang X, Ma Y, Zhang W, Li Z (2022). Open-domain dialog generation grounded with dynamic multi-form knowledge fusion. doi:10.48550/arXiv:2204.11239v1

29. Lan Y, Jiang J. Modeling transitions of focal entities for conversational knowledge base question answering. In: *Proceedings of the 59th annual meeting of the association for computational linguistics and the 11th international joint conference on natural l anguage processing*, 1 (2021). Long Papers.

30. Qin L, Galley M, Brockett C, Liu X, Gao X, Dolan B, et al. Conversing by reading: Contentful neural conversation with on-demand machine reading. In: *Proceedings of the 57th annual meeting of the association for computational linguistics* (2019).

31. Madotto A, Wu C, Fung P. Mem2seq: Effectively incorporating knowledge bases into end-to-end task-oriented dialog systems. In: *Proceedings of the 56th annual meeting of the association for computational linguistics, ACL 2018*, 1. Melbourne, Australia (2018). p. 1468–78. July 15-20, 2018Long Papers.

32. Xing C, Wu Y, Wu W, Huang Y, Zhou M. Hierarchical recurrent attention network for response generation. In: S A McIlraith K Q Weinberger, editors. *Proceedings of the thirty-second AAAI conference on artificial intelligence, new orleans, Louisiana, USA, february 2-7, 2018* (2018). p. 5610–7.

33. Kingma D P, Ba J. Adam: A method for stochastic optimization. In: *3rd international conference on learning RepresentationsICLR*. San Diego, CA, USA (2015). *May 7–9*.

34. Papineni K, Roukos S, Ward T, Zhu W-J. Bleu: A method for automatic evaluation of machine translationk. In: Proceedings of the 40th annual meeting on association for computational linguistics; 2002 July 6–12; Philadelphia, PA. Stroudsburg, PA: Association for Computational Linguistics (2002). p. 311–8.

35. Denkowski M, Lavie A. Meteor universal: Language specific translation evaluation for any target language. In: *Proceedings of the ninth workshop on statistical machine translation*. Baltimore, Maryland USA (2014). p. 376–80. *June 26–27*.

36. Dinan E, Roller S, Shuster K, Fan A, Auli M, Weston J. Wizard of wikipedia: Knowledge-powered conversational agents. In: *7th international conference on learning RepresentationsICLR*. New Orleans, LA, USA (2019). *May 6–9*.

37. Zhou K, Prabhumoye S, Black A W. A dataset for document grounded conversations. In: *2018 conference on empirical methods in natural l anguage processing*. Brussels, Belgium (2018). p. 708–13. October 31–November 4.

38. Kuribayashi T, Oseki Y, Ito T, Yoshida R, Asahara M, Inui K. Lower perplexity is not always human-like. In: C Zong, F Xia, W Li, R Navigli, editors. *Proceedings of the 59th annual meeting of the association for computational linguistics and the 11th international joint conference on natural l anguage processing, ACL/IJCNLP 2021, (volume 1: Long papers), virtual event, august 1-6, 2021*. Stroudsburg, PA: Association for Computational Linguistics (2021). p. 5203–17. doi:10.18653/v1/2021.acl-long.405

frontiers | Frontiers in Physics

TYPE Original Research
PUBLISHED 04 October 2022
DOI 10.3389/fphy.2022.1019118

OPEN ACCESS

EDITED BY
Xuzhen Zhu,
Beijing University of Posts and Telecommunications, China

REVIEWED BY
Yuexia Zhang,
Beijing Information Science and Technology University, China
Run-Ran Liu,
Hangzhou Normal University, China
Shimin Cai,
University of Electronic Science and Technology of China, China

*CORRESPONDENCE
Yi Chen,
00195035@wzut.edu.cn

SPECIALTY SECTION
This article was submitted to Social Physics,
a section of the journal
Frontiers in Physics

RECEIVED 14 August 2022
ACCEPTED 29 August 2022
PUBLISHED 04 October 2022

CITATION
Ye J and Chen Y (2022), Social contagion influenced by active-passive psychology of college students.
Front. Phys. 10:1019118.
doi: 10.3389/fphy.2022.1019118

Social contagion influenced by active-passive psychology of college students

Jianmeng Ye[1] and Yi Chen[2]*

[1]College of Artificial Intelligence, Zhejiang College of Security Technology, Wenzhou, China, [2]WenZhou University of Technology, Wenzhou, China

Educational behavioral psychology refers to the fact that college students within campus networks have various psychological cognition toward novel information and behavior. This is hardly ever taken into account or theoretically examined in weighted network research. According to psychological traits and a student's willingness to adopt fresh behaviors, we categorize students' behaviors into the active and passive. On this basis, a threshold models is established for the behavior of active and passive students in weighted networks, and the influence behavioral psychology on information propagation is discussed. In order to qualitatively investigate the information propagation mechanism, a partition theory based on edge-weight and behavioral psychology is developed. Active students encourage the acceptance of new behaviors and the spread of information, according to theoretical study and simulation results. However, the phase transition intersected was more significant. When the percentage of enrolled pupils is high, a continuous phase transition is present in the growth pattern of the final adoption size. In contrast, as the proportion of active students declines, the increasing pattern alterss to discontinuous phase transition. In addition, weight distribution heterogeneity facilitates the dissemination of information and does not alter phase transition pattern. Finally, the theoretical analysis is in good agreement with the simulation results.

KEYWORDS

complex network, behavioral propagation, active-passive psychology, phase transition, crossover phenomena

1 Introduction

The campus socialization of college students has been paid more and more attention as a result of the gradual improvement of higher education. In campus socialization, students' online information dissemination is becoming more and more crucial. The information propagation theory can be used to describe a variety of behaviors of college students, including social recommendation, online learning, online entertainment, among others.

For information propagation, researchers have investigated numerous potential influences on the information propagation mechanisms in depth studies for

information propagation models, including node distribution structures [1, 2], memory effects [3, 4], and heterogeneous adoption thresholds [5, 6].

Numerous research have shown that the spread of knowledge demonstrates social reinforcement or affirmation [7, 8]. One of the traditional models for describing social reinforcement is the threshold model based on non-Markov processes, in which the adoption of individual behavior demonstrates memory effects [9]. Additionally, a number of threshold models that are accurate to the network have been proposed to test their influence on information transmission, including binary adoption probability [10], truncated normal adoption probability [11], gate-like adoption probability [12], and sigmoid adoption probability [13]. It is worth noting that in the course of information propagation, the non-redundant feature, i.e., the prohibition of repetition of information propagation at the same edge, cannot be ignored.

The distribution of information is also greatly impacted by the variability of individual closeness in genuine social networks. People are more likely to obtain information from their friends and family than from complete strangers. The influence of intimacy heterogeneity on information dissemination was confirmed by the researchers, who built the connective links between people as edges with diverse weight distribution [14, 15].

Existing literature has suggested that populations are heterogeneous because different people have different attitudes toward the same action, for example [16–18]. Behavioral psychology is rarely considered in college educational studies. On campus, for example, students' psychological heterogeneity is common. College students often send and receive messages on social networks, and their adoption behavior can be influenced by personal psychology. Some students are very interested in new information and are willing to adopt and disseminate it when the information around them is not universally accepted. However, some students are more passive. They are willing to adopt information only when there are more adoptors around them. They are always hesitant about popular behavior, verifying information multiple times before adopting it. Therefore, according to the students' different psychological factors, they can be divided into active and passive individuals. Psychologically active students become interested in their own behavior once they have access to information. They gradually increase their willingness to accept behavior as they learn more information. But students with passive psychology will verify this information several times before taking action. In other words, a student's psychology has something to do with the likelihood that they would pick up a new behavior on campus.

Taking these factors into account, we investigated the effects of behavioral heterogeneity on weighted network information propagation. Only a small percentage of p students were active, while others were passive. To capture the behavioral variability of students, two adoption threshold probability functions that correspond to active and passive students are presented. To further examine the information propagation mechanism, a partition theory based on edge-weight and population heterogeneity is developed. Finally, the simulation outcomes demonstrate that the predictions of the theory are consistent with the information transmission under behavior heterogeneity. This article's remaining sections are organized as follows. The second section establishes an information transmission model that makes use of behavior heterogeneity on weighted networks. A partition theory based on edge-weight and behavior heterogeneity is demonstrated in Section 3. Section 4 of the report discusses the experiment's findings. Finally, Section 5 presents the conclusions.

2 Propagation model with behavioral heterogeneity

We build a weighted social network model with N individuals and a degree distribution of $p(k)$ to investigate the impact of population heterogeneity on the mechanism for information propagation. Our methodology uses the uncorrelated configuration model to prevent intra-degree correlations. A generalized SAR (susceptible-adopted-recovered) model to depict the information propagation mechanism in weighted social network models is shown in Figure 1. Each node in the SAR model is constantly in one of three states: the sensitive state (S-state), the adopted state (A-state), and the restored state. The S-state node is able to communicate with its neighbors and does not adopt this behavior. This behavior has been adopted by A-state nodes, and they are eager to spread information among their neighbors. R-state nodes stop taking an active interest in behavior and stop spreading information.

Additionally, edges with a weight distribution are used to indicate individual correlations. Then, in order to reflect the heterogeneity of edge, the distribution of edge weights is introduced. The edge-weight distribution is denoted by a function $f(\omega)$, and the edge-weight between two neighboring nodes i and j is denoted by the symbol ω_{ij}. Indicate the likelihood that an S-state node will learn something from its A-state neighbor node by using the following notation:

$$\lambda_{\omega} = \lambda\left(\omega_{ij}\right) = 1 - \left(1 - \beta\right)^{\omega_{ij}}, \tag{1}$$

where β is the probability of propagation per unit of information. If $\omega_{ij} = 1$, it is demonstrated by $\lambda_{\omega} = \beta$ that edge weight has no impact on the transmission of information. Additionally, $\lambda(\omega_{ij})$ increases monotonically as ω_{ij} increases.

Let m represent the total amount of data that the S-state node has successfully received. In weighted social networks, information does not initially spread because $m_j = 0$ (j for the S-state node). The total number of the node j's message blocks increases by one at each step, m_j right arrow $m_j + 1$, following the successful receipt of a message from the A-state neighbor I I across the relevant edge.

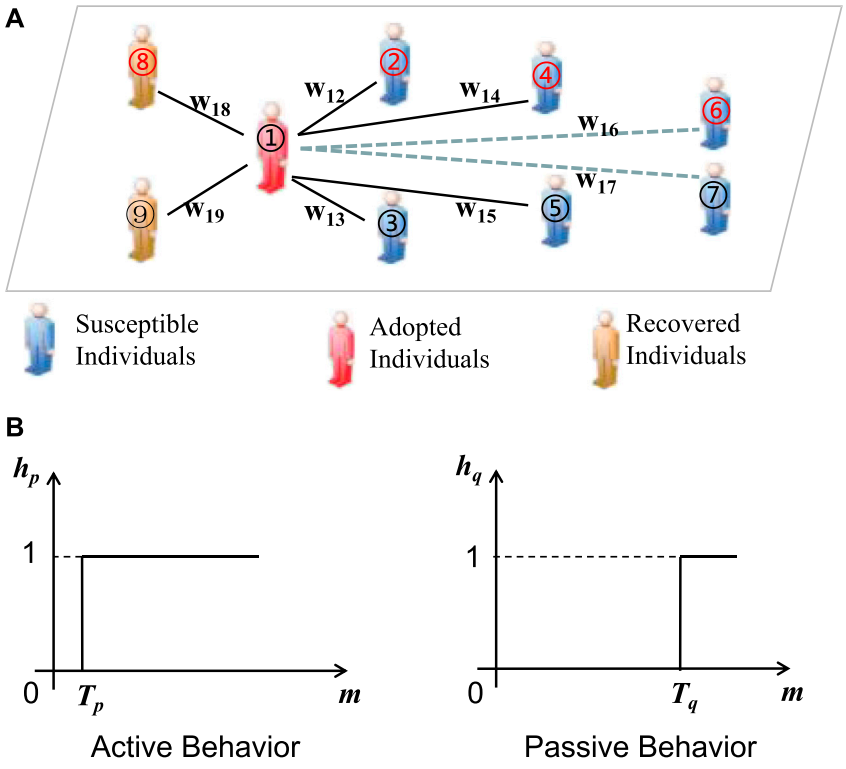

FIGURE 1
(A) SAR model description on weighted networks. Red labels represent active students, such as Nos. 2, 4, 6 and 8. Black labels represent passive students such as students 3, 5, 7, 9. The symbol ω is edge-weight. At t, A-State Student 1 disseminates information to his/her classmates or friends. Information cannot be transferred over the edge, as indicated by the dotted lines. Information is not sent across the corresponding borders of solid lines, as indicated. **(B)** The left subgraph shows the behavior of active students using a threshold model. The right subgraph is a threshold threshold model passive student behavior adoption. $m$is the sum of all the information that S-level students have successfully obtained. $p$and $q$are the scores of active and passive students, respectively.

Additionally, two functions are suggested to illustrate the threshold for individual behavior in order to describe the effects of behavior heterogeneity on the dissemination of information, as shown in Figure 1. The function that depicts the behavior adoption threshold for active students is denoted by

$$h_p(m, T_p) = \begin{cases} 0, & 0 < m \le T_p, \\ 1, & m \ge T_p. \end{cases} \quad (2)$$

The behavior adoption threshold function for conservatives is represented by

$$h_q(m, T_q) = \begin{cases} 0, & 0 < m \le T_q, \\ 1, & m \ge T_q, \end{cases} \quad (3)$$

only a small percentage of students with p are active, and only a small percentage of students with q are passive. $p + q = 1$. In fact, for active students, they are a very high willing to adopt the behavior. When small messages are received, their willingness to act this way is very low. Passive students will adopt behavior only if there are more adoptors around them.

The following is a summary of the information propagation details in weighted networks. First, we chose a few of p students at random to operate as active nodes, while the remaining students served as passive nodes. Then, we choose a subset of ρ_0 students at random to serve as the A-state node (seed) and all other nodes as the S-state. This information is transmitted from the A-state node to all neighbors through corresponding edge. The likelihood $\lambda(\omega_{ij})$ is matched by a weight of ω_{ij} when the S-State node j successfully gets information from the A-State neighbor node i. The collection block of the message is $m_j \rightarrow m_j + 1$ when the S-state node j is successful in receiving it. Information will not be repeated through the same edges due to the non-redundancy of information propagation. Additionally, with a chance of h_p (m, T_p), if j is active, it adopts the behavior and changes to the A status. A state changes to A if j is passive with the probability h_q (m, T_q). The A-state node loses interest in the behavior after information transmission and changes to R-state with a probability of γ. Information no longer propagates once there are no A-state nodes left in the weighted network.

3 Propagation theory based on edge-weight and behavioral heterogeneity

The study of nonredundant information memory with behavioral heterogeneity on weighted networks is based on citations. On the basis of this, this paper puts forward a theory of information partition based on behavioral heterogeneity and analyzes the mechanism of personal information dissemination. Assume that the node in a cavity state [19] implies that it can receive information from its neighbors and cannot send information externally.

The probability that the node will not get information from the following node is t because of the random distribution of the edge weights.

$$\theta(t) = \sum_{\omega} f(\omega)\theta_w(t), \tag{4}$$

where the likelihood that the side of the ω weight does not spread information to its S-country neighbors is given by $\theta_w(t)$.

The likelihood that the S-state nodes i and k_i will collectively get a m pieces communication from their neighbor at time t may be written as

$$\phi(k_i, m, t) = \binom{k_i}{m}\theta(t)^{k_i - m}[1 - \theta(t)]^m. \tag{5}$$

Think about the threshold functions for behavior adoption and behavioral heterogeneity. If the S-state node i is active, it will still be in S-sate at time t with a likelihood of not adopting the behavior after cumulatively accepting m bits of information.

$$\begin{aligned} s_p(k_i, m, t) &= \sum_{m=0}^{k_i} \phi(k_i, m, t) \prod_{l=0}^{m} \left[1 - h_p\left(l, T_p\right)\right] \\ &= \sum_{m=0}^{T_p - 1} \phi(k_i, m, t) \prod_{l=0}^{m} \left(1 - \frac{l}{T_p}\right). \end{aligned} \tag{6}$$

The likelihood that the quantity of the aggregate information pieces by time t is computed by for the active S-state node i is then

$$\eta_p = \sum_{k_i} P(k_i) s_p(k_i, m, t). \tag{7}$$

After receiving m bits of information cumulatively, if the S state node i is passive, it has not yet exhibited this behavior and is still in the S-state in terms of time t probability.

$$\begin{aligned} s_q(k_i, m, t) &= \sum_{m=0}^{k_i} \phi(k_i, m, t) \prod_{l=0}^{m} \left[1 - h_q\left(l, T_q\right)\right] \\ &= \sum_{m=0}^{T_q - 1} \phi(k_i, m, t). \end{aligned} \tag{8}$$

Following that, i and t are the probabilities of the total amount of information blocks in a passive S-state node. calculated by

$$\eta_q = \sum_{k_i} P(k_i) s_q(k_i, m, t). \tag{9}$$

The likelihood that the S-state node i receives m pieces of information and maintains S-state, then, up until time t, is given by

$$s(k_i, t) = (1 - \rho_0)\left[p s_p(k_i, m, t) + q s_q(k_i, m, t)\right]. \tag{10}$$

As a result, we can write the proportion of S-state nodes in a weighted network at time t as

$$S(t) = \sum_{k} P(k) s(k, t) = (1 - \rho_0)\left[p\eta_p + q\eta_q\right]. \tag{11}$$

We start by taking into account the $\theta_\omega(t)$ before calculating $S(t)$. Because all nodes in a network have only three states, $\theta_\omega(t)$ can be broken down to

$$\theta_\omega(t) = \psi_{S,\omega}(t) + \psi_{A,\omega}(t) + \psi_{R,\omega}(t), \tag{12}$$

where the probability that the S-state node i contacts an A-state neighbor j through the appropriate edge of weight ω and has not successfully received information from the A-state node j by time t is denoted by the symbol $\psi_{A,\omega}(t)$. The chance that the S-state node i contacts a S (or R)-state neighbor j via the matching edge with weight ω is known as $\psi_{S,\omega}(t)$ (or $\psi_{R,\omega}(t)$).

Then, we compute $\psi_{S,\omega}(t)$ first. The cavity theory's influence prevents the node i from transmitting data to nearby nodes. Therefore, the S-state node j with k_j neighbors can obtain information from those $k_j - 1$ in addition to the node i. Consequently, the likelihood that node j will accumulate to acquire n bits of information from its surrounding nodes by time t is

$$\phi\left(k_j - 1, n, t\right) = \binom{k_j - 1}{n}\theta(t)^{k_j - 1 - n}[1 - \theta(t)]^n. \tag{13}$$

Think about the threshold functions for behavior adoption and behavioral heterogeneity. If the S-state node j is active, it will still be in S-sate at time t with a likelihood of not adopting the behavior after cumulatively accepting n bits of information.

$$\begin{aligned} \Theta_p\left(k_j, t\right) &= \sum_{n=0}^{k_j - 1} \phi\left(k_j - 1, n, t\right) \prod_{l=0}^{n} \left[1 - h_p\left(l, T_p\right)\right] \\ &= \sum_{n=0}^{T_p - 1} \phi\left(k_j - 1, n, t\right) \prod_{l=0}^{n} \left(1 - \frac{l}{T_p}\right). \end{aligned} \tag{14}$$

After cumulatively accepting n pieces of information, if the S-state node j is passive, it has not yet adopted the behavior and will likely still be in S-sate by time t.

$$\begin{aligned} \Theta_q\left(k_j, t\right) &= \sum_{n=0}^{k_j - 1} \phi\left(k_j - 1, n, t\right) \prod_{l=0}^{n} \left[1 - h_q\left(l, T_q\right)\right] \\ &= \sum_{n=0}^{T_q - 1} \phi\left(k_j - 1, n, t\right). \end{aligned} \tag{15}$$

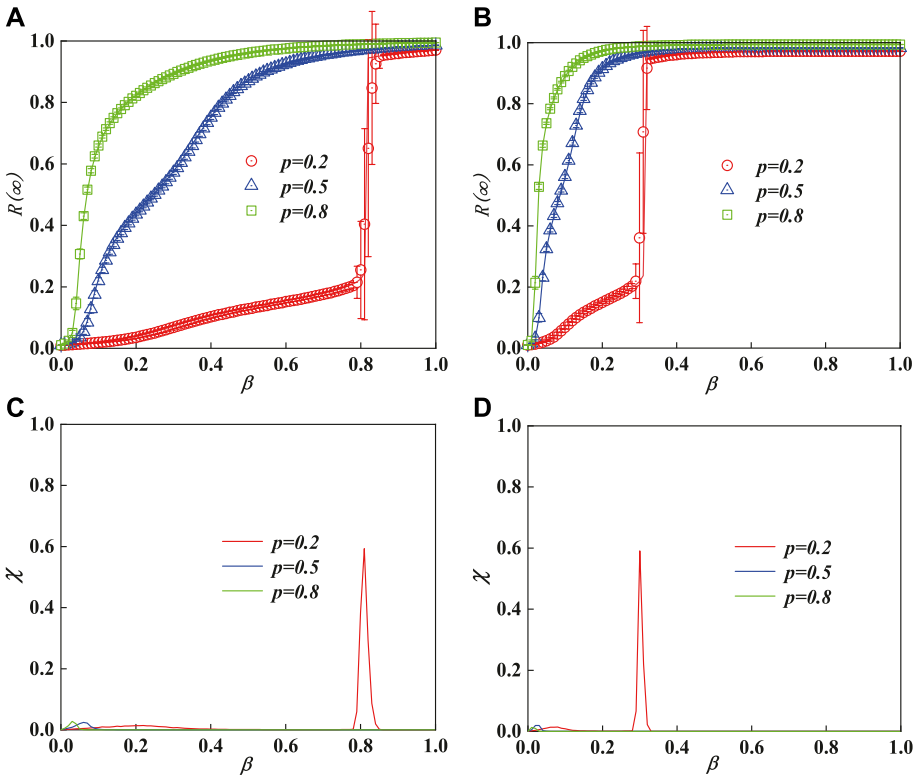

FIGURE 2
Unit propagation probability's impact on the final adaptive size of nodes in a weighted ER network with various percentages of active nodes, in beta. The phase transition is shown to be impacted by the heterogeneity of the weight distribution in (a1) (α_ω = 2) and (b1) (α_ω = 3). The relative variances and thresholds in subparagraphs **(A)** and **(B)**, respectively, are indicated in subparagraphs **(C)** and **(D)**. Additionally, the theoretical predictions (dotted lines) in subparagraphs **(A,B)** are in good agreement with the simulation results (symbols). Other parameters are ρ_0 = 0.01, T_p = 1, and T_q = 5.

Consequently, the likelihood that the node j remains in the S-state after receiving n bits of information cumulatively is

$$\Theta\left(k_j,t\right) = p\Theta_p\left(k_j,t\right) + q\Theta_q\left(k_j,t\right). \tag{16}$$

With the corresponding weight margin ω, the likelihood that the node i will link to the S-state node j is given by

$$\psi_{S,\omega}(t) = \left(1-\rho_0\right)\frac{\sum_{k_j} k_j P\left(k_j\right)\Theta\left(k_j,t\right)}{\langle k\rangle}, \tag{17}$$

where $k_j P(k_j)/\langle k\rangle$ indicates the probability that node i connects to node j with degree k_j, and $\langle k\rangle$ is the average degree of the network.

The evolutionary equation of $\psi_{R,\omega}(t)$ and $\psi_{A,\omega}(t)$ is then examined. With a probability of λ_ω, the S-state node i successfully takes the information from its A-state neighbor j via the appropriate edge of weight ω. Thus, $\theta_\omega(t)$ development can be described by

$$\frac{d\theta_\omega(t)}{dt} = -\lambda_\omega \psi_{A,\omega}(t). \tag{18}$$

On the other hand, the R-state node may transition from the A-state with a probability of γ if the A-state node loses interest in information propagation. Therefore, it is possible to determine the evolution of $\psi_{R,\omega}(t)$ by

$$\frac{d\psi_{R,\omega}(t)}{dt} = \gamma\psi_{A,\omega}(t)\left(1-\lambda_\omega\right). \tag{19}$$

When the initial conditions $\theta_\omega(0) = 1$ and $\psi_{R,\omega}(0) = 0$ are combined with Eqs. 18, 19, we may obtain the evolution of $\psi_{R,\omega}(t)$

$$\psi_{R,\omega}(t) = \gamma[1-\theta_\omega(t)]\left(\frac{1}{\lambda_\omega}-1\right). \tag{20}$$

Substituting Eq.17–20 into Eq. 12, we can obtain

$$\begin{aligned}\psi_{A,\omega}(t) &= \theta_\omega(t) - \psi_{S,\omega}(t) - \psi_{R,\omega}(t)\\ &= \theta_\omega(t) - \left(1-\rho_0\right)\frac{\sum_{k_j} k_j P\left(k_j\right)\Theta\left(k_j,t\right)}{\langle k\rangle}\\ &\quad -\gamma[1-\theta_\omega(t)]\left(\frac{1}{\lambda_\omega}-1\right).\end{aligned} \tag{21}$$

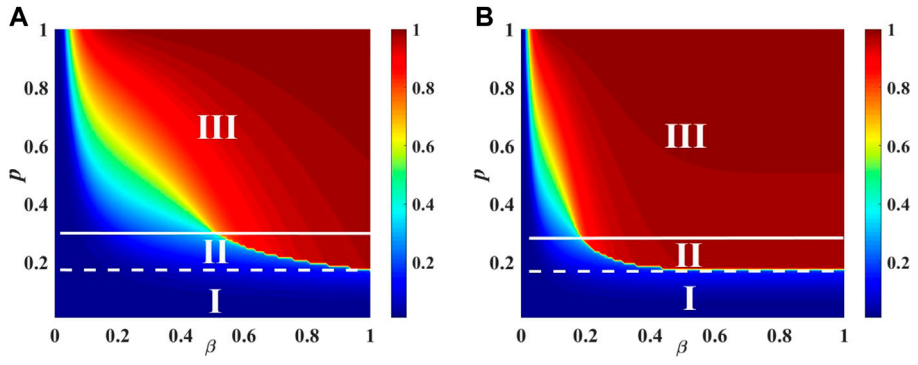

FIGURE 3
The final adoption size of a single weighted ER network is affected by the interaction of the unit propagation probability of beta and the active student part of p. There was no global behavior outbreak, discontinuous phase transition, or continuous phase transition in regions I, II, or III as described in subparagraphs **(A)** and **(B)** (α_ω = 2 and 3, respectively). Other parameters are ρ_0 = 0.01, T_p = 1, and T_q = 5.

Substituting Eq. 21 into Eq. 18, the evolution of $\theta_\omega(t)$ can be rewritten as

$$\begin{aligned}\frac{d\theta_\omega(t)}{dt} &= -\lambda_\omega\left\{\theta_\omega(t) - (1-\rho_0)\frac{\sum_{k_j} k_j P(k_j)\Theta(k_j,t)}{\langle k^X\rangle}\right.\\ &\left.-\gamma[1-\theta_\omega(t)]\left(\frac{1}{\lambda_\omega}-1\right)\right\}\\ &= (1-\rho_0)\lambda_\omega\frac{\sum_{k_j} k_j P_X(k_j)\Theta(k_j,t)}{\langle k\rangle} + \gamma(1-\lambda_\omega)\\ &-[\gamma+\lambda_\omega(1-\gamma)]\theta_\omega(t).\end{aligned} \tag{22}$$

Throughout the network, the density variation of each state can be expressed as

$$\frac{dR(t)}{dt} = \gamma A(t), \tag{23}$$

and

$$\frac{dA(t)}{dt} = -\frac{dS(t)}{dt} - \gamma A(t). \tag{24}$$

So, by combination and iteration Eq.11 and 23, and Eq.24, $S(t)$, $A(t)$and $R(t)$, i.e., you can calculate the density of each state at any given time step length.

There are only S-state and R-state nodes in the network when $t \to \infty$. The maximum size of behavior adoption is $R(\infty)$. Let $\frac{d\theta_\omega(t)}{dt}|_{t=\infty}$ go to zero. The likelihood that information propagation did not occur in the weighted ω at this moment is

$$\theta_\omega(\infty) = \frac{(1-\rho_0)\lambda_\omega\sum_{k_j} k_j P(k_j)\Theta(k_j,\infty) + \langle k\rangle\gamma(1-\lambda_\omega)}{\langle k\rangle\gamma + (1-\gamma)\lambda_\omega\langle k\rangle}. \tag{25}$$

$S(\infty)$ and $R(\infty)$ can be derived by combining and iterating Eq. 11 and 25, and $A(\infty) = 0$.

4 Results and discussions

We conduct comprehensive numerical simulations and theoretical studies on weighted Scale-Free (SF) [20] and Erdő-Rényi (ER) [21] networks, respectively, to validate the theoretical study presented above. The network size is 10^4; that is, there are at least 10^4 dynamically independent persons in the network. The network's average degree is $\langle k\rangle = 10$. The wight distribution follows $g_X(\omega) \sim \omega^{-\alpha_\omega}$ with $\omega^{\max} \sim N^{\frac{1}{\alpha_\omega - 1}}$ and the average weight is $\langle\omega\rangle = 8$. In addition, the probability of recovery is $\gamma = 1.0$.

In our simulations, we employed the relative variance $\mathcal{X}$ Refs. [22, 23], which denotes the probability of critical unit propagation and critical conditions

$$\mathcal{X} = N\frac{\langle R(\infty)^2\rangle - \langle R(\infty)\rangle^2}{\langle R(\infty)\rangle}, \tag{26}$$

where the ensemble average is represented by $\langle\cdots\rangle$. The key moment of information global propagation is represented by the highest values of relative variance.

4.1 Information propagation on weighted ER network

We start by investigating how information spreads on a weighted ER network. The nodes of the ER network are subject to Poisson distribution, i.e., $P(k) = e^{-\langle k\rangle}\frac{\langle k\rangle^k}{k!}$.

In a weighted ER network, Figure 2 investigates the impact of a unit propagation probability *beta* on the final adaptation size of various proportions of active nodes. The initial seed percentage is *rho*0 = 0.01. The adoption criteria are T_p = 1 and T_q = 5, respectively. Figures 2A,B illustrate how the final adoption size, $R(\infty)$, increased to global adoption as β increased.

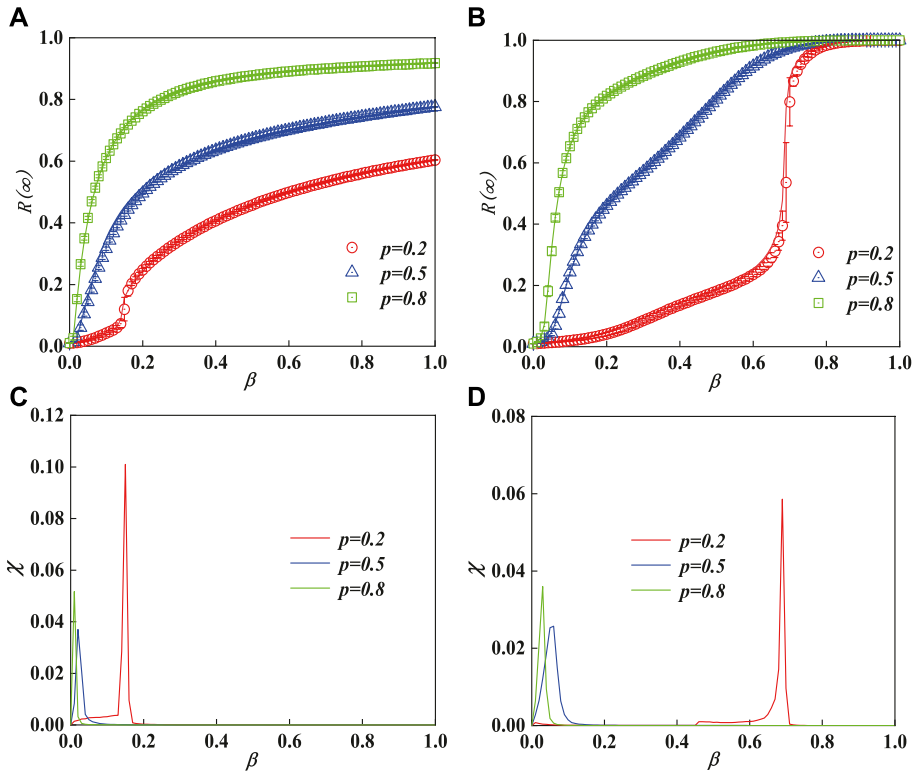

FIGURE 4
Effect of β per unit propagation probability and p active student portion on the final adoption size of weighted SF network individuals. the vertical subgraphs utilizes the same degree distribution index, i.e., the subgraph from first column to third column corresponds to v = 2, 4. Subgraphs **(A)** and **(B)** present the impact of β and p on the size of final individual adoptions with degree distribution heterogeneity. Figure **(C)** and **(D)** present the relative variances and thresholds for **(A,B)**, respectively. Theoretical analysis (dotted line) is in good agreement with simulation values (symbol). Other parameters are ρ_0 = 0.01, α_ω = 2, T_p = 1, and T_q = 5.

Additionally, as the percentage of students who are actively enrolled rises, so does the eventual adoption size, or R (∞). The adoption of the behavior can be encouraged by p. There is a crossover: the R (∞) growth pattern exhibits a continuous phase transition with a sizable p component (between p = 0.5 and p = 0.8). However, the growth pattern of R (∞) shows that the phase transition is discontinuous when the p dollar is small (i.e., p = 0.2). Figure 2 3) and 4) simultaneously display the crucial propagation probabilities and relative variance of 1) and (b), respectively. Phase transition and the adoption of global behavior take place at this crucial time. Additionally, there was a rise in the weighted weighted distribution exponent earlier outbreak of information propagation outbreak as compared to subparagraphs 1) and (b). However, the phase transition pattern is unaffected by the weight distribution. The findings of the simulation accord well with the theoretical prediction (line) (symbol).

The co-effect of p per fashionista and *beta* per unit of propagation probability is examined in Figure 3 for the weighted ER network R (∞). The effects of the weighted heterogeneity of the weight heterogeneity plane (β, p) on R (∞) are shown in Figure 3 1) (α_ω = 2) and 2) (α_ω = 3). The initial fraction of seeds ρ_0 = 0.01. The adoption thresholds are T_p = 1 and T_q = 5. The crossover phenomena appears when β increases. There are three areas in the parameter plane (β, p). There is no widespread trend of adopting new behaviors in region I, and the percentage of trendy people is quite low (p). The cause of this is that students' lack of passion to participate in information propagation during the earliest stages of information dissemination prevents information propagation. In area II, the growing pattern of R (∞) illustrates the discontinuous phase transition as the proportion of active students p increases. The growth pattern of R (∞) displays a persistent phase change in area III. In fact, the dissemination of information and the adoption of passive behavior are dominated by active students in the III district. Additionally, the weight distribution's heterogeneity speeds up information transfer without altering the phase transition pattern.

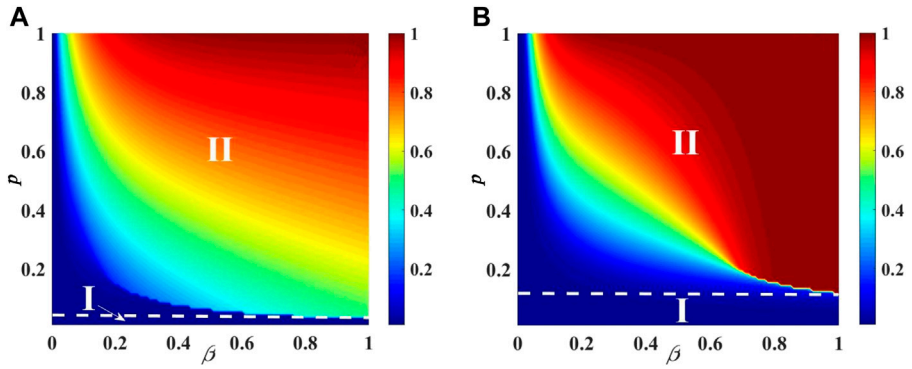

FIGURE 5
The combined impact of active student score and unit propagation probability on the final adoption size of weighted SF network users. The effects of (β, p) on the ultimate adoption size at v = 2.4 are shown in subparagraphs **(A)** and **(B)**, respectively. In **(A,B)**, two regions appeared: region I experienced a sustained phase shift while region II did not experience a worldwide behavior outbreak. Other parameters are ρ_0 = 0.01, α_ω = 2, T_p = 1, and T_q = 5.

4.2 Information propagation on weighted SF network

The degree index v and the heterogeneity of node degree distribution in SF networks are negatively associated. Nodes' degree follows a power-law distribution. The degree exponent of the SF network is presented by equation $p(k) = \xi k^{-v}$, where $\xi = 1/\sum_k k^{-v}$. The minimum and maximum degrees are, respectively, $k_{\min} = 4$ and $k_{\max} \sim 100$.

Figure 4 illustrates the effect of unit propagation probability of β and active student portion of p on individual final adoption size in weighted SF networks with degree distribution heterogeneity. the vertical subgraphs utilizes the same degree distribution index, i.e. the subgraph from first column to third column corresponds to v = 2, 4. The initial fraction of seeds ρ_0 = 0.01. The weight distribution exponent α_ω = 2. The adoption criteria are T_p = 1 and T_q = 5, respectively. With the increase of beta, R (∞) becomes more widely used. Additionally, p encourages the adoption of the behavior. The growth pattern of the final adoption size exhibits a continuous and phase transition with the increase in the percentage of active students. Additionally, when subgraphs 3) and 4) are compared, it can be seen that degree distribution heterogeneity facilitates information dissemination without changing the growth patterns that ultimately result in adoption size. Additionally, in Figure 4A, the global adoption size increases with the percentage of enrolled students when the degree distribution index is 2.

For a weighted SF network with v = 2, 4, respectively, Figures 5A,B examine the fluctuation of R (∞) on the information propagation parameter plane (β, p). The initial seed percentage is ρ_0 = 0.01. Alpha α_ω = 2, which is the exponent of weight heterogeneity. The adoption criteria are T_p = 1 and T_q = 5, respectively. Phase transitions occur as a result of the crossover phenomenon when beta increases. Even more exciting, when the degree distribution heterogeneity is highly heterogeneous, at v = 2, the eventual size of individual adoptions rises slowly as the proportion of students in work increases. But when the degree distribution heterogeneity is less heterogeneous, at v = 4, the eventual size of individual adoptions increases rapidly with the proportion of active students. In Zone I, there has been no global outburst behavior adoption. In region II, the growth model of R (∞) exhibits a sequential phase transition in phase II. In fact, in the II District (Figures 5A,B), active students dominate the dissemination of information and stimulate the adoption of passive behavior.

5 Conclusion

This paper discusses the influence of behavioral psychology on the dissemination on campus sociality. We randomly select a small percentage of p students as active, while others were passive. We also take individual intimacy heterogeneity into account, which is depicted in the campus network as the edge-weight. Then, in order to demonstrate the behavioral psychology, we provide two adoption threshold functions. For active students, they are willing to receive and disseminate information if the information around them is not universally accepted. But passives are willing to adopt information if only when there are more adoptors around them. They are always hesitant about popular behavior, verifying information multiple times before adopting it. A threshold model based on edge weight and heterogeneity is suggested to conceptually investigate the impacts of psychology heterogeneity. We discover several fascinating information transmission phenomena through theoretical investigation and simulation findings. First, engaged

students encourage the spread of knowledge and the adoption of new behaviors. The phase transition crossover phenomenon also manifests. The growth pattern of R (∞) changes has transitioned from a discontinuous phase to a continuous phase with an increase in p. In addition, the distribution of weights facilitates the dissemination of information without altering the pattern of phase transition pattern. Despite being essential to the spread of information, behavioral psychology lacks thorough theoretical modeling and study. The effects of behavior psychology on weighted work are modeled and analyzed qualitatively and quantitatively. By considering behavior psychology on weighted networks, this paper reveals the intrinsic mechanism of campus social.

Data availability statement

The original contributions presented in the study are included in the article/supplementary material, further inquiries can be directed to the corresponding author.

Author contributions

JY and YC designed and performed the research and wrote the manuscript.

Conflict of interest

The authors declare that the research was conducted in the absence of any commercial or financial relationships that could be construed as a potential conflict of interest.

Publisher's note

All claims expressed in this article are solely those of the authors and do not necessarily represent those of their affiliated organizations, or those of the publisher, the editors and the reviewers. Any product that may be evaluated in this article, or claim that may be made by its manufacturer, is not guaranteed or endorsed by the publisher.

References

1. Duan B, Chen H, Sun L, Tang Q, Tian S, Xie M. Identifying influential spreaders in complex networks by propagation probability dynamics. *Chaos* (2019) 29(3):033120. doi:10.1063/1.5055069

2. Pang S, Wen X, Fei H. Controllability limit of edge dynamics in complex networks. *Phys Rev E* (2019) 100(2):022318. doi:10.1103/physreve.100.022318

3. Williams OE, Lillo F, Latora V. Effects of memory on spreading processes in non-markovian temporal networks. *New J Phys* (2019) 21(4):043028. doi:10.1088/1367-2630/ab13fb

4. Dodds P, Watts J. Universal behavior in a generalized model of contagion. *Phys Rev Lett* (2004) 92(21):218701. doi:10.1103/physrevlett.92.218701

5. Peng H, Peng W, Zhao D, Wang W. Impact of the heterogeneity of adoption thresholds on behavior spreading in complex networks. *Appl Mathematics Comput* (2020) 386:125504. doi:10.1016/j.amc.2020.125504

6. Wang W, Tang M, Shu P, Wang Z. Dynamics of social contagions with heterogeneous adoption thresholds: Crossover phenomena in phase transition. *New J Phys* (2016) 18(1):013029. doi:10.1088/1367-2630/18/1/013029

7. Wang W, Tang M, Zhang H, Lai Y. Dynamics of social contagions with memory of nonredundant information. *Phys Rev E* (2015) 92(1):012820. doi:10.1103/physreve.92.012820

8. Han L, Lin Z, Tang M, Zhou J, Zou Y, Guan S. Impact of contact preference on social contagions on complex networks. *Phys Rev E* (2020) 101(4):042308. doi:10.1103/physreve.101.042308

9. Wang W, Shu P, Zhu YX, Tang M, Zhang YC. Dynamics of social contagions with limited contact capacity. *Chaos* (2015) 25(10):103102. doi:10.1063/1.4929761

10. Granovetter M. Threshold models of collective behavior. *Am J Sociol* (1978) 83(6):1420–43. doi:10.1086/226707

11. Yang Q, Zhu X, Tian Y, Wang G, Zhang Y, Chen L. The influence of heterogeneity of adoption thresholds on limited information spreading. *Appl Mathematics Comput* (2021) 411:126448. doi:10.1016/j.amc.2021.126448

12. Zhu X, Wang W, Cai S, Stanley H. Optimal imitation capacity and crossover phenomenon in the dynamics of social contagions. *J Stat Mech* (2018)(6) 063405. doi:10.1088/1742-5468/aac914

13. Fink C, Schmidt AC, Barash V, Kelly J, Cameron C, Macy M. Investigating the observability of complex contagion in empirical social networks. In: Tenth International AAAI Conference on Web and Social Media (2016).

14. Zhu X, Yang Q, Tian H, Ma J, Wang W. Contagion of information on two-layered weighted complex network. *IEEE Access* (2019) 7:155064–74. doi:10.1109/access.2019.2948941

15. Zhu X, Ma J, Su X, Tian H, Wang W, Cai S. Information spreading on weighted multiplex social network. *Complexity* (2019) 2019:5920187. doi:10.1155/2019/5920187

16. González M, HidalgoCésar A, Barabási A-L. Understanding individual human mobility patterns. *Nature* (2009) 453:238–782. doi:10.1038/nature07850

17. Perc M. Does strong heterogeneity promote cooperation by group interactions? *New J Phys* (2011) 13(12):123027. doi:10.1088/1367-2630/13/12/123027

18. Wang W, Tang M, Zhang HF, Gao H, Do Y, Liu ZH. Epidemic spreading on complex networks with general degree and weight distributions. *Phys Rev E* (2014) 90(4):042803. doi:10.1103/physreve.90.042803

19. Yuan X, Hu Y, Stanley H, Havlin S. Eradicating catastrophic collapse in interdependent networks via reinforced nodes. *Proc Natl Acad Sci U S A* (2017) 114(13):3311–5. doi:10.1073/pnas.1621369114

20. Catanzaro M, Boguná M, Pastor-Satorras R. Generation of uncorrelated random scale-free networks. *Phys Rev E* (2005) 71(2):027103. doi:10.1103/physreve.71.027103

21. Paul E, Rényi A. On the evolution of random graphs. *Publ Math Inst Hung Acad Sci* (1960) 5(1):17–60.

22. Shu P, Wei W, Ming T, Do Y. Numerical identification of epidemic thresholds for susceptible-infected-recovered model on finite-size networks. *Chaos* (2015) 25(6):063104. doi:10.1063/1.4922153

23. Chen X, Wang W, Cai S, Eugene SH, Braunstein LA. Optimal resource diffusion for suppressing disease spreading in multiplex networks. *J Stat Mech* (2018) 5(5):053501. doi:10.1088/1742-5468/aabfcc

frontiers | Frontiers in Physics

TYPE Original Research
PUBLISHED 05 October 2022
DOI 10.3389/fphy.2022.1019643

OPEN ACCESS

EDITED BY
Xuzhen Zhu,
Beijing University of Posts and Telecommunications (BUPT), China

REVIEWED BY
Yong Wang,
Beijing Technology and Business University, China
Huan Wang,
Beijing Technology and Business University, China
Zhao Wang,
Tsinghua University, China

*CORRESPONDENCE
Jing Zhang,
zhangjing01@caas.cn
Mengshuai Zhu,
zhumengshuai@caas.cn

†These authors have contributed equally to this work and share first authorship.

SPECIALTY SECTION
This article was submitted to Social Physics, a section of the journal Frontiers in Physics

RECEIVED 15 August 2022
ACCEPTED 07 September 2022
PUBLISHED 05 October 2022

CITATION
Shen C, Chi L, Wang X, Han S, Zhang J and Zhu M (2022), A spatial network analysis of vegetable prices based on a partial granger causality approach. *Front. Phys.* 10:1019643. doi: 10.3389/fphy.2022.1019643

A spatial network analysis of vegetable prices based on a partial granger causality approach

Chen Shen[1†], Liang Chi[1†], Ximeng Wang[2], Shuqing Han[1], Jing Zhang[1*] and Mengshuai Zhu[1*]

[1]Agricultural Information Institute, Chinese Academy of Agricultural Sciences, Beijing, China, [2]Cyber Finance Department, Postal Savings Bank of China, Beijing, China

The spatial difference in agricultural product prices is a crucial factor affecting the benefits of related stakeholders. This study aims to analyze the mechanisms of spatial price transmission. In this paper, taking garlic as an example, we present a vector autoregression model analyzing relations of the price transmission between producing and selling cities. The partial Granger causality test is used to determine the direction and path of price transmission between the main producing areas and the main consuming areas. We find that the prices in different areas have a complex transmission network and fluctuate in correlation with each other. The results reveal the characteristics of agricultural product price transmission in China and provide reasons and evidence for market regulation.

KEYWORDS

spatial network, agricultural product price, vector autoregression, vegetable, garlic, price transmission

1 Introduction

Analyzing price forming mechanism is a critical means to guide farmers' behaviors, regulate economic activities and reduce risks, and price transmission is one important reason to affect marketing prices. Asymmetric price transmission is a rule in economic activity [1] and it is of great meaning to analyze price transmission. The main forms of price transmission include vertical and horizontal types. Vertical price transmission is the price linkage through value chains, and horizontal price transmission is spatial and cross-commodity price connections [2], both of which are common in markets.

Scholars have studied price transmission in the agricultural market for decades. Many people analyze agricultural market price transmission at the national level such as pork, beef, maize, rice, and pangasius in the US, Ghana, Vietnam, China, etc., [3–8]. Some other people, such as Bekkers [9] and Luo [10], also study international price transmission. Kim [11] use recursive methods across 100 food commodities and conclude that price linkages are strong. They all conclude that price transmission is universal in the market.

Price transmission could also link with other factors to affect prices. Information propagation is thought greatly important for relationships [12]. Food inflation and price transmission are critical on macroeconomic dimensions [13]. Market integration and structure are linked with price transmission in consumer markets of developing countries [14, 15]. Distance and border have a great effect on price transmission [16]. Improving marketing, information, and transportation technology have strengthened the links between prices [17]. Oligopoly and oligopsony power do not necessarily lead to imperfect price transmission [18].

Researchers should study price transmission with caution about methodologies [19, 20]. There is a wider range of methods to assess linkages and connections [21–23]. Also, the methods to measure price transmission has been progressing, and the econometric model is the most used method in past years, such as the error correction model (ECM), stationarity and integration tests, and autoregressive distributed lag (ARDL) models, generalized autoregressive conditional heteroskedasticity (GARCH). Table 1 lists some examples of measuring price transmission with different methodologies.

In this paper, we focus on vegetable price transmission in China. China is the biggest vegetable producer and consumer. Vegetable prices have attracted a lot of attention over the years because vegetable plays a vital role in daily life while their prices fluctuate greatly. The violent fluctuations of vegetable prices influence farmers' income and affect consumers' benefits. In recent years, the Chinese government issued various policies to keep vegetable prices within a reasonable range [39], but still did not solve the problem. Especially for some small varieties, like scallion, ginger, and garlic [40, 41], the total output value is relatively low, so the production guidance and price prediction are quite difficult.

We choose garlic as an example to analyze the price transmission of vegetables in China. On the one hand, the research on garlic price transmission in China is of great significance for the garlic industry both domestically and internationally. China plants about 800,000 ha and produces more than 19 million tons of garlic, with more than 70% output and 62.8% international market share. As the main producing, consuming and exporting country, the relative stability of the garlic planting scale is the basis for the sustainable development of the garlic industry. Studying the characteristics of garlic price transmission is of great significance in guiding farmers to make scientific decisions, stabilizing garlic prices and promoting the stable development of the garlic industry. On the other hand, the special trait of garlic makes its price a hot issue in China. Garlic could be kept for a few months in storage, so it is always processed and refrigerated by dealers after being harvested and sold out at a high

TABLE 1 Literature review of price transmission methods.

Author	Region	Variety	Period	Methodology
Kinnucan and Forker (1987) [24]	US	Major Dairy Products	1971–1981	Chow-type test, Houck procedure
Cramon-Taubadel (1998) [3]	Germany	Pork	1990–1993	Error correction representation
Goodwin and Holt (1999) [4]	US	Beef	1981–1998	Cointegration and Threshold Testing
Abdulai (2000) [5]	Ghana	Maize	1980–1997	Threshold cointegration tests
Sanjuan and Dawson (2003) [25]	United Kingdom	Meat	1986–2000	Cointegration procedure of Johansen
Bakucs and Fertō (2005) [26]	Hungary	Pork	1992–2002	Stationarity and Integration Tests, Granger causality
Ihle et al. (2009) [27]	Tanzania and Kenya	Maize	2000–2008	Markov-switching vector autoregression
Brummer (2009) [28]	Ukraine	Wheat and flour	2000–2004	Markov-switching vector error-correction
Cudjoe et al. (2010) [29]	Ghana	Food	2007–2008	Threshold cointegration
Xu et al. (2012) [8]	China	Swine	1994–2011	Market-Chain Cooperated Model
Santeramo (2012) [30]	Europe	Tomatoes and cauliflowers	1996–2006	Asymmetric threshold autoregressive econometric specification
Weldesenbet (2013) [31]	Slovakia	Liquid milk	1993–2010	Granger causality and the Johansen cointegration
Acosta and Valdes (2014) [32]	Panama	Milk	1991–2011	Two-Step ECM
Singh (2015) [2]	Thai	Aquaculture	2001–2010	Unit-root, Granger causality, and cointegration
Hatzenbuehleer (2016) [33]	Nigeria	Crop	2002–2008	Comprehensive price transmission analysis
Fousekis et al. (2016) [6]	US	Beef	1990–2014	Nonlinear ARDL
Usman and Haile (2017) [34]	Ethiopia	Cereal	2000–2011	Asymmetric error correction models
Rezitis (2018) [35]	Finland	Dairy product	2002–2015	Nonlinear ARDL
Dong et al. (2018) [36]	China	Pork	1994–2016	Asymmetric error correction and autoregressive moving average
Pham et al. (2018) [37]	Vietnam to Poland	Pangasius	2010–2014	Vector error correction model
Ricci et al. (2019) [38]	Italy	Wheat	1999–2011	Cointegration methodology
Thong et al. (2020) [7]	Vietnam to Germany	Pangasius	2007–2012	Johansen cointegration
Luo and Tannka (2021) [10]	10 countries	Food	2005–2019	GARCH, DCC

market price. In practice, market information such as supply and demand, price trends, circulation costs, and information transmission can all have an impact on price transmission.

Before determining the research area, we comprehensively analyzed the distribution of the garlic industry in China. In terms of production, according to the statistics of 2016, the garlic output of Shandong, Henan and Jiangsu provinces accounted for 57.58% of the total national output. The garlic output of Shandong, Henan and Jiangsu provinces accounted for 27.83%, 18.90%, and 10.86% of the total national output, respectively. The garlic output of Sichuan, Yunnan and Guizhou provinces accounted for 7.74% of the total national output, accounting for less than 1/10 of the total national output. The garlic output of Sichuan, Yunnan and Guizhou provinces accounted for 3.51%, 2.77%, and 1.45% of the total national output, respectively. In terms of planted area, the area of garlic in Shandong, Henan and Jiangsu provinces accounted for 52.64% of the total area of China, accounting for more than half of the total area. The area of garlic in Shandong, Henan and Jiangsu provinces accounted for 25.25%, 14.91%, and 12.48% of the total area of China, respectively. The area of garlic in Sichuan, Yunnan and Guizhou provinces accounted for 12.01% of the total area of China, accounting for only about 1/10 of the total area. The area of garlic in Sichuan, Yunnan and Guizhou provinces accounted for 4.59%, 3.78%, and 3.64% of the total area of China, respectively.

The main purpose of price transmission is to study the relationship between prices. At first, we introduce a methodology to measure price transmission, which is proposed by Krishna [42] and shows great appropriateness in results. Secondly, we analyze the mechanism of vegetable price transmission in China and take garlic as an example. The results reveal that the garlic market in northern China has been highly integrated. There is a causal relationship in the garlic wholesale prices between the main producing areas and important consuming areas. The change of the price in one region will cause the change of garlic wholesale prices in other regions. We also find that the wholesale prices of garlic in China show the characteristics of the bidirectional transmission.

The rest of the paper is organized as follows. In Section 2 we provide materials and methods. In Section 3 we demonstrate the results. In Section 4, we summarize and discuss the results, and analyze these conclusions in combination with the actual situation of the industry.

2 Materials and methods

2.1 Data

In this study, we have collected and aggregated ten-day prices from 2015 to 2019 in the wholesale markets of China's main garlic-producing areas and important consuming cities in northern China. The producing areas include Jinxiang County in Shandong Province, Qixi County in Henan Province, and Pizhou City in Jiangsu Province. The consuming cities include Beijing, Shijiazhuang, Taiyuan, Zhengzhou, and Qingdao, which are all big cities with huge populations.

Figure 1 depicts the trend of wholesale garlic prices. The garlic prices not only vary greatly from year to year but also show relatively seasonal characteristics. The wholesale price data of garlic in Beijing, Shijiazhuang, Taiyuan, Zhengzhou, and Qingdao are from China Agricultural Information Network. And the wholesale price data of Jinxiang County, Qixi County, and Pizhou City are from China Vegetable Association. We take Logarithmic processing of the original price sequences in order to eliminate the heteroscedasticity.

2.2 Partial granger causality approach

Granger causality has been widely used in economic analyses nowadays. According to the Granger causality theory, if the

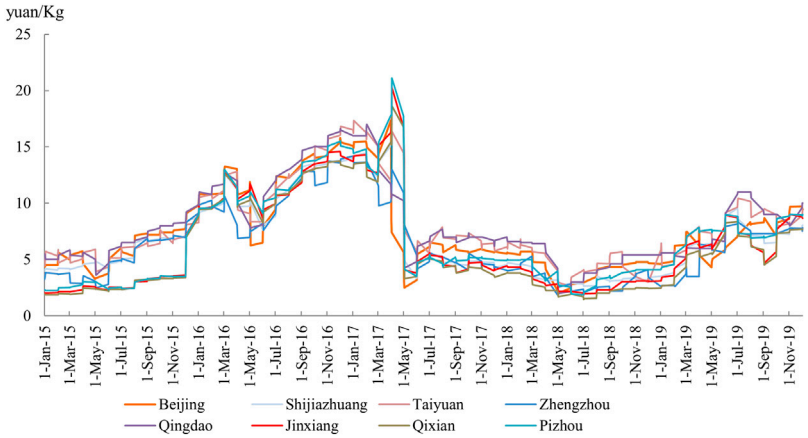

FIGURE 1
Prices of several cities in China from 2015–2019.

TABLE 2 Results of the ADF unit root test for price series.

Variables	Form	Critical value at 5%	Test statistic	*p*-value
p_t^{bj}	(C,0,1)	−2.88	−2.45	0.13
p_t^{sjz}	(C,0,2)	−2.88	−1.75	0.40
p_t^{qd}	(C,0,1)	−2.88	−2.47	0.12
p_t^{zz}	(C,0,0)	−2.88	−1.75	0.41
p_t^{ty}	(C,0,0)	−2.88	−1.95	0.31
p_t^{jx}	(C,0,1)	−2.88	−1.89	0.34
p_t^{pz}	(C,0,1)	−2.88	−2.02	0.28
p_t^{qx}	(C,0,2)	−2.88	−2.05	0.27
Δp_t^{bj}	(C,0,1)	−1.94	−10.95	0.00
Δp_t^{sjz}	(0,0,1)	−1.94	−9.13	0.00
Δp_t^{qd}	(0,0,0)	−1.94	−8.89	0.00
Δp_t^{zz}	(0,0,1)	−1.94	−13.56	0.00
Δp_t^{ty}	(0,0,0)	−1.94	−13.41	0.00
Δp_t^{jx}	(0,0,0)	−1.94	−9.71	0.00
Δp_t^{pz}	(0,0,0)	−1.94	−8.62	0.00
Δp_t^{qx}	(0,0,0)	−1.94	−8.98	0.00

TABLE 3 Criterion of optimal lag order in model.

Lag	AIC	SC	HQ	FPE
0	−16.400	−16.25430*	−16.341	0.000
1	−17.333	−16.021	−16.80057*	4.10e-18*
2	−17.33348*	−14.855	−16.328	0.000
3	−17.264	−13.618	−15.785	0.000
4	−17.123	−12.311	−15.171	0.000
5	−16.820	−10.842	−14.395	0.000
6	−16.782	−9.637	−13.883	0.000

Note: * indicates the optimal lag order corresponding to the criterion.

prediction of one process can be improved by incorporating its past information as well as the past information of the other process, then the second process is said to cause the first process. Granger causality test could be demonstrated as follows in Eqs 1, 2.

$$F_{Y\to X|Z} = ln\left(\frac{S_{11} - S_{12}S_{22}^{-1}S_{21}}{\sum XY - \sum XYZ\sum_{zz}^{-1}\sum ZXY}\right) \tag{1}$$

$$\begin{aligned} S &= \begin{bmatrix} var(\varepsilon_{1t}) & cov(\varepsilon_{1t},\varepsilon_{2t}) \\ cov(\varepsilon_{1t},\varepsilon_{2t}) & var(\varepsilon_{2t}) \end{bmatrix} \\ &= \begin{bmatrix} S_{11} & S_{12} \\ S_{21} & S_{22} \end{bmatrix}, \sum = \begin{bmatrix} var(\varepsilon_{3t}) & cov(\varepsilon_{3t},\varepsilon_{5t}) \\ cov(\varepsilon_{3t},\varepsilon_{5t}) & var(\varepsilon_{5t}) \end{bmatrix} \\ &= \begin{bmatrix} \sum XY & \sum XYZ \\ \sum ZXY & \sum ZZ \end{bmatrix} \end{aligned} \tag{2}$$

ε_{1t} and ε_{2t} are prediction errors. Eqs 3, 4 give the past information of the variables. Variance ε_{3t} measures the strength of prediction error. If $Var(\varepsilon_{3t}) < Var(\varepsilon_{1t})$, then Y_t influences X_t.

$$X_t = \sum_{i=1}^{\infty} a_{2i}X_{t-i} + \sum_{i=1}^{\infty} c_{2i}Y_{t-i} + \varepsilon_{3t}, \tag{3}$$

$$Y_t = \sum_{i=1}^{\infty} b_{2i}Y_{t-i} + \sum_{i=1}^{\infty} d_{2i}X_{t-i} + \varepsilon_{4t}. \tag{4}$$

For a network having multiple entities, one entity can be influenced by another directly or indirectly. Thus, a multivariate model using information from all entities in the system, makes it possible to verify whether two entities share direct causal influence while considering the effect of other entities. Krishna and Guo proposed a partial Granger causality test approach [42].

Now consider two processes X_t and Z_t. Eqs 5, 6 show the joint autoregressive representation for X_t and Z_t.

$$X_t = \sum_{i=1}^{\infty} a_{1i}X_{t-i} + \sum_{i=1}^{\infty} c_{1i}Z_{t-i} + \varepsilon_{1t}, \tag{5}$$

$$Z_t = \sum_{i=1}^{\infty} b_{1i}Z_{t-i} + \sum_{i=1}^{\infty} d_{1i}X_{t-i} + \varepsilon_{2t}. \tag{6}$$

Let $S = \begin{bmatrix} var(\varepsilon_{1t}) & cov(\varepsilon_{1t},\varepsilon_{2t}) \\ cov(\varepsilon_{1t},\varepsilon_{2t}) & var(\varepsilon_{2t}) \end{bmatrix}$ be covariance matrix, *var* and *cov* be variance and co-variance, the vector autoregressive including X_t, Y_t and Z_t can be written as Eqs 7, 8, 9.

$$X_t = \sum_{i=1}^{\infty} a_{2i}X_{t-i} + \sum_{i=1}^{\infty} b_{2i}Y_{t-i} + \sum_{i=1}^{\infty} c_{2i}Z_{t-i} + \varepsilon_{3t}, \tag{7}$$

TABLE 4 Results of VAR model.

Variables	Δp_t^{bj}	Δp_t^{sjz}	Δp_t^{ty}	Δp_t^{qd}	Δp_t^{zz}	Δp_t^{jx}	Δp_t^{qx}	Δp_t^{pz}
Constant	0.003	0.001	0.001	0.002	0.001	0.005	0.005	0.004
Δp_{t-1}^{bj}	0.099	0.104	0.013	0.211	−0.111	0.138	0.100	0.119
Δp_{t-1}^{sjz}	−0.271	0.225	0.138	−0.115	−0.028	0.256	0.320	0.148
Δp_{t-1}^{ty}	0.019	0.012	−0.245	0.092	−0.141	0.002	0.008	0.045
Δp_{t-1}^{qd}	0.091	0.179	0.324	0.262	0.280	0.269	0.295	0.231
Δp_{t-1}^{zz}	0.089	0.062	0.139	0.307	−0.090	0.068	0.085	0.109
Δp_{t-1}^{jx}	−0.142	−0.024	−0.221	0.184	0.400	−0.457	−0.277	−0.236
Δp_{t-1}^{qx}	0.445	0.142	0.283	0.005	−0.208	0.465	0.200	0.101
Δp_{t-1}^{pz}	−0.101	0.243	−0.050	−0.161	0.110	0.236	0.362	0.522
Δp_{t-2}^{bj}	0.081	0.092	0.117	0.143	0.122	0.122	0.139	0.090
Δp_{t-2}^{sjz}	−0.304	−0.095	0.066	−0.130	0.159	−0.196	−0.292	−0.145
Δp_{t-2}^{ty}	−0.118	−0.044	−0.143	0.023	−0.072	0.047	−0.010	0.003
Δp_{t-2}^{qd}	0.065	−0.163	0.036	−0.221	−0.119	−0.310	−0.349	−0.188
Δp_{t-2}^{zz}	0.049	−0.053	−0.043	−0.029	−0.150	−0.052	0.000	−0.032
Δp_{t-2}^{jx}	0.291	0.088	−0.253	0.150	0.171	0.213	0.428	0.186
Δp_{t-2}^{qx}	−0.251	−0.111	0.305	−0.209	−0.021	−0.222	−0.450	−0.239
Δp_{t-2}^{pz}	−0.104	-0.105	−0.063	−0.030	0.018	0.013	−0.036	−0.101
R-squared	0.161	0.546	0.233	0.428	0.220	0.409	0.430	0.409
Adj. R-squared	0.078	0.500	0.156	0.371	0.142	0.350	0.373	0.350
F-statistic	1.925	12.019	3.040	7.484	2.826	6.926	7.533	6.924
p-value	0.022	0.000	0.000	0.000	0.000	0.000	0.000	0.000

TABLE 5 Values of the partial Granger causality test statistics for garlic prices.

Variables	Δp_t^{bj}	Δp_t^{sjz}	Δp_t^{ty}	Δp_t^{zz}	Δp_t^{qd}	Δp_t^{jx}	Δp_t^{qx}	Δp_t^{pz}
Δp_t^{bj}	—	0.825	0.203	−0.099	0.796	2.149	2.236	1.447
Δp_t^{sjz}	0.337	—	0.170	0.085	0.371	1.997	2.024	1.119
Δp_t^{ty}	0.309	0.668	—	0.106	0.178	1.930	2.002	1.054
Δp_t^{zz}	0.358	0.912	0.275	—	0.611	2.084	2.275	1.269
Δp_t^{qd}	0.266	0.975	0.223	0.207	—	2.091	2.277	1.309
Δp_t^{jx}	0.324	0.785	0.203	0.133	0.347	—	1.231	1.078
Δp_t^{qx}	0.406	0.883	0.262	0.192	0.443	1.250	—	1.263
Δp_t^{pz}	0.328	0.764	0.188	0.107	0.376	1.887	2.082	—

$$\boldsymbol{Y}_t = \sum_{i=1}^{\infty} \boldsymbol{d}_{2i}\boldsymbol{X}_{t-i} + \sum_{i=1}^{\infty} \boldsymbol{e}_{2i}\boldsymbol{Y}_{t-i} + \sum_{i=1}^{\infty} \boldsymbol{f}_{2i}\boldsymbol{Z}_{t-i} + \boldsymbol{\varepsilon}_{4t}, \tag{8}$$

$$\boldsymbol{Z}_t = \sum_{i=1}^{\infty} \boldsymbol{g}_{2i}\boldsymbol{X}_{t-i} + \sum_{i=1}^{\infty} \boldsymbol{h}_{2i}\boldsymbol{Y}_{t-i} + \sum_{i=1}^{\infty} \boldsymbol{k}_{2i}\boldsymbol{Z}_{t-i} + \boldsymbol{\varepsilon}_{5t}. \tag{9}$$

Now let $\sum = \begin{bmatrix} \boldsymbol{var}(\boldsymbol{\varepsilon}_{3t}) & \boldsymbol{cov}(\boldsymbol{\varepsilon}_{3t}, \boldsymbol{\varepsilon}_{4t}) & \boldsymbol{cov}(\boldsymbol{\varepsilon}_{3t}, \boldsymbol{\varepsilon}_{5t}) \\ \boldsymbol{cov}(\boldsymbol{\varepsilon}_{3t}, \boldsymbol{\varepsilon}_{4t}) & \boldsymbol{var}(\boldsymbol{\varepsilon}_{4t}) & \boldsymbol{cov}(\boldsymbol{\varepsilon}_{4t}, \boldsymbol{\varepsilon}_{5t}) \\ \boldsymbol{cov}(\boldsymbol{\varepsilon}_{3t}, \boldsymbol{\varepsilon}_{5t}) & \boldsymbol{cov}(\boldsymbol{\varepsilon}_{4t}, \boldsymbol{\varepsilon}_{5t}) & \boldsymbol{var}(\boldsymbol{\varepsilon}_{5t}) \end{bmatrix}$ indicate the new covariance matrix, $\boldsymbol{F}_{Y\to X|Z} = \boldsymbol{ln}(\boldsymbol{S}_{11} - \boldsymbol{S}_{12}\boldsymbol{S}_{22}^{-1}\boldsymbol{S}_{21}/\sum \boldsymbol{xy} - \sum \boldsymbol{xyz} \sum \sum \boldsymbol{zxy}_{zz}^{-1})$ can be used to test partial causality if $\boldsymbol{F}_{Y\to X|Z} > \boldsymbol{0}$. It means the partial causality from Y_t to X_t. We have $\boldsymbol{S} = [\boldsymbol{var}(\boldsymbol{\varepsilon}_{1t}) | \boldsymbol{cov}(\boldsymbol{\varepsilon}_{1t}, \boldsymbol{\varepsilon}_{2t}) / \boldsymbol{cov}(\boldsymbol{\varepsilon}_{1t}, \boldsymbol{\varepsilon}_{2t}) | \boldsymbol{var}(\boldsymbol{\varepsilon}_{2t})] = [\boldsymbol{S}_{11} | \boldsymbol{S}_{12} / \boldsymbol{S}_{21} | \boldsymbol{S}_{22}]$, $\sum = [\boldsymbol{var}(\boldsymbol{\varepsilon}_{3t}) | \boldsymbol{cov}(\boldsymbol{\varepsilon}_{3t}, \boldsymbol{\varepsilon}_{5t}) / \boldsymbol{cov}(\boldsymbol{\varepsilon}_{3t}, \boldsymbol{\varepsilon}_{5t}) | \boldsymbol{var}(\boldsymbol{\varepsilon}_{5t})] = [\sum \boldsymbol{XY} | \sum \boldsymbol{XYZ} / \sum \boldsymbol{ZXY} | \sum \boldsymbol{ZZ}]$.

Then we use the VAR model (vector autoregressive model) including multiple entities in Eq. 10.

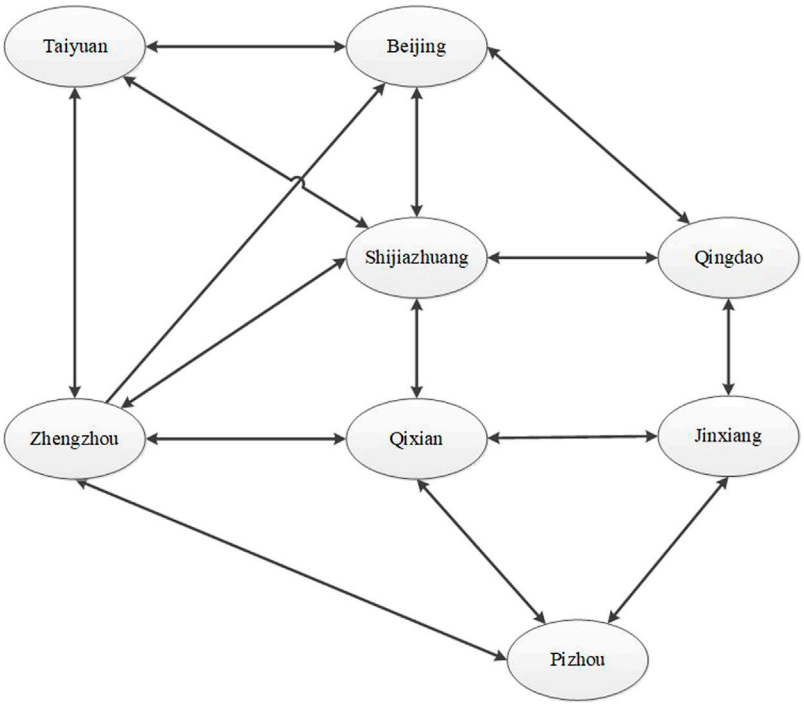

FIGURE 2
Directions of garlic price transmission.

$$\begin{bmatrix} x_{1t} \\ x_{2t} \\ \vdots \\ x_{mt} \end{bmatrix} = \begin{bmatrix} c_1 \\ c_2 \\ \vdots \\ c_m \end{bmatrix} + \begin{bmatrix} \alpha_{11} & \alpha_{12} & \cdots & \alpha_{1m} \\ \alpha_{21} & \alpha_{22} & \cdots & \alpha_{2m} \\ \vdots & \vdots & \ddots & \vdots \\ \alpha_{m1} & \alpha_{m2} & \cdots & \alpha_{mm} \end{bmatrix} \begin{bmatrix} x_{1t-1} \\ x_{2t-1} \\ \vdots \\ x_{mt-1} \end{bmatrix} + \begin{bmatrix} \beta_{11} & \beta_{12} & \cdots & \beta_{1m} \\ \beta_{21} & \beta_{22} & \cdots & \beta_{2m} \\ \vdots & \vdots & \ddots & \vdots \\ \beta_{m1} & \beta_{m2} & \cdots & \beta_{mm} \end{bmatrix} \begin{bmatrix} x_{1t-2} \\ x_{2t-2} \\ \vdots \\ x_{mt-2} \end{bmatrix} + \cdots \begin{bmatrix} \delta_{11} & \delta_{12} & \cdots & \delta_{1m} \\ \delta_{21} & \delta_{22} & \cdots & \delta_{2m} \\ \vdots & \vdots & \ddots & \vdots \\ \delta_{m1} & \delta_{m2} & \cdots & \delta_{mm} \end{bmatrix} \begin{bmatrix} x_{1t-p} \\ x_{2t-p} \\ \vdots \\ x_{mt-p} \end{bmatrix} + \begin{bmatrix} \varepsilon_1 \\ \varepsilon_2 \\ \vdots \\ \varepsilon_m \end{bmatrix}. \tag{10}$$

To build VAR model, time-series should be weakly stationary. We use the ADF unit root test to test stationarity and Akaike Information Criterion (AIC) to determine the optimal lag order.

$$AIC(p) = 2log(|\sigma|) + \frac{2m^2p}{n}. \tag{11}$$

3 Results

3.1 Stationarity tests

Table 2 shows the results of the ADF unit root test for each price series. In the variables, let bj, sjz, qd, zz, ty, jx, pz, qx denote the cities of Beijing, Shijiazhuang, Qingdao, Zhengzhou, Taiyuan, Jinxiang, Pizhou, Qixian, p denote price, and t denote current period. We use AIC statistics with the minimum point for examination. The null hypothesis of the ADF test is that the series is stationary. The *p*-value of the price series test statistics is more than 0.05, so we reject the null hypothesis. This indicates that none of the garlic wholesale price series examined is stationary. So, the original price series is differenced and then tested for stationarity. The results show that the *p*-value are less than 0.01. It indicates that the differenced series are all stationary and match the criteria for building the VAR model.

3.2 Building VAR model

After testing the series' stationarity, we build a VAR model using the post-differential price series. We use AIC criterion to determine the optimal lag order and set the maximum lag time at 6. Table 3 displays the optimal lag order for several criteria, with the findings indicating that the 2-lags model fits best.

The VAR (2) model is constructed and estimated. Table 4 shows the results. The variable in the top row of the table represents the current period's wholesale price for each location, which is assigned as the dependent variable in the VAR model. The values in each column represent the coefficients of the relevant varibles' regression. For all equations, the *p*-value of the F-statistic is less than 0.05. It

shows that the variables are statistically significant and can provide a better fit for each local price change.

3.3 Partial granger causality test

The partial Granger causality test requires the construction of the VAR model. According to Krishna [42], the partial Granger causality test statistic between two variables could be obtained by using regression residuals for each equation which can be derived using the VAR model. Table 5 shows the results of the partial Granger causality test for garlic. The values in the table represent the partial Granger causality test value for the effect of the row price on the column price. If the value is bigger than zero, the column price with change following the row price. Figure 2 describes the direction of garlic price transmission according to the magnitude of the test statistic used.

4 Conclusion and discussion

Using the stationarity test and the VAR model, we conducted a partial Granger causality test on wholesale price series in the major garlic-producing regions and the important northern cities in China from 2015 to 2019. The primary conclusions are as follows.

The Northern garlic market in China has been highly consolidated. Garlic wholesale prices are all causally connected between the major producing areas and the major consumption areas. Changes in the wholesale price of garlic in one place can induce price changes in another, which we think is resulted from the improvement of transportation and communication conditions in China in recent years. The ever-improving highway network has linked the main garlic production areas with major consumption areas, which promotes the spread of garlic circulation.

The wholesale prices of garlic show the characteristic of bidirectional transmission. The wholesale prices in producing areas could affect that of the consuming areas, and vice versa. The causal effect of wholesale price in important consuming areas on the main producing areas and the causal effect among the main producing areas are more significant, just as the value of the partial Granger causality test statistic shows. Only one unidirectional connection is the transmission from Zhengzhou to Beijing, which means that the price changes in Zhengzhou could affect the price in Beijing, but not vice versa.

Also, there are some limitations in our analysis. The first shortcoming is that we only choose some big producing areas and consuming cities in northern China. Price transmission exists in every city and the linkages should be much more complex. Secondly, we only consider spatial price transmission among cities and do not examine vertical price transmission along supply chains. Vertical and horizontal price transmissions may interact and lead to various results. Besides, just as Von Cramon-Taubadel and Meyer's view [19], the method should be considered with caution. People using different methods may get contrary outcomes. The method innovation is very important when studying price transmission.

Data availability statement

The original contributions presented in the study are included in the article/Supplementary Material, further inquiries can be directed to the corresponding authors.

Author contributions

Conceptualization, MZ and CS; Data curation, CS and LC; Formal analysis, LC and XW; Methodology, CS, LC, and JZ; Validation, LC, XW, and SH; Writing–MZ and LC; draft, MZ and JZ; Writing–review and editing, SH and JZ.

Funding

This research was funded by National Natural Science Foundation, Grant Number 71703159 and Central Public interest Scientific Institution Basal Research Fund of China, Grant Number JBYW-AII-2022-13 and JBYW-AII-2022-40.

Conflict of interest

The authors declare that the research was conducted in the absence of any commercial or financial relationships that could be construed as a potential conflict of interest.

Publisher's note

All claims expressed in this article are solely those of the authors and do not necessarily represent those of their affiliated organizations, or those of the publisher, the editors and the reviewers. Any product that may be evaluated in this article, or claim that may be made by its manufacturer, is not guaranteed or endorsed by the publisher.

Supplementary material

The Supplementary Material for this article can be found online at: https://www.frontiersin.org/articles/10.3389/fphy.2022.1019643/full#supplementary-material

References

1. Peltzman S. Prices rise faster than they fall. *J Polit Economy* (2000) 108: 466–502. doi:10.1086/262126

2. Singh K, Dey MM, Laowapong A, Bastola U. Price transmission in Thai aquaculture product markets: An analysis along value chain and across species. *null* (2015) 19:51–81. doi:10.1080/13657305.2015.994236

3. Cramon-Taubadel SV. Estimating asymmetric price transmission with the error correction representation: An application to the German pork market. *Eur Rev Agric Econ* (1998) 25:1–18. doi:10.1093/erae/25.1.1

4. Goodwin B K, Holt M T. Price transmission and asymmetric adjustment in the U.S. Beef sector. *Am J Agric Econ* (1999) 81:630–7. doi:10.2307/1244026

5. Abdulai A. Spatial price transmission and asymmetry in the Ghanaian maize market. *J Develop Econ* (2000) 63:327–49. doi:10.1016/S0304-3878(00)00115-2

6. Fousekis P, Katrakilidis C, Trachanas E. Vertical price transmission in the US beef sector: Evidence from the nonlinear ARDL model. *Econ Model* (2016) 52: 499–506. doi:10.1016/j.econmod.2015.09.030

7. Thong NT, Ankamah-Yeboah I, Bronnmann J, Nielsen M, Roth E, Schulze-Ehlers B. Price transmission in the pangasius value chain from Vietnam to Germany. *Aquacult Rep* (2020) 16:100266. doi:10.1016/j.aqrep.2019.100266

8. Xu S, Li Z, Cui L, Dong X, Kong F, Li G. Price transmission in China's swine industry with an application of MCM. *J Integr Agric* (2012) 11:2097–106. doi:10.1016/S2095-3119(12)60468-7

9. Bekkers E, Brockmeier M, Francois J, Yang F Local Food Prices and International Price Transmission. *World Development* (2017). Amsterdam, 96. p. 216–30. doi:10.1016/j.worlddev.2017.03.008

10. Luo P, Tanaka T. Food import dependency and national food security: A price transmission analysis for the wheat sector. *Foods* (2021) 10:1715. doi:10.3390/foods10081715

11. Kim H, Ward R W. Price transmission across the U.S. food distribution system. *Food Policy* (2013) 41:226–36. doi:10.1016/j.foodpol.2013.05.006

12. Xiong F, Shen W, Chen H, Pan S, Wang X, Yan Z. Exploiting implicit influence from information propagation for social recommendation. *IEEE Trans Cybernetics* (2020) 50:4186–99. doi:10.1109/TCYB.2019.2939390

13. Lloyd T. Forty years of price transmission research in the food industry: Insights, challenges and prospects. *J Agric Econ* (2017) 68:3–21. doi:10.1111/1477-9552.12205

14. Baquedano FG, Liefert WM. Market integration and price transmission in consumer markets of developing countries. *Food Policy* (2014) 44:103–14. doi:10.1016/j.foodpol.2013.11.001

15. Bakucs Z, Fałkowski J, Fertő I. Does market structure influence price transmission in the agro-food sector? A meta-analysis perspective. *J Agric Econ* (2014) 65:1–25. doi:10.1111/1477-9552.12042

16. Mengel C, von Cramon-Taubadel S. Distance and border effects on price transmission: A meta-analysis. *J Agric Econ* (2016) 67:255–71. doi:10.1111/1477-9552.12145

17. von Cramon-Taubadel S, Goodwin BK. Price transmission in agricultural markets. *Annu Rev Resource Econ* (2021) 13:65–84. doi:10.1146/annurev-resource-100518-093938

18. Weldegebriel HT. Imperfect price transmission: Is market power really to blame? *J Agric Econ* (2004) 55:101–14. doi:10.1111/j.1477-9552.2004.tb00082.x

19. Von Cramon-Taubadel S, Meyer J. *Asymmetric price transmission: Fact or artefact?* (2000).Citeseer

20. Meyer J, Cramon-Taubadel S. Asymmetric price transmission: A survey. *J Agric Econ* (2004) 55:581–611. doi:10.1111/j.1477-9552.2004.tb00116.x

21. Xiong F, Wang X, Pan S, Yang H, Wang H, Zhang C. Social recommendation with evolutionary opinion dynamics. *IEEE Trans Syst Man, Cybernetics: Syst* (2020) 50:3804–16. doi:10.1109/TSMC.2018.2854000

22. Li Z, Xiong F, Wang X, Chen H, Xiong X. Topological influence-aware recommendation on social networks. *Complexity* (2019) 2019:e6325654. doi:10.1155/2019/6325654

23. Zhu M, Chen H, Wang X, Wang Y, Shen C, Zhu C. Firms' investment behaviours in temperature-controlled supply chain networks. *Complexity* (2021) 20211–1. doi:10.1155/2021/5359819

24. Kinnucan HW, Forker OD. Asymmetry in farm-retail price transmission for major dairy products. *Am J Agric Econ* (1987) 69:285–92. doi:10.2307/1242278

25. Sanjuán AI, Dawson PJ. Price transmission, BSE and structural breaks in the UK meat sector. *Eur Rev Agric Econ* (2003) 30:155–72. doi:10.1093/erae/30.2.155

26. Bakucs LZ, Fertõ I. Marketing margins and price transmission on the Hungarian pork meat market: Marketing Margins and Price Transmission. *Agribusiness* (2005) 21:273–86. doi:10.1002/agr.20047

27. Ihle R, von Cramon-Taubadel S, Zorya S, Zonya S. Markov-switching estimation of spatial maize price transmission processes between Tanzania and Kenya. *Am J Agric Econ* (2009) 91:1432–9.

28. Brümmer B, von Cramon-Taubadel S, Zorya S. The impact of market and policy instability on price transmission between wheat and flour in Ukraine. *Eur Rev Agric Econ* (2009) 36:203–30. doi:10.1093/erae/jbp021

29. Cudjoe G, Breisinger C, Diao X. Local impacts of a global crisis: Food price transmission, consumer welfare and poverty in Ghana. *Food Policy* (2010) 35: 294–302. doi:10.1016/j.foodpol.2010.01.004

30. Santeramo FG. Price transmission in the European tomatoes and cauliflowers sectors: Price transmission in the EUROPEAN tomatoes and cauliflowers sectors. *Agribusiness* (2015) 31:399–413. doi:10.1002/agr.21421

31. Weldesenbet T. Asymmetric price transmission in the Slovak liquid milk market. *Agric Econ* (20132013) 59:512–24. doi:10.17221/150/2012-AGRICECON

32. Acosta A, Valdés A. Vertical price transmission of milk prices: Are small dairy producers efficiently integrated into markets?: Vertical price transmission of milk prices. *Agribusiness* (2014) 30:56–63. doi:10.1002/agr.21357

33. Hatzenbuehler PL, Abbott PC, Abdoulaye T. Price transmission in Nigerian food security crop markets. *J Agric Econ* (2017) 68:143–63. doi:10.1111/1477-9552.12169

34. Usman MA, Haile MG. Producer to retailer price transmission in cereal markets of Ethiopia. *Food Sec* (2017) 9:815–29. doi:10.1007/s12571-017-0692-0

35. Rezitis AN. Investigating price transmission in the Finnish dairy sector: An asymmetric NARDL approach. *Empir Econ* (2019) 57:861–900. doi:10.1007/s00181-018-1482-z

36. Dong X, Brown C, Waldron S, Zhang J. Asymmetric price transmission in the Chinese pork and pig market. *BFJ* (2018) 120:120–32. doi:10.1108/BFJ-02-2017-0056

37. Pham TAN, Meuwissen MPM, Le TC, Bosma RH, Verreth J, Lansink AO. Price transmission along the Vietnamese pangasius export chain. *Aquaculture* (2018) 493:416–23. doi:10.1016/j.aquaculture.2017.04.028

38. Ricci EC, Peri M, Baldi L. The effects of agricultural price instability on vertical price transmission: A study of the wheat chain in Italy. *Agriculture* (2019) 9:36. doi:10.3390/agriculture9020036

39. Lu H, Bai Y, Ren H, Campbell DE. Integrated emergy, energy and economic evaluation of rice and vegetable production systems in alluvial paddy fields: Implications for agricultural policy in China. *J Environ Manage* (2010) 91: 2727–35. doi:10.1016/j.jenvman.2010.07.025

40. Wang B, Liu P, Zhang C, Wang J, Peng L. Prediction of garlic price based on ARIMA model. In: *Cloud computing and security*. p. 731–9. doi:10.1007/978-3-030-00006-6_66

41. Zhang X-X, Liu L, Su C-W, Tao R, Lobonț O-R, Moldovan N-C. Bubbles in agricultural commodity markets of China. *Complexity* (2019) 2019:e2896479. doi:10.1155/2019/2896479

42. Krishna R, Guo S. A partial granger causality approach to explore causal networks derived from multi-parameter data. In: *Computational methods in systems biology*. p. 9–27. doi:10.1007/978-3-540-88562-7_6

frontiers | Frontiers in Physics

TYPE Original Research
PUBLISHED 13 October 2022
DOI 10.3389/fphy.2022.1017951

OPEN ACCESS

EDITED BY
Fei Xiong,
Beijing Jiaotong University, China

REVIEWED BY
Jianjuan Liu,
Henan University of Technology, China
Ye Tian,
Shenyang Ligong University, China
Biao Leng,
Beihang University, China

*CORRESPONDENCE
Mengjie Gong,
sqt2000405081@
student.cumtb.edu.cn

†These authors have contributed equally to this work

SPECIALTY SECTION
This article was submitted to Social Physics,
a section of the journal
Frontiers in Physics

RECEIVED 12 August 2022
ACCEPTED 20 September 2022
PUBLISHED 13 October 2022

CITATION
Yang J, Gong M, Dong X, Liang J and Wang Y (2022), MPDNet: A Transformer-based real-time passenger detection network in metro stations. *Front. Phys.* 10:1017951.
doi: 10.3389/fphy.2022.1017951

MPDNet: A Transformer-based real-time passenger detection network in metro stations

Jun Yang[1,2†], Mengjie Gong[2*†], Xueru Dong[2†], Jiahua Liang[2†] and Yan Wang[2†]

[1]Big Data and Internet of Things Research Center, China University of Mining and Technology, Beijing, China, [2]Key Laboratory of Intelligent Mining and Robotics, Ministry of Emergency Management, Beijing, China

We propose a passenger flow detection method for dense areas of subway stations to address the current situation that existing pedestrian detection models cannot meet the real-time performance requirements in subway applications and lack validation in multiple subway scenarios. First, we designed the MPDNet model, which uses PVT-small to extract features and an improved feature pyramid network (FPN) for upsampling using the adaptively spatial feature fusion (ASFF) algorithm to retain more local information in the output of the FPN. Second, to better evaluate the performance of models in the metro, we collected subway surveillance video data and proposed the MetroStation dataset. Finally, we trained and evaluated the performance of the MPDNet model on the MetroStation dataset. We compare our method with several common object detection models on the MetroStation dataset, using mAP and frames per second (FPS) to verify its accuracy. The experiments on the MetroStation dataset demonstrated that the MPDNet performed well and satisfied inference speed requirements in metro passenger flow detection.

KEYWORDS

passenger detection, metro station, surveillance video, deep learning network, transformer

Introduction

The demand for transportation capacity increases with the continuous expansion of the scale of cities. As an integral part of public transportation in large cities, the metro system plays an important role in improving traffic capacity and relieving traffic pressure. Therefore, metro construction has become the focus of many cities. Rail transportation has gradually won the approval of passengers because of its high capacity, punctuality, safety, and comfort.

At present, the scale of the metro network is expanding. It shows the uneven distribution of passenger flow in the metro network, with high traffic volume and passenger flow during the morning and evening rush hours. This means the instantaneous passenger flow of a metro station has a large peak that could lead to trampling accidents during the peak period. This peak affects the safe and stable operation of the subway. Therefore, obtaining passenger flow data in a timely and accurate method

plays an important role in supporting operational decisions and ensuring the safe and efficient operation of the metro.

The automatic fare collection system (AFC) is the most common and widely used method to get passenger flow information. The core of the AFC is to collect data from gate machines and then process the data to obtain the location and timing of passengers entering and exiting the stations, thus analyzing the spatial and temporal distribution of passenger flow. The flow data obtained in this way is accurate, but it takes time to process and analyze after collecting raw data from the AFC. In addition, this method cannot obtain the passenger flow data from internal areas of stations such as station halls, transfer channels, and platforms.

In China, metro stations are fully covered by video surveillance systems. Many metro operators assign specialized staff to observe the surveillance video in real time to obtain information about the passenger flow in each area of the station [1]. This labor-based approach not only relies heavily on staff experience but also does not enable quantifying passenger flow data. Moreover, this type of passenger flow information contains subjective information that can produce bias in the information propagation [2]. Therefore, many researchers have began to use real-time surveillance video systems to get passenger flow data. Hu et al. [3] proposed a crowd counting method on subway platforms. It combined a weighted area feature that considers perspective and an improved gradient feature that could indicate crowd density to calculate the number of passengers. This method solves the problem of overlapping passengers and calculates the number of people in a dense crowd more accurately. However, its performance is easily affected by the quality of the images and different crowd density levels. Xie et al. [4] used the Dempster–Shafer theory (D–S theory) to improve the average background model for background modeling, reduced the weight of irrelevant background caused by moving objects, and then used the feature of image connected domain for passenger flow recognition. This method has fast inference speed but is greatly influenced by the environment and has different performance under different passenger flow densities.

With the concepts of intelligent transportation and the development of deep learning in recent years, many researchers have started to use convolutional neural network (CNN) methods for passenger flow detection. The deep learning-based methods have greatly improved the accuracy of passenger flow detection and reduced the influence of environmental changes on the performance of models. Zhang et al. [5] proposed MPCNet, which uses CNN to extract features and then uses a multi-column atrous CNN with atrous spatial pyramid pooling to estimate the crowd size. It can aggregate multi-scale contextual information in crowded scenes. This method has high detection accuracy but slow inference speed, so it is difficult to meet the requirement of real-time detection in metro stations. Later, Guo et al. [6] proposed MetroNet to detect highly obscured passengers efficiently and also proposed Tiny MetroNet to achieve a better balance of accuracy, memory, and speed on resource-constrained platforms. Liu et al. [7] designed a novel MSAC block to generate informative and semantic convolutional features and proposed MetroNext based on MSAC. This method can achieve real-time detection of passengers on and off the subway by combining MetroNexts and an optical flow algorithm. Yang et al. [8] used the attention mechanism CBAM to improve yolov4 and decrease the effect of light on the detection performance. The passenger flow detection methods in these studies are based on CNNs owing to their good trainability and generalization capabilities. Getting real-time passenger flow data both reduces the risk of emergencies and influences passengers' travel decisions through social network propagation [9]. However, many of these methods do not satisfy the required real-time performance in metro applications and lack validation in the context of multiple metro scenes.

In response to the above problems, we propose the metro passenger detection network (MPDNet) based on a transformer model. It can achieve dense passenger flow detection in metro stations with multiple scenes, focusing on the passenger distortion caused by the installation angle of the metro video surveillance system and inter-passenger occlusion problems. We implement pyramid vision transformer (PVT) as the feature extraction network on RetinaNet. We also improve the feature fusion module with the adaptively spatial feature fusion (ASFF) algorithm. This improvement compensates for the loss of spatial information caused by PVT. Finally, we replace an L1 loss with a generalized intersection over union (GIoU) loss as the regression loss of the bounding box. In addition, we propose the MetroStation dataset based on the video surveillance system data of Beijing metro stations. The MetroStation dataset fills the gap of lacking station scene data in metro station passenger flow detection. The dataset contains images from different camera angles of various areas within the rail stations, with passengers at different sparsity levels labeled in each image. This dataset is of great value for improving the performance and robustness of the model in metro passenger flow detection. Finally, we test our model on the MetroStation dataset and compare it with various other object detection models. The experiments show that our method has both better accuracy and good real-time performance.

Related work

CNN-based objection detection

The development of object detection algorithms can be divided into two stages: methods based on manual feature construction and methods based on deep learning models. After 2012, the performance of manual feature methods became saturated, and methods based on manual feature

construction entered a bottleneck. The emergence of AlexNet [10] changed the situation. AlexNet was the first method to adopt convolutional neural networks for image classification tasks and achieved better performance than the manual feature-based methods. Since then, computer vision has entered a new era dominated by CNNs. In 2014, Girshick et al. [11] proposed region-based CNN (RCNN), a representative of the two-stage method, which first applied convolutional neural networks to object detection. Later, Fast RCNN [12], and Faster RCNN [13] were proposed to have better detection accuracy and inference speed than RCNN. However, the two-stage method based on classification has a serious drawback of slow inference speed despite its high detection accuracy, so it is not suitable for real-time object detection. This restriction was later removed by YOLO [14]. It directly regresses all information of the bounding box in the output layer and greatly improves the inference speed. After YOLO, one-stage detectors, such as SSD [15] and RetinaNet [16], have emerged continuously. Their excellent detection performance is based on high resolution and multi-scale feature maps.

Transformer-based objection detection

Transformer is a self-attention-based model originally applied in natural language processing (NLP). The excellent performance of bidirectional encoder representations from transformers (BERT) and generative pre-trained transformer 3 (GPT-3) in NLP demonstrates that transformer-based methods have strong computational performance and scalability. Based on the existing model growth, transformer methods show no sign of saturation. Considering the great success of transformer methods in the field of NLP, many researchers started to think about introducing it in computer vision tasks. Carion et al. proposed DETR [17], a full end-to-end detector. It abandoned the anchor generator and non-maximum suppression (NMS) that were commonly used in previous CNN-based detectors and used the transformer encoder-decoder structure to directly consider object detection as a direct set prediction problem. Inspired by the transformer in NLP, vision transformer (ViT) [18] was proposed, which was the first to introduce pure transformer methods in image classification tasks. ViT divides an image into a patch sequence and considers patches as tokens (words) in the NLP task. It was proved that ViT obtains the same or even better results than CNN-based methods for supervised training on large datasets (14 –300 million images). This shows that transformer methods can replace CNN applications as a fundamental component in computer vision. After ViT, research on adopting transformer methods in target detection tasks has sprung up. The Swin transformer [19] is a hierarchical structure that progressively shrinks the output resolution, expanding the receptive field by layer like a CNN. Instead of performing multi-head attention on patch sequences like ViT, the Swin transformer introduced the concept of windows into the transformer to implement the localization of CNN. This approach also reduced the computational complexity caused by self-attention. PVT [20] introduced the pyramid structure into transformer methods and presented a pure transformer backbone for dense prediction tasks. PVT added spatial reduction operation to multi-head attention to form spatial-reduction attention (SRA). SRA greatly reduced the computational and memory cost required for attention operation while keeping the resolution of the feature map and the global receptive field. Replacing ResNet50 with PVT-small as the backbone network of RetinaNet gained better performance at COCO VAL2017, showing that PVT performed better than CNN under the same number of parameters.

Proposed methods

MPDNet structure

Lin et al. [16] attributed the lower detection accuracy of the one-stage detector compared to the two-stage detector to the extremely unbalanced ratio of positive to negative samples. Therefore, they proposed a simple but practical function called focal loss and designed the RetinaNet for object detection. This enables the one-stage detector to match or even surpass the two-stage detector in accuracy.

In this study, we built a RetinaNet detector on the MMDetection framework. As shown in Figure 1, the model structure can be divided into three parts: backbone, neck, and head.

RetinaNet is a detection model with better and faster detection performance. It uses ResNet50 as the backbone network, as proposed by He et al. [21] in 2015. ResNet50 is the first to address the progressive degradation of neural networks caused by increasing depth with the residual module. After inputting the processed image, ResNet outputs four different scale feature maps into a feature pyramid network (FPN). The FPN [22] upsamples the bottom map and fuses it with the same scale feature map. The outputs of FPN have high resolution and strong semantic features. RetinaNet is an anchor-based algorithm that generates nine anchors with three scales and three aspect ratios at every position of a feature map. The RetinaHead has two branches. One calculates the category, and the other calculates the regression parameters of the bounding box. Focal loss as classification loss is the core of the RetinaNet; it is an improvement of cross-entropy (CE) loss for binary classification.

$$CE(p, y) = \begin{cases} -log(p), & if\ y = 1, \\ -log(1-p), & otherwise. \end{cases} \tag{1}$$

In the equation above, $y \in \{\pm 1\}, p \in [0, 1]$ is the estimated probability for class with label $y = 1$. Therefore, define p_t:

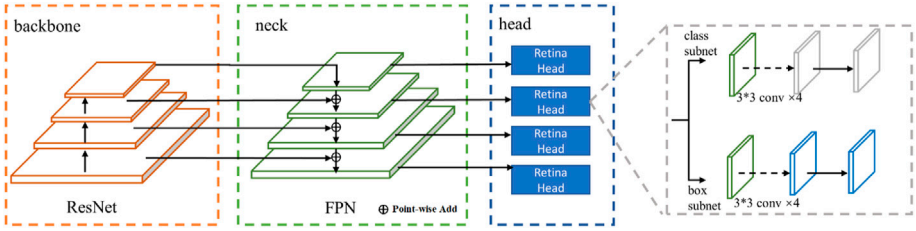

FIGURE 1
The structure of RetinaNet.

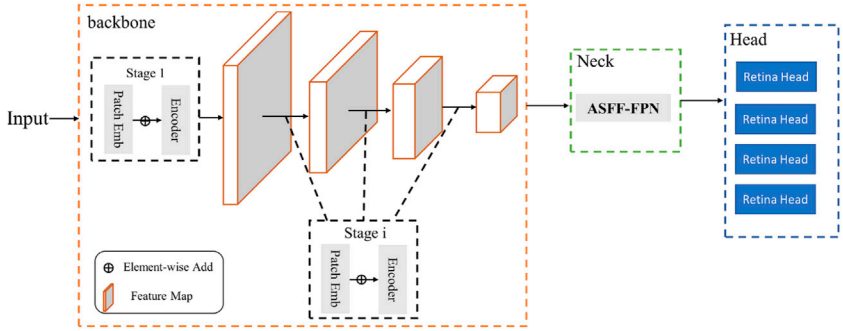

FIGURE 2
The structure of MDPNet.

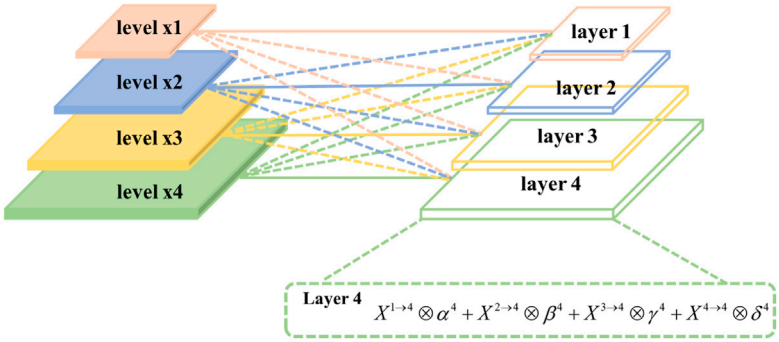

FIGURE 3
The structure of improved FPN.

$$p_t = \begin{cases} p & , \quad if\ y = 1 \\ 1 - p & , \ otherwise \end{cases} \tag{2}$$

Then, rewrite $CE(p, y) = CE(p_t) = -log(p_t)$.

A common solution to class imbalances is to add a weight factor. Set $\alpha \in [0, 1]$ for class 1 and $1 - \alpha$ for class −1. Then, we write α-balanced CE loss as:

$$CE(P_t) = -\alpha_t log(p_t) \tag{3}$$

During training, many easily classified negatives dominate in the loss. But α can only balance positive/negative examples and cannot distinguish between easy and hard examples. To address that, a modulating factor $(1 - p_t)^y, y \geq 0$ is added in CE loss. The equation is

FIGURE 4
Comparison of MetroStation with other pedestrian detection datasets. **(A)** CrowdHuman, **(B)** CityPerson, **(C)** CUHK occlusion, and **(D)** MetroStation.

TABLE 1 Size of each subset in MetroStation.

	Stairs	Escalator	Gate	Platform
Image	676	748	470	229
People	4,905	3,004	3,097	1968

$$CE(p_t) = -(1 - p_t)log(p_t). \tag{4}$$

Combining Eqs 3, 4, the focal loss can be written as:

$$FL(p_t) = -\alpha_t (1 - p_t)^{\gamma} log\ (p_t). \tag{5}$$

The application of focal loss greatly improves the detection accuracy of the one-stage detector, making the one-stage detector comparable to the two-stage detector in terms of detection accuracy while maintaining inference speed. However, RetinaNet does not have a special network structure design. Therefore, it can be improved according to the changeable lighting conditions, and the characteristics of dense passenger flow in subway stations so as to improve the robustness of the model.

According to experiments [20], when using RetinaNet for object detection, the PVT-based model performs better on COCO Val2017 than ResNet50. In this study, we implemented PVT-small as a backbone network in RetinaNet. The overall network structure is shown in Figure 2.

The transformer encoder is an important part of stages in PVT-small. Each encoder contains an attention layer and a feed-forward layer. PVT replaced the multi-head attention (MHA) layer in the traditional encoder [23] with an SRA layer. In ViT, the calculation of attention can be expressed as follows:

$$\text{Attention}(q, k, v) = \text{Softmax}\left(\frac{qk^T}{\sqrt{d_{head}}}\right)v. \tag{6}$$

Here, q is query, k is key, v is value, and SRA performs spatial reduction in the spatial scale of K, V before attention operation. The calculation of SR is:

$$SR(x) = \text{Norm}\left(\text{Reshape}(x, R_i)W^S\right). \tag{7}$$

Here, $x \in (H_i W_i) \times C_i$ is an input sequence. R_i is the reduction ratio in stage i. $Reshape(x, R_i)$ represents the operation of reshaping x into a sequence of size $\frac{H_i W_i}{R_i^2} \times (R_i^2 C_i)$. $W^S \in \mathbb{R}^{(R_i^2 C_i) \times C_i}$ is a linear projection. Therefore, the attention operation in every head is calculated as:

$$head_j = \text{Attention}\left(QW_j^Q, SR(K)W_j^K, SR(V)W_j^V\right) \tag{8}$$

$W_j^Q \in \mathbb{R}^{C_i \times d_{head}}, W_j^K \in \mathbb{R}^{C_i \times d_{head}}, W_j^V \in \mathbb{R}^{C_i \times d_{head}}$. $\text{Attention}(\cdot)$ is the same as Eq. 6.

SRA adopts the same concatenation operation for the head as MHA. According to Eqs 6, 7, the computation of SRA is R_i^2 times smaller than that of MHA, so it can process larger images with the same resources.

The improvement of FPN

The CNN-based model has a local receptive field and hierarchical structure that can extract features from local to global. The transformer-based model shows strong modeling

FIGURE 5
The types of scenes in the MetroStation dataset: **(A)** platform, **(B)** stairs, **(C)** escalator, and **(D)** gate.

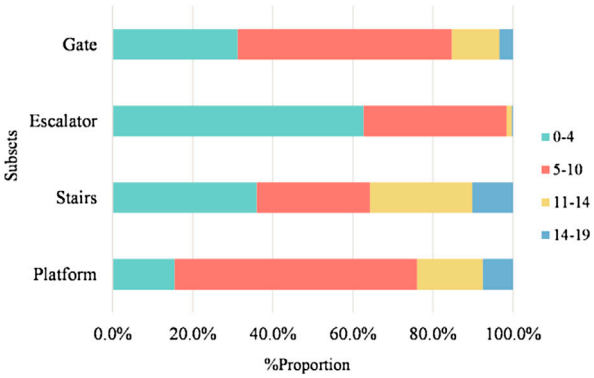

FIGURE 6
The proportions of different densities in the MetroStation subset.

performance with its global modeling ability. However, they are not designed to make full use of the spatial information in images, so they need other means to compensate for this lack. In addition, a mechanism called a heuristic-guided feature selection usually exists when adopting feature pyramids for object detection. In feature maps, large objects are usually associated with upper-level features and small ones with lower-level features. In the process of FPN upsampling, the large instance of the upper feature is regarded as the background in the lower feature map. When there are objects of different scales in the image, this inconsistency between features will interfere with the gradient calculation during training and lower the performance of the pyramidal feature map. Therefore, we adopted the ASFF algorithm to improve FPN. The detailed implementation is shown in Figure 3.

We assigned weight coefficients to different levels of feature maps and retained useful information for combination. The weight coefficients allowed the model to learn spatial fusion weights of different feature maps adaptively and enhanced the feature fusion. Each layer will be processed as follows: First, we modified the feature maps for each level by up-sampling or down-sampling to achieve the same size as the corresponding layer. For example, $X^{3\to4}$ denotes that x^3 is up-sampled by nearest-neighbor interpolation, and the feature map is scaled to the same size as x^4. Second, α^4, β^4, γ^4, and δ^4 indicate the important spatial weights at four levels to layer 4, which are adaptively learned through standard back-propagation by the network. Also, we specified that $\alpha^4 + \beta^4 + \gamma^4 + \delta^4 = 1$ and $\alpha^4, \beta^4, \gamma^4, \delta^4 \in [0, 1]$. Third, after the dot product operation of feature maps and weights, a summation is performed to obtain the final feature maps. This method not only addresses the inconsistency of FPN in training but also compensates for the missing spatial information after PVT-small.

Loss optimization

RetinaHead calculates bounding box loss with L1 loss in the location subnet. L1 loss is also called mean absolute error (MAE). It calculates the loss of the four coordinates of the prediction box and the ground truth box, respectively, and then sums them. It does not consider the correlation between directions and coordinates, so it is not suitable for passenger detection in metro stations.

TABLE 2 Density comparison of MetroStation and its subsets.

	MetroStation	Stairs	Escalator	Gate	Platform
Image	2,123	676	748	470	229
People	12,974	4,905	3,004	3,097	1968
People/image	6.11	7.26	4.02	6.59	8.59

TABLE 3 Comparison of different methods on MetroStation from mAP and FPS.

Model	mAP @0.5	FPS
Retina-r50	92.3	35.4
MPDNet	94.0	34.3
YOLO x	83.2	62.4
SSD	82.4	39
Faster RCNN-r50	93.1	29.9

To address the shortcomings of L1 loss, we improved bounding box loss with GIoU [24] loss:

Predicted B^p and ground truth B^gbounding box coordinates:

$$B^p = (x_1^p, y_1^p, x_2^p, y_2^p), \quad B^g = (x_1^g, y_1^g, x_2^g, y_2^g).$$

For the predicted box B^p, ensuring $x_2^p > x_1^p$ and $y_2^p > y_1^p$:

$$\hat{x}_1^p = min(x_1^p, x_2^p), \quad \hat{x}_2^p = max(x_1^p, x_2^p), \hat{y}_1^p = min(y_1^p, y_2^p), \quad \hat{y}_2^p = max(y_1^p, y_2^p).$$

The area of B^p and B^g:

$$A^g = (x_2^g - x_1^g) \times (y_2^g - y_1^g), \quad A^p = (\hat{x}_2^p - \hat{x}_1^p) \times (\hat{y}_2^p - \hat{y}_1^p). \tag{9}$$

Thus, the intersection between B^p and B^g:

$$x_1^\iota = max(\hat{x}_1^p, x_1^g), \quad x_2^\iota = min(\hat{x}_2^p, x_2^g), y_1^\iota = max(\hat{y}_1^p, y_1^g), \quad x_2^\iota = min(\hat{y}_2^p, y_2^g),$$
$$I = \begin{cases} (x_2^\iota - x_1^\iota) \times (y_2^\iota - y_1^\iota), & \text{if } x_2^\iota > x_1^\iota,\ y_2^\iota > y_1^\iota \\ 0 & \text{otherwise} \end{cases} \tag{10}$$

The coordinates of smallest enclosing box B^c are calculated as:

$$x_1^c = min(\hat{x}_1^p, x_1^g), \quad x_2^c = max(\hat{x}_2^p, x_2^g), y_1^c = min(\hat{y}_1^p, y_1^g), \quad y_2^c = max(\hat{y}_2^p, y_2^g).$$

The area of B^c is:

$$A^c = (x_2^c - x_1^c) \times (y_2^c - y_1^c). \tag{11}$$

According to Eqs 9, 10:

$$IoU = \frac{I}{U}, \quad U = A^p + A^g - I, \tag{12}$$

$$GIoU = IoU - \frac{A^c - U}{A^c}. \tag{13}$$

The loss functions based on intersection over union (IoU) and GIoU are:

$$L_{IoU} = 1 - IoU, \quad L_{GIoU} = 1 - GIoU. \tag{14}$$

Compared with the L1 loss, IoU is scale invariant, and the output of IoU loss is always between 0 and 1, which reflects the inference performance of the prediction box and ground truth. GIoU addresses the problem that the gradient cannot be calculated when the two boxes overlap under the IoU. It also adds a minimum outsourcing box as the penalty term. This method can better reflect the proximity of the two boxes, and it is better for predicting box regression in the case of dense object detection.

Experiment

Dataset

With the continuous development of deep learning, model training has placed more requirements on the quality and quantity of datasets. Therefore, the quality of data is extremely helpful in model training and the generalization ability of the model. KITTI [25], CityPersons [26], and Caltech-USA et al. [27] are the mainstream large-scale pedestrian detection datasets. However, these datasets are still slightly inadequate for passenger flow detection in a metro station. For example, the KITTI and Caltech-USA datasets have less than one person per image on average. CityPersons, as a subset of the Cityscapes dataset [28], has an average of about six people per image, but this density still does not simulate the density of metro traffic very well. CrowdHuman [29] and CUHK Occlusion [30] are pedestrian detection datasets for dense, occlusive scenes. These two datasets are mainly oriented to streets, squares, and other open areas with good lighting conditions. However, in metro stations, the quality of images often suffers from diverse perspectives and insufficient lighting due to the restrictions of camera installation. Therefore, the existing pedestrian detection datasets can not fully simulate the subway operation scene in terms of density, perspective and light conditions. To address that, we proposed a new dataset named MetroStation. Our goal is to represent different

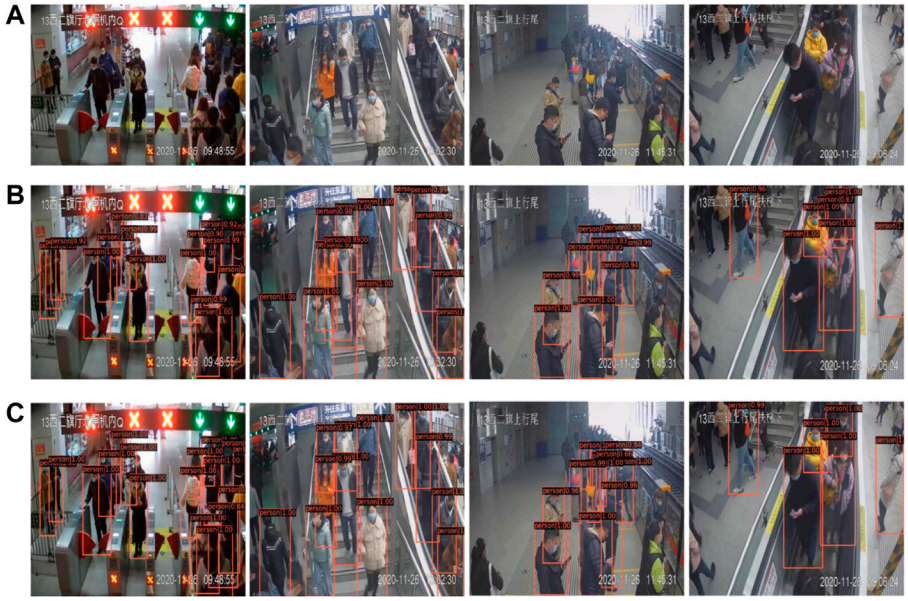

FIGURE 7
Comparison of practical application effects between RetinaNet and MPDNet. **(A)** The original images. **(B)** The results of RetinaNet. **(C)** The results of MPDNet.

TABLE 4 Experimental results of ASFF-FPN.

Model	mAP
Retina-r50*	92.3
Retina-r50	92.5
MPDNet*	87.9
MPDNet	94.0

operation scenes in MetroStation as comprehensively as possible, including different camera angles, different lighting conditions and different traffic densities. The original data of the MetroStation dataset were obtained from the surveillance video of Beijing subway stations. Depending on the speed of passenger movement in different areas of the stations, we draw frames at different time intervals.

The dataset contains 2,123 annotated images of size 640×480 pixels with 12,974 labels. The training set contains 1,699 images, and the remaining 424 images are validation and test images. The comparison between our dataset and other datasets is shown in Figure 4.

Diversity and size

Diversity is one of the important indicators of the dataset. Depending on the different video sources, the whole dataset can be divided into four subsets: Stairs, Escalator, Gate and Platform. The number of images and labels in each subset is shown in Table 1.

The Stairs subset comes from videos of two cameras installed in the stairs area during three different periods. The Escalator subset comes from the cameras facing four different escalators. The Gate subset consists of four time slots from two gates, and the Platform subset consists of seven time slots from five cameras. We display four types of scenes in our datasets in Figure 5.

Density

In terms of density, the average density in MetroStation is 6.1 people per image. However, the density of each subset varies due to different passenger flow characteristics and camera perspectives in different station areas, as shown in Table 2.

The average density of MetroStation can reach 6.11 people per image. The Platform subset has the highest density of all subsets, with an average density of 8.59 people per image. We show the distribution of images with different densities in Figure 6.

Experiments on the MetroStation dataset

In this study, we used two NVIDIA GeForce GTX 1080Tis to train on MMDetection 2.20, an object detection framework. We

used a step learning rate schedule with 24 epochs and the AdamW optimization algorithm.

We evaluated the performance of our method on the MetroStation dataset. We randomly divided MetroStation into a training set and test set according to an 8:2 ratio and used mean average precision (mAP) as the accuracy indicator. We compared several common object detection models on the MetroStation dataset in terms of accuracy. We took frames per second (FPS) as the indicator of inference speed. The experiment results are shown in Table 3.

Table 3 shows that our model has reached 94.0% passenger detection accuracy. Compared with other methods in Table 3, our detection accuracy is even better than the two-stage detector. The FPS of MPDNet is 34.3, which is capable of real-time detection in a metro station.

Figure 7 shows the application of RetinaNet and MPDNet in four subsets. The number of false positive samples in MPDNet is less, and MPDNet performed better in identifying passengers from a highly occluded crowd.

Ablation experiments

In this section, we performed ablation experiments on the MetroStation dataset to verify the effectiveness of ASFF-FPN. In this experiment, every model was improved by GIoU. Table 4 shows that using the ASFF algorithm to optimize the FPN model can effectively improve accuracy. "*" indicates the FPN was not improved by the ASFF algorithm.

The accuracy of the models improved by ASFF was lifted, with RetinaNet improved by 0.2% and MPDNet improved by 6.1%. The reason is that the features extracted by the backbone in these two models have different components of spatial information. The purpose of FPN is to pass the higher-layer feature down layer by layer. This will complement the semantic information of the lower layer to obtain high resolution and strong semantic features. In RetinaNet, the feature in the lower layer is more related to localization information, and the feature in the upper layer is more related to the characteristics of the object. In this case, the purpose of ASFF-FPN is almost the same as that of FPN, so the performance of ASFF-FPN in RetinaNet is not significant. Meanwhile, in MPDNet, PVT-small is a network based on a self-attention mechanism. It reshapes the image into a patch sequence and calculates the correlation between each patch. Even though the shape of feature maps is pyramidal, it still focuses more on global information. Thus, the feature contains more global information and less local information. The ASFF algorithm assigned higher weights to feature maps that contained more local information, making the output feature maps have a larger proportion of local information from upper layers. In this case, MPDNet improved with ASFF and performed better than the MPDNet* that was not improved. Moreover, the transformer-based method can extract more localization information than the CNN-based method from the principle, making MPDNet have higher accuracy than RetinaNet.

Conclusion

This research focused on using surveillance video data to detect passenger flow in various areas of metro stations. We proposed the MetroStation dataset based on surveillance video from metro stations. Compared with other pedestrian detection datasets, this dataset reflects multiple scenes from metro stations. We also introduced MPDNet, a real-time passenger flow detector based on RetinaNet. The experiment on MetroStation showed that MPDNet performed well on passenger flow detection in dense, occluded scenes of metro stations.

Although our model performed well in dense passenger flow detection, we still hope to have better computational efficiency. Therefore, our future work will focus on the 2D position embedding method in the transformer-based model to make it more suitable for objection detection tasks and increase its inference speed. We will continue to enrich the density and diversity of the MetroStation dataset.

Data availability statement

The MetroStation dataset now is available in https://doi.org/10.6084/m9.figshare.20521848.

Author contributions

All authors listed have made a substantial, direct, and intellectual contribution to the work and approved it for publication.

Funding

This study is supported in part by the National Key R&D Program of China (2020YFC0833104); the Beijing Municipal Natural Science Foundation (L201015) and Safe Mining of Coal Resources (Grant No. 52121003).

Conflict of interest

The authors declare that the research was conducted in the absence of any commercial or financial relationships that could be construed as a potential conflict of interest.

Publisher's note

References

1. ling YX, Xie Z, Wang AL. Real-time monitoring system for passenger flow information of metro stations based on intelligent video surveillance. In: B Liu, L Jia, Y Qin, Z Liu, L Diao, M An, editors. Proceedings of the 4th International Conference on Electrical and Information Technologies for Rail Transportation (EITRT); Singapore (2019). p. 329–35. doi:10.1007/978-981-15-2914-6_31

2. Xiong F, Shen W, Chen H, Pan S, Wang X, Yan Z. Exploiting implicit influence from information propagation for social recommendation. *IEEE Trans Cybern* (2020) 50:4186–99. doi:10.1109/TCYB.2019.2939390

3. Hu X, Zheng H, Wang W, Li X. A novel approach for crowd video monitoring of subway platforms. *Optik* (2013) 124:5301–6. doi:10.1016/j.ijleo.2013.03.057

4. Zhengyu X, Limin J, Li W. Passenger flow detection of video surveillance: A case study of high-speed railway transport hub in China. *ElAEE* (2015) 21:48–53. doi:10.5755/j01.eee.21.1.9805

5. Zhang J, Zhu G, Wang Z. Multi-column atrous convolutional neural network for counting metro passengers. *Symmetry* (2020) 12:682. doi:10.3390/sym12040682

6. Guo Q, Liu Q, Wang W, Yuanqing Z, Kang Q. A fast occluded passenger detector based on MetroNet and Tiny MetroNet. *Inf Sci* (2020) 534:16–26. doi:10.1016/j.ins.2020.05.009

7. Liu Q, Guo Q, Wang W, Zhang Y, Kang Q. An automatic detection algorithm of metro passenger boarding and alighting based on deep learning and optical flow. *IEEE Trans Instrum Meas* (2021) 70:1–13. doi:10.1109/TIM.2021.3054627

8. Yang J, Zheng Y, Yan K, Liu H, Jin K, Fan W, et al.SPDNet: A real-time passenger detection method based on attention mechanism in subway station scenes. *Wireless Commun Mobile Comput* (2021). doi:10.1155/2021/7978644

9. Xiong F, Wang X, Pan S, Yang H, Wang H, Zhang C. Social recommendation with evolutionary opinion dynamics. *IEEE Trans Syst Man Cybern Syst* (2020) 50:1–13. doi:10.1109/TSMC.2018.2854000

10. Krizhevsky A, Sutskever I, Hinton GE. ImageNet classification with deep convolutional neural networks. In: *Advances in neural information processing systems* (2022)

11. Girshick R, Donahue J, Darrell T, Malik J. Rich feature hierarchies for accurate object detection and semantic segmentation. In: Proceedings of the IEEE Conference on Computer Vision and Pattern Recognition (CVPR) (2014). p. 580–7. doi:10.1109/CVPR.2014.81

12. Girshick R. Fast R-CNN. In: 2015 IEEE International Conference on Computer Vision (ICCV); 07-13 December 2015; Santiago, Chile (2015). p. 1440–8. doi:10.1109/ICCV.2015.169

13. Ren S, He K, Girshick R, Sun J. Faster R-CNN: Towards real-time object detection with region proposal networks. *IEEE Trans Pattern Anal Mach Intell* (2017) 39:1137–49. doi:10.1109/TPAMI.2016.2577031

14. Redmon J, Divvala S, Girshick R, Farhadi A. You only look once: Unified, real-time object detection. In: 2016 IEEE Conference on Computer Vision and Pattern Recognition (CVPR); Las Vegas, NV, USA (2016). p. 779–88. doi:10.1109/CVPR.2016.91

15. Liu W, Anguelov D, Erhan D, Szegedy C, Reed S, Fu C-Y, Berg AC. Ssd: Single shot MultiBox detector. In: European Conference on Computer Vision (2016). p. 21–37. doi:10.1007/978-3-319-46448-0_2

16. Lin T-Y, Goyal P, Girshick R, He K, Dollár P. Focal loss for dense object detection (2018). Available at: http://arxiv.org/abs/1708 (Accessed June 2, 2022).

17. Carion N, Massa F, Synnaeve G, Usunier N, Kirillov A, Zagoruyko S. End-to-End object detection with transformers (2020). Available at: http://arxiv.org/abs/2005.12872 (Accessed April 30, 2022).

18. Dosovitskiy A, Beyer L, Kolesnikov A, Weissenborn D, Zhai X, Unterthiner T, et al.An image is worth 16x16 words: Transformers for image recognition at scale (2020). Available at: http://arxiv.org/abs/2010 (Accessed April 30, 2022).

19. Liu Z, Lin Y, Cao Y, Hu H, Wei Y, Zhang Z, et al.Swin transformer: Hierarchical vision transformer using shifted windows. In: 2021 IEEE/CVF International Conference on Computer Vision (ICCV); Montreal, QC, Canada (2021). doi:10.1109/ICCV48922.2021.00986

20. Wang W, Xie E, Li X, Fan D-P, Song K, Liang D, et al.Pyramid vision transformer: A versatile backbone for dense prediction without convolutions. In: 2021 IEEE/CVF International Conference on Computer Vision (ICCV); Montreal, QC, Canada (2021). p. 548–58. doi:10.1109/ICCV48922.2021.00061

21. He K, Zhang X, Ren S, Sun J. Deep residual learning for image recognition. In: 2016 IEEE Conference on Computer Vision and Pattern Recognition (CVPR); Las Vegas, NV, USA (2016). p. 770–8. doi:10.1109/CVPR.2016.90

22. Lin T-Y, Dollar P, Girshick R, He K, Hariharan B, Belongie S. Feature pyramid networks for object detection. In: 2017 IEEE Conference on Computer Vision and Pattern Recognition (CVPR) (2017). p. 936–44. doi:10.1109/CVPR.2017.106

23. Vaswani A, Shazeer N, Parmar N, Uszkoreit J, Jones L, Gomez AN, et al.Attention is all you need. In: *Advances in neural information processing systems*. Curran Associates, Inc. (2022).

24. Rezatofighi H, Tsoi N, Gwak J, Sadeghian A, Reid I, Savarese S. Generalized intersection over union: A metric and A loss for bounding box regression (2019). Available at: http://arxiv.org/abs/1902.09630 (Accessed June 4, 2022).

25. Geiger A, Lenz P, Urtasun R. Are we ready for autonomous driving? The KITTI vision benchmark suite. In: 2012 IEEE Conference on Computer Vision and Pattern Recognition (2012). p. 3354–61. doi:10.1109/CVPR.2012.6248074

26. Zhang S, Benenson R, Schiele B. CityPersons: A diverse dataset for pedestrian detection. In: 2017 IEEE Conference on Computer Vision and Pattern Recognition (CVPR (2017). p. 4457–65. doi:10.1109/CVPR.2017.474

27. Dollar P, Wojek C, Schiele B, Perona P. Pedestrian detection: A benchmark. In: 2009 IEEE Conference on Computer Vision and Pattern Recognition (2009). p. 304–11. doi:10.1109/CVPR.2009.5206631

28. Cordts M, Omran M, Ramos S, Rehfeld T, Enzweiler M, Benenson R, et al.The Cityscapes dataset for semantic urban scene understanding. In: 2016 IEEE Conference on Computer Vision and Pattern Recognition (CVPR); Las Vegas, NV, USA (2016). p. 3213–23. doi:10.1109/CVPR.2016.350

29. Shao S, Zhao Z, Li B, Xiao T, Yu G, Zhang X, Sun J. CrowdHuman: A benchmark for detecting human in a crowd (2018). Available at: http://arxiv.org/abs/1805.00123 (Accessed May 1, 2022).

30. Ouyang W, Wang X. A discriminative deep model for pedestrian detection with occlusion handling. In: 2012 IEEE Conference on Computer Vision and Pattern Recognition (2012). p. 3258–65. doi:10.1109/CVPR.2012.6248062

frontiers | Frontiers in Physics

TYPE Original Research
PUBLISHED 20 October 2022
DOI 10.3389/fphy.2022.1045555

OPEN ACCESS

EDITED BY
Xuzhen Zhu,
Beijing University of Posts and Telecommunications (BUPT), China

REVIEWED BY
Guanghua Zhang,
Hebei University of Science and Technology, China
Baozhen Li,
Nanjing Audit University, China
Anmin Fu,
Nanjing University of Science and Technology, China

*CORRESPONDENCE
Shaoqing Lv,
lvsq3601@xupt.edu.cn

SPECIALTY SECTION
This article was submitted to Social Physics, a section of the journal Frontiers in Physics

RECEIVED 15 September 2022
ACCEPTED 30 September 2022
PUBLISHED 20 October 2022

CITATION
Lv S, Xiang J, Li Y, Ren X and Lu G (2022), MERP: Motifs enhanced network embedding based on edge reweighting preprocessing. *Front. Phys.* 10:1045555. doi: 10.3389/fphy.2022.1045555

MERP: Motifs enhanced network embedding based on edge reweighting preprocessing

Shaoqing Lv[1]*, Ju Xiang[2], Yiyang Li[3], Xincheng Ren[4] and Guangyue Lu[1]

[1]Shaanxi Key Laboratory of Information Communication Network and Security, Xi'an University of Posts and Telecommunications, Xi'an, China, [2]School of Computer Science and Engineering, Central South University, Changsha, China, [3]School of Foreign Studies, Northwestern Polytechnical University, Xi'an, China, [4]Shaanxi Key Laboratory of Intelligent Processing for Big Energy Data, Yan'an University, Yan'an, China

Network embedding has attracted a lot of attention in different fields recently. It represents nodes in a network into a low-dimensional and dense space while preserving the structural properties of the network. Some methods (e.g. motif2Vec, RUM, and MODEL) have been proposed to preserve the higher-order structures, i.e., motifs in embedding space, and they have obtained better results in some downstream network analysis tasks. However, there still exists a significant challenge because original motifs may include redundant noise edges, and embedding entire motifs into embedding space may adversely affect the performance in downstream tasks. To overcome this problem, we propose a motifs enhancement framework for network embedding, based on edge reweighting. Through edge reweighting, the weight of redundant noise edges between motifs is decreased. Therefore, the effect of redundant noise edges will be reduced in the embedding space. We apply the edge reweighting as a preprocessing phase in network embedding, and construct the motifs enhanced network by incorporating enhanced motifs structures with the original network. By doing this, the embedding vectors from the motifs enhanced network can achieve better performance in downstream network analysis tasks. Extensive experiments are performed on two network analysis tasks (community detection and node classification) with synthetic and real-world datasets. The results show that our framework outperforms state-of-the-art network embedding methods.

KEYWORDS

network embedding, motifs, edge reweighting, random work, network mining

1 Introduction

Network embedding, also known as network representation learning, maps the nodes in a network to vectors in a low-dimensional and dense space while preserving various structures and connectivity patterns between nodes [1, 2]. These vectors can be used with existing machine learning algorithms to accomplish downstream network analysis tasks--e.g., node classification [3], link prediction [4], community detection [5],

recommendation [6], and anomaly detection [7]. Due to the excellent performance in different network analysis tasks, network embedding has attracted a lot of attention.

From academia and industry. And various network embedding methods have been proposed from different perspectives [1]. To capture the higher-order structural patterns between nodes, lots of works have been presented to integrate higher-order structures into network embedding [8, 9]. As the most common higher-order structures, network motifs are considered building blocks for a complex network, and have been found in various networks--e.g., the networks of neurology, ecology, and biochemistry [10, 11]. Studying network motifs is effective for understanding structures and functions in real-world complex networks [12]. Therefore, lots of network embedding algorithms have been designed to preserve network motifs, such as motif2Vec [13], RUM [14], and MODEL [15], which achieved excellent performance in different network analysis tasks.

However, all these methods are implemented to embed entire network motifs into the embedding space including some redundant noise edges, which may affect the performance of network embedding. We illustrate this situation with an example in Figure 1. Figure 1A shows an original undirected network with two communities. Figure 1B is the motifs from the network in Figure 1A, and we set the triangle to be the motifs of interest. To retain higher-order relationships, previous works preserved all these four motifs in embedding space. However, among these motifs, $m3$ is constituted by nodes from different communities. Hence, preserving motif $m3$ will make the distances between nodes 3, 4, and five which belong to different communities closer in embedding space and this may adversely affect the performance in downstream tasks. Therefore, incorporating entire network motifs including redundant noise edges into embedding space will impact the performance of network embedding in downstream tasks.

In this paper, we propose MERP, a Motifs enhanced network embedding based on Edge Reweighting Preprocessing to overcome the above-mentioned problem of the existing methods. Specifically, we first construct the motifs weighted network by incorporating the higher-order structures--i.e., motifs, with first-order structures. Then an iteration motifs enhancement algorithm is designed based on a random walk to re-assign the weights of edges in the motifs weighted network. By edge reweighting, we decrease the weight of redundant noise edges in the motifs. Through iteratively processing this procedure, we obtain the motifs enhanced network. Finally, the final embedding vectors are obtained by projecting the motifs enhanced network with existing network embedding methods. Experiments on synthetic and real-world networks demonstrate that our framework achieves better performance than existing network embedding algorithms in community detection and node classification.

To summarize, the main contributions in this paper are as follows:

- We propose a new framework to incorporate enhanced motifs in network embedding to overcome the problem of preserving redundant noise edges in embedding space, which is commonly existing in previous works.
- We apply an iteration edge reweighting algorithm based on a random walk to re-assign the weight of edges in motifs before network embedding and our algorithm is a general technique that can be easily combined with existing network embedding methods.
- We perform experiments with two typical network analysis tasks, community detection, and node classification, on synthetic and real-world networks to evaluate our approach. Experimental results show that our method improves the state-of-the-art baselines by 0.65%–10.79% (NMI) in community detection task, and 0.21%–2.29% (micro-F1) in node classification task.

The rest of the paper is organized as follows. In section 2, we summarize network embedding research specifically related to network embedding methods with the network motifs. Then we propose our framework with enhanced motifs based on edge reweighting preprocessing in section 3. Section 4 outlines the experimental results on two network analysis tasks: community detection and node classification. Finally, section 5 presents our conclusions and discussions with future works.

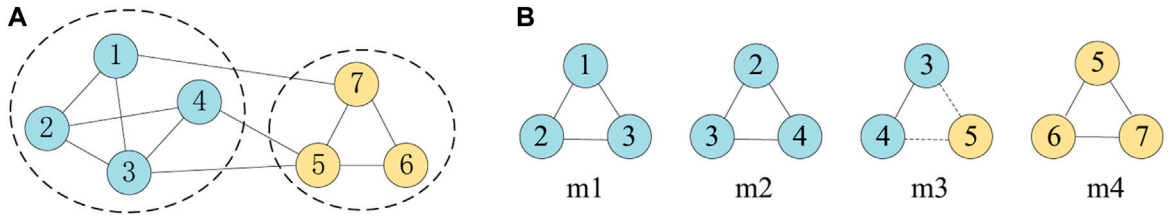

FIGURE 1
An example of network motifs and redundant noise edges. **(A)** Original network. **(B)** The motifs of original network.

2 Related works

Network embedding has attracted a lot of attention in recent years. It learns the low-dimensional representations of nodes in a network and preserves the structure information which aims to close the gap between network analysis and machine learning technologies. In this section, we briefly review the related works. Several comprehensive surveys could refer to [1, 2, 16, 17].

Network motifs have been proven to play an important role in describing the higher-order structural information between nodes in networks. Therefore, preserving the network motifs can improve the performance of network embedding in downstream network analysis tasks. And some works have been proposed to incorporate network motifs in network embedding. Dareddy et al. proposed the motif2Vec [13], which transformed the original heterogeneous network into a motif network by computing the motif adjacency matrices. Through the skip-gram model, the final embedding vectors were obtained and achieved better results in node classification and link prediction tasks. Yu et al. designed a new strategy MotifWalk in RUM to represent the motifs [14], which used each motif as a new node to construct an auxiliary network. The embedding vectors were obtained by executing a random walk on the auxiliary network and had better performance in node classification and network reconstruction. Wang et al. proposed the MODEL algorithm to preserve the network motifs by autoencoder [15]. In MODEL, the first-order similarities were redefined according to common motifs between nodes, and the second-order similarities were determined by the neighbors between the nodes. In the work of HONE [18], Rossi et al. constructed a series matrix to represent network motifs, such as the weighted motif adjacency matrix, the motif transition matrix, the motif Laplacian, and the normalized motif Laplacian. The final embedding vectors were got by solving a minimization problem with different matrices. In MBRep [19], Qian et.al proposed a generalized motif-based higher-order representation learning method. It learned triangle motif embedding in a heterogeneous network using a SkipGram model and had a better performance in link prediction. Ping et.al presented an algorithm LEMON [20] to bridge connectivity and structural similarity in a uniform network representation *via* motifs.

Although these methods preserve network motifs in different ways and have good performance in different network analysis tasks, all of them incorporate entire network motifs in embedding space. As we have mentioned earlier, there are some redundant noise edges in network motifs making the performance of these methods still have space to improve. In our work MERP, we conduct an iteration algorithm to decrease the weight of redundant noise edges in motifs before incorporating the network motifs in the embedding space. In this way, our method achieves better results in different tasks than the existing methods.

With the development of deep learning in various domains, network embedding based on the deep neural network has drawn increasing research attention and tremendous related works have been proposed [1, 16]. Such as InfoMotif [21], GSN [22], and MBHAN [23], these works incorporated subgraphs or attributed structural roles in GNN and achieved notable performance gains compared with state-of-art GNNs. There are also some network embedding methods designed for specific networks, such as signed networks [24–26], bipartite networks [27–29], dynamic networks [30, 31], and heterogeneous networks [32–34]. In this paper, we mainly focus on the most essential case where only the static, homogeneous network is available.

3 Motifs enhanced network embedding based on edge reweighting preprocessing

The framework of MERP is shown in Figure 2, which includes three steps. The first step is the extraction and representation of network motifs. In this step, network motifs containing redundant noise edges are extracted and represented as the motifs weighted network. The second step is network motifs enhancement, which constructs the motifs enhanced network by reweighting redundant noise edges in motifs through multiple iterations of the random walk-based method. The third step is network embedding, which projects the motifs enhanced network by existing network embedding methods and preserves the enhanced motifs structures into the embedding space.

3.1 Motifs weighted network construction

Given an undirected and unweighted network G= (V, E), we can construct the adjacency matrix A from node list V and edge list E, where A is a symmetric matrix and represents the first-order structures of the network G. To get the higher-order structure information of motifs, we can use some existing motifs detection algorithms such as FANMOD [35]. With these tools, the motifs set $M = \{m_1, m_2, m_3 \ldots m_l\}$ is extracted from the network G, where each m_i is a motif. By the motifs set M, we construct the motifs adjacency matrix W^M, where the value of each element $w^M_{i,j}$ in W^M is the number of times that node i and node j appear together in the motifs set M.

For example, in Figure 1A, node *two* and node three appear in motif $m1$ and motif $m2$, so the value of $w^M_{2,3}$ is 2. The motifs adjacency matrix W^M contains all the motifs structures in the network G. However, W^M may have different dimensions with A because some nodes may not be contained in any motif. Furthermore, W^M does not preserve the first-order relationships between nodes. Therefore, we construct the motifs weighted matrix W' that combines the adjacency

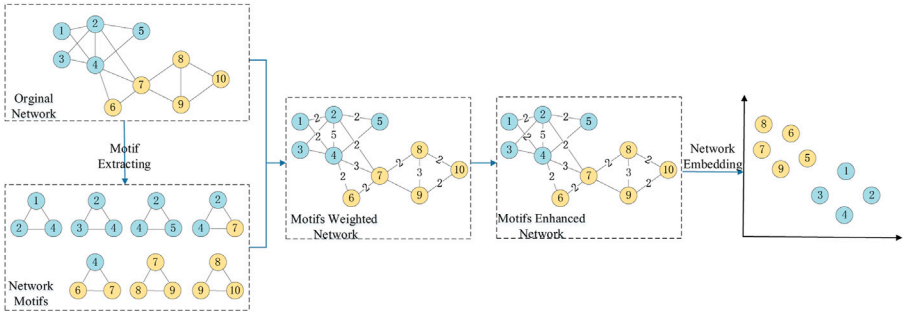

FIGURE 2
The framework of MERP.

matrix A and the motif adjacency matrix W^M to keep the same nodes set as in the original network and to preserve the first-order structures between nodes.

$$W' = A + W^M \tag{1}$$

The motifs weighted matrix W' not only retains the motifs structures, but also the first-order information between nodes. Some previous motifs-aware network embedding approaches are based on the motifs weighted network and can achieve better results than traditional network embedding methods in some network analysis tasks. However, the motifs weighted matrix W' contains the entire motifs including some redundant noise edges. These inter-community motifs cut will be retained in the network embedding vectors, which deteriorates the performance in downstream tasks. Therefore, it needs to filter the noises and reduce the weight of redundant noise edges in motifs. To achieve this goal, we re-assign the weights in the motifs weighted matrix by motifs enhancement.

3.2 Motifs enhancement

As we have described earlier, some motifs are conducted by nodes from different communities, and the edge between these nodes are the redundant noise edges for these edges would make the communities more obscure in the embedding space.

To reduce the influence of redundant noise edges in the motifs weighted matrix, we propose a motifs enhancement method to reduce the weight of these edges.

We use the dynamic behavior of nodes to determine whether two nodes in the motifs belong to the same community. It has proved that a random walker will be stuck for a longer time in the same community than between communities. Thus, random walkers starting from nodes in the same community will behave in a similar way when they randomly walk across the networks. Generally, nodes belonging to the same community have similar dynamic behaviors, while the dynamic behaviors of nodes belonging to different communities have lower similarities. Therefore, the weight between the nodes can be reweighted by the dynamic behavior similarity of the two nodes. If the dynamic behavior similarity between two nodes is low, it means that the two nodes have a high probability of belonging to different communities. The weight of the edges between them can be reduced. Many methods can be used to describe the dynamic behaviors of nodes [36–40]. In this paper, we use the k-step random walk for calculation simplicity [39].

Specifically, the k -step random walk in the network can be calculated by the k -order adjacency matrix. Therefore, for the motifs weighted matrix W', we first calculate its diagonal matrix D with the elements shown as follows:

$$d_{ij} = \begin{cases} \sum_p W'_{i,p} & i = j \\ 0 & i \neq j \end{cases} \tag{2}$$

Then the transition probability matrix P of motifs weighted network is defined as:

$$P = D^{-1}W' \tag{3}$$

Each element p_{ij} in P is the transition probability from node v_i to v_j within one step in motifs weighted network.

Then we can calculate the k-step transition probability matrix as following:

$$P^k = P \cdots P \tag{4}$$

Each element P^k_{ij} in P^k records the probability that node v_i reaches v_j through k steps random walk. Each row of P^k--i.e., $P^k_{i\cdot}$, can be regarded as a vector in n-dimensional space and can be used to represent the dynamic behavior of node v_i. To capture all behaviors from order one to order k, we use the transition probability of the first $1\sim k$ order vectors as the behavior of the node. Therefore, the behavior representation of all nodes can be represented by the sum of the first k-order transition probabilities:

$$R^k = \sum_{i=1}^{k} P^i \tag{5}$$

To measure the similarity of the dynamic behavior between nodes, we can choose a variety of similarity calculation methods, such as Euclidean distance, correlation coefficient, and cosine similarity. Here we use cosine similarity to calculate the behavior similarity between nodes for the cosine similarity can well capture the difference between two vectors in high-dimensional space. Therefore, the dynamic behavior similarity calculation based on cosine similarity is as follows:

$$Sim(v_i, v_j) = \frac{R_i^k \cdot R_j^k}{\| R_i^k \| \| R_j^k \|} \tag{6}$$

If the behavior vector of node v_i and node v_j have high similarity, the corresponding similarity calculation $Sim(v_i, v_j)$ is close to 1, otherwise, if the behavior vectors of node v_i and node v_j have large differences, the corresponding similarity calculation $Sim(v_i, v_j)$ is close to 0. Therefore, the similarity Sim can be used to measure whether the edge between two nodes is a redundant noise edge.

For each edge (v_i, v_j) existing in the motif weighted network, we set its weight to the value of the similarity $Sim(v_i, v_j)$. In this way, we get a new motifs-weighted network. Then in this new motifs-weighted network, the above weights calculation process is repeated. Through I iterations of calculation, the motifs structures in the motifs weighted network are continuously enhanced. For convenience, we call the final network as the motifs enhanced network and the weights in the motifs enhanced network are marked as $\tilde{W}$, which incorporates the enhanced motifs information between nodes. The outline of motifs enhancement by edge reweighting preprocessing is demonstrated in Algorithm 1.

Whereas, it is time-consuming to calculate R^k in real applications, especially for large-scale networks. To speed up the calculation, we take advantage of the characteristics of network G. Since network G is a general network, the adjacency matrix A is a symmetric matrix. Then both the motifs adjacency matrix W and the motifs weighted matrix W' are symmetric matrices.

Although the transition probability matrix P is an asymmetric matrix, P has a symmetric structure. Since

$$D^{1/2} P D^{-1/2} = D^{-1/2} W' D^{-1/2} \tag{7}$$

The symmetric matrix $D^{-(1/2)}W'D^{-(1/2)}$ has eigen-decomposition $Q\Lambda Q^T$ and Q is orthogonal matrix, $\Lambda = diag(\lambda_1, \ldots \lambda_n)$.

And we have the equations:

$$D^{1/2} P D^{-1/2} = D^{-1/2} W' D^{-1/2} = Q\Lambda Q^T \tag{8}$$

$$D^{1/2} P^k D^{-1/2} = \left(D^{\frac{1}{2}} P D^{-1/2}\right)^k = \left(Q\Lambda Q^T\right)^k = Q\Lambda^k Q^T \tag{9}$$

So, Equation 4 can be rewritten as:

$$P^k = D^{-1/2}\left(Q\Lambda^k Q^T\right) D^{-1/2} \tag{10}$$

And Equation 5 can be calculated as:

$$R^k = \sum_{i=1}^{k} P^i = \sum_{i=1}^{k} D^{-1/2}\left(Q\Lambda^i Q^T\right) D^{-1/2} = D^{-1/2} Q \left(\sum_{i=1}^{k} \Lambda^i\right) Q^T D^{-1/2} \tag{11}$$

3.3 Complexity analysis

The time complexity of our algorithm is primarily dominated by the cost of calculating the eigen-decomposition of the transition probability matrix P. For a large-scale network, we could use some algorithms to calculate the first h eigenpairs to approximate the eigen-decomposition of matrix P, such as the Lanczos algorithm [40]. Hence the time complexity for eigen-decomposition is $O(t \times n^2)$ in the worst case, where t is the average number of nonzero elements in rows of the matrix. And in most instances, transition probability matrix P is sparsity and $t \ll n$. Furthermore, given a network G, the eigen-decomposition step can be calculated offline. The time complexity to calculate cosine similarity between each pair of nodes is $O(n^2)$. The total time complexity of MERP is $O((t + L) \times n^2 \times I)$, where L is the edges number of network and I is the iteration number. And the iteration number I is small, mostly less than 10.

Input: Network $G = (V, E)$, adjacency matrix A of the network G, motifs set M of the network G, step for random walk k, iteration I
Output: weighted matrix $\tilde{W}$ with motifs enhanced information

Construct the motifs adjacency matrix W^M from M
$W' = A + W^M$
for $m = 0$ to I **do**
  Calculate the degree matrix D by Equation 2
  Calculate the transition probability matrix P by $P = D^{-1}W'$
  for $n = 1$ to k **do**
    $R^n += P^n$
  end for
  for each edge (i, j) in E **do**
    Calculate the similarity $Sim(v_i, v_j)$ of node v_i and v_j by Equation 6
    $w'_{ij} = Sim(v_i, v_j)$
  end for
end for
Calculate the final motifs enhanced matrix $\tilde{W} = W'$
Return $\tilde{W}$

Algorithm 1. Motifs enhanced by edge reweighting

4 Experiments

To evaluate the performance of our method, we perform two different experiments on network analysis tasks: community detection and node classification.

4.1 Community detection

Community detection is to divide nodes into different clusters according to the connection between nodes, which is one of the most important network analysis tasks [41]. There are dense connections between nodes in the same community, while the connections between nodes in different

Communities are relatively sparse. To test the effectiveness of our method, we conducted community detection experiments on both synthetic and real-world datasets. Similar to the community detection experiments involved in NE-MRF [42], we first use different network embedding to map the nodes into low-dimensional space. Then these node vectors are clustered into different clusters using the k-means algorithm. To avoid the sensitivity of k-means clustering to the initial centroid, we perform each experiment 5 times and calculated its average value as the final result. With the ground truth community information of these data, we use normalized mutual information (NMI) as the results evaluation metric. The higher the NMI, the closer the result obtained by the method is to the ground truth.

4.1.1 Synthetic datasets

To evaluate the effectiveness of our algorithm, we use the LFR framework to obtain six synthetic networks with known community information [43]. In the LFR framework, both the degree distribution of nodes and the size of communities satisfy the power-law distribution, which is consistent with most real-world networks. We set the main parameters in the LFR framework to construct synthetic networks in our experiments as follows: 1) the number of nodes is 1,000, 2) the average node degree is 20, 3) the maximum node degree is 50, 4) the minimum number of nodes in the community is 50, 5) the maximum number of nodes in the community is 80. The main difference between these six synthetic networks is λ, which is used to control the ratio of a node's edges connecting to other nodes in different communities. And the values of λ are [0.2, 0.5, 0.6, 0.65, 0.7, 0.8]. The higher the value, the more the node is connected with the nodes in different communities, and the more difficult the community detection task is.

We compare the framework proposed in this article with three well-known network representation learning algorithms (deepWalk [3], node2vec [44], and GraRep [45]). The methods combined our.

Framework with deepWalk, node2vec, and GraRep are called: MERP-D, MERP-N, and MERP-G respectively. We use the default parameters in these algorithms as the setting parameters in our experiments. All embedding dimensions in our experiments are set to 128.

The results of the community detection for synthetic datasets are shown in Figure 3. Compared with traditional methods, our proposed framework has achieved the best results in all six synthetic datasets. On the whole, when λ <0.6, both our proposed method and traditional methods can obtain good performance in community detection for the community structures are obvious in LFR networks. When λ > 0.7, the community structures are not prominent enough in synthetic networks and the motifs contain more redundant noise edges, making the task of community detection more difficult. However, our method can still achieve marginally better performance than the original algorithms. When $0.6 \leq \lambda \leq 0.7$, our method can achieve better results than traditional algorithms. Specifically, MERP-N can achieve 44.15% higher NMI than the original node2vec method when $\lambda = 0.65$. And MERP-D can get 4% NMI higher than the original deepWalk algorithm. Meanwhile, MERP-G is 2% higher than the GraRep method, although GraRep is also a method based on a k-step transition probability matrix.

4.1.2 Real-world datasets

In this section, we evaluate the performance of our proposed method on eight real-world datasets with ground truth in the community detection task. The attributes of these eight real-world datasets are shown in Table 1. In this experiment, we compare our framework with deepWalk, node2Vec, GraRep, and MRF-based methods [42]. The MRF-based method incorporates the Markov random field with network embedding and can achieve better performance than other traditional algorithms (e.g. SNMF [46], MNDP [47]) in community detection tasks. And we use the results described in the original paper of the MRF-based method because getting better results by this method requires adjusting a lot of parameters. The community detection results of all methods are shown in Table 2. We see that our methods MERP-D, MERP-N, and MERP-G acquire better results compared with the original methods. We also find that our approach performs better on five out of six networks compared with the MRF-based method. From the experiment results in table 2, we can conclude that our method has comparable performance on the community detection task compared with other higher-order structures preserving network embedding methods.

4.1.3 Parameter analysis

To evaluate the effect of k and I parameters in our framework on community detection tasks, we perform

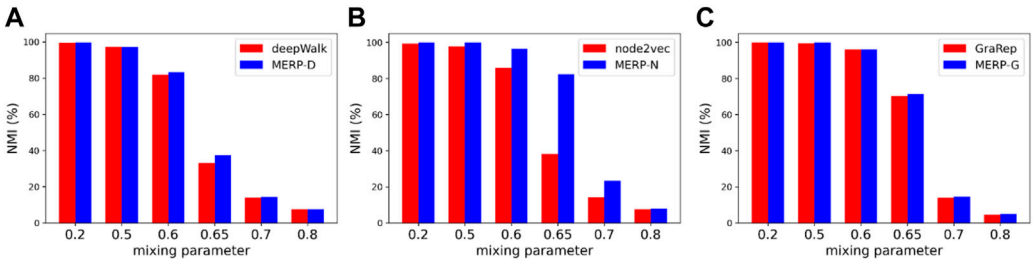

FIGURE 3
Comparison of our method with three embedding methods, **(A)** deepWalk, **(B)** node2vec, and **(C)** GraRep, on LFR benchmark networks with different mixing parameters.

TABLE 1 Statistics of real-world datasets.

Datasets	|V|	|E|	#Communities
Friend6	69	220	6
Friend7	69	220	7
Polbook	105	441	3
Football	115	613	12
Polblogs	1,222	16,717	2
Core	2,707	5,429	7
Email	1,005	25,571	42
DBLP	13,184	48,018	5

experiments on real-world datasets. In these experiments, the value of random walk step k was changed from 3 to 6, because previous works have shown that community structures in a random walk would more clearly when the step size is less than 6. For different networks having similar performance, we just exhibit the results of our method MERP-N on Friend6 and Cora networks. We show the community detection results NMI (%) with respect to k and I in Figure 4.

As shown in Figure 4, community detection results have a little change and the performance is relatively stable. Furthermore, we also find that with different parameters MERP-N on both networks still shows competitive performance compared with other methods. As shown in Figure 4B, the worst result is 44.04%, but this result is still better than other results obtained by most of the traditional methods.

4.2 Node classification

To evaluate our framework in different network analysis tasks, we perform experiments on multi-label node classification. We use three widely used networks for node classification in this section. The details of these networks are shown in Table 3.

BlogCatalog [48] is an online social network of bloggers, where nodes are bloggers and edges are the friendship network among the bloggers. Node labels represent topics of interest to the bloggers.

Protein-Protein Interactions (PPI) [49] is a subgraph of the PPI network for *Homo* Sapiens. Nodes represent human proteins and edges represent physical interaction between proteins. Node

TABLE 2 Performance comparison of different methods on real-world networks (the MRF-based method did not give results on Email and DBLP networks; we mark these with 'N/A').

Datasets	deepWalk	node2vec	GraRep	MRF	MERP-D	MERP-N	MERP-G
Friend6	91.55	87.31	83.82	95.21	**95.67**	95.21	84.35
Friend7	90.27	91.05	84.63	94.55	**94.61**	93.24	87.91
Polbook	56.36	56.31	52.96	58.61	**59.29**	58.15	55.9
Football	91.93	92.03	92.47	**93.91**	92.69	92.69	92.71
Email	69.18	70.13	68.04	*N/A*	**70.35**	71.03	68.49
Polblogs	73.79	**75.53**	71.17	74.27	74.44	72.74	71.17
Cora	38.7	44.91	38.17	45.68	42.24	**45.91**	41.69
DBLP	72.17	70.06	60.38	*N/A*	**74.44**	72.74	71.17

The bold values are the highest performance in each dataset.

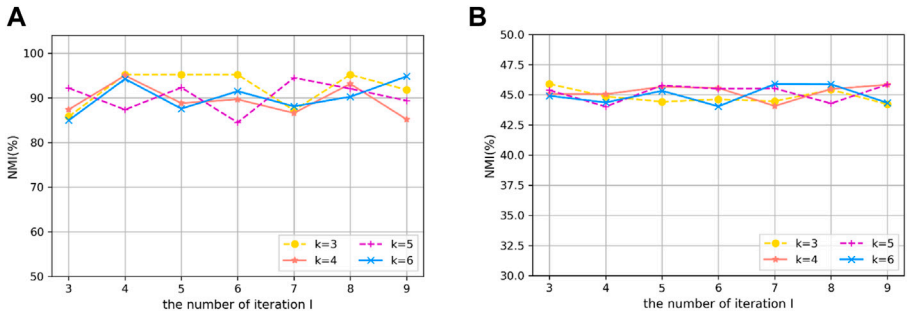

FIGURE 4
Effect of parameters *k* and *l* on community detection task on **(A)** Friend6 and **(B)** Cora.

TABLE 3 Statistics of benchmark datasets.

Dataset	|V|	|E|	#Labels
BlogCatalog	10,312	333,983	39
PPI	3,890	76,584	50
Wikipedia	4,777	184,812	40

labels stand for biological states obtained from the hallmark gene sets.

Wikipedia[1] is a words co-occurrence network from the first million bytes of the Wikipedia dump. Nodes are Wikipedia pages and edges are hyperlinks between pages. Labels represent the part-of-speech (POS) tags of pages which are inferred using the Stanford POS-Tagger [50].

And our experimental settings in this section were the same as the NetMF [51]. Firstly, we randomly sampled a ratio of nodes as the training set and the others as the test set. The ratio was changed from 0.1 to 0.9 with the step size being 0.1. Then, we used the one-vs-rest logistic regression model LIBLINEAR[2] as the classification algorithm. The experiment procedure was repeated 10 times to reduce the effect of different training set and test set. The performance is evaluated in terms of average micro-F1. We also compare our framework with deepWalk, node2vec, and GraRep. Our framework with deepWalk, node2vec, and GraRep are also called MERP-D, MERP-N, and

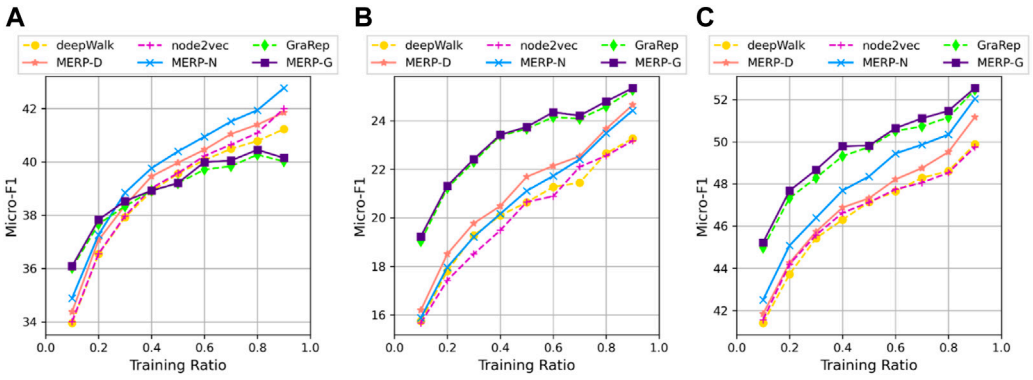

FIGURE 5
Performance evaluation with varying the ratio of training data on three real-world networks with different methods. **(A)** BlogCatalog network, **(B)** PPI network, and **(C)** Wikipedia network.

1 http://mattmahoney.net/dc/text.html.

2 https://www.csie.ntu.edu.tw/\~cjlin/liblinear/.

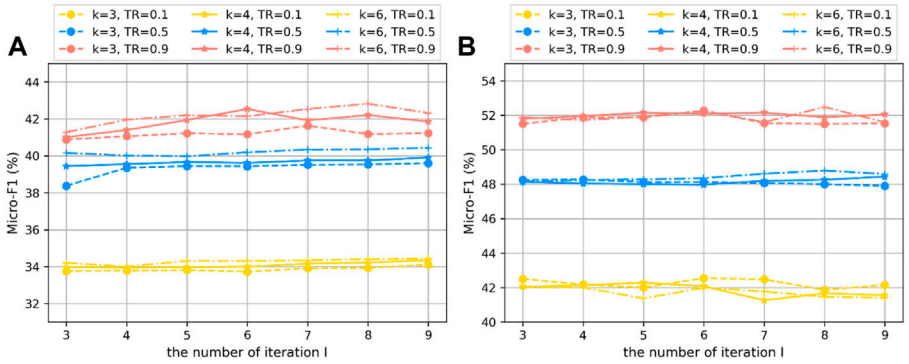

FIGURE 6
Effect of parameters *k* and *I* on node classification task on real-world dataset **(A)** BlogCatalog and **(B)** Wikipedia.

MERP-G, respectively. Finally, Figure 5 shows the results on the three networks in terms of micro-F1.

From the results and the curves in Figure 5, we find that our methods (MERP-D, MERP-N, and MERP-G) can achieve a better (or at least similar) micro-F1 than the original methods (deepWalk, node2vec, and GraRep) on all three real-world datasets.

Furthermore, we can make some interesting observations from Figure 5. We find that GraRep has a better performance than random walk-based methods (node2vec and deepWalk) no matter the ratio of the training set on Wikipedia and PPI networks. And our method MERP-G is still better than the original GraRep on all three networks in all training ratios. In all three networks, the original methods deepWalk and node2vec have similar results. However, in our model, MERP-N has the best results on BlogCatalog and Wikipedia networks while MERP-D has the best performance on the PPI network. To summarize, our proposed method incorporating enhanced motifs in network embedding can achieve significant improvements compared with the original network embedding methods on the node classification task.

4.2.1 Parameter analysis

To analyze the effect of parameters *k* and *I* on node classification, we also conducted experiments with MERP-N on the BlogCatalog and Wikipedia datasets. The training ratios varied in the range [0.1, 0.5, 0.9]. The steps *k* changed in the range [3, 4, 6], and the number of iterations *I* varied from three to 7.

The node classification results are shown in Figure 6 in terms of micro-F1. From Figure 6, we can see our framework exhibit stable performance with different parameters.

Specifically, with the same training ratio, the micro-F1 results range within 2\% on all three datasets. This demonstrates that the performance of our method on node classification is insensitive to the setting of the parameters.

5 Conclusion and discussions

In this paper, we proposed a novel motifs enhancement network embedding framework (MERP) based on edge reweighting preprocessing. MERP framework is used to incorporate the enhanced motifs information with local structure information in the original network. By an iteration motifs enhanced algorithm, the weights of motifs between nodes in different communities are decreased. In this way, we reduce the effect of redundant noise edges in motifs. And we applied edge reweighting as a preprocessing stage making nodes' embedding vectors useful to all kinds of downstream network analysis tasks. Moreover, MERP can be effortlessly applied with the most available network embedding algorithms. Compared with other higher-order structures preserved network embedding methods such as M-NMF [8] and Cosine [9], our method embeds motifs in the network embedding space which is proven to contain rich information and can reveal semantic information of vertices. The experimental results for downstream network analysis tasks: community detection and node classification, as well as the parameters analysis, illustrate that MERP achieves remarkable improvements compared with the existing network embedding methods.

In this study, we mainly focused on normal networks and neglected other different types of networks, such as signed networks, bipartite networks, and heterogeneous networks. And all these networks have been proven to exist motifs. Furthermore, we only analyzed the static networks and not considered dynamic networks which are common in the real world. For future work, we plan to investigate the effects of motifs-enhanced based network embedding on these networks with different types of nodes and edges.

Our method can effectively improve the structure of original networks to enhance the ability of network embedding algorithms. Due to the improvement of network structure, some problems of other network analysis algorithms may also be solved or improved, such as the resolution limit in community detection [52, 53]. Some studies have shown that network enhancement can mitigate the

resolution limit and improve traditional community detection algorithms [35, 54]. So, our method can also enhance the ability of traditional algorithms in community detection.

Data availability statement

The raw data supporting the conclusion of this article will be made available by the authors, without undue reservation.

Author contributions

SL and JX conceived and planned the experiments. SL and YL carried out the experiments. XR and GL contributed to the interpretation of the results. SL took the lead in writing the manuscript. All authors provided critical feedback and helped shape the research, analysis and manuscript.

Funding

This work was supported in part by the National Natural Science Foundation of China under Grant 60832019 and 61702054, in part by the National Science Foundation of Shaanxi Province under Grant 2020GY-081 and 2022JQ-675, in part by the Shaanxi Key Laboratory of Intelligent Processing for Big Energy Data Open Fund Project under Grant IPBED10, and in part by the Scientific Research Program Funded by Shaanxi Provincial Education Department under Grant 21JK0918.

Conflict of interest

The authors declare that the research was conducted in the absence of any commercial or financial relationships that could be construed as a potential conflict of interest.

Publisher's note

All claims expressed in this article are solely those of the authors and do not necessarily represent those of their affiliated organizations, or those of the publisher, the editors and the reviewers. Any product that may be evaluated in this article, or claim that may be made by its manufacturer, is not guaranteed or endorsed by the publisher.

References

1. Li B, Pi D. Network representation learning: A systematic literature review. *Neural Comput Appl* (2020) 32:16647–79. doi:10.1007/s00521-020-04908-5

2. Cui P, Wang X, Pei J, Zhu W. A survey on network embedding. *IEEE Trans Knowl Data Eng* (2018) 31(5):833–52. doi:10.1109/tkde.2018.2849727

3. Bryan P, Al-Rfou R, Skiena S. Deepwalk: Online learning of social representations. In: Proceedings of the 20th ACM SIGKDD international conference on Knowledge discovery and data mining; August, 2014; New York, USA. (2014). p. 701–10.

4. Wang Z, Chen C, Li W. Predictive network representation learning for link prediction. In: Proceedings of the 40th international ACM SIGIR conference on research and development in information retrieval; August, 2017; Tokyo, Japan. (2017). p. 969–72.

5. Lv S, Xiang J, Feng J, Wang H, Lu G, Li M. Community enhancement network embedding based on edge reweighting preprocessing. *J Stat Mech* (2020) 2020(10): 103403. doi:10.1088/1742-5468/abb45a

6. Zhang F, Yuan NJ, Lian D, Xie X, Ma W-Y. Collaborative knowledge base embedding for recommender systems. In: Proceedings of the 22nd ACM SIGKDD international conference on knowledge discovery and data mining; August, 2016; San Francisco, CA, USA. (2016). p. 353–62.

7. Ding K, Li J, Bhanushali R, Liu H. Deep anomaly detection on attributed networks. In: Proceedings of the 2019 SIAM International Conference on Data Mining; May, 2019; algary, Alberta, Canada (2019). p. 594–602.

8. Wang X, Cui P, Wang J, Pei J, Zhu W, Yang S. Community preserving network embedding. In: Proceedings of the Thirty-First AAAI Conference on Artificial Intelligence; February, 2017; Hilton San Francisco. (2019).

9. Zhang Y, Lyu T, Zhang Y. Cosine: Community-preserving social network embedding from information diffusion cascades. In: Proceedings of the Thirty-Second AAAI Conference on Artificial Intelligence; Feburuary, 2018; Orleans, Louisiana, USA (2018).

10. Milo R, Shen-Orr S, Itzkovitz S, Kashtan N, Chklovskii D, Alon U. Network motifs: Simple building blocks of complex networks. *Science* (2002) 298(5594): 824–7. doi:10.1126/science.298.5594.824

11. AustinBenson R, David Gleich F, Leskovec J. Higher-order organization of complex networks. *Science* (2016) 353(6295):163–6. doi:10.1126/science.aad9029

12. Jiang J, Hu Y, Li X, Bin C, Fangcheng F, Zhitao W, Wen O. Analyzing online transaction networks with network motifs. In: Proceedings of the 28th ACM SIGKDD Conference on Knowledge Discovery and Data Mining; August, 2022; Washington, DC (2022). p. 3098–106.

13. Reddy Dareddy M, Das M, Yang H. motif2vec: Motif aware node representation learning for heterogeneous networks. In: proceedings of the 2019 IEEE International Conference on Big Data (Big Data); December, 2019; Los Angeles, CA.(2019). p. 1052–9.

14. Yu Y, Lu Z, Liu J, Zhao G, Wen J-rong. Rum: Network representation learning using motifs. In: Proceedings of the 2019 IEEE 35th International Conference on Data Engineering (ICDE); April, 2019; Macau, SAR, China. IEEE (2019). p. 1382–93.

15. Wang L, Ren J, Xu B, Li J, Luo W, Xia F. Model: Motif-based deep feature learning for link prediction. *IEEE Trans Comput Soc Syst* (2020) 7(2):503–16. doi:10.1109/tcss.2019.2962819

16. Hou M, Ren J, Zhang D, Kong X, Zhang D, Xia F. Network embedding: Taxonomies, frameworks and applications. *Comput Sci Rev* (2020) 38:100296. doi:10.1016/j.cosrev.2020.100296

17. Xue G, Zhong M, Li J, Chen J, Zhai C, Kong R. Dynamic network embedding survey. *Neurocomputing* (2022) 472:212–23. doi:10.1016/j.neucom.2021.03.138

18. Rossi RA, Ahmed NK, Koh E. Higher-order network representation learning. In: Proceedings of the Companion Proceedings of the The Web Conference 2018; April, 2018; Lyon, France. (2018). p. 3–4.

19. Hu Q, Fan L, Wang B. MBRep: Motif-based representation learning in heterogeneous networks. *Expert Syst Appl* (2022) 190:116031. doi:10.1016/j.eswa.2021.116031

20. Shao P, Yang Y, Xu S, Wang C. Network embedding via motifs. *ACM Trans Knowl Discov Data* (2021) 16(3):1–20. doi:10.1145/3473911

21. Bouritsas G, Frasca F, Zafeiriou S, Bronstein M. Improving graph neural network expressivity via subgraph isomorphism counting. *IEEE Trans Pattern Anal Mach Intell* (2022) 1. doi:10.1109/tpami.2022.3154319

22. Sankar A, Wang J, Krishnan A, Sundaram H. Self-supervised role learning for graph neural networks. *Knowl Inf Syst* (2022) 64(8):2091–20121. doi:10.1007/s10115-022-01694-5

23. Hu Q, Lin W, Tang M, Jiang J. Mbhan: Motif-based heterogeneous graph attention network. *Appl Sci* (2022) 12(12):5931. doi:10.3390/app12125931

24. Yu L, Yuan T, Zhang J, Chang Y. Learning signed network embedding via graph attention. In: Proceedings of the Thirty-Fourth AAAI Conference on Artificial Intelligence; April, 2020; Louis, USA (2020). p. 4772–9.

25. Lee Y-C, Seo N, Han K, Kim S-W Asine: Adversarial signed network embedding. In: Proceedings of the 43rd International ACM SIGIR Conference on Research and Development in Information Retrieval; July, 2020. Xi'an, China,(2020) 609–18.

26. Amin J, Tyler D, Esmailian P, Tang J, KevinChang C-C. Rose: Role-based signed network embedding. In: Proceedings of The Web Conference 2020; April, 2020; Taipei Taiwan (2020). p. 2782–8.

27. Gao M, Chen L, He X, Zhou A. Bine: Bipartite network embedding. In: Proceedings of the The 41st International ACM SIGIR Conference on Research & Development in Information Retrieval (2018). p. 715–24.

28. Huang W, Li Y, Yuan F, Fan J, Yang H. Biane: Bipartite attributed network embedding. In: Proceedings of the 43rd international ACM SIGIR conference on research and development in information retrieval; July, 2020; Xi'an, China (2020). p. 149–58.

29. Cao J, Lin X, Guo S, Liu L, Liu T, Wang B. Bipartite graph embedding via mutual information maximization. In: Proceedings of the 14th ACM International Conference on Web Search and Data Mining; March, 2021; Israel (2021). p. 635–43.

30. Hou C, Zhang H, Shan H, Tang K. Glodyne: Global topology preserving dynamic network embedding. In: Proceeding of the IEEE 38th International Conference on Data Engineering; May, 2020; Kuala Lumpur, Malaysia (2020).

31. Ma L, Zhang Y, Li J, Lin Q, Bao Q, Wang S, et al.Community-aware dynamic network embedding by using deep autoencoder. *Inf Sci* (2020) 519:22–42. doi:10.1016/j.ins.2020.01.027

32. Wang X, Lu Y, Shi C, Wang R, Cui P, Mou S. Dynamic heterogeneous information network embedding with meta-path based proximity. *IEEE Trans Knowl Data Eng* (2020) 34:1117–32. doi:10.1109/tkde.2020.2993870

33. Li X, Shang Y, Cao Y, Li Y, Tan J, Liu Y. Type-aware anchor link prediction across heterogeneous networks based on graph attention network. In: Proceedings of the Thirty-Fourth AAAI Conference on Artificial Intelligence; February, 2020; New York, USA (2020). p. 147–55.

34. Wang R, Shi C, Zhao T, Wang X, Ye YF. Heterogeneous information network embedding with adversarial disentangler. *IEEE Trans Knowl Data Eng* (2021) 1. doi:10.1109/tkde.2021.3096231

35. Wernicke S, Rasche F. Fanmod: A tool for fast network motif detection. *Bioinformatics* (2006) 22(9):1152–3. doi:10.1093/bioinformatics/btl038

36. Xiang J, Zhang J, Zheng R, Li X, Li M. Nidm: Network impulsive dynamics on multiplex biological network for disease-gene prediction. *Brief Bioinform* (2021) 22:bbab080. doi:10.1093/bib/bbab080

37. Zhang Z-K, Liu C, Zhan X-X, Lu X, Zhang C-X, Zhang Y-C. Dynamics of information diffusion and its applications on complex networks. *Phys Rep* (2016) 651:1–34. doi:10.1016/j.physrep.2016.07.002

38. Masuda N, Porter MA, Lambiotte R. Random walks and diffusion on networks. *Phys Rep* (2017) 716:1–58. doi:10.1016/j.physrep.2017.07.007

39. Lai D, Lu H, Nardini C. Enhanced modularity-based community detection by random walk network preprocessing. *Phys Rev E* (2010) 81(6):066118. doi:10.1103/physreve.81.066118

40. Parlett BN, Scott DS. The lanczos algorithm with selective orthogonalization. *Math Comput* (1979) 33(145):217–38. doi:10.1090/s0025-5718-1979-0514820-3

41. Wang J, Zhong J, Chen G, Li M, Wu F-xiang, Pan Y. Clusterviz: A cytoscape app for cluster analysis of biological network. *Ieee/acm Trans Comput Biol Bioinform* (2014) 12(4):815–22. doi:10.1109/tcbb.2014.2361348

42. Jin D, You X, Li W, He D, Cui P, Fogelman-Souli´e F¸coise, Chakraborty T. Incorporating network embedding into markov random field for better community detection. In: Proceedings of the AAAI Conference on Artificial Intelligence; Feburary, 2019; Hawaii, USA (2019). p. 160–7. doi:10.1609/aaai.v33i01.3301160

43. Lancichinetti A, Fortunato S, Radicchi F. Benchmark graphs for testing community detection algorithms. *Phys Rev E* (2008) 78(4):046110. doi:10.1103/physreve.78.046110

44. Grover A, Leskovec J. node2vec: Scalable feature learning for networks. In: Proceedings of the 22nd ACM SIGKDD international conference on Knowledge discovery and data mining; August, 2016; San Francisco California USA (2016). p. 855–64.

45. Cao S, Lu W, Xu Q. Grarep: Learning graph representations with global structural information. In: Proceedings of the 24th ACM international on conference on information and knowledge management; October, 2015; Melbourne. (2015). p. 891–900.

46. Wang F, Li T, Wang X, Zhu S, Ding C. Community discovery using nonnegative matrix factorization. *Data Min Knowl Discov* (2011) 22(3):493–521. doi:10.1007/s10618-010-0181-y

47. Jin D, Chen Z, He D, Zhang W. Modeling with node degree preservation can accurately find communities. In: Proceedings of the Twenty-Ninth AAAI Conference on Artificial Intelligence; January, 2015; Austin, Texas. (2015).

48. Tang L, Liu H. Relational learning via latent social dimensions. In: Proceedings of the 15th ACM SIGKDD international conference on Knowledge discovery and data mining; July, 2009; Paris France. (2009). p. 817–26.

49. Stark C, Bobby-Joe B, Chatr-Aryamontri A, Boucher L, Oughtred R, Livstone MS, et al.The biogrid interaction database: 2011 update. *Nucleic Acids Res* (2010) 39(1):D698–D704. doi:10.1093/nar/gkq1116

50. Toutanova K, Klein D, Manning CD, Singer Y. Feature-rich part of-speech tagging with a cyclic dependency network. In: Proceedings of the 2003 conference of the North American chapter of the association for computational linguistics on human language technology; May, 2003; Stroudsburg, PA, U.S.A (2003). p. 173–80.

51. Qiu J, Dong Y, Ma H, Li J, Wang K, Tang J. Network embedding as matrix factorization: Unifying deepwalk, line, pte, and node2vec. In: Proceedings of the Eleventh ACM International Conference on Web Search and Data Mining; Feburary, 2018; Los Angeles, California (2018). p. 459–67.

52. Xiang J, Wang Z-Z, Li H-J, Zhang Y, Li F, Dong L-P, et al.Community detection based on significance optimization in complex networks. *J Stat Mech* (2017) 2017(5):053213. doi:10.1088/1742-5468/aa6b2c

53. Xiang J, Tang Y-N, Gao Y-Y, Liu L, Yi H, Li J-M, et al.Phase transition of surprise optimization in community detection. *Physica A: Stat Mech its Appl* (2018) 491:693–707. doi:10.1016/j.physa.2017.09.090

54. Xiang J, Hu K, Zhang Y, Bao M-H, Tang L, Tang Y-N, et al.Enhancing community detection by using local structural information. *J Stat Mech* (2016) 2016(3):033405. doi:10.1088/1742-5468/2016/03/033405

frontiers | Frontiers in Physics

TYPE Original Research
PUBLISHED 24 October 2022
DOI 10.3389/fphy.2022.1016535

OPEN ACCESS

EDITED BY
Shirui Pan,
Monash University, Australia

REVIEWED BY
Guanghui Song,
Xidian University, China
Yujie Yang,
Henan Normal University, China
Xiangchun Liu,
Minzu University of China, China

*CORRESPONDENCE
Jinming Ma,
jmma@bupt.edu.cn

SPECIALTY SECTION
This article was submitted to Social Physics,
a section of the journal
Frontiers in Physics

RECEIVED 11 August 2022
ACCEPTED 04 October 2022
PUBLISHED 24 October 2022

CITATION
Hao J, Li Z, Wu Z and Ma J (2022), Role of degree and weighted coreness based on endpoints in link prediction.
Front. Phys. 10:1016535.
doi: 10.3389/fphy.2022.1016535

Role of degree and weighted coreness based on endpoints in link prediction

Jiaqi Hao[1], Zheng Li[2], Zhanhe Wu[3] and Jinming Ma[1]*

[1]School of Artificial Intelligence, Beijing University of Posts and Telecommunications, Beijing, China, [2]Network Department of China Mobile Wenzhou Branch, Wenzhou, China, [3]Holley Technology Ltd., Hangzhou, Zhejiang, China

Many researchers propose link prediction models based on node similarity. Among all models, researchers found that the endpoint influence plays an important role in evaluating the similarity between endpoints. For endpoint influence, we consider that an endpoint possessing a large and extensive maximum connected subgraph can strongly attract other nodes. After thorough research, we found that the coreness can describe the aggregation degree of neighbors and the endpoint degree may be used to describe the largest connected subgraph of an endpoint. In order to create a model, we repeat our experiments on eight real benchmark datasets after combining endpoint degree and weighted coreness. The experimental results illustrate the positive role of synthetical endpoint degree and weighted coreness for measuring endpoint influence in link prediction.

KEYWORDS

complex network, link prediction, endpoint degree, weighted coreness, synthetical influence of endpoints

1 Introduction

With the application of and dependence on networks, human life gradually becomes virtualization. Through networks, people can carry out social activities, shopping transactions, information retrieval, and so on. Link prediction has emerged as a key technical tool for investigating the properties of complicated networks. Link prediction technology can precisely recommend goods in e-commerce networks [1–3], recommend friends in social networks [4–6], plan routes in transportation networks [7], find the relations between proteins in biological networks [8, 9], mine base station information in power networks, [10] and so on. In addition, link prediction can also reveal the structure growth or formation mechanism of complex networks [11, 12].

For the research studies in link prediction, more researchers consider the topological similarity of networks to build the models. For example, models based on common neighbors, such as CN (common neighbor) [13], AA (Adamic–Adar) [14], and RA (resource allocation) [15], become the first link prediction approaches. These models mainly consider the local structure of the networks, such as the number, node degree or node influence of common neighbors, the influence of target nodes, and the paths between nodes. They show simplicity and effectiveness, but still need to be further classified. The

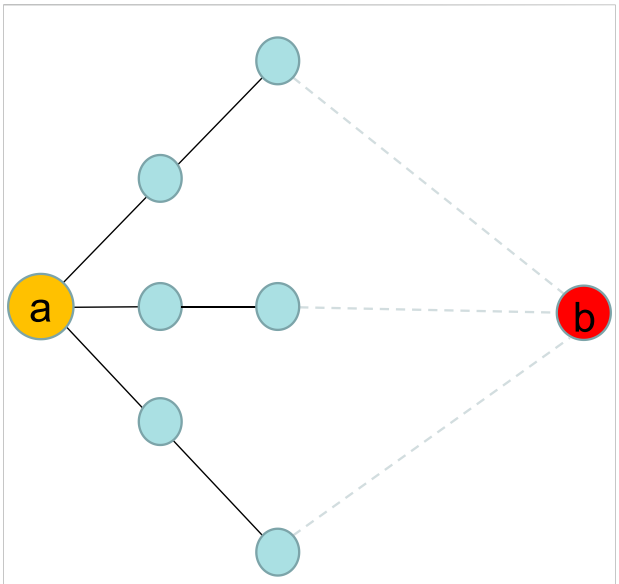

FIGURE 1
(Color online). Diagram of endpoint influence based on degree and coreness. Endpoint **(A)** represents a source node, which has degree = 3 and coreness = 3. Endpoint **(B)** represents a target node. All solid and dashed lines indicate existing links and potential links, respectively.

link prediction models based on global information consider the global structure of the networks, involving the impact of different length paths on the node similarity, such as Katz [16], ATC (average commute time) [17], and so on. These models improve the prediction accuracy, but they cannot be applied to large networks due to the high computational complexity. The models based on quasi-local information eliminate the long paths and redundant information, while considering the local information of the networks, reducing the computational complexity and improving the prediction accuracy. These models consider short paths between nodes and initial degree distribution of endpoints, such as LP (local path) [15], LRW (local random walk) [18], and SRW (superposed random walk) [18],, which have been the focus of many researchers.

As of now, link prediction models that take endpoint influence into account mostly concentrate on the role of endpoint degree in gauging endpoint similarities, such as Sørensen [19], LHN [20], LRW [18], and SRW [18]. Since the endpoint degree simply takes into account the number of its neighbors, endpoint influence is not adequately taken into account. This means that while it can characterize the endpoint influence's breadth, it cannot describe the degree to which neighbors are aggregated. Through consulting literatures, Zhu et al. [21] discussed the role of degree, H-index, or coreness through improving SRW in link prediction. Further research reveals that an endpoint with a high endpoint degree and coreness can have a larger maximal connected subgraph, which attracts more nearby nodes.

Figure 1 shows the roles of endpoint degree and coreness in link prediction. The degree and coreness of endpoint a are 3 and 3, respectively. The influence of endpoint a is described as 3 when we only consider the endpoint degree, leading to a weak attraction of endpoint a. However, the influence of endpoint a should be described as 9 when we exploit the product of degree and coreness, illustrating that endpoint a has a large influence and easily attracts the target endpoint b. As a result, by computing the synthetic degree and coreness of endpoints in link prediction, we may uncover more potential relationships between nodes.

The real world reveals the roles of synthetical degree and coreness on individuals. For example, a celebrity with large and concentrated fans has more influence in one place. The number of fans can be described as the endpoint degree, and the concentration degree of fans represents the coreness of endpoints in the networks. The phenomenon appears on the internet celebrity in online social networks, popular goods in shopping networks, and classic articles in citation networks. Through abundant research studies, we find the endpoint degree plays a fundamental role in each individual. Meanwhile, the coreness describes the different influence intensities on different individuals. Therefore, we consider weighted coreness to apply in different typological networks.

The rest of this article is organized as follows: In section 2, we propose a link prediction model based on the weighted synthetical influence of endpoint degree and coreness (WSIDC). In section 3 and section 4, we show the eight benchmark experiment datasets and methods, including eight mainstream baselines and a metric. The findings of the experiment are covered in Section 5. Section 6 provides the conclusion.

2 Description and structure of models

The superposed random walk model (SRW) mainly considers the endpoint degree as the endpoint influence to evaluate the similarity between endpoints. In order to replace endpoint degree with synthetical endpoint degree and weighted coreness to characterize the endpoint influence, we designed a new link prediction model on SRW using the explanation given in section 1. This section will introduce the concept of SRW and building WSIDC. In the undirected simple network G (V, E), where V and E stand for sets of nodes and links, respectively, all models in this study are proven. We removed multiple linkages and self-connections on all network datasets. We constructed a similarity score (s_{xy}) and rank the scores in descending order for each pair of unlinked nodes, x, $y \subset V$, to assess how similar they are to one another. The links with the highest L ratings show that

there is a higher likelihood that two disconnected nodes will eventually form a link.

2.1 Superposed random walk model (SRW)

The probability of a node's influence resource randomly moving from node x to node y in a single step is indicated by the Markov chain equation $p_{xy} = a_{xy}/k_x$, where k_x denotes the node's degree. Thus, $a_{xy} = 1$ if node x has connected y and $a_{xy} = 0$ if not. The order of nodes between x and y with a t-step can be expressed as $\{x = x_0 = y_t, x_1 = y_{t-1}, \ldots, x_{t-1} = y_1, x_t = y_0 = y\}$. Accordingly, the t-step transition probability from x to y can be denoted by $\pi_{xy}(t) = \prod_{i=0}^{t-1} p_{x_i x_{i+1}}$ and $\pi_{yx}(t) = \prod_{i=0}^{t-1} p_{y_i y_{i+1}}$. Thus, considering the endpoint degree as the influence of endpoints, the similarity between nodes x and y, with path of length l from 2 to t into consideration, is modeled as

$$s_{xy}^{SRW}(t) = \sum_{l=2}^{t}\left[\frac{k_x}{2|E|} \times \pi_{xy}(l) + \frac{k_y}{2|E|} \times \pi_{yx}(l)\right], \quad (1)$$

where k_x and k_y represent the degree of node x and y, respectively. $|E|$ represents the number of links in the networks. $\frac{k_x}{2|E|}$ and $\frac{k_y}{2|E|}$ describe the influence resource of node x and y, respectively.

2.2 Weighted hybrid influence of degree and coreness

Through investigations and analysis, we discover that the hybrid endpoint degree and coreness are sufficient to effectively explain the endpoint effects, and the endpoint degree plays a fundamental role in the hybrid influence of endpoints. Therefore, we first introduce a simple (unweighted) hybrid influence of degree and coreness based on the endpoint model (DCHI) [22] as follows,

$$s_{xy}^{DCHI} = \sum_{l=2}^{t}\left[\frac{\sqrt{k_x \times c_x}}{2|E|} \times \pi_{xy}(l) + \frac{\sqrt{k_y \times c_y}}{2|E|} \times \pi_{yx}(l)\right], \quad (2)$$

where $\frac{\sqrt{k_x \times c_x}}{2|E|}$ and $\frac{\sqrt{k_y \times c_y}}{2|E|}$ describe the simple hybrid influence resource of node x and y, respectively.

We developed a link prediction model by enhancing the weighted hybrid impact of degree and coreness (WDCHI) model, where coreness is exponentially suppressed by the inhibitory factor β. The new model can, therefore, be identified as

$$s_{xy}^{WDCHI} = \sum_{l=2}^{t}\left[\frac{\sqrt{k_x \times c_x^{\beta}}}{2|E|} \times \pi_{xy}(l) + \frac{\sqrt{k_y \times c_y^{\beta}}}{2|E|} \times \pi_{yx}(l)\right], \quad (3)$$

where $\frac{\sqrt{k_x \times c_x^{\beta}}}{2|E|}$ and $\frac{\sqrt{k_y \times c_y^{\beta}}}{2|E|}$ describe the synthetic influence resources of nodes x and y, respectively. Also, $\beta \in [0, 1]$, depressing the role of coreness on the synthetical influence of endpoints.

TABLE 1 Twelve benchmark networks' fundamental topological characteristics.

Nets	$\|V\|$	$\|E\|$	$\langle k\rangle$	$\langle d\rangle$	C	r	H
USAir	332	2,128	12.81	2.74	0.749	-0.208	3.36
Power	4,941	6,594	2.669	15.87	0.107	0.003	1.45
Metabolic	453	2025	8.940	2.664	0.647	-0.226	4.485
NS	1,461	2,742	3.75	5.82	0.878	0.461	1.85
Email	1,133	5,451	9.62	3.61	0.254	0.078	1.94
Ucsocial	1893	13,825	14.62	3.06	0.138	-0.188	3.81
Infec	410	2,765	13.49	3.63	0.467	0.226	1.39
CE	453	2025	8.94	2.66	0.655	-0.225	4.49

The properties are as follows: $|V|$ denoting the number of nodes, $|E|$ denoting the number of links, $\langle k\rangle$ denoting the average degree, $\langle d\rangle$ denoting the average distance, C denoting the clustering coefficient, r denoting the assortativity coefficient, and H denoting the degree heterogeneity and defined as $H = \frac{\langle k^2\rangle}{\langle k\rangle^2}$

3 Network datasets

To show the prediction performances of the model proposed, we produce experiments on eight network datasets [23], which are introduced as follows: 1) US Air97 (USAir) [24] represents the US airline network. 2) The electrical power transmission system for western US is represented by Power Grid (Power) [25]. 3) The C. *elegans* worm's neural network is represented by metabolic [26]. 4) Network Science (NS) [27] is an example of collaboration among researchers who publish articles on the topic of networks. 5) The email communication network for University Rovira I Virgili (URV) in Tarragona, Spain, is represented by Email [28]. 6) The social media website UC Irvine addresses social network issues (UCsocial) [29] and is created by University of California, Irvine students. 7) The face-to-face interaction network of visitors at the 2009 exhibition "Infectious:Stay Away" at the Science Gallery in Dublin is represented by Infectious (Infec) [30]. 8) Another network of neurons in the C. *elegans* worm is represented by C. *elegans* (CE) [26]. Due to the various fundamental topological properties, the metabolic and CE neural networks are two distinct neuronal networks. The main topological characteristics of the aforementioned networks are shown in Table 1.

Each original dataset is randomly split into a training set E^T, which contains 90% of the connections, and a testing set E^P, which contains 10% of the links, for the experiments. Unsurprisingly, $E^T \cup E^P = E$ and $E^T \cap E^P = \varnothing$. We divide each dataset into 30 separate, independent divisions; check each division for connectedness in E^T; and then average the prediction performances.

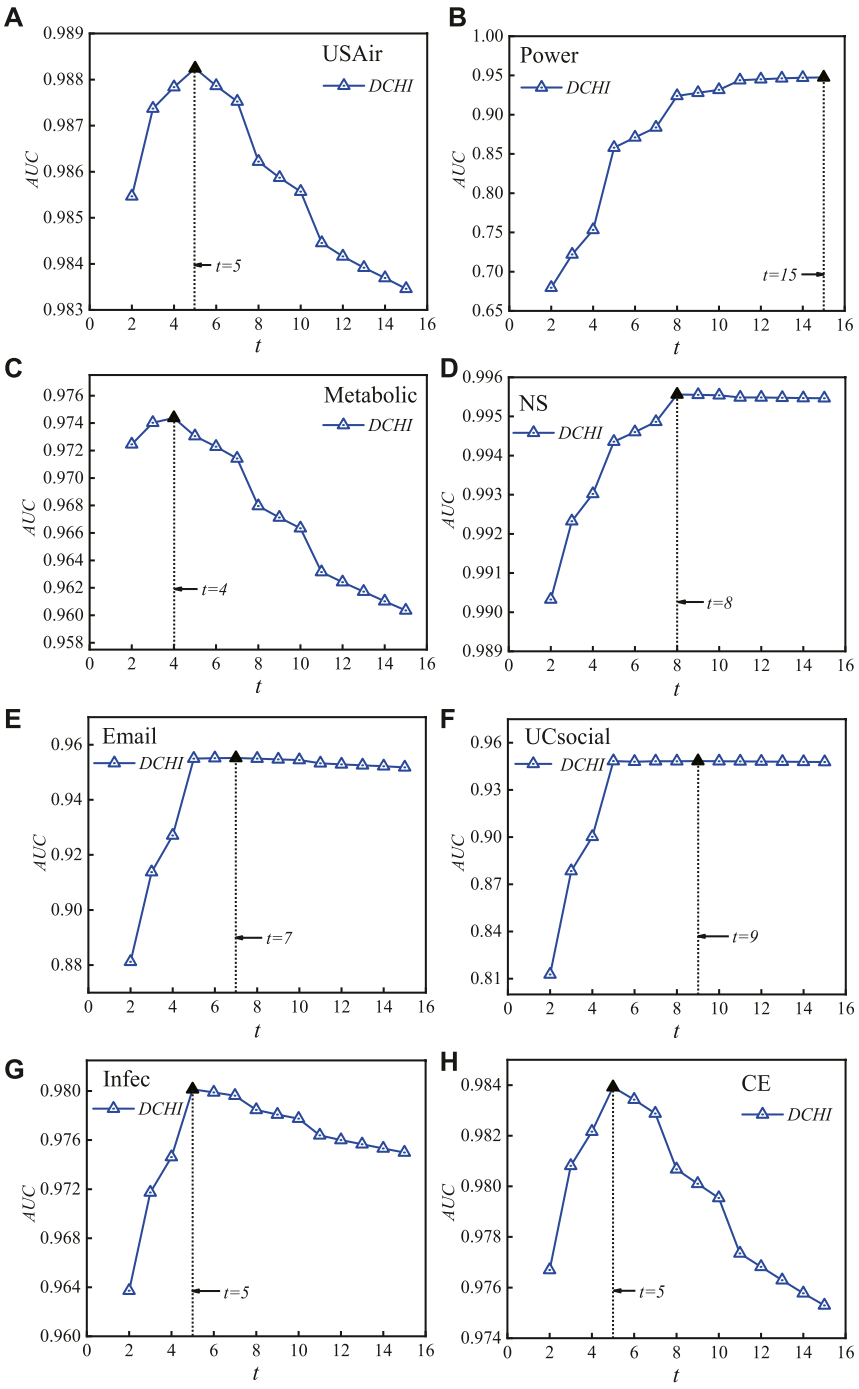

FIGURE 2
(Color Online) Pattern illustration of accuracy metric AUC on the number of random-walk steps t on eight datasets. With the fewest steps, DCHI achieves the most ideal AUC values, which is 5 in **(A)** USAir, 15 in **(B)** power, 4 in **(C)** Metabolic, 8 in **(D)** NS, 7 in **(E)** email, 9 in **(F)** UCsocial, 5 in **(G)** Infec, and 5 in **(H)** CE.

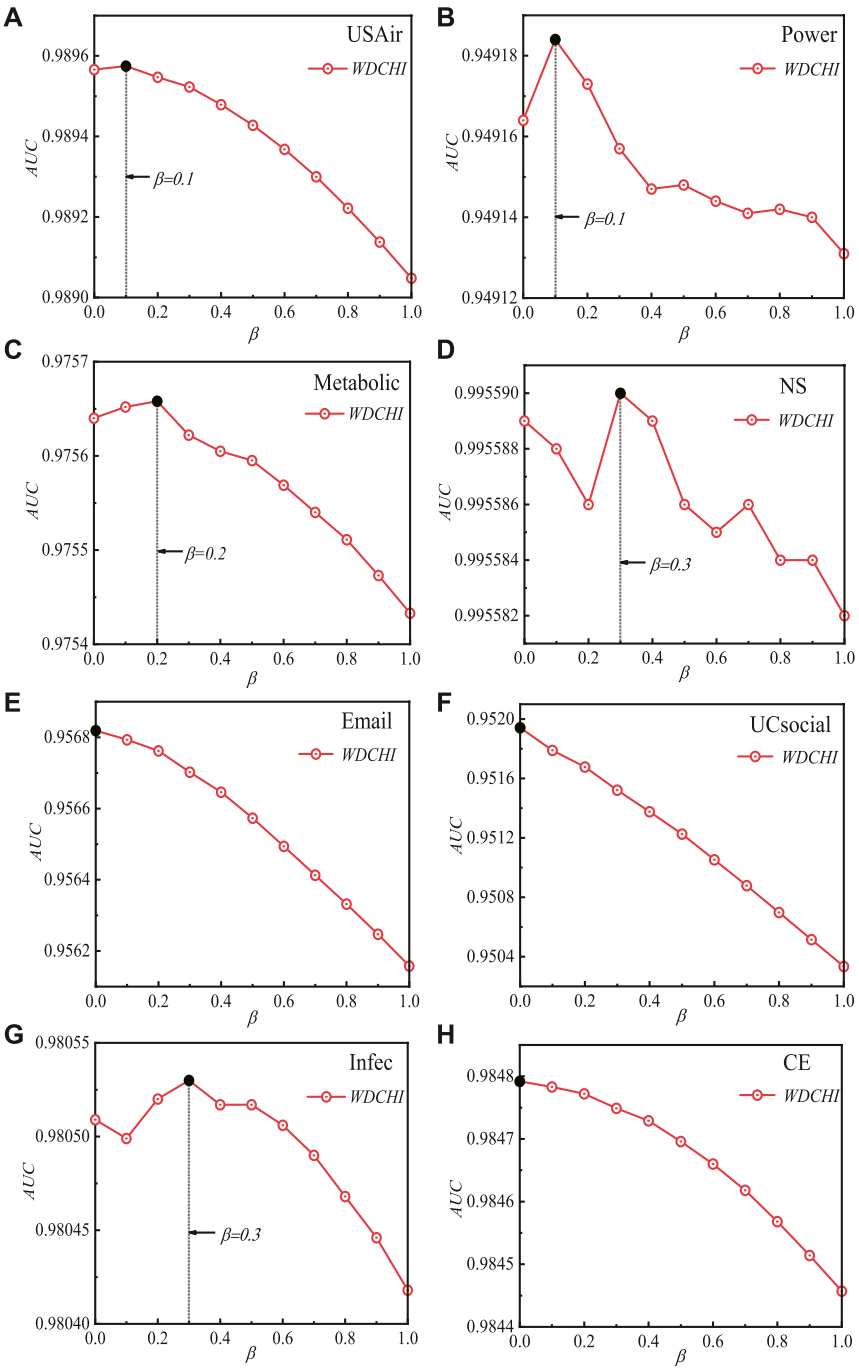

FIGURE 3
(Color Online) AUC's sensitivity to the levels of the inhibitory factor β with L = 100. In this study, the training and testing sets are divided 30 times in a completely random manner. The average of the 30 runs is the outcome.

TABLE 2 AUC on the twelve benchmark networks with L = 100 as the line rate. Each data point represents the average of more than 30 independent realization methods, with each point being a random 90%–10% division of the training set and testing set.

AUC	DCHI	WDCHI
USAir	0.989,048 (5)	**0.989,575(5, 0.1)**
Power	0.949,131 (15)	**0.949,184(15, 0.1)**
Metabolic	0.975,433 (4)	**0.975,658(4, 0.2)**
NS	0.995,582 (8)	**0.99559(8, 0.3)**
Email	0.956,158 (7)	**0.956,819(7, 0)**
UCsocial	0.950,344 (9)	**0.951,942(9, 0)**
Infec	0.980,418 (5)	**0.98053(5, 0.3)**
CE	0.984,457 (5)	**0.984,792(5, 0)**

The values on DCHI enclosed in parentheses represent the equivalent ideal number of steps t. The numbers in parentheses on the WDCHI represent the appropriate ideal step size t and ideal inhibitory factor β. By modifying the coefficients, all of the current findings demonstrate the best-case scenarios. The bold values represnet optimal parameter.

4 Experimental methods

4.1 Metric

AUC [30], a metric of accuracy, can be interpreted as the probability that a potential link (a link in E^P) ranks a higher score than a nonexistent link (a link in $U \setminus E$, where U denotes the universal link set). In the particular implementation, the overall score increases by n' and $0.5n''$ if the prospective connection performs better among n independent comparisons n' times and equally to the non-existent link n'' times. The average score across n-time comparisons is, therefore, expressed as

$$AUC = \frac{n' + 0.5 \times n''}{n}. \tag{4}$$

A model's performance is assessed globally by *AUC*. The value should be equal to 0.5 if each score comes from an independent, identical distribution. The degree to which the accuracy exceeds 0.5 thus indicates how much better a model outperforms random chance.

4.2 Baselines

Comparatively, we introduce the following eight fundamental models as follows:

1. Common neighbors (CN) [13] determines the quantity of common neighbors, which is used to represent how related two endpoints are

$$s_{xy}^{CN} = \left|\Gamma(x) \cap \Gamma(y)\right|, \tag{5}$$

where the collection of neighbors of endpoint x is represented by the expression $\Gamma(x)$, $x \in \{x, y\}$. The number of neighbors that endpoints x and y has in common is denoted by the symbol $|\Gamma(x) \cap \Gamma(y)|$.

2. The inverse logarithm, which is used by Adamic/Adar (AA) [14], which is based on CN, significantly reduces the contributions of shared neighbors

$$s_{xy}^{AA} = \sum_{z \in \Gamma(x) \cap \Gamma(y)} \frac{1}{\log(k_z)}, \tag{6}$$

where k_z represents the degree of node z.

3. Similar to AA, by using the reciprocal of the degrees of common neighbors, resource allocation (RA) [15] lowers the high degree of common neighbors, defined as

$$s_{xy}^{RA} = \sum_{z \in \Gamma(x) \cap \Gamma(y)} \frac{1}{k_z}. \tag{7}$$

4. The two-step paths are favored when comparing the similarity of two-step and three-step approaches between endpoints using local path (LP) [15], where the two-step paths are defined as

$$s^{LP} = A^2 + \varepsilon \times A^3, \tag{8}$$

where the adjacency matrix is represented by A, and the punishment parameter is ε.

5. In Section 2, the superposed random walk (SRW) [18] is shown.
6. The degree of influence in SRW is replaced by the coreness in CSRW [21], which also quantifies the impact of the endpoint,

$$s_{xy}^{CSRW}(t) = \sum_{l=2}^{t} \left[\frac{c_x}{2|E|} \times \pi_{xy}(l) + \frac{c_y}{2|E|} \times \pi_{yx}(l) \right]. \tag{9}$$

where c_x and c_y represent the coreness of node x and y, respectively.

7. HSRW [21] replaces the degree influence in SRW with the H-index and measures the influence of the endpoint,

$$s_{xy}^{HSRW}(t) = \sum_{l=2}^{t} \left[\frac{h_x}{2|E|} \times \pi_{xy}(l) + \frac{h_y}{2|E|} \times \pi_{yx}(l) \right]. \tag{10}$$

where h_x and h_y represent the H-index of node x and y, respectively.

8. The degree influence in SRW is replaced by the simple hybrid influence (SHI) [18], which uses degree and H-index as the synthetical influences. The model is denoted by

TABLE 3 AUC on the twelve benchmark networks with $L = 100$ as the line rate. Every data point is a random 90%–10% divide of the training set and testing set, with each point being an average of over 30 independent realization procedures.

AUC	CN	AA	RA	LP	SRW	CSRW	HSRW	SHI	WDCHI
USAir	0.977,771	0.984,243	0.986,611	0.966,917	0.988,464 (4)	0.987,171 (6)	0.987,346 (5)	0.987,975 (5)	**0.989,575(5, 0.1)**
Power	0.679,613	0.679,723	0.67968	0.763,982	0.888,964 (15)	0.888,625 (15)	0.888,724 (15)	0.888,844 (15)	**0.949,184(15, 0.1)**
Metabolic	0.94913	0.971,743	0.973,661	0.921,503	0.9742 (3)	0.974,185 (5)	0.974,053 (4)	0.974,244 (4)	**0.975,658(4, 0.2)**
NS	0.990,227	0.990,345	0.990,355	0.993,998	0.994,864 (15)	0.994,783 (15)	0.994,802 (15)	0.994,836 (15)	**0.99559(8, 0.3)**
Email	0.881,955	0.883,162	0.882,471	0.942,283	0.947,927 (15)	0.946,909 (15)	0.947,445 (15)	0.947,803 (15)	**0.956,819(7, 0)**
UCsocial	0.813,094	0.817,405	0.81764	0.948,516	0.939,542 (15)	0.936,628 (15)	0.937,387 (15)	0.938,368 (15)	**0.951,942(9, 0)**
Infec	0.962,318	0.964,223	0.964,209	0.970,787	0.977,274 (8)	0.976,935 (10)	0.977,107 (9)	0.977,311 (9)	**0.98053(5, 0.3)**
CE	0.951,545	0.977,089	0.97905	0.932,316	0.982,963 (5)	0.982,176 (7)	0.982,329 (6)	0.982,663 (5)	**0.984,792(5, 0)**

The values in parentheses on WDCHI denote the corresponding ideal number of steps t, whereas the numbers in parentheses on WDCHI denote the corresponding ideal inhibitory factor β. By (if any) changing the coefficients, all of the results in this study represent the best-case scenarios. The bold values represnet optimal parameter.

$$s_{xy}^{SHI}(t) = \sum_{l=2}^{t}\left[\frac{\sqrt{k_x \times h_x}}{2|E|} \times \pi_{xy}(l) + \frac{\sqrt{k_y \times h_y}}{2|E|} \times \pi_{yx}(l)\right], \quad (11)$$

where $\frac{\sqrt{k_x \times h_x}}{2|E|}$ and $\frac{\sqrt{k_y \times h_y}}{2|E|}$ indicate the combined influence of nodes x and y based on their respective synthetic degrees and H-indices.

5 Results and discussions

In this part, we demonstrate how well WDCHI predicts outcomes when compared to baselines such as CN, AA, RA, LP, SRW, CSRW, and HSRW. These are the outcomes.

We believe that the synthetical endpoint degree and coreness play a significant role in characterizing the influence of endpoints and improve the link prediction performances, as explained in section 1 and section 2. For verification, we propose a new link prediction model WDCHI by synthesizing the endpoint degree and weighted coreness, with inhibitory factor β to adjust the optimal contributions of coreness in the different networks. Because WDCHI considers the hybrid influence of endpoints on the random walk steps t, we should first obtain the optimal random walks t of DCHI when $\beta = 1$ (removing the impact of inhibitory factor β). Figure 2 shows the accuracy metric AUC for the total number of random-walk steps t across eight datasets. DCHI generates the best AUC values in the fewest steps for (a) USAir, (b) power, (c) metabolic, (d) NS, (e) Email, (f) UCsocial, (g) Infec, and (h) CE. Then, using an interval of 0.1, we traverse the inhibitory factor *beta* from 0 to 1 in the various datasets after setting the inhibitory factor on coreness. We discover that in the majority of datasets, the weighted synthetical influence of endpoints with coreness suppressed exhibits greater prediction accuracy. In Figure 3, we display the AUC's reliance on the value of β.

Figure 3 displays the optimal AUC values for WDCHI for various inhibitory factors of $\beta \in [0, 1)$ on the ideal number of random-walk steps of t in various datasets, i.e., $\beta = 0.1$ in (a) USAir, $\beta = 0.1$ in (b) Power, $\beta = 0.2$ in (c) Metabolic, $\beta = 0.3$ in (d) NS, $\beta = 0$ in (e) Email, $\beta = 0$ in (f) UCsocial, $\beta = 0.3$ in (g) Infec, and $\beta = 0$ in (h) CE. However, WDCHI shows the optimal AUC values at $\beta = 0$ in email, UcSocial, and CE networks, illustrating the negative roles of coreness in these networks.

We first display the AUC values of WDCHI and DCHI in Table 2 to demonstrate the significance of the weighted coreness, where DCHI stands for the unweighted synthetic influence of endpoints. Table 2 contains the mean outcomes of our 30 separate divisions, each represented by a value. For WDCHI, the values in parenthesis reflect the optimal inhibitory factor *beta* and the optimal number of random-walk steps t, respectively. The values in parentheses for DCHI represent the optimal number of random-walk steps t. In WDCHI and DCHI, the ideal numbers of random walk steps are equivalent. The fact that WDCHI can achieve higher AUC than DCHI shows that the weighted coreness contributes to link prediction.

The eight link prediction models CN, AA, RA, LP, SRW, CSRW, HSRW, and SHI are then put up against WDCHI in comparison. We display the averaged AUC values for all models across 30 simulations in Table 3 to illustrate the experimental findings. While the underlined bold fonts on WDCHI reflect the best AUC values in each dataset, the numbers in parenthesis on WDCHI show the corresponding optimum number of steps (t) and the ideal inhibitory factor (β). The optimal random-walk steps t are indicated by the numbers in parenthesis. In comparison to other models, WDCHI exhibits optimal values on all datasets, as shown in Table 3. The synthetical endpoint degree and weighted coreness, thus, provide a superior contribution to evaluating endpoint influence, as shown by the results of Figure 3.

In addition, more simplified computation is a critical condition for link prediction. The product's time complexity of two $N \times N$ matrices is $O(N^3)$. From the definitions of the baselines, CN, AA, and RA possess the time complexity of $O(N^3)$, and LP, SRW, CSRW, HSRW, and SHI have $M \times O(N^3)$ with coefficient M. Though WDCHI has an identical time complexity as the baselines, WDCHI shows a significant improvement. Most

importantly, the proposed scheme achieves satisfactory performance without increasing the complexity.

6 Conclusion

Traditional link prediction models place more emphasis on the influence of the terminus. More researchers, however, just take degree into account when describing endpoint influence, which is often inappropriate. Through investigations and study, we have discovered that the weighted coreness and synthetical endpoint degree are accurate ways to characterize the influence of the endpoint. Consequently, we suggest a weighted hybrid influence model based on the degree and coreness (WDCHI). On eight real datasets, we compare the prediction results of the WDCHI with those of CN, AA, RA, LP, SRW, CSRW, HSRW, and SHI. As a result, we demonstrate that WDCHI exhibits the same computational complexity and outperforms other models on the metric AUC. The remarkable gain in accuracy demonstrates the weighted coreness and synthetic endpoint degree as endpoint influence can uncover the potential links between two disconnected endpoints and can accurately represent the most linked subgraph. Additionally, our findings can be used to improve social, computer, e-commerce, communication, transportation, and other types of networks.

Data availability statement

The datasets presented in this study can be found in online repositories. The names of the repository/repositories and accession number(s) can be found in the article/Supplementary Material.

Author contributions

JH and ZL: conceptualization, methodology, software, and editing the original draft. ZW: validation. JM: reviewing.

Conflict of interest

ZW was employed by Holley Technology Ltd.

The remaining authors declare that the research was conducted in the absence of any commercial or financial relationships that could be construed as a potential conflict of interest.

Publisher's note

All claims expressed in this article are solely those of the authors and do not necessarily represent those of their affiliated organizations, or those of the publisher, the editors, and the reviewers. Any product that may be evaluated in this article, or claim that may be made by its manufacturer, is not guaranteed or endorsed by the publisher.

Supplementary material

The Supplementary Material for this article can be found online at: https://www.frontiersin.org/articles/10.3389/fphy.2022.1016535/full#supplementary-material

References

1. Linyuan L, Medo M, Yeung CH, Zhang Y-C, Zhou T, Zhang Z-K. Recommender systems. *Phys Rep* (2012) 519(1):1–49. doi:10.1016/j.physrep.2012.02.006,

2. Wang W, Liu Q-H, Liang J, Hu Y, Zhou T. Coevolution spreading in complex networks. *Phys Rep* (2019) 820:1–51. doi:10.1016/j.physrep.2019.07.001

3. Mahdi J, Sajad A, Maliheh I, Parham M, Salehi M. Evaluating collaborative filtering recommender algorithms: A survey. *IEEE Access* (2018) 6:74003–24. doi:10.1109/access.2018.2883742

4. Aiello L, Schifanella R, Cattuto C, Markines B. Friendship prediction and homophily in social media. *ACM Trans Web* (2012) 6(2):1–33. doi:10.1145/2180861.2180866

5. Pan L, Zhou T, Linyuan L, Hu C-K. Predicting missing links and identifying spurious links via likelihood analysis. *Sci Rep* (2016) 6:22955. doi:10.1038/srep22955

6. Linyuan L, Pan L, Zhou T, Zhang YC, Stanley H. Toward link predictability of complex networks. *Proc Natl Acad Sci U S A* (2015) 112(8):2325–30. doi:10.1073/pnas.1424644112

7. Leicht EA, Holme P, Newman M. Vertex similarity in networks. *Phys Rev E* (2006) 73(2):026120. doi:10.1103/physreve.73.026120

8. Angeles Serrano M, Sagues F. Network-based scoring system for genome-scale metabolic reconstructions. *Bmc Syst Biol* (2011) 5:76. doi:10.1186/1752-0509-5-76

9. Chen X, Wang R, Yang D, Xian J, Li Q. Effects of the awareness-driven individual resource allocation on the epidemic dynamics. *Complexity* (2020) 2020:1–12. doi:10.1155/2020/8861493

10. Essa FA, Elaziz MA, Elsheikh Ammar H. Prediction of power consumption and water productivity of seawater greenhouse system using random vector functional link network integrated with artificial ecosystem-based optimization. *Process Saf Environ Prot* (2020) 144:322–9. doi:10.1016/j.psep.2020.07.044

11. Wang W, Zhang Q, Zhou T. Evaluating network models: A likelihood analysis. *Europhysics Lett (Epl)* (2011) 98(2):28004–9. doi:10.1209/0295-5075/98/28004

12. Zhu B, Xia Y. Link prediction in weighted networks: A weighted mutual information model. *PloS one* (2016) 11(2):e0148265. doi:10.1371/journal.pone.0148265

13. Newman MEJ. Clustering and preferential attachment in growing networks. *Phys Rev E* (2001) 64(2):025102. doi:10.1103/physreve.64.025102

14. Adamic LA, Adar E. Friends and neighbors on the web. *Social networks* (2003) 25(3):211–30. doi:10.1016/s0378-8733(03)00009-1

15. Zhou T, Linyuan L, Zhang Y-C. Predicting missing links via local information. *Eur Phys J B* (2009) 71(4):623–30. doi:10.1140/epjb/e2009-00335-8

16. Katz L. A new status index derived from sociometric analysis. *Psychometrika* (1953) 18(1):39–43. doi:10.1007/bf02289026

17. Klein DJ, Randić M. Resistance distance. *J Math Chem* (1993) 12:81–95. doi:10.1007/bf01164627

18. Liu W, Linyuan L. Link prediction based on local random walk. *Europhys Lett* (2010) 89(5):58007. doi:10.1209/0295-5075/89/58007

19. Sørensen TJ. A method of establishing groups of equal amplitude in plant sociology based on similarity of species content and its application to analyses of the vegetation on Danish commons. *Biol Skar* (1948) 5:46.

20. Zhu X, Yang Y, Li L, Cai S. Roles of degree, h-index and coreness in link prediction of complex networks. *Int J Mod Phys B* (2018) 32(16):1850197. doi:10.1142/s0217979218501977

21. Tian Y, Wang Y, Tian H, Cui1 Q. The comprehensive contributions of endpoint degree and coreness in link prediction. *Complexity* (2021) 2021: 1544912–9. doi:10.1155/2021/1544912

22. Batajelj V, Mrvar A. Pajek datasets (2006). Datasets are freely downloaded from the following web sites Available at: http://vlado.fmf.uni.lj.si/pub/networks/data/.

23. Batagelj V, Mrvar A. (1998), *Pajek-program for large network analysis*. Berlin, Germany: Springer.

24. Watts Duncan J, Strogatz Steven H. Collective dynamics of 'small-world'networks. *Nature* (1998) 393:440–2. doi:10.1038/30918

25. Jordi D, Arenas A. Community detection in complex networks using extremal optimization. *Phys Rev E* (2005) 72:027104. doi:10.1103/physreve.72.027104

26. Holme P, Newman M. Nonequilibrium phase transition in the coevolution of networks and opinions. *Phys Rev E* (2006) 74(5):056108. doi:10.1103/physreve.74.056108

27. Guimera R, Danon L, Diaz-Guilera A, Giralt F, Arenas A. Self-similar community structure in a network of human interactions. *Phys Rev E* (2003) 68(6):065103. doi:10.1103/physreve.68.065103

28. Blagus N, Subelj L, Bajec M. Self-similar scaling of density in complex real-world networks. *Physica A: Stat Mech its Appl* (2012) 391(8):2794–802. doi:10.1016/j.physa.2011.12.055

29. Isella L, Stehle J, Barrat A, Cattuto C, Pinton J-F, Van den Broeck W. What's in a crowd? Analysis of face-to-face behavioral networks. *J Theor Biol* (2011) 271(1): 166–80. doi:10.1016/j.jtbi.2010.11.033

30. Kitsak M, Gallos LK, Havlin S, Liljeros F, Muchnik L, Eugene Stanley H, et al.Identification of influential spreaders in complex networks. *Nat Phys* (2010) 6(11):888–93. doi:10.1038/nphys1746

frontiers | Frontiers in Physics

TYPE Original Research
PUBLISHED 24 October 2022
DOI 10.3389/fphy.2022.1019380

OPEN ACCESS

EDITED BY
Wei Wang,
Chongqing Medical University, China

REVIEWED BY
Xiaoyue Zhang,
Capital University of Economics and Business, China
Guocan Wu,
Beijing Normal University, China
Zigang Chen,
Chongqing University of Posts and Telecommunications, China

*CORRESPONDENCE
Lin Zhang,
zhanglin2011@bupt.edu.cn

SPECIALTY SECTION
This article was submitted to Social Physics, a section of the journal Frontiers in Physics

RECEIVED 15 August 2022
ACCEPTED 16 September 2022
PUBLISHED 24 October 2022

CITATION
Wang L and Zhang L (2022), Hawkes processes for understanding heterogeneity in information propagation on Twitter. *Front. Phys.* 10:1019380. doi: 10.3389/fphy.2022.1019380

Hawkes processes for understanding heterogeneity in information propagation on Twitter

Liwen Wang and Lin Zhang*

School of Science, Beijing University of Posts and Telecommunications, Beijing, China

Social platforms make information propagation anywhere anytime. Large quantity data recording information spreading is available for further understanding the intrinsic mechanism within these stochastic processes. Based on the empirical spreading trees of tweets on Twitter, the heterogeneity of Twitter users is explored, turning out the burstiness in the spreading process. A few super spreaders can significantly change the trends of information spreading. Moreover, an improved Hawkes process is designed in this study to better investigate users' heterogeneity during information propagation. Verification is provided for accuracy and stability of the improved Hawkes model in simulating propagation patterns revealed in empirical sequential data, predicting spreading trends, and predicting probability of information outbreaks. Our improved Hawkes model is an effective spreading model for detecting and quantifying super spreaders during the propagation process, which may shed light on the control and prediction of information spreading in social media.

KEYWORDS

Hawkes process, heterogeneity, information propagation, super-spreader, bursts

Introduction

In modern society, information develops at a high speed. Online social networks such as Twitter, Micro-blog, and WeChat provide a free and fast access to all kinds of information, allowing all users to produce and propagate contents. As a result, information today is propagated regardless of any temporal and spatial factors and will have a great influence on individuals and society. Therefore, understanding the patterns and mechanisms within information propagation is of crucial importance nowadays. However, it is challenging to describe and investigate all ingredients during the spreading, such as network topology, features of information, and characteristics of various users.

Information propagation is a rich and active research area. Research perspectives mainly include three aspects: mining spreading patterns, predicting spreading popularity, and information traceability. The methodology is mainly based on a descriptive analysis and construction of models based on data. There are mainly three ways for modeling

propagation: network topology–based, user state–based, and stochastic process–based models [1, 2].

The classical user state–based models are mainly borrowed from the infectious disease models aiming at modeling the epidemiological processes. The two common models are SIR and SIS [3, 4], where S stands for susceptibility, I for infection, and R for recovery. In both models, nodes in class S switch to class I with a fixed probability β. However, the SIS model and the SIR model assume that each node connects to another node with the same probability so that the connections within the population are made randomly. The relationship between nodes, that is, between users, is very important for information propagation, so the assumption made by the contagion model is unrealistic.

To investigate the influence of topology on information propagation, the Independent Cascade (IC) [5]or Linear Threshold (LT) [6] models are commonly used. These models utilize directed graphs on which there are two types of node states, namely, active and inactive and assume that node states can only be transferred from inactive to active states. When applied to analyze the information propagation process, a node transferring from an inactive state to an active state indicates that the user node has propagated information and can propagate information to surrounding users. The model based on network topology has some shortcomings. One is that the weights between nodes in the model are usually assumed to be the same or identically distributed values, but the relationship between users in the actual situation is difficult to be described uniformly, which is the same as the shortcoming of the contagion model. The second is that it obtains the static structure at a certain moment, which cannot keep up with the rapid changes of information propagation, so the timeliness of the model is insufficient.

The Hawkes process, first defined by Hawkes, is a class of point processes whose intensity depends on the history of the process [7]. It has been widely used in recent years to model earthquakes, terrorist attacks, finance, and so forth. [8, 9, 10, 11, 12]. They are ideal models to describe information cascades because each new retweet of a certain piece of tweet not only increases its cumulative retweet count by one but also gains new followers who may further retweet the tweet. In comparison with the aforementioned topology-based and user state–based models, the Hawkes process makes up for the shortcomings of the aforementioned models by not making assumptions about user relationships and by obtaining the complete tweet propagation state.

Research on spreading patterns, prediction of spreading trends, and information traceability by the Hawkes process has been fruitful in the analysis. However, there are still some limitations in the research. One of the most noteworthy is the phenomenon of information bursts, which is the main reason for the significant impact of information propagation on individuals and society. Therefore, the causes of the burst phenomenon, its fitting, and prediction need to be urgently considered and solved.

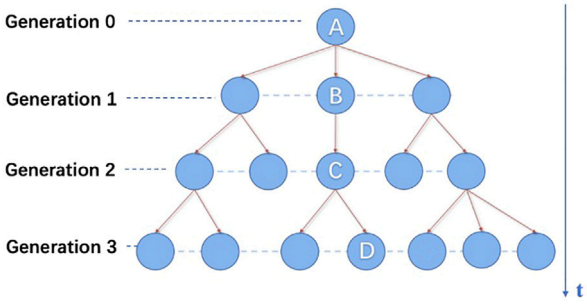

FIGURE 1
Illustration of the propagation tree.

Based on Hawkes processes, this study provides an empirical analysis and modeling of information propagation and the exploration and analysis of the information burst phenomenon. In terms of empirical analysis, we analyze the spreading process from micro to macro based on real spreading data, obtain the emergence of the information propagation process, and focus on the heterogeneity of spreading users. To better portray the burst of the spreading process, an improved Hawkes model is constructed to simulate and predict the development trend and burst phenomenon of the information spreading process, to restore the real spreading process.

Characterization of the propagation process

In this section, the dataset used in this study is described first, and then the characteristics within the empirical propagation process from micro to macro are illustrated and ended up with well-founded reasoning of peaks in the propagation sequence, which is the inspiration of our improved Hawkes processes.

Data description and processing

The data in our study is based on a set of 4626 tweets on Twitter in 2015 and 2016, with their complete retweet trees. Each retweet item includes tweet ID, ID of the retweeted, ID of the retweeter, posting time, and retweeting time, where the posting time refers to the time when the retweeters retweeted the tweet.

Tweets with at least 300 retweets are picked for further analysis and modeling to obtain a sufficient amount of data to study the propagation and to eliminate the noise in the data. Finally, 150 tweets are selected for exploratory analysis, and four

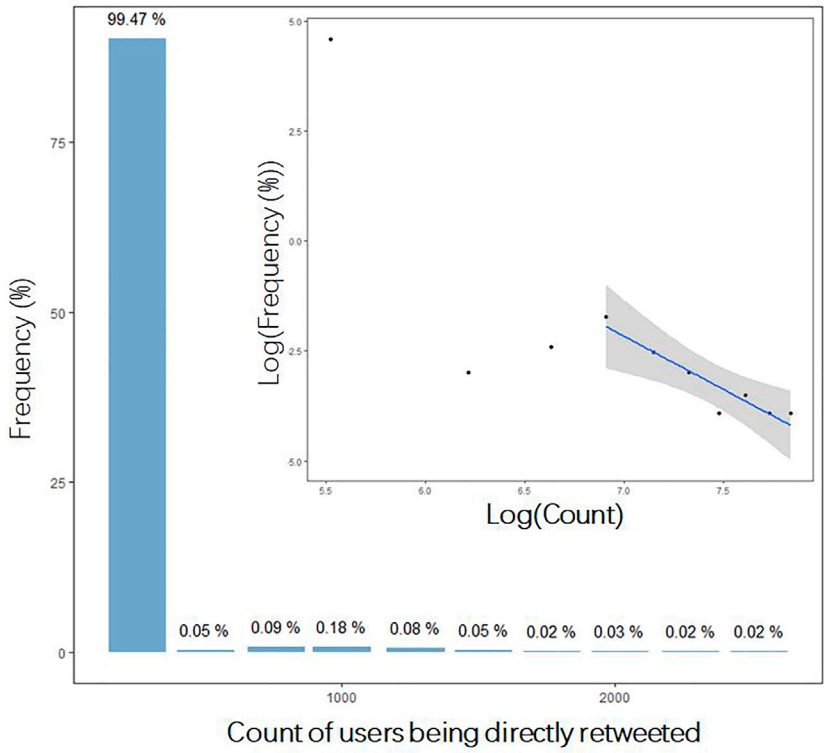

FIGURE 2
Distribution of the count of users being directly retweeted. The inserted is the distribution in log-log scale. The fitted line is log(frequency) = 6.256–0.3664*log(count), with R^2 = 0.8853.

of them are chosen as representative tweets for illustration and visualization.

User heterogeneity analysis

The whole process of information propagation is formed by users' secondary transmission on social platforms. Therefore, the features of different users greatly affect the propagation process. The influence of a certain user can be expressed by the speed and range of information propagation stimulated. Highly influential users can make the content, read, and re-post fast and vast; therefore, the information is highly propagated. In topology-based models, the degree centrality, the proportion of users who are directly connected to the user node, is widely used to measure the average influence of an individual on his/her friends [13].

The retweeting relationship is illustrated in Figure 1. User A created the origin tweet. Then it was retweeted by User A's direct followers, User B is one of them, as shown in Figure 1. User C retweeted the content directly after User B and so forth.

Based on the characteristics of our dataset, the influence of a user is measured by the number of times he or she directly retweeted. If User B retweets User A directly, it means that User A and User B are connected on the social platform, that is, User B is a follower of User A or they follow each other. If User A's influence is high, more users will see that A retweeted a tweet and will retweet this tweet with relatively high probability, resulting in more direct retweets of User A's tweet.

TABLE 1 Quantile of the count of users being directly retweeted.

Percentile ratio	0%	20%	40%	60%	80%	100%
Direct retweet counts	1	1	1	2	2	2530

The number of time that each user's tweet was directly retweeted is analyzed to investigate users' influence. Figure 2 shows the distribution of the number of time users's tweets were directly retweeted, indicating that the users' influence is highly skewed distributed, where 99% of the users's tweets were directly retweeted less than 100 times. The inset figure shows the distribution in the log-log scale, and the fitting line for the tail has slope −0.3664 and R^2 = 0.8853, respectively. The straight line fitted in the log-log scale provides the power law tail of user

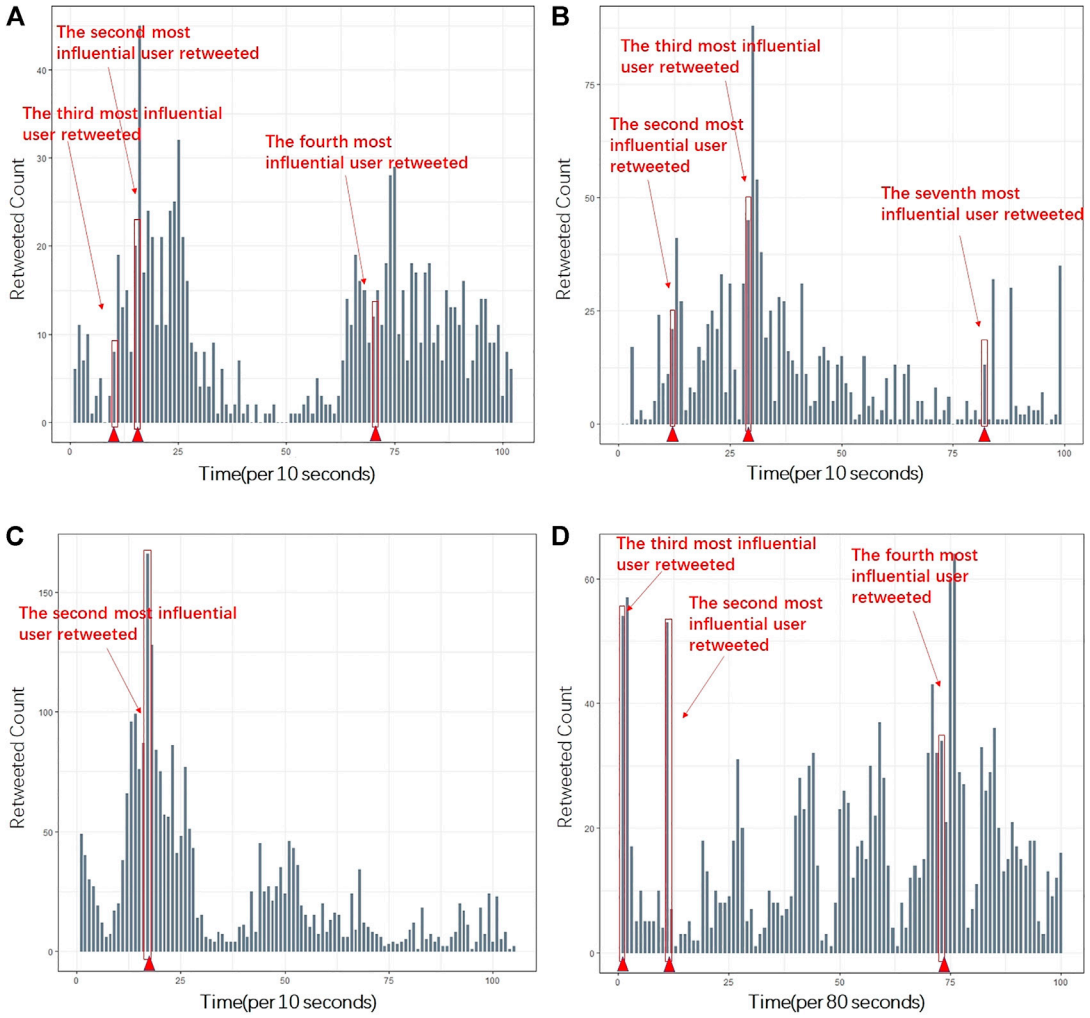

FIGURE 3
Four representative sequences of tweets propagation with top super spreaders marked. Panel **(A)**, **(B)**, **(C)**, and **(D)** corresponds to tweet (a), (b), (c), (d) respectively. Due to different total time lengths of the tweets under consideration, the unit of the horizontal axes in A, B, C, and D are 10 s, 10 s, 10 s, and 80 s, respectively. **(A)** shows stable propagation and slight fluctuations. The relative silence period may be due to circadian. **(B)** illustrates a burst due to the third most influential user. **(C)** is similar to **(B)** with only one burst appearing at early stage of the transmission. **(D)** consists of multiple bursts, which may appear at any stage during the spreading.

influence in a linear scale. The power–law distribution is highly uneven, that is, the scale of direct retweets varies widely, meaning most direct retweets are small and a few are quite large. Therefore, the fitted straight line indicates that there is significant variation in user influence during the dissemination process, with most of the users having low influence and a few users having high influence, and users being heterogeneous. Moreover, as shown in Table 1, 80% of the users' tweets were directly retweeted only twice. However, there are a few users who get many retweets, even up to 2000. Therefore, there are a few "super spreaders" with great influence in the spreading process, and their influence is much higher than that of ordinary users, showing high heterogeneity among spreaders.

Peak analysis

Due to various influence factors, the sequential data of information propagation shows different characteristic patterns. Yasuko et al. investigated the rise and fall patterns of information propagation through clustering [14]. Inspired by their results, four representative time sequences are selected from our sequential data. Figure 3 shows the four propagation sequences of information (a), (b), (c), and (d).

The peaks within one sequence are significant for the overall trend and hotness of information propagation. Reasons leading to the peaks in the information propagation sequence come from the heterogeneity of users' influence. In Figure 3, top influential users are labeled referring to the time they retweeted the tweet,

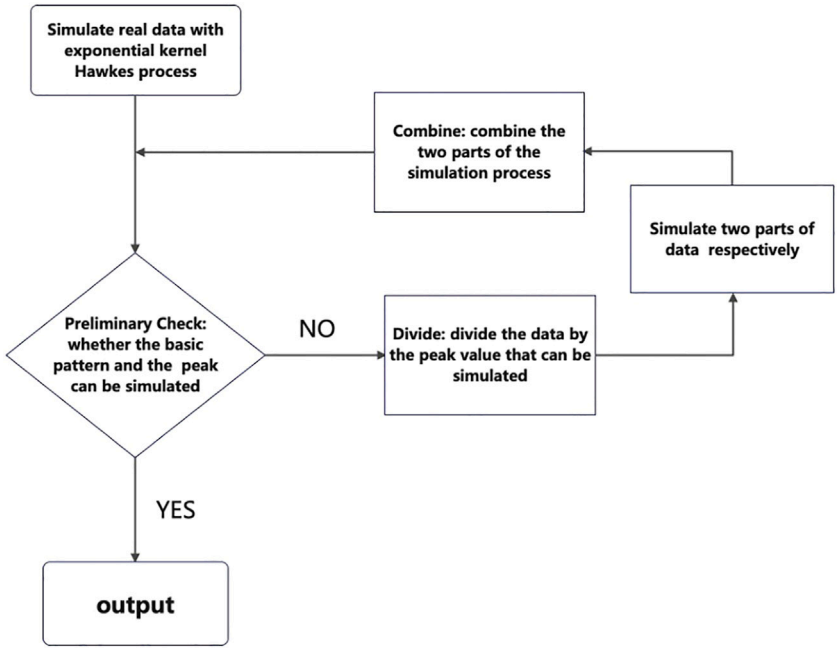

FIGURE 4
Flow chart of Algorithm 1.

which is at or right before the time intervals bursts appeared. Therefore, the posting or retweeting of information by high-influential users during the propagation process can significantly impact the hotness and trend of the information, which is the main reason for a large fluctuation phenomenon within information propagation.

Modeling information propagation by Hawkes processes

In order to quantify the burstiness and further predict and control the propagation process, standard Hawkes processes are introduced and then improved in this section. We will describe how to build an information propagation model based on the Hawkes process, and introduce a Hawkes process simulation method and parameter estimation. Furthermore, the Hawkes model is improved according to the characteristics of real propagation data, and the steps of the improved Hawkes model to simulate the propagation process are given.

Model description

Information propagation is considered as a random process of users' retweeting information. User' retweeting is influenced by two factors. One is the background factor, that is, different content of information has different intensity of attraction to users. The other is the self-exciting effect, that is, if the retweet counts in the previous period is high, the popularity of the spread increases and users will see and retweet the tweet with a higher probability. Thus, information spreads as a random process whose intensity varies with time, and the intensity consists of background factors and self-exciting effects, which is in line with the Hawkes process.

We refer to the point process whose future evolution depends on its own history as the self-exciting point process, that is, the Hawkes process [7]. The Hawkes process can be defined in two ways: one by defining it as a marked Poisson cluster process, where the clusters are generated by a certain branching structure, and the other by using conditional intensity function. The conditional intensity is defined as shown in the following equation:

$$\lambda(t|H_{t^-}) = \mu(t) + \int_0^t g(t-u)N(\mathrm{d}u) = \mu(t) + \sum_{i:\ 0<t_i<t} g(t-t_i). \tag{1}$$

Here, the exponential kernel Hawkes process proposed by Hawkes is used to model the process [7]. Assume that t_i is the time when the ith retweet occurs then the intensity of retweeting at moment t is as follows:

$$\lambda(t) = \mu + \sum_{i:\ 0<t_i<t} \alpha e^{-\beta(t-t_i)}. \tag{2}$$

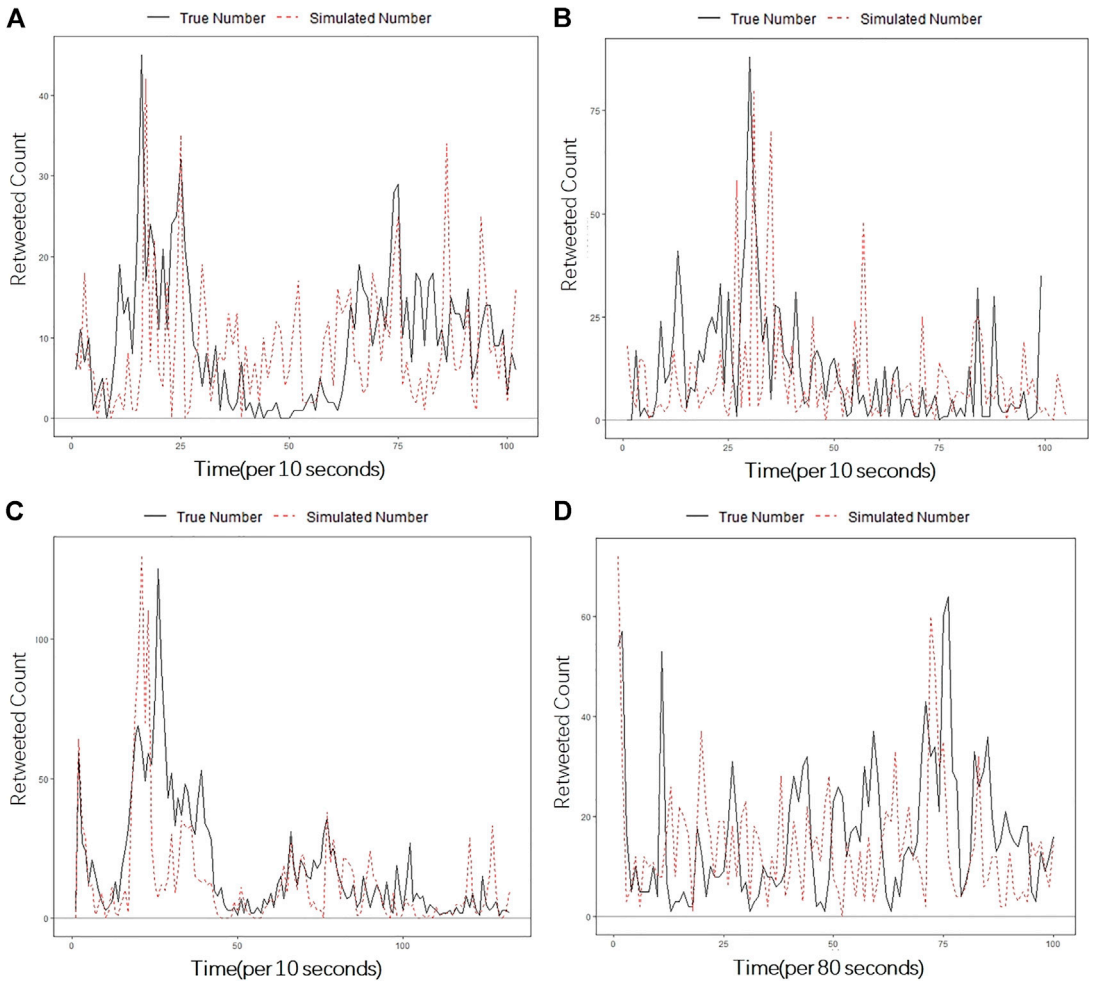

FIGURE 5
Fitting results for the four representative tweets by the improved Hawkes model. Panel **(A)**, **(B)**, **(C)**, and **(D)** corresponds to the fitting results of tweet (a), (b), (c), (d) respectively.

TABLE 2 Parameter estimation for the four tweets.

Tweet	μ_1	α_1	β_1	μ_2	α_2	β_2
(a)	0.333	0.646	0.929			
(b)	0.507	2.827	4.786	0.184	16.639	18.856
(c)	0.061	0.155	0.183	0.017	0.592	0.597
(d)	0.411	0.068	0.094	0.001	0.250	0.252

The parameter μ in the model is the background strength of the tweet. The background strength of the same tweet is a constant, that is, the propagation process generated by the attraction of the tweet itself is a homogeneous Poisson process of strength μ; β is the decay rate, indicating that the influence of the previous retweets is exponentially decayed over time with the parameter β; and α is the cumulative strength, indicating the cumulative influence of the previous retweets, and a retweet is expected to trigger retweet counts of size α.

Moreover, the branching structure in Figure 1 and the Hawkes process can be viewed as the duality of each other. They are both continuous time stochastic processes with non-negative integers as the state space. In the Hawkes process, each point may excite future point, as the retweeting events do. Therefore, the intensity at time t is defined in Eq. 1. Meanwhile, in the branching process, each retweet may cause further retweets, which can be regarded as its children.

Model simulation algorithm

There are two simulation methods for the Hawkes model: intensity-based methods and clustering-based methods [15]. Here, intensity methods for simulation are adopted.

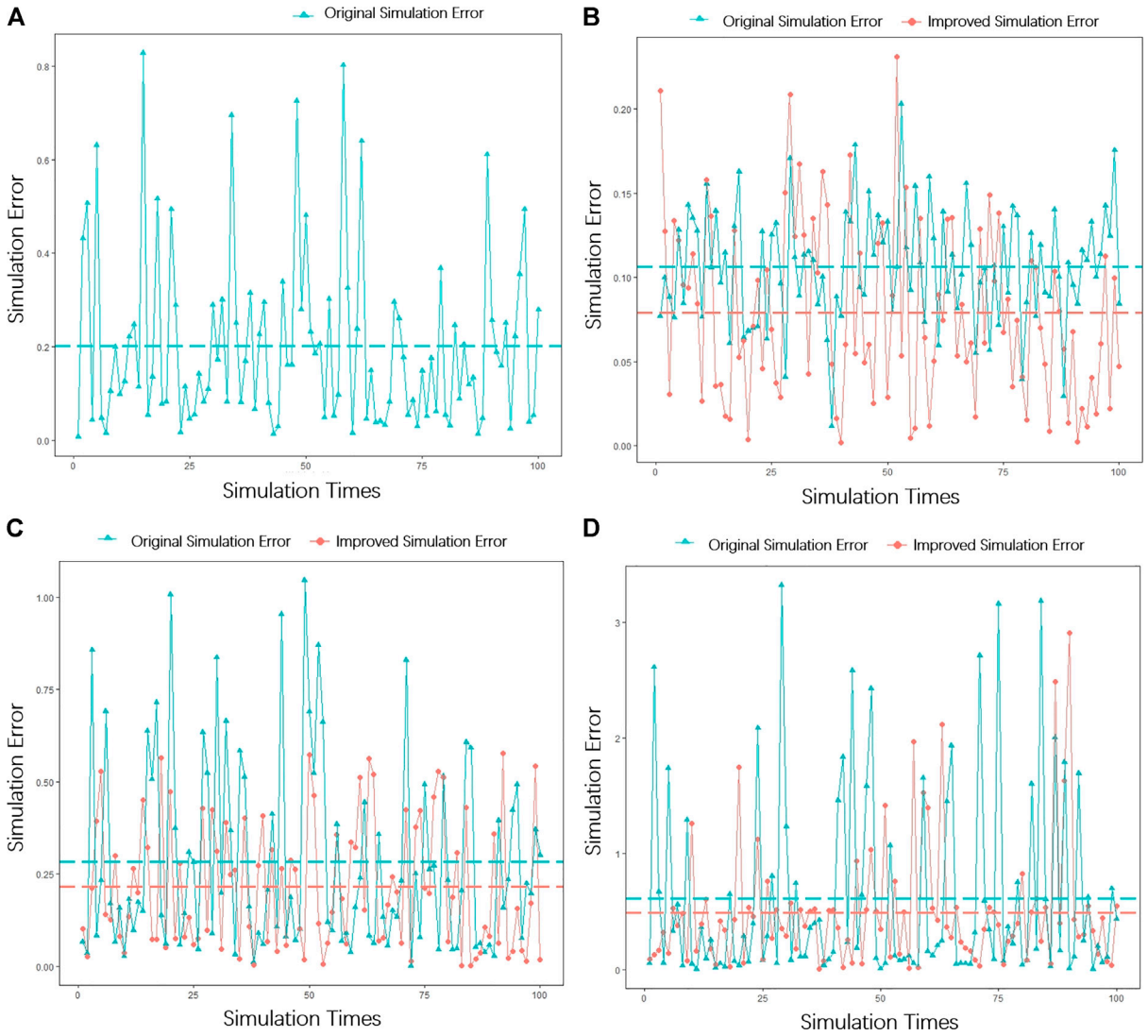

FIGURE 6
Scatter plot of simulation error. Panel **(A)**, **(B)**, **(C)**, and **(D)** corresponds to the scatter plot of simulation error of tweet (a), (b), (c), (d) respectively.

The main idea of the simulation algorithm is to first initialize the intensity λ using the background intensity μ, generating an exponentially distributed random variable as the time when the new event point occurs, and in practice as the distance of the trigger intensity function increases, $\lambda(t)$ in the interval should keep decreasing to accept this new point with a certain probability, and if the point is rejected then the simulation continues to generate a new point.

Model parameters solving

There are two types of methods for estimating the parameters of the Hawkes model: kernel density method and maximum likelihood method. Here, the maximum likelihood estimation method is used to estimate the model parameters in this study [16].

For the Hawkes process with a trigger intensity function of$\alpha e^{-\beta t}$, the log-likelihood is as follows [17]:

$$\log(L(t_1,\ldots,t_n)) = -\mu t_n + \sum_{i=1}^{n}\frac{\alpha}{\beta}\left(e^{-\beta(t_n-t_i)}-1\right) + \sum_{i=1}^{n}\log\left[\mu + \alpha\sum_{t_j<t_i} e^{-\beta(t_i-t_j)}\right]. \tag{3}$$

The maximum likelihood estimation of the parameters is obtained by solving the parameter values in Eq. 3 by finding the

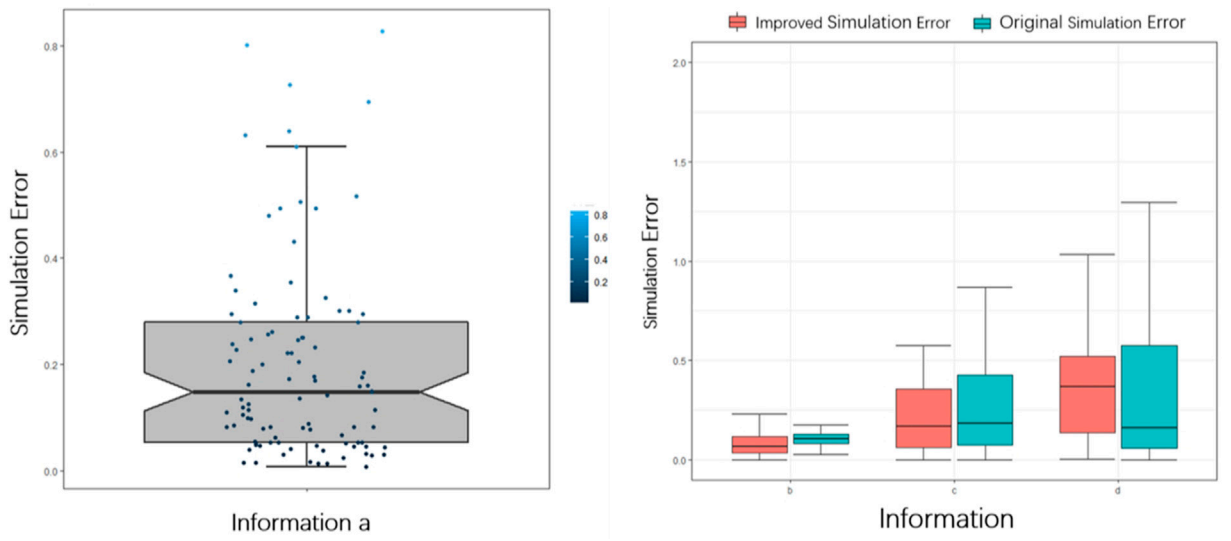

FIGURE 7
Box plots of simulation errors of tweet (a), (b), (c), and (d). The left figure corresponds to the box plot of simulation error of tweet (a), and the right figure corresponds to the box plot of simulation error of tweet (b), (c), (d) respectively. The distribution of the intensity error of tweet (a) simulated by the improved Hawkes model ranges from 0.1 to 0.3, with a mean value of about 0.2; the distribution of the simulation error of tweet (b) ranges from 0.1 to 0.2, with a mean value of about 0.1; the distribution of the simulation error of tweet (c) ranges from 0.1 to 0.4, with a mean value of about 0.26; for tweet (d), which has more burst peaks in the information propagation, the simulation error is enlarged, and it is mainly concentrated between 0.1 and 0.4, but the simulation error still maintains the mean value of 0.35. The stage on the left side of the vertical dashed line and the prediction stage on the right side.

partial derivatives of μ, α, and β, respectively, so that the partial derivatives of the three are zero.

Improved Hawkes information propagation model

It is revealed that the overall pattern of the real information propagation process is consistent with the smooth Hawkes model, but the Hawkes model lacks consideration of peaks, resulting in some peaks in the propagation sequence that cannot be fitted by the smooth Hawkes model. Since peaks play a crucial role during the spreading process, the standard Hawkes model needs improvement to model high peaks, and then modeling the heterogeneity in the stochastic process.

It is found in Figure 3 that peaks are information bursts generated by high-influential users who have retweeted the tweet. Based on this, the propagation process is divided into two propagation sub-processes: one is the "burst" propagation process, which consists of the peak data that cannot be fitted by the smooth Hawkes process, and the other is the "smooth" propagation process, which consists of the remaining propagation data. The propagation process is the superposition of these two processes. The parameters of the sub-processes are estimated separately by the maximum likelihood estimation method, and then the simulated points are obtained by simulating the real propagation data. Finally, the fitted points are combined to obtain the fitted results. If the propagation process simulated after dividing the data is still unable to simulate the retweeting peak continue the process of "divide→ simulate→ combine→ check" until the highest point of the retweeting sequence can be simulated. The algorithm is listed in Algorithm 1, and the algorithm flow chart is shown in Figure 4

The microscopic user heterogeneity characteristics in the real propagation process make the propagation process show the macroscopic characteristics of non-smooth peaks, which are not consistent with the smooth Hawkes model. Therefore, according to the characteristics of the real propagation process, we innovatively divide the propagation process and use the Hawkes process to simulate different parts of the propagation process separately to obtain the improved Hawkes process. Compared with the Hawkes process, in terms of data, the improved Hawkes process overcomes the drawback that the Hawkes process cannot fit the non-smooth peaks and makes the simulation process fit the real propagation process to the maximum extent. In a practical sense, it takes into account the heterogeneity of users and portrays the pattern characteristics of the propagation process, which is important for us to understand and grasp the intrinsic nature of the propagation process.

The improved Hawkes process that we propose has the following advantages in modeling the propagation process:

(1) Unified capability: Information propagation is a stochastic process whose intensity varies with time. Moreover, there are

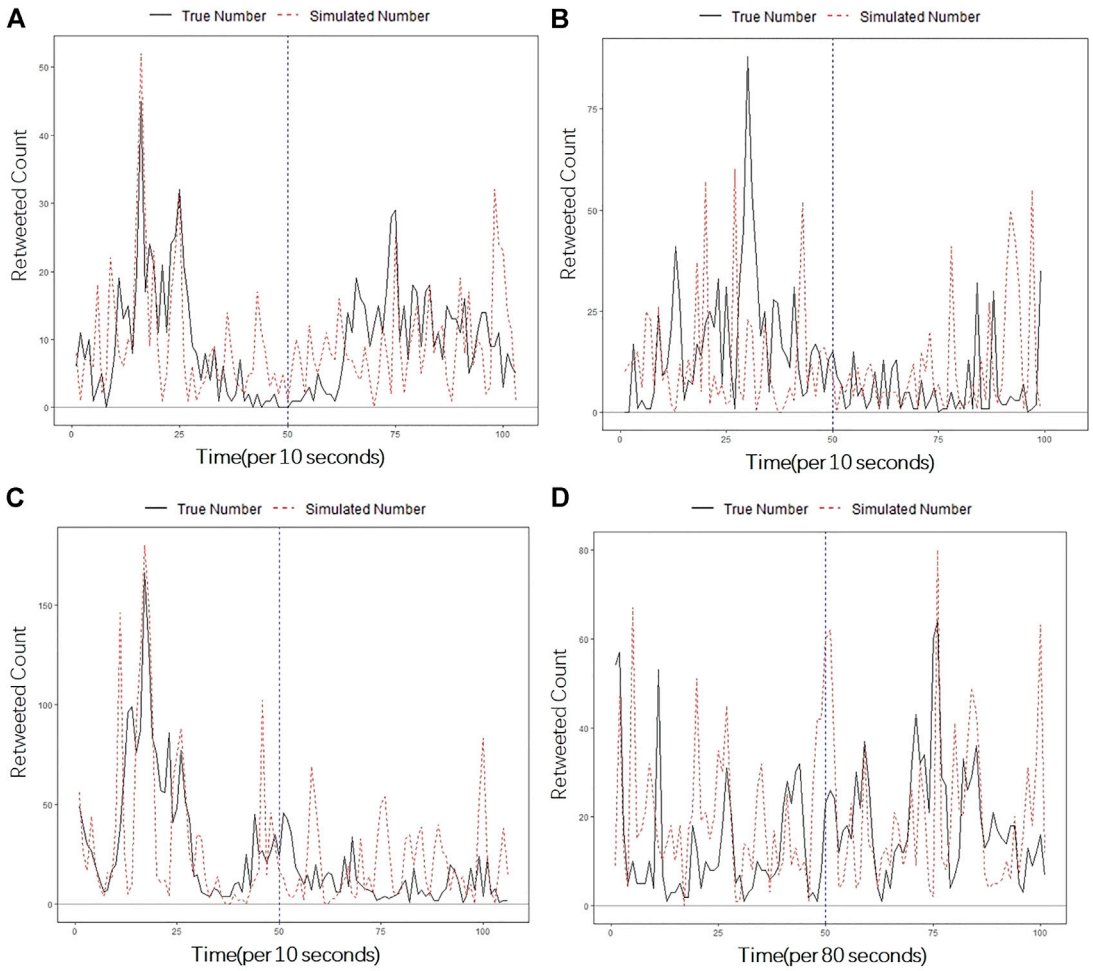

FIGURE 8
Prediction results of the real propagation model and the improved Hawkes model. Panel **(A)**, **(B)**, **(C)**, and **(D)** corresponds to the prediction results of tweet (a), (b), (c), (d) respectively.

a few "super spreader" in the communication process, and their retweets can significantly change the trend and heat of information dissemination, so the real propagation process is non-stationary. By using the improved Hawkes process to build a model, the non-smoothness of the real communication process is depicted, and the stationary and bursty parts during propagation are simulated, respectively, resulting in more accurate description of the propagation process.

(2) Flexibility and scalability: The improved Hawkes process considers the random outbursts in the propagation process. Moreover, it simulates and predicts the varying density and outbursts through the four steps procedure: "divide→ simulate→ combine→ check".

(3) Practicality: By controlling the participation of detected "super spreaders" in the propagation process, the dissemination of information can be facilitated or inhibited; the improved Hawkes model has a high prediction rate for the trend of the propagation process and the information outburst, which is conducive to the identification of information outburst, timely detection of abnormalities, and scientific intervention.

(4) Simplicity: It only needs three model parameters, and then the propagation process can be simulated and predicted.

Experimental results and analysis

The effectiveness of the improved Hawkes model is validated in this section. Moreover, the evaluation index is defined to test the effectiveness of our improved model. Finally, the prediction ability of the improved Hawkes model for the information burst phenomenon is discussed and compared with the standard one.

1. Input: input the time point of each retweet in the real propagation process: $\{t_i, i = 1 \ldots N\}$;
2. Model the propagation process with an exponential kernel Hawkes process to obtain simulated event points: $\{\hat{t}_i, i = 1 \ldots N\}$;
3. Preliminary check simulation effect: check the current simulation situation, whether the basic pattern of the propagation process and the highest peak value can be simulated, if it fails, go to step 3, if it passes, go to step 6;
4. Divide data: If the current model does not simulate the mode and peak of the propagation process, the data will be divided by the peak that can be simulated, and the propagation will be divided into the superposition of two propagation processes $\{t_{1i}, i = 1 \ldots N_1\}, \{t_{2i}, i = 1 \ldots N_2\}$, and if the data has been divided, the part containing the highest peak value will be divided in priority;
5. Simulate the propagation process respectively, and the parameters are estimated by maximum likelihood method for the divided data, and the simulation points are generated by model simulation$\{\hat{t}_{1i}, i = 1 \ldots N_1\}, \{\hat{t}_{2i}, i = 1 \ldots N_2\}$;
6. Combine process: Combine simulation points to generate propagation process $\{\hat{t}_{11}, \ldots \hat{t}_{1i} \ldots, \hat{t}_{1N_2}, \hat{t}_{21}, \ldots, \hat{t}_{2j}, \ldots \hat{t}_{2N_2}, i = 1 \ldots N_1, j = 1 \ldots N_2, \ldots\}$, and then go to step 2;
7. Output: Output the parameters of the model and the simulated propagation process.

Algorithm 1 Improved Hawkes model simulation propagation process.

Evaluation index

In order to analyze the improved Hawkes model and the simulation algorithm, an evaluation index of model fitting, APE (Absolute Percentage Error) is introduced in the SEISMIC model constructed by Zhao et al. as a metric to evaluate the fitting degree of the model to the final popularity count [18]. APE is defined as follows:

$$APE(W,T) = \frac{|\hat{R}_\infty(w,t) - R_\infty(w)|}{R_\infty(w)}, \tag{4}$$

where R is the number of retweets, and Eq. 4 is the ratio of the absolute error of the final number of retweets to the true value, that is, the relative error of the number of retweets.

When simulating the propagation process, the most direct way to test the simulation effect is to consider the average intensity of propagation. Here. the error of the model simulation is defined according to the same pattern as APE, and the final retweet numbers are replaced by the average intensity of the propagation process for further accurate measurement of the simulation effect. The average intensity of the real propagation process is as follows:

$$\bar{\lambda} = \frac{R_\infty}{T}. \tag{5}$$

The average intensity of the simulated propagation process is as follows:

$$\hat{\bar{\lambda}} = \frac{\widehat{R_\infty}}{\hat{T}}. \tag{6}$$

Simulation error is defined as follows:

$$Error = \frac{\left|\frac{R_\infty}{T} - \frac{\widehat{R_\infty}}{\hat{T}}\right|}{\frac{R_\infty}{T}} = \frac{\left|\hat{\bar{\lambda}} - \bar{\lambda}\right|}{\bar{\lambda}}. \tag{7}$$

Error represents the error of the simulation, which is actually relative error of intensity. Here, R_∞ is the actual final retweet count, T is the actual propagation duration of tweet, $\widehat{R_\infty}$ is the model's estimate of final retweet count, and $\hat{T}$ is the model's estimate duration of tweets.

Model simulation experiment

The purpose of simulation experiments is to evaluate whether the improved Hawkes model can fit the real information propagation process and simulate different patterns of information propagation. Algorithm 1 is applied to simulate the four selected representative tweets, and Figure 5

TABLE 3 Predicted peaks of the propagation process.

Information	Actual number of peaks in the prediction stage	Hawkes model prediction		Improved Hawkes model prediction	
		Probability of occurrence of peak (probability of number > 0)	Average number of occurrence of peak	Probability of occurrence of peak (probability of number > 0)	Average number of occurrence of peak
(b)	1	0.44	0	0.78	3
(d)	9	0.84	2	0.92	4

The number of occurrences of peaks is taken as the largest integer not greater than the value.

shows the fitting results by the improved Hawkes model. Tweet (a) needs no division, and the peak of information can be simulated by Hawkes model. (b), (c) and (d) are divided once. Parameters for the four empirical sequences are shown in Table 2.

The improved Hawkes model can better describe the overall trend and represent the fluctuations in the propagation process. In addition, our model can simulate the bursts of information propagation. (b), (c), and (d) in Figure 4 are the results of simulating with two sub-models after one division, that is, there are peaks in the information propagation process that cannot be fitted by standard Hawkes model. It can be seen that almost all the peaks appear during the propagation of (b), (c), and (d) are simulated by the improved Hawkes model, and the rising and falling patterns of the peaks can be well simulated.

Accuracy and stability of model simulation

For the model simulation results, it is described from two aspects of simulation accuracy and simulation stability. Simulation accuracy can be reflected by the numerical value of the simulation error. The smaller the error value is, the closer the simulated average propagation intensity is to the real average intensity, the more the simulated propagation process fits the real propagation process, the higher the simulation accuracy. The stability of the simulation can be described by the fluctuation range of the simulation error, the larger the fluctuation range of the error, the greater the difference in the simulation effect, the higher the instability of the simulation.

In order to measure the simulation effect of the improved Hawkes model and compare it with standard Hawkes model, 100 simulations were performed for tweets (a), (b), (c), and (d) based on standard Hawkes model and the improved Hawkes model, respectively, where (a) does not need to be divided and does not need the improved Hawkes. The simulation errors of the four tweets are calculated, and the error scatter plots (Figure 6) and box plots (Figure 7) of the four tweets are plotted to evaluate the simulation accuracy and simulation stability, and the dashed lines in Figure 6 are the mean error values.

From Figures 6, 7, it is shown that the simulation error of the improved Hawkes model is smaller, the simulated intensity is close to the real value, the fitting accuracy is higher, and the fluctuation range is smaller, so the simulation stability is higher. Moreover, the improved Hawkes model effectively improves the simulation effect and stability of the information propagation process with burst peaks, especially in the case with Tweet (d).

From the error analysis, it can be seen that the improved Hawkes model can simulate different information propagation processes with higher accuracy and stability, and for the information propagation process where the burst phenomenon occurs, the improved Hawkes model has a better simulation effect and better robustness compared with Hawkes model.

Model prediction experiments and discussion

In order to evaluate the prediction ability of the improved Hawkes model and test its application in real life, four information propagation processes are predicted. The data of the first 50 time intervals of the propagation process are used as the learning stage to learn the model parameters using the maximum likelihood estimation method, and the later time is used as the prediction stage to compare with the predicted propagation process generated by the model. Figure 8 gives the comparison of the true propagation pattern of the four tweets with the predicted results, with the learning.

In addition, the difference between the improved Hawkes model and the Hawkes model lies in its simulation of peaks in the propagation sequence. In order to test the prediction ability of the improved Hawkes model for peaks, the occurrence of information peaks in the prediction stage and the number of occurrences are predicted. The 90 percentile of retweets count per unit time interval in the learning stage is taken as the information peak threshold, and the retweet count greater than this threshold is regarded as a peak. After testing, two of them, b and d, the real propagation process of information appeared in the prediction stage with information peaks, and Table 3 gives the results of 50 times of prediction peaks by Hawkes model and improved Hawkes model.

The improved Hawkes model can quickly learn and accurately predict the propagation trends and fluctuations. The information peaks and small fluctuations are well fitted. In the prediction stage, the improved Hawkes model predicted the subsequent development patterns of the tweet based on the learning results, in which the smooth fluctuations in the later part of (a) and (c) and the peaks appearing in the later part of (b) and (d) are predicted.

The improved Hawkes model can predict the peaks in the propagation process with higher accuracy compared to the Hawkes model. The results in Table 3 show that, compared with the standard Hawkes model, in terms of peak occurrence probability, the improved Hawkes model is more accurate in predicting peak occurrence if a peak occurs in the subsequent stages of information propagation. In terms of the count of peak occurrences, the improved Hawkes model predicted more peaks than the Hawkes model which means it is more sensitive in terms of early warning.

Conclusion and discussion

Aimed at mining the propagation law, this study starts from analyzing the real propagation data, gives the micro and macro

characteristics of the propagation process, and then constructs the improved Hawkes model, focusing on the pattern and explosion phenomenon of the propagation process.

It is found that the direct forwarding relationship among users reflects the connection between users, and the number of users being directly forwarded reflects the influence of users, showing great heterogeneity among users. This is the main reason for the information explosion phenomenon is that people with high influence forward information. After selecting four representative tweets according to the classical propagation pattern, an improved Hawkes process is established to quantify the evolving patterns, which is an effective and quantitative propagation model that accurately and concisely describes the information propagation process.

However, regarding the construction of the propagation model, the exponential kernel adopted here is a simple case of point processes. In real life, the situation may not be homogeneous, and the intensity is not necessarily exponentially decaying, which needs further investigation.

Data availability statement

The original contributions presented in the study are included in the article/Supplementary Material; further inquiries can be directed to the corresponding author.

Author contributions

LZ carried out the concepts and design of this study. LW carried out the analysis of data, and interpretation of model and simulation. LW drafted the manuscript. All authors read and approved the final manuscript.

Funding

This work was jointly supported by the National Natural Science Foundation of China (Grant Nos. 11971074, 61671005).

Acknowledgments

The authors would like to thank the editors and reviewers for their enthusiastic help and constructive comments.

Conflict of interest

The authors declare that the research was conducted in the absence of any commercial or financial relationships that could be construed as a potential conflict of interest.

Publisher's note

References

1. Xu H, Zhang Q. A review of epidemic dynamics on complex networks[J]. *Inf Sci* (2020) 38(10):159–67.

2. Hu CJ, Xu WW, Hu Y, Fang MZ, Liu F Review of information diffusion in online social networks[J]. *J Electron Inf Tech* (2017) 39(04):794–804.

3. Herbert W. Hethcote. The mathematics of infectious diseases[J]. *SIAM Rev* (2006) 42(4):599–653.

4. Newman MEJ. The structure and function of complex networks[J]. *SIAM Rev* (2006) 45(2):167–256.

5. Goldenberg J, Libai LE, Muller E. Talk of the network: A complex systems look at the underlying process of word-of-mouth[J]. *Marketing Lett* (2001) 12(3): 211–23. doi:10.1023/a:1011122126881

6. Kempe D, Kleinberg J, Tardos E. Maximizing the spread of influence through a social network[J]. *Theor Comput* (2003)(4) 137–46.

7. Hawkes AG. Spectra of some self-exciting and mutually exciting point processes. *Biometrika* (1971) 58(1):83–90. doi:10.1093/biomet/58.1.83

8. Tita G, Ridgeway G. The impact of gang formation on local patterns of crime. *J Res Crime Delinquency* (2007) 44(2):208–37. doi:10.1177/0022427806298356

9. Lewis E, Mohler G, Brantingham PJ, Bertozzi AL Self-exciting point process models of insurgency in Iraq[J]. *Security J* (2010) 25(3):244–264.

10. Bacry E, Dayri K, Muzy JF. Non-parametric kernel estimation for symmetric Hawkes processes. Application to high frequency financial data[J]. *The Eur Phys J B* (2012) 85(5):1–12. doi:10.1140/epjb/e2012-21005-8

11. Chen F, Hall P. Inference for a nonstationary self-exciting point process with an application in ultra-high frequency financial data modeling. *J Appl Probab* (2013) 50(4):1006–24. doi:10.1239/jap/1389370096

12. Fox EW, Short MB, Schoenberg FP, Coronges KD, Bertozzi AL. Modeling E-mail networks and inferring leadership using self-exciting point processes. *J Am Stat Assoc* (2016) 111(514):564–84. doi:10.1080/01621459.2015.1135802

13. Wu XD, Li Y, Li L. Influence analysis of online social networks[J]. *Chin J Comp* (2014) 37(4):18.

14. Yasuko M, Yasushi S, Prakash AB. Rise and fall patterns of information diffusion: Model and Implications[C]. *Proc 18th ACM SIGKDD Int Conf Knowledge Discov Data Mining* (2012) 6–14. 10.1145/2339530.2339537 (Accessed January, 2022).

15. Dassios A, Zhao H. Exact simulation of Hawkes process with exponentially decaying intensity[J]. *LSE Res Online Documents Econ* (2013) 18(18):1–13. doi:10.1214/ecp.v18-2717

16. Ogata Y. On Lewis' simulation method for point processes. *IEEE Trans Inform Theor* (1981) 27(1):23–31. doi:10.1109/tit.1981.1056305

17. Rubin I. Regular point processes and their detection. *IEEE Trans Inform Theor* (1972) 18(5):547–57. doi:10.1109/tit.1972.1054897

18. Zhao Q, Erdogdu MA, He HY, Rajaraman A, Leskovec J SEISMIC: A self-exciting point process model for predicting tweet popularity[C]. *Proc 21th ACM SIGKDD Int Conf Knowledge Discov Data Mining* (2015) 1513–22. 10.1145/2783258.2783401 (Accessed December, 2021).

frontiers | Frontiers in Physics

TYPE Original Research
PUBLISHED 02 November 2022
DOI 10.3389/fphy.2022.1042900

OPEN ACCESS

EDITED BY
Xuzhen Zhu,
Beijing University of Posts and Telecommunications (BUPT), China

REVIEWED BY
Yang Xu,
Hunan University, China
Caihong Liu,
Jiaxing University, China
Xiaofan Lai,
Shenzhen University, China

*CORRESPONDENCE
Jianjia He,
hejianjia@usst.edu.cn
Shengxue He,
lovellhe@usst.edu.cn

SPECIALTY SECTION
This article was submitted to Social Physics,
a section of the journal
Frontiers in Physics

RECEIVED 13 September 2022
ACCEPTED 17 October 2022
PUBLISHED 02 November 2022

CITATION
Liu J, He J, Qiu Z and He S (2022), An opinion dynamics model based on affinity and social noise.
Front. Phys. 10:1042900.
doi: 10.3389/fphy.2022.1042900

An opinion dynamics model based on affinity and social noise

Jusheng Liu[1], Jianjia He[2,3,4]*, Zhiping Qiu[5] and Shengxue He[2]*

[1]School of Economics and Management, Shanghai University of Political Science and Law, Shanghai, China, [2]Business School, University of Shanghai for Science and Technology, Shanghai, China, [3]Center for Supernetworks Research, Shanghai, China, [4]Shanghai Institute of Public Diplomacy, Shanghai, China, [5]School of Economics and Management, Dongguan University of Technology, Dongguan, China

Most previous works have studied the evolution of opinions based on the Hegselmann–Krause model, the Deffuant–Weisbuch model, and the Sznajd model. However, the influence of social influence on opinions is discussed less. Based on the social influence theory and the Hegselmann–Krause model of opinion dynamics, we introduce the affinity and social noise in the Hegselmann–Krause model of opinion dynamics and propose an affinity and social noise Hegselmann–Krause model (ASNHK). The influence of affinity degree, affinity threshold, social noise, and personnel heterogeneity on opinion evolution is discussed in experimental analysis. Experimental results show that the affinity between people can improve opinions to form a consensus positively, but the affinity threshold has a negative role contrarily. Moreover, when the social noise increases, the opinions will form a consensus. When it increases to a certain value, the opinion will be decentralized. Furthermore, personnel heterogeneity has different effects on opinion evolution. Open-minded individuals are more likely to form a unified opinion, while closed-minded individuals have difficulty unifying their opinions. Overall, this research provides a clearer explanation of the group opinion evolution from social influence.

KEYWORDS

group opinion evolution, Hegselmann–Krause model, social influence, affinity, social noise, bounded confidence

1 Introduction

Opinion is people's insights and understanding of something. It is a kind of idea, opinion, judgment, or emotion generally held by the public [1]. Exploring the evolution of public opinion can help people understand the evolution mechanism of opinion and behavior, respond to public opinion crises, and guide public opinion dissemination. At present, scholars have carried out relevant research on the evolution of ideas, but the behavior and opinions of the public still need to be further explored. For example, with the advent of COVID-19, it was believed that the Shuanghuanglian oral liquid can act on the COVID-19 virus, based on an internet finding, and then many people began to form opinions. What is the mechanism behind this phenomenon and how are the opinions

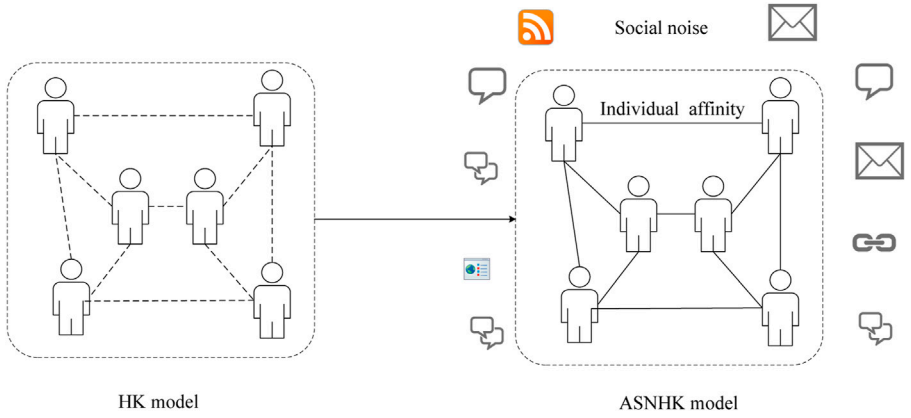

FIGURE 1
Illustration of the affinity and social noise Hegselmann–Krause model.

affected and formed? What factors play a role? To our best knowledge, there is still no research that can provide a clear explanation.

Until now, scholars have researched group opinion dynamics from different perspectives [2–5]. According to the type of opinion, the opinion dynamic model can be divided into many types, such as the continuous model, the discrete model, and the continuous opinions and discrete actions model (CODA model). The common continuous model contains the Hegselmann–Krause model (HK model) [6–9], the Deffuant–Weisbuch model (DW model) [10–12], and other models. In terms of the Deffuant–Weisbuch model, [13] proposed an adaptation of the Deffuant–Weisbuch model that incorporates both implicit and explicit opinions; [14] discussed the higher-order interactions that destroy phase transitions in the Deffuant–Weisbuch opinion dynamics model; based on the Deffuant model, [1] considered attitude-hiding behaviors and proposed an agent-based model of opinion dynamics with attitude-hiding behaviors. The common discrete model contains the Sznajd model [15–18], the Voter model [19–21], and the Majority model [22, 23].

Current scholars have explored different opinion models from different perspectives. However, few researchers consider the social influence. In fact, the study of opinions is often inseparable from the individual and the environment in which the individual lives, but existing research has not observed this. Social influence theory indicates that proximity to others and the social environment can affect people's opinions comprehensively. On one hand, people cannot survive independently, and it is necessary to establish a relationship with people around [24]; on the other hand, it is impossible for people to escape from the social environment. Therefore, relationship and social environment are two important factors that can influence people's behavior [25]. To express conveniently, we use affinity and social noise to indicate the relationship and social environment. If the relationship among people is good, the affinity is large; on the contrary, if the relationship is not good, the affinity is small. Similarly, if the influence of the social environment is strong, the social noise is large; on the contrary, the social noise is small. To explore opinion evolution under the influence of social influence theory, this study discussed the evolution mechanism of group opinion by introducing affinity and social noise. Finally, an experimental analysis is carried out, and the simulation results are discussed. The illustration of the affinity and social noise Hegselmann–Krause model is shown in Figure 1.

There are the following contributions to this research. First, this study extends the Hegselmann–Krause model and conforms the opinion evolution more to human interaction activities. Second, affinity and social noise are introduced to the Hegselmann–Krause model based on the social influence theory. Third, this research will shed light on and help people understand the opinion evolution mechanism well. Moreover, distinct from the HK model, this research used mathematical models and equations to portray affinity and social noise, and it enriched the opinion dynamics model greatly and can be applied to the fields of public opinion governance, intervention, and control. The research considers interpersonal and environmental influences in the evolution of opinion and further extends the boundaries of opinion dynamics.

The article is arranged as follows: the introduction is shown in Section 1. In this part, we introduce the current research on the opinion dynamic models; the related works on the Hegselmann–Krause model, social influence theory, affinity in public, and social noise are introduced in Section 2; in Section 3, the affinity and social noise Hegselmann–Krause model (ASNHK) construction is described; section 4 presents the experimental analysis of the ASNHK model. Finally, we

discuss the experimental results and summarize the conclusion in Section 5 and Section 6, respectively.

2 Related work

2.1 Opinion dynamics in the Hegselmann–Krause model

As a kind of bounded confidence group opinion dynamics, the HK model has attracted the research interests of many scholars since it was put forward by Hegselmann and Krause [6] in 2002. After that, scholars used different methods to extend this model. [26] integrated the Hegselmann–Krause model into the process of product improvement and explored the relationship among the evolution of opinion, product scheme, and design iteration; [27] proposed a bounded confidence model which considered the opinion priority of leaders and divided the group into "opinion leaders" and ordinary people groups; based on the HK model, [28] considered social learning and explored the agent's opinion evolution when they are influenced by the truth or a conflicting source. In addition, some researchers discussed the consensus and convergence in the HK model [29, 30]. The aforementioned research provided some insights to the following scholars on the HK model, and these research studies broaden the research boundary of opinion dynamics.

2.2 Social influence theory

As a kind of sociological and psychological theory, social influence theory has been given more and more attention by scholars [31]. Social influence comes from two aspects. On one hand, an agent will be influenced by the role of another. Under the influence of others, an individual will more or less change in one way or another. On the other hand, the surrounding environment will form a kind of normative force, promoting members' psychology to form a kind of group pressure and making its members be in line with the group [4, 32]. In terms of social influence, [33] explored the effect of social influence based on the Durkheimian opinion dynamics by constructing a social influence function with the social ranking (SR) and the distance; [34] also introduced individuals' social influences in social networks to highlight the heterogeneity of individuals in opinion evolution; [35] considered the individuals' influential power and explored the authority effect and the Matthew effect in opinion dynamics. In addition, some researchers also explored individuals' social influence on themselves in opinion dynamics [36].

2.3 Affinity in public

As an indicator of people's estrangement, affinity is an important factor that influences people's attitudes and behavior. In opinion dynamics, [37] proposed a model to simulate the process of opinion formation and explored the role of mutual affinity between interacting agents; [38] developed a statistical method to find affinity relations in a large opinion network; [39] took the mutual affinity between agents into the model and explored the process of opinion formation in an open community; [40] used the opinion dynamics to explore the partisan conflicts in recent America and discuss the change of affinity among co-partisans; [41] explored the nonlinear interaction of ideological affinity with the psychological reaction of agents in the frame of a multiparametric mathematical model of opinion dynamics. It can be seen from the aforementioned research that affinity has gradually gained the attention of scholars and has been applied to sociology, opinion dynamics, and other fields.

2.4 Social noise

In addition, in the process of evolution, social noise can also influence people's behavior or opinions [42]. At present, [43] explored the HK model under the influence of noise and found that the fragmentation of HK dynamics tends to vanish when persistent noise was present; [44] explored the influence of noise on the HK model and found that the system presented an orderly to disordered phase transition with the increase of noise in the HK model; [45] also found that noise was helpful in adjusting the split phenomenon of viewpoint through the study of HK model noise; [46] used an agent-based modeling and a computational social science approach to explore the opinion evolution with various noise levels; [47] introduced the noise into the Degroot framework and proposed a new Degroot-type social learning model.

The aforementioned scholars explored opinion dynamics from different perspectives. Few studies have explored the affinity and social noise in opinion dynamics based on social influence theory systematically. To bridge this gap, this study takes the affinity and noise into the HK model and constructs an affinity and social noise Hegselmann–Krause model. In this model, we explore opinion evolution and propose the evolutionary rules and algorithm. After that, experimental analysis is carried out, and some conclusions are discussed.

3 Model formulation

3.1 Introduction of the Hegselmann–Krause model

Within the limited confidence threshold, we assume that there is a set A, $A = [1, 2, 3, \ldots, i, j, N]$, the set A has N individuals, and the opinion of individuals i and j is assigned as x_i^t and x_j^t and x_i^t and $x_j^t \in [0, 1]$, respectively; if $|x_i^t - x_j^t| \leq \varepsilon$, then:

$$x_i^{t+1} = \sum_{j:\,|x_i^t - x_j^t|} \alpha_{ij} x_j^t, \tag{1}$$

where the aforementioned model [Eq. (1)] is the Hegselmann–Krause model of opinion dynamics[6], x indicates the individual's opinion, α_{ij} is the influence weight of individual i on the individual j, $\alpha_{ij} \in [0, 1]$, and $\sum_{j=1}^{N} \alpha_{ij} = 1$. If the α_{ij} is larger, it indicates that one individual's influence on other individuals is more obvious; ε is the opinion threshold, and the smaller the ε is, it is difficult for an individual's opinions to influence each other. In addition, the aforementioned model is a simplified model; it ignores the order in which ideas are presented and is suitable for simultaneous group updates, such as a group meeting and an exchange within a forum.

3.2 Affinity and social noise Hegselmann–Krause model

Based on the HK model, according to the group opinion dynamics' characteristics, we focus on the affinity and social noise in the opinion evolution. Affinity always exists in the relationship among people. If the relationship between two individuals is good, the affinity is large; on the contrary, if the relationship between two individuals is bad, the affinity is small. To take into account the affinity, we use the r_{ij}^t to indicate the degree of opinion influence:

$$r_{ij}^t = \frac{max\left(R_{ij} - \left(|x_i^t - x_j^t| - \varepsilon_i\right), 0\right)}{max\left(|x_i^t - x_j^t|, \varphi\right)}, \tag{2}$$

where $R_{ij} \in [0, 1]$ is a real number of $N \times N$ nonnegative and asymmetric matrix of R, and it indicates the affinity degree between people. If the R_{ij} is smaller, the relationship between them is worse; instead, if the R_{ij} is larger, the relationship between them is good. x_i^t is the opinion value of i, and x_j^t is the opinion value of j. r_{ij}^t is the degree of opinion influence, which indicates the influence degree of individual j on i in the t round. φ is a number that is not equal to 0. To avoid the denominator being equal to 0, we set φ as a minimal number, here $\varphi = 0.001$. Especially, if $|x_i^t - x_j^t| > \varepsilon_i \& R_{ij} < \delta$, the opinion influence weight is 0, and to measure the degree of opinion influence weight, we define ρ_{ij} is the opinion influence weight, which is given by Eq. 3. Here, the δ is the affinity threshold, and this parameter shows that if the opinion difference between two individuals does not exceed the opinion influence threshold, the affinity between individuals can also affect the evolution of opinion.

$$\rho_{ij} = \begin{cases} r_{ij}^t, & otherwise \\ 0, & if\,|x_i^t - x_j^t| > \varepsilon_i \& R_{ij} < \delta \end{cases} \tag{3}$$

By standardizing the influence degree of the aforementioned opinions, the following Φ_{ij}^{t+1} indicates the opinion influence weight of individual j on individual i.

$$\Phi_{ij}^{t+1} = \begin{cases} 0, & \sum_{\kappa \in N} \rho_{ik}^t = 0 \& i \neq j \\ \dfrac{\rho_{ij}^t}{\sum_{\kappa \in N} \rho_{ik}^t}, & \sum_{\kappa \in N} \rho_{ik}^t \neq 0 \\ 1, & \sum_{\kappa \in N} \rho_{ik}^t = 0 \& i = j \end{cases} \tag{4}$$

Furthermore, to take into account the social noise, the extended HK equation in opinion dynamics can be constructed as follows.

$$x_i^*(t) = \mu_i x_i(t) + \left(1 - \mu_i\right) \sum_{j \in N(i, x(t))} \Phi_{ij} x_j(t) + \xi_i(t), \tag{5}$$

where μ_i indicates the initial opinion persistence, ξ_i is the social noise, and it obeys the random uniform distribution. Moreover, the social noise is independent and identically distributed (i.i.d.) with $E\xi_1(1) = 0$, $E\xi_1^2(1) > 0$ [48,49]. μ_i is the persistence of individual i, and $1 - \mu_i$ indicates the sensitivity of individuals to the opinions of the public around them. The initial persistence generally follows the normal distribution, that is to say, most people's persistence of opinions is neutral, and the persistence of few individuals is extreme. When the mean value of the normal distribution is large, it is easy to form multiple opinion clusters, but not easy to form a consensus. On the contrary, if the majority of people's opinions is amiable, individuals' opinions are easily influenced by other individuals and finally form a consistent opinion.

The conditions for the evolution of opinion are as follows:

$$N(i, x(t)) = \left\{(j \in \nu) | x_j(t) - x_i(t)| \leq \varepsilon\right\}, \quad \varepsilon \in (0, 1]. \tag{6}$$

At the $t + 1$, the opinion evolution equation is as follows:

$$x_i(t+1) = \begin{cases} 1, & x_i^*(t) > 1 \\ x_i^*(t), & x^* \in [0, 1], \forall i \in N, t \geq 0 \\ 0, & x_i^*(t) < 0 \end{cases} \tag{7}$$

To clearly explain the algorithm, we have shown the calculation process of the affinity and social noise Hegselmann–Krause model in Figure 2.

Based on the aforementioned model construction, the affinity and social noise Hegselmann–Krause model is built, and the specific parameter note is shown in Table 1.

4 Experimental analysis

4.1 Experiment setup

Generally speaking, in real life, the persistence of opinion is neutral, and the opinion of small people is extremely close to 0 or 1. Therefore, we can assume that the distribution of people's opinion persistence belongs to normal distribution. Default settings for the parameters used in the experiments are shown in Table 2.

Algorithm 1 The affinity and social noise Hegselmann-Krause model

Input: opinion value x, opinion persistence μ, opinion threshold ε, affinity threshold δ, social noise ξ
Output: final opinion status
initialize parameters;
initialize the opinion value;
build an affinity matrix;
while $\frac{1}{N}\sum_{i=1}^{N}|x_i^{t+1}-x_i^t|>\varepsilon$ **do**
  $x_i^*(t)=\mu_i x_i(t)+(1-\mu_i)\sum_{j\in N(i,x(t))}\Phi_{ij}x_j(t)+\xi_i(t)$;
  standardize the opinion influence weight;
  start to update the opinion values;
  if $|x_i^t-x_j^t|>\varepsilon_i \& R_{ij}<\delta$ **then**
    $\rho_{ij}=0$;
    if $i=j$ **then**
      $\Phi_{ij}^{t+1}=1$;
    else
      $\Phi_{ij}^{t+1}=0$;
    end
  else
    $\rho_{ij}=r_{ij}^t$;
    $\Phi_{ij}^{t+1}=\frac{\rho_{ij}^t}{\sum_{\kappa\in N}\rho_{ik}^t}$;
  end
end

FIGURE 2
Algorithm of the affinity and social noise Hegselmann–Krause model.

TABLE 1 Parameters in the model.

Parameters	Range	Explanation
R	[0,1]	Affinity among public
x	[0,1]	Opinion value
Φ	[0,1]	Opinion influence weight
ξ	[0,1]	Social noise from public
μ	[0,1]	Opinion persistence
δ	[0,1]	Affinity threshold
ε	[0,1]	Opinion threshold
φ	Constant	A constant on the denominator

TABLE 2 Default settings for the parameters used in the experiments.

Parameter	Default setting
R	Non-negative and asymmetric matrix between 0 and 1
x	Random uniform distribution 0 and 1
Φ	Between 0 and 1
ξ	Random uniform distribution between 0 and 1
μ	Normal distribution between 0 and 1
δ	Constant between 0 and 1
ε	Constant between 0 and 1
φ	0.001

4.2 Influence of affinity degree on opinion evolution

In the proposed model, the first analysis is performed by simulating the influence of affinity degree on opinion evolution. In terms of parameter setting, we set the affinity degree R_{ij} to 0.1, 0.5, and 0.9. At this moment, the threshold of the affinity is 0.8 and the opinion numbers are 100. Also, we keep other parameters unchanged, and the simulation result is shown in Figure 3.

As shown in Figure 3A, we find that the opinion evolution is related to the affinity degree. In Figure 3A, when R_{ij} = 0.1, the opinion will be stable at 200 steps, and the opinion will form six opinion clusters; when R_{ij} = 0.5, the opinion will be stable at 50 steps, and the opinion will form five opinion clusters in Figure 3B; as the affinity continues to increase, when the affinity degree increases to 0.9, at this moment, the opinion will form one opinion cluster in Figure 3C. Based on the aforementioned simulation results, we can see that affinity can improve the opinion to tend to an agreement, and the result is

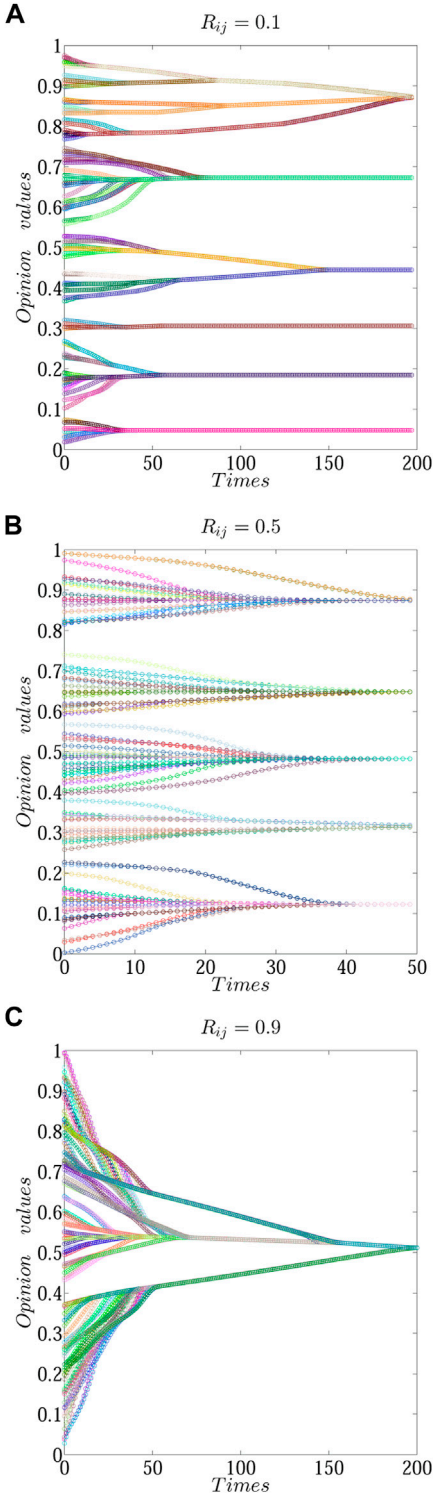

FIGURE 3
Opinion evolution result under the different affinities R_{ij}. **(A)** R_{ij} = 0.1, **(B)** R_{ij} = 0.5, and **(C)** R_{ij} = 0.9.

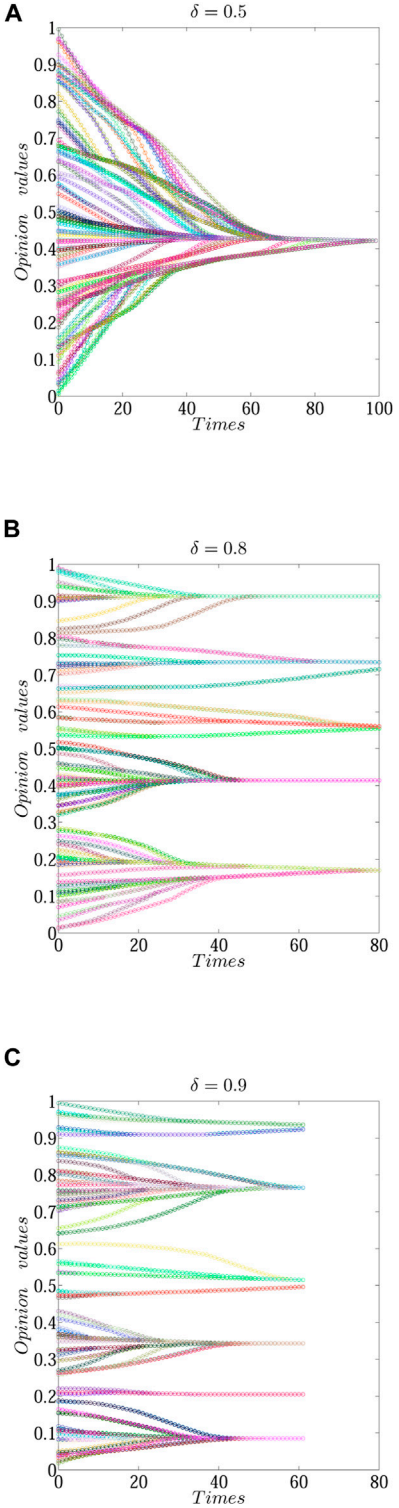

FIGURE 4
Opinion evolution result under different thresholds of affinity, **(A)**δ = 0.5, **(B)** δ = 0.8, and **(C)** δ = 0.9.

also consistent with the social influence theory. Meanwhile, the aforementioned results indicate that affinity among people has a positive effect on opinions. If the affinity among individuals increases, the opinion will be easier to reach an agreement.

4.3 Influence of threshold of affinity on opinion evolution

Different thresholds of affinity may have different influences on opinion evolution. To further explore the influence of the threshold of affinity on opinion evolution, we carried out a related simulation about the threshold of affinity. In the simulation, we set the affinity as 0.5, and the thresholds of affinity are 0.5, 0.8, and 0.9. Keeping other parameters unchanged, the simulation result is shown in Figure 4.

As shown in Figure 4, opinion evolution has different results when the threshold of affinity takes different values. In Figure 4A, when $\delta = 0.5$, at this moment, the affinity is equal to the threshold of affinity, the opinion will be stable at 100, and the opinion will form one opinion cluster finally. As shown in Figure 4B, when the threshold increases, for instance, if $\delta = 0.8$, we can find that the opinion will be stable at 80, and the opinion will form six opinion clusters, compared with Figure 4A. This result indicates that the larger difference between affinity and the threshold will prevent opinions from forming a consensus and lead to a split of opinion. In Figure 4C, when the $\delta = 0.9$, at this moment, the difference between affinity and the threshold is increasing continuously, and the opinion will form more clusters. It indicates that if the difference between affinity and the threshold is larger, the opinion will be more dispersed.

4.4 Influence of social noise on opinion evolution

In the ASNHK model, social noise is an important factor that can affect opinion evolution. In terms of social noise, as an external factor, social noise can give individuals some pressure or influence and promote the evolution of individual opinion. To explore the influence mechanism of social noise, we set the affinity to 0.5, set the threshold to 0.8, and kept other parameters unchanged. Moreover, we set the interval of social noise distribution to $\xi_i \in [-0.01, 0.01]$, $\xi_i \in [-0.02, 0.02]$, and $\xi_i \in [-0.03, 0.03]$ uniformly. The simulation result is shown in Figure 5.

As shown in Figure 5, we find that the opinion will form different evolution results when the social noise increases to different values. In Figure 5A, when there is no noise in opinion dynamics, the opinion will be stable at 95 steps and form five opinion clusters. Based on Figure 5A, when the interval of social

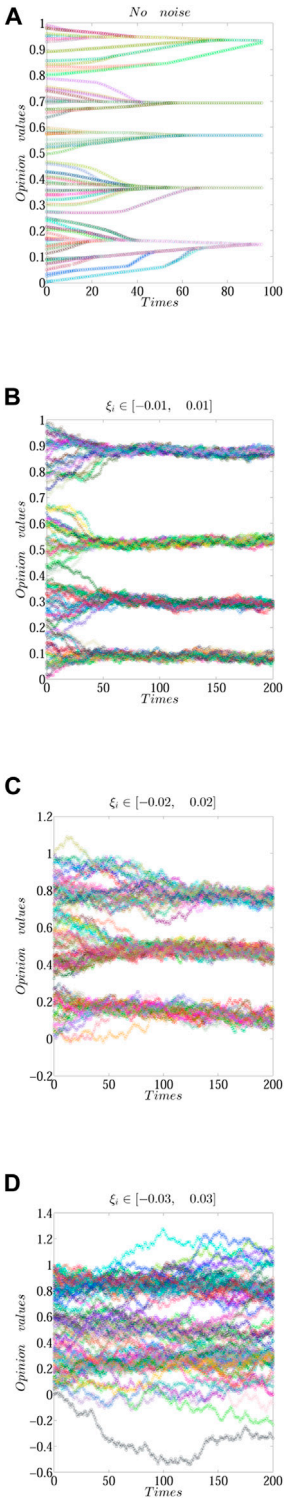

FIGURE 5
Opinion evolution result under different social noises, **(A)** No noise, **(B)** $\xi_i \in [-0.01,0.01]$, **(C)** $\xi_i \in [-0.02,0.02]$, and **(D)** $\xi_i \in [-0.03,0.03]$.

10.3389/fphy.2022.1042900

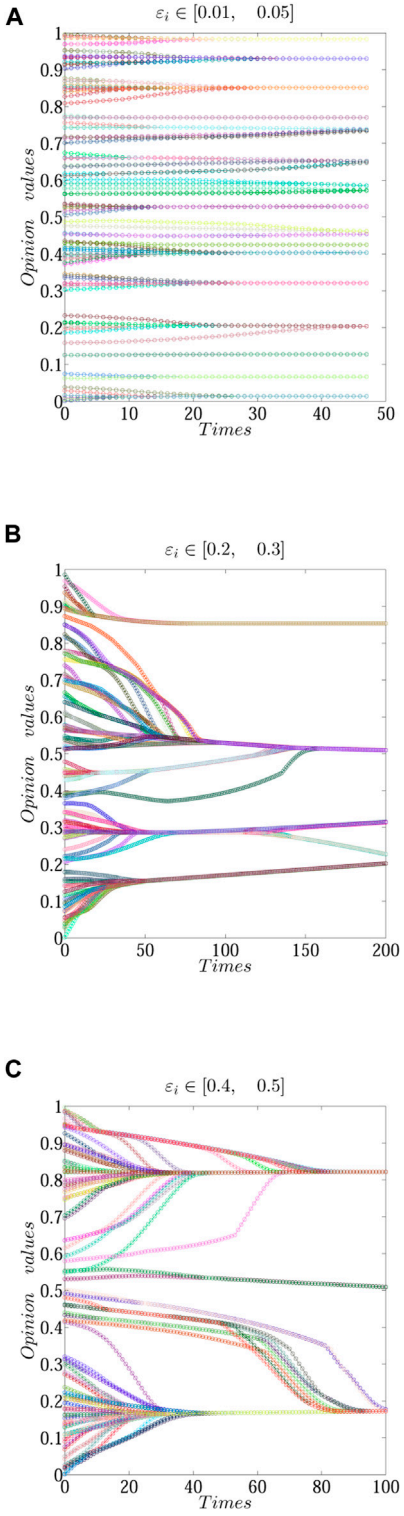

FIGURE 6
Opinion evolution result under different personnel heterogeneity, **(A)** $\varepsilon_i \in [0.01,0.05]$; **(B)** $\varepsilon_i \in [0.2,0.3]$; **(C)** $\varepsilon_i \in [0.4,0.5]$; **(A–C)** are the results of the opinion evolution.

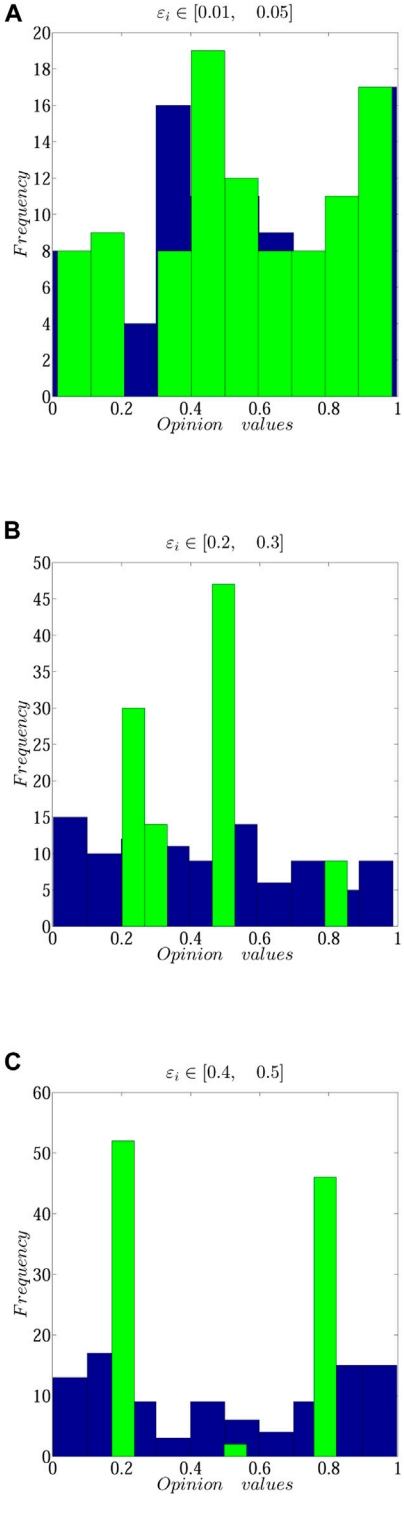

FIGURE 7
Opinion evolution result under different personnel heterogeneity, **(A)** $\varepsilon_i \in [0.01,0.05]$; **(B)** $\varepsilon_i \in [0.2,0.3]$; **(C)** $\varepsilon_i \in [0.4,0.5]$; **(A–C)** are the histograms of the opinion evolution.

noise distribution increases to [− 0.01, 0.01], the simulation result is shown in Figure 5B. As shown in Figure 5B, the number of final opinion clusters is 4. This result indicates that social noise can urge the people to form more consensus opinions. Furthermore, in Figure 5C, when the interval of social noise distribution increases to [− 0.02, 0.02], the number of the final opinion cluster is reduced from 4 to 3, and the opinion gets more close. As the social noise increases continuously, for example [− 0.03, 0.03], the simulation result is shown in Figure 5D. From Figure 5D, we can find that the final opinion is disorderly, dispersed, and inconsistent. The possible explanation is that social noise has a critical influence. When social noise is greater than the critical value, an individual's opinion will get dispersed. It also indicates that a phase transition exists under the influence of social influence. The aforementioned conclusions are also consistent with those of the research of Su et al.[43, 45].

4.5 Influence of personnel heterogeneity on opinion evolution

In the process of opinion evolution, because people have different characteristics, people react differently to opinions, that is to say, people's character has certain heterogeneity [50]. According to the heterogeneity, people can be divided into three types roughly: closed, easygoing, and open. We set the opinion thresholds $\varepsilon_i \in [0.01, 0.05]$, [0.2, 0.3], and [0.4, 0.5] separately. $\varepsilon_i \in [0.01, 0.05]$ indicates that people are closed; $\varepsilon_i \in [0.2, 0.3]$ indicates that people are easy-going; and $\varepsilon_i \in [0.4, 0.5]$ indicates that people are open. To explore the influence of different heterogeneity in the opinion evolution and keep other parameters unchanged, we perform the related simulations on the personnel heterogeneity. In addition, to make the evolution of ideas clearer, we also use the histogram to display the result of opinion evolution. The specific result is shown in Figures 6, 7.

As shown in Figures 6, 7, we can find that different heterogeneity can cause different evolution results. In Figure 6A, when the opinion threshold $\varepsilon_i \in [0.01, 0.05]$, it indicates that people are closed in the community. At this moment, the opinions will form nine clusters, and the convergence steps will stabilize at 49. We also find that the final opinion will distributed in [0, 1] almost uniformly in Figure 7A; From Figure 6B, when the opinion threshold increases continuously, for example, $\varepsilon_i \in [0.2, 0.3]$. This threshold indicates that people are easygoing in the community. The evolution result forms four opinion clusters, and convergence steps will stabilize at 200. The final opinions will be distributed around 0.5 in Figure 7B. In Figure 6C, when the opinion threshold $\varepsilon_i \in [0.4, 0.5]$, it indicates that people are open in the community, the opinions will form three opinion clusters, and the steps will stabilize at 200. The final opinions are distributed around 0.2 and 0.8 in Figure 7C. At this moment, people's opinions are easier to form an agreement.

5 Discussion

Opinion dynamics has been explored by most scholars in recent years [51–53]. However, few researchers explored the opinions of affinity and social noise systematically. As a kind of social influence, affinity and social noise affect an individual's opinion and have an impact on others and the environment. Considering the aforementioned two factors, this study built an affinity and social noise Hegselmann–Krause model and explored the influence of affinity, the threshold of affinity, social noise, and personnel heterogeneity on opinion dynamics. The research result will extend the boundary of opinion dynamics and has certain practical significance. First, affinity has a positive effect on opinion dynamics. If the affinity among individuals increases, the opinion will quickly tend to be consistent. Compared with the HK model, the affinity can accelerate the integration and alignment of opinions. Thus, affinity is important to be considered in opinion evolution. Second, social noise has a critical influence on opinion dynamics. Within a certain range, when the social noise increases, the opinions will be convergent. Once the social noise exceeds the critical value, the opinions will be divergent [44], implying that social noise has an important influence on opinion dynamics, and it should be reasonably controlled and guided in public opinion management. Third, personnel heterogeneity has different effects on opinion evolution. When the opinion evolves, public opinion management should develop individualized strategies for guiding public opinion, as the heterogeneity of groups can affect the evolution of opinions.

6 Conclusion

Group opinion evolution is an interesting research topic. At present, scholars have carried out some research about it. However, few types of research focus on the influence of affinity and social noise comprehensively. Based on the Hegselmann–Krause model of opinion dynamics, this study constructs the ASNHK model by introducing affinity and social noise from the perspective of social influence. Then, it explores the influence of affinity degree, affinity threshold, social noise, and personnel heterogeneity on opinion evolution. The results show that first of all, affinity between people can improve the opinion to form a consensus positively, but the affinity threshold has a negative role on the contrary. When people's affinity increases, it is easier for them to form an agreement on their opinions. Moreover, when the social noise increases, the opinions will form a consensus. When it increases to a certain value, the opinions will get decentralized. Furthermore, personnel heterogeneity has different effects on opinion evolution. Open-minded individuals are more likely to form a consistent opinion, while closed-minded personalities make it difficult to form a consensus. The research extends the opinion

dynamics from social influence and will shed light on the interdisciplinary study of psychology, sociology, and opinion evolution dynamics.

This study explored opinion evolution based on the social influence theory. It introduced the affinity and social noise in the opinion dynamics model. In this research, the influence of affinity degree, affinity threshold, social noise, and personnel heterogeneity on opinion evolution is discussed. Although we obtained some valuable conclusions, there are still some limitations given as follows. First, in terms of research content, this study explored the influence of affinity, social noise, and personnel heterogeneity on opinion evolution. However, it does not consider the network structure of people. Different network structures of people may have a different social influence on opinion evolution. Thus, in the future, the network structures of people will be introduced to the model. Second, this study constructed a new model based on social influence theory and carried out some simulation analysis. However, no algebraic analysis was carried out. Future work will focus on the numerical analysis, and some convergence values will be calculated. Third, although some simulation analyses are mentioned in this article, the real data need to be considered in the opinion evolution. Future work will use real opinion data from some media to explore opinion evolution.

Overall, this research explored the model of opinion dynamics from social influence and provided some theoretical and practical insights for the following research. In theory, this study introduced the affinity and social noise in the Hegselmann–Krause model of opinion dynamics, provided a new perspective on the social influence theory, and enriched the application of this theory to opinion dynamics. In practice, this study explained the mechanism of influence of affinity in interpersonal relationships and social noise from the external environment. It provided some methods for managing public opinion; for example, improving interpersonal relationships and affinity between people can be conducive to a convergence of opinions. Moreover, reasonable control of external noise can facilitate a consistent opinion. In conclusion, this research can provide some new perspectives on the study of opinion dynamics and public opinion management.

Data availability statement

The original contributions presented in the study are included in the article/Supplementary Material; further inquiries can be directed to the corresponding authors.

Author contributions

JL: conceptualization, methodology, software, writing—original draft, and investigation. JH: methodology, supervision, and validation. ZQ: methodology and Investigation. SH: supervision and validation.

Funding

This work was supported by the National Natural Science Foundation Project (grant no. 71871144) and the Science and Technology Development Program of the University of Shanghai for Science and Technology (grant no. 2020KJFZ046).

Conflict of interest

The authors declared that there was no competing financial interest, all authors made substantial contributions and agreed to the final manuscript.

Publisher's note

All claims expressed in this article are solely those of the authors and do not necessarily represent those of their affiliated organizations, or those of the publisher, the editors, and the reviewers. Any product that may be evaluated in this article, or claim that may be made by its manufacturer, is not guaranteed or endorsed by the publisher.

References

1. Zhu J, Yao Y, Tang W, Zhang H. An agent-based model of opinion dynamics with attitude-hiding behaviors. *Physica A: Stat Mech its Appl* (2022) 603:127662. doi:10.1016/j.physa.2022.127662

2. Shang L, Zhao M, Ai J, Su Z. Opinion evolution in the sznajd model on interdependent chains. *Physica A: Stat Mech its Appl* (2021) 565:125558. doi:10.1016/j.physa.2020.125558

3. Hou J, Li W, Jiang M. Opinion dynamics in modified expressed and private model with bounded confidence. *Physica A: Stat Mech its Appl* (2021) 574:125968. doi:10.1016/j.physa.2021.125968

4. Weimer CW, Miller J, Hill RR, Hodson DD. An opinion dynamics model of meta-contrast with continuous social influence forces. *Physica A: Stat Mech its Appl* (2022) 589:126617. doi:10.1016/j.physa.2021.126617

5. Botte N, Ryckebusch J, Rocha LE. Clustering and stubbornness regulate the formation of echo chambers in personalised opinion dynamics. *Physica A: Stat Mech its Appl* (2022) 599:127423. doi:10.1016/j.physa.2022.127423

6. Hegselmann R, Krause U. Opinion dynamics and bounded confidence models, analysis and simulation. *J Artif Societies Soc Simulation* (2002) 5:1–2.

7. Su W, Gu Y, Wang S, Yu Y. Partial convergence of heterogeneous Hegselmann-Krause opinion dynamics. *Sci China Technol Sci* (2017) 60:1433–8. doi:10.1007/s11431-016-0615-x

8. Zhao Y, Zhang L, Tang M, Kou G. Bounded confidence opinion dynamics with opinion leaders and environmental noises. *Comput Operations Res* (2016) 74:205–13. doi:10.1016/j.cor.2015.07.022

9. Jiang L, Liu J, Zhou D, Zhou Q, Yang X, Yu G. Predicting the evolution of hot topics: A solution based on the online opinion dynamics model in social network. *IEEE Trans Syst Man Cybern Syst* (2018) 50:3828–40. doi:10.1109/TSMC.2018.2876235

10. Deffuant G, Neau D, Amblard F, Weisbuch G. Mixing beliefs among interacting agents. *Adv Complex Syst* (2000) 03:87–98. doi:10.1142/S0219525900000078

11. Zhang J, Hong Y. Opinion evolution analysis for short-range and long-range Deffuant–Weisbuch models. *Physica A: Stat Mech its Appl* (2013) 392:5289–97. doi:10.1016/j.physa.2013.07.014

12. Chen G, Su W, Mei W, Bullo F. Convergence properties of the heterogeneous Deffuant–Weisbuch model. *Automatica* (2020) 114:108825. doi:10.1016/j.automatica.2020.108825

13. Luo Y, Li K, Sun C, Cheng C. Adapted deffuant–weisbuch model with implicit and explicit opinions. *Physica A: Stat Mech its Appl* (2022) 596:127095. doi:10.1016/j.physa.2022.127095

14. Schawe H, Laura H. Higher order interactions destroy phase transitions in deffuant opinion dynamics model. *Commun Phys* (2022) 5:32–9. doi:10.1038/s42005-022-00807-4–

15. Sznajdweron K, Sznajd J. Opinion evolution in closed community. *Int J Mod Phys C* (2000) 11:1157–65. doi:10.1142/S0129183100000936

16. Araujo MS, Vannucchi FS, Timpanaro AM, Prado CPC. Mean-field approximation for the Sznajd model in complex networks. *Phys Rev E* (2015) 91:022813. doi:10.1103/PhysRevE.91.022813

17. Karan FSN, Srinivasan AR, Chakraborty S. Modeling and numerical simulations of the influenced Sznajd model. *Phys Rev E* (2017) 96:022310. doi:10.1103/PhysRevE.96.022310

18. Calvelli M, Crokidakis N, Penna TJ. Phase transitions and universality in the sznajd model with anticonformity. *Physica A: Stat Mech its Appl* (2019) 513:518–23. doi:10.1016/j.physa.2018.09.023

19. Hsu J, Huang D. Mean-field theory of modified voter model for opinions. *Physica A: Stat Mech its Appl* (2014) 416:371–7. doi:10.1016/j.physa.2014.09.009

20. Tang S, Yan S, Pei S, Zheng Z. Evolutionary dynamics of the weighted voter model with opinion strength on complex networks. *J Korean Phys Soc* (2015) 66:1783–8. doi:10.3938/jkps.66.1783

21. Klamser PP, Wiedermann M, Donges JF, Donner RV. Zealotry effects on opinion dynamics in the adaptive voter model. *Phys Rev E* (2017) 96:052315. doi:10.1103/PhysRevE.96.052315

22. Pasi G, Yager RR. Modeling the concept of majority opinion in group decision making. *Inf Sci* (2006) 176:390–414. doi:10.1016/j.ins.2005.07.006

23. Vilela ALM, Stanley HE. Effect of strong opinions on the dynamics of the majority-vote model. *Sci Rep* (2018) 8:8709. doi:10.1038/s41598-018-26919-y

24. Javarone MA. Social influences in opinion dynamics: The role of conformity. *Physica A: Stat Mech its Appl* (2014) 414:19–30. doi:10.1016/j.physa.2014.07.018

25. Nowak A, Szamrej J, Latané B. From private attitude to public opinion: A dynamic theory of social impact. *Psychol Rev* (1990) 97:362–76. doi:10.1037/0033-295x.97.3.362

26. Dou R, Zhang Y, Nan G. Iterative product design through group opinion evolution. *Int J Prod Res* (2017) 55:3886–905. doi:10.1080/00207543.2017.1316020

27. Zhu M, Xie G. Leader's opinion priority bounded confidence model for network opinion evolution. In: AIP Conference Proceedings (2017). p. 020060. 1864. doi:10.1063/1.4992877

28. Glass CA, Glass DH. Opinion dynamics of social learning with a conflicting source. *Physica A: Stat Mech its Appl* (2021) 563:125480. doi:10.1016/j.physa.2020.125480

29. Bernardo C, Altafini C, Vasca F. Finite-time convergence of opinion dynamics in homogeneous asymmetric bounded confidence models. *Eur J Control* (2022) 100674. doi:10.1016/j.ejcon.2022.100674

30. Lanchier N, Li H-L. Consensus in the hegselmann–krause model. *J Stat Phys* (2022) 187:20–13. doi:10.1007/s10955-022-02920-8

31. Dong Y, Zhan M, Kou G, Ding Z, Liang H. A survey on the fusion process in opinion dynamics. *Inf Fusion* (2018) 43:57–65. doi:10.1016/j.inffus.2017.11.009

32. Li C-Y. Persuasive messages on information system acceptance: A theoretical extension of elaboration likelihood model and social influence theory. *Comput Hum Behav* (2013) 29:264–75. doi:10.1016/j.chb.2012.09.003

33. Kaur R, Kumar R, Bhondekar AP, Kapur P. Human opinion dynamics: An inspiration to solve complex optimization problems. *Sci Rep* (2013) 3:3008–7. doi:10.1038/srep03008

34. Diao S-M, Liu Y, Zeng Q-A, Luo G-X, Xiong F. A novel opinion dynamics model based on expanded observation ranges and individuals' social influences in social networks. *Physica A: Stat Mech its Appl* (2014) 415:220–8. doi:10.1016/j.physa.2014.07.072

35. Lu X, Mo H, Deng Y. An evidential opinion dynamics model based on heterogeneous social influential power. *Chaos, Solitons & Fractals* (2015) 73:98–107. doi:10.1016/j.chaos.2015.01.007

36. Glass CA, Glass DH. Social influence of competing groups and leaders in opinion dynamics. *Comput Econ* (2021) 58:799–823. doi:10.1007/s10614-020-10049-7

37. Franco B, Carletti T, Duccio F, Alessio G, Andrea G. Dynamical affinity in opinion dynamics modeling. *Phys Rev E* (2007) 76:066105. doi:10.1103/PhysRevE.76.066105

38. Blattner M, Zhang Y, Maslov S. Exploring an opinion network for taste prediction: An empirical study. *Physica A: Stat Mech its Appl* (2007) 373:753–8. doi:10.1016/j.physa.2006.04.121

39. Carletti T, Fanelli D, Guarino A, Bagnoli F, Guazzini A. Birth and death in a continuous opinion dynamics model. *Eur Phys J B* (2008) 64:285–92. doi:10.1140/epjb/e2008-00297-3

40. Ishii A, Okano N, Nishikawa M. Social simulation of intergroup conflicts using a new model of opinion dynamics. *Front Phys* (2021) 9:640925. doi:10.3389/fphy.2021.640925

41. Abrica-Jacinto NL, Kurmyshev E, Juárez HA. Effects of the interaction between ideological affinity and psychological reaction of agents on the opinion dynamics in a relative agreement model. *J Artif Soc Soc Simul* (2017) 20:1–12. doi:10.18564/jasss.3377

42. Pineda M, Toral R, Hernández-García E. The noisy hegselmann-krause model for opinion dynamics. *Eur Phys J B* (2013) 86:490–10. doi:10.1140/epjb/e2013-40777-7

43. Su W, Chen G, Hong Y. Noise leads to quasi-consensus of Hegselmann–Krause opinion dynamics. *Automatica* (2017) 85:448–54. doi:10.1016/j.automatica.2017.08.008

44. Wang C, Li Q, Weinan E, Chazelle B. Noisy hegselmann-krause systems: Phase transition and the 2R-conjecture. *J Stat Phys* (2016) 166:1209–25. doi:10.1007/s10955-017-1718-x

45. Su W, Guo J, Chen X, Chen G, Li J. Robust fragmentation modeling of Hegselmann–Krause-type dynamics. *J Franklin Inst* (2019) 356:9867–80. doi:10.1016/j.jfranklin.2019.09.012

46. Mansouri A, Taghiyareh F. Phase transition in the social impact model of opinion formation in log-normal networks. *J Inf Syst Telecommunication* (2021) 1:1–14. doi:10.52547/jist.9.33.1

47. Vaidya T, Chotibut T, Piliouras G. Broken detailed balance and non-equilibrium dynamics in noisy social learning models. *Physica A: Stat Mech its Appl* (2021) 570:125818. doi:10.1016/j.physa.2021.125818

48. Liu Y, Mo L. Noise-induced truth seeking of heterogeneous Hegselmann-Krause opinion dynamics. *Adv Math Phys* (2018) 2018:1–6. doi:10.1155/2018/8702152

49. Su W, Wang X, Chen G, Yu Y, Hadzibeganovic T. Noise-based synchronization of bounded confidence opinion dynamics in heterogeneous time-varying communication networks. *Inf Sci* (2020) 528:219–30. doi:10.1016/j.ins.2020.04.018

50. Su J, Liu B, Li Q, Ma H. Trust, evolution, and consensus of opinions in a social group. *Acta Phys Sin* (2014) 63:050501. doi:10.7498/aps.63.050501

51. Liang H, Li C, Dong Y, Jiang Y. The fusion process of interval opinions based on the dynamic bounded confidence. *Inf Fusion* (2016) 29:112–9. doi:10.1016/j.inffus.2015.08.010

52. Dong Y, Chen X, Liang H, Li C. Dynamics of linguistic opinion formation in bounded confidence model. *Inf Fusion* (2016) 32:52–61. doi:10.1016/j.inffus.2016.03.001

53. Li K, Liang H, Kou G, Dong Y. Opinion dynamics model based on the cognitive dissonance: An agent-based simulation. *Inf Fusion* (2020) 56:1–14. doi:10.1016/j.inffus.2019.09.006

frontiers | Frontiers in Physics

TYPE Original Research
PUBLISHED 15 November 2022
DOI 10.3389/fphy.2022.1044919

OPEN ACCESS

EDITED BY
Xuzhen Zhu,
Beijing University of Posts and Telecommunications (BUPT), China

REVIEWED BY
Qiong Hu,
University of Colorado Denver, United States
Fei Gao,
Shanghai Jiao Tong University, China
Xinning Wang,
Ocean University of China, China

*CORRESPONDENCE
Wenjing Yan,
yanwenjing@butbu.edu.cn

SPECIALTY SECTION
This article was submitted to Social Physics, a section of the journal Frontiers in Physics

RECEIVED 15 September 2022
ACCEPTED 27 October 2022
PUBLISHED 15 November 2022

CITATION
Zhang Q, Wei S, Li Z and Yan W (2022), Combining NSP and NER for public opinion event extraction model. *Front. Phys.* 10:1044919. doi: 10.3389/fphy.2022.1044919

Combining NSP and NER for public opinion event extraction model

Qingchuan Zhang, Siwei Wei, Zihan Li and Wenjing Yan*

National Engineering Research Centre for Agri-Product Quality Traceability, Beijing Technology and Business University, Beijing, China

Event extraction in the field of public opinion aims to extract important event arguments and their corresponding roles from the moment-to-moment generated opinion reports. Most of the existing research methods divide the task into three subtasks: event trigger extraction, event type detection, and event argument extraction. Despite the remarkable achievements of the event argument extraction paradigm combining part-of-speech (POS) and event trigger features, the performance of POS features in combinatorial event argument extraction tasks is struggling due to its inherent semantic diversity in Chinese. In addition, previous research work ignored the deep semantic interaction between event trigger and text. To address the aforementioned problems, this paper proposes an opinion event extraction model (NN-EE) combining NSP and NER, which alleviates the lack of performance of combinatorial event argument extraction by introducing NER technology. Meanwhile, the event trigger features are incorporated into the NSP mechanism of the pre-trained language model BERT to prompt the model to learn the deep semantic interaction between the event trigger and original text. The results of the self-constructed food opinion report dataset (FD-OR) in this paper show that the NN-EE model achieves optimal performance.

KEYWORDS

event extraction, event argument extraction, NSP, NER, BERT

1 Introduction

With the rapid development of the Internet, more and more people choose to share what they see and hear around them through social media. In the face of massive data dissemination, quickly, accurately, and automatically extracting event types and their core arguments from the data has become an urgent problem in the field of public opinion event analysis. A key technology in the field of information extraction, event extraction has attracted extensive attention in recent years, aiming at identifying event types from unstructured texts and extracting important arguments with different roles from them manually or automatically. As shown in Figure 1, for a given input text, the event extraction model first identifies the event trigger "Crack down" contained in the text and uses this as an important clue to judge the event type the text belongs to: "Counterfeit." Then, using the previously identified trigger "Crack down" and the named entities

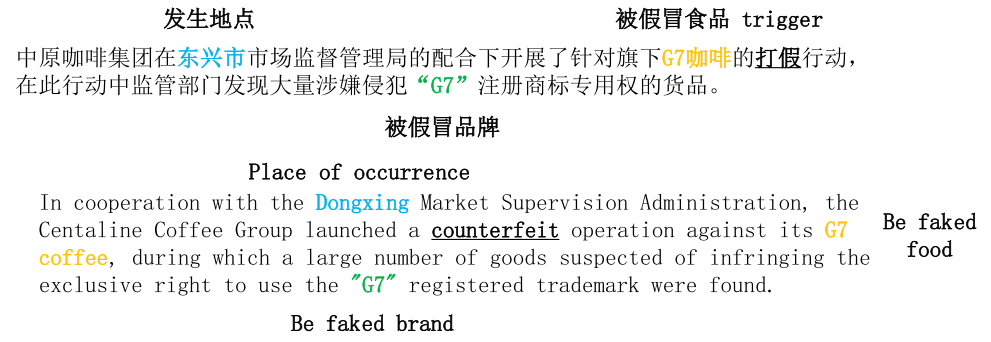

FIGURE 1
Example of event extraction task. There is a “Counterfeit” event in this text, where “Crack down” is an event trigger, and other colored and bold words are important arguments in “Counterfeit” events, with their corresponding roles in bold font mentioned previously.

identified in the text as clues, the event argument and their corresponding roles of the event “Counterfeit” is extracted from the text by the event argument extraction model, that is, {“Place of occurrence”: “Dongxing,” “Counterfeit food”: “G7coffee,” “Counterfeit brand”: “G7”}.

To automatically extract the core event arguments and their corresponding roles from the text, most of the early research methods used the pipeline-based event extraction framework [1–4]. Under this framework, the task was divided into three subtasks, event trigger extraction, event type extraction, and event argument extraction. Although the pipeline-based framework has good flexibility, the results of event argument extraction tasks are completely dependent on the performance of the event trigger extraction task. At the same time, because the execution of the three subtasks is completely independent, the error propagation between models is irreversible, and the model has a serious error accumulation problem.

In view of the aforementioned problems of the pipeline framework, in recent years, a large number of end-to-end joint event extraction frameworks have been proposed and have achieved excellent performance [5–9]. The extraction of event triggers and event arguments can be performed simultaneously by the joint framework. Although this framework can avoid the error accumulation problem, to the best of our knowledge, none of the joint frameworks make good use of semantic dependencies and ignore the relationship between event triggers and event arguments.

Currently, neural networks are widely used in the research of event extraction tasks, and by introducing pre-trained models, syntactic features, and semantic features, the performance of neural network models has been continuously improved, and they even perform well on multilingual event extraction tasks [11–15]. However, the POS feature, a grammatical feature commonly used in event extraction, does not perform well in the task of extracting combined event arguments in the Chinese text [3].

In this paper, we propose a novel approach to use the triggers from the already well-performing event-triggered word extraction task with the original text as input to the NSP task by the NSP mechanism, thus prompting the model to learn the deep semantic interactions between the event trigger and original text. In addition, we also introduce the named entity recognition (NER) technology to solve the problem that the model does not perform well for combinatorial event argument extraction in Chinese. In turn, an event extraction framework combining Next Sentence Predict (NSP) and NER is developed, which solves the difficulty that the commonly used POS features make it difficult for the model to accurately identify Chinese combinatorial event arguments and deep semantic interaction between event trigger features and text. Extensive comparative experiments were conducted on the self-constructed dataset, and the results show that the NN-EE model proposed in this paper achieves optimal performance, proving the effectiveness of the event extraction model combining the NSP mechanism with the NER technique, and the model performance is improved.

The main contributions of this paper are summarized as follows:

(1) In this paper, we proposed an event argument extraction model combining the NSP mechanism to deepen the deep semantic interaction between event triggers and text by introducing the NSP mechanism.
(2) Unlike previous research methods that only use POS features to stitch with word-embedding vectors, this paper stitches entity-type label-embedding vectors with word-embedding vectors, which can significantly improve the accuracy of the event argument extraction model in identifying Chinese combinatorial event arguments.
(3) In this paper, we constructed a dataset for the food opinion reporting domain (FD-OR) with a complex syntactic structure and wide semantic coverage of the corpus, and our model achieves optimal performance on this dataset.

2 Related work

Previous research work can be divided into two frameworks according to different stages of task execution, one is the pipeline framework and the other is the joint framework.

2.1 Pipeline framework

DMCNN framework: Ref. [2] proposed a method based on a dynamic multi-pooling convolutional neural network (DMCNN), which uses dynamic multi-pooling layers according to event triggers and candidate arguments to capture sentence-level clues without using complex NLP tools and more comprehensively retain information. However, this method is not flexible enough to cope with the situation where there is only one event in a sentence but multiple occurrences of the same trigger, which often occurs in real texts.

QA-based framework: Proposed a method to transform event trigger extraction and event argument extraction into a question answering (QA) task to extract event arguments in an end-to-end manner. This method can extract event arguments that appear during training. Meanwhile, Ref. [4] proposed a method to transform the event extraction task into a multi-round question-and-answer task. Ref. [13] proposed a method to transform the event extraction task into a machine reading comprehension task. However, they all ignored the deep semantic interaction between event triggers and original text.

2.2 Joint framework

JMEE framework: Ref. [14] proposed a novel multiple-event extraction (JMEE) framework. By introducing synchronous shortcut arcs to enhance information flow and an attention-based graph convolution network to simulate graph information, multiple event triggers and parameters and their roles can be jointly extracted. However, the joint framework mentioned above makes good use of semantic dependencies and ignores the deep relationship between event triggers and event arguments.

Cas EE framework: Ref. [15] proposed a method to extract overlapping events by cascading decoding. This method carries out event type detection, event trigger extraction, and event parameter extraction in turn, in which all subtasks learn together in a framework, so that the dependency between subtasks can be captured, which successfully solves the overlapping problem in event extraction. Meanwhile, Ref. [16] proposed a deep learning model using a bidirectional recurrent neural network (RNN) to induce shared hidden representations of words in sentences for all three subtasks, and the method could improve the performance of event extraction using the interactions between subtasks. However, while all the aforementioned models learn deep relationships between event triggers and text, no other semantic or syntactic features are used to improve the overall performance of the models.

3 Methods

The purpose of EE is to extract event triggers and detect the event types, event arguments, and their corresponding roles contained in a sentence. In this paper, the event extraction task is modeled using the pipeline framework and is divided into three subtasks: event trigger extraction, event type detection, and event argument extraction.

In this paper, the event type detection task is considered a multi-label classification task and the event trigger extraction task as a NER task. This paper also uses the BERT–BLSTM model combining the sigmoid function as the event type detection model and the BERT–BLSTM–CRF model as the event trigger extraction model, which has been shown to perform excellently in previous NER tasks [17]. The models for both of these tasks already have F1 values above 99% on the FD-OR dataset constructed in this paper, and there is little room for further optimization. Therefore, in this study, we only optimize the event argument extraction models with poorer performance. This study mitigates the lack of performance of combinatorial event argument recognition in the event argument extraction task by introducing the NER technique; at the same time, by incorporating event triggers into the NSP mechanism of the pre-trained language model Bidirectional Encoder Representations from Transformer (BERT) [18], the event argument extraction model is motivated to learn the deep semantic interactions between the event trigger and the original text. The improvement in performance of the event argument extraction model is achieved by the aforementioned method.

Denoted by $S = \{c_1, c_2, c_3, \ldots, c_n\}$, a sentence of length n, where c_i denotes the *i*th character; by $E = \{e_1, e_2, e_3, \ldots, e_k\}$, the k entities in the sentence, where k is the total number of entities in the sentence; by $V = \{v_1, v_2, \ldots, v_m\}$, the m events in the sentence, where m is the total number of events occurring in the sentence; by T the event trigger word corresponding to the m events in the sentence; and by using BIO annotation to label each token c_i with corresponding label y_i, to indicate the case where the event argument corresponding to the event type consists of one or more consecutive characters.

The NN-EE model proposed in this paper is an improvement on the BERT–BLSTM–CRF model, which consists of the following two main modules: (i) char encoder, which represents sentences with vectors and improves the performance of the model for combinatorial event argument extraction by introducing the entity type label feature; (ii) the event argument extraction decoder, which enhances the model's learning of deep semantic interactions between the event trigger and the original text by using event

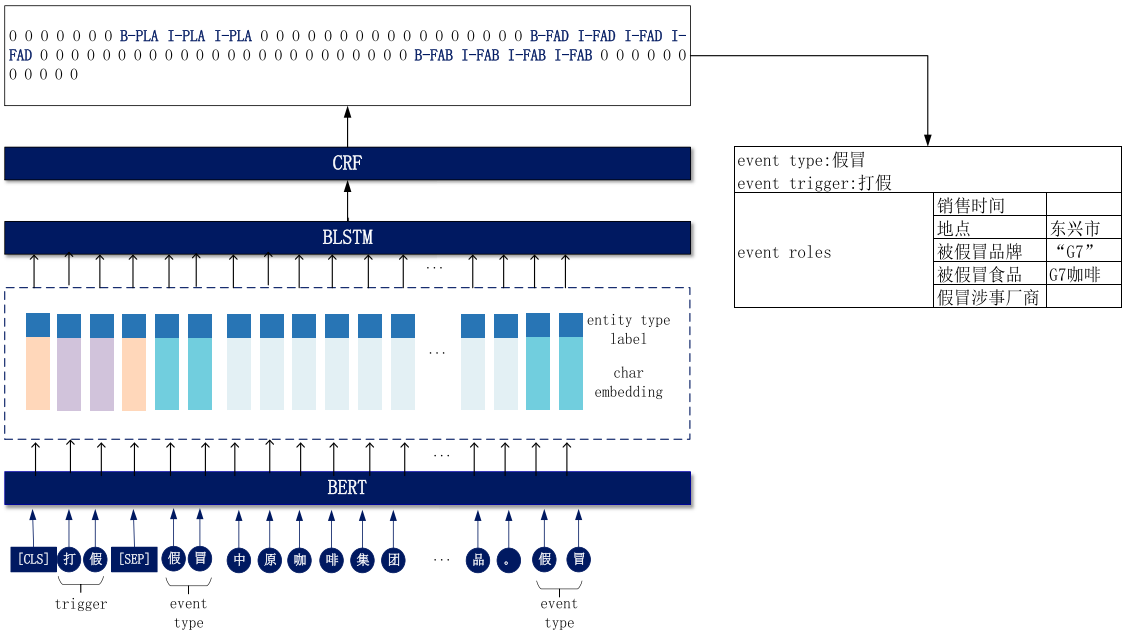

FIGURE 2
Structure diagram of the event argument extraction model. It illustrates the event argument extraction process for one sentence.

triggers as the text1 of the NSP mechanism. We first obtained the encoding of the input text through the BERT layer and stitch it with the NER features, and finally got the current event type corresponding to the event arguments and its role through the BLSTM + CRF layer, as shown in Figure 2.

3.1 Char encoder

In the char encoder, the char embedding corresponding to each token c_i in the sentence is obtained by the BERT pre-training model. In order to solve the problem of unsatisfactory performance in the event extraction task for the recognition of combinatorial event arguments in Chinese, this paper splices the char embedding with the entity-type label-embedding vector, thus transforming c_i into a real-valued vector x_i.

- Character vector for c_i: When a character passes through the BERT model, character vectors $Z = \{z_1, z_2, z_3, \ldots, z_n\}$ are generated, as shown in the following equation:

$$Z = \{z_1, z_2, z_3, \ldots, z_n\} = \text{BERT encoder}(S). \quad (1)$$

where $S = \{c_1, c_2, \ldots, c_n\}$, is a sentence of length n.

- Entity-type label feature for c_i: This is used to extract the required entity types by using the public NER model in the open-source Chinese natural language processing tool HanLP to identify the event arguments that occur in the sentence. The entities appearing in the sentence are then labeled with their entity type at the position corresponding to the characters, and “O” at other positions. The entity type labels are then transformed by the embedding layer into a real-valued vector $B = \{b_1, b_2, b_3, \ldots, b_n\}$.

Then, the method of obtaining the representation X of the token used for argument extraction is needed, as shown in the following equation:

$$X = [Z; B], \quad (2)$$

where [-;-] denotes the splicing of the vectors.

The conversion x_i from token c_i to a real-valued vector is to convert the input sentence $S = \{c_1, c_2, c_3, \ldots, c_n\}$ into a string of real-valued vectors $X = \{x_1, x_2, x_3, \ldots, x_n\}$. The sentence vectors are then used as input to the next model in turn, so that the model learns a more efficient vector representation for the event argument extraction task.

3.2 Event argument extraction decoder

In order to enhance the connection between the preceding and following subtasks in the pipeline framework, this paper uses the output of the event trigger extraction task and the event type detection task as priori knowledge to play a role in the event argument extraction task. In this paper, we use the BIO annotation method to annotate each c_i in a sentence with its corresponding label y_i.

In this paper, the BLSTM–CRF model is used to complete the decoding of the event argument extraction task, and the aforementioned real-valued vector $X = \{x_1, x_2, x_3, \ldots, x_n\}$ is the input of the BLSTM layer. After the BLSTM layer outputs the hidden layer vector $H = \{h_1, h_2, h_3, \ldots, h_n\}$, the vector dimension is changed to the total number of label categories to be identified through the fully connected layer, thus obtaining the input $P = \{p_1, p_2, p_3, \ldots, p_n\}$ of the CRF layer. The output of the fully connected layer can only obtain the relationship between $S = \{c_1, c_2, c_3, \ldots, c_n\}$ and the tagged BIO labels, but lacks the consideration of the relationship between BIO labels, thus some invalid BIO labels are predicted. With the conditional random field (CRF) method, the predicted BIO tags can be constrained to reduce the probability of predicting invalid BIO tags, and the final output is a sequence of tags $L = \{l_1, l_2, l_3, \ldots, l_n\}$ consisting of each token c_i corresponding to tag l_i predicted by the model. The loss function of the model is as shown in the following equation:

$$LOSS = \sum_{i=1}^{n} l(CRF(p_i), y_i), \tag{3}$$

where $l(CRF(p_i), y_i)$ is the negative log *likehood* of the comparison between the predicted value $CRF(p_i)$ of the entity model and the true value y_i of the sequence labeling.

To improve the precision of the BLSTM–CRF model in extracting event arguments corresponding to event types, in this paper, event type names are spliced on both sides of the original sentence and encoded as part of the input sentence. By acting through the BLSTM layer, the event type names on both sides of the input sentence cause the hidden layer vectors corresponding to the characters in the original sentence to learn information about the event type, thus improving the overall performance of the model.

Because in the FD-OR constructed in this study, important event arguments often appear before and after the trigger (Figure 1), "Counterfeit food" appears at a position one character away from the trigger word, making deep semantic interaction between the event trigger word and the original sentence, which is crucial to improve the performance of event argument extraction.

TABLE 1 Pre-defined event schema of FD-OR.

Event type	Event role
Counterfeit (fake)	Sales time (sell time), (place), counterfeit brand (be faked brand), counterfeit food (be faked food), and fake the manufacturer involved (fake factory)
Exceed the standard (exceeded)	Sales time (sell time), (place), counterfeit brand (over standard food), counterfeit food (over standard item), and manufacturers involved in exceeding the standard (over standard factory)
Presence of foreign body (have foreign substance)	Sales time (sell time), (place), presence of foreign body food (food with foreign substance), foreign body present (foreign substance), and manufacturers involved in foreign bodies (foreign substance-related factory)

In order to solve the challenge, this paper introduces the approach of combining the NSP task in BERT to capture the relationship between the event trigger and the original sentence as mentioned in Ref. [10]. The NSP task in the BERT model is to predict whether two sentences are preceding or following sentences, and the similarity between two sentences text1 and text2 is calculated by the text similarity task; if they are similar, then it is considered that text2 is the next sentence of text1, and *vice versa*. In this process, the long-distance interdependent features in the sentences are captured by BERT's multi-headed self-attention mechanism, which enables deep semantic interaction between text1 and text2 and captures the relationship between text1 and text2. The attention formula is:

$$\text{Attention}(Q, K, V) = \text{softmax}\left(\frac{QK}{\sqrt{d_k}}\right)V, \tag{4}$$

where Q (query) is the query vector, K (key) is the queried vector, V (value) is the content vector, and d_k is the dimensionality of Q,K. In the self-attention mechanism, Q is x_i and K, V is $X = \{x_1, x_2, x_3, \ldots, x_n\}$. Multi-headed self-attention is a mechanism that divides Q, K, and V into multiple branches to learn different features.

There are two special symbols [CLS] and [SEP] in BERT. [CLS] indicates that the feature is used in a classification model; for non-classification models, this symbol can be omitted. The [SEP] symbol is used to break the two sentences of text1 and text2 of the input. After splicing the event argument names and performing the input processing for the NSP task in this paper, the input to the model is shown in Figure 2.

The NSP task is applied to the proposed event argument extraction model by using the event trigger word as text1 in the NSP task and the original sentence as text2. The NSP task enables deep semantic interaction between the event trigger and the original sentence, thus improving the performance of the event argument extraction model. In addition, the entity type labels of the two parts mentioned previously are complemented with "O" for the corresponding characters.

4 Experimental results

4.1 Experimental dataset

In this paper, Chinese food opinion report data were constructed as the experimental dataset. The corpus of news reports in the experimental dataset was particularly sourced from China Quality News Network, which is under the supervision of the State Administration for Market Regulation of China, and the

TABLE 2 Experimental dataset.

Dataset		Training	Validation	Test	Event type
FD-OR	Number of sentences	1800	257	514	3
	Avg event argument	3	2	3	-

Chinese mainstream news platforms Baidu News and Today's Headlines. The dataset is available at http://180.76.244.155:8080/FD-OR.zip. Three event types were included in the dataset. Different event types corresponding to different event arguments are as shown in Table 1.

In the ratio of 7:2:1, the experimental dataset is divided into three parts: training set, testing set, and validation set. The specific dataset division is shown in Table 2.

Another dataset is the food safety news reports dataset (FD-SR). Five event types were included in the dataset. Different event types corresponding to different event arguments are shown in Table 3.

TABLE 3 Pre-defined event schema of FD-SR.

Event type	Event role
Food sampling announcement	(food name), (time), (testing unit), and (units involved)
Malignant emergencies	(time), (position), (consequences), (number of people affected), and (units involved)
Food quality defects	(food name), (manufacturer), (quality defects), and (food purchase source)
Production environment exposure	(time), (place), (unit involved), (type of production environment), and (exposure issues)
Off-line dining complaints	(time), (place), (unit involved), (complaint food), and (complaint type)

4.2 Evaluation standard setting

In this paper, the experimental results of precision, recall, and F1 score are used as model performance measures.

The formula for calculating the precision is:

$$P = \frac{TP}{TP + FP}, \tag{5}$$

where TP indicates the number of classes that are themselves positive and that the model correctly predicts as positive, and FP indicates the number of classes that are themselves negative and that the model predicts as positive.

The formula for calculating the recall is:

$$R = \frac{TP}{TP + FN}, \tag{6}$$

where TP is the same as the aforementioned formula and FN indicates the number of classes that are themselves positive but that the model predicts as negative.

The formula for calculating the F1 score is:

$$F1 = \frac{P^*R^*2}{P + R}. \tag{7}$$

The FD-OR constructed in this paper is a balanced dataset, and precision and recall are two contradictory metrics. The F1 score is essentially the summed average of precision and recall, so in order to better evaluate the performance of the model, the F1 value is used as the overall evaluation metric to balance precision and recall, and the loss function during the training process is shown in Figure 3.

4.3 Experimental parameter settings

In terms of experimental parameter settings, the main parameter information of the model in this paper is finalized by experience, continuous experimentation and adjustment, and corpus specifics. The hidden layer of the BERT model has 12 layers and its output vector dimension is 768; the hidden layer of the BLSTM model has an output vector dimension of 256, and the dimension of the entity type label vector is 80. One of the open-source deep learning frameworks, PyTorch (https://pytorch.org/), was used to build the experimental platform to develop deep learning models. In the experiments, the values of the main parameters of the proposed model in this paper are as shown in Table 4. The hyperparameters in the experiments were determined by the specifics of the experiments and the corpus. Following the empirical value, we set the output vector dimension of the BLSTM model as 256, when the parameter is set to dimensions of entity-type label vector as 80, epochs as 40, max length as 150, and learning rate as 1e-5, the model obtains the optimal performance.

4.4 Experimental results and analysis

Through the following experiments, the NN-EE model proposed in this paper is compared with the following neural network-based event argument extraction models.

1) Baseline: This model is the BLSTM–CRF model.
2) BERT–BLSTM–CRF: This model is the BERT + Baseline model.

FIGURE 3
Loss function during the training process.

3) BERT–BLSTM–CRF + NER: This model is based on the BERT + Baseline model, where all entities appearing in the sentence are annotated, and then the entity type labels are encoded to be spliced with the output of the BERT layer, which is then input to the BLSTM layer.
4) Baseline + NSP: The model is based on the BERT + Baseline model and introduces the NSP mechanism from the BERT model. In this mechanism, the event trigger is used as text1 for this task, the symbol " [SEP]," and the original sentence are spliced together and used as model input.
5) NN-EE: The model is a combination of the BERT + Baseline + NER model and the BERT–BLSTM–CRF + NSP model described previously.

Table 5 shows the overall performance of the aforementioned models on the FD-OR, a self-constructed dataset in this paper. In addition, to demonstrate the stability of our proposed model, we conducted comparative experiments on another dataset of food safety news reports (FD-SR). From the results, we can observe that our proposed model combining NSP and NER for public opinion event extraction (NN-EE) achieves the best F1 score across all the compared methods. NN-EE improves the F1 score to 96.83%, which is an improvement of 1.11% compared to the baseline model. It can be observed from experiments 1 and 2 that the recall of the model increased and the precision decreased, and from experiments 1 and 3 that the recall, precision, and F1 score of the model decreased when combining the NSP mechanism, and from experiments 1 and 4 that the precision, recall, and F1 score of the model increased. This shows that using either the NSP mechanism or the NER technique model performance alone will decrease the performance of the model. The reason is that the NSP mechanism inherent in the BERT model can capture the semantic similarity between text_a and text_b. In this paper, the NSP mechanism can prompt the model to focus on the semantics of different parts of the text in the face of different trigger words and event types, alleviating the semantic interaction between the three that has been ignored in previous research work and improving the NER model's targeted extraction of relevant entities' capability of the NER model. Our NN-EE achieves optimal performance and demonstrates the effectiveness of combining the NSP mechanism with the NER model.

A specific event extraction example is presented to further explain our model, as shown in Figure 4. We first obtained the

TABLE 4 Experimental parameter setting.

Parameter	Value
Epochs	40
Batch size	8
Dimensions of entity-type label vector	80
Maximum length	150
Learning rate	1e-5
Layer of BERT	12
Dimensions of BERT	768
Function of BERT	Tanh
Layer of BLSTM	2 layers
Dimensions of BLSTM	256
Function of BLSTM	ReLu tanh

TABLE 5 Experimental results of event extraction.

Model	FD-OR data			FD-SR data		
	P (%)	R (%)	F1 (%)	P (%)	R (%)	F1 (%)
Baseline	92.64	83.22	87.66	79.32	74.21	76.67
BERT + Baseline	97.11	94.37	95.72	85.12	84.77	84.94
BERT + Baseline + NER	97.82	95.51	96.65	88.47	84.33	86.35
BERT + Baseline + NSP	96.93	95.22	96.36	92.64	83.22	87.66
NN-EE (ours)	**98.19**	**95.51**	**96.83**	**89.22**	**86.75**	**87.96**

P, R, F1 have been mentioned in the section Evaluation standard setting. The explanation of FD-OR data, FD-SR data has been given in section Experimental dataset.

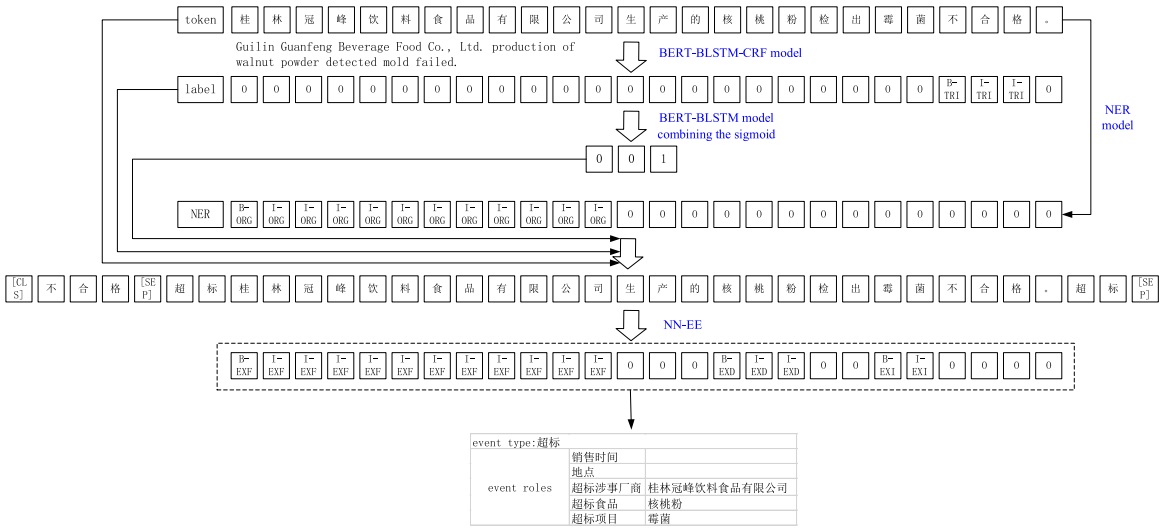

FIGURE 4
Case study.

initial input event trigger word: 不合格 (failure) by the BERT–BLSTM–CRF trigger word extraction model, while regretting the use of the BERT–BLSTM event type detection model combined with the sigmoid function to obtain the event type: exceedance, and also the initial input sequence of named entities $N = \{O, O, O, \cdots, B-TRI, I-TRI, I-TRI, O\}$. Then, we formed the token sequence $S = \{[CLS], hit, fake, [SEP], fake, w_1, \ldots., w_n, fake, [SEP]\}$ by splicing the event trigger, event type, and input text according to the input format of the BERT model and obtain the event arguments and their roles in it using our proposed NN-EE model. For example, {manufacturer involved in exceeding the standard: Guilin Guanfeng Beverage and Food Co., Ltd., exceeding the standard food: walnut powder, exceeding the standard item: mold}. Finally, we combined the obtained entity results with the trigger words and event types obtained from the upstream task to complete the event extraction for this text.

5 Conclusion and discussion

In this paper, we propose an opinion event extraction model (NN-EE) combining NSP and NER, which solves the problem of insufficient performance in recognizing combinatorial event arguments in Chinese text by introducing NER technology. At the same time, by incorporating event trigger word features into the NSP mechanism of the pre-trained language model BERT, the model is motivated to learn the deep semantic interactions between the event trigger and original text. The model achieves optimal performance on FD-OR, a self-constructed food opinion reporting dataset in this paper, and the experiments demonstrate the effectiveness of the model. In the future, we will optimize the performance of the model in handling event arguments that are nested entities.

Data availability statement

The datasets presented in this study can be found in online repositories. The names of the repository/repositories and accession number(s) can be found in the article/Supplementary Material.

Author contributions

QZ contributed significantly to theoretical analysis and manuscript preparation. SW performed the experiments, and contributed to the conception of the study and model formulation. ZL provided many promising insights during the revision process. WY performed the data analyses and helped perform the analysis with constructive discussions. All authors contributed to the article and approved the submitted version.

Funding

This research was supported by Beijing Natural Science Foundation (grant no. 4202014), the National Key Technology R and D Program of China (grant no. 2021YFD2100605), the Natural Science Foundation of China (grant nos. 62006008 and 61873027), Humanity and Social Science Youth Foundation of Ministry of Education of China (grant no. 20YJCZH229), Open Project Program of National Engineering Laboratory of Agri-Product Quality Traceability (grant no. AQT-2020-YB6), the Social Science Research Common Program of Beijing Municipal Commission of Education (grant no. SM202010011013), and Research Foundation for Youth Scholars of Beijing Technology and Business University (grant no. QNJJ2020-28).

Conflict of interest

The authors declare that the research was conducted in the absence of any commercial or financial relationships that could be construed as a potential conflict of interest.

Publisher's note

References

1. Zhang Z, Xu W, Chen Q. Joint event extraction based on skip-window convolutional neural networks. In: Natural Language Understanding and Intelligent Applications (2016). p. 324–34.

2. Ji H, Grishman R. Refining event extraction through cross-document inference. In: Proceedings of ACL-08: Hlt (2008). p. 254–62.

3. Hong Y, Zhang J, Ma B, Yao J, Zhou G, Zhu Q. Using crossentity inference to improve event extraction. In: Proceedings of the 49th Annual Meeting of the Association for Computational Linguistics: Human Language Technologies (2011). p. 1127–36.

4. Ritter A, Etzioni O, Clark S. Open domain event extraction from twitter. In: Proceedings of the 18th ACM SIGKDD International Conference on Knowledge Discovery and Data Mining (2012). p. 1104–12.

5. Huang L, Cassidy T, Feng X, Ji H, Voss C, Han J, Sil A. Liberal event extraction and event schema induction. In: Proceedings of the 54th Annual Meeting of the Association for Computational Linguistics (2016). p. 258–68.

6. Zhang T, Ji H, Sil A. Joint entity and event extraction with generative adversarial imitation learning. *Data Intell* (2019) 1(2):99–120. doi:10.1162/dint_a_00014

7. Chen Y, Xu L, Liu K, Zeng D, Zhao J. Event extraction via dynamic multi-pooling convolutional neural networks. In: Proceedings of the 53rd Annual Meeting of the Association for Computational Linguistics and the 7th International Joint Conference on Natural Language Processing (2015). p. 167–76.

8. Nguyen TH, Cho K, Grishman R. Joint event extraction via recurrent neural networks. In: Proceedings of the 2016 Conference of the North American Chapter of the Association for Computational Linguistics: Human Language Technologies (2016). p. 300–9.

9. Wang H, Zhu T, Wang M, Zhang G, Chen W. A prior information enhanced extraction framework for document-level financial event extraction. *Data Intelligence* (2021) 3(3):460–76. doi:10.1162/dint_a_00103

10. Kan Z, Qiao L, Yang S, Liu F, Huang F. Event arguments extraction via dilate gated convolutional neural network with enhanced local features. *IEEE Access* (2020) 8:123483–91. doi:10.1109/access.2020.3004378

11. Du X, Cardie C. Event extraction by answering (almost) natural questions. In: Proceedings of the 2020 Conference on Empirical Methods in Natural Language Processing. Association for Computational Linguistics (2020).

12. Li F, Peng W, Chen Y, Wang Q, Pan L, Lyu Y, Zhu Y. Event extraction as multi-turn question answering. In: Findings of the Association for Computational Linguistics: EMNLP 2020 (2020). p. 829–38.

13. Liu J, Chen Y, Liu K, Bi W, Liu X. Event extraction as machine reading comprehension. In: Proceedings of the 2020 Conference on Empirical Methods in Natural Language Processing (EMNLP) (2020). p. 1641–51.

14. Liu X, Luo Z, Huang H. Jointly multiple events extraction via attention-based graph information aggregation. In: Proceedings of the 2018 Conference on Empirical Methods in Natural Language Processing, Brussels, Belgium, October 31–November 4, 2018 (2018). p. 1247–1256. Available at: https://aclanthology.info/papers/D18-1156/d18-1156.

15. Sheng J, Guo S, Yu B, Li Q, Hei Y, Wang L, et al. CasEE: A joint learning framework with cascade decoding for overlapping eventextraction. In: Findings of the Association for Computational Linguistics: ACL-IJCNLP 2021, Association for Computational Linguistics, Online (2021). p. 164–174. Available at: https://aclanthology.org/2021.findings-acl.14

16. Nguyen TM, Nguyen TH. One for all: Neural joint modeling of entities and events. *Proc AAAI Conf Artif Intelligence* (2019) 33:6851–8. doi:10.1609/aaai.v33i01.33016851

17. Luo Y, Xiao F, Zhao H. Hierarchical contextualized representation for named entity recognition. *Proc AAAI Conf Artif intelligence* (2020) 34:8441–8. doi:10.1609/aaai.v34i05.6363

18. Devlin J, Chang M-W, Lee K, Toutanova K. Bert: Pre-training of deep bidirectional transformers for language understanding. arXiv preprint arXiv: 1810.04805 (2018).

Frontiers in Physics

Investigates complex questions in physics to understand the nature of the physical world

Addresses the biggest questions in physics, from macro to micro, and from theoretical to experimental and applied physics.

Discover the latest Research Topics

See more →

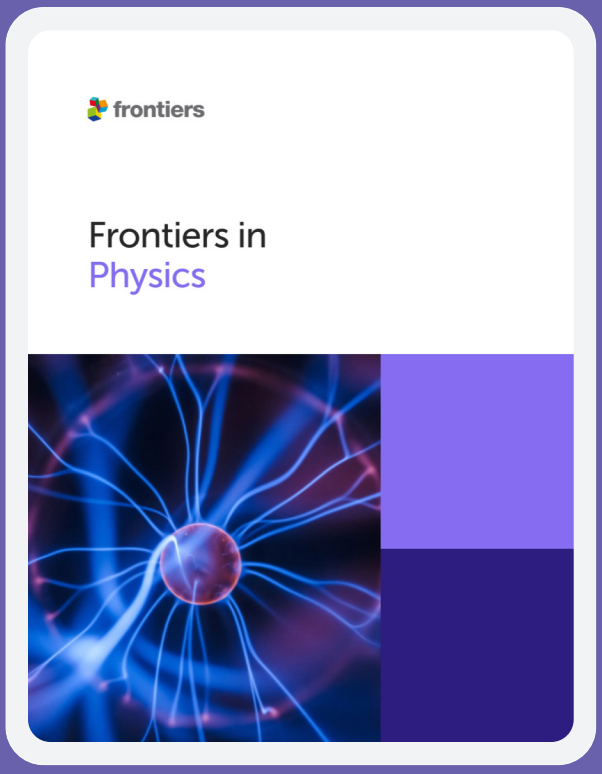

Frontiers

Avenue du Tribunal-Fédéral 34
1005 Lausanne, Switzerland
frontiersin.org

Contact us

+41 (0)21 510 17 00
frontiersin.org/about/contact